PROCEEDINGS OF THE FOURTH INTERNATIONAL SYMPOSIUM ON

CLEANING TECHNOLOGY IN SEMICONDUCTOR DEVICE MANUFACTURING

Editors

Richard E. Novak
SubMicron Systems, Inc.
Allentown, Pennsylvania

Jerzy Ruzyllo
The Pennsylvania State University
University Park, Pennsylvania

Assistant Editors

A. Bowling
R. Helms
M. Heyns
T. Ohmi
L. Shive

ELECTRONICS DIVISION

Proceedings Volume 95-20

THE ELECTROCHEMICAL SOCIETY, INC.,
10 South Main St., Pennington, NJ 08534-2896

Copyright 1996 by The Electrochemical Society, Inc.
All rights reserved.

This book has been registered with Copyright Clearance Center, Inc.
For further information, please contact the Copyright Clearance Center,
Salem, Massachusetts.

Published by:

The Electrochemical Society, Inc.
10 South Main Street
Pennington, New Jersey 08534-2896
Telephone (609) 737-1902
Fax (609) 737-2743

Library of Congress Catalog Number: 95-61593

ISBN 1-56677-115-3

Printed in the United States of America

PREFACE

The Fourth International Symposium on Cleaning Technology in Semiconductor Device Manufacturing was held during the Fall Electrochemical Society meeting in Chicago, Illinois, October 1995. This was a very successful meeting which attracted world-class speakers and a large audience active in wafer cleaning. The meeting was the fourth in the series that began in the Fall of 1989 during the Hollywood, Florida, ECS meeting. Since that time the Symposium has attracted an increasing number of papers, as well as attendees. The Fourth International Symposium had paper submissions grow to the limit of the meeting. Future increase in the number of papers will necessitate the use of poster sessions. Each year the quality of papers, in terms of scientific content, has grown. This Symposium has established itself as one of the premier forums for presentation of state-of-the-art work on wafer cleaning while simultaneously offering the opportunity to meet informally with others working in the field.

This proceedings volume contains the papers presented at the Fourth International Symposium on Wafer Cleaning Technology in Semiconductor Device Manufacturing. Ninety percent of those presented at the meeting are contained in this volume. As one reads these papers it is hoped that information contained in these pages will help improve the wafer cleaning processes for which you are responsible, as well as providing fundamental information that may lead to new or improved processes. These are the aspirations of a successful meeting.

Wafer cleaning has transitioned from an "art" to the science we know today. There are clearly challenges ahead to make successful 0.25 m, 0.18 m and 0.13 m type devices. A number of these challenges are in the area of surface preparation. We are delighted that the Electrochemical Society forum has provided the catalyst to bring together the science and the manufacturing technology so that, together, improved device yield can be attained.

We would like to thank all the symposium authors, session chairmen and participants for making this meeting a success. We would particularly like to thank the invited speakers for sharing their expert knowledge with the rest of us. Our colleagues who assisted in editing this volume are warmly thanked, also. We look forward to the next symposium in this series which is scheduled to be held at the Paris Electrochemical Society meeting in August of 1997.

Richard E. Novak
Jerzy Ruzyllo

TABLE OF CONTENTS

Preface *iii*

LIQUID-PHASE CLEANING -- *Parts I & II*

PROPOSAL OF ADVANCED WET CLEANING OF SILICON SURFACE 1
Tadahiro Ohmi

CONTAMINATION EFFECTS ON OXIDE BREAKDOWN PROPERTIES 13
Jennifer Sees, Lindsey Hall, Jagdish Prasad, Anthony Schleisman and John Niccoli

THE EFFECTS OF DILUTE SC-1 AND SC-2 CHEMISTRIES ON DIELECTRIC BREAKDOWN FOR PRE GATE CLEANS 21
Shelley M. Smith, Mohan Varadarajan and Kurt K. Christenson

RCA OPTIMISATION FOR SUB - 0.5 m CMOS TECHNOLOGIES 28
Alain Fleury, Kathy Barla, Didier Levy and Laurens Kwakman

QUANTITATIVE MODEL FOR THE SC-1 CLEANING 39
Steven Verhaverbeke, Jennifer W. Parker and Chris F. McConnell

OPTIMIZATION OF HF AND OXIDANT WET CLEANINGS BEFORE 7nm GATE OXIDE 49
F. Tardif, T. Lardin, C. Paillet, J. P. Joly, A. Fleury, P. Patruno, D. Levy and K. Barla

THE EFFECTS OF REVERSING WAFER-SURFACE WETTING PROPERTIES OF SULFURIC ACID:HYDROGEN PEROXIDE WAFER-CLEANING SOLUTIONS 60
W. Syverson, M. Fleming and P. Schubring

SULFURIC ACID/HYDROGEN PEROXIDE RINSING STUDY 66
P. J. Clews, G. C. Nelson, C. A. Matlock, P. J. Resnick, C. L. J. Adkins and N. C. Korbe

EQUIPMENT FOR WAFER CLEANING PARALLEL DOWN FLOW RINSE 74
Yutaka Hiratsuka, Nobuyuki Fujikawa

THE APPLICATION OF THE OZONATED DI WATER AT THE PRE GATE OXIDATION WET CLEANING FOR THE PREVENTION OF WATER MARKS 82
Jin-Goo Park and Michael F. Pas

THE USE OF ULTRASOUND ENERGY IN PHOTORESIST STRIPPING APPLICATIONS 90
Ismail I. Kashkoush

RADICAL ACTIVATION OF DI WATER AND CLEANING SOLUTION BY MEGASONIC 99
Masayuki Toda and Masayuki Kato

STUDY ON MEGASONIC IN ADVANCED WET CLEANING PROCESS 107
K. Kubo, S. Ojima, M. Toda and T. Ohmi

GAS-PHASE CLEANING

IN-SITU VAPOR PHASE PROCESSES IN AN INTEGRATED CLUSTER SYSTEM FOR PRE-GATE OXIDE SILICON SURFACE CLEANING 115
Y. Ma and M. L. Green

THE REACTION OF VAPOR HF WITH CHEMICALLY FORMED SILICON OXIDE: PRODUCTION OF STABLE HYDROGEN-TERMINATED SURFACES 126
J. M. Barnett, P. A. Grothe, J. S. Martin, R. A. Carpio, B. W. Fowler, Vasu Atluri and Nicole Herbots

A STUDY OF THE EFFECTIVENESS OF VAPOR PHASE CLEANS FOR ADVANCED GATE OXIDATION 134
J. K. Tong, G. F. Hanger, D. S. Becker and D. J. Syverson

COMPARISON OF HC1 GAS-PHASE CLEANING WITH CONVENTIONAL AND DILUTE WET CHEMISTRIES 142
C. Elsmore, T. Q. Hurd, J. Clarke, M. Meuris, P. W. Mertens and M. M. Heyns

UV/CL2 ETCHING AND CLEANING OF WAFER SURFACES 150
A. Scott Lawing, Anthony J. Muscat, Herbert H. Sawin and Jeffrey W. Butterbaugh

METAL REMOVAL WITH A CIF3 BEAM AT ROOM TEMPERATURE 158
Jane P. Chang, Zhe Zhang, Han Xu, Herbert H. Sawin and Jeffrey W. Butterbaugh

SUB-MONOLAYER IRON AND COPPER REMOVAL BY EXPOSURE TO 1,1,1,5,5,5-HEXAFLUORO-2,4-PENTANEDIONE (H+hfac) 166
S. E. Beck, M. A. George, K. M. Young, D. A. Moniot, D. A. Bohling, A. A. Badowski and A. P. Lane

REACTION OF 1,1,1,5,5,5-HEXAFLUORO-2,4-PENTANEDIONE (h+hfac) WITH IRON OXIDE THIN FILMS 175
M. A. George, D. W. Hess, S. E. Beck, K. M. Young, D. A. Roberts, R. Vrtis, G. Voloshin, D. A. Bohling and A. P. Lane

MONITORING OF SILICON SURFACE AFTER REACTIVE ION ETCHING 184
D. K. Hwang, J. Ruzyllo and E. Kamieniecki

SELECTIVE ETCHING FOR MAKING CYLINDRICAL CAPACITORS USING ANHYDROUS HF VAPOR PHASE CHEMISTRY 194
Jitesh R. Mehta, Tim Rogers and Satoshi Kikuchi

EVOLUTION OF Si SURFACES AFTER ANHYDROUS HF:CH3OH ETCHING
K. Torek, A. Miechkowski and J. Ruzyllo 208

OPTIMIZATION OF PHOTORESIST AND POLYMER REMOVAL IN A VIA ETCH PROCESS 214
Steve Marks, Sandra W. Graham, Tinal Uk, C. C. Chang, Claudia Geller and Chiu Tse

DAMAGE DURING ASHING: A CHARACTERIZATION OF SEVERAL MODERN ASHERS 225
Lee M. Loewenstein, Srikanth Krishnan and George A. Brown

REMOVAL OF POLYMERIC/SILICATE RESIDUES AND REDUCTION OF CONTACT RESISTANCE FOR INTER-METAL VIA HOLES BY VAPOR PHASE HF CLEANING 235
J. K. Tong, J. S. Martin, T. C. Rogers and D. J. Syverson

ANALYSIS AND REMOVAL OF POLYSILICON ETCH RESIDUE 243
Chang Weon Lee, Sang Jun Choi, Jae Jeong Kim, Hong Seok Kim, Woo Shik Kim, Jong Dae Lee and Jong Wan Lee

SPECIALTY GAS INTERACTIONS WITH ULTRACLEAN SILICON SURFACES 251
Yasuyuki Shirai, Masakazu Nakamura and Tadahiro Ohmi

LIQUID-PHASE CLEANING -- *Part III*
IMPURITIES ON Si SURFACES
ELECTROCHEMICAL DEPOSITION AND REMOVAL OF METALLIC IMPURITIES ON SILICON SURFACES 257
Hitoshi Morinaga and Tadahiro Ohmi

METAL ADSORPTION MECHANISM ON SI WAFER 269
Y. Takahara, A. Saito and H. Oka

METAL INTERACTIONS WITH SILICA (SiO2) SURFACES: ADSORPTION AND ION EXCHANGE 277
T. Q. Hurd, H. F. Schmidt, A. L. P. Rotondaro, P. W. Mertens, L. H. Hall, M. M. Heyns

IMPACT OF THE ELECTROCHEMICAL PROPERTIES OF SILICON WAFER SURFACES ON COPPER OUTPLATING FROM HF SOLUTIONS 284
I. Teerlinck, H. F. Schmidt, A. L. P. Rotondaro, T. Q. Hurd, L. Mouche, P. W. Mertens, M. Meuris, M. M. Heyns, D. Vanhaeren and W. Vandervorst

ANALYSIS OF Cu ADHESION ONTO SILICON WAFER SURFACE USING ELECTROCHEMICAL IMPEDANCE MEASUREMENT 292
Kenichi Uemura and Kengo Shimanoe

THE EFFECT OF METALLIC CONTAMINATION AND SURFACE ROUGHNESS ON GATE OXIDE STRENGTH AND PRODUCT YIELD 300
Thomas Roche, Steve Adler, Rick Cosway, Stephen Schauer and Lisa Liu

SURFACE METAL CONTAMINATION ON SILICON WAFERS MEASURED BY *SurfaceSIMS* 308
Stephen P. Smith, C. J. Hitzman and R. S. Hockett

DEPTH PROFILE OF METALLIC CONTAMINATION DEPOSITED ON Si and SiO2 SURFACES IN APM SOLUTION 316
Mikio Tsuji, Yoshinori Muramatsu and Nahomi Aoto

CHARACTERIZATION & MONITORING -- *Part I*

ON SILICON WAFER SURFACES
ANALYTICAL METHODS FOR ORGANIC IMPURITIES ADSORBED 323
Ayako Shimazaki, Makiko Tamaoki and Yumi Sasaki

NON-CONTACT ELECTRICAL CHARACTERIZATION OF SILICON SURFACES FOR TRUE IN-LINE MONITORING OF CLEANING PROCESSES 332
Emil Kamieniecki

MONITORING OF Fe CONTAMINATION ON Si SURFACES USING NON-CONTACT SURFACE CHARGE PROFILER 344
P. Roman, I. Kashkoush, R. E. Novak, E. Kamieniecki and J. Ruzyllo

IN-LINE MONITORING OF WET CLEANING PROCESSES USING RADIO FREQUENCY PHOTOCONDUCTANCE DECAY 350
G. J. Norga, K. A. Black, M. R. Black, J. Michel and L. C. Kimerling

A METHOD FOR NATIVE OXIDE THICKNESS MEASUREMENT 358
K. Vepa, K. Baker and L. W. Shive

CHEMICAL OXIDE CHARACTERIZATION 366
C. Paillet, J. P. Joly, F. Tardif, K. Barla, P. Patruno, D. Levy

CHARACTERIZATION OF SILICON OXIDE ETCHING IN GAS PHASE HF/VAPOR MIXTURES 371
Anthony J. Muscat, A. Scott Lawing, Herbert H. Sawin, Jeff Butterbaugh, Dan Syverson and Fred Hiatt

THE APPLICATION OF SURFACE ANALYSIS TECHNIQUES FOR MONITORING HYDROGEN TERMINATION CLEANING PROCESSES 379
Ronald A. Carpio, Burt W. Fowler, Vasu Atluri, Nicole Herbots and Philip R. Brierley

TRACE MOISTURE MEASUREMENT IN Hcl USING NEAR-INFRARED LASER ABSORPTION SPECTROSCOPY 387
Yoshio Ishihara, Hiroshi Masusaki, Shang-Qian Wu, Koh Matsumoto and Tetsuya Kimijima

CHARACTERIZATION, PROPERTIES AND ANALYSIS OF VIA VEILS 395
K. Mocala, P. Crabtree, E. Mocala, R. Hegde, K. Lao and P. Laberge

DEFECT CHARACTERIZATION ON A BATCH CLEAN PROCESS USED AFTER PLASMA METAL ETCHING 401
K. E. Mautz

LIQUID PHASE CLEANING -- *Part IV*

DOUBLE-SIDE WAFER SCRUBBING BEYOND POST-CMP CLEANING 409
Wilbur C. Krusell, Igor J. Malik, Fred Mohr and Diane J. Hymes

WATER CONSUMPTION AND RINSE CONSIDERATIONS IN SEMICONDUCTOR WET PROCESSING 421
Chris McConnell, Huw Thomas, Steven Verhaverbeke, Steve Bay and Jennifer W. Parker

ETCH UNIFORMITY OF THERMAL OXIDE DURING HF-WET PROCESSES 429
I. Kashkoush, R. E. Novak, B. Rajaram and F. Carrillo

SMOOTHING OF Si (100) SURFACE MICROROUGHNESS BY A NEW ETCHING SOLUTION BHF/H2O2 436
Yoshinori Muramatsu, Mikio Tsuji and Nahomi Aoto

DETERMINATION OF THE H-PASSIVATION BUILD-UP TIME IN DHF-TREATMEN 444
M. Meuris, H. Izumi, K. Kubo, S. Ojima, T. Ohmi and M. M. Heyns

CHEMICAL OXIDE GROWTH AND ITS INFLUENCE ON SUBSEQUENT HF CLEANING 449
L. Li, E. Grieger, K. Griffiths, S. Byrne and R. C. Hawthorne

MECHANISM FOR THE CHEMISORPTION OF CONTAMINANTS ON HYDROGEN-TERMINATED SILICON SURFACES 455
Christopher E. D. Chidsey and Matthew R. Linford

REMOVAL OF THERMALLY GROWN SILICON DIOXIDE FILMS USING WATER AT ELEVATED TEMPERATURE AND PRESSURE 464
Geoffrey L. Bakker and Dennis W. Hess

IMPROVEMENT OF A POST-OXIDE CMP CLEANING PROCESS THROUGH THE USE OF DESIGNED EXPERIMENTS 472
Raj Shah, Jeanine Herrera, Shelley Peterman

CHARACTERIZATION & MONITORING -- *Part II*

IN SITU AND REAL TIME STUDIES OF WET CHEMICAL SILICON SURFACE CLEANING REACTIONS 480
H. F. Schmidt, I. Teerlinck, W. Storm, H. Bender and M. M. Heyns

SURFACE ANALYSIS OF Si(100) WAFERS PROCESSED IN VANADIUM SPIKED DILUTE HF SOLUTIONS 492
Jagdish Prasad, Jennifer Sees, Lisa Lester, Monte Douglas, Allen Templeton and Lindsey Hall

SURFACE SIMS ROUND ROBIN FOR NA, AL AND K ON SILICON WAFERS 500
R. S. Hockett and Alain Diebold

FEASIBILITY OF ANALYSIS OF SILICON SURFACE CLEAN TIME-OF-FLIGHT SECONDARY ION MASS SPECTROMETRY 508
S. D. Hossain-Pas, M. F. Pas and M. A. Douglas

ANALYSIS OF SUBMICRON ALUMINUM AND ALUMINA PARTICLES BY TIME-OF-FLIGHT SECONDARY ION MASS SPECTROMETRY (TOF-SIMS) 518
Patricia M. Lindley, Bruno W. Schueler, Alain C. Diebold, Richard S. Hockett and George Mulholland

WET PROCESSING OF VIAS AND TRENCHES 526
Jennifer Parker, Steven Verhaverbeke and Chris McConnell

DEVELOPMENT OF ADVANCED CORROSION FREE ORGANIC STRIPPERS FOR ULSI PROCESSING 537
A. L. P. Rotondaro, K. Honda, T. Maw, D. Perry, M. Lux, M. M. Heyns, C. Claeys and I. Darakchiev

ETCHING SiO2 FILMS IN AQUEOUS 0.49% HF 544
Sean O'Brien and Ambika Somashekar

SURFACE EFFECTS DURING PROXIMITY RAPID THERMAL DIFFUSION OF PHOSPHORUS IN SILICON 552
S. Montandon, W. Zagozdzon-Wosik, Jia Li, W. T. Taferner and B. Bensaoula

PARTICLES

PARTICLE CONTAMINATION DURING WET CLEANING PROCESS ONTO VARIOUS WAFER SURFACES 560
Yasuki Sakata, Akihiro Ohnishi, Gunji Kishi, Shouzou Izumo, Hiroyuki Kondou and Akihiro Tomozawa

EFFECTS OF SEQUENTIAL CHEMISTRIES ON PARTICLE REMOVAL 567
K. K. Christenson, S. M. Smith, S. Nelson, B. Carlson, C. Bode and K. Johnson

PARTICLE IMPACT ON 7 nm GATE OXIDES 575
C. Paillet, A. M. Papon, J. P. Joly, F. Tardif, D. Levy, K. Barla and P. Patruno

ASPECTS OF ALUMINA PARTICLE DEPOSITION ONTO CVD TUNGSTEN WAFERS RELEVANT TO POST CMP CLEANING 581
Joong S. Jeon, Chilkunda Raghunath, Emil A. Kneer and Srini Raghavan

A STUDY OF LIGHT POINT DEFECT REMOVAL BY SC-1 CHEMISTRIES 589
P. J. Resnick, C. L. J. Adkins, C. A. Matlock, M. J. Kelly, P. J. Clews, N. C. Korbe

EFFECTS OF SC-1 DILUTION AND TEMPERATURE ON VARIOUS PARTICLE REMOVAL CHALLENGES 597
K. K. Christenson, S. M. Smith, C. Bode and K. Johnson

FIRST OBSERVATION OF 0.1 m SIZE COPS AND DUSTS ON THE BARE Si WAFERS BY USING AFM WITH OPTIMAL SCATTERING SYSTEM 605
Naohiko Fujino, Isamu Karino, Junji Kobayashi, Kazuo Kuramoto, Masashi Ohomori, Masatoshi Yasutake and Shigeru Wakiyama

EXPLORATORY USE OF MICRO-XANES FOR PARTICLE DETECTION AND ANALYSIS ON SI WAFERS 613
C. R. Brundle, Y. Uritsky, A. Warwick, R. S. Hockett, A. Craig and C. Ayre

AUTHOR INDEX 621

SUBJECT INDEX 624

FACTS ABOUT THE ELECTROCHEMICAL SOCIETY, INC.

The Electrochemical Society, Inc., is an international, nonprofit, scientific, educational organization founded for the advancement of the theory and practice of electrochemistry, electrothermics, electronics, and allied subjects. The Society was founded in Philadelphia in 1902 and incorporated in 1930. There are currently over 6000 scientists and engineers from more than 60 countries who hold individual membership; the Society is also supported by more than 100 corporations through Patron and Sustaining Memberships.

The Technical activities of the Society are carried on by Divisions and Groups. Local Sections of the Society have been organized in a number of cities and regions.

Major international meetings of the Society are held in the Spring and Fall of each year. At these meetings, the Divisions and Groups hold general sessions and sponsor symposia on specialized subjects.

The Society has an active publications program which includes the following:

Journal of The Electrochemical Society - The Journal is a monthly publication containing technical papers covering basic research and technology of interest in the areas of concern to the Society. Papers submitted for publication are subjected to careful evaluation and review by authorities in the field before acceptance, and high standards are maintained for the technical content of the JOURNAL.

Interface - Interface is a quarterly publication containing news, reviews, advertisements, and articles on technical matters of interest to Society Members in a lively, casual format. Also featured in each issue are special pages dedicated to serving the interests of the Society and allowing better communication between Divisions, Groups, and Local Sections.

Meeting Abstracts *(formerly Extended Abstracts)* - Meeting Abstracts of the technical papers presented at the Spring and Fall Meetings of the Society are published in serialized softbound volumes.

Proceedings Series - Papers presented in symposia at Society and Topical Meetings are published from time to time as serialized Proceedings Volumes. These provide up-to-date views of specialized topics and frequently offer comprehensive treatment of rapidly developing areas.

Monograph Volumes - The Society has, for a number of years, sponsored the publication of hardbound Monograph Volumes, which provide authoritative accounts of specific topics in electrochemistry, solid state science, and related disciplines.

For more information on these and other Society activities, visit the ECS Home Page at the following address on the World Wide Web:

http://www.electrochem.org.

PROPOSAL OF ADVANCED WET CLEANING OF SILICON SURFACE

Tadahiro Ohmi
Department of Electronics, Faculty of Engineering, Tohoku University,
Sendai 980, Japan

Ultraclean wafer surface is crucial for high quality processing in Si technologies. Cleaning of Si wafer surface has been provided by RCA wet cleaning for this quarter century, where there exist high temperature processes consisting of $H_2SO_4/H_2O_2/H_2O$, $NH_4OH/H_2O_2/H_2O$ and $HCl/H_2O_2/H_2O$ treatment. Thus, RCA cleaning requires a large number of processing steps, resulting in requirements of huge consumption volume of liquid chemicals and ultrapure water, and simultaneously huge volume of clean air exhaust to suppress chemical vapor getting into clean room.

Total room temperature wet cleaning consisting of five cleaning steps has been developed for Si wafer surface, where consumption volume of liquid chemicals and ultrapure water has been reduced dramatically less than 1/20 compared to that of RCA cleaning. The newly developed cleaning technology has been confirmed to contribute to future simplified and low cost manufacturing of ULSI.

INTRODUCTION

It is the ultraclean substrate surface which enables us to take the first step ahead toward materialization of the advanced process. Without ultraclean substrate surface, high-quality semiconductor process will never be realized however thoroughly other process steps may be controlled. Figure 1 shows reflection electron diffraction image of sputtering Si epitaxial thin films obtained at 300℃ (1). In the case of Figure 1(a), the Si substrate is treated, immediately before film deposition, with very low energy Ar ion bombardment to remove moisture molecules adsorbed on its surface. The film shown in Figure 1(b) is deposited on the Si substrate which is not treated with very low energy Ar ion bombardment. Figure 1 (a) shows clear Kikuchi lines which demonstrate that the Si film is composed of perfect crystal while Figure 1(b) shows streak patterns which indicate that the Si film is made from extremely-defective single crystal. As shown in Figure 1, however, perfect single-crystal thin film can not be grown at low temperatures such as 300℃ if moisture molecules remain on the substrate surface.

The ultraclean surface is defined as the surface which is free from contaminants such as particles, metals, organic, and moisture molecules as well as native oxide, and which features atomic-order surface smoothness and hydrogen termination of surface dangling bonds. When the substrate surface is exposed to the air in cleanroom, moisture of several tens of molecular layers adsorbs within a second (2)-(4). Bond energy between moisture molecules and that between moisture molecule and hydrogen-terminated Si surface are the same at 0.12 eV (2.7 kcal/mol), which is higher by about 4.5 times than the thermal energy at room temperature of 0.026 eV. This is why either high-temperature baking or low-energy ion bombardment is necessary to remove adsorbed moisture from substrate surface. For these ten years, author has argued "the biggest enemy in realizing the advanced process is moisture."

REMOVAL MECHANISM OF SURFACE CONTAMINANTS

In order to remove metallic and organic contaminants from the Si surface, it is necessary to use a solution featuring high redox potential or deep energy level. This solution captures electrons from metallic and organic contaminants to oxidize them. In this process, metals are ionized to be dissolved into the solution while organic impurities are decomposed to CO_2, H_2O etc. This is why the conventional surface cleaning process employs H_2SO_4 : H_2O_2 (SPM) solution (4:1, 120 - 150℃) and HCl : H_2O_2 : H_2O (HPM) solution (1:1:6, 80 - 90 ℃), both of which feature high redox potential (5)-(10).

Following two requirements must be simultaneously satisfied to remove particles from the surface (11)-(13) :

- Zeta potential of the substrate surface and particles is in the same polarity in the solution in order to exhibit repulsive electric force between surface and particles.
- The substrate surface is slightly etched (over 0.25 nm/min).

The in-process Si wafer surface is covered with thin films of SiO_2, Si_3N_4, Al alloy, and photoresist as well as Si, while particles are composed of various materials. It is alkaline solution so far where all these materials exhibit zeta potential of the same polarity (negative potential) (as shown in Figure 2) (11). This is why the particle removal step of the conventional cleaning process employs NH_4OH : H_2O_2 : H_2O (APM) solution (1:1:5 [RCA], 0.05:1:5 [Tohoku University], 80-90℃) which can slightly etch the Si surface (14)-(16). Thus the mechanism to remove contaminants adsorbed on the surface has been scientifically revealed.

RCA cleaning uses chemicals and ultrapure water in large volume at high temperature. As a result, it generates huge amount of chemical vapor, which increases loads on clean air exhaust and make-up air for fresh air intake as well as on scrubber. As chemicals and ultrapure water are evaporated in large volume in RCA cleaning, chemical composition of the cleaning solution can not be maintained at a constant level, which inevitably deteriorates accuracy and reproducibility of the cleaning process. The new surface cleaning technology, therefore, is essentially needed to satisfy the followings :
(1) All cleaning process steps are performed at room temperature so as to almost perfectly suppress evaporation of chemicals and ultrapure water, which makes it possible to accurately maintain chemical composition.
(2) The number of process steps is reduced as small as possible and consumption volume of chemicals and ultrapure water is minimized.
(3) Chemical wastes are perfectly recovered and regenerated so as to make semiconductor manufacturing environmentally friendly.

Removal of metallic and organic impurities from wafer surface requires a solution featuring high redox potential or deep energy level. Figure 3 shows redox potential and energy level as a function of pH in HCl, HNO_3, H_2SO_4, HCl/KClO, H_2SO_4, Na_2SO_4, and KOH. It also shows redox potential and pH of ultrapure water with O_3, O_2, and H_2 injected (9)(20). Redox potential (E) which has been used in the solution chemistry can be converted to energy level (ϵ)as follows :

$$\epsilon = -(4.44 + E)\ (\mathrm{eV}) \qquad [1]$$

Using Equation [1], it is possible to convert Figure 3 to Figure 4 which shows energy level of solution as a function of pH. In Figure 4, dotted lines stand for energy levels at the bottom of conduction band and at the top of valence band of Si. As shown in Figure 4, energy level of acid solutions with pH of 6 or less is deeper than that at the top of the Si valence band. This means that acid solutions are capable of taking electrons in valence band to weaken Si-Si covalent bond on the surface contacting with acid solution. In acid solutions, therefore, the Si surface easily gets oxidized in a short time.

All that is required in organic impurity removal is capability to oxidize organic impurities to decompose them into CO_2, H_2O etc. To remove metallic impurities, on the other hand, a solution featuring high positive redox potential is satisfactory as it can oxidize metals (take electrons form metals) to get ionized metals dissolved. A solution featuring strong

oxidizing force, in other words, a solution featuring high positive redox potenmtial, i.e., deep energy level is expected fully satisfy this requirement. It is obvious that the conventional cleaning method employs H_2SO_4, HCl, and H_2O_2 to control redox potential of the solutions. Redox potential can be controlled in the range of +1.3 V to -0.35 V, as shown in Figure 2 and 3, by injecting O_3, O_2, or H_2 into ultrapure water in ppm order. Ozonized ultrapure water features higher redox potintial than those of H_2SO_4, HCl, and HNO_3 with very high concentration. Ultrapure water with O_3 of several ppm can dissolve metals including Cu and Ag at room temperature which feature higher electronegativity than Si (6)(7)(10).

Figures 5 (a) and (b) show residual Cu and Ag on the Si wafers which are treated with ozonized ultrapure water. The wafers are initially contaminated with Cu at around 1×10^{13} and with Ag at around 1×10^{14} atoms/cm^2. Cu removal is found hardly dependent on O_3 concentration. Although O_3 concentration is varied from 1.8 ppm - 13.1 ppm, Cu of about 10^{12} atoms/cm^2 remains in chemical oxide formed by ozonized ultrapure water. On the other hand, amount of residual Ag is below TRXRF detection limit of 1×10^{11} atoms/cm^2 when O_3 concentration is kept at higher than 0.6 ppm. Ozone concentration is decided around at 5 ppm because surface microroughness increases for ozone concentration of 10 ppm. Cu included in chemical oxide can be removed in the succeeding FPM cleaning. As shown in Figure 6, amount of residual Cu is reduced below detection limit of 1.8×10^9 atoms/cm^2, where H_2O_2 of more than 0.1% is injected to 0.5% HF. It has been proved in experiments that ozonized ultrapure water and FPM cleaning steps are extremely effective in removing noble metals such as Cu and Ag featuring higher electronegativity than Si.

In order to remove particles from the substrate surface, it is required to get every material to feature zeta potential of the same polarity in a solution. Even in acid solutions, it is possible to meet this requirement if ionic surfactant is added to get them adsorbed onto the material surface (See Table 1) (14). The $HF:H_2O_2:H_2O$ (FPM) cleaning is a remarkable cleaning method which can remove SiO_2 film and metals such as Cu simultaneously (22)(23), and it is also capable for slightly etching the Si surface (9). Figure 7 shows Si surface etching with FPM with and without surfactant. Initial etching rate is 0.3 nm/min at 25℃. When a surfactant is injected, etching rate is lowered less than 1/10.

It is speculated that particles as well as oxides and metals must be removed simultaneously if megasonic with frequency of around 1 MHz is applied to surfactant-added FPM solution. Figure 8 shows particle removal efficiency of various solutions. The Si wafer is intentionally contaminated with 3000 - 4000 particles with size of 0.3 μm or more. DHF, FPM, and surfactant-added FPM (FPMS) are found hardly effective in removing particles. Particle re. oval efficiency of high-temperature APM cleaning is exceeded at room

temperature only when megasonic is applied to surfactant-added FPM solution (FPMS+MS). We have found at last the method which can replace the APM cleaning, a core of the conventional RCA cleaning. The APM cleaning process uses extremely volatile ammonia. Evaporation of ammonia makes it impossible to control chemical composition accurately.

Figure 9 (a) shows the newly-proposed Si surface cleaning process in which every step is performed at room temperature. Figure 9 (b) shows the conventional RCA cleaning process. The new cleaning process is composed of five room-temperature steps. Chemicals used in the new process are just HF and H_2O_2 where chemical concentration is maintained less than 1%. By keeping humidity around chemical bathes at higher than 80%, evaporation of chemicals and ultrapure water can be suppressed at a very low level. Consequently, chemical composition can be controlled in an extremely accurate level, which enables us to realize the wet process featuring extremely high accuracy and perfect reproducibility. Figure 10 demonstrates an aspect of the accurate and reproducible process (24). It shows etching depth as a function of etching time when thermal oxide formed in 1000℃ dry oxidation is etched with BHF (NH_4F/HF) whose chemical composition and temperature are accurately controlled. Etching rate is kept around 0.11 nm/min. Figure 11 shows samples for Z-axis calibration of Atomic Force Microscope (AFM) which are prepared by using this precise etching method (24). In this wet etching, samples are prepared so as to have steps of about 0.5 nm difference in height each other.

The FPMS process with megasonics is followed by ozonized ultrapure water shower or dip cleaning in order to recover FPM solution from the wafer and the wafer carrier surface. As surfactant is added to FPM solution, FPM solution adheres on wafers and carriers : about 0.8 gram of FPM solution adheres on a 200-millimeter wafer on average. In the ozonized ultrapure water shower or dip cleaning, this adhering FPM is cleaned off to be introduced to the recovery/regeneration process. Additionally this shower or dip cleaning step can minimize chemicals carried over to the final parallel down flow rinsing bath, which can reduce rinsing duration and ultrapure water consumption as small as possible. The shower or dip cleaning employs ozonized ultrapure water having a 1 ppm concentration in order to remove surfactant molecules which may not be removed merely with ultrapure water. The new cleaning process employs the DHF cleaning at the final stage in order to remove chemical oxide grown in previous ozonized ultrapure wafer treatment and to terminate the bare Si surface with hydrogen.

In the parallel down flow rinsing process, ultrapure water is introduced from the top of cleaning bath while it is pumped out from the bottom which is equipped with media with relatively high pressure drop such as a PTFE membrane filter. The ultrapure water flows

uniformly between wafers regardless of wafer diameter and spacing since the distribution of the flow is determined by the uniformity of the media (See Figure 12). In addition, stagnant layer on the substrate surface can be substantially eliminated by applying megasonic, which further enhances efficiency of the rinsing process. In the conventional overflow rinsing process, ultrapure water flows out from the peripheral of the top of cleaning bath. As wafer diameter gets larger and wafer to wafer spacing gets smaller, smaller amount of ultrapure water is introduced between wafers and water mainly flows around wafers. This is why the conventional overflow rinsing process consumes large amount of ultrapure water (27).

HF solution has been usually handled with fluorocarbon container or vessels. Megasonic is considerably attenuated, however, when it goes through fluorocarbon container, or vessel wall. Quartz vessel usually used for other chemicals is dissolved when it comes in contact with HF. Without a metal vessel which withstands FPMS solution, the FPMS+megasonic cleaning can not be realized. A metal vessel having NiF_2 passivation film can be used for acid solutions including diluted HF and FPM. NiF_2 film formed on pure Ni or Ni-P plating surface through direct reaction of F_2 gas is 50 - 150 nm in thickness, and it is perfectly resistant to acid solutions (28). Thus the newly-proposed room-temperature wet cleaning has become perfectly practical.

Basic technologies for new wet cleaning have been completely established to be implemented into new wet station.

IMPACT OF NEW WET CLEANING ON SEMICONDUCTOR MANUFACTURING

The new wet cleaning process drastically reduces load on make-up air system as it remarkably reduces clean air exhaust by suppressing chemical vapor evaporation, considerably reducing the number of steps from 12 steps to 5 steps, and reducing wet station in size. Besides load on scrubber is almost eliminated as exhaust from wet station scarcely contains chemical vapor. The HF recovery technology has already been established (25)(26). There is no environment-related problem.

The number of ultrapure water rinsing steps is drastically reduced from 5 or 6 times to once. In addition, parallel down flow rinse with megasonic irradiation replaces the conventional overflow rinse, which reduces ultrapure water consumption in a single rinsing step to 1/4 or less. Consequently total ultrapure water consumption can be decreased to at least 1/20. Chemical consumption volume is also reduced to 1/20 or less in the new surface cleaning method. These figures demonstrate a dramatic improvement in economic benefits

of the new method in semiconductor manufacturing.

The conventional semiconductor plant usually consumes water of 10,000 tons or more and chemicals of several tens of tons or more on the daily basis. Therefore, this limits potential sites for semiconductor plant. By introducing the new wet cleaning technology which reduces water consumption volume to 1/20 or less, it is possible to remarkably increase the number of site candidates for semiconductor plant. And this will also fundamentally change design concept of equipment layout in a plant as it almost eliminates generation of chemical vapor. The current wet process needs to be centralized at a certain location in a plant in order to effectively exhaust generated chemical vapor. Due to this layout, wafers, which are treated with the cleaning and drying process, need to be transported for a long distance to a succeeding processing equipment.

Introduction of the new wet cleaning technology will enable us to install wet station and other process equipment right adjacent to the following process steps. Wafers with perfectly clean surface can be loaded to processing equipment as they are. Equipment layout in a plant will be designed for minimizing wafer flow path throughout the entire process. Semiconductor industry is planning to establish volume production of ULSI with minimized feature size by introducing large diameter wafer such as 300 mm and 500 mm. Therefore, wafer flow path minimum throughout the entire process is key design concept for large diameter wafer volume production plant having a capability of high throughput and low cost production with 100% yield.

CONCLUSION

Total room temperature wet cleaning technology consisting of five cleaning steps has been developed for Si wafer surface. Cleaning technology is used in Si ULSI manufacturing to obtain ultraclean wafer surface which is free from contaminants such as particles, organic impurities and metallic impurities, and, moreover, characterized by atomic order flatness, no native oxide and hydrogen termination. The newly developed cleaning technology consists of following simplified five process steps, i.e., 1) ozonized ultrapure wafer cleaning to remove organic impurities and part of metallic impurities, 2) diluted HF/H_2O_2 cleaning with ionic surfactant in conjunction with megasonics to remove particles, most of metallic impurities and native/chemical oxide film, 3) ozonized ultrapure water shower rinse to eliminate previous cleaning solution adhered to the wafer of about 0.8 gram/wafer, 4) diluted HF treatment to remove chemical oxide resulting in hydrogen termination and 5) ultrapure water parallel down flow rinse. Highlight of this new wet cleaning is particle removal procedure by diluted HF/H_2O_2 with ionic surfactant in conjunction with megasonics. An

addition of ionic surfactant makes it possible to exhibit same polarity of zeta potential for all materials in diluted HF/H_2O_2 solution, resulting in an appearance of electric repulsive force between wafer surface and particles. This is most important key issue to remove particles from wafer surface. An application of megasonics to diluted HF/H_2O_2 solution with surfactant goes to reduce the effect of stagnant layer on the wafer surface, resulting in supporting surface slight etching capability of the solution, i.e., electron repulsive force greater than van der Waals force.

The consumption volume of liquid chemicals and ultrapure water in the new wet cleaning is dramatically reduced to less than 1/20 compared to that of RCA cleaning. Moreover, there does not generate chemical vapor in the new wet cleaning, resulting in an elimination of clean air exhaust from wet station. Thus, the new wet cleaning technology will introduce drastic change of concept of semiconductor fab construction, i.e., fab. location and equipment layout in the fab.

Right now, semiconductor fab. location is free from the regulation to have a capability to supply much volume of high quality water, and layout of manufacturing line must be designed to basically follow the processing steps in semiconductor fab., where the wet cleaning station is set just adjacent to succeeding process equipment.

Wafer flow path minimum through entire process is most important key concept for large diameter wafer manufacturing line with high throughput and low cost production capability.

REFERENCES

1. T. Ohmi, T. Ichikawa, H. Iwabuchi, and T. Shibata, J. Appl. Phys., **66**, 4756(1989).
2. T. Ohmi, Y. Nakagawa, H. Aomi, and J. Takano, Rev. Sci. Instrum., **64**, 2683(1993)
3. Y. Nakagawa, H. Izumi, S. Miyoshi, T. Kojima and T. Ohmi, Proceedings of Microcontamination 93, San Jose, p.586(1993).
4. H. Izumi, Y. Nakagawa, S. Miyoshi and T. Ohmi, Extended abstracts of 1994 International Symposium on Semiconductor Manufacturing, Tokyo, p. 211(1994).
5. T. Ohmi, T. Imaoka, I. Sugiyama and T. Kezuka, J. Electrochem. Soc., **139**, 3317 (1992)
6. T. Ohmi, T. Isagawa, T. Imaoka and I. Sugiyama, J. Electrochem. Soc., **139**, 3336 (1992)
7. T. Ohmi, T. Isagawa, M. Kogure and T. Imaoka, J. Electrochem. Soc., **140**, 804(1993).
8. T. Ohmi, T. Imaoka, T. Kezuka, J. Takano and M. Kogure, J. Electrochem. Soc., **140**, 811(1993)
9. H. Morinaga, M. Suyama and T. Ohmi, J. Electrochem. Soc., **141**, 2834 (1994)

10. N. Yonekawa, S. Yasui, F. Kunimoto, F. W. Kern, Jr. and T. Ohmi, Extended Abstracts, 184th Electrochemical Society Meeting, New Orleans, Abstract No. 346, pp.569-570 (1993)
11. M. Itano, F. W. Kern, Jr., R. W. Rosenberg, M. Miyashita, I. Kawanabe and T. Ohmi, IEEE Trans. Semicond. Manufact, **5**, 114(1992)
12. M. Itano, F. W. Kern, Jr., M. Miyashita and T. Ohmi, IEEE Trans. Semicond. Manufact, **6**, 258(1993)
13. M. Itano, T. Kezuka, M. Ishii, T. Unemoto, M. Kubo and T. Ohmi, J. Electrochem. Soc., **142**, 971(1995)
14. T. Ohmi, M. Miyashita, M. Itano, T. Imaoka and I. Kawanabe, IEEE Trans. Electron Devices, **39**, 537(1992).
15. W. Kern and D. A. Puotien, RCA Review, **31**, 187(1970)
16. H. Mishima, T. Yasui, T. Mizuniwa, M. Abe and T. Ohmi, IEEE Trans. Semicond. Manufact, **2**, 69 (1989)
17. H. Kikuyama, N. Miki, K. Saka, J. Takano, I. Kawanabe, M. Miyashita and T. Ohmi, IEEE Trans. Semicond. Manufact, **3**, 99(1990)
18. H. Kikuyama, N. Miki, K. Saka, J. Takano, I. Kawanabe, M. Miyashita and T. Ohmi, IEEE Trans. Semicond. Manufact, **4**, 26(1991)
19. H. Kikuyama, M. Waki, M. Miyashita, T. Yabune, N. Miki, J. Takano and T. Ohmi, J. Electrochem. Soc., **141**, 366(1994)
20. H. Morinaga, T. Futatsuki, T. Ohmi, E. Euchita, M. Oda and C. Hayashi, J. Electrochem. Soc., **142**, 966(1995)
21. N. Sato,*Denkyokukagaku*, Nittetsu Joho Center, Tokyo, 1993 (in japanese)
22. T. Shimono, M. Morita, Y. Muramatsu and M. Tsuji, in Proceedings of 8th Workshop on ULSI Ultra Clean Technology, p.59, Tokyo(1990)
23. T. Shimono and M. Tsuji, Extended Abstracts of Electrochemical Society, Vol. 91-1, pp.278, Washington, DC, (1991)
24. T. Ohmi and S. Aoyama, Appl. Phys. Lett., **61**, 2479(1992)
25. N. Miki, M. Maeno, T. Fukudome, M. Miyashita and T. Ohmi, in Contamination Control and Defect Reduction in Semiconductor Manufacturing I, PV92-21., D. N. Schmidt, Editor, p.375, The Electrochemical Society, Pennington, NJ, (1992)
26. M. Maeno, N. Miki, T. Fukudome, M. Miyashita and T. Ohmi, Contamination Control and Defect Reduction in Semiconductor Manufacturing I, PV92-91, D. N. Schmidt, Editor, PV92-21, pp.375, The Electrochemical Society, Pennington, NJ, (1992).
27. Y. Hiratsuka and N. Fujikawa, Proceedings of 24th Symposium on ULSI Ultra Clean Technology, p.92, Tokyo(1995)
28. M. Maeno, R. Hirayama, H. Izumi, K. Chiba, Y. Mikasa, H. Matsushita and T. Ohmi, J. Electrochem.Soc., **139**, 1865(1992)

Table 1 Relationship between zeta potential of both polystyrene latex particles and Si wafer surface and deposition of polystyrene latex particles onto Si wafer surfaces in 0.5% HF solution.

	PSL zeta potential (mV)	Si zeta potential (mV)	Particle Deposition particles/4inch wafer
without surfactant	+39	-23	>10000
anionic A	-67	-32	470
anionic B	-65	-27	380
anionic C	-62	-24	790
cationic A	+78	+63	9600
cationic B	+40	+34	9300
cationic C	+79	+62	9000
nonionic A	-52	-19	1900
nonionic B	+15	+3	9600
nonionic C	+27	+1	5300

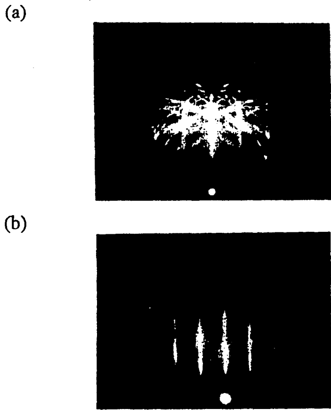

Figure 1 Reflection electron diffraction pattern of epitaxial silicon. (a) with removal process of adsorbed moisture by low - energy Ar ion and (b) without removal process of adsorbed moisture.

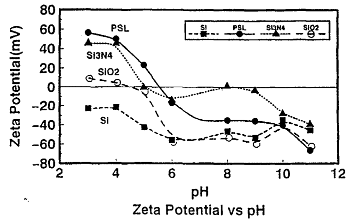

Figure 2 Zeta potentials of various substrate (Si, Si_3N_4, SiO_2) and polystyrene latex particles as a function of solution pH. Acidity / basicity was controlled by the addition of either HCl or NaOH.

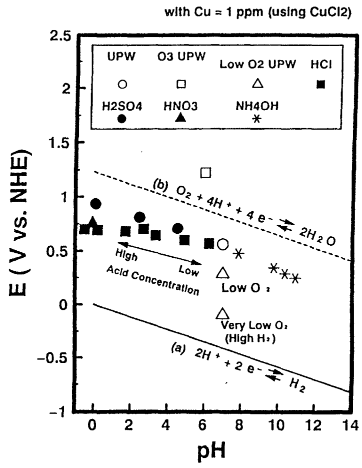

Figure 3 The relationship between pH and redox potential of various solutions (potential - pH diagram).

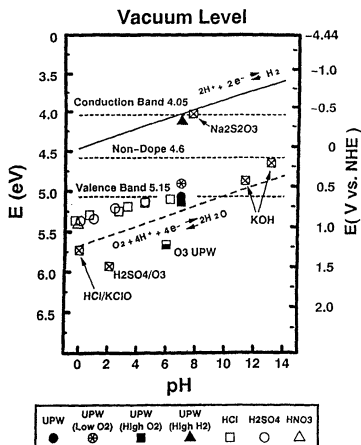

Figure 4 Redox potential-pH diagram is converted to energy level. Redox potential of ultrapure water is controlled by adding O_3, O_2 and H_2.

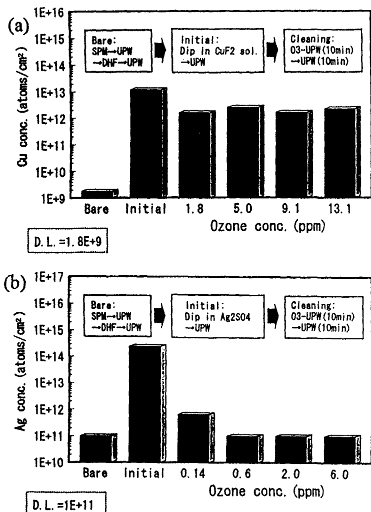

Figure 5 The Cu (a) and Ag (b) removal efficiency on the wafer surface with the change of ozone concentration in UPW.

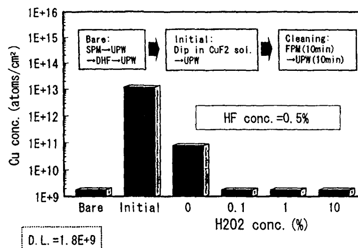

Figure 6 The Cu removal efficiency on the wafer surface with the change of H_2O_2 concentration in FPM solution.

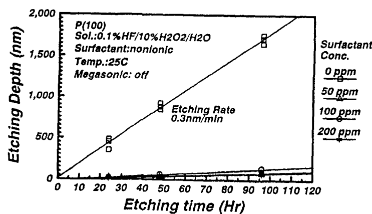

Figure 7 Si surface etching depth with HF : H_2O_2 : H_2O (FPM) as a function of time and the effect of surfactant addition.

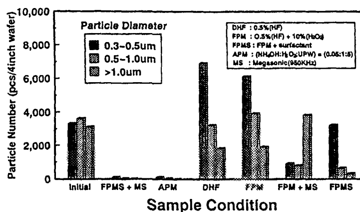

Figure 8 The particle removal efficiency on the wafer surface with various cleaning methods.

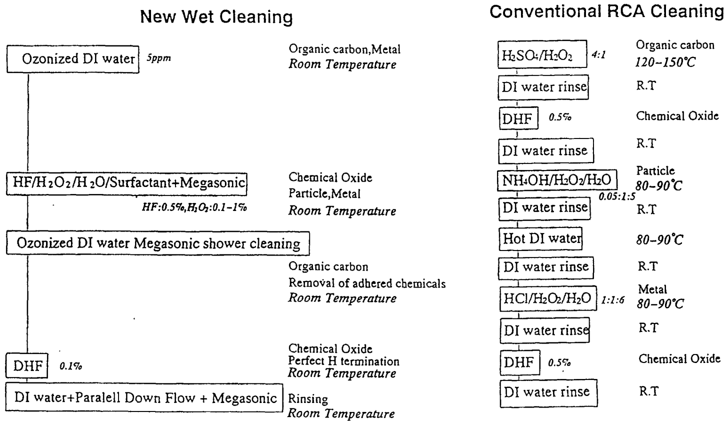

Figure 9 New total room temperature wet cleaning procedure vs. conventional RCA cleaning procedure.

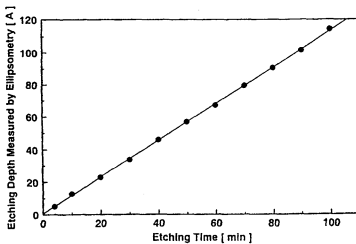

Figure 10 The etching characteristic of thermal oxide by extremely low etching rate BHF.

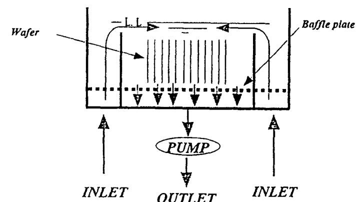

Figure 12 Schematic diagram of parallel down flow rinse system.

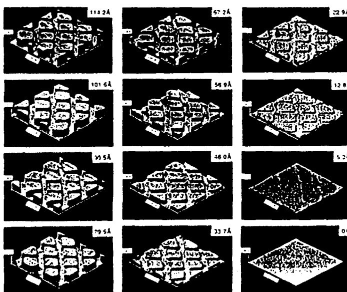

Figure 11 AFM images of standard samples of various etching depth.

CONTAMINATION EFFECTS ON OXIDE BREAKDOWN PROPERTIES

Jennifer Sees, Lindsey Hall, Jagdish Prasad,
Anthony Schleisman, and John Niccoli
P.O. Box 650311, Mail Station 301
Texas Instruments, Inc., Dallas, TX 75265

The results of an evaluation of varying purity levels of H_2O_2 and NH_4OH (SC1) and HF chemicals for wafer cleaning are documented. Chemical purity, gate oxide integrity (V_{bd}), and GOI scrap rate were monitored. Lower metals in SC1 resulted in a lower scrap rate. Higher purity HF resulted in baseline GOI improvements. Lower carbon content was found in higher purity HF. Wafers exposed to higher purity HF showed fewer deposited particles and lower surface carbon as revealed by XPS analysis.

INTRODUCTION

Many studies have documented the relationship between metallic impurities in semiconductor process chemicals and device electrical characteristics (1-4). It is not always clear, however, what level of chemical purity is necessary for maximum yield in semiconductor manufacturing. A minimum level of chemical purity is necessary because contamination remaining on a wafer surface from chemical processing can cause a variety of adverse effects which will depend on the nature of the impurity. For example, particles present during film growth or deposition can lead to pinholes and microvoids and if sufficiently large or conductive, will cause shorting between conductor lines (5). Metallic contamination left from chemical processing will contribute to the increase of current leakage at the p-n junction, decrease of oxide breakdown voltage, and deterioration of minority carrier lifetime (MCLT) (6).

This study documents the relationship between device electrical characteristics and impurities found in cleaning chemicals during a long term, production scale evaluation of various qualities of chemicals. The chemicals evaluated during the study included Standard Clean 1 (SC1) and hydrofluoric acid (HF). Because of its impact during this study, the HF chemistry was evaluated further to determine which of its qualities are important in semiconductor manufacturing.

An eight month evaluation of various grades of SC1 and HF chemistry was performed in a wafer fab manufacturing 0.8μm logic devices. Chemicals introduced for wafer cleaning during the evaluation included:

1. Standard grade SC1 chemicals
2. Two different sources of ultrahigh purity (UHP) grade SC1 chemicals
3. Standard grade 0.5% and 5% HF
4. UHP grade 0.5% and 5% HF

The terms "standard" grade and "UHP" grade are defined by levels of impurities found in them. SC1 refers to a 1:1:5 mixture of hydrogen peroxide (H_2O_2), ammonium hydroxide (NH_4OH) and deionized (DI) water, as described by Kern (5,7). SC1 chemistry is typically used in semiconductor cleaning processes for surface particle removal (5,7). HF-last processes are attractive in processing because of the superior gate oxide integrity (GOI) and minority carrier lifetime (MCLT) they provide (8).

A summary of the evaluation is included in Figure 1: the first switch of chemicals involved a change from standard grade to Source 1 UHP SC1. This combination was in place for 3½ months. In the second switch, the source of UHP SC1 was changed, and HF was upgraded to UHP. During the evaluation, GOI was characterized by measurement of breakdown voltage (V_{bd}). Chemical purity and GOI scrap rate were also monitored. Finally, an investigation of properties of standard and UHP 5% HF was undertaken. In this study, relative carbon content was determined, particles deposited from HF baths were monitored, and chemical states of adsorbed impurities, specifically carbon, were measured.

EXPERIMENTAL

During the evaluation, GOI (V_{bd}) was measured on all production lots. GOI was measured by exponentially ramping current in an I-V test until the oxide could no longer support the voltage drop across it. Breakdown field strength, as measured in MV/cm, was normalized to oxide thickness. P<100>, 11-15Ωcm silicon wafers were processed during the evaluation. One wafer per lot was measured with four sites tested. V_{bd} values were recorded for each of the four sites. Chemical purity was monitored with a Varian SpectrAA 300/400 series graphite furnace atomic absorption spectrometer (GFAAS) and a Fisons Instruments PQS model inductively coupled plasma-mass spectrometer (ICP-MS).

After the evaluation, a more complete study of HF properties was undertaken. First, a carbon analysis of 5% standard grade and UHP grade HF was performed. The carbon analysis was determined with a Fisons Instruments ARL3520 inductively coupled plasma-atomic emission spectrometer (ICP-AES) at 247.856nm. Because no attempt was made

to separate the HF matrix from the carbon analyte, a PTFE spray chamber corrosion resistant nebulizer and an alumina injector torch were required to prevent etching of the usual glass and quartz components by the HF. A direct analysis approach was deemed the fastest way to get relative carbon values on these samples.

Next, P<100>, 8-10Ωcm silicon wafers were exposed to static, 10 minute standard and UHP grade 5% HF baths and then analyzed for surface particles with a Tencor Instruments Surfscan 6200 surface particle analyzer.

Similarly prepared wafers were also analyzed for chemical states of adsorbed surface impurities with a VG Scientific ESCAlab Mark II x-ray photoelectron spectrometer (XPS). A Mg Kα anode was used for the excitation. Sample size was 1 cm^2. After the samples received the chemical exposure, they were all introduced at the same time into the sample preparation chamber, and then into the main analysis chamber which was pumped to a base pressure of 10^{-9} Torr.

RESULTS AND DISCUSSION

A dramatic reduction in GOI scrap rate was observed with the switch from standard grade to Source 1 UHP SC1 chemicals (switch 1), Figure 2. This can be correlated to a reduction in metallic impurities in the H_2O_2 and NH_4OH. Reductions in impurity levels for Ca, Na, Fe, and Al in the SC1 ranged from 74% to 97%, Table I.

Table I. Impurities in SC1 during evaluation (standard deviation in parentheses).

ppb	Standard	UHP, Source 1	UHP, Source 2
Ca	0.85	0.21 (0.29)	0.15 (0.07)
Fe	0.63	0.10 (0.02)	0.13 (0.03)
Na	1.55	0.14 (0.07)	0.05 (0.04)
Zn	1.64	0.19 (0.06)	0.30 (0.15)
Al	0.92	0.03 (0.01)	0.01 (0.01)

Previous research has documented the effect of metallic contamination on oxide breakdown properties. Specifically, IMEC research has revealed the detrimental effects of Ca, Fe, and Al on the breakdown of thermal oxides (1-3). In the IMEC research, Ca was incorporated into the thermal oxide and degraded GOI by inducing surface roughness. Additionally, it was found that SC1 solutions with the highest Ca content also promoted the most surface roughening during clean up. Fe degraded oxide integrity by formation of defect spots during oxidation. Zinc was found to diffuse into the silicon substrate, or evaporate in the oxidation ambient, and therefore have essentially no effect on oxide

integrity (1). In the present study, Ca averaged 0.85 ppb in the standard grade SC1, 0.21 ppb in Source 1 UHP SC1, and 0.15 ppb in the Source 2 UHP SC1.

Baseline improvements in GOI as measured by V_{bd} were observed with the switch from Source 1 to Source 2 UHP SC1 chemicals, and from standard to UHP HF (switch 2), Figure 3. Further, but less dramatic, impurity reductions were seen in the SC1 chemicals (with the exception of Zn and Fe), Table I.

In order to isolate the cause of baseline GOI shifts, other tests were run, and improvements always correlated to the introduction of UHP HF. Impurity outplating from HF is important because several critical steps in the fab use HF for oxide stripping. In these steps, the oxide is completely stripped and the silicon substrate exposed to the HF solution, making HF purity particularly significant. No significant differences in metallic impurities monitored during the evaluation were observed between the two sources of HF, Tables II and III, so tests were undertaken to quantify any other differences between the two. First, an ICP-AES analysis for carbon content was conducted on standard and UHP grade 5% HF. A carbon analysis was considered important because an organic type of residue was observed during analysis of standard grade but not UHP grade HF. The ICP-AES analysis revealed that the standard grade HF contained at least 3 to 5 times more carbon than did the UHP grade HF. Only relative values are reported because of the difficulty in obtaining good analytical results at the low ppb level by the ICP-AES method. Difficulties include high background levels and possible discrimination of organic species in the sample introduction process. However, only a relative confirmation of carbon levels was needed to confirm that the residue from the standard grade acid contained significantly higher levels of carbon.

Table II. Impurities in 0.5% HF during evaluation (standard deviation in parentheses).

ppb	Standard 0.5% HF	UHP 0.5% HF
Ca	0.18 (0.32)	0.19 (0.31)
Fe	0.33 (0.24)	0.32 (0.20)
Na	0.03 (0.03)	0.06 (0.05)
Al	0.11 (0.05)	0.11 (0.05)
K	0.01 (0.01)	0.01 (0.01)

Table III. Impurities in 5% HF during evaluation (standard deviation in parentheses).

ppb	Standard 5% HF	UHP 5% HF
Ca	0.02 (0.03)	0.02 (0.02)
Fe	0.26 (0.21)	0.49 (0.48)
Na	0.03 (0.05)	0.02 (0.01)
Al	0.03 (0.02)	0.02 (0.02)
K	0.02 (0.02)	0.01 (0.01)

Wafers were later exposed to static, 10 minute standard and UHP 5% HF baths and analyzed for surface particles. Control wafers (no chemical treatment) averaged 2.8 light point defects (LPDs) per wafer, standard grade HF wafers averaged 58.1 LPDs, and UHP HF wafers averaged 4.5 LPDs, Figure 4. Currently, research is underway to reveal the composition of these particles.

X-ray photoelectron spectroscopy (XPS) analysis of a set of similarly prepared wafers was undertaken to reveal chemical states of adsorbed impurities. A carbon 1s peak at 7 times the area of the Si 2p peak was observed at binding energy 285.0eV on standard grade HF-treated wafers. No carbon peak was found on UHP HF-treated wafers. No other impurities were detected by XPS analysis, probably because impurities (if present) were present at less than the monolayer coverage (10^{15}atoms/cm^2) needed for detection with this method.

CONCLUSIONS

The introduction of improved-quality (lower impurity) SC1 chemicals into the fab for wafer cleaning was strongly correlated to a reduction in GOI scrap rate. This was attributed to lower levels of several impurities in the SC1, specifically Ca, Fe, Na, Zn, and Al. This correlation between reductions in Ca, Al, and Fe content in SC1 chemicals and improved GOI is consistent with previously published data that shows a direct relationship between these specific impurities and GOI (1-3).

The introduction of UHP HF was correlated to baseline GOI improvements as measured by V_{bd}. No major differences in levels of metallic impurities were measured in the standard grade and UHP grade 0.5% and 5% HF, so in relation to this study, it is impossible to correlate any particular impurity in HF to device performance. A significant difference in carbon content, however, was found between the standard and UHP grade HF. Carbon was 3-5 times higher in standard HF than in the UHP material. Carbon was also found by XPS analysis on the surface of standard HF-treated wafers, while none was detected on the surface of UHP HF-treated wafers.

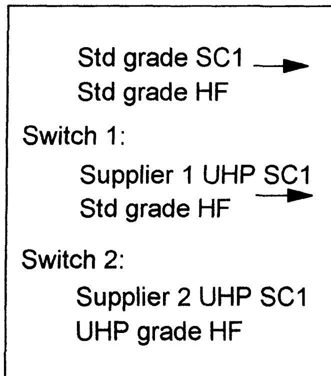

Figure 1. Summary of chemical evaluation.

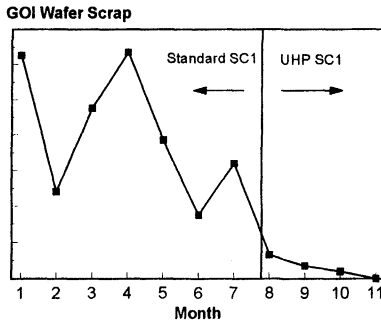

Figure 2. GOI scrap rate during chemical evaluation.

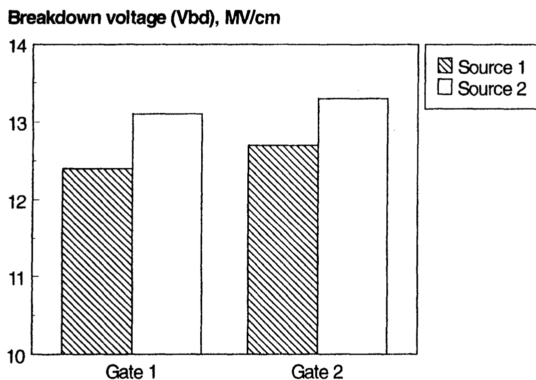

Figure 3. GOI during evaluation.

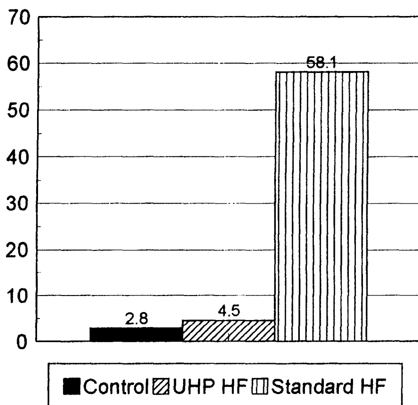

Figure 4. LPDs found on HF-exposed wafers.

ACKNOWLEDGMENTS

The authors would like to gratefully acknowledge Asadd Hosein and Jeff Smith for surface particle characterization and Valerie Sewall for ICP-MS analysis.

REFERENCES

1. S. Verhaverbeke, P. Mertens, M. Meuris, M. Heyns, A. Schnegg, A. Philipossian, in the Technical Conference SEMICON Europe 92, Zurich (1992).

2. W. Bergholz, in Proceedings of the Silicon Ultra Clean Processing Workshop, Oxford (1991).

3. M. Heyns, C. Hasenack, R. De Keersmaecker, R. Falster, in Proceedings of The Electrochemical Society Meeting (1989).

4. P. Mertens, M. Meuris, S. Verhaverbeke, M. Heyns, A. Schnegg, D. Graf, A. Philipossian, in Proceedings of the Institute of Environmental Sciences 38th Annual Technical Meeting, p. 475 (1992).

5. W. Kern, Overview and Evolution of Semiconductor Wafer Contamination and Cleaning Technology, in Handbook of Semiconductor Wafer Cleaning Technology, W. Kern, Editor, Noyes Publications (1993).

6. T. Ohmi, T. Imoaka, I. Sugiyama, T. Kezuka, J. Electrochem. Soc., **139**, 3317 (1992).

7. W. Kern, D. Poutinen, RCA Review, **31**, 187 (1970).

8. J. Park, M. Pas, J. Electrochem. Soc., **142**, 2028 (1995).

THE EFFECTS OF DILUTE SC-1 AND SC-2 CHEMISTRIES ON DIELECTRIC BREAKDOWN FOR PRE GATE CLEANS

Shelley M. Smith*, Mohan Varadarajan**,
and Kurt K. Christenson*
*FSI International,
MS 3-8045, 322 Lake Hazeltine Dr., Chaska, MN 55318
**Motorola MOS 5
2200 West Broadway Road, Mesa, AZ 85202

The effects of changing the temperatures and concentrations of the SC-1 and SC-2 chemistries in a pre gate clean were studied. Based on the dielectric breakdown, metals added, and surface roughness data, both the cold, dilute and hot, concentrated chemistries yielded identical results within the noise of the experiment.

INTRODUCTION

The SC-1 (or APM) and SC-2 (or HPM) standard cleans, as published by Kern in 1970, have been the primary means of removing particles, trace organics, and metals in pre diffusion cleans for over 20 years (1,2). While optimized to meet the cleanliness requirements of the earlier bipolar devices with the available chemicals, the details of the APM and HPM chemistries are being reevaluated in the light of modern chemical purities and current MOS device structures. To this end we have extensively studied the effects of dilution and temperature on the APM and HPM chemistries for a variety of wafer metrics (3-6). These studies have shown that diluting the chemical concentrations and decreasing the solution temperature will improve the process results as well as lower the operating costs. A DOE was conducted in an acid spray processor to compare the performance of dilute chemistries versus the standard pre gate clean. The metrics used for comparison were dielectric breakdown, metals added, and surface haze.

EXPERIMENT

A 3x2x2 screening DOE was performed in an FSI MERCURY® MP acid spray processor in which the following factors were varied:

- Chemical flow rates of NH_4OH, H_2O_2, and HCl (20, 120, 200 cc/min.)
- Temperature of the hot DI water heater (65 & 90° C)
- Temperature of the DI water for the APM step (hot & cold/ambient)

A total of thirteen runs were made: the twelve runs of the 3x2x2 matrix and one duplicated run as an indication of noise level and run-to-run repeatability. The run order, given in Table I, was randomized as much as possible, although all the low flow runs (20 cc/min.) had to be done together due to constraints in the system. Because the flow pickups cannot operate as low as 20 cc/min., it was necessary to dilute the chemicals in the canisters for those runs. The chemicals were diluted to 1/10th their concentration (1:9 chemical:H_2O) and the flow pickups were programmed to 200 cc/min. Also, in all the runs the DI water flow rate during the APM and HPM steps was set to 1000 cc/min.

The pre gate clean used the following sequence:

- 90 sec Wafer pre-wet with DI H_2O
- 90 sec SPM (4:1 H_2SO_4:H_2O_2)
- 505 sec Cold Rinse
- 50 sec HF (1:7.9 HF: H_2O)
- 200 sec Cold Rinse
- 30 sec Cold Diluted H_2O_2 (1:5 H_2O_2:H_2O)
- 105 sec APM (1:1:5 NH_4OH:H_2O_2:H_2O)
- 165 sec Hot Rinse
- 110 sec HPM (1:1:5 HCl:H_2O_2:H_2O)
- 390 sec Hot Rinse
- 435 sec Final Dry

Run 3 corresponded to the current standard process to which the other runs were compared. The basic differences between the runs were the APM and HPM ratios; the temperature of both the hot DI rinse water and the DI water used in the APM step; and whether hot or cold water was used in the APM step.

Several 5" p-type (100) wafers were processed with each run: one TTDDB (Time To Dielectric Die Break-down) electrical test wafer, and four bare silicon wafers. The four bare Si wafers were tested for metals added using a variety of analysis techniques. The first two wafers were analyzed using Total Reflection X-ray Fluorescence (TXRF) at Motorola's Materials Characterization Lab, and then further analyzed for surface haze using a Tencor Surfscan 6200 at FSI's lab. The next wafer was analyzed using O-leak dynamic SIMS, and the last wafer was analyzed at Motorola's Lab using quadrupole SIMS. Although the former is a more sensitive test, it was decided to do the latter as well because of the quicker turn around time.

It was decided not to study metals removal efficiency for the DOE on deliberately contaminated wafers because of the slight risk of contaminating a production tool. Thus the scope of the study was limited to studying the effects of metals added only.

RESULTS

The TTDDB results are given in Table II. Note that the gate oxide thickness was 116 A. The results ranged from 59.6-67.6 seconds, with the standard deviations ranging from 6.85-14.24. Since the standard deviation results were similar to the 8 second range in the TTDDB results, t-tests were done to compare run results (using n=19 dies). These tests showed that all of the runs are not statistically different from each other within a 80-95% confidence level, depending on which runs were compared. The only exception is that the highest result and the lowest result are significantly different at the 98% confidence level.

The fact that no particular set of conditions was significantly better is still encouraging, because it demonstrates that the factors that were varied (Heater Temperature, Flow Rate, APM Temperature) can all be reduced without affecting the product results. However, it needs to be emphasized that further work needs to be done to optimize the recipes for these factors.

The TXRF results for metals added also showed little difference between the runs, and in fact little was detected above the detection limits (10^{10} atoms/cm^2). The only metals seen for these runs were Ni, Cu, and Zn. Three sites were analyzed on each wafer, and the average result of each wafer is given in Table III.

A few wafers had higher results, Run 8 Wafer 2, Run 9 Wafer 2, and Run 11 Wafer 1, but in all such cases the duplicate wafer did not have unusually high levels. It should be pointed out that the wafers were initially very clean, so it would be easy to reduce the contamination levels below the TXRF limits.

After TXRF analysis, these two sets of wafers were then measured for surface haze on a Tencor Surfscan 6200 at FSI's Lab. The results are given in Table IV. There appears to be a break in the data between Runs 2 and 3 and between Runs 8 and 9. Although the first break cannot be explained, the second break occurs when a new box of wafers was started. Analyzing the results using the DOE software gave no significant model. This means that the differences between the results can be attributed to noise and no conclusions can be made based on this data. In the future, the noise level can be reduced by measuring the initial haze level on the wafers before processing, and using the change in haze as the response. (When this experiment was started, the Tencor was not available to measure the initial haze level.)

The first sets of SIMS wafers were analyzed using a quasi-static SIMS technique on a PHI 6600 quadrupole-based SIMS instrument at Motorola's Materials Characterization Laboratory. Two sites were analyzed on each wafer. Typical surface contaminants of

boron, hydrocarbons, fluorine, sodium, and calcium were detected on all of the wafers. No unusual contamination was detected on any of the wafers (detection limit of 10^{12} atoms/cm^2), except for Al and Na (detection limit of 10^{10} atoms/cm^2).

Based on the lack of detectable results with the quad SIMS, and in order to minimize cost, it was decided to only send two wafers to Charles Evans for O-leak dynamic SIMS profiling. The two wafers were chosen at the processing extremes: Run 3 (90° C Heater Temperature, 200 cc/min. chemical flow, Hot APM) and Run 10 (65° C Heater Temperature, 20 cc/min. chemical flow, Cold APM). In order to get a broad spectrum of possible contaminants, it was decided to profile for Mg, Al, Na, Ca, Fe, Cu, and Zn. The results are given below in Table V.

There appears to be no differences in the average contamination levels for the two processing extremes. The only possible exception is Cu, and in that case the cold dilute chemistries are better than the hot concentrated chemistries.

CONCLUSIONS

Within the resolution of the experiment, all the processes gave identical results. The electrical results showed no significant difference between the different processes. The TXRF and SIMS data showed no significant metals added to any of the wafers. Although this report did not include metals removal results, it has been shown elsewhere that deliberately contaminated wafers clean comparably in both dilute and concentrated B CLEAN solutions (3,4). Finally, the surface haze results were not sufficiently above the noise level to detect any differences in the processes. However, we have shown elsewhere (6) that colder and more dilute APM blends produce less surface roughening. In the future, any surface haze experiments must include pre and post measurements. Using only post measurements is not adequate due to initial variations in wafer surface conditions.

From this data, it can be concluded that cold, dilute chemistries give equivalent results to hot, concentrated chemistries. The fact that cold, dilute chemistries did not show obvious process improvements is not discouraging and should not be a reason to abandon further efforts in this direction. On the contrary, between the financial savings and ecological impact of decreasing chemical consumption by as much as 10x, it is essential to continue these efforts.

ACKNOWLEDGMENTS

We would like to acknowledge the generosity of the Motorola Corporation and FSI International whose support made this work possible. We thank Dennis Werho and Joy Watanabe for their efforts in analyzing the wafers; Brian Clark and MOS 5 for allowing us use of their facilities; and finally, the MOS 5 operators without whose help the experiments would never have been completed.

REFERENCES

1. W. Kern and D. Puotinen, RCA Review, **31**, 187-206 (1970).
2. W. Kern, Proceedings of the First International Symposium on Cleaning Technology in Semiconductor Device Manufacturing, **PV 90-9**, pp. 3-19, The Electricalchemical Society, Pennington, NJ, (1990).
3. K. Christenson, S. Smith, and D. Werho, Proceedings of the Semiconductor Pure Water and Chemical Conference/1994, pp. 84-92, Balazs Analytical Laboratory, Sunnyvale, CA, (1994).
4. K. Christenson, S. Smith, and D. Werho, Microcontamination Magazine, pp. 47-53, June, 1994.
5. S. Smith, K. Christenson, and D. Werho, Proceedings of the Semiconductor Pure Water and Chemical Conference/1995, pp. 295-328, Balazs Analytical Laboratory, Sunnyvale, CA, (1995).
6. K. Christenson, S. Smith, "Effects of SC-1 Dilution and Temperature Variations on Etch Rate and Surface Haze," Ultraclean Semiconductor Processing Technology and Surface Chemical Cleaning and Passivation, San Francisco, CA, MRS Spring Meeting (1995) (to be published).

Table I. Process run order for the DOE.

Run #	Heater Temp °C	Flow cc/min.	APM Temp
1	65	200	Cold
2	65	120	Hot
3	90	200	Hot
4	90	120	Cold
5	90	200	Cold
6	90	120	Hot
7	65	120	Cold
8	65	200	Hot
9	65	20	Hot
10	65	20	Cold
11	90	20	Cold
12	90	20	Hot
13	65	20	Hot

Table II. Average TTDDB results (seconds). The Gate TOX=116 A.

Run #	Heater Temp °C	Flow Rate cc/min.	APM Temp	TTDDB Mean	TTDDB Std Dev
1	65	200	Cold	63.4	6.851
2	65	120	Hot	62.5	9.902
3	90	200	Hot	64.6	6.85
4	90	120	Cold	65.3	7.556
5	90	200	Cold	63.1	7.694
6	90	120	Hot	63.2	8.672
7	65	120	Cold	67.1	7.674
8	65	200	Hot	67.2	8.972
9	65	20	Hot	62.8	10.87
10	65	20	Cold	67.6	6.006
11	90	20	Cold	64	10.71
12	90	20	Hot	62.54	7.771
13	65	20	Hot	59.6	14.24
			Average	63.5	7.491

Table III. Metals Added By TXRF (10^{10} atoms/cm^2). Detection Limits given in final row.

Run #	Ni Waf 1	Ni Waf 2	Ni Ave	Cu Waf 1	Cu Waf 2	Cu Ave	Zn Waf 1	Zn Waf 2	Zn Ave
1	1.0	1.3	1.2	1.3	1.0	1.2	0.7	0.5	0.6
2	1.3	0.9	1.1	1.0	1.0	1.0	0.5	0.5	0.5
3	1.0	0.9	0.9	1.3	1.0	1.2	0.7	0.5	0.6
4	1.0	0.9	0.9	1.0	1.0	1.0	0.5	0.5	0.5
5	1.0	0.9	0.9	1.0	1.0	1.0	0.5	0.5	0.5
6	0.9	1.0	0.9	1.7	1.3	1.5	0.5	0.5	0.5
7	0.9	1.0	0.9	1.0	1.0	1.0	0.5	0.5	0.5
8	0.7	1.3	1.0	1.0	3.3	2.2	0.5	0.8	0.7
9	1.0	1.7	1.3	1.0	2.0	1.5	0.5	0.5	0.5
10	0.9	1.0	0.9	1.0	1.0	1.0	0.5	0.5	0.5
11	1.3	1.0	1.2	4.0	1.0	2.5	1.3	0.5	0.5
12	1.0	1.3	1.2	1.0	1.3	1.2	0.5	0.5	0.5
13	1.0	0.9	0.9	1.3	1.0	1.2	0.5	0.5	0.5
D.L.	0.6	0.6	0.6	0.5	0.5	0.5	0.5	0.5	0.5

Table IV. Surface Haze (ppm) results.

Run #	Wafer 1 Haze	Wafer 2 Haze	Haze Average
1	0.519	0.520	0.520
2	0.612	0.540	0.576
3	0.400	0.404	0.402
4	0.401	0.402	0.402
5	0.401	0.497	0.449
6	0.406	0.411	0.409
7	0.393	0.401	0.397
8	0.469	0.405	0.437
9	0.524	0.514	0.519
10	0.519	0.507	0.513
11	0.508	0.521	0.515
12	0.538	0.544	0.541
13	0.611	0.518	0.565

Table 5. Average Metals Added By O-leak dynamic SIMS (10^{10} atoms/cm^2).

Run #	Mg	Al	Na	Ca	Fe	Cu	Zn
3	1.05	0.399	2.43	0.412	0.752	8.24	12.0
10	0.956	0.125	1.51	0.440	0.680	0.755	18.3

RCA OPTIMISATION FOR SUB - 0.5 μm CMOS TECHNOLOGIES

Alain FLEURY, Kathy BARLA, Didier LEVY, Laurens KWAKMAN

Centre Commun CNET - SGS THOMSON Microelectronics
850 rue Jean Monnet, BP 16, 38921 CROLLES Cedex, FRANCE

ABSTRACT

A Design Of Experiment (DOE) has been used to improve the particle removal efficiency of a SC1 wet chemical cleaning step in a recirculated and filtrated Wet-Bench bath dedicated to the front-end cleaning of 8" (200mm) wafers. The mathematical analysis of the DOE shows that within the studied process window the influences of temperature, time, megasonic power and frequency on the particle removal efficiency of SC1 are about 50%, 20%, 25% and 15% respectively.

The modified RCA clean, including the optimized SC1, has been qualified in terms of particle removal efficiency for critical cleaning steps after locos oxide or nitride layer etching, but also in terms of Gate Oxide Integrity at the pre-gate oxide clean for Sub - 0.5 μm CMOS integrated circuits.

Finally, the surface microroughness of wafers after this RCA-clean has been correlated to the electrical defectivity of 7 nm gate oxides grown on these substrates.

INTRODUCTION

In this work, critical RCA - last processes used for front-end cleaning of sub - 0.5 μm CMOS integrated circuits on 8" wafers are analysed.

Nowadays process flows used for the manufacturing of submicron CMOS and BiCMOS integrated circuits, include at least ten cleaning operations prior to the growth of the gate oxide. Some of these cleans are needed to ensure low particle levels even after (wet) etch processes such as e.g. used for PBL nitride removal, that are notorious for potential particle generation. Other cleans are needed to ensure lowest metallic and organic contamination levels required for e.g. high quality gate oxide fabrication. From a production point of view, having one unified cleaning process that can fulfil both requirements is desirable. Historically, the RCA clean has been successfully used as such general cleaning process and at present it still can be considered as an industrial standard.

The study presented in this paper focuses on the first step of a full RCA clean, the SC1 clean whose main properties are its ability to remove particles on highly polluted wafers, and at the same time, its particle neutrality on initially clean wafers. The evaluation of these features of SC1 is possible by the study of the Particle Removal Efficiency (η) for the first characteristic and the Adder To Zero (Δ_0) for the second characteristic. Clearly, the robustness of the cleaning process is only guaranteed when $\eta \sim 1$ and $\Delta_0 \sim 0$.

In this work, an optimisation of η and Δ_0 is realised based on a Design Of Experiments in which the influences of the control parameters for a recirculated-filtrated SC1 Megasonic bath are evaluated. From the analysis of the DOE responses, optimised SC1 process settings are selected and subsequently tested in a second campaign of experiments in which the cleaning efficiency on different types of wafers, prepared according to our standard submicron process flow, is evaluated.

Finally, metallic contamination, surface roughness and Gate Oxide Integrity are measured to ensure that this optimised SC1 in the RCA process is not only efficient in terms of particle removal but also meets all stringent production criteria at the pre-gate oxidation cleaning stage.

EXPERIMENTAL

Process tool description

The process tool used in this study is a fully automated Wet Bench offering the capability of multi batch processing with different recipes. This Wet Bench is dedicated to the front-end cleaning of submicron CMOS/BiCMOS device technologies and is configured accordingly (H_2SO_4 : O_3, Dilute HF, SC1 Megasonic, SC2, Final Rinse Megasonic, IPA Vapour Dryer). The SC1 module is a four sided scalloped/knife edge overflow Megasonic quartz tank. The 800 W Megasonic transducer has a concave shape and is located at the bottom of the tank. The bath is prepared directly in the process tank where ammonia and peroxide solutions are dispensed in hot DI water from pre-weighted reservoirs. The bath is then recirculated and filtrated at 0.1 µm in a loop to a remote cabinet. The total loop volume for each recirculated bath is about 60 litres.

Periodic spikes of ammonia and hydrogen peroxide are automatically injected into the tank using the pre-weighted reservoirs to compensate for the concentration decay of these chemicals and to extend the bath lifetime. The injection rate for ammonia at different bath temperatures has been selected using the curves shown in figure 1 (1). On the other hand, since the metallic content is found to be temperature independent, the injection rate of hydrogen peroxide (grade : 0.8 ppb) has been fixed independent from the bath temperature to approximately 2% per hour (2).

All tests presented in this paper for the characterisation of the particle removal efficiency of SC1 use a cleaning recipe that includes the SC1 tank and its dedicated hot DI rinse tank (Quick Dump and overflow cascade), the final rinse tank (overflow cascade

to a 15 MΩ.cm resistivity) and the IPA Vapour Dryer. Furthermore, in each experiment the second Megasonic located in the Final Rinse has been set up to operate at 1.2 MHz, 800 W.

SC1 production setting and performance at 35°C

The original SC1 process used in production before this study is described in table I. Chemicals used are ULSI grade (< 10 ppb). Figure 2 gives the results obtained with this process step setting on intentionally polluted wafers (3). When data are approximated by a straight line, the two parameters that are of particular interest are easily estimated :

- The Particle Removal Efficiency, η, represented by the slope of the linear regression and defined as :

$$\eta = \frac{Bp - Ap}{Bp} \qquad [1]$$

  where Bp and Ap represent particle counts on wafers before and after cleaning, respectively .
- The Adder To Zero, Δ_0, represented by the Y axis intercept of the linear regression.

Correct interpretation of both parameters is important in the judgement of the bath performance. In case of incoming wafers that are seriously contaminated, the final particle count approaches Δ_0 if $\eta \sim 1$ and exceeds Δ_0 if $\eta < 1$. In case the incoming wafers are essentially clean ($Bp < 10$), the final particle count is not necessarily given by Δ_0, but depends on the exact mechanism responsible for the particle removal and/or addition. If two independent mechanisms account for particle removal and addition, the final particle count can be estimated by Δ_0 / η. On the other hand, if it is assumed that no particle addition mechanism is active but that the removal efficiency brakes down at low particle levels, the final particle count will approach the initial particle count and the bath can be considered as "particle neutral".

According to figure 2, the SC1 at 35°C is characterised by $\eta = 63$ % and $\Delta_0 = 308$. These values are indicative for a very moderate particle removal performance, however, when analysing the experimental particle data at low Bp values, it is obvious that the bath does not add a significant amount of particles but becomes essentially particle neutral.

Both η and Δ_0 are strongly dependent on the exact process conditions as will be shown later.

DESIGN OF EXPERIMENT MATRIX

The Design Of Experiment has been set up to distinguish between the influences that the Megasonic and the chemistry of SC1 may have on the final particle level after the cleaning step. Table II summarises all key parameters and setting ranges on which the

Design Of Experiment is based, i.e. process time, process temperature, megasonic power, frequency and, finally, the initial particle count. The NH_4OH/H_2O_2 ratio, although most likely an important parameter, is not considered in the DOE due to practical constraints.

Since the DOE includes five input factors and should primarily serve as a first process screening, a two-level linearplus fractional-factorial design is selected that requires the execution of eight experiments. The randomised experimental matrix is presented in table III. The values for the initial particle count listed in table III represent the mean value of particle counts on five intentionally contaminated wafers in order to improve the statistical relevance of the model prediction. After completion of the experiments in the randomised order given in table III, the results (final particle counts, i.e. Ap values) are entered in RS Discover, the analysis method used for the calculation of the response surface Ap = f(t, T, P, ν, Bp).

RESULTS AND DISCUSSIONS

RS/Discover mathematical analysis of the experimental results yields a relationship between Ap and Bp that can be expressed as :

$$Ap = K_1\, Bp + K_2 \qquad [2]$$

where :

$K_1 = 0.06$

and

$$K_2 = 61.28 - 6.04\left(\frac{t-10}{5}\right) - 27.83\left(\frac{T-52.5}{17.5}\right) - 12.78\left(\frac{P-400}{400}\right) + 8.25\nu \qquad [3]$$

with :

t = process time, T = process temperature, P = megasonic power, ν = +1 (High frequency) or -1 (Low frequency).

Analysis of the Particle Removal Efficiency

The Particle Removal Efficiency is evaluated using [1] and [2] :

$$\eta = \left(1 - K_1\right) - \frac{K_2}{Bp} \qquad [4]$$

Using the Bp values from Table III in equation [4], the contribution of each parameter in SC1 is calculated and represented in figure 3, and can be summarised as follows :

The cleaning efficiency

- improves significantly at higher process temperature (up to 42% at 70 °C),

- is strongly affected by the process time at 35 °C (up to 48%) but much less at 70°C (up to 18%),
- improves up to 25% at 70°C due to the Megasonic effect,
- is slightly better using a low frequency rather than a high frequency (up to 10%).

Analysis of the Adder to Zero

Since Δ_0 is defined as the particle addition on initially clean wafers, i.e. Bp -> 0, it follows that :

$$\Delta_0 = K_2 \quad [5]$$

Again, using expression [3], the contribution of each parameter in SC1 is calculated and represented in figure 4.
The Adder To Zero

- is significantly reduced at higher process temperature (56% at 70°C),
- is reduced by the Megasonic effect (26% at 800W),
- is slightly better using a low frequency rather than a high frequency (17% gain),
- is little affected by the increase of the process time (12% gain at 15 min).

Within the parameter range studied, it can be concluded that the particle removal efficiency of the SC1 is dominated primarily by its chemical and not by its physical (megasonic) action. However, the megasonic action speeds-up the particle removal and as such offers the potential benefits of a short process time (less oxide etching, less surface micro roughening). Finally, since the tuning of the SC1 parameters improves both η and Δ_0 , the optimised SC1 will yield reproducible performance not depending on the initial particle level of wafers. The selected final process settings to be used in production are :

- Temperature : 70 °C,
- Process time : 5 min,
- Megasonic Power : 800W,
- Frequency : 0.8 MHz.

Experimental verifications

The optimised SC1 process condition has been tested on various types of substrates (on silicon, on silicon after a sacrificial oxide removal, and on oxide after nitride etch) to confirm its high particle removal efficiency and to check etch rates. It is found that the SC1 only etches 0.7 nm of SiO_2 instead of 2 nm commonly described in literature (4).
Figure 5 gives SC1 cleaning results obtained on bare silicon wafers. The correlation between experimental data and the model prediction for Particle Removal Efficiency and Adder To Zero is apparent (less than 2% error).
Finally, figure 6 shows the results obtained with a SC1 clean following a nitride etch. Also in this particular case a particle removal efficiency > 90% minimum is obtained.

ELECTRICAL RESULTS AND PROCESS INTEGRITY

In order to apply this process as the pre-gate oxidation clean in a 0.5 μm CMOS device flow, the complete RCA clean (SC1 + SC2) is analysed in terms of particles, metallic contamination and Gate Oxide Integrity (10 nm for this particular experiment). The results are presented in figures 7-9. As shown in figure 7, the particle levels after a RCA clean including the new SC1 process are low (< 0.05 particles/cm^2) and identical to the results obtained before the process change. Although the metallic contamination as measured by TXRF (see figure 8) after SC1 increases as a function of the SC1 temperature and process time to levels in the 10^{11} at/cm^2 range, it is found that the SC2 consequently removes these metals to a level below the 10^{10} at/cm^2 range.
In terms of electrical defectivity, no significant differences are observed between old and new RCA recipe.

SURFACE ROUGHNESS AND 7 NM GATE OXIDE

The Silicon surface roughness after SC1 and full RCA cleaning is measured using Atomic Force Microscopy (AFM). The results show that when a higher SC1 temperature is used, the surface roughness as measured after SC1 increases from 0.13 nm (RMS) at 35 °C to 0.19 nm at 70 °C. On the other hand, the surface roughness as measured after a full RCA clean (SC1 + SC2) does no longer reveal the SC1 temperature effect and becomes 0.22 nm for both SC1 temperatures. Interestingly, it is found that extending the SC1 process time from 5 to 60 minutes does not change the surface roughness significantly : at 70 °C the surface roughness measured after the SC1 increases from 0.19 nm (t = 5 min) to 0.21 nm (t = 60 min).

In parallel to the AFM measurements, the electrical defectivity of 7 nm gate oxides grown on substrates treated by the various SC1 and RCA is studied. While a defectivity increase is observed (SC1 only clean) when the SC1 time is increased from 5 to 60 minutes, this is not the case when a full RCA clean is used. In the latter case, values are in the same range of defectivity obtained for a 10 nm gate oxide.

Hence, it can be concluded that the optimised RCA clean does preserve the gate oxide integrity for 0.35 μm CMOS integrated circuits.

CONCLUSIONS

A Design Of Experiment has been used to improve the particle removal efficiency of a RCA - last clean for sub - 0.5 μm technologies.

An optimised and production worthy process has been obtained by raising the temperature of the SC1 bath to 70°C, using a 800W Megasonic at a low frequency (0.8 MHz) and maintaining a short process time of 5 minutes.

Using this full RCA-last clean at different critical process steps (i.e. sacrificial oxide removal, pre-gate oxide clean and PBL nitride etch), a Particle Removal Efficiency of 90 - 98 % with an "Adder To Zero" around 20 particles at 0.2 μm is achieved. At the same time, low metallic contamination and surface micro roughness are preserved which is also confirmed by the electrical characterisation of 7-10 nm gate oxides.

It is, therefore, concluded that the RCA clean will continue to play an important role at critical steps in the fabrication of state of the art CMOS/BiCMOS devices.

ACKNOWLEDGEMENTS

We are grateful to Emmanuelle Robert for her help on the processing and analysis of the wafers. We also thank Elie Andre for all AFM measurements and Paul Patruno for his stimulating discussions.

REFERENCES

1. Courtesy of Submicron System Inc., 1994.
2. H. F. Schmidt, M. Meuris, P. W. Mertens, A. L. P. Rotondaro, M. M. Heyns, T. Q. Hurd and Z. Hatcher, J. Appl. Phys., **34**, 727 (1995).
3. C. J. Gow, R. E. Smith, W. A. Syverson, R. F. Kunesh, E. D. Buker, K. B. Albaugh and L. S. Whittingham, **PV 92-12**, p.366, The Electrochemical Society Proceedings Series, Pennington, NJ (1993).
4. Marc Meuris, Marc M. Heyns, Paul W. Mertens, Steven Verhaverbeke, and Ara Philipossian, J. Microcontamination, **10-5**, 31 (1992).

SC1 PARAMETERS	SET-UP
Ratio (NH_4OH : H_2O_2 : H_2O)	0.25 : 1 : 5
NH_4OH Spike	0.625 liter / hour
H_2O_2 Spike	0.2 liter / hour
Process Temperature	35 °C
Process time	5 min
Megasonic Power	800 W
Megasonic Frequency	1.2 MHz

Table I : Initial SC1 Set-Up.

Parameters	Controlled	Limits
Process time	Yes	5' - 15 '
Process temperature	Yes	35°C - 70°C
Megasonic power	Yes	0W - 800W
Megasonic frequency	Yes	0.8 MHz - 1.2 MHz
Initial particle count	No	N/A

Table II : Parameter (factor) list for the Design Of Experiment

Experiment Number	Process Time	Process Temp.	Megasonic Power	Megasonic Frequency	Bp (part/wfr)
1	5	35	0	Low	159
2	15	35	0	High	423
3	15	35	800	Low	429
4	5	35	800	High	581
5	15	70	800	High	495
6	5	70	0	High	195
7	15	70	0	Low	540
8	5	70	800	Low	579

Table III : Design Of Experiment Matrix

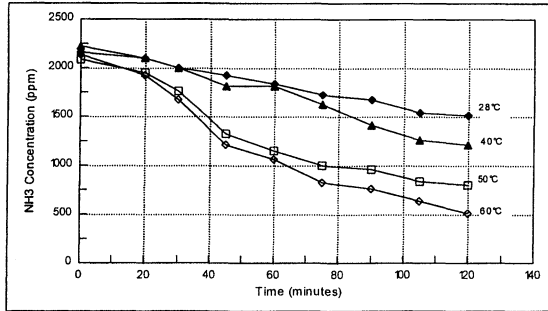

Figure 1 : SC1 Ammonia Concentration versus Bath Lifetime

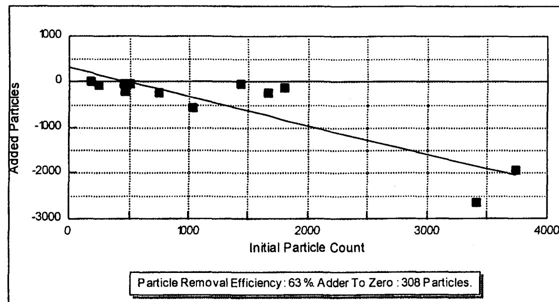

Figure 2 : SC1 Particle Removal Efficiency On Silicon For Particle size > 0.2 µm.
Process conditions : t = 5 min, T = 35°C, P = 800W, ν = 1.2 MHz.

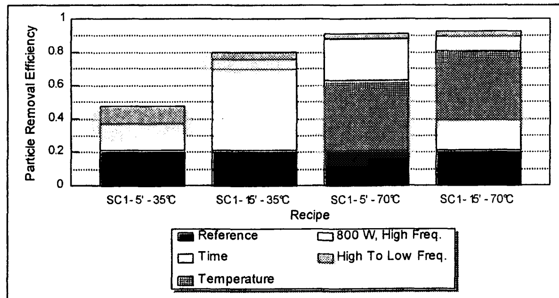

Figure 3 : Effects of SC1 Parameters on the Particle Removal Efficiency
Initial Process (reference) conditions : t=5 min, T=35°C, No Megasonic Power.

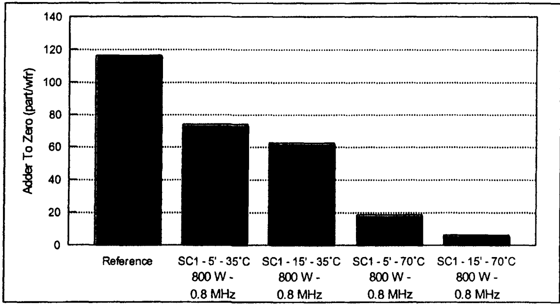

Figure 4 : Effects of SC1 Parameters on the Adder to Zero.
Initial Process (reference) conditions : t=5 min, T=35°C, No Megasonic Power.

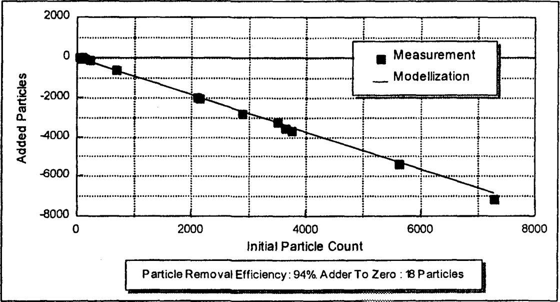

Figure 5 : Particle Removal Efficiency On Silicon For Particle size > 0.2 µm.
Process conditions : t = 5 min, T = 70°C, P = 800W, ν = 0.8 MHz.

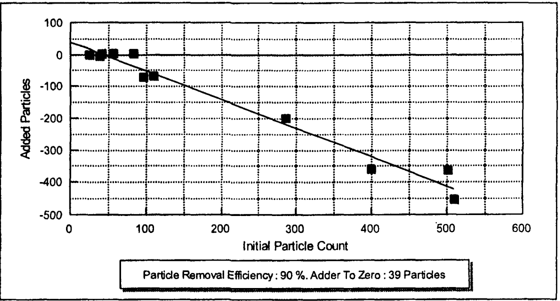

Figure 6 : Particle Removal Efficiency After Nitride Etch For Particle size > 0.2 µm.
Process conditions : t = 5 min, T = 70°C, P = 800W, ν = 0.8 MHz.

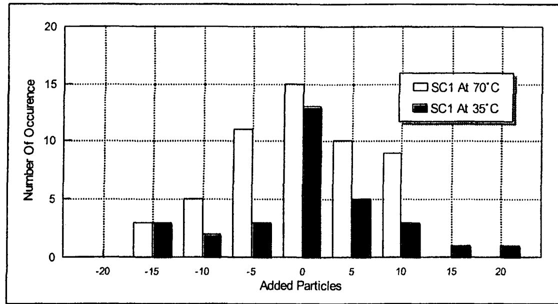

Figure 7 : RCA Monitoring - SC2 (0.25 : 1 : 5) at 50°C. Mean Added Particles and 3σ variance : 1.6 +/- 30 (SC1 at 35°C), -0.3 +/- 21 (SC1 at 70°C).

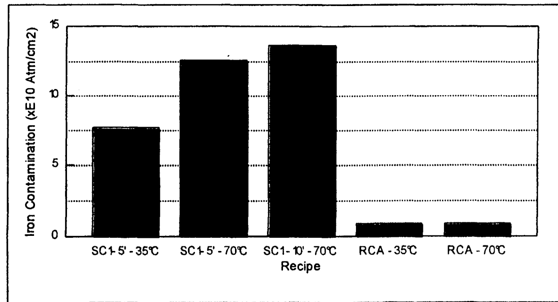

Figure 8 : Iron Contamination (TXRF results) on wafers after RCA clean . SC2 (0.25 : 1 : 5) conditions: t = 5 min, T = 50°C.

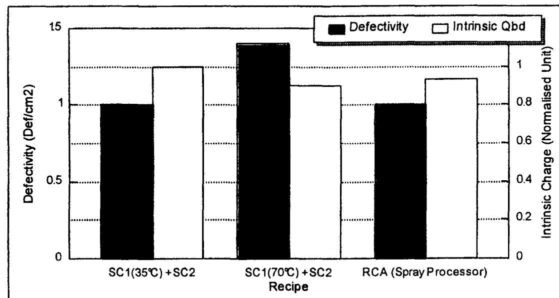

Figure 9 : Electrical Results after Current Constant Stress at 200 mA/cm^2 - Sample Surface = 0.6 mm^2 - Defectivity at 0.1 C/cm^2

QUANTITATIVE MODEL FOR THE SC-1 CLEANING

Steven Verhaverbeke, Jennifer W. Parker and Chris F. McConnell
CFM Technologies Inc., 1381 Enterprise Drive, West Chester, PA 19380

Equations detailing the equilibrium chemical compositions for SC-1 solutions are developed and solved. Approximate analytical expressions are derived for the $[OH^-]$ concentration and ionic strength; these expressions are accurate within 10% for $[OH^-]$ and 15% for the ionic strength over a large concentration domain. Additionally, the temperature dependence of [OH-] and ionic strength is presented. As a result of this study, the ratio NH_4OH/H_2O_2 was found to be the most important parameter for optimizing SC1 solutions, since this ratio determines the OH^- concentration. Additionally, the product of the ammonium hydroxide and hydrogen peroxide concentrations should be minimized to minimize the ionic strength and thereby, reduce particle deposition. Higher temperatures are optimal since the ionic strength decreases as a function of temperature for similar OH^- concentrations.

INTRODUCTION

The RCA Standard Clean, developed by W. Kern and D. Puotinen in 1965 and disclosed in 1970 (1) is extremely effective for removing contamination from silicon surfaces and has become the industry standard (2). The first step of the RCA Standard Clean, the Standard Clean 1, is the most efficient method for removing particles from semiconductor wafers found to date. The Standard Clean 1 (SC1) consists of a mixture of ammonium-hydroxide (NH_4OH), hydrogen-peroxide (H_2O_2) and water. A complete understanding of the solution chemistry occurring in the SC1 mixture is necessary for process optimization of SC1 cleaning. Earlier attempts have been made to solve the reaction equilibria (3,4). To date, however, no extensive analysis of the SC1 solution has been published. In this paper, a quantitative model for the SC1 cleaning is presented and discussed with respect to process optimization and control. Additionally, approximations to the quantitative model are developed and compared to the rigorous model.

EQUILIBRIUM ANALYSIS OF THE SC1 CLEANING SOLUTION

Equilibrium Equations

SC1 solutions, comprised of water, H_2O_2, and NH_4OH, are currently used in semiconductor manufacturing in concentrations ranging from 5:1:1 (H_2O:H_2O_2: NH_4OH) to 600:2:1. In order to quantify the chemistry occurring in SC1 solutions, the dissociation reactions for these three components must be accounted for:

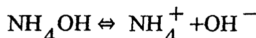

$$NH_4OH \Leftrightarrow NH_4^+ + OH^-$$

$$H_2O_2 \Leftrightarrow HO_2^- + H^+$$

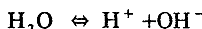

$$H_2O \Leftrightarrow H^+ + OH^-$$

In addition, NH_4OH can be oxidized by powerful oxidizing agents. Such oxidation leads to the formation of dissolved HNO_2, NO_2^- and NO_3^- and gaseous N_2, N_2O and NO. In particular, H_2O_2 will oxidize ammonia solutions into nitrite (NO_2^-) by forming ammonium nitrite (NH_4NO_2). The nitrite (NO_2^-) is subsequently slowly converted into nitrate (NO_3^-) (6). These oxidative processes are quite slow and for short solution-lifetimes the quantity of the resulting by-products is insignificant. Therefore, the oxidation of NH_4OH by H_2O_2 is neglected in our model.

The three dissociation reactions can be expressed in terms of equilibrium constants and the activity coefficients of each species, a_i, as follows:

$$a_{NH_4^+} \cdot a_{OH^-} = K_b \cdot a_{NH_4OH} \quad [1]$$

$$a_{HO_2^-} \cdot a_{H^+} = K_a \cdot a_{H_2O_2} \quad [2]$$

$$a_{H^+} \cdot a_{OH^-} = K_w \quad [3]$$

The relation between the activities, a_i and the concentrations $[C_i]$ for species i is:

$$a_i = f_i \cdot [C_i]$$

The activity coefficient of an electrolyte, f_i, is dependent on the ionic strength of the solution. According to the Debye-Huckel equation:

$$-\log f_i = \frac{0.5 z_i^2 \sqrt{\mu}}{1 + 3.3 r_i \sqrt{\mu}}$$

where z_i is the ionic charge and r_i is the ionic radius in nm. The activity coefficient f_i tends to 1 if the ionic strength, μ, tends to 0 (i.e., very dilute solutions). Consequently, we assume that molar concentrations can be used instead of activities in the equilibrium solutions for the purpose of our model. This assumption will be validated by calculating the ionic strength of solutions considered in our analysis.

The three equilibrium reactions can be written in terms of the molar concentrations of the chemical species, [Ci], as follows:

$$[NH_4^+] \cdot [OH^-] = K_b \cdot [NH_4OH] \quad [1]$$

$$[HO_2^-] \cdot [H^+] = K_a \cdot [H_2O_2] \quad [2]$$

$$[H^+] \cdot [OH^-] = K_w \quad [3]$$

Additionally, equations can be written for the conservation of charge as well as stochiometric balances for ammonia and hydrogen-peroxide:

$$[NH_4^+] + [H^+] = [OH^-] + [HO_2^-] \quad [4]$$

$$[NH_4OH] + [NH_4^+] = c_{NH_3} \quad [5]$$

$$[H_2O_2] + [HO_2^-] = c_{H_2O_2} \quad [6]$$

Equations 1-6 provide a set of 6 equations with 6 unknowns, the molar concentrations. The parameters that are known in equations 1-6 are the equilibrium constants K_b, K_a and K_W, expressed in molarities, and the initial concentrations of ammonia, c_{NH3}, and hydrogen peroxide, c_{H2O2}. The initial concentrations can be calculated from the extent of dilution of the of ammonium-hydroxide, hydrogen-peroxide, and water solution.

Equilibrium Constants

The equilibrium constants K_b, K_a and K_W are required to solve the six simultaneous equations. The equilibrium constants at infinite dilution are available in the literature (7, 8, 9, 10) for a number of temperatures. These literature values were extrapolated or interpolated for those temperatures where no data was found. The general temperature variation for the ionization of mono-acidic bases (11) was used to determine dissociation constant ammonium hydroxide for temperatures higher than 75°C:

$$\frac{-d(pK_{a(NH3)})}{dT} = \frac{pK_{a(NH_3)} - 0.9}{T} \quad [7]$$

where,

$$pK_b = pK_w - pK_{a(NH_3)} \qquad [8]$$

Linear extrapolation was used to calculate dissociation constants for H_2O_2 at temperatures higher than 50°C. The literature and calculated values for Kb, Ka, and Kw are given in Table 1.

The dissociation of water is an endothermic reaction and K_W is highly temperature dependent. At 70°C, K_W is 15 times its value at 25°C. In contrast, the dissociation constant for ammonium hydroxide is almost temperature independent. At 70°C, the Kb value for NH_4OH is only 6% higher than the Kb value at 25°C. Finally, the K_a value for H_2O_2 is a factor of 4 higher at 70 °C than at 25°C. Clearly, K_w has a strong influence on the temperature dependency of the solution chemistry.

EXACT AND APPROXIMATE SOLUTIONS TO THE EQUILIBRIUM EQUATIONS

SC1 chemistry is dominated by $[OH^-]$; the concentration of OH- determines the etch rate of the oxide and therefore, the particle removal efficiency. Consequently, solving Equations 1-6 for $[OH^-]$ is necessary for process optimization. The resulting equation is 4th order in $[OH^-]$:

$$\begin{aligned} &K_a[OH^-]^4 + (K_aK_b + K_w + K_a c_{H2O2})[OH^-]^3 + \\ &(K_aK_b c_{H2O2} - K_aK_w c_{NH3} - K_aK_w + K_bK_w)[OH^-]^2 \\ &+(-K_aK_bK_w - K_w^2 - K_bK_w c_{NH3})[OH^-] - K_bK_a^2 = 0 \end{aligned} \qquad [9]$$

Equation 9 was solved exactly for the ranges of c_{NH3} = 0.025 mol/l - 2.5 mol/l and of c_{H2O2}= 0 mol/l -1.25 mol/l at 25°C. Once $[OH^-]$ is known, all the other concentrations can readily be determined from Equations 1-6. The solution to Equation 9 at 25°C is shown in Figure 1 for the concentration domain indicated above. The results in Figure 1 clearly show that $[OH^-]$ increases with c_{NH_3} and decreases with $c_{H_2O_2}$ concentration.

For the range of concentrations considered in our analysis, Equation 9 can be simplified by neglecting all terms that are 2 or more orders of magnitude smaller than the largest as follows:

$$\begin{aligned} &\cancel{K_a[OH^-]^4} + (\cancel{K_aK_b} + \cancel{K_w} + K_a c_{H_2O_2})[OH^-]^3 + \cancel{(K_aK_b c_{H_2O_2} - K_aK_b c_{NH_3} - K_aK_w + K_bK_w)[OH^-]^2} \\ &+(\cancel{-K_aK_bK_w - K_w^2} - K_bK_w c_{NH_3})[OH^-] - \cancel{K_bK_a^2} = 0 \end{aligned}$$

This simplification yields an approximate expression for $[OH^-]$:

$$[OH^-] = \sqrt{\frac{K_bK_w}{K_a}\frac{c_{NH_3}}{c_{H_2O_2}}} \qquad [10]$$

The relative error between the approximation and the exact solutions is shown in Figure 2. As can seen in this figure, the approximation yields a value for $[OH^-]$ that is generally within a 5% error margin and always within a 10% error margin throughout the ranges considered. The largest absolute error is found for low hydrogen peroxide concentrations and high ammonia concentrations.

Chemical Concentration Error

The SC1 solution used in semiconductor fabrication is generally mixed from ammonium hydroxide in a 28-30 % by weight of ammonia (NH3) solution and a 30-32 % solution by weight of hydrogen peroxide (H_2O_2). The concentrations of these chemicals, as received from the supplier, were measured at the IBM Burlington site over the period of 2 years (5). Throughout this time, the concentration of ammonium hydroxide was found to be 28.95 w-% +/- 0.40 w-% and the hydrogen peroxide concentration was found to be 31.2 w-% +/- 0.34 w-%. Thus, the relative accuracy for the NH_4OH

and the H_2O_2 concentrations 1.4% and 1.1% for 1σ, respectively. Within the 2 year time period, however, all concentrations within the 28-30 w-% range for NH_4OH and 30-32 w-% range for H_2O_2 were encountered. These ranges convert into relative accuracy of 3.4 % for c_{NH_3} and 3.2% for $c_{H_2O_2}$.

Mixing the chemicals to obtain the desired process concentrations will further increase the error of c_{NH_3} and $c_{H_2O_2}$. Thus, the 10% error resulting from using Equation 10 as an approximation for [OH] is quite acceptable given the current chemical standards.

pH Effects

The [OH-] concentration determines the pH by the following equation:

$$pH = Kw - pOH \qquad [11]$$

where - log [OH-] = pOH. The pH values at 25°C are plotted in Figure 3 as a function of $[OH^-]$. Figure 3 shows that the pH value falls between 10 and 11 with an average of 10.5 for most of the concentration domain; These results agree with previous findings (4). When comparing solutions of different temperatures, the use of pH in SC1 solutions can be misleading, since similar pH values at different temperatures correspond to different $[OH^-]$ concentrations.

IONIC STRENGTH

The ionic strength of SC1 solutions is also an important parameter in determining particle removal efficiency. The ionic strength determines thickness of the electrostatic double layer surrounding particles and the wafer surface. The double layer thickness effects the separation distance between a sub-micron particle and the wafer surface (12). Lower ionic strengths lead to larger separation distances and consequently, lower particle adhesions. Consequently, optimal particle performance with SC1 processing is obtained with solutions with minimized ionic strength. Additionally, the approximation of molar activities by molar concentration is only valid at low ionic strength.

The ionic strength, μ, is defined as:

$$\mu = \frac{1}{2}\sum_{1}^{n} z_i^2 c_i \qquad [12]$$

with z_i the charge and c_i the molar concentration of the ions in solution. Therefore, the ionic strength of the SC1 solution can be calculated as:

$$\mu = \frac{1}{2}\left([HO_2^-] + [NH_4^+] + [H^+] + [OH^-]\right) \qquad [13]$$

The ionic strength as a function of c_{NH_3} and $c_{H_2O_2}$ is shown in Figure 5 using the exact solution to Equation 9. For H_2O_2 concentrations higher than 0.125 mol/l, 99% or more of the ionic strength results from NH_4^+ and HO_2^- alone. The OH^- concentration is negligible compared to the HO_2^- concentration. Even for concentrations of H_2O_2 down to 0.025 mol/l, more than 90% of the ionic strength is made up of NH_4^+ and HO_2^-. In the absence of H_2O_2, almost half of the ionic strength is made up of NH_4^+ and half is made up of OH^-.

Substituting the approximation for [OH] (i.e., Equation 10) yields a simplified approximation for ionic strength:

$$\mu = \frac{c_{NH_3}}{1 + \sqrt{\frac{K_w}{K_a K_b}\frac{c_{NH_3}}{c_{H_2O_2}}}} \qquad [14]$$

As with [OH], the error resulting from using the approximation for μ can be determined. The error is shown in Figure 7. If Equation 14 is used for the ionic strength, then throughout most of the concentration domain shown in Figure 7, the error

is within 10% of the exact solution obtained by solving the Equations 1-6. At the extremes of the concentration domain, the error increases up to 15 % with the use of Equation 14.

Equation 14 can be simplified further without increasing the error when (Kw / KaKb) 1/2 >>1:

$$\mu = \sqrt{\frac{K_a K_b}{K_w} c_{NH_3} c_{H_2O_2}} \qquad [15]$$

Equation 15 shows that the ionic strength is primarily dependent on the product of the ammonium hydroxide and hydrogen peroxide concentration.

TEMPERATURE DEPENDENCE

The influence of temperature on the composition of the solution can be determined since the dissociation constants are known as functions of temperature. Equations 1-6 have been solved exactly and 50 °C as well as at 25 °C. The approximate expressions have also been analyzed at the higher temperature. The same qualitative conclusions with respect to $[OH^-]$ and μ are true at 50 °C as found were 25 °C. At 50°C, the errors introduced by using the approximate expressions for $[OH^-]$ and μ are smaller than at 25 °C. Therefore, these approximations will be used to study the effect of temperature on SC1 composition.

The temperature dependence of $[OH^-]$ and μ can be calculated by using Equations 10 and 14. Since c_{NH3} and c_{H2O2} are independent of temperature, the resulting expressions for $[OH^-]$ and μ as a function of temperature are :

$$\frac{[OH^-]}{[OH^-]_{25°C}} = \sqrt{\frac{K_{b_t} K_{w_t} K_{a_{25°C}}}{K_{a_t} K_{b_{25°C}} K_{w_{25°C}}}} \qquad [16]$$

$$\frac{\mu_t}{\mu_{25°C}} = \sqrt{\frac{K_{w_{25°C}} K_{a_t} K_{b_t}}{K_{w_t} K_{a_{25°C}} K_{b_{25°C}}}} \qquad [17]$$

The temperature dependence of [OH-] is shown in Figure 6. As seen in this figure, the [OH-] concentration is twice as high at 70 °C than at 25 °C for the same bath composition.. A linear regression of the data in Figure 6, yields an expression for the $[OH^-]_t / [OH^-]_{25°C}$ ratio:

$$[OH^-] = [OH^-]_{25°C} * (0.25 + 0.025 * t) \qquad [18]$$

where t is in °C.

Similarly, the temperature dependence of μ is given in Figure 7. As can be seen from this figure, the ionic strength is lower at higher temperature for the same bath composition. Again, an analytical expression for the $\mu_t / \mu_{25°C}$ ratio can be obtained with linear regression:

$$\mu_t = \mu_{25°C} * (1.30 - 0.0112 * t) \qquad [19]$$

where t is in °C.

Figures 6 and 7 clearly indicate that at higher temperatures $[OH^-]$ increases, whereas μ decreases. These results provide great incentive for using higher temperatures, since the same OH^- concentration can be obtained for much lower ionic strengths by raising the temperature. For example, at 70 °C, the ionic strength is only half of the ionic strength at room temperature, whereas $[OH^-]$ is almost double.

As mentioned earlier, the ionic strength is almost entirely determined by the $[NH_4^+]$ and the $[HO_2^-]$ concentration. At 25 °C, The dissociation of NH_4OH and H_2O_2 depends on pH according to the following reactions:

$$\log\frac{[NH_4OH]}{[NH_4^+]} = -9.25 + pH \qquad [20]$$

$$\log\frac{[HO_2^-]}{[H_2O_2]} = -11.62 + pH \qquad [21]$$

where 9.25 and 11.62 are the pK_a values for NH_4OH and H_2O_2, respectively. The pK_W value at 25°C is 13.995. At 50 °C, the pK_a values for NH_4OH and H_2O_2 values decrease to 8.55 and 11.21, respectively, and the pK_W value decreases to 13.275. The effect of the temperature dependency of these parameters on the composition is schematically illustrated in Figure 8. At higher temperatures, the difference between of pK_a values of NH_3 and H_2O_2 is greater and therefore the ionic strength will be lower (i.e., less ionization will occur). Additionally, the increase in $[OH^-]$ at higher temperatures results from the fact that the dissociation of H_2O_2 increases less at higher temperatures than the increase of the dissociation of water (change in pK_W).

CONCLUSIONS

In the past few years, considerable effort has been spent optimizing the NH_4OH concentration in SC1 solutions, while keeping the H_2O_2 concentration constant. This study, in contrast, shows that the ratio of NH_4OH/H_2O_2 is the most important parameter for process optimization of SC1 solutions. The ratio of c_{NH3} and c_{H2O2}, not the absolute values of the chemical concentrations, determine the OH^- concentration. The OH- concentration should be optimized to obtain a certain etch rate of the oxide, depending on the particular application and whether or not megasonic energy is used during processing.

The product of the ammonium hydroxide and hydrogen peroxide concentrations should be minimized to diminish the ionic strength. In general, the concentration of both components should be as low as possible, because of the effect of ionic strength. The tolerance on the initial chemical concentration and the mixing becomes critical in highly dilute solutions. Thus, the optimum SC-1 mixture is a solution of NH_4OH and H_2O_2 with a optimized ratio but at minimal concentration of NH_4OH and H_2O_2.

Finally, higher operating temperatures are favorable, since the ionic strength decrease for the same $[OH^-]$ concentrations as temperature increase.

Table 1 : The pK ($pK = -\log K$) values for the equilibrium constants K_b, K_a and K_W expressed in molarities as a function of temperature.

Temperature (°C)	pKw	pKb	pKa
25	13.995	4.751	11.620
30	13.836	4.740	11.550
35	13.685	4.733	11.340
40	13.542	4.730	11.297
45	13.405	4.726	11.253
50	13.275	4.723	11.210

Temperature (°C)	pKw	pKb	pKa
55	13.152	4.730	11.167
60	13.034	4.727	11.123
65	12.921	4.725	11.080
70	12.814	4.726	11.037
75	12.712	4.726	10.993
80	12.613	4.725	10.950

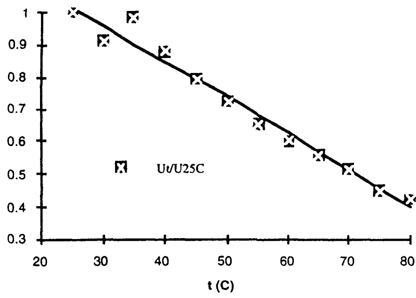

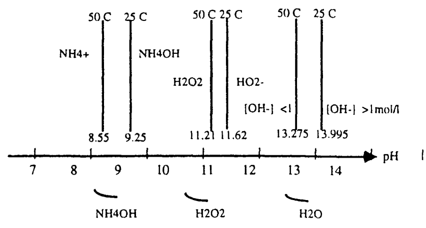

Fig. 7 - Temperature dependence of the ionic strength μ. The ratio of μ_t/μ_{25oC} is shown as a function of temperature ranging from 25 ^oC up to 80 ^oC.

Fig. 8 - Composition of the SC-1 solution as a function of pH.

REFERENCES

1. W. Kern and D. Puotinen, RCA Rev. 31, 187 (1970).
2. W. Kern, J. Electrochem. Soc. 137, 1887 (1990).
3. G.S. Higashi, J. Rosamilia, K. Hanson, J. Sapjeta, L. Psota-Kelty, T. Boone, I. Kashkoush and R.W. Grant, unpublished results.
4. D. L. Rath, F. Abramovich, S. L. Cohen, C. Gow, M. Hevey, G. Ouimet, unpublished results.
5. S. Cohen et al., IBM Burlington Chemical Analysis (1994).
6. M. Pourbaix and N. De Zoubov, Atlas of Electrochemical Equilibria in Aqueous Solutions (NACE, Houston, TX, 1974), p. 501.
7. D. Lide, edt., Handbook of Chemistry and Physics (CRC, Boca Raton, Fl, 1995), p. 8-57.
8. D. Lide, edt., Handbook of Chemistry and Physics (CRC, Boca Raton, Fl, 1984), p. D-167.
9. E. Högfeldt, Stability Constants of Metal-Ion Complexes, Part A : Inorganic Ligands (Pergamon, Oxford, 1971).
10. D.D. Perrin, Ionization Constants of Inorganic Acids and Bases in Aqueous Solution (Pergamon, Oxford, 1982).
11. A. Albert and E. Serjeant, The Determination of Ionization Constants (Chapman and Hall, London, 1971).
12. M. Itano, F.W. Kern, R.W. Rosenberg, M. Miyashita, I. Kawanabe and T. Ohmi, IEEE Tans. on Semic. Manuf. Vol. 5, No.2, May 1992, p. 114.

FIGURES

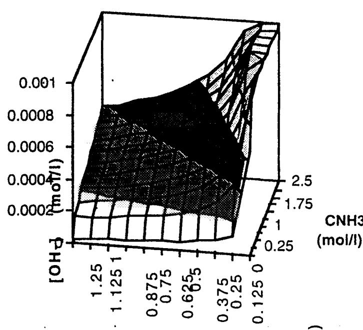

Fig. 1 - Calculated [OH$^-$] concentration as a function of the formal concentration of NH_4OH and H_2O_2 at 25°C. The [OH$^-$] concentration was calculated by solving the reaction equilibria equations.

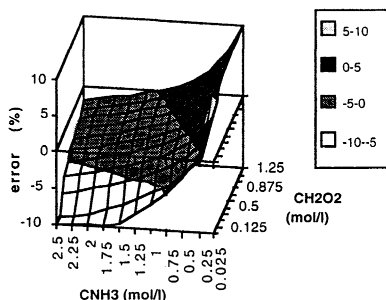

Fig. 2 - Relative error (%) between the approximated [OH-] and the [OH-] concentration as a result of solving the complete set of equilibria equations at 25°C.

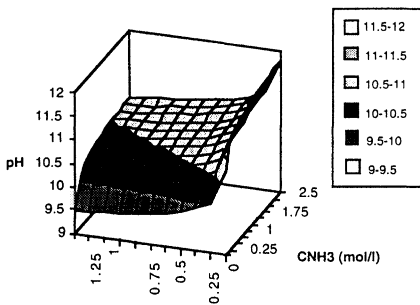

Fig. 3 - Calculated pH as a function of formal NH_3 and H_2O_2 concentration.

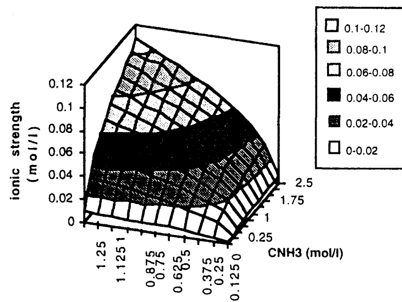

Fig. 4 - Ionic strength (mol/l) as a function of formal NH_3 and H_2O_2 concentration.

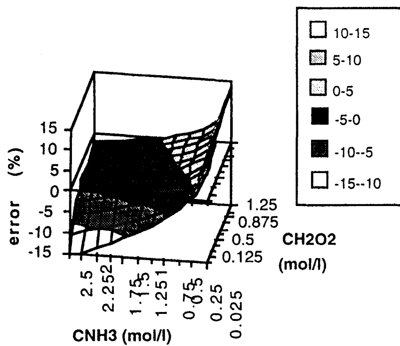

Fig. 5 - Relative error on the ionic strength (%) when using the approximative expression versus the exact solution to the equations as a function of NH_3 and H_2O_2 concentration.

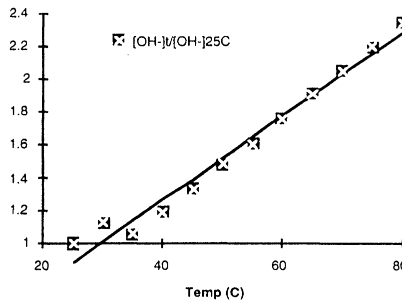

Fig. 6 - Temperature dependence of $[OH^-]$ concentration.

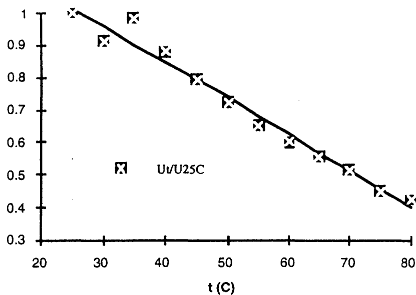

Fig. 7 - Temperature dependence of the ionic strength μ. The ratio of μ_t/μ_{25^oC} is shown as a function of temperature ranging from 25°C up to 80°C.

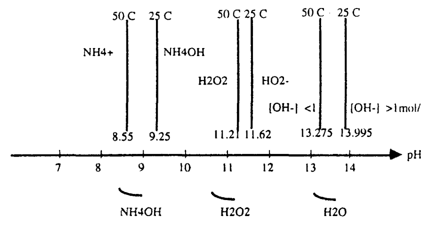

Fig. 8 - Composition of the SC-1 solution as a function of pH.

OPTIMIZATION OF HF and OXIDANT WET CLEANINGS BEFORE 7 nm GATE OXIDE

Introduction to "DDC" : Diluted Dynamic Clean

F. Tardif, T. Lardin, C. Paillet, JP. Joly
GRESSI LETI (C.E.A.), CEN/G, 17 rue des Martyrs / F-38054 Grenoble Cedex 9

A. Fleury, P. Patruno, D. Levy, K. Barla
SGS/Thomson, Centre Commun, F-38290 Crolles

Using very diluted chemicals is a possible way of satisfactorily removing particles and metals before gate oxidation. The ideal thin gate oxide integrity obtained with HFlast cleanings can also be achieved by adding a simple ozonized Di water final dip leading to a better process robustness. A new concept for processing diluted chemistries called "DDC" : Diluted Dynamic Clean is proposed. One tank is dedicated to HF chemistries, the other one is constituted by a conventional overflow where the chemicals are injected into the continuous flow of Di water.

INTRODUCTION

Usual RCA based pre-gate cleaning recipes give satisfactory performances even for the most advanced IC manufacturing technologies (lower than 0.35 µm) when they are performed in state of the art equipment. But they are more and more expensive because of the use of ultra clean chemicals and sophisticated tools. (From our recent estimation, wet processing represents nowadays about 10% of the total cost of IC fabrication). The next challenge is to reach the same good performances but at a lower price and with a lower environmental impact. The use of chemicals diluted with ultra pure Di water can potentially solve at the same time the problems of costs, purity and environmental considerations.
This study reviews the optimization of the conventional cleaning steps performed before gate oxidation including : sacrificial oxide removal, particle removal, metallic removal and final passivation. Their performances are compared with those obtained with diluted chemistries. A new concept called "DDC" Diluted Dynamic Clean is also proposed.

EXPERIMENTS

The tests were performed in Leti facilities on CZ, (100) p type 14-22 Ω.cm 4" wafers, using 1ppb level grade chemicals. Seven nm thick gate oxides are grown under wet conditions at 750°C without TCA or HCl. All the thermal steps including wafer loading are performed under partial oxygen pressure. The test vehicle used here is constituted by flat capacitors only (no lateral isolation). A previous silicon surface conditioning is performed in order to remove major crystalline defects due to oxygen precipitates by a 1100 °C out-diffusion process. Nevertheless, using epi wafers as major IC manufacturers do at present would certainly lead to better electrical results due to the high silicon crystalline quality of epitaxial layers. On the other hand, CZ wafers enhance the phenomena and can furthermore to a certain extent be representative of the behaviour of stressed epi silicon areas.

OPTIMIZATION OF SACRIFICIAL OXIDE REMOVAL

Most of the time, the cleaning process before gate oxidation has to start with sacrificial oxide removal. This step, already performed by a diluted HF based chemistry, is in fact potentially highly damaging and therefore has to be carefully optimized.

Impact of HF bath pH : An overetch of the locos or PBL edges can drastically degrade the gate oxide intrinsic properties in terms of QBD[1] by disclosing the disturbed peripheral area. It is therefore necessary to use diluted HF (1%) in order to better control the overetch. But in this case the relatively high pH can favour silicon etching by HF_2^- species leading to Si-monohydride terminations on the (100) oriented silicon[2]. The addition of a strong acid such as HCl even at diluted concentration (1%) enables the pH to be decreased from 1.9 to 0.5 and leads to a lower RMS roughness as measured by tapping mode AFM (see figure 1). This effect is confirmed by the results of intrinsic QBD obtained on 7 nm gate oxide shown in figure 2. The use of HF baths spiked with 1% HCl is therefore recommended.

Impact of dissolved oxygen : Silicon is also oxidized by dissolved oxygen as shown in figure 3 where the effects of non especially treated and partially degassified DI water are measured in terms of tapping mode AFM measurements. This effect seems to be particularly active in the first minutes of the overetch. It is therefore necessary to use degassifiers both in the HF bath and in the associated rinsing bath.

Protection of HF baths against noble metal contamination effects : Another potential risk is due to the plating phenomena of noble metals (Pt, Au, Ag, Cu, FeIII, ...)[3] which in parallel dissolve silicon atoms increasing the roughness. The addition of traces of a strong oxidant such as H_2O_2 or the presence of a residual dissolved oxygen content reoxidizes the just deposited metals back to the solution but leaves the associated roughness which is unfortunately probably the most detrimental effect. No solutions are industrially available today to protect the silicon surface from the roughening effect of a noble metal contamination in HF except to closely monitor the bath contamination content. Chemical purifiers constituted for example by high specific area silicon represent one of the solutions for the near future. In this case the use of oxidant species will be prohibited as they will re-dissolve the captured noble metals.

To remove the sacrificial oxide, we therefore propose to use the so-called "%" : 1%HF+1%HCl diluted mixture, continuously degassified, filtered and chemically purified as far as noble metals are concerned.

Furthermore, the HF bath purity can be partially protected from the external noble metal contamination brought about by the surface wafer contamination using a previously diluted 3ppm O_3+0.01%HCl bath. Indeed, according to Pourbaix Diagrams, this diluted mixture is thermodynamically liable to remove Au, Cu, FeIII, and probably Ag which is just at the corrosion limit area. Tests are in progress to check the kinetic aspect. Using this protecting cleaning, the organic contamination will also be removed as shown by Ohmi et al [4], but for the sacrificial oxide removal step this is probably not very relevant.

OPTIMIZATION OF PARTICLE REMOVAL

Sacrificial oxide deglaze is theoretically liable to remove particles by under-etching mechanism. Al_2O_3 particles in the 0.8 µm range were intentionally deposited on wafers by dipping them in spiked Di water. Al_2O_3 particles were selected for their highly positive Zeta potential (iso electrical point pH = 7.4). As silicon substrates are negatively charged even at fairly low pH, the use of a highly positively charged particle represents the most unfavorable case during the particle/substrate separation step. The particle contamination was performed before the sacrificial oxidation simulating a poor sacrificial oxidation cleaning and after the sacrificial oxidation in order to simulate a particle contamination in the furnace.

Figure 4 shows that the sacrificial oxide deglaze performed with 1% HF is unable to remove a satisfactory level of particles especially when the particles are initially deposited before sacrificial oxidation and therefore pre-sealed in this oxide. An (O.25,1,5) SC1 clean performed after the HF etching improves the final level of residual particles. Even if the presence of anionic surfactant could probably improve the particle removal efficiency[5] of the diluted HF bath, a more powerful cleaning step anyway seems to be necessary. Taking the worst case (Al_2O_3 particles deposited before the sacrificial oxidation), conventional chemistries were tested after the sacrificial oxide removal process : SC1 (1,1,5) and (0.25,1,5) with or without megasonics, 70°C, 10'. These mixtures were compared with two-step cleanings which mechanism was first explained by IMEC[6] : CARO 4/1 10' followed by a 1%HF+IPA dip or 1%HF+1%HCl dip (in order to avoid roughening effects) and their diluted ozonized (3 ppm in Di water) equivalents. Figure 5 shows the typical results obtained on different tests. All the different tested cleanings lead to the same residual particle removal. In this case, the diluted chemistries remove the deposited particles with the same efficiency as the conventional cleaning processes. (In the general case, we have already shown that CARO/HF is slightly more powerful than O_3/HF[7]). The commonly reached decontamination level is only perfectible by the mechanical effect of a scrubber which is not possible on processed wafers. Nevertheless, these proposed diluted processes induce one more HF step which is always potentially highly damaging as stipulated before. The lateral isolation process has to be adapted in this case.

OPTIMIZATION OF METALLIC REMOVAL

In order to replace the conventional Kern's (1,1,5), 70°C SC2, diluted cleaning mixtures are tested on intentionally contaminated wafers in the 10^{12} at/cm^2 range. The wafers are initially contaminated in spiked SC1. Then, (1.1.5) SC2 is compared to 1%HF+1%HCl mixture or 1' in 1% HF followed by a variable time in 1%HCl (the roughening effect of 1%HCl is acceptable as demonstrated in figure 1). The results are given in terms of residual contamination measured by VPD-TXRF (figures 6,7,8) or in terms of minority carrier lifetime for Fe as measured by ELYMAT (figure 9).

Except for the case of Cu as representative of noble metals, the HF based mixtures lead to a faster metallic kinetic removal than SC2. A 30" HF process time removing the contaminated oxide leads to even better results than an SC2 performed during 300". The cleaning process which consists of an HF dip followed by HCl gives even slightly better results. The metallic removal is therefore in practice performed during the necessary minimum overetch time of the sacrificial oxide deglaze.

The use of the above proposed "%" diluted (1%HF+1%HCl) mixture during this step can therefore be considered as the metallic removal clean as well.
After cleaning the wafers, the following steps have also to keep the wafers clean. Especially during the rinse steps where the pH is close to 7 a slight accidental contamination (<< 1ppb) can produce a heavy $Fe(OH)_3$ deposition among others [3]. This phenomenon can be easily avoided by adding traces (0.01 %) of HCl or HNO_3 in the Di water. Figure 10 shows experimental results obtained after a 10' rinsing bath for which the flush frequency was not enough (analytical tools were not able to detect any change in the Di water purity). The HCl dynamic spiking at 0.01% in the incoming Di water was sufficient to avoid Fe deposition (the same results were obtained with HNO_3). A convenient way of protecting the cleaning tool from the rinsing deposition consists in continuously injecting traces of HCl in the incoming Di water or only during the processes performed at neutral pH (rinsing, O_3 in Di water, ...).

PASSIVATION STEP

The last cleaning step is particularly critical as it conditions the chemical state of the silicon surface before oxidation. HFlast cleanings, performed under ideal conditions, lead to high intrinsic gate oxide performances. Nevertheless, they make the associated thermal process more sensitive as they produce very reactive surface to hydrocarbon and particle contaminations and heterogeneous island re-oxidation. We performed both optimization of HF cleanings to approach the ideally perfect silicon state as close as possible (100% hydrogen terminated, perfectly atomically flat, ...) and also optimization of a last oxidant passivation step.

Optimization of HFlast cleanings :

Impact of waiting delay between HFlast cleaning and furnace loading : A short time delay between a conventional 1%HF dip of 100" followed by a rinse and furnace loading modifies the reactive silicon surface and consequently drastically affects the extrinsic properties of 7 nm gate oxide (see figure 11). The maximum acceptable delay can fluctuate with the over-etch time and the gaseous environment of the wafers. It was fixed at a maximum of 20 minutes for all the experiments.

Impact of HF bath time and rinsing : In this experiment, 1%HF bath time and the presence of a final 10' rinse are studied. Figure 12 shows an optimal 1%HF bath time at about 100 seconds. We can imagine that before this time, the silicon atoms at the surface are not all hydrogenated as indicated by contact angle measurements also reported by Alay et al[8]. This surface non-homogeneity could cause detrimental effects by local differential oxidation kinetics of the first monolayers. After the optimum, the roughening effects described above could explain the obtained results (use of non degassified DI water). The shape of the QBD curve is the result of the competition between these two mechanisms. If we assume that the etching process continues to a lesser extent in the rinsing tank, we can explain why the rinsing step improves the oxide QBD when the process time is not sufficiently long and degrades the QBD when the rinsing step exceeds the optimum time. Over-etching in the HF bath therefore has to be limited and optimized according to the oxygen content in the HF bath and in the associated rinsing tank.

Optimization of oxidant cleanings :

Bath temperature impact on conventional oxidant cleanings : After a 1% HF treatment, different cleanings are tested : SC2 (1 HCl, 1 H_2O_2, 5 H_2O) 10', Aqua regia (2 HCl, 1 HNO_3) 10', CARO 3/1 (3 H_2SO_4, 1 H_2O_2) 10' and CARO 2/1 (2 H_2SO_4, 1 H_2O_2) 10'. As depicted in figure 13, the process temperature of conventional cleaning steps seems to be one of the main parameters which govern thermal oxide quality.
An optimum mean breakdown field is obtained close to 100 °C for both CARO and SC2. The performances are equivalent to the optimized HFlast process acting as reference. In figure 14, a correlation can be seen between the mean breakdown field of capacitors and RMS roughness measured by AFM contact mode. Even though this relation is usually verified in our tests, we do not know if the AFM roughness acts directly or is combined with another actually detrimental phenomenon.

Bath temperature impact on ozonized oxidant cleanings : Ozone is a potentially good oxidant candidate for replacing water peroxide. Ozone is a much stronger oxidant than H_2O_2 (the electrochemical potentials at 25 °C are respectively equal to +2.07 and +1.78 V) and is consequently able to oxidise silicon even at room temperature. Chemical oxidation of silicon depends on the oxidant concentration in the bath and also on the diffusion capacity of the oxidant species through the first monolayers of the chemical oxide. The latter parameter is facilitated by the temperature, but a high temperature also limits the absorbed ozone concentration. Therefore, competition occurs between these two phenomena which does not exist in the case of use of water peroxide. This antagonism can restrict the silicon oxidation power of ozone chemistry. Different cleaning processes are tested according to the bath temperature (see figure 15). The O_3 content is assumed to be near the saturation limit for each media as we inject ozone continuously at the bottom of the bath. The optimized 1%HF last process is compared with O_3/H_2O 10' in a static heating bath, O_3/H_2SO_4 (3 H_2SO_4, 1 H_2O) 10' and O_3/HCl (1 HCl, 1 H_2O, 5 H_2O) 10'. The last two recipes present the same acid concentrations as CARO 3/1 and SC2 (1,1,5). O_3/H_2O cleaning gives a better oxide integrity at room temperature. In this case, the intrinsic performances of 7 nm gate oxide measured on a small capacitor area are close to the optimal value indicated by the 1%HF reference, but the mean breakdown fields measured on large capacitors are lower than for the other cleanings. For O_3/H_2SO_4, the best results are obtained at 80 or 140 °C. In the case of O_3/HCl cleaning, the optimum temperature as for O_3/H_2O mixtures is 20 °C. The chemical differences between water peroxide and ozone chemistries described above could explain the different evolutions of thin oxide properties with the process temperature (figures 13 and 15).

Comparison between optimized conventional and ozonized cleanings

Optimized cleanings using water peroxide and ozone are tested after the two main particle removal recipes : conventional (1,1,5) SC1 or CARO followed by 1%HF. The tested recipes are SC2 (1,1,5) 10', CARO 3/1 10' and their ozonized equivalents with the same acid concentrations and also the simple O_3/H_2O 10' cleaning processed in an overflow tank (O_3 is adjusted to 3 ppm) or in a static bath (see figure 16). Ozonized Di water gives good results on clean HF treated surfaces especially when performed in an overflow bath. This difference could be attributed to the high purity of the always new Di water of the overflow tank. After the polluting SC1, O_3/H_2O cleaning does not give satisfactory results.

This behaviour could be attributed to its lack of efficiency to remove most of the metallic contamination due to its neutral pH. The use of a final O_3/H_2O step is therefore only possible on clean wafers and if the DI water is absolutely pure. The chlorinated chemistries SC2 and O_3/HCl also give good intrinsic thin oxides when performed on initially clean wafers. (But in this test O_3/HCl gives bad results on large capacitors). After polluting SC1, the low process temperature of O_3/HCl does not enable enough contamination to be removed as proved by Elymat measurements. This is a well known phenomenon already published[7], within the scope of SC2 process temperature optimization. In the case of sulphuric acid cleanings, the best results are obtained for traditional CARO 3/1 performed at 100 °C.
So the best passivation of the wafers in terms of following thermal process robustness and electrical performances is given by a simple dip in a 3 ppm ozonized Di water performed in dynamic mode (overflow). We propose to spike the ozonized Di water with 0.01% HCl in order to prevent recontamination due to a DI water quality failure. The residual traces of HCl left on the silicon surface evaporate rapidly due to its high volatility.

DILUTED CLEANING ADAPTED TO GATE OXIDE PROCESS

Taking the above described results into account, we tested the intrinsic performances of some diluted recipes compared to conventional RCA as reference.

Table 1 : Tested diluted cleaning recipes

#	Sac. Ox. deglaze	Particle removal		Passivation
1	1%HF 3'	SC1 (0.25,1,5) 10' 70°C		SC2 (1,1,5) 70°C, 10'
2	1%HF 3'	CARO4/1 10'	1%HF 1' then 1%HCl 3'	3ppm O_3 10'.
3	1%HF 3'	3ppm O_3 10'	1%HF 1' then 1%HCl 3'	3ppm O_3 10'.
4	1%HF 3'	3ppm O_3 10'	1%HF + 1%HCl 4'	3ppm O_3 10'.
5	1%HF 3'			3ppm O_3 10'

The test was carried out on 7 nm gate oxide flat capacitors in terms of Charge to Breakdown. A 12 nm sacrificial oxide was first removed in 1%HF during 3'. The 2 batches processed gave the same conclusion : on flat capacitors the performances of the diluted chemistries are comparable with the performances given by a conventional RCA. Only process 3 gave repeatedly bad results for unexplained reasons.
Based on the previously exposed results, table 2 proposes an example of a full diluted cleaning recipe suited to gate oxidation.

Table 2 : Example of a diluted cleaning sequence adapted to gate oxide process

Step	Process		Action
0 (optional)	(3 ppm O_3 in 0.01% HCl)		Protect the bath and remove the organics
1	1%HF + 1%HCl	30" overetch	Sacrificial oxide deglaze and metallic removal
2	3 ppm O_3 in 0.01% HCl	10'	Separation of the particles from the silicon
3	1%HF + 1%HCl	4'	Particle under-etching and removal
4	3 ppm O_3 in 0.01% HCl	10'	Final passivation

Some of the durations are indicative and tests are in progress to reduce them. Nevertheless it would be difficult to propose a definitive value as the process times depend drastically on the optimization state of the bath hydrodynamics. This still perfectible cleaning recipe consumes much less chemical products compared to a conventional RCA.

ADVANCED EQUIPMENT FOR DILUTED CLEANING PROCESS : INTRODUCTION TO "DDC" : DILUTED DYNAMIC CLEAN

The use of very diluted chemicals at room temperature enables new technological concepts to be envisaged. In order to perform the diluted chemistry cleanings, we propose a new concept we call at Leti "DDC": Diluted Dynamic Clean. The main idea consists in using a conventional quartz overflow rinsing tank in which small amounts of reactives are injected alternately or together into the continuous flow of Di water. As the quantity of chemicals is negligible in the case of diluted clean, the overflow can still be connected directly to the drain. In this case, the purity of the chemicals is very high (especially if the reactives are gases) and the interfacial particle deposition contribution is reduced[9]. This bath can be used to run different processes and rinsing steps as well. Of course, the hydrodynamics of the bath have to be optimized in order to reduce the consumptions of DI water and chemicals. Since for environmental considerations IC manufacturing has to limit its fluoride wastes, another bath dedicated to HF based chemistries completes the whole concept. This bath is constituted by a conventional HF recirculated/filtered bath including an oxygen desorption device and a chemical purifier to remove noble metals. The DDC concept is constituted by the association of the two baths represented in figure 18. This minimum configuration thus constitutes a cleaning tool suitable for low throughputs. Higher throughputs can be achieved by juxtaposing several DDC modules, the total footprint always being reduced mainly due to elimination of the rinsing baths.

CONCLUSION

On CZ wafers, HF treatments used to remove the sacrificial oxide can be improved by adding 1%HCl, by reducing the dissolved oxygen content and by decreasing the over-etch time. Particles can be advantageously removed by the diluted two-step cleanings : O_3/H_2O followed by a diluted HF dip. Major metallic contamination can be rapidly eliminated during the necessary overetch of the sacrificial oxide removal using the diluted "%" mixture : 1%HF+1%HCl. In terms of final passivation the drastic consequences induced by a too long waiting time after HFlast cleaning enable the advantages of passivating the silicon during a last oxidant step to be appreciated, particularly in the industrial context where process robustness is a key parameter. The ideal thin gate oxide integrity obtained with HFlast cleanings can also be achieved by a final optimized oxidant cleaning step such as a simple 3 ppm ozone/H_2O final step performed in an overflow rinsing tank at room temperature. This diluted solution gave better results than the optimized conventional chemistries (optimized CARO or SC2) and their ozonized equivalents.
So a cleaning sequence using only diluted chemicals at room temperature can be proposed for gate oxide applications. Nevertheless, this chemistry require one more 1%HF step than a conventional RCA which can cause some detrimental effects if the locos or PBL edge is not especially designed.
The very low quantities of chemicals involved opens up the possibility of drastically simplifying the existing wet benches. We propose a new concept called DDC : "Diluted

Dynamic Clean" where the chemicals are injected into the continuous DI water flow of a conventional overflow rinsing tank. Another recirculated tank is devoted to diluted HFbased chemistry.

REFERENCES

1. M. Gardner, J. Seaton, J. Fulford ECS Meeting, extended abstract 137, May 1994
2. S. Verhaverbeke - IMEC thesis - June 1993
3. L. Mouche, F. Tardif, J. Derrien ECS June 1995
4. S. Yasui, N. Yonekawa and T. Ohmi Semiconductor Pure Water and Chemicals conferences, San Jose, pp 66-73, March 1994
5. M. Itano, T. Kesuka, M. Ishii, T. Unemoto, M. Kubo, T. Ohmi, J. Electrochem. Soc, Vol 142, N° 3, March 1995
6. S. Verhaverbeke, H. Schmidt, M. Meeuris, P. Mertins, M. Heyns - Semi./Europa 93
7. F. Tardif et al, UCPSS's 94 conferences, Bruges Belgium, September 1994
8. J.L. Alay, S. Verhaverbeke, W Vandervost & M. Heyns Jpn.J.Appl.Phys.-Jan 93
9. L. Mouche, F. Tardif, J. Derrien ECS Vol 141, N° 6 June 1994

ACKNOWLEDGEMENTS

Special thanks to JL. di Maria (Leti), C. D'Assenza (Soitec), M. Druges (ST), A. Tonti (ST), M. Alessandri (ST), E. Bellandi (ST) for their active contributions.

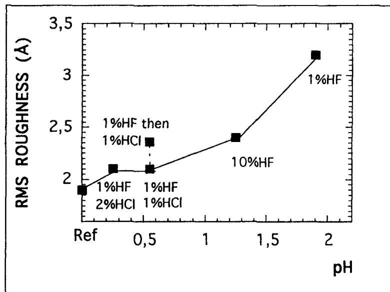

Figure 1 : pH Impact of HF based mixture treated wafers on the RMS roughness (Tapping mode AFM, process time : 10')

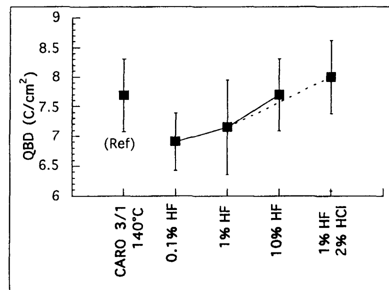

Figure 2 : pH Impact of HF based mixture treated wafers obtained on 7 nm gate oxide (Process time : 100", area = 0.05 mm^2)

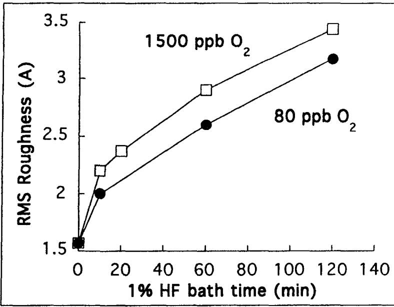

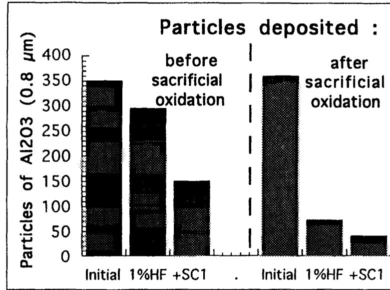

Figure 3 : AFM tapping mode roughness obtained in 1%HF as a function of time and dissolved oxygen content (Process time : 5')

Figure 4 : Particle removal efficiency achieved by the sacrificial oxide deglaze treatment

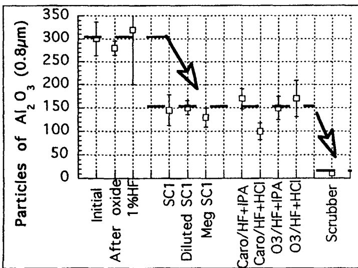

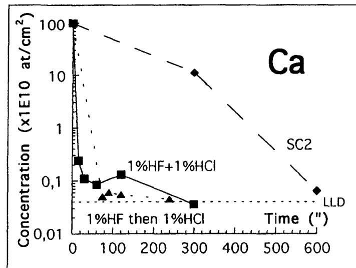

Figure 5 : Particle removal efficiency of different cleaning processes performed after 1%HF deglaze when Al_2O_3 particles are deposited before sacrificial oxidation.

Figure 6 : Ca removal efficiency versus process time (as measured by VPD-TXRF)

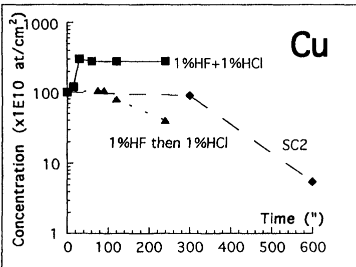

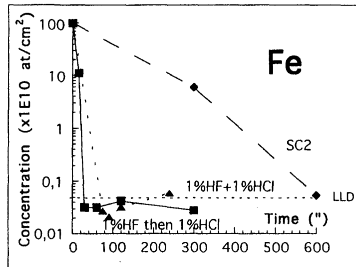

Figure 7 : Cu removal efficiency versus process time (as measured by TXRF)

Figure 8 : Fe removal efficiency versus time (as measured by VPD-TXRF)

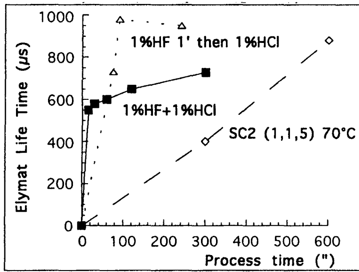

Figure 9 : Fe removal efficiency in terms of ELYMAT Life Time versus process time

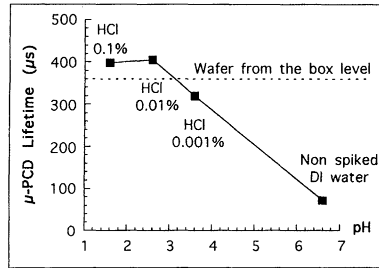

Figure 10 : Minority Carrier Life Times (Fe) obtained after a simple 10' dipping in DI water spiked with HCl

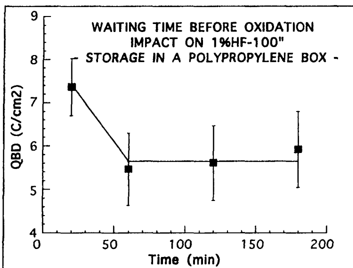

Figure 11 : Impact of waiting time between HFlast dip and furnace loading in terms of charge to breakdown (QBD) (7 nm gate oxide and 0.05 mm^2 capacitors)

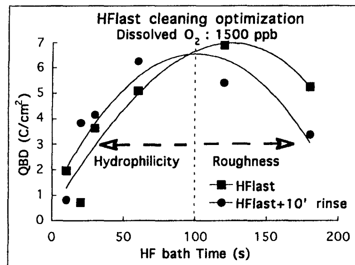

Figure 12 : Impact of 1% HF bath time and final rinse on 7 nm gate oxide integrity (capacitor area = 0.05 mm^2)

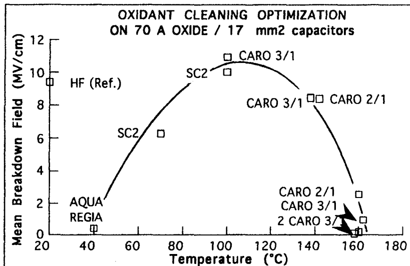

Figure 13 : Bath temperature impact for conventional oxidant cleanings

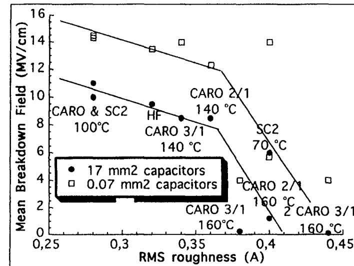

Figure 14 : 7 nm gate oxide integrity versus AFM roughness (contact mode)

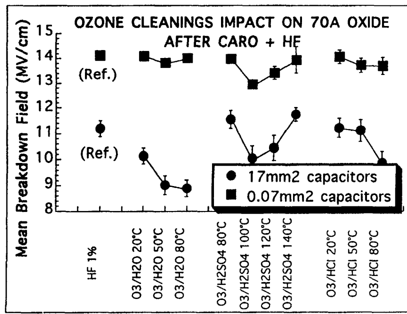

Figure 15 : Performances of 7 nm oxide with different ozone cleanings

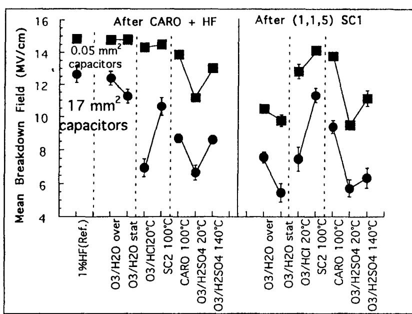

Figure 16 : Compared performances of best water peroxide and ozone recipes, in terms of 7 nm gate oxide integrity.

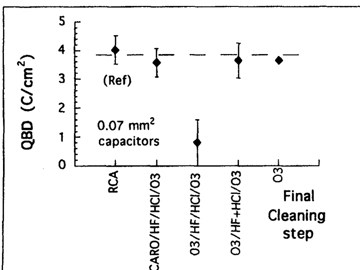

Figure 17 : Test of diluted chemistries before 7 nm gate oxidation

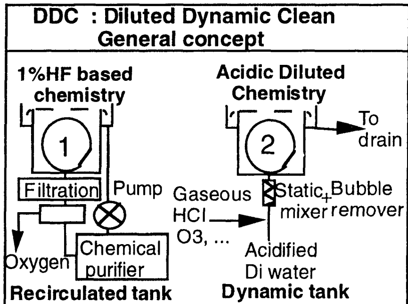

Figure 18 : General concept of DDC : "Diluted Dynamic Clean"

THE EFFECTS OF REVERSING WAFER-SURFACE WETTING PROPERTIES OF SULFURIC ACID:HYDROGEN PEROXIDE WAFER-CLEANING SOLUTIONS

W. Syverson, M. Fleming, P. Schubring
IBM Microelectronics Division
Essex Junction, VT 05452

INTRODUCTION

Sulfuric acid:hydrogen peroxide (S/P) solutions are commonly used to clean organic materials and metal residues from semiconductor wafer surfaces. But they are highly chemophilic and readily adhere to wafer surfaces when brought into contact with them. The viscous nature of the S/P solution traps suspended contaminants at a wafer surface despite extensive DI water rinsing. However, by adding a small quantity of dilute hydrofluoric acid (DHF) to an S/P solution, wafer-surface wetting properties are reversed and DHF-modified S/P solution (spiked piranha) becomes highly chemophobic. Spiked piranha solution remaining on wafers after immersion immediately beads and drains from wafers as they are removed from a process tank filled with the solution. This paper describes several process-engineering findings pertaining to the reversal of wafer-surface wetting properties of tank-S/P wafer-cleaning solutions.

STANDARD S/P VS SPIKED PIRANHA SOLUTION

A standard S/P solution is a nominal mixture of sulfuric acid and hydrogen peroxide in any of a variety of chemical proportions. The S/P solution is highly chemophilic in that the solution readily adheres to wafer surfaces. For use in dip-tank applications, the S/P solution is typically heated and controlled to an elevated temperature (e.g., 95C). In chemical-spray applications, the temperature is controlled by the chemical proportions used and chemical atomization pressures. In both applications, the S/P solution is used to clean organics and some metals from wafer surfaces. Spiked piranha is identical to an S/P solution but includes a very small quantity of DHF during initial mixing. Spiked piranha is formulated specifically to minimize wafer surface etching and to clean wafers better than S/P solutions.

WAFER-SURFACE WETTING PROPERTIES

A standard S/P solution is highly chemophilic when brought into contact with wafer surfaces. The solution is extremely viscous, readily adheres to wafer surfaces and requires extensive rinsing with DI water to minimize acid residuals. The spiked piranha solution is highly chemophobic when brought into contact with either a bare silicon or a SILICON DIOXIDE wafer surface. While still viscous, the solution will

not adhere to wafer surfaces. Spiked piranha easily beads and drains from wafer surfaces as the wafers are removed from a solution-containing process tank. Any droplets of residual solution are easily rinsed with DI water.

TIME-DEPENDENT WAFER HAZING

Development of a time-dependent wafer haze on wafer surfaces exposed to an S/P solution is a common observation. While not apparent immediately after exposure to the S/P solution, a haze can develop in a room ambient environment from 8-12 hours to several days after exposure to the solution. By using an optical dark-field microscope, the haze can typically be observed as light-point defects on the wafer surface (Figure 1). If the haze is highly developed, exposure to monochromatic light will make it visible to the unaided eye. While the amount of time required for haze development may vary with the method of exposure to an S/P solution (dip tank, spray, etc.) and extent of subsequent DI water rinsing, the time-dependent haze will usually occur.

The time-dependent haze on a wafer can be made to disappear by simply heating the wafer in an oven or on a hot plate, but the haze will reappear in a similar density and approximate amount of time as when it originally occurred. Simply rinsing a hazed wafer with DI water will prevent haze from reappearing.

The time-dependent wafer haze is difficult to observe with a standard scanning electron microscope (SEM). When highly magnified with an SEM, the haze defects disappear from view. To observe the haze defects, a thin film of gold must be deposited over the hazed wafer surface. Using this technique, the haze defects appear to be similar to small puddles of a liquid on the wafer surface (Figure 2). However, under high SEM magnification, the gold-decorated haze defects appear to explode much like a balloon. These observations lead one to conclude that the time-dependent haze defects have a liquid-based aspect.

Wafers exposed to a spiked piranha solution did not develop any observable haze, even when thoroughly inspected up to 90 days after exposure.

WAFER-SURFACE FOREIGN MATERIAL

Highly chemophilic solutions can trap suspended contaminants at a wafer surface during DI water rinsing (Figure 3). Insoluble contaminants suspended in a viscous solution can be driven toward a wafer surface during subsequent DI water rinsing. Once in contact with the wafer surface, these contaminants are very difficult to remove and, if small enough, equally difficult to detect with traditional wafer-surface inspection techniques. However, very small particles can be magnified by using the conformal deposition characteristics of chemical vapor deposited films (Figure 4).

Wafer surfaces exposed to an S/P solution and extensively rinsed with DI water show little change in particle addition. Subsequent deposition of a nominal 4000 angstrom conformal film of intrinsic polysilicon reveals a high degree of random surface roughness significantly above that of the polysilicon grains (Figure 5a). Wafer surfaces exposed to the same S/P solution (after DHF has been added) and identically rinsed with DI water also show little, if any, particle addition. However, subsequent processing in the same intrinsic polysilicon deposition step reveals an extremely smooth surface almost completely devoid of random surface roughness (Figure 5b).

THEORETICAL MODEL

Given the above findings, a simple theoretical model is proposed. Figure 6 shows a wafer surface immersed in a viscous, hygroscopic liquid much like an S/P solution. A small particle is initially suspended in the liquid. As the liquid is rinsed from the wafer surface, the particle contacts the wafer surface due to laminar effects of the two solutions. The particle traps a small quantity of the viscous liquid in a meniscus between the particle and the surface. When exposed to an ambient room environment for a sufficient period of time, the hygroscopic liquid could absorb sufficient atmospheric moisture and swell in volume until it would appear as a wafer surface defect. Heating the surface would drive off a sufficient quantity of absorbed moisture to cause the defect to temporarily disappear. Similarly, rinsing a hazed wafer would significantly reduce the quantity of trapped, now-diluted liquid to a new equilibrium point where no subsequent absorption of atmospheric moisture would occur.

DI WATER RINSING

Clean bare silicon and silicon-dioxide wafers exposed to a standard S/P solution remain highly chemo/hydrophilic throughout the entire process cycle (S/P solution and all subsequent DI water rinses). Both the S/P solution and DI water thoroughly adhere to the wafer surface. Wafers exposed to the spiked piranha solution retain their chemo/hydrophobic characteristic in the chemical step but only for the first few seconds in the initial DI water rinse; thereafter, the wafers return to being hydrophilic, with DI water adhering to the wafer surface.

SILICON-DIOXIDE ETCH CHARACTERISTICS

Because of their high oxidizing strength, S/P solutions at standard process temperatures will not etch silicon-dioxide surfaces. In fact, S/P solutions are known to grow measurable chemical oxides (10-15 angstroms) on bare silicon or native oxide surfaces. However, the high process temperatures, coupled with the presence of sufficient amounts of DHF in the spiked piranha solution, can cause measurable thermal silicon-dioxide etch rates.

Figure 7 shows the thermal silicon-dioxide etch rates of selected DHF concentrations in a spiked piranha tank. In this experiment, quantities of 5% DHF were added to a freshly poured dip tank containing 22,000 ml of a 4:1 S/P solution at 95C. For all concentrations of DHF, a chemophobic reaction was observed on wafer surfaces exposed to the solution. However, at the concentrations of 1 ml and 5 ml of 5% DHF, no etching of the wafer surface was measured and only a minimal level of chemical oxide growth occurred. At higher concentrations of DHF, a significant level of thermal silicon-dioxide etching was observed.

CONCLUSIONS

Standard S/P solutions are highly chemophilic, as observed on wafer surfaces, and tend to adhere to wafers after immersion in a dip tank. This chemophilic nature makes wafer surfaces prone to time-dependent wafer hazing which is a potential source of very small liquid-borne wafer-surface foreign material. A spiked piranha solution is highly chemophobic and will quickly drain from wafer surfaces when the wafers are removed from the solution, which eliminates time-dependent wafer-surface hazing and the potential for suspended particle contamination of the wafer surface by the solution.

REFERENCES

1. United States Patent 5,294,570, March 15, 1994. Co-Inventors: M. Fleming, Jr., W. Syverson, E. White, all of IBM Corp. Title: "Reduction of Foreign Particulate Matter on Semiconductor Wafers."

Figure 1. Optical dark-field photograph of Piranha haze.

Figure 2. SEM Micrograph of gold-decorated Piranha wafer haze.

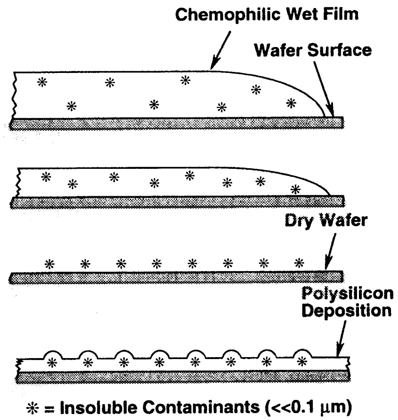

Figure 3. Diagram of insoluble contaminants in a chemical solution.

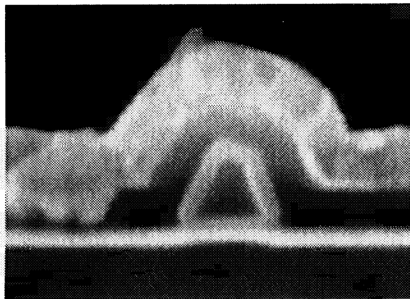

Figure 4. SEM micrograph of conformal magnification properties of polysilicon and CVD films.

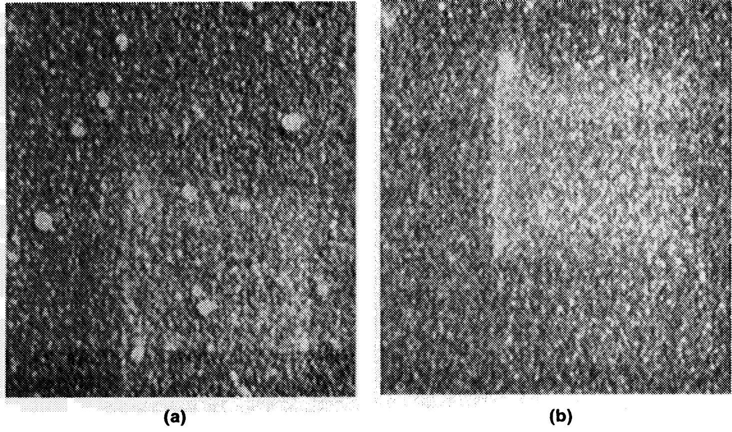

Figure 5. (a) SEM micrograph of tank Piranha cleaned wafer post polysilicon deposition. (b) SEM micrograph of tank spiked Piranha cleaned wafer post polysilicon deposition.

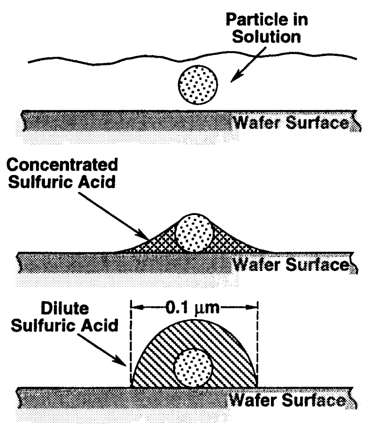

Figure 6. Diagram of suspected cause of Piranha haze.

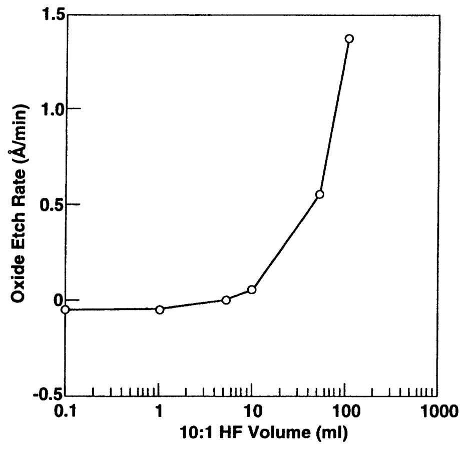

Figure 7. Graph of spiked Piranha thermal oxide etch rate vs. DHF concentration.

SULFURIC ACID/HYDROGEN PEROXIDE RINSING STUDY*

P. J. Clews, G. C. Nelson, C. A. Matlock, P. J. Resnick, C. L. J. Adkins, N. C. Korbe
Sandia National Laboratories
Albuquerque, NM 87185

ABSTRACT

Sulfuric acid hydrogen peroxide mixtures (SPM) are commonly used in the semiconductor industry to remove organic contaminants from wafer surfaces. This viscous solution is very difficult to rinse off wafer surfaces. Various rinsing conditions were tested and the resulting residual acid left on the wafer surface was measured. Particle growth resulting from incomplete rinse is correlated with the amount of sulfur on the wafer surface measured by Time of Flight Secondary Ion Mass Spectroscopy (TOF-SIMS). The amount of sulfur on the wafer surface after the rinse step is strongly affected by the wafer film type and contact angle prior to the SPM clean.

INTRODUCTION

Sulfuric acid/hydrogen peroxide mixtures (SPM) are widely used in the semiconductor industry for removing organic materials such as photoresist from wafer surfaces. This viscous mixture is not readily rinsed off the wafer surface even when using copious amounts of water. Conservation of water in semiconductor fabrication is becoming an important issue, especially in areas that do not have abundant water supplies. Reducing the amount of water required for wet processing can significantly reduce the cost-of-ownership of wet processing equipment.

Residual SPM contamination results in the growth of particles on the wafer surface after the wafers have been stored in a clean room environment for a period of time. These particles are easily rinsed off the wafer surface with deionized (DI) water. The particles will not regrow if they are given enough time to fully develop before they are rinsed off the wafer with water. If the particles are only allowed to grow for a short time, they will rinse off the wafer but new particles will regrow. It is not practical in a manufacturing environment to sufficiently delay rinsing wafers so that particles will not regrow because the delay increases cycle time. Wafers processed through ammonium hydroxide, hydrogen peroxide, water (SC1) or dilute hydrofluoric acid (HF) processes after the SPM clean

*This work was performed at Sandia National Laboratories, which is operated for the U.S. Department of Energy under contract no. DE-AC04-94AL85000. This work was funded through a cooperative research and development agreement with SEMATECH.

do not exhibit particle growth. HF or SC1 processing may not be practical due to extra processing equipment required. HF and concentrated SC1 solutions etch oxide which may not be acceptable in some manufacturing applications. Since processing in SPM last may be desirable in some applications, the SPM particle growth problem must be addressed using other means.

Several options to eliminate this residual contamination and reduce water usage have been reported in the literature. Adding small amounts of HF to the SPM mixture causes the silicon wafer surface to be hydrophobic after the clean. These wafers do not exhibit particle growth over time [1-2]. Rotondaro *et al.* reported that if SPM-cleaned wafers are placed in a isopropyl alcohol (IPA) bath prior to the DI water rinse step, particle growth is significantly reduced. It can be further reduced by heating the wafers with an infrared (IR) exposure to enhance particle growth, followed by a DI water rinse to remove the particles. No increase in particles is observed after one month of storage following the IR exposure and subsequent rinse step [3].

Methods to eliminate or reduce the particle growth on wafers cleaned in SPM without altering the chemicals the wafers are exposed to have also been investigated. M. Hall *et al.* [4] have demonstrated, by bulk resistivity measurements taken in the rinse tank, that megasonic power applied during an overflow rinse reduces the amount of water required to rinse wafers cleaned in a SPM. They also report that there is no advantage of using megasonic power during the rinse step of wafers cleaned in a SPM if the wafers are dump rinsed for 3 to 4 cycles prior to the overflow rinse. This work also demonstrated that megasonic power applied during an overflow or a dump rinse operation does not eliminate time-dependent particle growth on wafers cleaned in SPM. These researchers were able to significantly reduce time-dependent particle growth on wafers cleaned in a SPM by rinsing them in hot DI water [4].

The mechanism for particle growth and the composition of these particles are not well understood. Some researchers suggest that the particles are formed when residual acid on the wafer surface reacts with moisture from the air and over time the residual acid grows large enough to be detected as particles [4]. Other researchers suggest that contamination is trapped in the SPM chemical oxide, diffuses to the wafer surface and coalesces forming micro-crystals during storage. Given enough time most of the contamination diffuses to the surface and a simple rinse step can remove it preventing further particle formation [3]. We will refer to this as the SPM diffusion theory throughout this paper.

The purpose of our work is to gain a better understanding of the particle growth mechanism on SPM-cleaned wafers. We have demonstrated that megasonic power applied during the rinse step following a SPM clean removes particles added during the clean but does not aid in the removal of sulfur (S) contamination from the wafer surface. Comparison of Time of Flight Secondary Ion Mass Spectroscopy (TOF-SIMS) and/or

Total Reflectance X-Ray Fluorescence Spectroscopy (TXRF) measurements with particle measurements shows a correlation between sulfur concentration and particle growth. Higher sulfur concentration on wafers cleaned in SPM is correlated with faster particle growth. We found that hydrophobic thermal oxide wafers cleaned in SPM do not exhibit particle growth but hydrophilic oxide and hydrophobic or hydrophilic silicon wafers do. We suggest another mechanism for SPM particle growth.

EXPERIMENTAL DETAILS

Rinsing studies were performed using 6-inch n-type (100) silicon wafers and 100 Å thermally oxidized silicon wafers. The contact angle of the thermal oxide and silicon wafers was altered prior to the SPM clean by processing these wafers through either a 100:1 HF dip, a 64:4:1 (H_2O:H_2O_2:NH_4OH) SC1 clean, a 5:1:1 (H_2O:H_2O_2:HCl) SC2 clean, or a combination of these chemistries. A full cassette of wafers was cleaned in a 5:1 or 10:1 (H_2SO_4:H_2O_2) SPM solution at 95°C for 10 minutes. The SPM temperature and time were standard for all experiments. Wafers were rinsed in a Verteq Turbo Sunburst Quick Dump Rinse (QDR) tank. The rinsing parameters used for each experiment are described in the experimental results section. Bulk resistivity of the water was monitored during the rinsing process. Light point defect (LPD) measurements, to monitor particle growth, were made on these wafers using a Tencor SFS-6200. Wafers were measured periodically until the SFS-6200 failed to scan the entire wafer. The SFS-6200 will fail to scan a wafer if there are too many particles on the wafer surface. TOF-SIMS and/or TXRF measurements were taken to compare LPD growth with the amount of sulfur left on the wafer surface. These data were used to evaluate the effectiveness of the rinse step.

EXPERIMENTAL RESULTS

Effect of Megasonic Power on Surface Contamination

Multiple experiments rinsing SPM-cleaned wafers with and without megasonic power were performed. The 6-inch silicon wafers used in these experiments were precleaned in a SC1 solution followed by a 100:1 HF strip to remove the chemical oxide formed during the SC1 clean. This procedure established the same initial starting condition on all wafers. A fresh 5:1 SPM solution was poured for each experiment to eliminate any differences that might result due to aging of the SPM solution. A full cassette of wafers was cleaned in the 5:1 SPM solution and rinsed in the Verteq QDR using 5 dump cycles with spray followed by an overflow rinse for 20 minutes of total rinse time. Duplicate runs with and without megasonic power applied during the rinse step were performed.

TXRF data shown in Figure 1 indicate that the concentration of sulfur on the wafer surface is approximately the same for all wafers rinsed with or without megasonic power. The TOF-SIMS S/O_2 peak height ratio data, shown in Figure 2, also indicate that megasonic power applied during the rinse step does not reduce the amount of residual sulfur on the wafer surface. However, the number of light point defects measured immediately after the SPM clean, shown in Figure 3, indicates that megasonic power applied during the rinse step significantly reduces the amount of particulate contamination added to the wafers during this cleaning step. All wafers used in these experiments failed the SFS-6200 scan less than 24 hours after the SPM clean. This failure indicates that megasonic power applied during the rinse step does not eliminate the growth of particles on wafers cleaned in SPM. Nor does resistivity data taken during the experiment indicate an advantage of using megasonic power during the rinse. These data are consistent with that presented by Hall *et al.* [4]. If contamination remains bound to the surface and therefore does not contribute to the conductivity of the water, a high resistivity will not necessarily be indicative of a clean wafer surface. In summary, megasonic power applied during the rinse step of SPM-cleaned wafers removes particles added during the clean but does not aid in the removal of sulfur contamination from the wafer surface.

Effect of Si and SiO_2 Wafer Contact Angle Prior to SPM Clean on Ease of Rinse

In order to determine if the diffusion of contaminants trapped in the chemical oxide grown during the SPM clean is the cause of particulate growth, both Si and SiO_2 wafers were cleaned in the same 5:1 SPM solution and then rinsed together. No chemical oxide should be grown on thermally oxidized wafers during an SPM clean. These oxide wafers should not experience growth of particles if the SPM diffusion theory [3] is correct. The contact angle, and therefore surface termination, of the wafers prior to the SPM clean was varied by exposing the wafers to SC1, SC2, HF, or a combination of these solutions. The SiO_2 wafers were exposed to either 1) an SC1 clean, 2) an SC2 clean, 3) an SC1 followed by an SC2 clean, or 4) a 1 second HF dip to remove approximately 8 Å of oxide. One group of thermally oxidized wafers did not receive any post furnace processing. Silicon wafers were exposed to 1) an SC1 clean, 2) an HF dip followed by an SC2 clean, or 3) an SC1 followed by an SC2 clean. Wafers of each type were evenly spaced throughout the cassette. This full cassette of wafers was cleaned in a 5:1 SPM solution and rinsed with no megasonic power for 5 dumps followed by an overflow rinse for a total rinse time of 10 minutes.

Sulfur concentration on the wafers used in this experiment was measured by TXRF. The results are shown in Figure 4. The thermally oxidized wafers that received no post-furnace processing (SiO_2+none) and the ones that received only an SC2 process (SiO_2+SC2) prior to the SPM clean have significantly less sulfur on the wafer surface than the other wafers processed in this experiment. These wafers were hydrophobic prior to the SPM clean and had a water contact angle of 33° and 19°, respectively. These wafers also did not exhibit SPM particle growth even after one month of storage. The remaining

wafers in this experiment were hydrophilic prior to the SPM clean. All had significantly more sulfur on the wafer surface than the SiO_2+none and SiO_2+SC2 wafers. They also exhibited SPM particle growth that caused the SFS-6200 to fail to scan these wafers within 17 hours after the SPM clean.

These data indicate that the SPM diffusion theory [3] does not fully explain particle growth. A chemical oxide should not have grown on thermally oxidized wafers cleaned in a SPM and therefore particles should not have grown if diffusion from an SPM oxide is the source of sulfur. It appears that the SPM residual contaminant is more tightly bound to the surface of hydrophilic SiO_2 than to hydrophobic SiO_2 wafer surfaces.

Hydrophobic Si wafer surfaces were not included in this experiment although they were included in the megasonic rinsing experiments described earlier. Silicon wafers dipped in HF to make the wafer surface hydrophobic prior to the SPM clean were used in the megasonic experiment. Hydrophobic silicon wafers exhibited particle growth within 24 hours after the SPM clean. Sulfur concentrations on hydrophobic Si wafers, shown in Figure 1, are comparable to the sulfur concentrations on the hydrophilic Si wafers shown in Figure 4. Since the sulfur concentration is similar and since both hydrophobic and hydrophilic Si wafers exhibited SPM particle growth, one can conclude that contact angle on Si wafers prior to the SPM clean does not significantly influence the effectiveness of rinsing SPM-cleaned silicon wafers.

Correlation of Sulfur Concentration and Particle Growth

The Si/SiO_2 contact angle experiment described above suggests that particle growth is caused by elevated sulfur concentrations on the wafer surface. We performed an additional experiment to confirm this apparent correlation. Si wafers precleaned in an SC1 solution and SiO_2 wafers with no post furnace processing were cleaned in a 10:1 SPM solution at 95°C for 10 minutes. Wafers were rinsed with no megasonic power for 5 dumps followed by an overflow rinse. Wafers of each type were removed after 5 minutes and 20 minutes of total rinse time. Table I indicates that as the TOF-SIMS S/O_2 peak height ratio increases there is a corresponding increase in the number of light point defects (LPD) added to the wafers 17 hours after the SPM clean.

Table I. TOF-SIMS and LPD measurements on 10:1 SPM-cleaned wafers.

Wafer Type	Rinse Time (minutes)	TOF-SIMS S/O_2 peak height ratio	SFS-6200 LPD increase 17 hours after SPM clean (SPM particle growth)
SiO_2 + none	5	0.06	22
SiO_2 + none	20	0.07	40
Si + SC1	20	0.50	137
Si + SC1	5	0.63	7551

Caution must be exercised when using SFS-6200 measurements for evaluating the effectiveness of the rinse process because we have found that altering the storage conditions of the wafers can drastically alter the particle growth. For example, wafers stored in a very humid environment (storage box with small amount of DI water in the bottom) do not exhibit particle growth for as long as two weeks after the SPM clean. However, once the humid wafers are exposed to the clean room air, particles begin to grow very quickly. Wafers cleaned and rinsed at the same time as the wafers stored in the humid environment but stored in the normal clean room air exhibited particle growth and failed the SFS-6200 scan less than 24 hours after the SPM clean.

DISCUSSION

Some of our data conflicts with the existing theories for particle growth. For example, wafers stored in a humid environment did not exhibit particle growth. This observation contradicts the theory that residual contamination on wafers cleaned in SPM grow by absorbing moisture from the air [4]. We demonstrated that SiO_2 wafers, which are hydrophilic prior to the SPM clean, exhibit particle growth. This indicates that for oxide films, diffusion of contaminants trapped in the chemical oxide grown during the SPM clean cannot be the mechanism for particle growth because oxide wafers will not grow a chemical oxide during the SPM clean.

Other researchers have also made observations that conflict with the SPM diffusion theory. For example, Christenson [5] has stated that in an inert spray tool, SPM-cleaned wafers do not exhibit particle growth when stored in the inert environment for one day after the SPM clean. Particles start to grow on these wafers after they have been exposed to clean room air for a short time. This would indicate that diffusion is not the mechanism because diffusion should occur even in an inert environment. Christenson stated that a very dilute 30 second SC1 clean applied immediately after the SPM rinse prevents the growth of particles. This indicates that diffusion is not the mechanism because a dilute SC1 clean will remove less than 1 Å of the chemical oxide grown during the SPM clean. Christenson also found that a hot DI water rinse following the SPM clean in this inert spray tool is not effective in eliminating SPM particle growth. However, Hall *et al.* [4] found that hot DI water is very effective in eliminating SPM particle growth.

From the experimental results presented in this paper and from discussions with other researchers, we suggest another possible explanation for particle growth on SPM-cleaned wafers. We speculate that chemical contaminants in the clean room air react with residual sulfur left on the wafer surface after a SPM clean and form water soluble particles that can then be easily rinsed off the wafer surface. This explanation is consistent with the observation that particles do not grow in an inert spray tool until wafers are exposed to the clean room air. We believe that the mechanism for particle growth is a surface effect which is consistent with the fact that hydrophilic SiO_2 wafers exhibit particle growth. The

different hot DI water rinse results are explained by this mechanism. Contaminants in the clean room air could dissolve in the open tank hot DI rinse water and react with sulfur on the wafer surface forming a water soluble material which is then removed by the hot DI water. In the inert spray tool, the wafers and the hot rinse water are not exposed to the clean room air so this reaction can not take place to remove the sulfur contamination.

CONCLUSION

We have demonstrated that particle growth, as measured on the SFS-6200, correlates with the relative amount of sulfur on the wafer surface after a SPM clean. Megasonic power applied during the rinse step significantly reduces the amount of particles added to the wafer surface during the SPM cleaning process but does not reduce the amount of sulfur contamination on silicon wafer surfaces or eliminate the time-dependent SPM particle growth. We demonstrated that hydrophilic SiO_2 and hydrophobic and hydrophilic silicon wafers cleaned in a SPM exhibit growth of particles but hydrophobic thermal oxide wafers cleaned in the same SPM do not exhibit growth of particles. We have suggested another mechanism for SPM particle growth and are performing additional experiments to validate this theory.

ACKNOWLEDGMENTS

TXRF measurements contained in this study were performed at SEMATECH. The rinse tank was a demonstration unit supplied by Verteq. Authors wish to thank the following individuals for useful discussions: D.E. Beutler and R. Donovan - Sandia National Laboratories; K. Christenson - FSI International; W. Syverson and R. Gaylord - IBM Corporation; C. Silsby - Hewlett Packard; T. Nicolosi - Verteq; R.M. Hall - Santa Clara Plastics; S. Verhaverbeke and C. McConnell - CFM Technologies; and C.R. Helms Stanford University.

REFERENCES

1. "Reduction of Foreign Particulate Matter on Semiconductor Wafers", M. Fleming, Jr., W. Syverson, E. White, IBM Corporation, US Patent 5,294,570, March 15, 1994.
2. S. Verhaverbeke, R. Messoussi, T. Ohmi, UCPSS '94, Belgium, September 1994.
3. L.P. Rotondaro, H.F. Schmidt, M. Meuris, M.M. Heyns, C. Claeys and J. Mulready, UCPSS '94, Belgium, September 1994.
4. R.M. Hall, J.J. Rosato, P.G. Lindquist, T. Jarvis, T. Parry, J.D. Kelly, R.N. Walters, in Proceedings of Semiconductor Pure Water and Chemicals Conference 1995, M.K. Balazs (Ed), pp. 101-112.
5. Discussions with K. Christenson, FSI International.

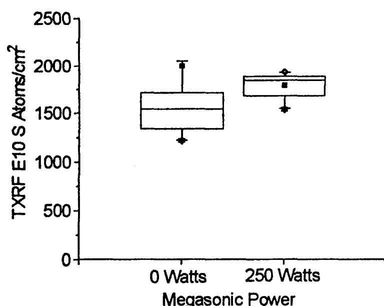

Figure 1. Boxplot of TXRF sulfur concentration on hydrophobic Si wafers cleaned in 5:1 SPM and rinsed with or without megasonic power.

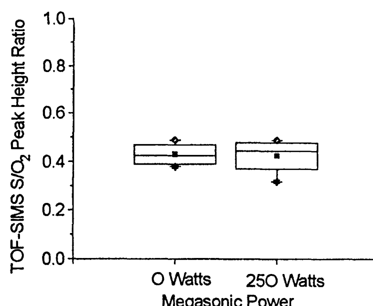

Figure 2. Boxplot of TOF-SIMS sulfur contamination on hydrophobic Si wafers cleaned in 5:1 SPM and rinsed with or without megasonic power.

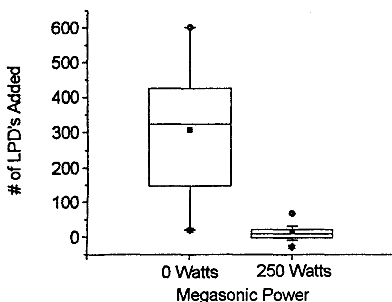

Figure 3. Boxplot of number of particles added to Si wafers cleaned in 5:1 SPM and rinsed with or without megasonic power. LPD measurements were made immediately following the SPM clean before measurable SPM particle growth could occur.

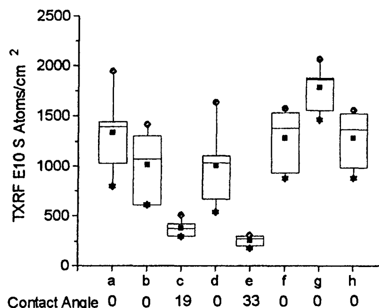

Figure 4. Boxplot of TXRF sulfur contamination levels measured on wafers processed through a 5:1 SPM and rinsed with no megasonic power. a) SiO_2 HF dip, b) SiO_2 SC1 clean, c) SiO_2 SC2 clean, d) SiO_2 SC1 + SC2 clean, e) SiO_2 no post furnace processing, f) Si SC1 clean, g) Si SC2 Clean, h) Si SC1 + SC2 clean.

EQUIPMENT FOR WAFER CLEANING PARALLEL DOWN FLOW RINSE

Yutaka Hiratsuka, Nobuyuki Fujikawa
Dan Science Co.,
Ohwadacho 1-9-2,Hachiohji,Tokyo,192,Japan

In order to save pure water used in wafer cleaning, we proposed parallel down flow rinse (PDR) instead of overflow rinse (OFR). Concept of PDR is to make uniform descending water flow continuously in a bath. That is, water supplied over the top edge of inner bath is pumped out from the bottom of the bath through the baffle plate with many tiny holes. PDR can reduce the quantity of water to displace the bath to half in comparison conventional OFR.

INTRODUCTION

The semiconductor manufacturing plant uses great amount of pure water in the wet cleaning process. Pure water consumption is expected to further increase, as long as the conventional technologies will be continuously employed, to cope with further device integration and larger-diameter wafers. Current pure water consumption has reached a level not only to make manufacturing cost of semiconductor devices too much excessive, but also to make it hard to secure water sources. Amid these circumstances, it is increasingly important to forcus our efforts on study to improve rinsing efficiency so as to reduce pure water consumption in the rinsing process.
In the case of overflow rinsing (OFR), only limited portion of delivered water runs into narrow gaps between wafers,which suppresses rinnsing efficiency and increases pure watter consumption. In this study, a parallel down flow rinsing technology has been developed which features higher rinsing efficiency than OFR.

EXPERIMENTAL METHOD

Visualization of Water Flow

Figure 1 shows overview of the experimental apparatus. Slit light is irradiated onto each side of a rinsing bath. Water flow in the bath is shot with a video camera placed in front of the bath (right-angled direction against incident light). Wafers and wafer carrier as well as the rinsing bath are made of transparent acrylic resin so as to observe water flow in the bath loaded with wafers. Tracer to visualize water flow in the bath is prepared by dispersing Al powder for paint use in water by means of surfactant. A syringe is mounted on the pure water deliver piping system to inject this tracer.
Another experiment is performed in this rinsing bath by dipping acrylic circular plates thinly coated with a paste. This paste is prepared by mixing Al powder and surfactant. Authors observe how water flow removes Al powder from the plate surface. This

rinsing bath is also used to observe contaminant displacement with fresh water. Wafer are first immersed into uranine, fluorescent dye, of 1g/1l. Then these wafers are dipped into the rinsing bath to observe how water colored with the fluorescent dye is displaced with pure water.

Conductivity Measurement to Evaluate Displacing Rate in Bath

Wafers are immersed into electrolyte (NaCl or SrCl2 100 g/l). They are withdrawn from the electrolyte and dipped into the rinsing bath. Conductivity of effluent drained out from the rinsing bath is measured and recorded with a small-sized electrode which authors have developed (Fig.2). To be more specific, output voltage from this electrode is measured, and it is converted into conductivity by using a calibration curve obtained with an electric conductivity meter which is available in the market.

EXPERIMENTAL RESULTS

Water Flow in OFR Bath

Conventional Overflow The carrier-supporting plate has holes of 20 mm in diameter with regular pitch through which water freely passes. Pure water is introduced to the bath at flow rate of 3 - 20 l/min. It is visualized that pure water does not go through narrow gaps between wafers, but it goes upward through wider gaps between wafer and side wall of the bath. Pure water introduced just beneath wafers, as shown in Figure 3, changes its direction horizontally, and joins the above-mentioned upward flow eventually. Water between wafers is pulled by the fast horizontal flow, and slowly runs downward. Majority of upward flow between wafer and side wall, when reaching the top, overflows from edge of the bath, but some portion flows toward the center of the bath, and joins downward flow between wafers. This creates outside-in circulating flow. Mainstream of introduced pure water does not directly contribute to wafer rinsing, but it is just drained out. What actually rinses wafers is slow downward flow between wafers which is generated by pulling-down action of the mainstream. Chemicals rinsed off from wafers by this downward flow meet the mainstream at the bottom of wafers, get diluted with the mainstream while flowing upward, and are drained out. Here again, not entire water to be drained is actually drained out. The circulating flow brings some portion back to gaps between wafers.

Improvement of OFR Bath In an attempt to make most of introduced water flow between wafers, authors have improved the carrier-supporting plate. The plate is modified so as to have holes distributed uniformly at aperture ratio (area of holes/area of bottom of the bath) of 10%. When this plate is installed in the bath, pure water passes through the holes as jet flow at 10 times faster velocity than average velocity, and flows straight upward even in narrow gaps between wafers. Due to fast upward flow, however, pure water in the vicinity of the bottom of the bath is pulled to underneath of wafers, as shown in Figure 4. This creates downward flow between wafer and side wall of the bath. Although most of upward flow, when reaching the top, flows horizontally to be overflowed, some portion is pulled by this downward

flow. As a result, an inside-out circulating flow is created, and some of chemicals rinsed off from wafers returns back. Stagnation of chemicals due to the circulating flow prolongs the rinsing process.This modified OFR method has a problem. Pitch of holes must precisely match with that of wafers. If upward jet flow does not properly pass through gaps between wafers due to misalignment of hole pitch, slow down flow is generated locally there due to neighboring upward jet flows as shown in Figure 5. This leads to insufficient rinsing.

Water Flow in PDR Bath.

Figure 6 shows the bath used in the experiment. It is equipped with a carrier-supporting plate with tiny holes uniformly distributed. Water is pumped out with a pump from the bottom of the bath. Pure water introduced into the bath gone up between an outer bath and inner bath, and flows into the inner bath from its top. When aperture ratio of the perforated plate is set at 10% or less, Al tracer goes straight down both in wide gaps between side wall of the inner bath and wafer and in narrow gaps between wafers. It passes through the perforated plate while hardly generating whirlpool. Al tracer coating circular plates (wafers) are removed little by little, and flows almost straight downward. No tracer is suspended around upper part of wafers, and only fresh pure water flows around.

Observation by Using Fluorescent Dye as Tracer

When wafers coated with dye are dipped in the baths, dye immediately gets diluted and mixed with pure water, and water in the baths gets colored. Pure water gradually displaces the colored water, as it is freshly introduced, and color in the bath gets lighter. There is a difference between the OFR bath and the PDR bath in terms of color fading progress. In the former case, coler gets lighter uniformly in the entire bath. In the latter case, color in upper part of the bath gets lighter first.

It can be observed that some dye remaining on wafer surface and in grooves of the wafer carrier is gradually removed as color in the bath gets lighter. In the case of the PDR bath, in particular, dye removed from wafer surface flows straight downward, and a thin colored layer is formed at the bottom of wafers. This experimental method enable us to observe how a boundary layer is formed and how it is rinsed off due to water flow to disappear.

Comparison of Displacement Characteristics by Means of Conductivity Measurement

With flow rate of pure water varied, rinsing time required for 99% displacement is studied by comparing the OFR bath and the PDR bath. Figure 7 shows the experimental result. It shows linear velocity on the horizontal axis because cross sectional area is different between the two bathes. Figure 7 shows almost linear relationship between linear velocity and rinsing time. Comparison between the OFR bath and the PDR bath in terms of this linear velocity has revealed that rinsing time required in the PDR bath is about a half of that in the conventional and improved OFR bathes. Coming in contact with the air, water absorbs CO_2, and consequently its

conductivity easily reaches 0.4 - 0.6 mS/m. Even when displacement of carried-over electrolyte practically proceeds and real electrolyte concentration gets low, therefore, the conductivity measurement method can not detect it. In an attempt to find out rinsing time required to completely remove contaminants remaining in the boundary layer, authors quantify electrolyte components in effluent with ICP-Emission Spectrometry. In this experiment,circular plates representing wafers are immersed to $SrCl_2$ instead of NaCl in order to suppress contamination introduced during measurement. Detection limit of Sr concentration is 0.002 ppm. Comparative experiment is performed between the OFR bath and the PDR bath, while setting cross sectional area and flow rate at the same level. Figure 8 shows concentration ratio (C/Co) in a logarithmic manner as a function of rinsing time. Up to 99.99% displacement, rinsing time in the PDR is kept half of that in the OFR.

Detailed Discussion of Parallel Down Flow Rinsing Bath

Perforated Plate Effect of aperture ratio of the perforated plete on rinsing efficiency is studied. Figure 9 shows experimental result. Aperture ratio is varied to 10% (hole size 4 ϕ), 1% (2 ϕ), and 0.1% (1 ϕ). Rinsing efficiency is found to be improved as aperture ratio is decreased. Between 0.1% and 10%, rinsing time is different by 1 minute for 99% displacement, and by over 2minutes for 99.9% displacement. With aperture ratio of 0.1%, wafers can be sufficiently rinsed even if wafer pitch is reduced to half of the conventional pitch.

Conditions for Pure Water Introduction Pure water is introduced at high speed through an inlet port. It is necessary to change irregular flow generated due to this fast pure water introduction to uniform upward flow. For this purpose, the perforated plate (aperture ratio of 10%) is installed in water path between the outer bath and the inner bath. Pure water runs upward along the water path while maintaining uniform velocity distribution, and flows into the inner bath over its top edge. In-flow velocity, therefore, depends on distance between water surface of the outer bath and top edge of the inner bath. Rinsing characteristics are studied by varying this distance to 5mm, 20mm, and 45mm. Rinsing efficency is found favorable when this distance is set at 20mm.

Shape of Subject to be Rinsed Rinsing time is studied by comparing the following two: a carrier available in the market loaded with wafers, and wafers held with a chuck used in carrier-less wafer transportation. The latter is found to increase rinsing efficiency as it disturbs water flow less than the former.

DISCUSSION

Application to Circulating-Filtration Cleaning Bath

When several batches of wafers are cleaned without changing the cleaning solution, circulating filtration unit is mounted on the cleaning bath in order to prevent acccumulation of contaminant particles carried over into the bath. Particle count in the

bath is reduced faster as circulating flow rate is increased. When flow rate is kept constant, however, reducing rate of particle count gets higher along with increase of liquid displacement efficiency. Displacement efficiency is higher in the PDR bath by two times than in the OFR bath. This means the PDR bath is appropriate as a circulating-filtration cleaning bath. Standard polystylene latex spheres of 0.5μm in size are suspended in solution. This solution is injected to a bath in which water circulation is halted. After stirring up and making PSL dispersion uniform, water in the bath is sampled from 10 cm below water surface, and evaluated with particle counter (RION KL-20) to find out initial particle count. Then pump operation is started up again to resume circulating filtration at flow rate of 10 l/min. Particle count is measured with a regular interval to obtain its reducing rate. Figure 10 shows this experimental result. When a diaphragm pump is used which generates pulsating flow, reducing rate of particle count is slightly low. Time required to remove particles by 99% in the PDR bath is half of that in the OFR bath.

Thermal oxide of 1000Å thick is deposited on fifty 5-inch Si wafers. They are held with a carrier-less chuck and immersed into DHF (0.5%) which is treated with circulating filtration. Uniformity of 10-minutes etching is evaluated by comparing the PDR bath and the OFR bath. As shown in Figure 11, variance of etching is more suppressed, either on the entire wafer surface or among wafers, in the PDR bath.

Improvement of Rinsing Efficiency of PDR

Displacement efficiency gets deteriorated due to boundary layer formation in the latter half of the rinsing process. Rinsing time will be further shortened if boundary layer can be eliminated. In an attempt to eliminate boundary layer, megasonic is irradiated from side of the PDR bath. Figure 12 shows the experimental result. At the initial stage of displacement, megasonic irradiation is found not effective. When displacement reaches about 99.9%, however, megasonic irradiation works effectively to shorten rinsing time. Study is now under way to find out optimum conditions for megasonic irradiation onto the PDR process.

CONCLUSION

The PDR bath has been developed by using findings of the water flow visualization test performed in the OFR bath. By means of conductivity measurement and chemical analysis, characteristics to displace carried-over contaminats with fresh pure water are investigated. As a result, pure water consumpution in the PDR bath is found half of that in the OFR bath. Various studies have been performed in order to find out optimum bath configuration for practical use. It is necessary to find a way to eliminate boundary layer to further improve rinsing efficiency of the PDR bath. This system is considered effective as a circulating-filtration bath as well as a rinsing bath.

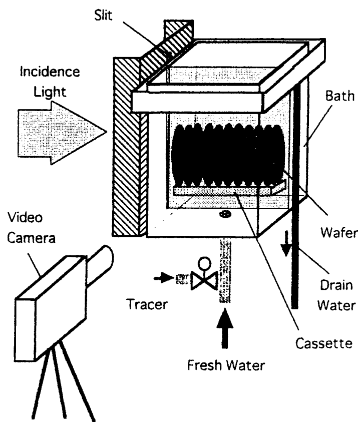

Fig. 1
VISUALIZATION OF LIQUID FLOW IN BATH.

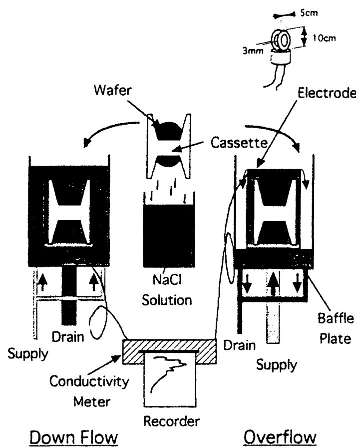

Fig. 2 CONDUCTIVITY MEASUREMENT FOR REPLACEMENT PERFORMANCE IN BATHS.

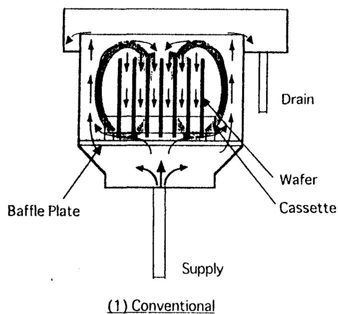

Fig. 3 THE SCHEMATIZED LIQUID FLOW IN A CONVENTIONAL OVERFLOW BATH.

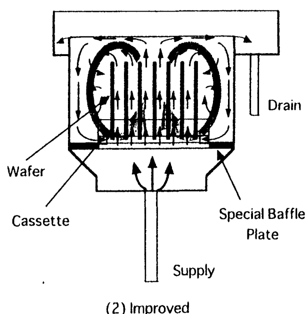

Fig. 4 THE SCHEMATIZED LIQUID FLOW IN AN IMPROVED OVERFLOW BATH.

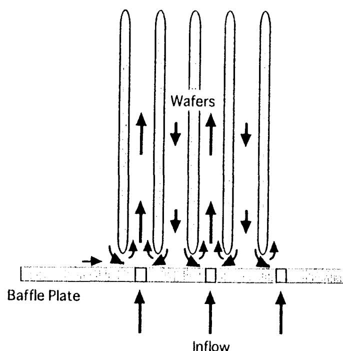

Fig. 5 THE SCHEMATIZED LIQUID FLOW WHEN WAFER GAPS AND HOLE POSITIONS OF BAFFLE PLATE DISAGREED.

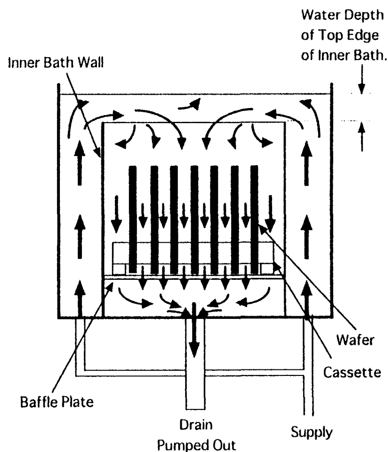

Fig. 6 THE SCHEMATIZED LIQUID FLOW IN A DOWN FLOW BATH.

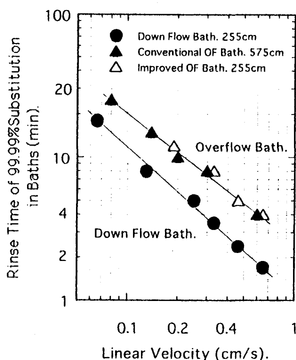

Fig. 7 COMPARISON OF RINSING PERFORMANCES BETWEEN OVERFLOW BATH AND DOWN FLOW BATH.

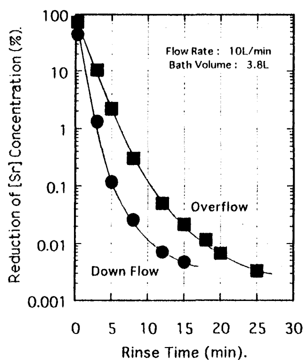

Fig. 8 COMPARISON WITH RINSING PERFORMANCE OF DOWN FLOW AND OVERFLOW MEASURED BY CHEMICAL ANALYSIS.

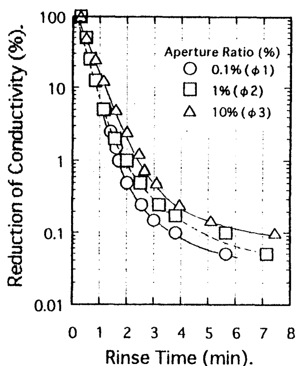

Fig. 9 EFFECT OF APERTURE RATIO FOR RINSE PERFORMANCE IN PARALLEL DOWN FLOW BATH.

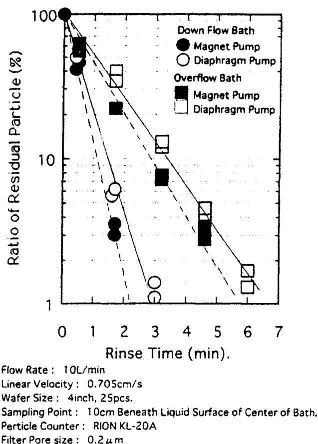

Fig.10 COMPARISON OF RESIDUAL PARTICLE(0.5μm PSL) BETWEEN DOWN FLOW BATH AND OVERFLOW BATH UNDER CIRCULATING FILTRATION.

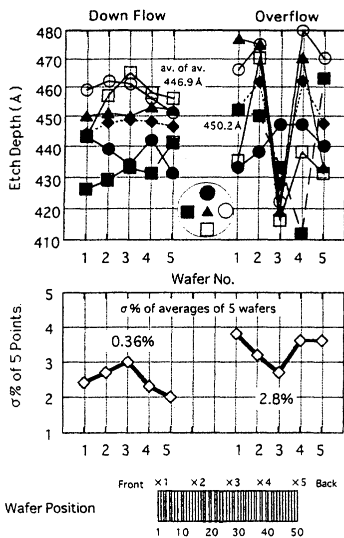

Fig.11 UNIFORMITY OF HF ETCHING.

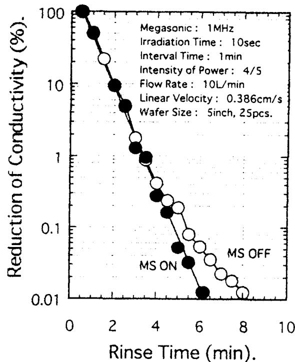

Fig. 12 EFFECT OF MEGASONIC FOR BOUNDARY LAYER OF PARALLEL DOWN FLOW RINSE.

THE APPLICATION OF THE OZONATED DI WATER AT THE PRE GATE OXIDATION WET CLEANING FOR THE PREVENTION OF WATER MARKS

Jin-Goo Park and Michael F. Pas*
Department of Metallurgy and Materials Engineering
Hanyang University, Ansan, 425-791, Korea

* Texas Instruments Inc.,
Dallas, Texas 75243

Ozonated DI water was evaluated and applied to pre gate oxidation wet cleaning processes after HF etching of silicon wafers for the prevention of water marks. No metallic contamination was observed not only in ozonated water cleaned wafer surfaces but also ozonated water itself. The oxide growth rate was faster than H_2O_2 based chemicals and reached the final oxide thickness of ~ 15 Å after 1 min. No water marks and particle addition were observed in ozonated water last cleaned wafers. Electrical evaluations of ozonated water last cleaned MOS device such as soft and hard breakdown of gate capacitors showed equivalent or better results than HF last cleaned wafers.

INTRODUCTION

The control of microcontamination such as residues and particles in semiconductor manufacturing has become one of the most important process issues due to their impacts on the device yield as the level of device integration increases. Even though there exists the drawbacks in wet chemical cleaning processes, they have been a major cleaning processes in semiconductor processes. It is well known that the wettability of wafers changes during the wet cleaning processes depending on the chemicals used [1]. Hydrophobicity/hydrophilicity of a silicon wafer surface is one of the most important parameters in understanding the source of microcontamination in wet chemical processes. Oxide coated and RCA cleaned wafer surfaces are hydrophilic and HF etched surfaces are hydrophobic due to the passivation by hydrogen termination [2]. The HF-last process is most attractive in terms of gate oxide integrity (GOI) and minority carrier lifetime (MCLT) in pre furnace wet processes. However, HF-last process introduces a highly hydrophobic and reactive surface created by HF etching of oxide on the wafer. This HF etched surface leaves defects called "water marks" after the drying process [3,4]. Water marks created before the gate oxidation can cause electrical failure due to locally thicker oxide formation. Also they can cause the thickness or concentration variation after implant, CVD, or plasma etch process and may result in the yield loss. The creation of water marks in HF last process has been attributed to the oxidation of silicon surfaces by dissolved oxygen in a water drop leaving hydrated oxide as a residue on the dried hydrophobic surface [3]. Drying methods are very important in controlling the formation of water marks. Spin drying tends to create more and larger water marks than IPA vapor drying. The patterned wafers with both hydrophilic and hydrophobic sites are vulnerable to the creation of water marks even in vapor dryers [4]].

A major concern is how water marks can be controlled in wet chemical clean up when HF etching is last cleaning sequence before dry is applied. The easiest way to prevent water marks is to make the silicon surface hydrophilic before a dry process. However the hydrophilization can cause the degradation of gate oxide integrity depending on the chemical used. The presence of metallic impurities in wet chemicals degrades GOI and MCLT when the last cleanup process involves RCA cleaning chemicals even though they can produce the hydrophilic surfaces.

Ozone has been applied not only in the film deposition [5] but also in wet/dry cleaning processes [6,7]. Ozone injected water has been applied to replace H_2SO_4 + H_2O_2 for the removal of residual organics [8]. Also ozonated DI water has been introduced into semiconductor wet processes in the place of H_2O_2 as a strong oxidant. The application of ozonated DI water added chemicals to wafer cleaning showed comparable particle removal and better metal removal performance than conventional H_2O_2 based RCA chemicals along with the organic removals.

The hydrophilization of HF etched surfaces without degrading GOI will be the best method in preventing water marks in semiconductor wet cleaning processes before gate oxidation. In this paper the application of ozonated DI water to HF etched wafer surfaces was evaluated whether it can prevent water marks from being created without degrading the gate oxide integrity of HF etched surfaces.

EXPERIMENTAL PROCEDURES

Ozone generator which was manufactured by Ozone Research and Equipment Co. was connected to a side of the final over flowing DI water rinse tank in an automatic wet station through the stainless steel tubing to produce the ozonated DI water. Ozone was produced at an oxygen flow of 6 l/min.

Chemical analysis of the Si surface was performed using a Riaku 3726 Transmission Reflection X-ray Fluorescence (TXRF) system. The angle of incidence is a few minutes of arc such that there is total reflection from the sample. The element capable of being detected are Na to U. The spot size for detection is about 1 cm in diameter. The wafers to be analyzed are kept whole during analysis.

X-ray Photoelectron Spectroscopy (XPS) analyses were performed on oxides grown in different oxidizing cleaning solutions. A Vacuum Generators ESCALAB Mark II electron spectrometer with a monochromatic aluminum ($K_{\alpha 1,2}$ = 1486.6 eV) anode as the x-ray excitation source was used in these measurements. Inductively Coupled Plasma Mass Spectroscopy (ICP-MS) was used to compare and analyze any trace metallic impurities in ozonated DI water.

In-line KLA 2111 and 2550 wafer inspection systems were used to measure and review the water marks on test wafer surfaces in different gate oxide cleaning processes. The patterns having hydrophilic and hydrophobic sites before the second gate oxidation were created using actual device fabrication steps for water marks tests [4]. Pre and post measurements and observation of defects on wafers were performed using KLA at the pre gate oxide cleaning processes to identify the formation of water marks. Both spin and IPA vapor dryers were used to observe the formation of water marks on wafers tested. For the measurements of particulate contamination on bare silicon wafers a WIS 8500 laser

particle scanner was used for measuring the particles larger than 0.2 μm before and after each different cleanings.

For the electrical evaluation minority carrier life time (MCLT) and Q_{bd} measurements were carried out. For the MCLT measurements the thermal oxide of 150Å was grown on high resistivity (>10 Ω•cm) silicon wafers to compare the effect of various cleanings. The oxidation process included 6% HCl in the horizontal furnace during oxidation. MCLT evaluation was done using a Leo Geiken Wafer Tau measurement tool which uses a contact-less photoconductive decay technique by applying the microwave reflection method. Wafers were prepared in an automatic wet station equipped with an IPA vapor dryer. All wafers were precleaned with SC1 combined with a megasonic power and HF at an automatic wet station. Before the cleaning splits, plain DI water rinse was performed to remove any HF chemicals left on the silicon wafers. H_2O_2, SC2, and ozone added DI water were used as a final clean up chemical with HF last cleaning. All experiments were done in a class 1 clean room and semiconductor grade chemicals and ultra high purity DI water were used in all experiments.

To electrically evaluate the cleaning processes, test device structures were fabricated on 6 in. (150 mm) p(100) wafers with 0.8 Ω•cm to obtain a MOS capacitor with a 150Å gate oxide, an isolation field oxide and doped polysilicon contacts. The area of the capacitor is 4.93×10^{-4} cm^2. All wafers went through same procedures except pre gate oxidation cleaning. To evaluate the electrical characteristics of oxide after various clean up, soft and hard breakdown of oxide were measured. In soft breakdown, the oxide recovers if the capacitor is not further stressed. The limit of GOI is usually set to 16V. In hard breakdown, the oxide breaks down destructively and can not be recovered. The limit for breakdown voltage and current are usually set by the limitations of the measurement instrument and the device oxide properties.

EXPERIMENTAL RESULTS AND DISCUSSION

Water mark tests were performed on patterned test wafers at pre gate oxidation clean up. As discussed previously the hydrophilization of HF etched silicon surfaces prevents water marks from being created in wet cleaning processes. No water marks were observed on ozone treated wafers not only in spin dries but also in IPA vapor dries. H_2O_2 based RCA chemical treated wafers did not also produce water marks at all. Ozonated DI water could be much purer than RCA chemicals due to the ultra high purity level of DI water. If ozone added into DI water can be proven to be pure without generating particles and metallic impurities the application of ozonated DI water will be favorable not only to maintain GOI level but also to prevent water marks from being created in HF last wet processes.

To measure the level of particulate and metallic contamination, both particles and trace metallic impurities were measured in DI water bath with and without ozone. No particle addition by introducing ozone to water was observed on bare silicon wafers when a laser particle scanner was used. The arc discharge is the most wildly accepted method in generating ozone radicals from oxygen. Metal electrode used in the ozone generator can produce the possible metallic species. In order to examine any metallic contamination in ozone added DI water, the trace metallic contamination was measured and compared to using TXRF on cleaned wafers. Wafers pre cleaned in SC1 and HF were rinsed in DI water with and without ozone for 5 min. They were then submitted for the trace metal

analysis. Table 1 shows the analysis results on each wafers. Other than higher concentration of S and Cl in ozone treated wafers, all other metals analyzed were below the detection limits. Also ICP-MS chemical analysis of the ozonated DI water was performed and compared to a baseline DI water. Other than a little higher concentration of Al not much differences in metallic concentrations were measured in the ozonated DI water as shown in Table 2.

To observe the oxidation reaction between ozone and silicon wafers in DI water, the rinsing of HF etched wafers in the ozonated DI water was carried out and the oxide thickness was measured as a function of the treatment time. Wafers were characterized using XPS to observe the oxidation states. After 1 min exposure to ozone, the hydrophobic silicon surface became hydrophilic and 15 Å of oxide thickness was measured by an ellipsometry. When the wafer was exposed to ozonated DI water to 20 min, there were no changes in oxide thicknesses. This indicates that the very short exposure of ozone oxidizes the HF etched surface and makes surface hydrophilic. Figure 1 shows the change of oxide thickness as a function of the rinse time in ozonated DI water. Also oxides formed from ozone and RCA chemical clean up were characterized by XPS. Comparing to H_2O_2 based chemical treated wafer, even 1 min ozone rinsed wafers resulted in a much stronger oxide peak (Si_{2p}). For ozone cleaned wafers surface became saturated with oxygen even after 1 min exposure to ozone and did not show much difference in the peak height in 10 min exposed wafers. It indicates that reduced final rinse time is possible in ozonated DI water rinse for the hydrophilization purpose. Figure 2 shows the XPS analysis of Si_{2p} peaks in ozone and H_2O_2 based chemical treated wafers. H_2O_2 based chemical treated wafers showed the progressive growth of oxides as a function of treatment time. The faster oxidation of silicon in ozone may be attributed to the stronger oxidation potential of ozone than H_2O_2 not only in acidic but also in basic solutions [9].

MCLT measurements can provide information on metallic contamination, crystal damage and/or trapping sites in silicon wafers. Most fabs measure MCLT in a routine basis for the monitor of wet and diffusion processes. Since the MCLT data depends quite heavily on the exact furnace used and furnace conditions, the most important observation is not the absolute values themselves but the relative trend comparison for a process condition. Figure 3 shows the measured MCLT results from different cleaning splits. The lowest MCLT value was measured at wafers cleaned with H_2O_2 solutions as the last cleaning chemical. This might be due to the highest metallic impurities left by H_2O_2. Ozonated DI water and SC2 chemical treated wafers resulted in higher values than in H_2O_2 solutions. The wafers etched with HF at the final clean step resulted in the highest MCLT values. Because the MCLT values includes lifetimes from both surface and bulk materials, it does not always relate the gate oxide quality of device. So other means of electrical characterization should be accompanied.

To evaluate the electrical characteristics of oxide after various cleanings, soft and hard breakdown of oxide was measured. Values reported in the results are labeled 'GOI' for the soft oxide breakdown, and 'V_{bd}' for the voltage and 'I_{bd}' for the current at which the hard breakdown occurs. Figure 4 (a) shows the measured GOI values on differently cleaned wafers before the gate oxidation. The very similar results were obtained on wafers cleaned in HF, H_2O_2, and ozone added DI water. Not like MCLT values, SC2 last cleaned wafers showed the lowest GOI values. Even though SC2 removes metallic contamination effectively, it can not remove particulate impurities. These particulate

impurities may play an important role in determining GOI. Also, it shows that MCLT measurements are not the absolute method in determining better processes or chemicals. Figure 4 (b) and (c) show the hard breakdown voltages and currents on differently cleaned wafers. They showed similar trends to GOI values as shown in Figure 4 (a). It is interesting to see that the highest values of Vbd and Ibd were observed in ozonated DI water cleaned wafers. It may prove the highest purity of ozonated water compared to the other chemicals used. HF last wet chemical processes before gate oxidation is the most favorable process but, it introduces water marks as residues after dry. Comparable results were observed in H_2O_2 last wet processes in charge to breakdown voltages without creating water marks. However MCLT showed the lowest values indicating metallic contamination on surfaces. Most promising data were obtained from ozonated water last wet processes. It resulted in no water marks and the best quality oxide layer.

CONCLUSIONS

Ozonated DI water was evaluated and applied to pre gate oxidation wet cleaning processes after HF etched silicon wafers for the prevention of water marks. No water marks and particle addition were observed in ozonated water last cleaned wafers. No metallic contamination was observed not only in ozonated water cleaned wafer surfaces but also the ozonated water itself when they were analyzed by TXRF and ICP-MS. The oxide growth rate was faster than H_2O_2 based chemicals due to higher oxidation potential of O_3 and reached the final oxide thickness of ~ 15 Å even after 1 min. The lowest MCLT value was measured at wafers cleaned with H_2O_2 solutions as the last cleaning chemical. Ozonated DI water and SC2 chemical treated wafers resulted in higher values than in H_2O_2 solutions. The wafers etched with HF at the final clean step resulted in the highest MCLT values. Not like MCLT values GOI, I_{bd} and V_{bd} evaluation of ozonated water last cleaned wafers showed the equivalent or better results than HF last cleaned wafers. Cleaning process including ozonated DI water can prevent the formation of water marks without degrading the oxide integrity compared to HF last cleaning process.

ACKNOWLEDGMENTS

We would like to thank Dr. R. M. Wallace for XPS analysis, Dr. L. -A. Files-Sesler for TXRF measurements and Mr. R. Clark of Texas Instruments for the experimental helps.

REFERENCES

1. J. -G. Park and S. Raghavan, *J. Adhesion Sci. Tech.*,7(**3**), 179 (1993)
2. V. A. Burrows, Y. J. Chabal, G. S. Higashi, K. Raghavachari, and S. B. Christman, *Appl. Phys. Lett.*, **53(11)**, 998 (1988).
3. M. Watanabe, M. Hamano and M. Harazono, *Mats. Sci. Eng.*, **B4**, 401 (1989).
4. J. -G. Park and M. Pas, *J. Electrochem. Soc.*, **142(6)**, 2028 (1995)
5. K. Fujino, Y. Nishimoto, N. Tokumasu, and K. Maeda, *J. Electrochem. Soc.*, **137(9)**, 2883 (1990)
6. J. R. Vig, in Handbook of Semiconductor Wafer Cleaning Technology, Ch. 6, W. Kern, Ed., Noyes Publications, 1993
7. J. T. Tong, D. C. Grant and C. A. Peterson, Proc. Second International Symposium on Cleaning Technology in Semiconductor Device Manufacturing, 92-12, pp. 18-25, J. Ruzyllo and R. E. Novak, Eds., The Electrochemical Society, Pennington, NJ (1992)

8. T. Ohmi, T. Isagawa, M. Kogure, and T. Imaoka, *J. Electrochem. Soc.*. **140(3)**, 804 (1993)
9. F. A. Cotton and G. Wilkinson, Advanced Inorganic Chemistry, 5th Ed., John Wiley & Sons, 1988

Table 1. TXRF Analysis of Trace Elements on Wet Cleaned Wafers

Element	Detection limit, atoms/cm^2	Baseline Wafer	DI water rinsed wafer w/o O_3 for 5 min	O_3 DI water rinsed wafer for 5 min
Ni	3.50E+10	<Det. Limit	4.08E+10	4.21E+10
Fe	5.00E+10	<Det. Limit	<Det. Limit	<Det. Limit
Cu	3.50E+10	<Det. Limit	<Det. Limit	<Det. Limit
Ca	2.50E+11	<Det. Limit	<Det. Limit	<Det. Limit
K	2.00E+11	<Det. Limit	<Det. Limit	<Det. Limit
Cr	1.00E+11	<Det. Limit	<Det. Limit	<Det. Limit
Ti	1.00E+11	<Det. Limit	<Det. Limit	<Det. Limit
Cl	8.00E+11	1.06E+12	1.25E+12	1.20E+12
S	5.00E+11	<Det. Limit	5.88E+11	8.32E+11
Zn	5.00E+10	1.74E+11	<Det. Limit	1.25E+11

Table 2 Elemental Analysis of DI water and Ozonated DI water by ICP-MS

Elements	D. L, ppb	DI Water	O_3-DI Water
Al	< 0.01	0.04	0.17
Ca	< 0.1	0.1	0.60
Cr	< 0.05	0.17	0.18
Cu	< 0.02	0.03	< DL
Fe	< 0.05	0.11	0.06
K	< 0.01	0.12	0.22
Mg	< 0.02	0.03	0.07
Mn	< 0.01	0.02	< DL
Mo	< 0.01	0.02	0.02
Na	< 0.01	14.42	15.31
Ni	< 0.02	0.26	0.27
Ti	< 0.01	0.02	0.03
V	< 0.01	0.01	< DL
Zn	< 0.02	0.14	0.08

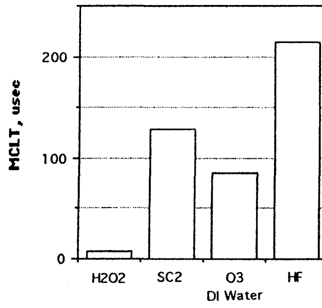

Figure 3. Minority carrier life time of wafers which went through different wet cleanings

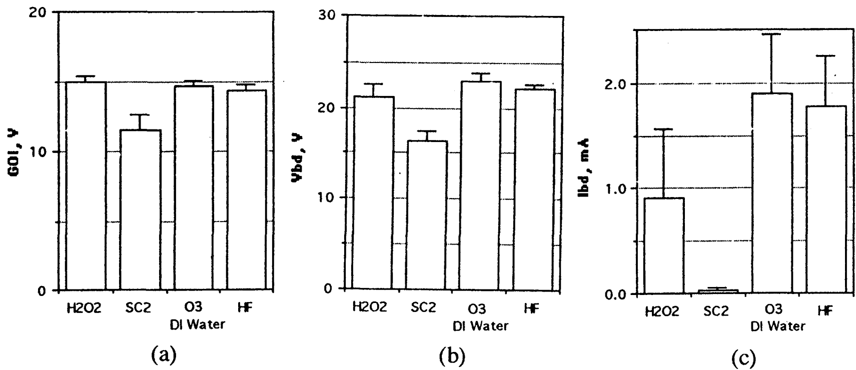

Figure 4. (a) GOI, (b) V_{bd} and (c) I_{bd} values measured on wafers cleaned in different wet chemicals.

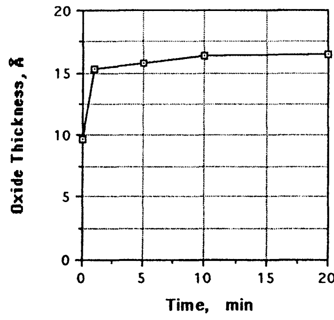

Figure 1. Change of oxide thickness as a function of ozonated DI water treatment time

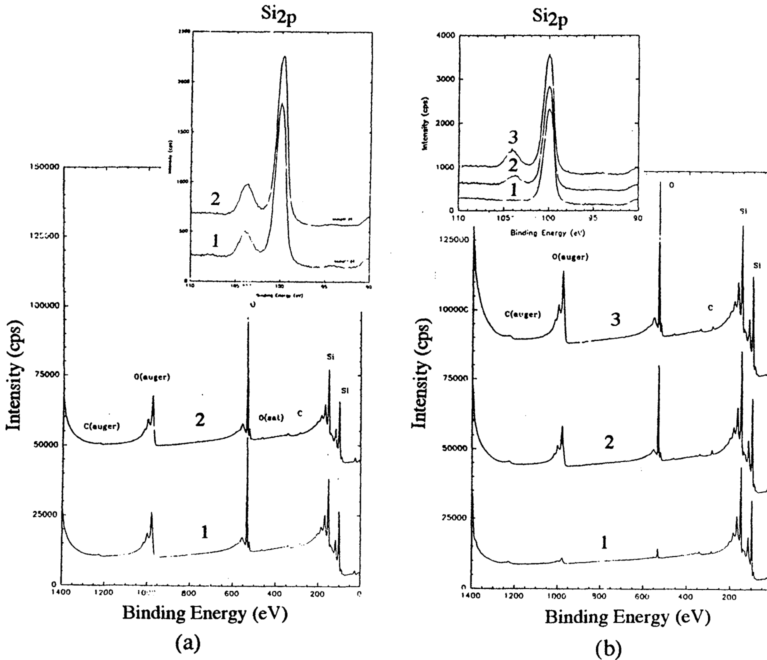

Figure 2. XPS analysis of (a) O_3 DI water (1: 1 min, 2: 10 min ozone treatment) and (b) hydrogen peroxide treated wafers (1: reference bare wafer, 2: 1 min, 3:10 min H_2O_2 treatment) as a function of time.

THE USE OF ULTRASOUND ENERGY IN PHOTORESIST STRIPPING APPLICATIONS

Ismail I. Kashkoush, Ph.D.

SubMicron Systems, Inc., 6330 Hedgewood Dr. Suite #150, Allentown, PA 18106.

Abstract

Using ultrasound energy in photoresist stripping applications is an effective method of removing heavy organic contaminants from silicon wafers. Traditionally, ultrasonic waves at 40 kHz are directed to the bottom of the process tank. It is thought that the cavitation bubbles implode and remove polymers from critical dimensions on patterned wafers. The optimization of this process was not well reported, nor was the use of high frequency sound waves (1 MHz) investigated. This paper investigates the effect of low (40 kHz) and high (1 MHz) frequency sound waves on the removal of polymeric materials from wafer surfaces. Test results showed that the megasonic energy effectively removes contaminants and enables the use of lower bath temperatures.

INTRODUCTION

Recently, work has been focused on the particle removal from silicon substrates using high frequency sound waves. Typically, sound waves between 800-1000 kHz are directed to silicon wafers immersed in an aqueous solution e.g. SC1. This technique has proven to be effective in removing particles as small as 0.13 μm in diameter [1], see figure 1.

The use of ultrasonic energy during post metal stripping is also common in IC manufacturing. The sonic energy enhances the removal of foreign material in critical areas, e.g. vias. Contaminants are removed from substrates by acoustic pressure forces, acoustic cavitation, and/or drag forces induced by localized microstreaming [2-9]. The role of these mechanisms in the contaminant removal process is not very well understood [2]. Contaminant removal can be caused by either one or all of these forces. The use of low frequency sound waves (40 kHz) must be optimized because substrates can be damaged when cavitation bubble implode. It was explained that high velocity liquid jets forming during the collapse of the bubble can cause damage to a solid surface [5].

Figure 2 shows a model of vibrating bubbles lifting a thin film from the substrate surface. High speed photography showed that the bubbles attack the edge of the gap between the

contaminant film and the surface being cleaned [2]. The bubbles attack the film, slip between the solid surface and the edge of the film and reside under the edge of the film (as shown schematically in figure 2). As the bubbles vibrate, a force begins to act upon the film (or possibly metal circuit lines), which tears the film away from the wafer surface. As the film separates, the bubbles slide toward the untouched part of the thin film and penetrate under it. This process continues until the entire film has been separated from the surface. The removed material will be carried away from the wafer surface by the localized streaming currents or the overall fluid flow. This paper investigates the use of low (40 kHz) and high (1000 kHz) frequency sound waves in the removal of photoresist and side wall polymer from silicon wafers. The effect of using high power megasonic energy to reduce the bath temperature was also investigated.

EXPERIMENTAL

The experimental setup consisted of an immersible transducer (provided by CREST Ultrasonics) operated at 40 kHz and 400 W of input power. The transducer was placed inside a glass tank full of room-temperature deionized water (10 gallons approx.). A silicon wafer coated with 1-2 μm resist layer was placed vertically 1 cm above the radiating surface of the transducer. The removal of the photoresist was monitored and taped using a video camera connected to a VCR. The experimental setup is schematically and photographically described in detail in ref. [2].

For solvent stripping experiments, a megasonic unit operating at 1 MHz and an input power level of 800 W was used. The volume of process tank was approximately 10 gallons. Patterned wafers were used with a resist layer of about 1.5 μm for this part of the study.

RESULTS AND DISCUSSION

a. Low frequency (40 kHz):

A 1-2 μm thick polymer layer (photoresist) was deposited on the wafer surface. Figure 3 shows the removal of the thin layer from the wafer surface after 15 seconds in a 40 kHz acoustic field. As the time increases, so does the removed area, as shown in figures 3 and 4. The dark areas in the figures indicate areas where the film has been removed. The other areas (bottom half) show the removal process is still taking place. Similar experiments were conducted at higher frequency ranges (65, 80, and 100 kHz). The film removal at those frequencies was observed also, but with a lower removal rate. The higher the frequency, the lower the removal rate of the film (i.e. longer time was needed to remove a similar film at 100 kHz). However, at a frequency of 850 kHz no film removal was observed. This suggests that if cavitation exists, it is not the primary contaminant removal force. Figure 5 shows the percentage of the cleaned area relative to the wafer surface area. The figure shows the cleaned area increases continuously with

time. A complete removal of the film was achieved after approximately 36 min. at 40 kHz. This result agrees with those obtained by Olaf [4].

At 40 kHz, the results suggest that cavitation is the contaminant removal mechanism in de-ionized water. As mentioned earlier, the cavitation limit in de-ionized water is low at low frequencies (40 kHz), but increases with frequency (see figure 6) [2]. Cavitation bubbles were observed attacking the thin film and separating it from the wafer surface. At frequencies high enough to exhibit no cavitation, the removal forces (drag and acoustic pressure) [2,9] are smaller than the adhesion force between the film and the wafer surface.

b. High frequency (1 MHz):

In the second application, a solvent stripper was used to remove resist and side wall polymer. Cavitation bubbles were not observed during this experiment. As shown in figure 7, the chemistry (solvent) alone was not sufficient to remove the contaminant effectively, even at temperatures as high as 85 °C.

The contaminant removal process was enhanced significantly by applying high frequency waves, as demonstrated in figures 7 and 8. In the absence of cavitation, the contaminant was removed by the pressure waves and carried away from the wafer surface by the acoustic streaming forces. This result is opposite to the result obtained in the first application. This may be explained by the fact that the specific gravity of the solvent is about 1.8. The speed of sound increases with the fluid density, so the wave transmission efficiency in the second application is higher than that in de-ionized water. More experiments are required to confirm this finding.

The effect of input power to the transducer on the contaminant removal effectiveness can be seen from figures 9 and 10. At 200 W, the megasonic energy was not very effective in removing the contaminants. Performance improved by increasing the input power to 400 W. The use of high input power also allows for wafer processing at lower temperature, which may be seen from figures 9 and 10. Better contaminant removal was obtained at 500 W and 70 °C as compared to 400 W and 90 °C. This results in a longer bath life, so less chemical consumption is expected.

CONCLUSIONS

Ultrasonics can accelerate the film lift-off process from silicon surfaces, enhancing the photoresist stripping processes. Also, the generated microstreaming currents can improve the efficiency of the recirculating baths. Certainly, the process will be more cost effective when reduced process time and lower chemical usage is considered.

Results showed that cavitation bubbles play an important role in penetrating under the film and initiating the film removal process in de-ionized water. The localized micro-streaming currents or the gross fluid flow remove the film to the liquid level, which carries it outside the process area. The removal of the thin film increases with time at 40 kHz. Thin film removal decreases with frequency (when time remains constant), and no film removal was observed at 850 kHz in de-ionized water at room temperature.

It has been demonstrated that the removal of resist and side wall polymers can be significantly enhanced using high frequency megasonic energy in solvent applications. The effectiveness of the polymer removal increases as power into the bath increases. In the absence of cavitation, the pressure forces and acoustic streaming are the removal forces. It has been demonstrated also that the bath temperature can be lowered when using high power/high frequency sound waves. By applying the megasonic energy, it was feasible to use lower temperature baths, which insures longer bath life and lower cost of ownership.

ACKNOWLEDGMENT

The author would like to acknowledge the cooperation by ACT/Ashland for hosting part of the experiments at their facility.

REFERENCES

1. Kashkoush, I., SMS Technical Report (unpublished), Jan. 1995.
2. Kashkoush, I.I., Ph.D. Thesis, Clarkson University, May 1993.
3. Busnaina, A., Kashkoush, I., and Gale, G., "An Experimental Study of Megasonic Cleaning of Silicon Wafers", J. Electrochem. Soc., 142(8), August 1995, pp. 2812-2817.
4. Olaf, J. "Oberfflachenreinigung mit Ultraschall", Acoustica, 7(5), 1957, pp. 253-263.
5. Bolle, H. and Lauterborn, W., "Experimental Investigation of Cavitation Bubble Collapse in the Neighborhood of a Solid Boundary", J. Fluid Mech., 72, Part 2, 1975, pp. 391-399.
6. Zarmebo, L.K. "Acoustic streaming", High Intensity Ultrasonic Fields, Edited by Rozenberg, L.D., Plenum Press, New York, 1971.
7. Neppiras, E.A., "Acoustic Cavitation", Physics Reports, 61, 1980, pp.159-253.
8. McQueen, D. H., "Frequency Dependency of Ultrasonic Cleaning", Ultrasonics, 24, Sept. 1986, pp.273-280.
9. Olson, L.G. "A Simplified Finite Element Model for Ultrasonic Cleaning", J. Sound and Vibration, 161(1), 1993, pp. 137-156.
10. ACT/Ashland Chemical, Allentown, PA, Private communications.

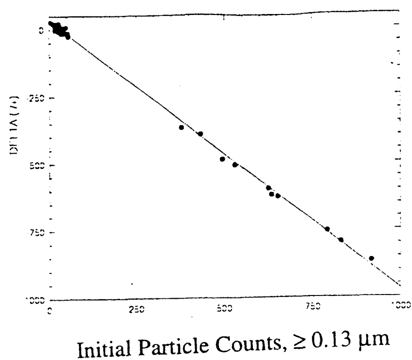

Figure 1: Particle Removal Efficiency in SC1/Megasonic Process (800 W, SC1:0.1:1:10 at 70 °C).

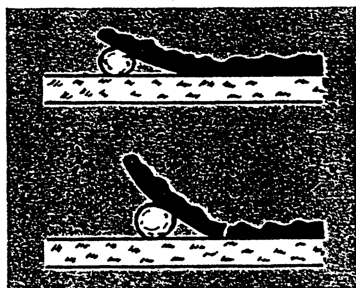

Figure 2: Model of A Vibrating Cavitation Bubble between a Thin Film and a Solid Surface [2].

Figure 3: The Removal of a Thin Polymer Film from a Silicon Surface in 40 kHz Acoustic Field in Water, Time = 90 sec.

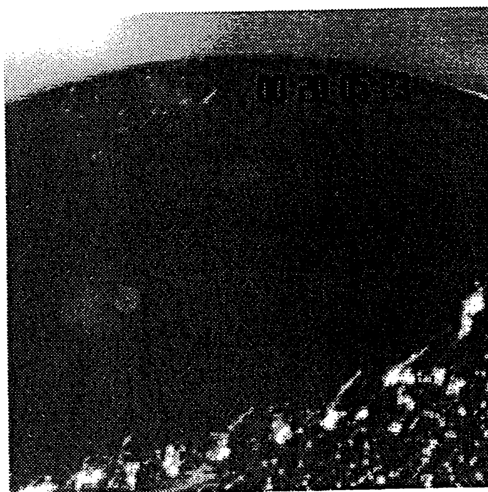

Figure 4: The Removal of a Thin Polymer Film from a Silicon Surface in 40 kHz Acoustic Field in Water, Time = 7.2 min.

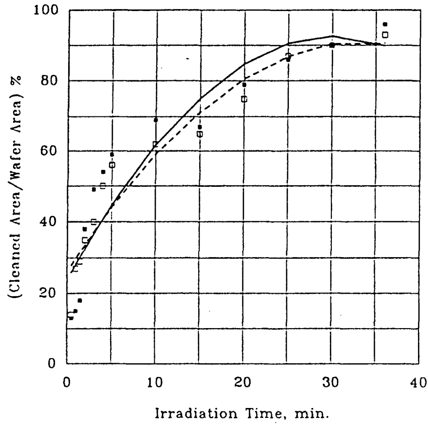

Figure 5: The Percentage Removed Area of a Photoresist under 40 kHz Acoustic Field in Water.

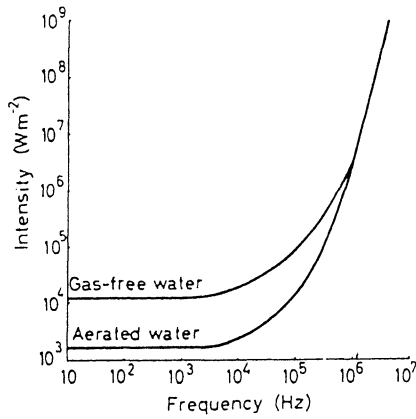

Figure 6: Variation of Cavitation Threshold with Frequency for Water at Room Temperature [2].

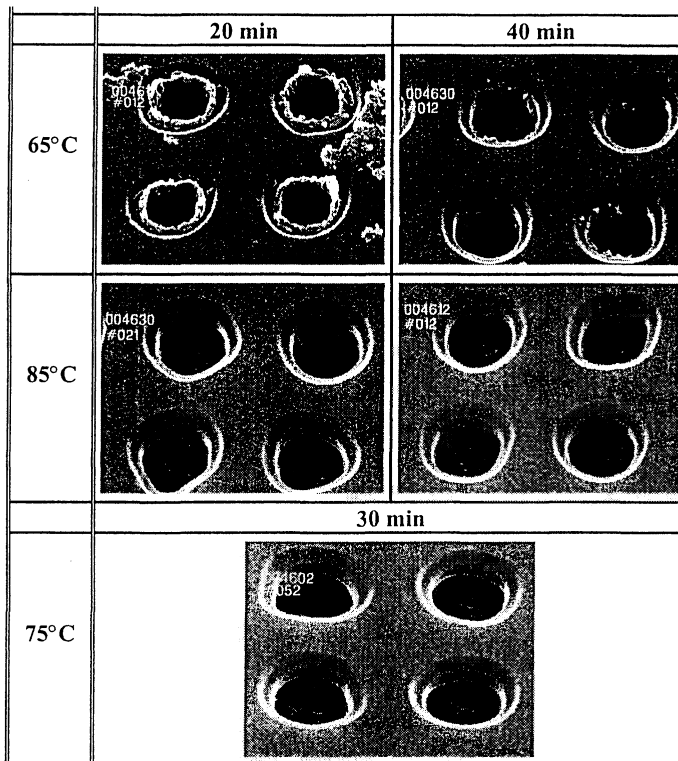

Figure 7: Photoresist Removal in Solvent at Different Process Temperatures and Times with no Megasonic (Courtesy from ACT/Ashland Chemical).

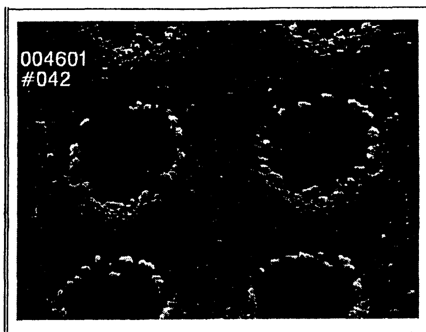

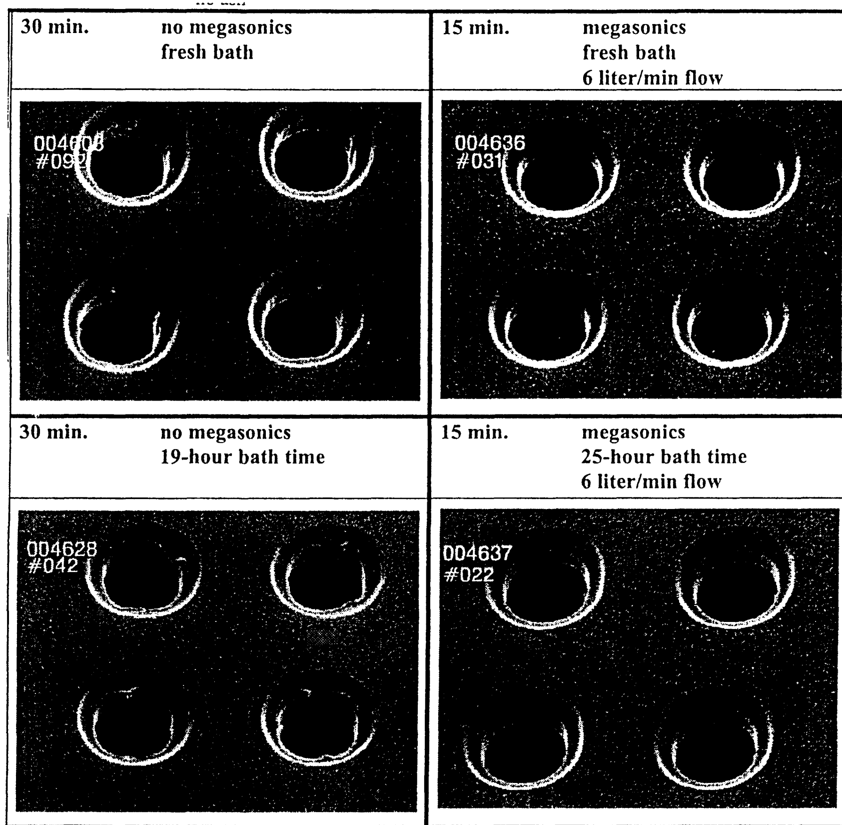

Figure 8: Photoresist Removal in a Solvent at 75 °C and 1 MHz Acoustic Field (Courtesy from ACT/Ashland Chemical).

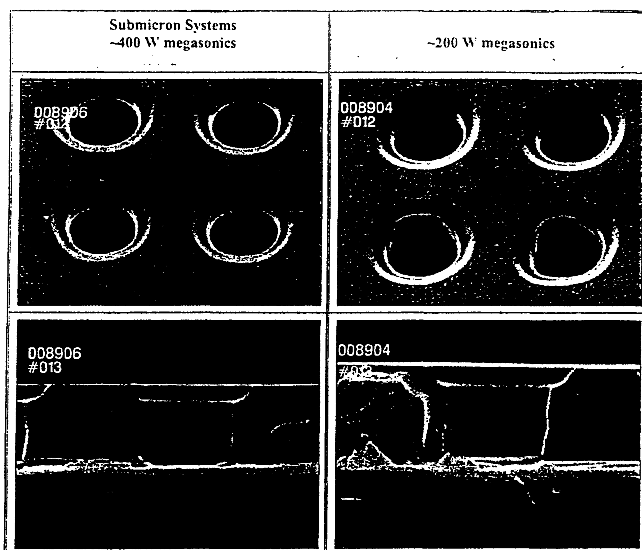

Figure 9: Effect of Megasonic Power on the Side Wall Polymer Removal.

- 70°-75°C processing
- Submicron Systems megasonics

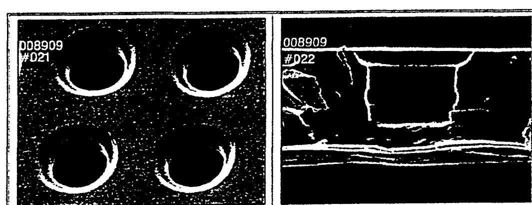

- 90°-95°C processing
- Submicron Systems megasonics

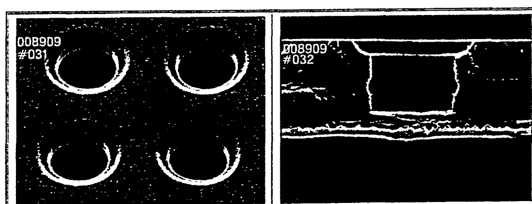

Figure 10: High Power Megasonic Enables the Use of Lower Bath Temperature.

RADICAL ACTIVATION OF DI WATER AND CLEANING SOLUTION BY MEGASONIC

Masayuki Toda and Masayuki Kato
Department of Materials Science and Engineering
Faculty of Engineering, Yamagata University
3 - 16, Jonan 4 chome, Yonezawa
Yamagata, Japan, 992
Kazuki Kubo, Senri Ojima and Tadahiro Ohmi
Department of Electronics
Faculty of Engineering, Tohoku University
Aza Aoba, Aramaki, Aoba-ku
Sendai, Japan, 980

The experimental study was performed to clarify the effectiveness of applying the megasonic to the cleaning of wafer surface. The quartz glass vessel having megasonic oscillators was used to apply 0.950 MHz megasonic wave to DI water. DMPO (5,5 - dimethyl - 1 - pyrroline - N - oxide) was added into the sample of DI water to adduct the formed free radicals, and the free radical formation was evaluated by X - Band ESR Spectrometer. Megasonic irradiation to DI water resulted in the H and OH radicals' formation and its quantities were found to be affected by composition of dissolved gases in DI water. It was also found that the formed free radicals were very effective to remove the organic contamination on silicon wafer.

INTRODUCTION

In advanced semiconductor manufacturing of next generation, not simply the size of wafer becomes large up to 30 cm, but also the geometry of semiconductor device is being reduced to deep sub micron order. It is supposed that the requirement for ultra cleanness of wafer surface becomes more strictness(1).

At present time, large amounts of chemicals and DI water are utilized for wet cleaning and the production cost of semiconductor device is now expensive for the one of reasons mentioned above. It is necessary to reduce the cleaning steps as much as possible and to try not to put too much load on clean room to decrease the production cost. Thus, the novel cleaning method offering the total room temperature processing is asked to reduce the production cost. From this point of view, the new advanced wet cleaning process we have developed utilizes DI water as a main cleaning agent and this new technology also facilitates to control the concentration of chemical solution perfectly. The new process steps are as follows;

(1) O_3/H_2O --- Removal of organic and metal contamination at room temperature
(2) $HF/H_2O_2/H_2O$/Surfactant + Megasonic
Removal of metal, particle and chemical oxide

HF = 0.5 % and H_2O_2 = 0.1~ 1% at room temperature

(3) Ozonized DI water Megasonic shower cleaning
Removal of organic carbon and adhered chemicals
at room temperature

(4) DHF ----- Removal of chemical oxide and perfect hydrogen
termination on silicon wafer
HF : 0.1 % at room temperature

(5) DI water + Parallel down flow + Megasonic
Rinsing at room temperature

In this new advanced cleaning process, megasonic is introduced to decrease the consumption of DI water and chemicals. Figure 1 shows the comparison of newly developed wet cleaning process with conventional RCA cleaning process. From this figure, the new process is very friendly to environment and the application of megasonic energy to wafer surface cleaning was known to be one of the key features in this proposed wet cleaning process. Therefore, the effect of megasonic on wafer surface cleaning should be comprehended to make this cleaning process most suitable. And for the effective operation of this process a right understanding of the relations between sonication and chemical reaction and/or radicals' formation in ultra pure water or in the cleaning solution is also necessary.

In this paper, both the production of free radicals in ultra pure water and cleaning solutions and the effect of megasonic on the wafer surface surface cleaning will be discussed.

EXPERIMENTAL APPARATUS AND PROCEDURES

The quartz glass vessel having megasonic oscillators of 1200 Watt was used to apply 0.95 MHz megasonic wave to DI water of 450 μl filled in a polyethylene micro-test-tube. DMPO(5,5-dimethyl-1-pyrroline-N-oxide) of 50 μl was added into a sample DI water to adduct the generated free radicals by spin-trap method. The free radicals' production was evaluated by X-Band ESR Spectrometer as shown in Fig.2 and the formed ions were also evaluated by ion-chromatography. To the quantitative analysis of radicals' formation, the stable radicals should be necessary for the standard materials. In general, TMPOL(4-Hydroxyl 2,2,6,6-Tetramethly Peridine-1-Oxyl), of which structure is shown in Fig.3, is used as the standard chemical materials.

Figure 3 shows the calibration line obtained by using TMPOL. It is clearly known that the number of radical is directly proportional to the characteristic value of ESR signal intensity.

Figure 4 shows the reaction of DMPO as spin trapping agent with H and OH radicals and also shows the unique ESR spectrum of products obtained by reaction. Therefore, the number of formed radical can be calculated by using the characteristic value obtained from this ESR spectrum as shown in Fig.4.

The same quartz glass vessel was also used to measure the removal of organic contamination on wafer surface. The quantity of removal of organic matter on wafer surface was evaluated by FT-IR Spectrometer.

RESULTS AND DISCUSSION

Figure 5 shows an example of ESR signal given by DMPO which reacts with H and OH radicals formed by megasonic irradiation in UPW bubbled with nitrogen gas. The remarkable signals correspond to H and OH radicals were observed from this figure.

Figure 6 shows the relationship between the number of OH radical and intensity of power supplied. At same time, the temperature variation caused by megasonic irradiation was shown in this figure. Number of OH radical was found to increase as increasing in the intensity of power supplied and then decrease. This is becasue DMPO has been decomposed by increasing temperature above 50 degree centigrade in vessel.

Figures 7(a) and 7(b) illustrate the effect of dissolved gas on H and OH radicals' formation by megasonic irradiation of 1.623 MHz, respectively. OH radical was extremely formed in ultra pure water containing oxygen gas. This is because OH radicals are formed by the reaction of [O] from O_2 on H radical from H_2O with the exception of formation of OH radicals from H_2O. In the figure, "no bubbling" means pure water containing nitrogen and oxygen gases. The quantity of OH radical formed under the condition of no bubbling is always smaller than that of oxygen bubbling condition. This is due to that oxygen concentration of no bubbling condition is smaller than that of oxygen bubbling condition. On the other hand, hydrogen radical was found to be formed in pure water containing Argon, Helium and Nytrogen gas. A lot of H radicalls' formation was found in pure water containing Argon gas. Consequently, the special effect of Argon gas can be considered. Previous paper(2) reported that hydroxyl radical was highly formed in pure water containing Xenon gas.

Formation of hydrogen peroxide in ultra pure water excited by megasonic was shown in Fig.8. In the case of ultra pure water containing Argon gas, hydrogen peroxide was formed immediately as megasonic irradiation was begun and the production of hydrogen radical was higher.compared with these in Nitrogen bubbling condition. In this case,[O] formed from H_2O_2, which is generated by recombination of OH radical in ultra pure water containing Argon gas, reacts on H_2O and generates H_2O_2 because of no formation of NH_3 from H radical and N_2 in this system. On the other hand, in the case of Nitrogen bubbling condition the formation of H_2O_2 is not found. It can be considered that H_2O_2 reacts on NH_3 from H radical and N_2. This NH_3 production was certified to analyze NH_3 ion in the excited ultra pure water by ion chromatography.

Figure 9 shows the effect of dissolved gas in ultra pure water on formation of ions. In this figure, Argon gas was utilized to discharge the dissolved N_2 from ultra pure water. In spite of the lower concentration of N_2 in this ultra pure water, $NH_4^+$is recognized to be high compared with the case of ultra pure water containing N_2. This is because in ultra pure water containing Argon, a lot of H radical is generated by megasonic irradiation. At the same time, generated H_2O_2 reacts on NH_4^+, and NO_2^- and NO_3^- are formed.

In advanced wet cleaning process, ozonized ultra pure water, of which dissolved gas concentration is controlled, will be utilized in 21st century. Figure 10 shows the formation of ions in ozonized ultra pure water by megasonic irradiation. In this figure, degassed ultra pure water was used to ozonize, and dissolved gas such as Nitrogen and Argon was used. Circumference around ultra pure water surface is atmosphere, Nitrogen and Argon, respectively. From this figure, the amount of formed ions was found to be very small.

After megasonic irradiation, it is found that as the concentration of dissolved Nitrogen in water is small, the amount of Nitric acid ion becomes small.

Figure 11(a) and 11(b) show the formation of oxygen and hydrogen molecules in degassed ultra pure water by megasonic irradiation. After megasonic irradiation in degassed ultra pure water, the amount of oxygen and hydrogen molecules increase along the time elapsed. In general, the formation of H and OH radicals from H_2O by megasonic was considered to be caused by cavitation effect in water. From figures 11(a) and 11(b), howevere, it can be considered that the decomposition of H_2O by megasonic is caused by the another factors. It is assumed that the space in original structure of water can be used to decompose H_2O.

The formation of H and OH radicals can be considered to be very effective to remove the organic contamination on the wafer surface. Figure 12 show the effect of megasonic irradiation on radical formation in each cleaning solutions. In this figure "+MS" means the irradiation of megasonic. OH radical was not found in "8.0ppm+UPW" as shown in Fig.12. Howevere, OH radical formations in another cleaning solution were found. After megasonic irradiation, free radical formation in all cleaning solutions were recognized.

Figures 13 and 14 show the removal of organic contamination from wafer surface by each cleaning solutions. In this figures, wafers on which surface the surfactant was adsorbed were used to measure the removal of organic contamination. From the comparison of the result obtained by ultra pure water containing ozone with ozonized ultra pure water excited by megasonic, the removal rate of ozonized ultra pure water excited megasonic was confirmed to be better than the other.cleaning solutions.

CONCLUDING REMARKS

H and OH radicals were confirmed to be generated in ultra pure water by megasonic irradiation. The formation of radicals is strongly affected by the dissolved gases. It was also found that generated H radical was very effective to remove the organic contamination on silicon surface. In the proposed wet cleaning process, the residual surfactant will be worried about in the step (2). Trace surfactant, however, is removed completely by the following cleaning step (4). This cleaning ability of the step (4) is understood by the present paper. The practical application of megasonic to the future cleaning is certified to be promising.

References

(1) T.Ohmi, "Future trends and application of ultra clean Technology", Tech. Dig., 1989 International Electron Devices Meeting,Washington D. C., pp.49 - 52
(2) T. Kondo, J. Gamson, J. B. Mitchell and P. Riesz, "Free radical formation and celllysis induced by ultrasound in the presence of different rare gases", Int. J. Radiat. Biol., Vol.54, No.6, pp.955 - 962 (1988)
(3) K.Makino, M.M.Mossoba and P.Riesz, "Chemical effect of ultrasound on Aqueous solutions. Formation of hydroxyl radical and hydrogen atoms", J. Phys. Chem., vol 87, pp1369 - 1377, (1983)

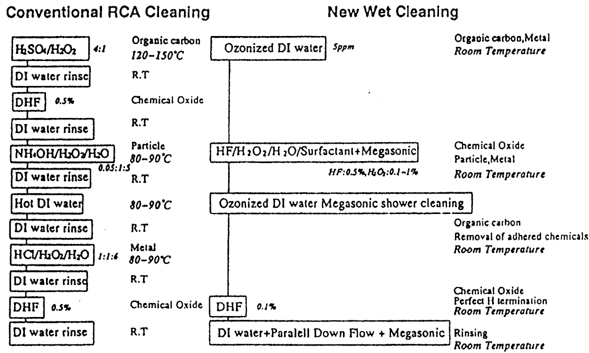

Fig. 1 Comparison of new wet cleaning process with conventional RCA cleaning process

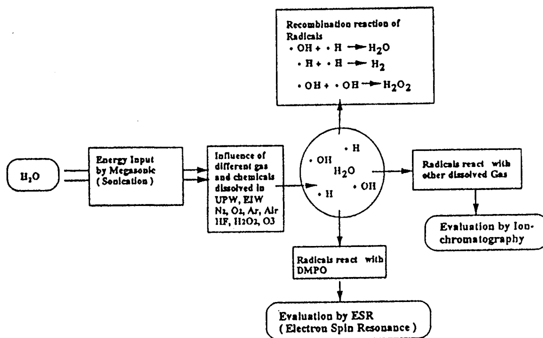

Fig. 2 Radicals' formation, Spin trapping by DMPO and evaluation of chemical products

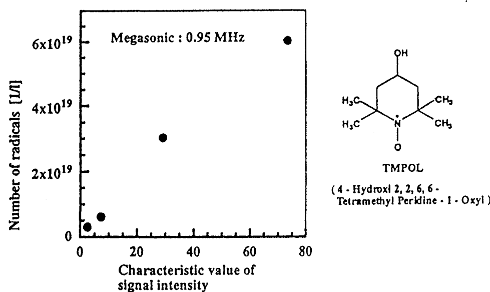

Fig. 3 Calibration line of OH-DMPO adduct

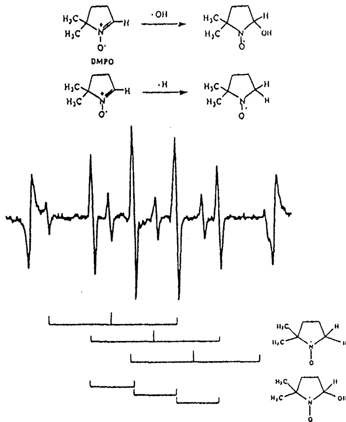

Fig. 4 ESR spectrum of aqueous solution purged by nitrogen with DMPO sonicated for 2 minutes

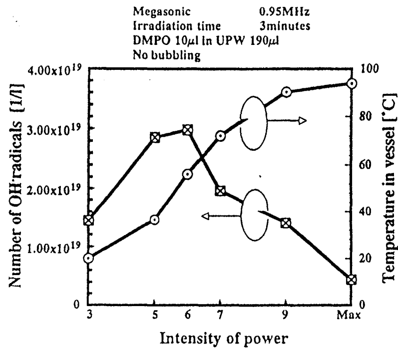

Fig. 6 Effect of temperature in vessel on OH radical formation

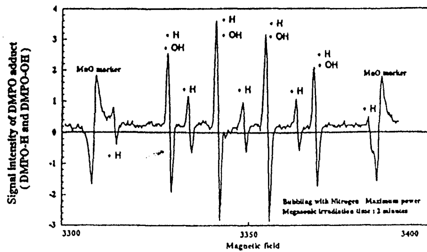

Fig. 5 Effect of N2 gas on radical formation in pure water excited by Megasonic

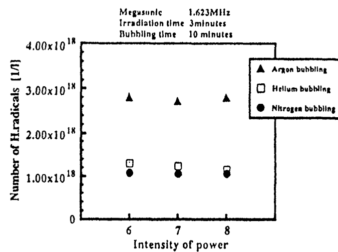

Fig. 7(a) Effect of dissolved gas on H radical formation

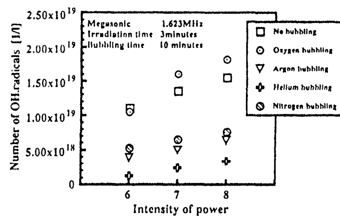

Fig. 7(b) Effect of dissolved gas on OH radical formation

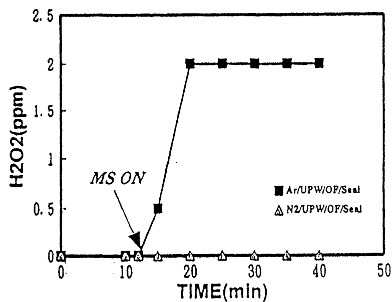

Fig. 8 Formation of hydrogen peroxide in ultra pure water by megasonic irradiation

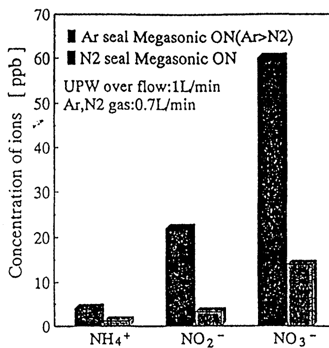

Fig. 9 Effect of dissolved gas in ultra pure water on production of ions

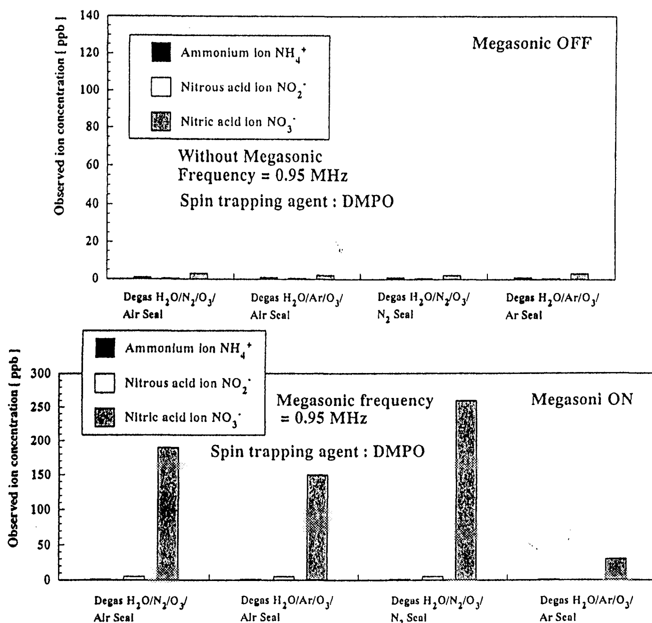

Fig. 10 Production of ions in ozonized ultra pure water by megasonic irradiation

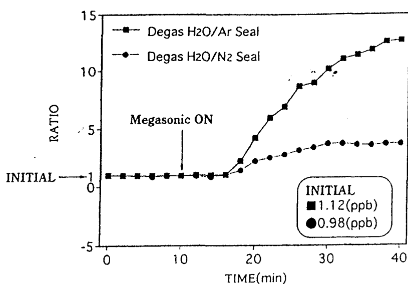

Fig. 11(a) Formation of hydrogen molecule in degassed ultra pure water by megasonic irradiation

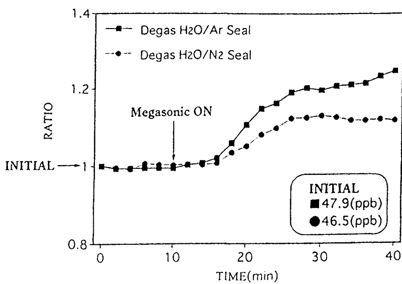

Fig. 11(b) Formation of oxygen molecule in degassed ultra pure water by megasonic irradiation

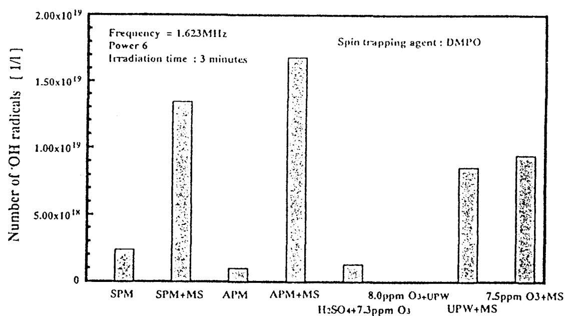

Fig. 12 Effect of megasonic irradiation on radical formation in each cleaning solutions

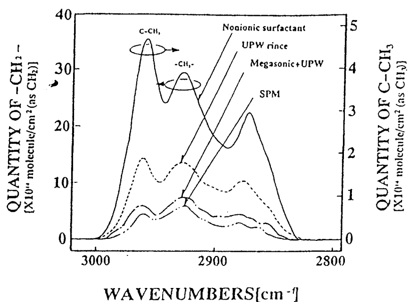

Fig. 13 Removal of organic contamination from wafer surface by UPW rince, UPW excited with megasonic and SPM

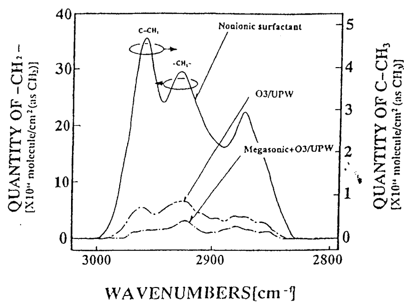

Fig. 14 Removal of organic contamination from wafer surface by Ozonized UPW and ozonized UPW excited with megasonic

STUDY ON MEGASONIC IN ADVANCED WET CLEANING PROCESS

K.Kubo, S.Ojima, M.Toda* and T.Ohmi
Department of Electronics, Faculty of Engineering, Tohoku Univ.
Aza Aoba, Aramaki, Aoba-ku, Sendai, Japan, 980
TEL:81-22-263-9395, FAX:81-22-263-9396
*Department of Materials Science and Engineering, Faculty Engineering, Yamagata Univ.
Jyonan, 4-Chome, Yonezawa, Japan
TEL:81-238-26-3165, FAX:81-238-26-3165

In this report we studied on influence of Ar, N2, and O3 dissolved ultra pure water with megasonic irradiation. We confirmed that the megasonic irradiation and the variation of dissolved gas drastically changes the characteristics of the ultra pure water, e.g., specific resistances, pH, ORP, dissolved hydrogen, etc. It is expected that the control of the amount and species of dissolved gas in the ultra pure water is capable for changing the effect on the Si wafer. For example, the removal efficiency of photo resist, prevention of oxidation in rinse water, etc. Furthermore, we made clear the effect and mechanism of hydrocarbon removal with megasonic irradiation. High removal efficiency of the organic contaminants by ozonized ultra pure water is further enhanced by the addition of megasonic irradiation. There is no relation between oxidation of the silicon surface and the decomposition of the organic contaminants. The radicals formed by the megasonic irradiation mainly contribute to the decomposition of the organic compounds.

INTRODUCTION

To keep the ultra clean wafer surface at anytime, it is necessary to control all process parameters perfectly[1]. Therefore, constant composition of cleaning solutions must be maintained. Fig.1 shows the total room temperature new wet cleaning process and conventional RCA cleaning process[2]. In conjunction with dramatic reduction of ultra pure water and chemicals, chemical vapor evaporation becomes negligibly small.

In the study reported on this article, it has been found that hydrocarbon contaminated on as-received wafer very heavy can be removed when the wafer is rinsed with ultra pure water dissolved O3, N2 and Ar gas with megasonic irradiation. We found the change of ultra pure water characters with megasonic irradiation. This is due to the only reaction process of radicals formed from ultra pure water oneself and dissolved gas with megasonic irradiation.

In the new cleaning process, ultra pure water is main cleaning agent. Therefore, it is necessary to make clear the influence of ultra pure water with megasonic irradiation and

dissolved gas.

EFFECT & MECHANISM OF HYDROCARBON REMOVAL

Measurement shown in Fig.2-4 was made for the wafer as-received, which is severely contaminated with hydrocarbons during the storage in plastic box, followed by the treatment with DHF.

Fig.2 shows the amount of hydrocarbon contamination on the wafer measured by FT-IR-ATR method. Furthermore, additional megasonic irradiation to the ozonized ultra pure water completely remove the organic contaminants down to the detection limit of the FT-IR-ATR method. This is the surprising fact that highly effective cleaning without strong acid SPM(H_2SO_4/H_2O_2) at high temperature is realized by the ozonized ultra pure water with the megasonic irradiation. Since this process requires much less equipment for the treatment of the chemical wastes and exhaust air, we can expect the drastic change in the semiconductor manufacturing process.

The FT-IR peaks of Si-Hx and SiO_2 on silicon substrate are shown in Fig.3 and Fig.4 respectively. Si wafer surface is oxidized immediately (within 1 second) by dipping in the SPM(H_2SO_4/H_2O_2) solution. The oxidation of the silicon substrate surface is much slower in the ozonized water. Especially, the oxidation does not proceed in the ozonized water with megasonic irradiation. Thus, there is no relation between the oxidization of silicon and the decomposition of organic contaminants, i.e., radicals formed by megasonic irradiation dominantly contributes to the decomposition of the organic compounds.

Fig.5 shows the amount of OH radicals and the redox potential of various cleaning solutions. The OH radicals were detected by ESR(Electron Spin Resonance) using 5,5-dimethyl-1-pyrroline-N-oxide (DMPO) as the spin trapping agent[3][4]. No radicals were detected in the ozonized water. However, OH radicals were detected for the first time in the SPM and APM solutions even without the megasonic irradiation. The megasonic irradiation to the ultra pure water and ozonized ultra pure water generates extremely high concentration of OH radicals, though the amount of OH radicals is remarkably small in SPM, APM, and SPM/O_3.

The OH radicals generated in the ultra pure water or ozonized ultra pure water are known to be capable of cleaning the C-C chemical bond directly and have high energy. Ozonized water with the megasonic irradiation perfectly removes the carbon contaminants by the attacks of radicals and synergistic effect of active oxygen. The radicals were not detected in the ozonized ultra pure water without the megasonic irradiation. Therefore, the organic compounds are estimated to be decomposed by the extraction of the electron in the solution which has high redox potential. When the megasonic is irradiated to the ozonized water, the contribution of the OH radicals is dominant rather than the redox potential.

INFLUENCE OF DISSOLVED GAS AND MEGASONIC

We found the radicals formation in ultra pure water with megasonic irradiation. Especially, in case of dissolved Ar gas in ultra pure water, we found the numbers of radicals(3.4×10^{18} pieces), in ultra pure water per 1 liter within 3 minutes megasonic irradiation. This was about twice radical formation numbers in dissolved N2 gas into the ultra pure water. It was able to expect the big influence of ultra pure water, when the many number of radicals formed in ultra pure water (without megasonic) have carbon removal efficiency on Si wafer. But we were able to expect that the much more effect of carbon removal efficiency with megasonic irradiation, in dissolved Ar or N2 gas into the ultra pure water. And so, we study on the character change of dissolved Ar, N2 or O3 into ultra pure water with megasonic.

Fig.6 shows the schematic diagram of experimental flow. At first, dissolved N2 gas, which was dissolved to remove the oxygen, was removed by the Film Degassing Unit and vacuum pump. Next, it is possible to dissolve the gasses such as Ar or N2 in a controlled manner using the Film Dissolved Gas Unit. In addition, O3 gas can be dissolved using the Mixing Ejector. The ultra pure water with controlled dissolved gassed such as Ar, N2, Ar+O3, and N2+O3 obtained as described above was introduced to quartz inner bath, which is irradiated by megasonic indirectly. The ultra pure water was analyzed by sampling from the inner bath using various monitors. The megasonic used is the frequency of 0.95 MHz and the maximum output of 1200W. The upper part of the megasonic bath was covered by the Gas Seal Shade, which is made of PFA. The remaining space was filled with Ar or N2 gas with the flow rate of 2 (l/min) to avoid the contamination from clean room air. The outer bath was filled with ultra pure water with the flow rate of 1.3 (l/min) to minimize the temperature rise by the megasonic irradiation. Inner bath volume is 5 (l) and outer bath volume is 10(l).

1. INFLUENCE FOR ULTRA PURE WATER

Fig.7 shows the variation of the redox potential of the degasified ultra pure water by megasonic irradiation. These are the case that Ar or N2 gas was dissolved into the degasified ultra pure water. The result shows that the dissolution of Ar makes the redox potential lower though the effect was not prominent.

The formation of hydrogen by megasonic irradiation is detected as shown in Fig.8. Especially, the amount of hydrogen is remarkable when Ar is dissolved degasified ultra pure water. Therefore the megasonic irradiation into the ultra pure water is generated the hydrogen by the recombination of H radicals which was formed by the megasonic It makes the redox potential lower, in other words, makes the ultra pure water slightly reducible.

Fig.9 show the time dependence on specific resistance in Ar or N2 dissolved degasified ultra pure water with megasonic irradiation. The data of specific resistances decrease very much in dissolved Ar into the degasified ultra pure water with megasonic irradiation.

Fig.10 shows the generation of H_2O_2. But in this case, ultra pure water which introduced to inner quartz megasonic bath, include original dissolved N_2 gas very much. Because, we did not run the film degassing unit. In case of sealed by Ar, it is possible to detect the H_2O_2. But in case of Sealed by N_2, it is no detect. In case of sealed by N_2, the generated radicals(·H, ·OH, [O]) with megasonic irradiation, react to dissolved N_2, which include ultra pure water, and generate the ions(NH_4^+, NO_3^-, NO_2^-). We think that the radicals (·H, ·OH, [O]) do not react on the recombination. In case of dissolved Ar in degasified ultra pure water, the megasonic irradiation generate the radicals very much. Therefore, it is possible to make recombination process. Of course, it make the ion generation process.

Fig.11 shows the ion generation in degasified ultra pure water with megasonic irradiation. It did not make the ion generation in case of clean room air exposure with megasonic irradiation. By reason of the selective dissolution from air for example O_2 and CO_2, which have a large number of solubility, the N_2 from air did not dissolve into the ultra pure water. Of course, the ultra pure water is include the very low volume of dissolved N_2 by film degassing unit. But in case of Ar and N_2 seal with megasonic irradiation, it makes a large number of ion generation. But in case of Ar seal with megasonic, it makes ions. When the megasonic irradiate to the dissolved Ar from seal gas into degasified ultra pure water, it generate the hydrogen radical(·H) very much. This hydrogen radical(·H) reacted on very small amount of dissolved remain N_2 gas, which can not remove completely from ultra pure water by film degassing unit. Namely, it is possible to suggest that the dissolved Ar in degasified ultra pure water with megasonic irradiation make the active state.

2. INFLUENCE FOR OZNIZED ULTRA PURE WATER

Fig.12 shows the amount of generated ion in degasified ultra pure water with O_3 and Ar, with O_3 and N_2 irradiated by megasonic. A large amount of ion generated by megasonic irradiation except Ar dissolved ultra pure water. Because the very little dissolved N_2 left in degasified ultra pure water was decreased by added Ar and O_3. But radicals were generated and there were no molecules and atoms to react, radicals reacted each other generated H_2, O_2, H_2O and H_2O_2. Much ions were generated in ozonized ultra pure water with megasonic irradiation under clean room air. And the phenomenon is different from ultra pure water as shown in Fig.12. This fact shows that megasonic irradiated ozonized ultra pure water make a large of active state.

Fig.13 shows the variation of the redox potential [E]. The dissolution of Ar has much larger effect to lower the potential than that of N_2.

Fig.14 shows the variation in the ozone concentration with the megasonic irradiation. In the case of ($Ar+O_3$)-dissolved water, the dissolved ozone molecules are completely decomposed by the megasonic irradiation. Though they still remain in the case of N_2-dissolved water. From this fact, we can attribute the lower redox potential of

Ar-dissolved water to the decomposition of the ozone molecules. The small change in the case of N2-dissolved water can be explained by the formation of HNO3. The decomposition of O3 itself and the transfer to the gas phase have to be considered. Quantitative analyses are one of the current subject of our research.

Fig.15 shows the reactions process. There are many and complicated reactions in the ultra pure water with dissolved Ar, N2 or O3 and with the megasonic irradiation. Furthermore, additional reactions are expected to occur with the dissolved O3 with megasonic irradiation e.g., spontaneous decomposition reactions proposed by J.Weiss[5]. It can be imagined that many processes are proceeding simultaneously and the it is considerably difficult problem to be fully understood.

CONCLUSION

Our study on the chemical side of the megasonic irradiation. has brought the knowledge which contributes extremely on the silicon wafer surface cleaning process. The results are summarized as follows:

(1) The megasonic irradiation and the variation of dissolved gas drastically changes the characteristics of the ultra pure water, e.g., , specific resistances, pH, ORP, dissolved oxygen, dissolved hydrogen, etc. It is expected that the control of the amount and species of dissolved gas in the ultra pure water is capable for changing the effect on the Si wafer. Give examples as follows:

<a> Ar·O3/H2O + Megasonic	: Removal efficiency of Photo resist
<b> H2O + Megasonic	: Prevention of oxidation in rinse
<c> Ar·H2/H2O + Megasonic	: Perfect hydrogen termination & Prevention of oxidation in rinse

(2) High removal efficiency of the organic contaminants by ozonized ultra pure water is further enhanced by the addition of megasonic irradiation.

(3) There is no relation between oxidation of the silicon surface and the decomposition of the organic contaminants, i.e., radicals formed by megasonic irradiation dominantly contributes to the decomposition of the organic compounds.

REFERENCES

[1] T.Ohmi, M.Miyashita, M.Itano and T.Imaoka, Proceedings of Microcontamination, **91**, 491(1991)

[2] W.Kern and D.A.Puotien, RCA Review, **31**, 187 (1970)

[3] M.Toda, M.Kato, K.Mitsumori and T.Ohmi, Proceedings of 25th Symposium on ULSI Ultra Clean Technology Sympo., Ultra Clean Society, pp.20-32,Tokyo(1995)

[4] T. Kondo, J. Gamson, J . B. Mitchell and P. Riesz, INT. J. RADIAT.BIOL, Vol.54, No. 6, pp. 955-962, (1988)

[5] J.Weiss, Transactions of the faraday Soc., **31**, 668, (1935)

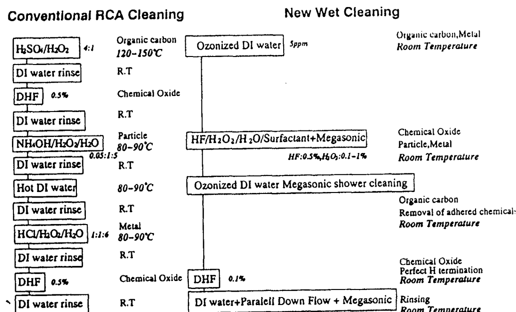

Fig.1 New total room temperature wet cleaning process vs. conventional RCA process

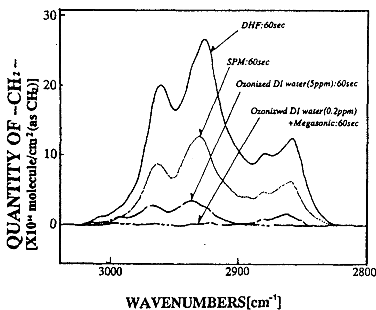

Fig.2 The FT-IR-ATR peaks of hydrocarbon contamination on silicon substrate

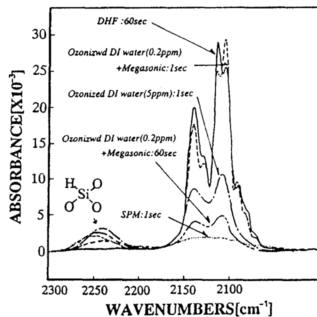

Fig.3 The FT-IR-ATR peaks of Si-Hx on silicon substrate

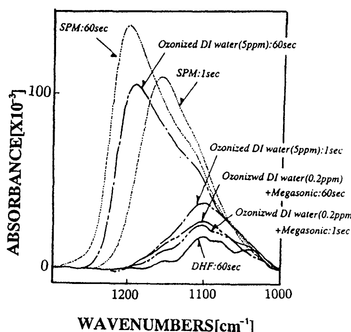

Fig.4 The FT-IR-ATR peaks of SiO2 on silicon substrate

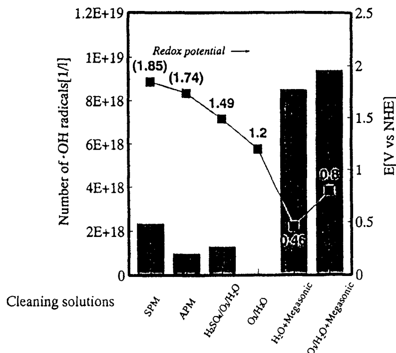

Fig.5 The amount of OH radicals and the redox potential of various cleaning solutions. The OH radicals were detected by ESR(Electron Spin Resonance) using 5,5-dimethyl-1-pyroline-N-oxide (DMPO) as the spin trapping agent.

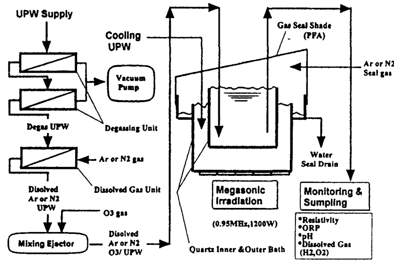

Fig.6 The schematic diagram of experimental system flow.

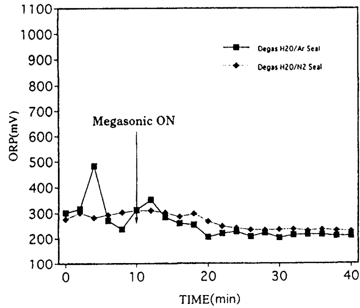

Fig.7 The variation of the redox potential of the degasified ultra pure water by the irradiation. of megasonic

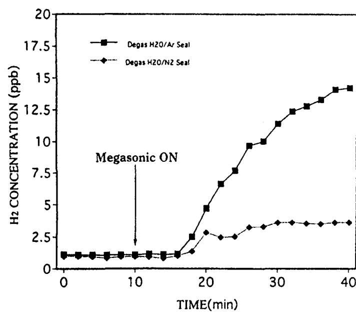

Fig.8 The formation of hydrogen gas in ultra pure water with megasonic irradiation.

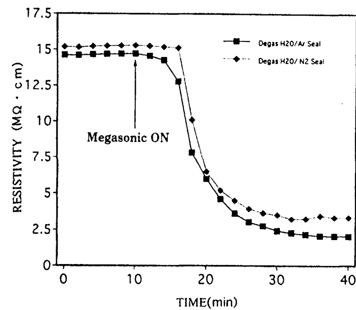

Fig.9 The time dependence on specific resistance in Ar or N2 dissolved degasified ultra pure water with megasonic irradiation.

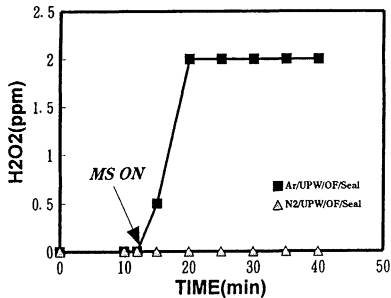

Fig.10 The generation of H2O2 with megasonic irradiation in ultra pure water.

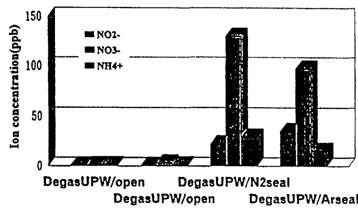

Fig.11 shows the ion generation in degasified ultra pure water with megasonic irradiation.

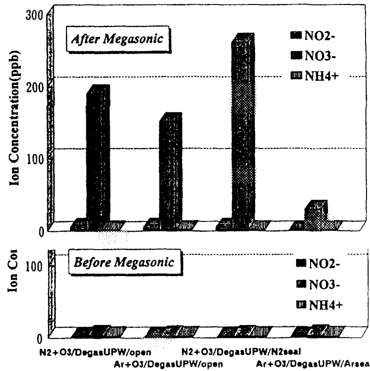

Fig.12 shows the amount of generated ion in degasified ultra pure water with O3 and Ar, with O3 and N2 irradiated by megasonic.

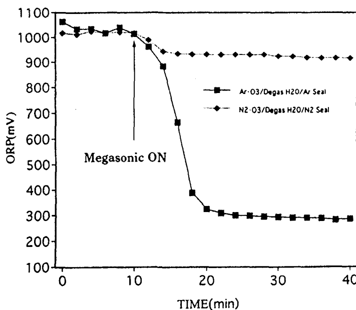

Fig.13 The variation of the redox potential [E] with the megasonic irradiation.

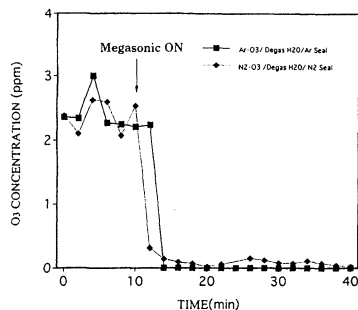

Fig.14 The variation in the ozone concentration with the megasonic irradiation.

■ Radical Formation Process

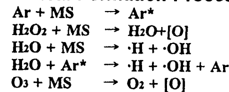

$Ar + MS \rightarrow Ar^*$

$H_2O_2 + MS \rightarrow H_2O + [O]$

$H_2O + MS \rightarrow \cdot H + \cdot OH$

$H_2O + Ar^* \rightarrow \cdot H + \cdot OH + Ar$

$O_3 + MS \rightarrow O_2 + [O]$

■ Recombination

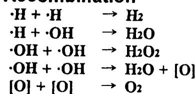

$\cdot H + \cdot H \rightarrow H_2$

$\cdot H + \cdot OH \rightarrow H_2O$

$\cdot OH + \cdot OH \rightarrow H_2O_2$

$\cdot OH + \cdot OH \rightarrow H_2O + [O]$

$[O] + [O] \rightarrow O_2$

■ Decomposition

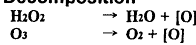

$H_2O_2 \rightarrow H_2O + [O]$

$O_3 \rightarrow O_2 + [O]$

■ Reaction

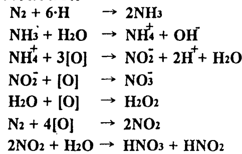

$N_2 + 6 \cdot H \rightarrow 2NH_3$

$NH_3 + H_2O \rightarrow NH_4^+ + OH^-$

$NH_4^+ + 3[O] \rightarrow NO_2^- + 2H^+ + H_2O$

$NO_2^- + [O] \rightarrow NO_3^-$

$H_2O + [O] \rightarrow H_2O_2$

$N_2 + 4[O] \rightarrow 2NO_2$

$2NO_2 + H_2O \rightarrow HNO_3 + HNO_2$

Fig.15 The reactions process. There are many and complicated reactions in the ultra pure water with dissolved Ar, N2 or O3 and with the megasonic irradiation.

IN-SITU VAPOR PHASE PROCESSES IN AN INTEGRATED CLUSTER SYSTEM FOR PRE-GATE OXIDE SILICON SURFACE CLEANING

Y. Ma,[a)] and M. L. Green

AT&T Bell Laboratories, Murray Hill, NJ 07974

Vapor phase pre-gate oxide surface preparation was studied in a high vacuum cluster tool. Sacrificial or native oxide was etched with vapor Hydrofluoride and trace metallic and Hydrocarbon contamination were removed with a UV/Cl_2 process. Surface residuals were analyzed with X-ray Photoluminescence Spectroscopy (XPS) and the surface morphology was investigated with Atomic Force Microscopy (AFM). Metal-Oxide-Semiconductor devices were fabricated on differently cleaned Si surfaces. The electrical properties of the SiO_2/Si interface and the SiO_2 integrity were characterized with Capacitance-Voltage (C-V) and Time-Dependent-Dielectric-Breakdown (TDDB) techniques.

I. INTRODUCTION

One of the most important processes in modern IC manufacturing is pre-gate oxide wafer surface preparation. It has been shown that the performance of Metal-Oxide-Semiconductor (MOS) devices depends on the cleaning processes prior to gate oxide growth.[1-5] However, with traditional manufacturing processes, wafers are transferred from tool to tool in a clean room after each process, as a result, exposed to the risk of re-contamination. For some critical process sequences such as gate oxide growth, the oxide should be grown immediately after wafer cleaning in order to reduce oxide defects and achieve high device yield.

To achieve contamination free manufacturing, clustering is one of the options. Cluster tools allow single wafer processing during which wafers are transferred under vacuum between process modules and the risk of re-contamination is reduced. Equipped with *in-situ* diagnostics, process stability can be better controlled. Single wafer processing becomes more and more appealing with larger wafer sizes. Vacuum compatible, vapor phase cleaning processes currently receive a lot of attention.[6-14] During vapor phase processes, oxides and other surface contaminants may be removed by reactions between reactive gases and surface layers/contaminants. Vapor phase processing also has the potential to clean smaller features, since wet processing is limited by solution surface tension. An additional advantage of vapor phase processing is the reduced chemical

---

[a)] Present address: AT&T Bell Laboratories, 9333 S. John Young PKWY, Orlando, FL 32819
E-mail address: orym@attme.cnet.att.com

consumption compared to wet batch processing. As a result, vapor phase processing is environmentally friendly.

In this paper, we report our study on *in-situ* vapor phase processing in a high vacuum integrated system. Silicon surface residuals, morphology after different process sequences were studied. Electrical properties of gate oxides and the SiO_2/Si interface formed by Rapid Thermal Oxidation (RTO) on the vapor phase cleaned surfaces were also investigated.

II. EXPERIMENTAL PROCEDURES

Substrates used were 5 inch Si(100) n-type with a resistivity of 3-5 Ω-cm. All samples were first subjected to a conventional Piranha cleaning procedure: H_2SO_4:H_2O_2=12.5:1 at 105°C for 10 minutes. Sacrificial oxides 100Å thick were grown in furnace at a temperature of 1000°C in O_2 atmosphere. Control wafers were given the standard wet clean: the sacrificial oxides were removed with 100:1 HF solution until hydrophobic, and RTO oxides was grown directly without any *in-situ* cleaning. All other wafers were loaded into the cluster tool (detail of the cluster tool was described elsewhere) [13] with the sacrificial oxides, after rinsing in DI water and spin drying in N_2. Reactive gases used for sacrificial oxides removal were Anhydrous HF (AHF) and methanol, with N_2 as a carrier gas. The flow rates of AHF, methanol and N_2 were 150 sccm, 200 sccm and 550 sccm, respectively. Process temperature was at 50°C and process pressure was at 200 Torr. With these process parameters, the oxide etch rate was 20Å/min. UV/Cl_2 cleaning took place at temperature of 100°C or 200°C for a period of 30 seconds to 10 minutes, at a pressure of 10 Torr, with a Cl_2 flow rate of 100 sccm. UV/O_3 process was accomplished at 50°C and 200 Torr with an O_2 flow rate of 1000 sccm. RTO oxides with nominal thickness of 55Å were grown at 1000°C in a pure O_2 atmosphere. Surface residues after cleaning were analyzed with XPS. Surface morphology was characterized with AFM. MOS structures of various sizes (0.0001-0.0016 cm^2) were then manufactured as the following: 2000Å of poly-Si was deposited and which was then subjected to a Phosphorous Ion Implantation at an energy of 40 KeV to a dose of $5x10^{15}/cm^2$; Aluminum was deposited as contacts after a dopants activation at 1030°C for 10 sec. in Ar atmosphere and drive-in process at 850°C for 60 min in N_2 with 2% O_2; MOS structures were then defined with a conventional lithographic procedure; Aluminum was deposited on back side of wafer for contacts; There was a post-metal forming gas annealing at 330°C for 30 min. SiO_2/Si interface trap densities were measured by C-V techniques while the integrity of the SiO_2 film was characterized by TDDB procedure where a constant current mode was used. C-V data were collected from three wafers of each process and 10 capacitors were measured on each wafer. The current density was 250 mA/cm^2 on capacitor dots with area of $4x10^{-4}$ cm^2. In the charge injection procedure, electrons were injected from the substrates with a positive gate bias.

III. RESULTS AND DISCUSSIONS

1. Surface Coverage

Si(100) surface after either aqueous HF or vapor HF etching is hydrophobic, indicating an Hydrogen passivated surface. Contrast to the monolayer Hydrogen surface coverage of an aqueous HF etched surface, a Multiple Internal Reflection Infrared study revealed a 2-3 monolayer Hydrogen surface coverage for a vapor HF etched one.[14] This implies a damaged Si surface structure and a strained Si-H surface bonding.

Surface residuals were characterized with XPS. Three typical cases are presented in Fig.1. Small amount (0.4 at %) of Fluorine (the peaks at 696.0 eV) was observed on an aqueous HF etched surface. The vapor HF process though left behind a much higher Fluorine, 3.6 at %, surface coverage. The Fluorine coverage disappeared after a following UV/Cl_2 process. Instead, surface was covered with Chlorine (see spectrum (c), peaks at 270.4 eV and 200.0 eV for Cl 2s and Cl 2p, respectively). The amount of the coverage was about 7.1 at %. The information about Oxygen and Carbon were not reliable since the XPS analysis was conducted in a separate analytical laboratory. Samples had to be taken out of the high vacuum chamber after *in-situ* surface cleaning. Care had been taken to minimize the contamination during the sample delivery. However, trace of hydrocarbon contamination was expected as indicated in the XPS spectra. The higher Carbon coverage from the UV/Cl_2 processed surface than both the aqueous and vapor HF cleaned surfaces was possibly due to the highly reactive nature of Chlorine.

2. Surface Morphology

Si/SiO_2 interfacial roughness usually results in higher leakage current or early dielectric breakdown of SiO_2 dielectric films.[15,16] Si surface microroughness can be increased during HF etching, chemical cleaning and even DI water rinse.[16,18,19] An atomically smooth surface is ideal for gate oxide formation.

As discussed above, the oxide etch rate fluctuates in the vapor HF oxide etching process. Overetching is required to guarantee a complete removal of the sacrificial oxide. Surface roughness due to the overetching is not desirable. Fig.2(a) is an AFM image from a Si(100) surface aggressively etched by vapor HF. The etching took place at 50°C, and at a chamber pressure of 200 Torr for a period of 3 minutes, equivalent to an oxide etch rate of 60Å/min. The Root-Mean-Square (RMS) roughness of this surface is 0.24 nm. As a comparison, the result from a Si(100) surface etched with 100:1 aqueous HF for 2 minutes is shown in Fig. 2(b). Here, the RMS value is 0.26 nm. Therefore, no difference has been observed between vapor and aqueous HF etched Si(100) surfaces.

Although the Vapor HF etching does not cause Si surface roughness, UV/Cl_2 process results in surface pitting. Small pits with diameter of 50-100 nm were formed on Si surface in just 30 second of UV/Cl_2 exposure. With longer UV/Cl_2 exposure period, pits grow from 100-150 nm (1 min) to about 500 nm (10 min). However, pits depth (measurable with AFM tip) changed little from 4.5 nm (2 minutes) to 4.0 nm (10 minutes) exposure. It is interesting to note however, that outside the pits area, surfaces are as smooth as a standard Si surface with an RMS of about 0.2 nm.

3. Electrical Properties of Si/SiO_2 Interface and SiO_2 Gate Dielectric

First, we present results from different cleaning sequences. The four basic in-situ cleaning sequences studied are: (a) single step vapor HF sacrificial oxide etching; (b) two step vapor HF followed by an UV/Cl_2 process; (c) two step vapor HF followed byUV/O_3;

and (d) three step vapor HF, UV/Cl_2 and UV/O_3. The samples prepared with these cleaning processes are identified as sample A, B, C and D, respectively, throughout the paper. Refer to Table I for definitions.

Table I. Mid-gap D_{it} at SiO_2/Si(100) interfaces and Q_{bd} of RTO oxides grown on both conventional and *in-situ* vapor phase cleaned Si surfaces

Sample Identification	Vapor Phase Cleaning Procedures	Mid-gap D_{it} (10^{10}/cm^{2}eV)	Q_{bd} at 50% cumulative failure (C/cm^2)
control	none	6.2	9.3
A	Vapor HF	5.2	4.8
B	Vapor HF + UV/Cl_2	8.0	12.5
C	Vapor HF + UV/O_3	4.2	7.6
D	Vapor HF + UV/Cl_2 + UV/O_3	5.7	11.6

Table I summarizes the mid-gap trap density (D_{it}) at SiO_2/Si interface inside Si band gap for all wafers. The mid-gap D_{it} for the control sample is 6.2 x 10^{10}/cm^{2}eV. This value is a little higher than optimized furnace grown oxide (normally 1-2 x 10^{10}/cm^{2}eV) but typical for RTO oxides.[20] For the four *in-situ* cleaned wafers, sample C shows the lowest mid-gap D_{it}, 4.2 x 10^{10}/cm^{2}eV. Samples A, B and D all display equivalent interface properties as compared to the control.

To further study the quality of the SiO_2/Si interface, MOS capacitors were electrically stressed with hot electron injection. The injection normally results in Si-H bond breakage and forms P_b type defects at the SiO_2/Si interface.[21] This effect will be reflected in an increase of interface trap density. An increase of interface trap density not only shift the device threshold voltage, more critically it reduces the device operation speed. In Fig.3, the increases of the mid-gap D_{it} after injection are plotted as a function of total injected charge density. Except for one case (sample D after a 0.25C/cm^2 charge injection), all *in-situ* cleaned wafers show a lower generation of interface trap density as a function of charge injection. The lower generation of interface trap density in samples A and C is mainly attributed to surface Fluorine coverage after vapor HF etching. Unlike a wet HF rinsed surface, the vapor HF etched Si surface has a much higher Fluorine surface coverage because no water is involved (see Fig.1). Fluorine mainly exists in the form of Si-F bonds. Since Si-F bonds (5.5 eV) are stronger than the Si-H bonds (3.0 eV), less P_b type defect formation is expected.[22] Sample C displays the same trend as sample A under electron injection. This can be attributed to the existence of Fluorine in the near region of SiO_2/Si interface even after UV/O_3 oxidation. This argument is supported by the fact that a small amount of Fluorine were detected at SiO_2/Si interface after RTO and is consistent

with the results from samples B and D where higher D_{it} were generated because Fluorine were lost during UV/Cl_2 process as shown in Fig.1.

MOS device cumulative failure is plotted as a function of Q_{bd} in Fig.4. Q_{bd} at 50% cumulative failure for the control sample is 9.3C/cm^2, a typical value for a 55Å oxide. [23] Although sample A has a better SiO_2/Si interface quality, its oxide integrity is degraded significantly (see Table I). According to Ohmi *et al*, traces of hydrocarbons were observed on the vapor HF etched Si surface.[16] The source of the Hydrocarbon could be Methanol used in the SiO_2 etching process. The hydrocarbons may be incorporated into the SiO_2 film during RTO which contributes to the degradation of SiO_2 integrity. However, with an additional UV/Cl_2 cleaning, the reliability of the oxide is significantly improved (sample B). The Charge-to-Breakdown was increased to 12.5 C/ cm^2. This is a surprising result. The AFM measurement has indicated that surface is roughened by a UV/Cl_2 process. An earlier dielectric breakdown is expected for the oxide grown on such rough surface. It is possible then that there are other factors in affecting SiO_2 integrity. We will discuss this issue in detail later in the paper. As compared with sample A, sample C shows an improvement of SiO_2 quality. Q_{bd} is increased to 7.6C/cm^2 with no early breakdowns observed, since there is no UV/Cl_2 induced surface damage. The UV/O_3 process normally removes hydrocarbon contamination and forms a thin SiO_2 layer, about 5-10Å. The result of sample C also indicates that the oxide formed during the UV/O_3 cleaning process has a high integrity. The effect of UV/O_3 after UV/Cl_2 is not obvious (sample D) because of the excellent cleaning consequence of the UV/Cl_2 process.

In order to further understand the cleaning effect from the UV/Cl_2 process, the cleaning period of UV/Cl_2 step in Process (b) was varied from 30 seconds to as long as 10 minutes. The interface trap densities (D_{it}) at Si mid-gap measured with C-V technique indicate a mid-10^{10}/cm^{2}eV. The D_{it} varies little with the cleaning period, except the 30 second cleaned one with a value of 1.8×10^{10}/cm^{2}eV. For all the samples, oxide fixed charge calculated from the flat band voltage is in the range of mid-10^{10}/cm^2.

The SiO_2/Si interface quality was studied with hot electron injection test. As indicated before, amount of mid-gap D_{it} increase under a current stress reflects the strength of SiO_2/Si interface. Fig.5 shows mid-gap D_{it} increase as a function of the total injected charge. To simplify the figure, only three cleaning period cases are presented as compared with the control sample. The 30 second cleaned sample indicates a lowest interface trap generation rate among the samples compared. With longer cleaning period, higher interface generation rate was observed. With increase the cleaning period longer than one minute, the interface quality began to degrade, a signature of damaged surface by the UV/Cl_2 process. However, up to 10 minutes cleaning, the interface still presented a reasonable behavior as capacitors.

The effect of surface roughness on the electrical property can be well characterized with the TDDB technique. The results of such characterization is shown in Fig.6, where MOS device cumulative failure is plotted as a function of total injected charge density. All the UV/Cl_2 cleaned samples show a higher charge-to-breakdown behavior (12-18 C/cm^2 at 50% failure) than the control sample (9.2 C/cm^2). The 30 second UV/Cl_2 cleaning results in an oxide with a Q_{bd} of 18 C/cm^2, almost a 100%

improvement to the control sample. Longer period UV/Cl_2 exposure degrades integrity of oxide (lower Q_{bd}), particularly in the lower charge injection range.

From a superficial look, our results are contradictory to the common knowledge about surface roughness, i.e., rougher surface results in a degraded SiO_2/Si interface as well as SiO_2 integrity. In studies of pre-gate oxide cleaning, two most addressed issues are the surface cleanliness and roughness. Our study indicates that surface roughness is not a controlling factor. The surface cleanliness also contributes significantly. In conventional gate oxide processing, surface cleaning and oxide growth are carried out in two different tools. The Si surface is most likely re-contaminated by, for example, hydrocarbons during samples transference. For an aqueous hydrogen fluoride rinsed Si surface, stable hydrogen passivated surfaces are obtained. However, trace metallic contamination and hydrocarbons are left behind on Si surface.[16,24] This contamination will contribute to the degradation of the SiO_2/Si interface and SiO_2 dielectrics. The degradation is most likely enhanced by a roughened surface, if there is any. In the vapor phase cleaning process, surface ultra cleanliness is provided by UV/Cl_2 process which eliminates both trace metallic contamination[9,13] and hydrocarbons.[14] This can be attributed to metal and hydrocarbon contamination removal capabilities of UV/Cl_2 process as reported before. Although the sacrificial oxidation procedure plays a role of metal contamination removal, Fujino *et al* [25] have reported that part of the contamination still existed at SiO_2/Si interface after the procedure. The hydrocarbon contamination left on the Si surface after vapor HF process was removed through the formation of volatile species such as Carbon Chlorides. The cleaned surfaces has never been exposed to a clean room atmosphere, as wafers are transferred under vacuum to an RTO chamber. The important issue is that Si surface maintains its cleanliness at the moment when oxidation starts. Oxides were grown on the "real" clean surface. Our results suggest that Si surface after UV/Cl_2 cleaning procedure is so clean that higher surface roughness can be accommodated.

IV. SUMMARY AND CONCLUSION

In summary, we have investigated vapor phase processing in a high vacuum integrated system. Silicon surface after vapor HF etching has a higher surface Fluorine coverage and is as smooth as an aqueous HF etched one. UV/Cl_2 process after the vapor HF etching eliminates the Fluorine coverage and causes surface pitting. MOS devices fabricated on vapor HF and UV/Cl_2 cleaned surface displays a superior quality of SiO_2 integrity in terms of charge-to-breakdown and a comparable SiO_2/Si interface quality in terms of the interface density and its generation rate under a current stress. Both surface roughness and cleanliness are critical to the integrity of gate oxide. However, with *in-situ* wafer processing, a reliable gate oxide can be achieved on even heavily roughed surface.

ACKNOWLEDGMENTS

The authors acknowledge J. Sapjeta, K. Konstadinidis, K. Hanson, R. Opila, L. C. Feldman, T. W. Weidman of AT&T Bell Laboratories and J. Ruzyllo, K. Torek of

Pennsylvania State University for their contribution to the paper; G. Higashi and L. Manchanda for beneficial discussions; K. Krisch for C-V measurement support; R. Shah and G. Smolinsky of SEMATECH for funding.

REFERENCES

1. W. Kern, J. Electrochem. Soc., **137**, 1887 (1990)
2. S. R. Kasi, M. Liehr, P. A. Thiry, H. Dallaporta and M. Offenberg, Appl. Phys. Lett., **59**, 108 (1991)
3. L. J. Huang and W. M. Lau, Appl. Phys. Lett., **60**, 1108 (1992)
4. T. Yasuda, Y. Ma, S. Habermehl and G. Lucovsky, Appl. Phys. Lett., **60**, 434 (1992)
5. X. L. Xu, R. T. Kuehn, M. C. Ozturk, J. J. Wortman, R. J. Nemanich, G. S. Harris and D. M. Maher, J. Electronic Material, **22**, 335 (1993)
6. B. E. Deal, M. A. McNeilly, D. B. Kao, and J. M. deLarios, *Proc. of the First International Symp. on Cleaning Technol. in Semicond. Dev. Manufacturing*, The Electrochemical Society Inc., Pennington, NJ, **90-9**, 121 (1989)
7. J. Ruzyllo, K. Torek, C. Daffron, R. Grant and R. Novak, J. Electrochem. Soc., **140**, L64 (1993)
8. A. Izumi, T. Matsuka, T. Takeuchi and A. Yamano, *Proceedings of the Second International Symp. on Cleaning Technol. in Semicond. Dev. Manufacturing*, p.260, 1991
9. T. Ito, R. Sugino, S. Watanabe, Y. Nara and Y. Sato, same as reference 6, 114 (1989)
10. M. Wong, M. M. Moslehi and R. A. Bowling, J. Electrochem. Soc. , **140**, 205 (1993)
11. R. Novak, Solid State Technology, March, 39(1988)
12. Y. Ma, M. L. Green, K. Torek, J. Ruzyllo, R. Opila, K. Konstadinidis, D. Siconolfi and D. Brasen, J. Electrochem. Soc., to be published
13. Y. Ma, M. L. Green, L. C. Feldman, J. Sapjeta, K. J. Hanson, and T. W. Weidman, J. Vac. Sci. Technol. **B 13**(4), 1460(1995)
14. Y. Ma, Y. J. Chabal, M. L. Green and S. B. Christman. (unpublished)
15. A. H. Carim and A. Bhattachayya, Appl. Phys. Lett., **46**, 872 (1985)
16. T. Ohmi, M. Miyashita, M. Itano, T. Imaoka, and I. Kawanabe, IEEE Trans. on Elect. Dev., Vol. 39, 537(1992)
17. T. Kitano, E. Hasegawa, M. Tsukiji, K. Akimoto, S. Kimura, S. Saito and K. Ikeda, Jpn. J. Appl. Phys., Vol. 32, p. L1581(1993)

18 G. S. Higashi, R. S. Becker, Y. J. Chabal and A. J. Becker, Appl. Phys. Lett., **58**(15) 1656(1991)

19 M. Mirose, M. Hiroshima, T. Yasaka and S. Miyasaki, J. Vac. Sci. Technol. **A12**(4) 1864(1994)

20 H. Fukuda, T. Arakawa and S. Ohno, IEEE Trans. Elect. Dev., **39**, 127 (1992)

21 E. H. Poindexter and P. J. Caplan, J. Vac. Sci. Technol., **A 6**, 1352 (1988)

22 T. P. Ma, J. Vac. Sci. Technol. **A 10,** 705(1992)

23 Y. Okada, P. J. Tobin, V. Lakhotia, W. A. Feil, S. A. Ajuria and R. I. Hegde, Appl. Phys. Lett. **63**(2), 194(1993)

24 Y. Ma, T. Yasuda, S. Habermehl, and G. Lucovsky, J. Vac. Sci. Technol. **A 10**, 781(1992)

25 N. Fujino, K. Hiramoto, M, Sano, K. Murakami, H. Horiye, Y. Oka and S. Sumita, Proceeding of Semiconductor Silicon, The Electrochemical Sociaty Inc., Pennington, New Jersey, **Vol. 90-7**, p.709 (1990)

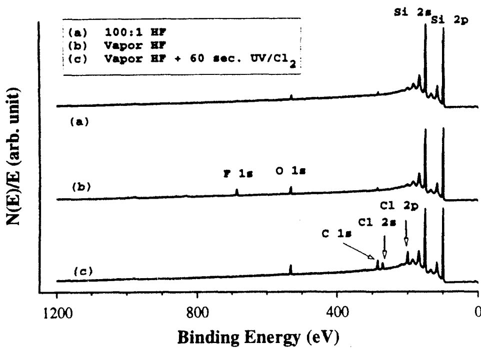

Fig.1, XPS spectra from (a) aqueous HF, (b) vapor HF and (c) UV/Cl_2 cleaned Silicon surface.

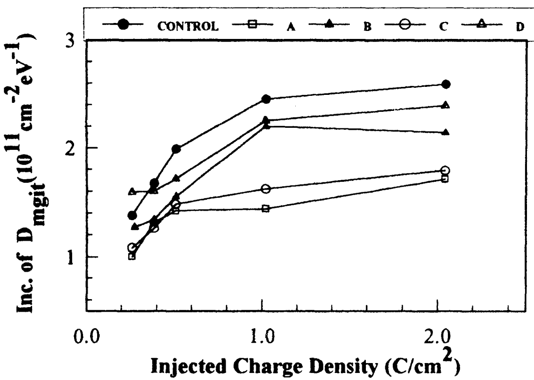

Fig.3, Increases of Si/SiO_2 interface trap density as a function of total injected charge density. Legends indicate the control sample and the samples with different in-situ cleaning procedures as defined in Table I.

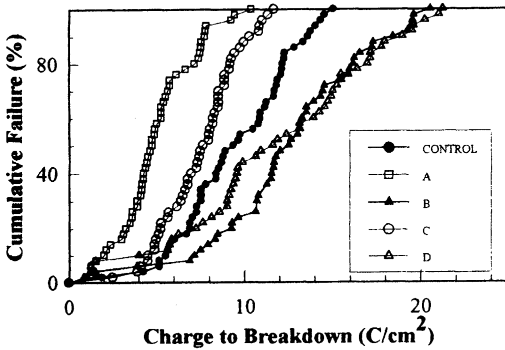

Fig.4, Cumulative failure of MOS devices as a function of Q_{bd}. Legends indicate the control sample and the samples with different in-situ cleaning procedures as defined in Table I.

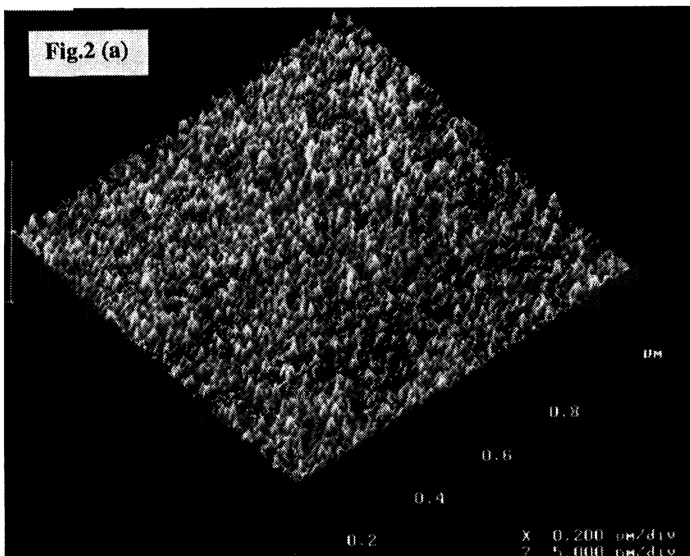
Fig.2 (a)
um
0.8
0.6
0.4
0.2
X 0.200 um/div
Z 5.000 nm/div

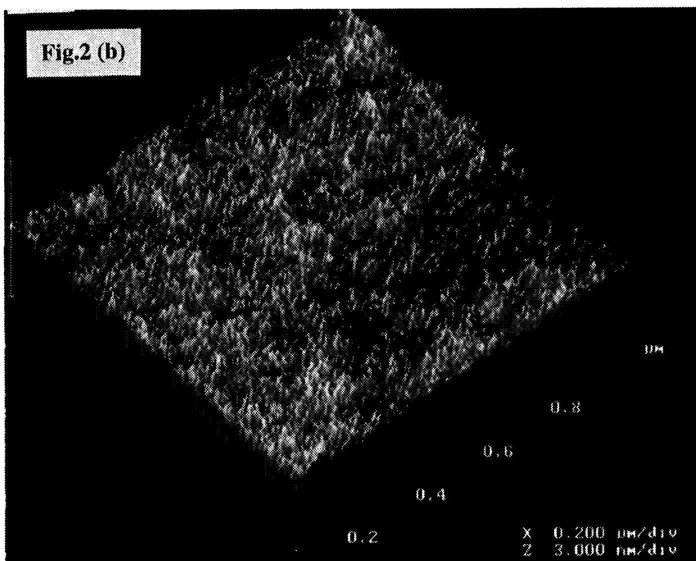
Fig.2 (b)
um
0.8
0.6
0.4
0.2
X 0.200 um/div
Z 3.000 nm/div

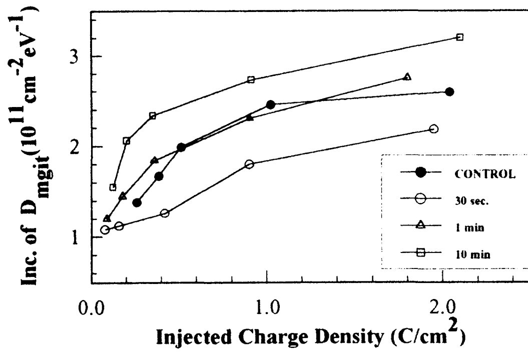

Fig.5, Increases of Si/SiO_2 interface trap density as a function of total injected charge density. Legends indicate the control sample and the samples with different UV/Cl_2 cleaning period.

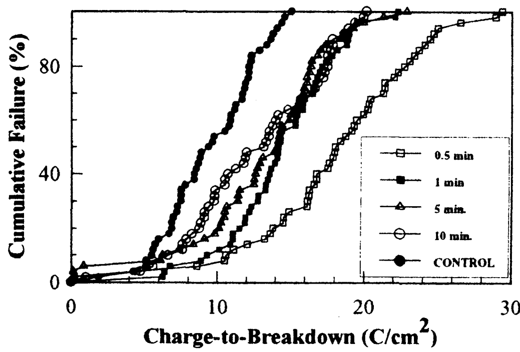

Fig.6, Cumulative failure of MOS devices as a function of Q_{bd}. Legends indicate the control sample and the samples with different UV/Cl_2 cleaning period.

THE REACTION OF VAPOR HF WITH CHEMICALLY FORMED SILICON OXIDE: PRODUCTION OF STABLE HYDROGEN-TERMINATED SURFACES

J. M. Barnett, P. A. Grothe, and J. S. Martin
FSI International, 322 Lake Hazeltine Dr., Chaska, MN 55318-1096

R. A. Carpio and B. W. Fowler
SEMATECH, 2706 Montopolis Dr., Austin, TX 78741

Vasu Atluri and Nicole Herbots
Department of Physics and Astronomy
Arizona State University, Tempe, AZ 85287

ABSTRACT

Surface infrared spectroscopic analysis reveals that processing a chemically grown oxide with a gaseous H_2O/HF mixture (vapor HF) produces hydrogen terminated silicon for standard 150 and 200 mm diameter Si(100) wafers; the infrared signal intensity is dominated by dihydrides, $-SiH_2$. An appreciable amount of trihydrides, $-SiH_3$, are also observed, but the intensity associated with monohydrides, -SiH, is small relative to that of the dihydride or trihydride. Subsequent to the vapor HF etch process, rinsing increases the amount of hydrogen terminated silicon. Simple chemical intuition can account for this observation. Two different rinse processes are compared: a standard water rinse and a proprietary rinse. While the amount of hydrogen terminated silicon is statistically equivalent for the two rinses, the measured contact angle increases to 75° with a proprietary rinse. The total atomic surface coverage measured by ion beam analysis did not correlate with contact angle measurements. Additionally, the $Si-H_x$ (x=1-3) surface infrared integrated intensities and contact angles did not exhibit a straightforward correlation.

INTRODUCTION

The impetus to advance silicon cleaning technology originates from the increasing complexity associated with silicon processing where approximately 300 process steps are involved in manufacturing a 256 megabit memory device. Because many processes leave the silicon surface in a reactive, uncharacterized, or "impure" state, a silicon surface may be incompatible with respect to the subsequent process. To circumvent this issue, a cleaning process is often introduced as a means to either preserve or restore the chemical and electrical integrity of the requisite surface.

In this regard, many cleaning steps employ a well-established etching reaction: that of hydrofluoric acid with silicon oxide, typically depicted phenomenologically as

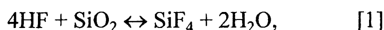

$$4HF + SiO_2 \leftrightarrow SiF_4 + 2H_2O, \qquad [1]$$

or as its variant,

$$6HF + SiO_2 \leftrightarrow H_2SiF_6 + 2H_2O, \qquad [2]$$

where Eqs. (1) and (2) convey only stoichiometry and not a mechanism. Concomitant with HF oxide dissolution, surface impurities and defects are removed, thereby restoring the uniquely favorable interfacial properties of the underlying silicon. Aqueous HF processing of oxidized silicon results in a hydrogen terminated surface; that is, aqueous HF processing transforms surface Si-O bonds into surface Si-H bonds. It is similarly known that a gaseous mixture of HF and H_2O, vapor HF, reacts with oxidized silicon; however, the propensity for this reaction to produce hydrogen terminated silicon has not been firmly established, and this issue is herein addressed.

Silicon surfaces etched in aqueous HF were initially thought to be fluorine terminated, but surface infrared spectroscopy (SIRS) proved such surfaces were hydrogen terminated (1). It is now known that thermodynamically stable Si-F bonds are kinetically unstable in an aqueous medium (2, 3); fluorine-terminated surfaces are thus largely an etching intermediate, and ultimately hydrogen terminated surfaces are produced, leaving behind a minority of sites where Si-F bonds might exist (4).

Polarized SIRS is a powerful surface probe because it discriminates between mono-, di-, and trihydrides, designated as -SiH, -SiH_2, and -SiH_3, respectively (5, 6, 7, 8, 9, 10, 11, 12). For a given polarization, each of the hydride species produces a spectral signature indicating not only ideally terminated silicon, but also the corresponding steps, kinks, and adstructures. Accordingly, polarized SIRS experiments can probe the resulting surface morphology and independently assess the relative contributions of -SiH, -SiH_2, and -SiH_3 resulting from the etching process (5, 6, 7, 8).

Utilizing polarized SIRS in conjunction with prototype Si(111) surfaces, it was demonstrated that steps and kinks are preferentially etched, yielding atomically flat Si(111) surfaces with remarkably few defects (7, 8). The prototype Si(111) surfaces were initially decorated with -SiH, -SiH_2, and -SiH_3, indicating an inhomogeneous surface with a root-mean-square (RMS) roughness of a few Angstroms. At high pH values, aqueous HF etched Si(111) oxide surfaces produce flat, ideally hydrogen-terminated surfaces where only the monohydride is observed. Higher solution pH produces a more perfect Si(111) interface, and this result seemingly implies that better device characteristics may be obtained by processing at higher pH, e.g., with buffered HF.

The promising results attained with Si(111) surfaces were not realized with Si(100) surfaces. Upon aqueous HF processing, Si(100) surfaces, like their Si(111) counterparts, are similarly hydrogen terminated (7, 13, 14). However, high pH HF etching solutions do not produce ideally terminated (dihydride) Si(100) surfaces. In fact, ideal hydride termination is unlikely as strain associated with an ideally terminated dihydride surface would produce instability (3). The etched Si(100) surfaces are therefore inherently rough, being decorated not only with -SiH_2, but also with -SiH and -SiH_3. The presence of the monohydride is interesting as this can indicate microfacetting along the (111) plane, particularly at high pH values (7, 13, 14). In any case, the resulting Si(100) surfaces are relatively stable and congruous with many processing steps; but, because of the geometric disparities resulting from the -SiH, -SiH_2, and -SiH_3 surface sites, they are rough on the scale of a few Angstroms RMS (7, 13, 14). In summary, aqueous HF treated Si(100) surfaces appear satisfactory for many processes, but ultimately it is desirable to ameliorate the atomic level roughness associated with aqueous HF treated Si(100).

Vapor HF processing is of interest in microchip fabrication, but the occurrence of hydrogen termination via a vapor HF process has not been firmly established. Toward this end, the ability of vapor HF to produce hydrogen-terminated 150 and 200 mm Si(100) wafers was characterized with a commercial vapor HF processing platform. Although the vapor HF platform utilizes the same active reagents as a wet process, HF and H_2O, these species are introduced near the wafer surface via a gaseous flow. As such, the vapor HF reaction is differentiated from a wet process by gas flow dynamics and nonequilibrium kinetics. Results from this study suggest that the vapor HF processed Si(100) wafers are hydrogen-terminated, and the primary surface terminating species is the dihydride. Because the vapor HF etch step can be implemented independent of water or proprietary rinses, the role of the post-etch rinse process was also investigated; either a water or proprietary rinse increases the amount of hydrogen-terminated silicon.

The above discussion has focused primarily on hydrogen termination; however, contact angle measurements afford an alternative view of the surface because, in addition to H, these measurements are sensitive to the presence of F, C, and O. In brief, contact angle probes surface wetting. For silicon surfaces considered here, wafer hydrophilicity (low contact angle) is associated with the presence of Si-O whereas wafer hydrophobicity (large contact angle) is associated with Si-H (15). To our knowledge, however, absolute H and O concentrations have not been measured. Additionally, as indicated above, contact angle is sensitive not only to Si-O and Si-H, but also F and C. To obtain a more complete view of the interfacial elemental composition, ion beam analysis was performed to quantify the H, O, and C coverages (16). By correlating the H, O, and C coverages with contact angle and integrated silicon hydride intensities, we attempted to address the relationship between contact angle and surface atomic coverage. Unfortunately, within the context of our experiments, this issue could not be resolved.

EXPERIMENTAL

Anhydrous HF processing was effected with two EXCALIBUR® ISR Vapor Phase Processing Systems (Fig. 1), one equipped for processing 150 mm diameter wafers and the other for processing 200 mm diameter wafers (17). The vapor pressure of HF and water is determined by independently controlling the water and HF temperatures. A mass-controlled flow of anhydrous HF vapor is admitted into a controlled nitrogen flow; independently, a mass-controlled flow of nitrogen is passed over a water bath, producing a controlled flow of humid nitrogen. The vapor HF and moisture are subsequently introduced into the processing chamber. An etch process is complete within a few seconds, the vapors are purged from the process chamber, and subsequently an optional rinse process may be implemented. The rinse is a dynamic process; the wafer is ramped to ~1000 revolutions per minute and a 0.5 litre per minute (LPM) flow rinses the wafer. The wafer is subsequently dried under ~ 15 LPM flow of nitrogen. After the vapor HF etch, either of two rinse processes were employed: a water rinse or a newly developed proprietary rinse. Thus, three process can be compared: an vapor HF etch, a vapor HF etch with a water rinse, and a vapor HF etch with a proprietary rinse.

Si(100), p-doped, 150 mm, prime wafers with a resistivity of 5-15 Ω cm were utilized. Prior to processing, all wafers were subjected to a standard "B-Clean" in a MERCURY® Spray Processor, thereby producing a clean, chemically oxidized surface. For each process, multiple wafers were utilized. Contact angle measurements were performed at several wafer sites and averaged. Both SIRS and ion beam analysis were performed at remote locations. For each process, multiple wafers were sealed under a nitrogen flow

and shipped to the analysis sites. Details regarding the ion beam analysis can be found elsewhere (16). The elapsed time between process and analysis was less than 24 hours. During process and surface analysis, the wafers experienced a minimum of two hours exposure to the ambient environment. Regarding infrared analysis, any observed silicon hydride signal implies the surface is stable for a minimum of two hours. The SIRS was performed on a Nicolet Model 800 Fourier Transform Infrared (FTIR) Spectrometer, equipped with a customized attenuated total reflection (ATR) apparatus, complete with a germanium ATR element and associated optics. Both p-polarized and unpolarized spectra were recorded, and each spectrum represents the numerical average of 256 scans at 4 cm^{-1} resolution. Spectra were referenced to a chemically grown oxide, and spectra were obtained at multiple wafer sites. The operations described above were repeated multiple times on different days. To further authenticate the results, 200 mm diameter wafers were twice processed at the SIRS analysis site and immediately analyzed.

RESULTS

Representative p-polarized spectra (Fig. 2) are displayed over the $Si-H_x$ (x=1-3) stretching region for each of the aforementioned processes. Unpolarized spectra revealed the same features and relative intensities as with those obtained using p-polarized light, albeit with a lower signal-to-noise ratio and slightly more inhomogeneous broadening. Thus, for simplicity, only p-polarized spectra were analyzed. For each process, spectral information is reduced by integrating the relative intensity within the $Si-H_x$ stretching region averaged over several wafers and wafer sites (Fig. 3). Wafer-to-wafer and site-to-site variations are estimated to be less than 20%. However, for a given process, the averaged absolute integrated signal intensities varied significantly for each data set. Average integrated peak intensities originating from different data sets could be compared only by normalizing the averaged relative intensities within each data set to that of etch plus water rinse process. As a result of the aforementioned 20% uncertainty, integrated intensities associated with the etch plus rinse processes are statistically indistinguishable. It is clear, however, that the integrated intensity associated with an etch (only) process, is smaller than for the corresponding HF etch plus rinse processes. The resulting process-specific contact angle measurements, averaged across several data sets and several wafer sites, are presented in Fig. 4. While measurements varied by perhaps 5°, the trend depicted in Fig. 4 was always observed.

DISCUSSION

Features associated with the Si(100) surfaces can generally be interpreted by the absorbing SiH_x frequencies. Monohydrides typically absorb in the range 2070-2090 cm^{-1}, dihydrides in the range 2090 to 2120 cm^{-1}, and trihydrides in the range 2120-2150 cm^{-1}. Given the above, Fig. 2 shows that for all processes, infrared signal intensity is dominated by dihydride species. However, recalling the introductory discussion, these are not the "ideal" dihydrides (3). Strong signal intensity is also observed for the trihydrides. While there is no rigorous rationale for the presence of trihydride adstructures, they are commonly observed on both Si(111) and Si(100) surfaces (7, 8, 9, 13, 14). Broadening below 2100 cm^{-1} is likely associated with the monohydride; yet, in relation to the di- and trihydrides, it is also likely present in a relatively small amount. Comparison of Fig. 2 with literature spectra (7, 9, 13) resulting from aqueous HF processing suggests that, relative to the corresponding di- and trihydrides, there is variability in the monohydride intensity. Based on the absence of a strong monohydride signal, one might suggest that vapor HF tends to minimize surface roughening; in the absence of a buffering agent, the

propensity for microfacetting is small (7, 9, 13). Vapor HF processes can produce surfaces with a 1.5 Angstrom RMS roughness (17), but, for vapor HF, the correlation between monohydride and roughening is unknown.

The overarching conclusion from the above is that vapor HF produces stable, hydrogen terminated Si(100) surfaces. As previously mentioned, the observation of SiH_x intensity requires stability for *at least* two hours. The stability of these surfaces is likely longer (9, 12). The presence of the trihydride and the monohydride imply atomic-level roughness. This atomic-scale roughness may be intrinsic to HF/Si(100) chemistry.

Integrated silicon hydride intensities are displayed in Fig. 3. This graph is telling: either a water or a proprietary rinse process markedly improves the extent of hydrogen termination. If one considers the HF process apart from a rinse, this is not surprising. For example, reaction intermediates and etch byproducts accumulate on the surface and likely hinder the operative reaction kinetics. These entities compete with reagents for active sites, and thus, the reaction rate may decrease with time as intermediates and products are generated. However, a rinse dramatically shifts the equilibrium as liquid jets across the wafer; new adsorption sites are exposed as etch byproducts are rinsed away and the reaction is reactivated as the reaction is forced toward products. It has been suggested that rinsing involves replacing Si-F bonds with Si-H bonds (12).

Process-specific contact angle data are displayed in Fig. 4. All vapor HF processes yield a hydrophobic surface as evidenced by the greater than 50° contact angles. It is significant that surfaces with a 75° contact angle can be prepared. Disparity among the contact angles (Fig. 4) suggests each process yields a unique surface and by conventional wisdom, this should be reflected in the integrated $Si\text{-}H_x$ intensity. Yet, when comparing Figs. 3 and 4, no correlation between the integrated $Si\text{-}H_x$ intensity and the measured contact angle appears. The integrated $Si\text{-}H_x$ intensity (Fig. 3) is a measure of $Si\text{-}H_x$, but surface wetting (Fig. 4) is also influenced by C, O, and F; this may account for differences between Fig. 3 and 4. Regarding Fig. 4, disparity between the etch (only) and the etch plus rinse processes may originate partly from fluorine-containing intermediates (12) and residues. As previously discussed, these may remain on the wafer in the absence of a rinse. To continue, the two post-etch rinse processes may yield differing amounts of suboxide (14) where Si atoms may exist with one, two, or three oxygen atoms. Suboxides are thought to remain even after a dilute HF process (14), and at submonolayer coverages, these suboxides may not be unambiguously observed by x-ray photoelectron spectroscopy or SIRS (14). This is particularly true for our surface infrared experiments as the spectra were referenced to a chemical oxide. In any case, byproducts, suboxides, and ambient contamination contribute to the disparity in Fig. 4, and it is difficult to compare Figs. 3 and 4. To arrive at a more complete understanding of the interfacial composition, we attempted to quantitatively relate contact angle data to the O, C, and H coverages. Ion beam analysis was performed; these measurements did not correlate with either contact angle or SIRS because we could not discriminate between the contributions of the various sources of C, O, and H toward the surface atomic coverage. In vacuo processing or isotopic substitutions might obviate this problem.

CONCLUSION

Vapor HF treatment produces hydrogen terminated Si(100) surfaces, and these surfaces are stable for at least two hours. The SIRS spectra are dominated by dihydrides, but trihydrides and monohydrides are also present, although the monohydride signal appears

relatively small. The presence of these species indicates atomic-level roughness, and from previous measurements we infer this is ~ 1.5 Angstroms RMS (17). This atomic-level roughness is completely consistent with previous HF processing studies and may be characteristic of HF/Si(100) processing. Rinsing produces more $Si\text{-}H_x$ species as rinsing likely shifts the equilibrium towards products, perhaps by replacing Si-F bonds with Si-H bonds. A notable feature of this work is the measured 75°contact angle associated with the etch plus proprietary rinse process. Interestingly, these experiments show no clear correlation between contact angle and the integrated $Si\text{-}H_x$ intensity. This is not surprising given that contact angle is sensitive not only to $Si\text{-}H_x$, but also to C, O, and F. A quantitative study of the interfacial atomic concentrations was unrevealing. The processing influence on the Si(100) surface could not be ascertained owing to the high C, O, and H background concentrations. Assessment of the interfacial atomic concentrations might benefit from isotopic substitutions.

ACKNOWLEDGMENTS

J.S.M. gratefully acknowledges John Evans, University of Minnesota, for his interest and unrequited contributions to this project. J.S.M. also acknowledges Herb Sawin, Massachusetts Institute of Technology, for commentary on this manuscript, and Brian Stallard, Sandia National Laboratories, for preliminary experimental work.

REFERENCES

1. E. Yablonovitch, D. L. Allara, C. C. Chang, T. Gmitter, and T. B. Bright, Phys. Rev. Lett. **57**, 249 (1986).
2. G. W. Trucks, K. Raghavachari, G. S Higashi, and Y. J. Chabal, Phy. Rev. Lett. **65**, 504 (1990).
3. G. S. Higashi and Y. J. Chabal, in *Handbook of Wafer Cleaning Technology*, W. Kern, Editor, p. 484, Noyes Publications, Park Ridge, NJ (1993).
4. T. Sunada, T. Yasaka, M. Takakura, T. Sugiyama, S. Miyazaki, and M. Hiroshe, Jpn. J. Appl. Phys. **29**, L2408 (1990).
5. Y. J. Chabal, Surf. Sci. Rep. **8**, 211 (1988).
6. Y. J. Chabal, in *Semiconductor Interfaces: Formation and Properties*/1987, G. Lelay, J. Derrien, and N. Boccara, Editors., **PV 22**, P. 301, Springer Proceedings in Physics Springer, Berlin (1987).
7. See reference 3, p. 433.
8. P. Jakob and Y. J. Chabal, J. Chem. Phys. **95**, 2897 (1991).
9. H. Bender, S. Verhaverbeke, and M. M. Heyns, J. Electrochem. Soc. **141**, 3128 (1994).
10. For an insightful polarized Raman study, see: M. A. Hines, Y. J. Chabal, T. D. Harris, and A. L. Harris, J. Chem. Phys. **101**, 8071 (1994).
11. R. A. Carpio, B. W. Fowler, V. Atluri, N. Herbots, and P. R. Brierley, this proceedings (1995).
12. L. Ling, S. Kuwabara, T. Abe, and F. Shimura, J. Appl. Phys. **73**, 3018 (1993).
13. P. Dumas, Y. J. Chabal, and P. Jakob, Surf. Sci. **269/270**, 867 (1992).
14. L. Zazzera and J. F. Evans, J. Vac. Sci. Technol. A **11**, 934 (1993).
15. S. Verhaverbeke, Ph.D. Dissertation, Katholieke Universiteit Leuven, Leuven, Belgium, 1993.
16. V. Atluri, N. Herbots, S. Bhagvat, S. Whaley, R. Carpio, and B. Fowler, submitted.
17. D. Syverson, J. Barnett, B. Bohannon, and B. Witowski, FSI Technical Report No. 403, FSI International, 1993.

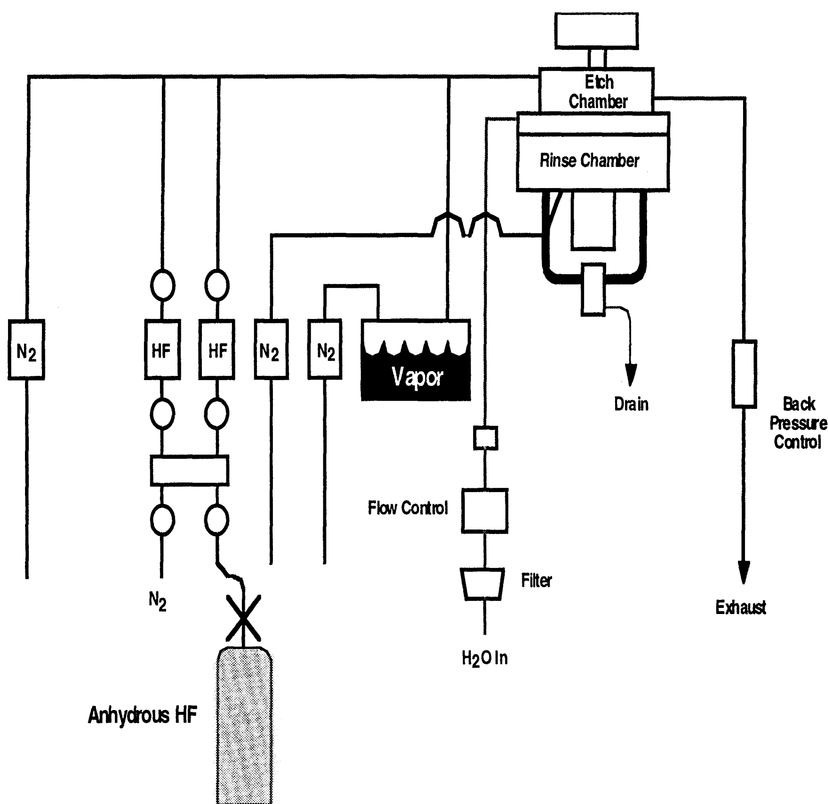

Figure 1. Flow schematic of a Standard EXCALIBUR® ISR Vapor Phase Processing Platform.

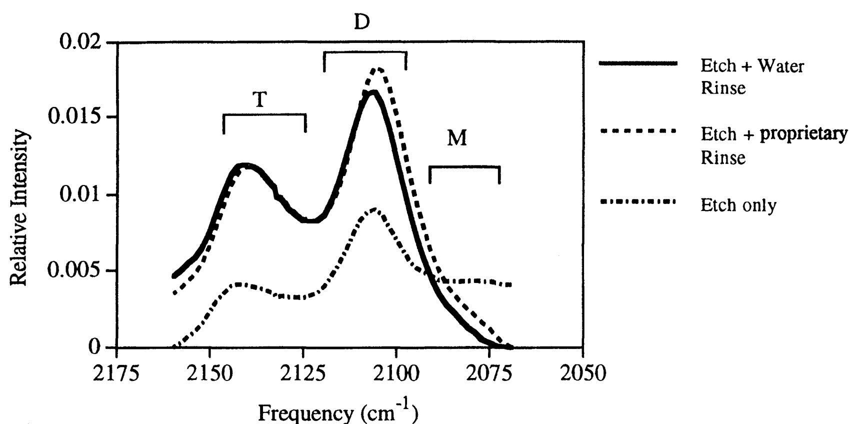

Figure 2. Infrared spectra of the silicon hydride stretching region for Si(100) wafers processed with vapor HF. Displayed spectra represent three processes collected using p-polarized light with 4 cm^{-1} resolution. The mono-, di-, and trihydride are denoted by M, D, and T, respectively.

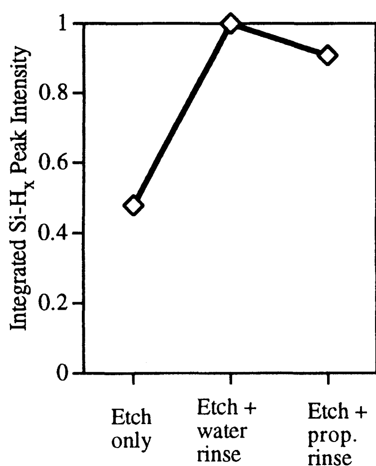

Figure 3. Integrated silicon hydride peak intensity for three vapor HF processes. See text.

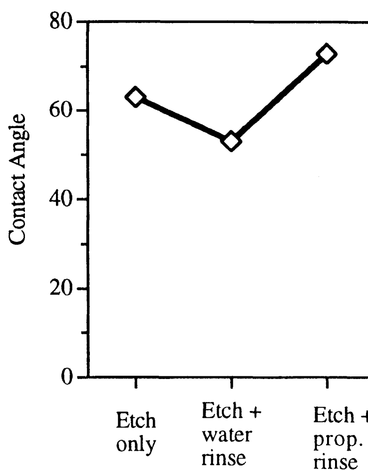

Figure 4. Contact angle for three vapor HF processes. Error bars are estimated to be ± 5°. See text.

A Study of the Effectiveness of Vapor Phase Cleans for Advanced Gate Oxidation

J. K. Tong, G. F. Hanger, D. S. Becker and D. J. Syverson

FSI International
322 Lake Hazeltine Drive
Chaska, MN 55318, U.S.A.

ABSTRACT

A cooperative project was conducted to evaluate the effectiveness of vapor phase cleaning processes utilizing vapor phase chemicals including O_3, Anhydrous HF and Anhydrous HCl for pre-gate oxidation cleaning. The project was conducted in comparison to the conventional aqueous chemicals based RCA cleans. Device electrical results such as gate oxide defect density, charge-to-breakdown, voltage-at-breakdown are collected using short loop, 90Å gate oxide test structures. Data indicates that pre-gate cleaning using vapor phase chemicals resulted in superior gate oxide electrical performance and oxide integrity.

INTRODUCTION

Gate oxidation is one of the most critical steps in ULSI MOS device manufacturing. The quality of gate oxide is largely determined by the cleanliness of the silicon surface to be oxidized to form gate oxide. Thus cleaning technology, prior to the gate oxidation, has continued to be one of the most focused areas for continuous performance improvement [1,2,3]. Conventional cleaning methods, namely the standard and modified RCA cleans, use aqueous based chemical solutions and cleaning processes are typically performed in a wet station. Tremendous amount of optimization has been done on these RCA cleans over the years. But due to their weaknesses in the various areas, as listed in table 1 for some of the typical chemical sequences, industry consensus indicates that newer cleaning technologies using gaseous and vapor phase chemicals are inevitably needed for the next generation devices with decreasing device geometry, increasing device density.

In this supplier-customer cooperative project, we evaluated the effectiveness of cleaning technology for pre-gate cleaning using vapor phase chemicals including O_3, Anhydrous HF (AHF), Anhydrous HCl (AHCl) and incorporated with insitu DI water rinse and spin dry. The respective analogy of the aqueous and vapor phase chemicals are listed in Table 2.

EXPERIMENT

Equipment

Figure 1 shows the simplified plumbing diagram of the single-wafer vapor phase cleaning equipment used for this study. O_3 gas is supplied by a corona discharge-type of ozone generator and AHF and AHCl gases are from semiconductor grade bottle sources. N_2 gas is used as carrier gas to introduce controlled amount of H_2O vapor into the Teflon PVDF-made process chamber. The process equipment also has wafer-spinning capability of up to 3000 RPM while offering virtually infinite combinations of vapor chemicals and DI water to be introduced onto the wafer surface. Industry-common instruments including Tencor 6200 Surfscan, Prometrix 200, Rigaku TXRF instrumentation, Perkin Elmer PHI-6300 SIMS and PHI-5400 ESCA were used for various measurements and monitoring during the study.

The process-of-record (POR) aqueous chemical cleans used for comparison in this study was a performed in a standard manual wet station with overflow rinse tanks and spin dryer using RCA chemistries.

Test Structures

Short loop 0.35μm technology-level CMOS silicon-oxide-polycide gate stack test structures with 90Å gate oxide, shown in Figure 2, were used for this study. Two types of structures were used: one has the gate oxide and polysilicon layers "terminated over the field oxide" and the other has the gate oxide and polysilicon "not terminated over the field oxide". The POR aqueous pre-gate cleaning, termed as STD hereafter, consisted of three chemical baths with DI water rinse in between and a final overflow rinse and spin dry. The chemical sequence are: Megasonic APM; SPM; Diluted HF. In this sequence, the APM and SPM are for the removal of particulate and organic contamination, the diluted HF is for the removal of the 150Å sacrificial oxide and producing a hydrophobic, ultra clean silicon surface for gate oxidation.

Process Splits

Split-lot experiments were performed comparing the vapor phase cleans with the conventional aqueous cleans. The process splits can be summarized as in Figure 3. Lot 1A and 1B went through the exact same process but the data collected were inconclusive due to equipment operation errors not related to the cleaning experiments . Test 3, inclusive of the same splits for Lot 1A and 1B, was the final experiment and the most equipment error-free and produced more conclusive data. Therefore discussion in this paper will be primarily focused on this last experiment. Four different vapor phase cleaning recipes were included in this evaluation and they are termed as VPC1, VPC2, VPC3 and VPC4. VPC1 is a direct replacement of the aqueous HF - Rinse/Dry in the pre-gate cleaning scheme. VPC2 was created by adding an additional rinse step where HCl gas and DI water was dispensed simultaneously onto the wafer surface. Thus VPC2 has the sequence of AHF - (AHCl+Rinse) - Rinse/Dry. With the addition of O_3, VPC3 is

a complete replacement of the whole aqueous pre-gate clean. VPC3 has the sequence of O_3 - AHF - (AHCl+Rinse) - Rinse/Dry. VPC4 is essentially the same as VPC1 except that the DI water rinse time was doubled.

RESULTS AND DISCUSSIONS

Understandably any successful gate cleaning sequence must be able to completely remove the sacrificial oxide without severe over etching and must be able to reveal a atomically flat silicon surface free of particulate, metallic or organic contamination. Figure 4 shows the representative data of the vapor phase cleaning for particle counts when processing bare Si wafers using a (AHF+AHCl) - Rinse/Dry process sequence, over a time frame of approximately two months. Shown in Figure 5 is the oxide etching performance with emphasis on etching depth repeatability and across wafer etching uniformity. In this case, the recipe was adjusted to target a etch depth of 200Å of thermal oxide. The data indicates that the across wafer etch uniformity is typically below 4% (calculated as [Etch Mean/Std. Dev.] x 100%) with the majority of the data points at or around 2%. Figure 6 represents the metals contamination removal capability of the vapor phase cleaning tool. Photoresist was selected as the metals removal challenge for this study due to nature of high metallic contamination in photoresist. In this case wafers coated with photoresist were first ashed in an oxygen asher (to remove the bulk resist) and then cleaned in the vapor phase cleaning tool using chemical sequences of AHF - Rinse/Dry and (AHF+AHCl) - Rinse/Dry. As expected, the AHF-Rinse/Dry effectively removed most of the metals, except Cu and Ni, to below the detection limit (1×10^{10} atoms/cm^2) of the TXRF instrument used in this experiment. The (AHF+AHCl)-Rinse/Dry process sequence effectively removed all of the metals, including Cu and Ni, to below detection limit level.

The electrical parameters that were evaluated include the Defect Density (D_o), Charge-to-Breakdown (Q_{bd}), Voltage-at-Breakdown (V_{bd}). Data was collected on test devices for both the "terminated over the field oxide" and the "not terminated over the field oxide" structures.

Figure 7 shows the normalized D_O data collected in Test 3. As shown, all four vapor phase clean recipes (VPC1-4) produced lower defect density on the gate oxide with the lowest defect density from recipe VPC2 . Shown in Figure 8 is the normalized Q_{bd} and V_{bd} for the "terminated over the filed oxide" test structure. VPC3 recipe seemed to performed better than the other vapor phase recipes in this case and was significantly better than the STD wet station process. Notice that VPC3, a chemical sequence of O_3 - AHF - (AHCl+Rinse) - Rinse/Dry, is a vapor recipe that completely replaced the wet station recipe which consisted chemical sequence of Megasonic APM - SPM - HF. This results strongly implies the feasibility of replacing both the Megasonic APM and SPM steps with the O_3 gas, a much stronger oxidant but much more environmentally friendly chemical due to its self-decomposition nature.

Shown in Figure 9 is the normalized Q_{bd} and V_{bd} data for the "not terminated over the field oxide" test structure. In this case, the performance difference between the recipes are not as dramatic but in general all of the vapor phase recipe still had slight improvement over the STD wet station process.

CONCLUSION

Process performance of vapor phase cleaning was compared with the conventional wet station cleaning for the pre-gate clean using 0.35μm CMOS silicon-oxide-polycide gate stack short loop test structures with 90Å gate oxide having both the "terminated over the field oxide" and "not terminated over the field oxide" test structures. The vapor phase cleans yield lower defect densities than the conventional aqueous clean. The vapor phase cleans yielded better Q_{bd} characteristics, most notably on the structures "terminated over the field oxide". In addition, the results strongly implies the feasibility of replacing both the Megasonic APM and SPM steps with the O_3 gas for improved gate characteristics.

REFERENCES

[1] Proceedings of the First Int'l Symp. on Cleaning Tech. in Semi. Device Manuf. (1989)
[2] Proceedings of the Second Int'l Symp. on Cleaning Tech. in Semi. Device Manuf. (1991)
[3] Proceedings of the Third Int'l Symp. on Cleaning Tech. in Semi. Device Manuf. (1993)
[4] Dielectric Breakdown in MOS Devices Part I: Defect Related and Intrinsic Breakdown, D. R. Wolters et al, Phillips J. Res. 40, 115-136
[5] Dielectric Breakdown in MOS Devices Part II: Conditions for the Intrinsic Breakdown, D. R. Wolters et al, Phillips J. Res. 40, 115-136

TABLE 1. Conventional RCA Cleans		
1. SC-1: $NH_4OH/H_2O_2/H_2O$ in 1:1:5 mixing ratio 2. SC-2: $HCl/H_2O_2/H_2O$ in 1:1:5 mixing ratio		
Chemical Cleaning Sequence	**Primary Strengths**	**Weaknesses**
HF - SC1 - SC2	Low particle counts Good metals reduction	Leaves residual chemical oxide
HF - SC2 - SC1	Low particle counts	Higher metals contamination Leaves residual chemical oxide
SC1 - SC2 - HF	Hydrophobic, oxide-free Si surface No ionic metals	High particle counts Could have higher atomic metals

TABLE 2. Vapor Phase Analog of RCA Cleaning Solutions

Targeted Contaminant Removal	RCA Cleaning Solutions	Analogous Vapor Phase Chemicals
Particles	HF SC1	AHF DI Rinse
Organics	$H_2SO_4/H_2O_2/H_2O$ (SPM) SC1	O_3
Silicon Oxides	HF, BOE EG/HF/NH_4F	AHF
Metallic contamination	HF SC2	AHF AHCl DI Rinse
Residues	HF EG/HF/NH_4F Solvents	AHF DI Rinse

FIGURE 1. Simplified Plumbing Diagram of the Vapor Phase Cleaning Equipment

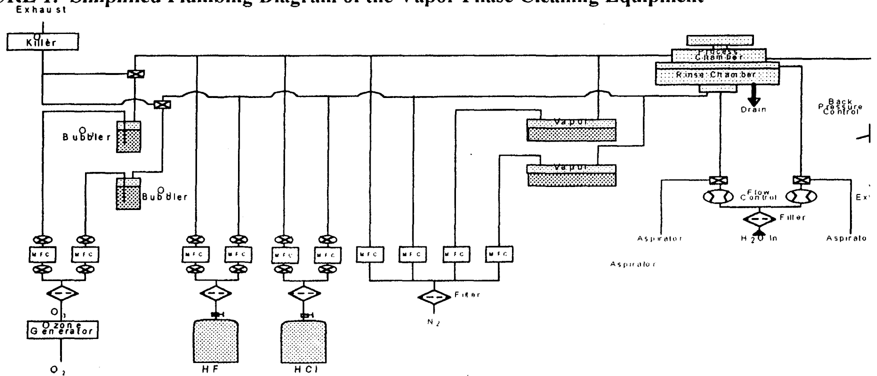

FIGURE 2. Cross-sectional Diagram of the Gate Oxide Zone Tester

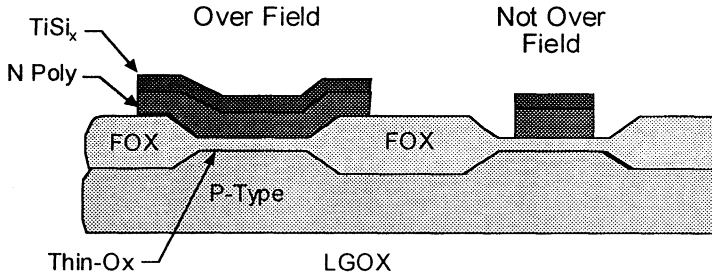

FIGURE 3. Process Splits Used in This Study

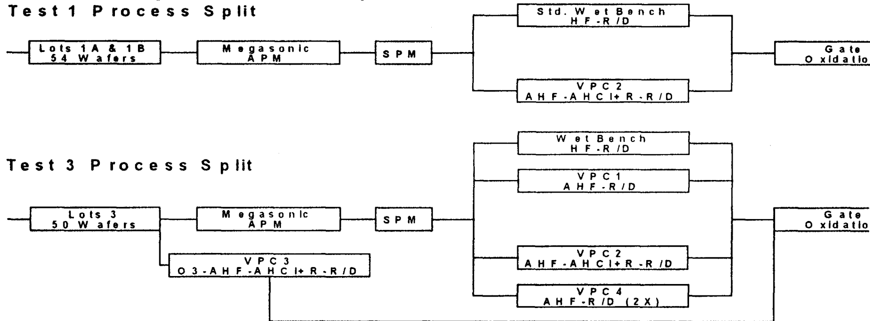

FIGURE 4. Representative Particle Counts of the Vapor Phase Cleaning Process Particles at ≥0.15μm and ≥0.20μm, (AHF+AHCl) - Rinse/Dry sequence

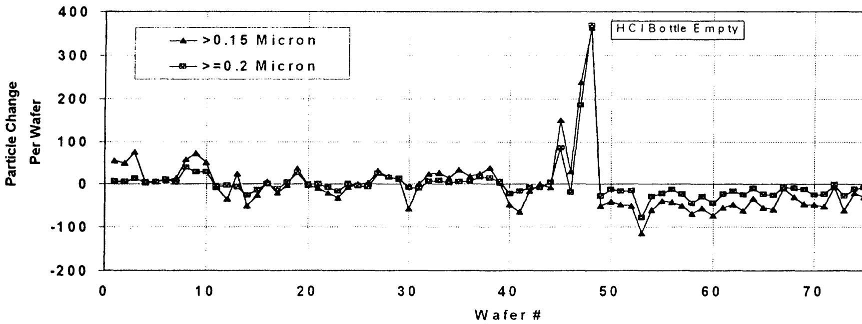

FIGURE 5. Representative Data for Oxide Etching Depth and Across Wafer Non-uniformity
Target Etching Depth 200Å, (AHF+AHCl) - Rinse/Dry sequence

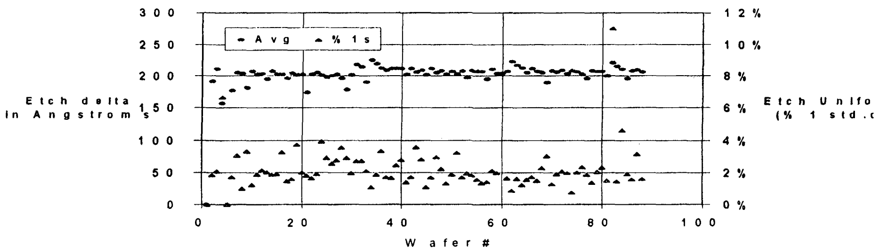

FIGURE 6. Metallic Contamination Removal by Vapor Phase Cleaning
Ashed photoresist used as metals contamination challenge

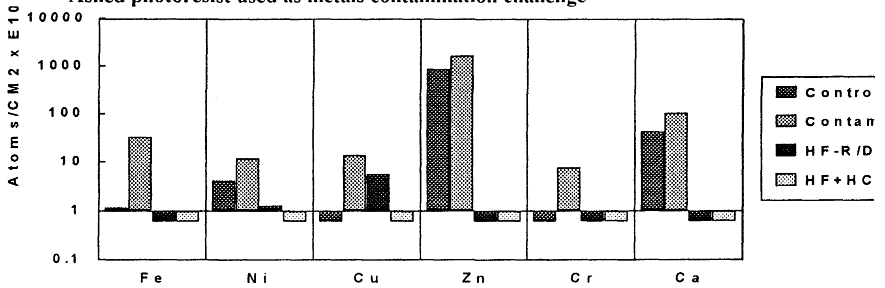

FIGURE 7. Normalized Gate Oxide Defect Density (D_o), Comparing Vapor Phase Cleaning and Conventional Aqueous Chemical Cleaning

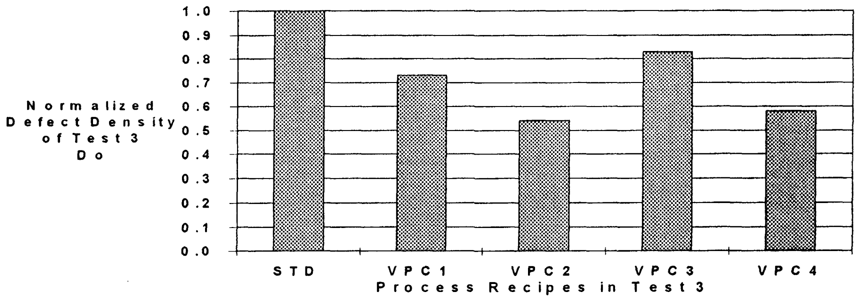

FIGURE 8. Normalized Gate Oxide Qbd and Vbd for the Structures "not terminated over the filed oxide)

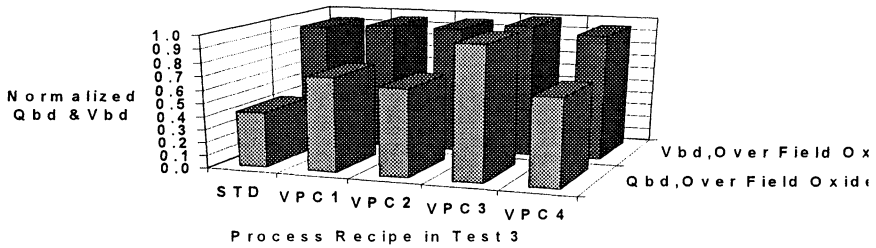

FIGURE 9. Normalized Gate Oxide Qbd and Vbd for the Structures "not terminated over the filed oxide)

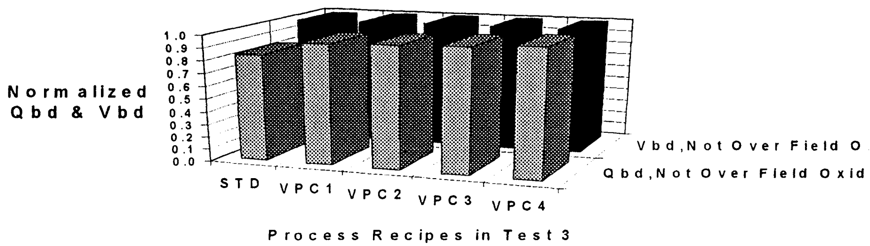

COMPARISON OF HCl GAS-PHASE CLEANING WITH CONVENTIONAL AND DILUTE WET CHEMISTRIES

C. Elsmore*, T.Q. Hurd#, J. Clarke†, M. Meuris,
P.W. Mertens & M.M. Heyns.

IMEC, Kapeldreef 75, B-3001 Leuven, Belgium.
* Currently assigned to IMEC from BOC Gases
# Currently assigned to IMEC from Texas Instruments
†MCNC, P.O.Box 12889, NC, 27709-2889, USA.

ABSTRACT

Dilute chemistries have emerged recently as alternatives to conventional wet cleans showing improved cleaning efficiency with reduced cost of ownership. In this paper HCl gas-phase cleaning is shown to be a promising alternative to SC1/SC2 cleans for a pre-gate oxidation clean, achieving good metal removals with no significant surface roughening. The dry clean is shown to be particle neutral and capable of achieving high capacitor yields when compared side-by-side with wet cleaning methods for similarly contaminated wafers. The integrity of the dry clean is shown to be sensitive to processing conditions, particularly temperature. Further understanding of the dry clean process and production testing is required to develop gas-phase cleaning into a workable process that competes with tried and tested wet cleans.

INTRODUCTION

A workable dry clean is needed more and more for several well known reasons; gases offer lower particle and higher purity levels at the wafer surface than conventional high grade chemicals. Vacuum environments reduce contamination during processing and prevent the wafer from coming into contact with clean room air. Finally, environmental problems and bulk liquid disposal costs make wet cleaning increasingly less attractive. Previously reported dry cleans(1-5) using Cl_2 gave good metal removal but suffered from surface roughening thought to be detrimental to gate oxide integrity (G.O.I.).

Several cleaning mediums reported earlier were investigated(6-7). From these trials, HCl was shown to produce the best overall results in terms of metal removal and surface condition. Therefore, the evaluation concentrated on HCl using different wafer contaminations with G.O.I. as the indicating step. As dry cleaning is a relatively new process aimed at replacing problematic wet steps, experiments were devised to compare wet and dry cleans side-by-side so that the true performance could be gauged. Dilute chemistries reported earlier(8) showed that metal removal could be maintained without paying the penalty of depositing particles. Dilute chemistries were compared since tightening environmental legislations and associated disposal costs mean that such cleans are possible replacements for traditional, full strength, wet processes, along with the dry clean.

EXPERIMENTAL TECHNIQUES

Monitor wafers were CZ, p-type, <100>, device wafers were either CZ or Epi. Elemental contamination levels and cleaning efficiencies were determined by Total X-Ray Fluorescence (TXRF) on an Atomika 8010. The detection limits of this method were lowered to 10^9 atoms/cm^2 by the use of the HF vapour-phase decomposition and droplet surface etch technique (VPD-DSE). Light point defects (LPDs), were monitored in the range of 0.12-1.5μm latex-sphere-equivalents using a CENSOR ANS100 light scattering particle counter. Surface charge profiling was carried out on the QC Solutions SCP.

Contamination: All wafers (monitor & device) were cleaned with a standard FSI-b clean to ensure all wafers were at the same baseline prior to contamination. The wafers were then coated with IX500 photoresist and baked for 30 minutes at 150°C. A standard Arsenic or Boron implantation followed, at typical dose and energy levels. Finally, the wafers underwent a PRS-800 plasma strip only, to leave resist residue on the surface. This contamination medium was used as opposed to wet spiking methods as it gives a wider range of contaminants than single spiked baths can provide. Typical contamination levels ranged from 10^{11} to 10^{13} atoms/cm^2. Time Of Flight Secondary Ion Mass Spectrometry (TOFSIMS) was used to ensure resist residues were not present on the surface of the wafer after cleaning.

Cleaning: All wafers were then split into lots for wet and dry cleans. After the respective cleans the wafers were re-grouped and sent to the furnace for gate oxidation within two hours of the cleans being finished. The combined lots then followed the same capacitor build process to termination.

The cleans tested were as follows:-

- Dry HCl
- Sulphuric Peroxide Mixture (SPM)
- Dilute SC2 (dSC2); 1:5:100
- SC1 + Dry HCl
- SC1 + dSC2
- SC1 + Dilute HCl (dHCl); 1:100
- No Clean; Initial conditions

A standard dry cleaning sequence utilised a pre-heat step, followed by a 60 second exposure of U.V.-activated HCl at temperatures between 100 & 240°C, chamber pressure of 100 Torr and completed with an extensive N_2 purge.

G.O.I.: 6.5nm gate oxide was grown in a dry oxidation using no Cl_2, to produce Al sputtered poly-si gates. E_{bd} was used to evaluate the integrity of the gate oxide as a function of the cleaning process.

Equipment: The wet cleans were carried out in a conventional wet bench.

A SubMicron Systems PRIMAXX was used for all of the dry cleaning experiments described here. A schematic is shown in figure 1. The silicon wafer is suspended on alumina pins in an alumina reactor, and is rotated during processing using a magnetically levitated spindle. Sapphire diffuser plates ensure adequate gas distribution and a sapphire window above the wafer allows wafer heating with halogen lamps and U.V. activation of the gases from external sources. Irradiation is normal to the wafer surface while process gases are directed parallel to the surface. The system pressure, gas flows, wafer temperature, U.V. activation and process time are independently controlled using a dedicated computer and custom software. Stainless steel components, electropolished where possible, and Ni coated near the reactor, are used for the gas supplies and vacuum connections. Wafers are loaded and unloaded from the system using an evacuated load lock equipped with a wafer manipulator.

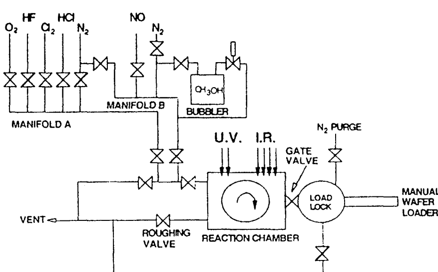

Figure 1 - Schematic of SMS Primaxx

RESULTS & DISCUSSION

Metals: Earlier work[6] showed high metal removal efficiencies with HCl as a single gas process at 200°C for Ca^{++}, Cu°, Cu^{++}, and Fe^{+++}, for samples contaminated by wet spiking. Figures 2 and 3 show the metal removals achieved with dry HCl, again at 200°C, on wafers contaminated with resist residue. The slight addition seen when processing the wafers under nitrogen is attributed to background noise from valves etc. Figures 4 & 5 show the metal levels for wet vs. dry cleans. The data shows that the SC1 cleans followed by the dilute chemistries give the best removal with promising results from the dry HCl clean. Overall the SC1+Dry HCl gave better results than the dry HCl alone.

Surface Roughening: Previously reported work[6&7] showed that increased temperature improved metal removal particularly for high levels of initial contamination. Atomic Force Microscopy (AFM) plots show surface roughening is not a problem for processing at elevated temperatures. Table 1 below shows a summary of the AFM data for the respective cleans clearly showing that dry cleaning roughens the surface less than SC1.

TABLE 1. Summary of AFM data for wet vs. dry cleans

Clean	RMS (Rq)	Ra
SC1 + Dry (200°C)	0.120	0.101
SC1	0.109	0.094
Dry HCl (200°C)	0.067	0.052
Dry HCl (100°C)	0.096	0.075
SC1 + dSC2	0.158	0.097
SC1 + dHCl	0.143	0.114
Initial	0.050	0.039

Particles: Figure 6 shows the LPD levels of the wet vs. dry cleans with an initial level of particles (>0.15μ) being >30,000 (overload). These levels are still quite high for the dry clean due to the nature of the contamination, however, the dry cleans do compare well with other metal removal steps and the SC1 + Dry HCl is particularly promising.

G.O.I: Figure 7 shows the yields obtained from the wet, dry and combined wet & dry cleans. The dry clean yields are promising but the traditional SPM and SC1 + Dry HCl give the most promising results. It must be noted though that the dry clean yields were not consistent with every run due to temperature control problems with Epi wafers. This phenomena was only seen with Epi wafers as they have a different emissivity value (used for temperature control) for the backside of the wafer which causes an offset in the process temperature. This problem can be overcome with a different method of temperature control or the inclusion of an adjustment factor for each wafer type.

Surface Condition: Previously reported ESCA data(7) showed the surface of the wafer after dry cleaning was similar to wafers post wet cleaning. Figure 8 shows a plot of Surface Charge Profiling (SCP) values showing that the dry cleans leave the wafer surface positively charged, whereas the wet cleans generally leave the surface negatively charged. It can be clearly seen from the error bars that the SCP values are far more consistent for dry cleaning and always positive, whereas the wet cleans can be positive or negatively charged depending upon the measurement position. It is not known at this stage what effects this phenomena has on downstream processing, if any.

Total Cost Of Ownership (TCOO): A COO model was produced† which is shown in figure 9. The figures for dilute SC2 alone are not shown due to the large values compared to the other cleans. The average cost of $26/wafer for this step arises from the large scrap value due to the low yield of ~80% shown from the dSC2 data. The graph shows that SPM has the lowest COO followed by Dry HCl and SC1 cleans alone. More statistics for each clean are required for the COO model since the yield is the dominating factor. Previous COO models were used as a filter to highlight the salient variables that required more work. Earlier comparisons(7) showed that the dry clean was more cost effective than an acid spray tool or conventional wet bench for a metal removal step up to 25,000 wafer starts/month, after which, throughput becomes the limiting factor.

Environmental Efficiency: Figure 10 shows the number of moles of HCl required to remove the respective number of metal atoms for each clean and dilution. The calculation accounts for the dry clean using 1 litre gas per wafer, normal cleans processing 200 wafers/bath, and the 1:100000 dilution only cleaning 25 wafers before metal loading becomes an issue.The graph clearly shows that in terms of environmental friendliness, only the heavily diluted chemistries can compete with the dry clean (note log scale).

CONCLUSIONS

The cleaning mechanism for the HCl dry clean is proposed as follows. The U.V. lamp used gives a wavelength of ~150nm so it is thought that the high power of the lamp is capable of breaking the H-Cl bond (431.9 kJ/mol = 277nm) to give Cl ions that can form metal chlorides, which are volatile at the increased temperature and reduced pressures used. Previous work(1) showed that Cl_2 used in conjunction with H_2 gives good metal removal without roughening the surface. It is thought that the H present after breaking the H-Cl bond serves the same purpose.

The dry clean compares well with conventional and dilute wet chemistries in terms of metal removal, particle levels, surface roughening and most importantly, device yield.

The "environmental efficiency" of the HCl dry clean can only be matched by the extreme dilute chemistries with the conventional wet cleans releasing 4-5 orders of magnitude more of HCl to the atmosphere.

The dry clean needs to be developed in a semi-production environment to increase run-to-run consistency and reduce the standard deviation of the data. The initial results are very promising and the HCl dry clean should be used on niche problematic steps to gain acceptance into fab. processing.

ACKNOWLEDGEMENTS

The author is grateful to SMS for sponsoring this paper and to P. Carr and R. Gluck for all of their initial work. To D. Vanhaeren for the AFM analysis and to G. Doumen, K. Kenis, I. Cornelissen and M. Baeyens for their experimental assistance. Also, J. Clarke at MCNC for extensive COO modelling used throughout the dry cleaning program.

REFERENCES

1. T. Ito et al, Proceedings of the First International Symposium on Cleaning Technology in Semiconductor Device Manufacturing, Proceedings Volume 90-9, The Electrochemical Society Inc., Pennington, N.J. 1989, pp. 114-120.
2. Y. Sato et al, Extended abstracts of the 22nd Conference on Solid State Devices and Materials, Sendai, 1990, pp. 1103-1106.
3. S. Watanabe et al, Jap. J. of Applied Physics, Vol. 28, No. 10, 1989, pp. 2167-2171.
4. R. Sugino et al, ECS Mtg. ext. abstract 512, Vol. 91-2, 1991, p. 762.
5. H. Fukuda, U.S. Patent 4,871,416.
6. C. Elsmore et al, Proceedings of the Second International Symposium on Ultra-clean Processing of Silicon Surfaces, Bruges, September 19-21, 1994, pp.125-129.
7. C. Elsmore et al, Proceedings of the 41st Annual Technical Meeting, Institute of Environmental Sciences, Anaheim, California, April 30-May 5,1995, pp.487- 493.
8. T.Q. Hurd et al, Proceedings of the Second International Symposium on Ultra-clean Processing of Silicon Surfaces, Bruges, September 19-21, 1994, pp.41-45.

FIGURES

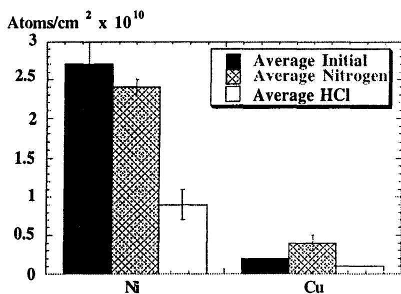

Figure 2. Ni & Cu removal levels using HCl @ 200°C for resist residue.

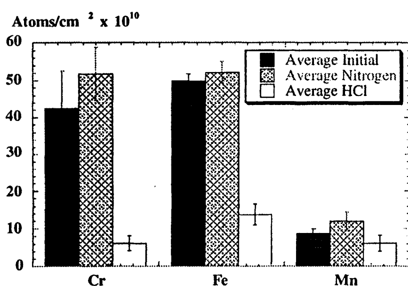

Figure 3. Cr, Fe & Mn removal levels using HCl @ 200°C for resist residue.

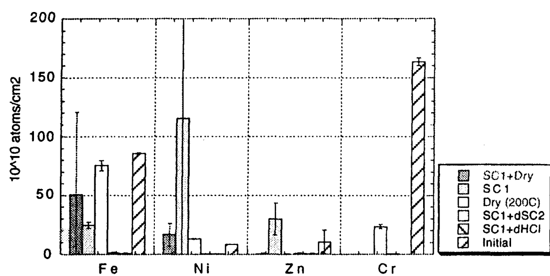

Figure 4. Comparison of wet vs. dry cleans for Fe, Ni, Zn & Cr

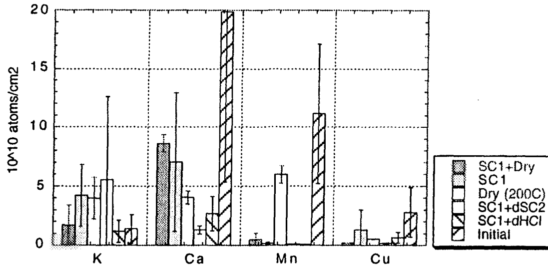

Figure 5. Comparison of wet vs. dry cleans for K, Ca, Mn & Cu

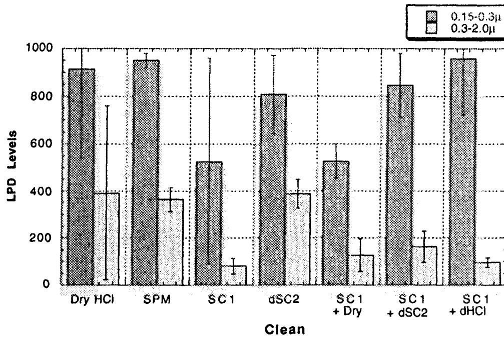

Figure 6. Comparison of LPD levels for wet vs. dry clean

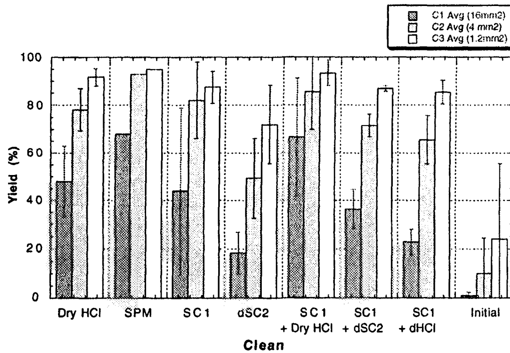

Figure 7. Comparison of capacitor yield for wet vs. dry clean

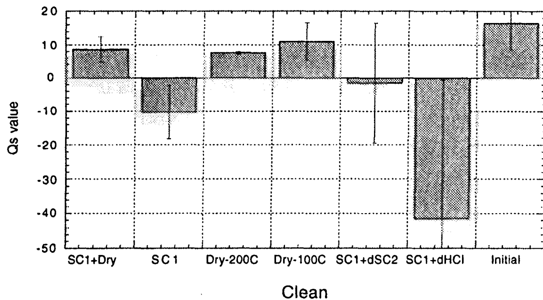

Figure 8. SCP plot of wet vs. dry cleans

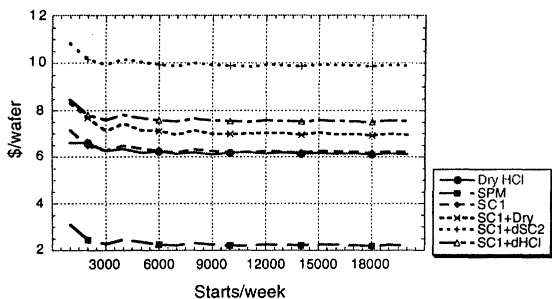

Figure 9. TCOO of wet vs. dry cleans as a function of wafer starts/week

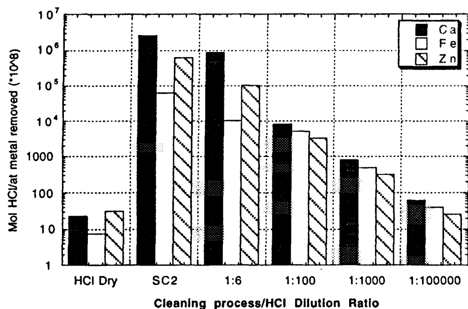

Figure 10. "Environmental Efficiency" comparison of SC2 vs. Dry HCl clean

UV/Cl_2 Etching and Cleaning of Wafer Surfaces

A. Scott Lawing, Anthony J. Muscat, Herbert H. Sawin
Massachusetts Institute of Technology
Department of Chemical Engineering
Cambridge, MA 02139

Jeffrey W. Butterbaugh
FSI International
Chaska, MN 55318

The UV/Cl_2 process has been demonstrated to be effective in removing metals from wafer surfaces. In order to be industrially applicable, metals must be removed while maintaining acceptable surface roughness. Using Response Surface Methodology (RSM), we have demonstrated that there is a significant parameter space where metals can be removed and surface integrity maintained. Silicon etching is accelerated by both gas phase and surface photolysis, with surface photolysis being by far the dominant mechanism. We have demonstrated copper removal to the detection limit of X-ray Photoelectron Spectroscopy (XPS) with UV/Cl_2. Copper is removed from both oxide and silicon surfaces with equal effectiveness at the same conditions. The mechanisms by which copper removal is enhanced by the UV/Cl_2 process are discussed.

Introduction

The UV/Cl_2 process has been demonstrated to be effective in removing metal contaminants from wafer surfaces (1,2,3,4). For the UV/Cl_2 process to be accepted by industry, it must be demonstrated that the surface remaining after the clean is amenable to subsequent processing. Of prime concern in this regard are the post-process surface roughness, which must be maintained below acceptable levels, and the amount of material removed during the process, which must be small enough not to effect device dimensions and performance. We have explored the parameter space of interest in UV/Cl_2 wafer cleaning to determine the silicon etch rates and post-process surface roughness. We have also performed some mechanistic studies to investigate the relative effects of surface and gas phase photolysis on the etching process.

The removal of copper from wafer surfaces with UV/Cl_2 has been investigated. It has been suggested that metal removal in this system occurs by the formation of $Si_XCl_YM_Z$ complexes (2,4,5) and that the volatilities of many of the metal chloride compounds are too low to explain the observed removal. We have investigated the mechanism by which copper removal is enhanced by UV exposure in the presence of chlorine.

Experimental

Our experimental apparatus is illustrated in Figure 1. Several reaction chambers are connected via a central transfer system, giving us the ability to perform multiple sequential cleaning processes without exposing the samples to ambient contamination, in effect mimicking a clustered process. We also have the ability to perform *in situ* surface analysis, including X-ray Photoelectron Spectroscopy (XPS) and ellipsometry. All of the XPS results reported here were obtained with Mg Kα radiation and a VG 100 AX electron energy analyzer.

The UV cleaning chamber consists of a 1 inch diameter quartz or sapphire tube (both were used at various stages in these experiments). The gas flows axially down the tube. The outside of the tube can be wrapped with heating tape to provide sample heating above ambient temperatures. The sample is introduced via a stainless steel transfer rod, with a stainless steel sheathed thermocouple mounted annularly in the rod such that the junction is within 1 cm of the sample surface. The sample holder and sample transfer fork used in the silicon etching studies were fabricated from Macor (a machinable ceramic) in an attempt to limit sample contamination due to reaction of chlorine radicals with metal surfaces. In these etching studies, samples were partially masked with a thermally grown oxide film. Etch depths and surface roughness were determined as described in the following paragraph. In the metal removal studies, samples were fixed to an alumina button. The mounting system allows for the sample to be rotated with respect to the incident UV light. The light source used is a Spectral Energy model 151 lamp housing with a 1000 watt high pressure Hg-Xe arc lamp. This system provides $\approx$ 500 milliwatts/cm^2 in the wavelength range of 260-320 nm. In the metal removal studies, a IR filter was utilized in an attempt to reduce sample heating due to light exposure. The Cl_2 gas used was 99.998 % purity (Matheson ULSI grade). Pressure was controlled via a throttle valve and capacitance manometer with a PID controller.

A series of response surface experiments were performed in an earlier version of the UV reactor in order to establish the response of surface roughness and etch rate to the input variables of Cl_2 pressure and UV exposure time. These experiments were performed with 1 cm x 1 cm p-type Si <100> 5-20 Ω-cm samples which were partially masked with photoresist. Etch depths were determined with a Dektak 8000 profilometer. Surface roughness measurements were obtained with a Topometrix Discoverer Scanning Probe Microscope (SPM). Reported values of roughness represent the mean of at least nine 5 μm square scans spanning a representative area of the sample surface. Generally, the standard deviation of rms roughness was $\approx$20 % of the mean value for a given sample. In these experiments, pressure was varied between 1 and 99 torr. Exposure time was varied between 30 and 120 seconds. A central composite design was used (6). All runs were initiated at room temperature. A temperature rise on the order of 30 °C per minute was observed due to light exposure.

Samples used in all other etching and cleaning experiments were 1 cm x 1 cm n-type Si <100> 1-5 Ω-cm. All samples were pre-cleaned before processing. The cleaning

sequence was as follows: 1) Aqueous HF dip for 60 seconds (5 % if a thermal oxide, 49 % if silicon), 2) 3/1 H_2SO_4/H_2O_2 (samples were allowed to sit in this solution until just prior to use), and 3) 49 % Aqueous HF (oxide samples were not subjected to step 3 so as to maintain total oxide coverage). All samples were rinsed in distilled H_2O before and after immersion into the cleaning solutions and blown dry with N_2 before insertion into the vacuum chamber. For the samples fixed to the alumina buttons, it was necessary to wipe them with IPA in order to remove "water marks" (presumably due to reaction of the torr-seal resin used for attachment with the cleaning solution). This cleaning sequence resulted in surfaces with a minimum amount of carbon contamination. Silicon surfaces subjected to this sequence exhibited strongly hydrophobic character, although small amounts of oxygen were evident under XPS analysis. The oxide component of the silicon peak was not observable on the silicon samples. Oxides of initial thickness 4000 Å were reduced to ≈ 2000 Å as a result of this cleaning procedure.

Controlled contamination was achieved via sputtering in the analytical chamber. A carousel of five ≈ 1 cm square metal targets was located adjacent to the sample. An argon ion beam is directed at the target of choice, which is biased at 1200 V, reducing the potential for sputtering unwanted metal contaminants from the adjacent targets. Metal was deposited at an argon pressure of 4×10^{-7} torr and a beam energy of 1.7 kV, resulting in a current of 1.8 $\mu A/cm^2$ to the sputtering target. In this manner, contamination rates on the order of 1 Å/min can be obtained.

Selected samples were contaminated *ex situ*. Copper was deposited on a silicon surface in an HF solution. The sample was cleaned by the aforementioned procedure and immersed in a 1000 ppm copper solution (Johnson Matthey Copper ICP standard) with 5 % HF for 15 minutes. The sample was then allowed to sit in air for 30 minutes.

Results and Discussion

Silicon Etching Studies

The response surface for surface roughness as a function of UV/Cl_2 etching is shown in Figure 2. These data were generated in an earlier version of our UV cleaning reactor, and these are the only data reported here that were not generated in the reactor depicted in Figure 1. The R^2 value of the fitted surface is 0.84, indicating the goodness of fit. From the figure, it is apparent that there is a significant parameter space where a cleaning process can be performed with minimal roughening. Most of the copper removal processes which will be reported subsequently in this paper where performed at 5 torr Cl_2 with a 1 minute UV exposure. From the figure, a process in this range will result in a surface roughness of less than 0.5 nm. For a point of reference, the surface roughness of a virgin silicon sample is between 1 and 2 Å rms as measured by our instrument. Figure 3 shows a SPM scan of a processed surface. The roughness of this sample is 0.62 nm rms. Note that the sample depicted in Figure 3 was processed at nominally 120 °C, while the response surface was generated at nominally 60 °C. This morphology is typical of what we observe at these conditions. The response surface for etch depth generated in the same set of experiments is qualitatively similar to the surface

depicted in Figure 2, indicating a correlation between the amount of silicon etched and the degree of surface roughening.

Figure 4 is a plot of surface roughness as a function of amount of silicon etched. These data represent a range of process conditions. There is a strong correlation between the degree of surface roughening and the amount of silicon removed. We observe that the surface is roughened on the order of 1 Å rms/ 100 Å etched.

In our apparatus, we have the ability to vary the orientation of the sample surface with respect to the light source. In this manner we can vary the UV fluence to the surface and study the relative effects of surface and gas phase photolysis. Figure 5 illustrates the results of one such experiment. The x-axis represents the normalized UV fluence to the surface and the y-axis the normalized etch depth, with both values normalized to the quantities at direct incidence. These data suggest that the UV/Cl_2 etching of silicon is not first order in the UV fluence. This is consistent with other investigations of UV activated etching processes (7,8). Not immediately obvious is that there is a small but measurable etch rate at parallel incidence, *i.e.* zero UV fluence. Since moderately doped silicon does not etch spontaneously in molecular chlorine at these conditions (9), this small rate represents the contribution of gas phase photolysis (the creation of reactive Cl radicals in the gas phase) to the etching process. The enhancement in the etch rate due to surface photolysis is approximately two orders of magnitude.

Copper Removal

We have calibrated our sputter deposition system. We performed a carefully controlled sequential deposition of copper on a SiO_2 substrate, measuring the copper, oxygen and silicon XPS signals after each deposition interval. The XPS peak intensities plotted versus time are shown in Figure 6. Initially all of the signals follow the exponential pattern of growth and decay predicted by the substrate/overlayer model (10), which models the XPS signals resulting from a homogeneous film over a substrate. At about the same time all of the signals exhibit a linear response, indicating island growth is taking place. Islands were in fact observed with the SPM on this sample. By fitting the exponential portion of the curve, the deposition time can be correlated with a thickness. In this manner, we have determined that the copper deposition rate is not more than 1 Å/min and not less than 0.5 Å/min at our standard conditions. Numbers quoted in this paper are based on the (more conservative) value of 1 Å/min.

The reaction mechanism between copper and Cl_2 gas without UV illumination is schematically illustrated in Figure 7. It has been reported that copper volatilizes as the trimeric species $(CuCl)_3$ (11,12) and that complete conversion of bulk copper to $CuCl_2$ is thermodynamically favored, especially in thin films (13,14). The kinetics of this reaction are such that a film of thickness on the order of monolayers is completely reacted in a few seconds or less at 5 torr (13).

Figure 7 also illustrates copper removal in the presence of Cl_2 without UV at 45 °C. The copper was allowed to react for 60 seconds to insure complete conversion of the metallic copper. In the vicinity of the monolayer regime, ≈ 50 % of the deposited copper

is removed. The copper that remains on the surface is entirely in the form of $CuCl_2$ and is stable and involatile. In the submonolayer regime, virtually no copper is removed, indicating that the mechanism of copper removal in the sub-monolayer regime is fundamentally different than that in the bulk. This observation is in agreement the work of Winters (11,12) who states that copper volatilizes in the form of the trimer $(CuCl)_3$ in the bulk, but that this trimer cannot form in the sub-monolayer (*i.e.* dispersed) regime. Winters also states that in the sub-monolayer regime copper volatilizes as the monomer CuCl.

Figure 8 illustrates copper removal from both silicon and oxide surfaces at 50 °C with the UV/Cl_2 process. In these cleaning experiments, Cl_2 gas was introduced to the chamber and the Cl_2 pressure was allowed to stabilize at 5 torr for 30 seconds prior to UV exposure. As discussed previously, the copper would be totally converted to $CuCl_2$ before UV exposure was initiated. After a timed exposure to Cl_2, the chamber was evacuated and the UV exposure was maintained for 3 minutes. During this post Cl_2 exposure, the temperature rise which resulted from UV exposure at pressure was reversed, and in fact the final sample temperature was lower than the initial temperature. The additional UV exposure did not result in additional copper removal, but was necessary to remove an interference peak in the XPS spectrum which we have not been able to assign to a specific chemical state. An initial coverage of $\approx 1.5 \times 10^{14}$ copper atoms/cm^2 (0.1 ML) is removed to the detection limit from both surfaces. In none of our experiments have we observed any significant difference between the removal efficiency of copper from oxide and silicon surfaces. Sugino *et.al.* (3) have reported that substrate etching does not occur through a chemically grown native oxide below 200 °C. This would indicate that silicon etch products are not critical to the copper removal process, and in fact we find it is not necessary to etch silicon in order to remove copper from the surface. In addition, since it is unlikely that the highly involatile product $CuCl_2$ could be removed from the surface, these results suggest that UV exposure results in the conversion of $CuCl_2$ to a more volatile product such as CuCl or $(CuCl)_3$.

Figure 9 gives further evidence that UV exposure results in the reduction of Cu(II) species to Cu(I) species. This sample was subjected to an aqueous deposition and allowed to oxidize. The as deposited surface exhibits copper in multiple oxidation states; Cu_2O and CuO, with a total coverage of $\approx 1 \times 10^{15}$ copper atoms/cm^2 (2/3 ML). After 1 minute of UV exposure, copper is present only as $CuCl_2$, and after two minutes of exposure, the copper is removed to the detection limit. Again, this suggests that the UV exposure is resulting in the reduction of higher oxidation states.

Our results to date suggest that copper is being removed as a chloride in the UV/Cl_2 system. It is unlikely that the highly involatile product $CuCl_2$ could be removed from the wafer surface. Also, the equilibrium vapor pressure of the monomer CuCl in air is too low to explain the observed removal efficiency. However, more reasonable volatilities are obtained if we consider the equilibrium pressure of CuCl in a chlorine atmosphere as determined by the reaction equilibrium (14,15):

$$Cu_{(s)} + 1/2\ Cl_{2(g)} \rightarrow CuCl_{(g)} \quad [1]$$

The pressures predicted by this treatment are shown in Figure 10. If one considers that a flux of 1 monolayer/second corresponds to a pressure of 1 x 10^{-6} torr the removal efficiencies observed here are not at all unreasonable. Another possibility is that UV exposure is enhancing the formation of the volatile trimer $(CuCl)_3$. As discussed previously, the trimer does not normally form in the submonolayer regime.

The results presented here are in contrast to other published investigations (2,3,4). We observe metal removal at less extreme conditions and to a greater extent than what has generally been observed. The most obvious difference in our experiments is the intensity of the light source. We have the ability to illuminate the sample with ≈ 500 milliwatts/cm^2 over the range of 260-320 nm, while Sugino *et.al.* (2,3,4), for instance, report a UV fluence of 22 milliwatts/cm^2 over the range 200-300 nm. This is a difference of more than 1 order of magnitude. By comparison, the silicon etching process would be enhanced by a factor of ≈ 100 with this increase in UV fluence. If the UV/Cl_2 metal removal process also exhibits this type of non-linear response to UV fluence these differences can be explained.

Conclusions

We have investigated the etching of silicon in the UV/Cl_2 system. We have found that there is a significant parameter space where a cleaning process can be performed while maintaining surface integrity. We have found evidence that the etching process is not first order in the UV fluence to the surface, and that surface photolysis dominates over gas phase photolysis in enhancing the etching process.

We have explored copper removal from both silicon and oxide surfaces in the UV/Cl_2 system. We have demonstrated that copper can be removed to the detection limit of our XPS (at least two orders of magnitude) at temperatures as low as 50 °C on both oxide and silicon surfaces. We have shown that the mechanism of removal in the submonolayer regime is fundamentally different than that in the bulk. We have not observed a dependence of removal efficiency on the composition of the surface, and in fact we do not need to etch silicon to remove copper. We have presented evidence that suggests that the UV is reducing higher oxidation states of copper as well as enhancing the volatility of copper chloride reaction products.

Acknowledgments

The research reported in this article was funded by FSI International. We would especially like to acknowledge the support and guidance of Fred Hiatt, Ty Fayfield and Dave Gray. We would also like to acknowledge the support of the NIST ATP program.

References

1. J. W. Butterbaugh, D. C. Gray, C. Fred Hiatt, H. H. Sawin, and A.S. Lawing, Proceedings of the Second International Symposium on Ultra Clean Processing of Silicon Surfaces, M. Heyns, M. Meuris, and P. Mertens eds., p. 229, Acco, Leuven, Belgium (1994).

2. Y. Sato, R. Sugino, T. Ito, Fujitsu Sci. Tech. J., **27**, 319 (1991).
3. R. Sugino, Y. Nara, H. Horie, T. Ito, J. Appl. Phys., **76**, 5498 (1994).
4. R. Sugino, Y. Okui, M. Shigeno, S. Okubo, K. Takasaki, and T. Ito, Proceedings of the 1995 International Symposium on Semiconductor Manufacturing, p. 262-265 (1995).
5. B.E. Deal and C.R. Helms, in Handbook of Semiconductor Wafer Cleaning Technology, W. Kern, ed., p. 316, Noyes Publications, Park Ridge, NJ (1993).
6. D.C. Montgomery, Design and Analysis of Experiments, p. 457, John Wiley and Sons, New York (1984).
7. F.A. Houle, J. Chem. Phys., **80**, 4851 (1984).
8. E. Ikawa, S. Sugito, and Y. Kurogi, Surface Science, **183**, 276 (1987).
9. E.A. Ogryzlo, D.L. Flamm, D.E. Ibbotson, and J.A. Mucha, J. Appl. Phys., **64**, 6510 (1988).
10. G. Ertl and J. Kuppers, Low Energy Electrons and Surface Chemistry, p. 65-83, VCH, Weinheim, FDR (1985).
11. H.F. Winters, J. Vac. Sci. Technol. A, **3**, 786 (1985).
12. H.F. Winters, J. Vac. Sci. Technol. B, **3**, 9 (1985).
13. W. Sesselman and T.J. Chuang, Surface Science, **176**, 32 (1986).
14. L.B. Pankratz, Thermodynamic Properties of Halides, p. 182-185, U.S. Bureau of Mines, Washington, DC (1984).
15. J.M. Smith and H.C. Van Ness, Introduction to Chemical Engineering Thermodynamics, p. 184-186, McGraw-Hill, New York (1975).

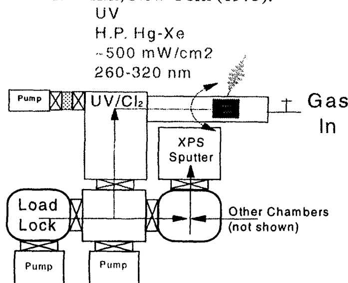

Figure 1 - Vacuum Chamber Schematic Diagram.

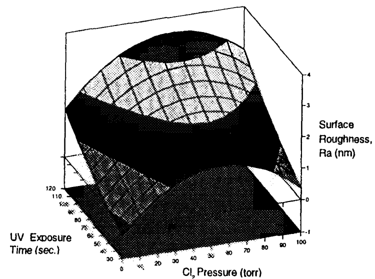

Figure 2 - Surface Roughness as a function of Cl_2 pressure and exposure time in UV/Cl_2 etching.

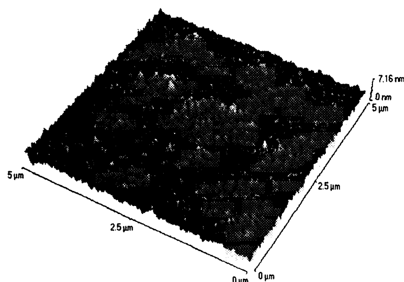

Figure 3 - SPM Image of Processed Wafer Surface. This sample was processed at 5 torr Cl_2 and 120 C, yielding a roughness of 6 Å rms.

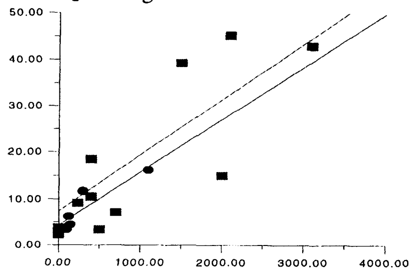

Figure 4 - Correlation Between Surface Roughness and Amount Etched. Y axis shows rms roughness (Å). X axis shows amount removed (Å).

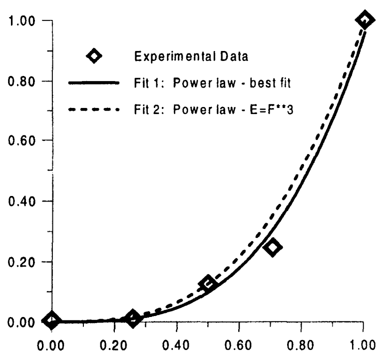

Figure 5 - Normalized Etch Rate vs. Normalized UV Fluence.

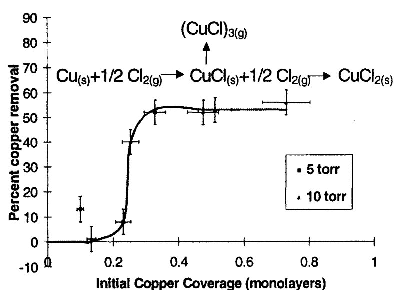

Figure 7 - Copper Removal with No UV as a function of surface coverage.

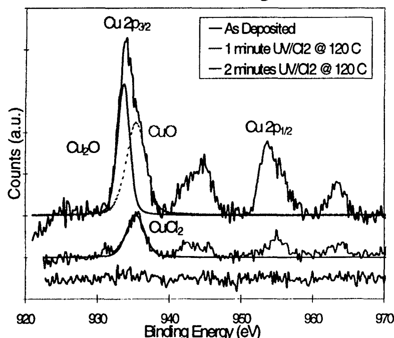

Figure 9 - Removal of Copper Deposited from Solution with UV/Cl_2. Note multiple oxidation states initially.

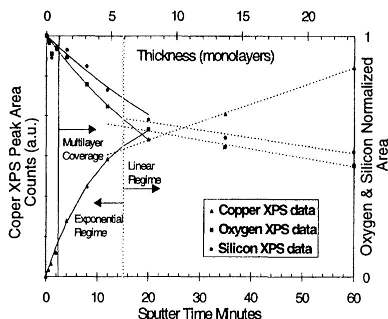

Figure 6 - Calibration Data for Copper Sputter Contamination.

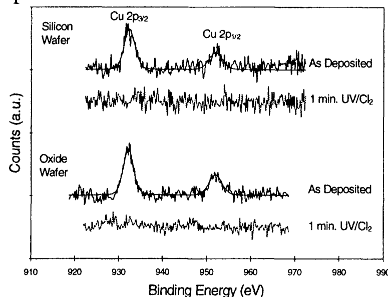

Figure 8 - Copper Removal from Oxide and Silicon Surfaces with UV/Cl_2 at 50 °C. This sample was sputter contaminated.

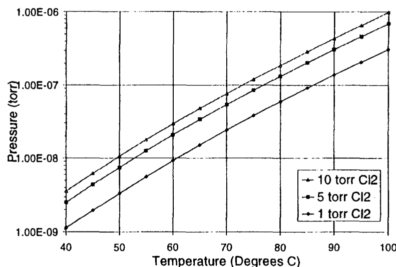

Figure 10 - Equilibrium Pressure of CuCl in a Chlorine Atmosphere. Parameter space shown is of interest for UV/Cl_2 cleaning.

Metal Removal with a ClF_3 Beam at Room Temperature

Jane P. Chang, Zhe Zhang, Han Xu and Herbert H. Sawin
Department of Chemical Engineering
Massachusetts Institute of Technology
Cambridge, MA. 02139

Jeffery W. Butterbaugh
FSI International
Chaska, MN. 55318

A room temperature ClF_3 molecular beam has been developed to remove metallic contaminants from wafer surfaces. Removal of sputter deposited copper and nickel from polysilicon and native oxide surfaces has been demonstrated. Copper removal occurs during the removal of less than 6 nm of silicon. The surface termination and surface roughening after the process have been investigated to evaluate its feasibility for metal contamination removal. Our results showed potential applicability for removing metallic contamination from wafer surfaces at room temperature.

Introduction

Wafer cleaning is a critical process in the fabrication of microelectronics especially when the feature sizes shrink down to sub-quarter-micron range. To incorporate cleaning process into the integrated-and-automated system, dry cleaning has been widely studied to replace the conventional wet etching process. Wet cleans to remove copper and other metal contaminants are used in the semiconductor industry. Developing dry etching process for etching copper or copper removal is therefore demanded. Surface termination, roughness, and residues are the few major factors used to assess the feasibility of dry cleaning processes.

Thermal beam has been studied due to its ability to achieve highly anisotropic and almost damage-free etching profiles[1]. ClF_3, which can etch silicon spontaneously at room temperature[2], has been expected as the cleaning gas for the apparatus after chemical vapor deposition and also etching gas for semiconductor substrates[3]. In this paper, we report the work using a ClF_3 beam at ambient temperature to clean monolayer metal contamination. The focus is on the copper removal; the other transition metals, such as nickel will also be discussed.

Experimental Setup

The apparatus used in this work is shown in Figure 1. The UHV analytical chamber

has the X-ray Photoelectron Spectroscopy (XPS) capability to analyze and determine the sample surface compositions. The analytical chamber is also equipped with an ion gun for sputtering cleaning samples and metal targets (1 cm square metal foils of Ni, Cu, Fe, and other materials) which rest on a carousel to contaminate the sample surface with metal deposition. Atomic Force Microscopy (AFM) is available *ex-situ* for surface roughness studies.

A multiple beam chamber is connected to the analytical chamber by vacuum corridors through which samples can be transferred between any chambers in the apparatus while maintaining base pressures in the 10^{-8} Torr range. Samples can be introduced through the load-lock chambers without exposing any of the process chambers to the atmosphere. Up to three beams can be simultaneously impinged on a sample surface in this chamber. The thermal beam source is currently constructed to generate neutral radicals pyrolytically. The beam consists of an alumina tube for introducing gas, a coiled heating filament, a cooling water jacket and a thermocouple for temperature control and measurement. Gases such as chlorotrifluoride (ClF_3), and chlorine (Cl_2) are currently being used. Feed gas can be heated to 1000°C to dissociate or excite the gas molecules like chlorine, while the highly reactive ClF_3 is used at room temperature. 99.0% pure ClF_3 gas was used in this work and the flux level is approximately $5x10^{16}$ cm^{-2} s^{-1}. The etching or deposition rates can be measured by laser interferometry or ellipsometry while product emissions can be monitored by mass spectrometry.

Both n-type and undoped polysilicon samples are studied in this work. Silicon samples with native oxide are pre-cleaned by ethanol before position into the chamber. Appreciable amount of carbon contamination is observed under XPS analysis. Silicon surface is generally yielded by *in situ* argon ion sputtering to remove the native oxide.

Up to 15 monolayers of copper can be sputter deposited on the sample surface using a 3kV Ar ion beam. The copper target is biased at 1.2 kV to achieve maximum copper deposition and minimize the sputtering of the adjacent targets. The amount of copper deposited on the sample surface is controlled by deposition time and detailed calibration can be found in the work of Lawing[4].

Results and Discussions

Copper removal from both Si and SiO_2 surfaces using a room temperature ClF_3 beam has been demonstrated. ClF_3 is a chemically unstable species which can be cracked at room temperature to yield fluorine atoms. An Arrhenius plot for the silicon etching rate of clean and copper contaminated samples is shown in Figure 2. The etching of silicon was measured for exposures to a room temperature ClF_3 beam with the polysilicon sample held at various temperatures. The etching of silicon is enhanced by copper and nickel (not shown) contamination of the sample. The apparent activation energies derived from the slope of Arrhenius plot are given, but are both small. The small apparent activation energies suggest that the rate limiting step does not have a high potential energy barrier, but can be affected by the presence of a metal contaminant.

Shown in Figure 3 is the XPS copper and silicon signals as a function of sputtered copper contamination levels. The XPS copper signal saturates for a dosage of approximately 1.5 monolayer while the underlying silicon substrate signal is not appreciably attenuated at dosages as great as 3 monolayer of copper. This strongly indicates that the sputtered copper forms islands rather than being uniformly dispersed on the surface.

Figures 4 and 6 show the XPS signals for the Cu(2p) emission from undoped polysilicon samples at 20°C and 250°C before and after exposure to the ClF_3 beam. It was found that to obtain quantitative information on the metal removal, it was necessary to lightly sputter the sample with an argon ion beam before XPS analysis. The light sputtering removed the adsorbed fluorine, but did not remove a significant amount of the metal. The plots indicate that approximately 55% and 80% of the copper is removed, respectively, and that the removal occurs with the etching of 6 nanometers or less polysilicon. Since the etching of more silicon does not decrease the copper contamination level and copper halides are not volatile, it strongly suggests that the copper islands are not etched by the ClF_3, but the dispersed copper is etched.

The peak area data from Figures 4 and 6 is computed and plotted in Figures 5 and 7 indicating the removal of the copper during the initial etching of the surface. The data points for beam flux intensities which differ by a factor of two are indicated accordingly. Two types of sample preparation were used and no effect was shown on the results. No significant dependency is observed for either the flux intensity of the ClF_3 beam or the amount of substrate being etching. This is consistent with the model that the beam removes the dispersed copper, but not the copper islands.

The XPS signals for the Cu(2p) emission from n-type polysilicon samples before and after exposure to a ClF_3 beam with the sample at 250°C are shown in Figure 8. In this case, the sample surface was exposed to a light argon ion bombardment after sputter deposition. The plots indicate that approximately 80% of the copper was removed from the Si sample; the same as was observed without the argon ion bombardment after copper sputter deposition. The results for differing sample preparations are shown in Figure 9. The plots indicate that approximately 60% of the copper was removed from the polysilicon sample at room temperature and that the removal occurred with the etching of 13 nanometers or less polysilicon. Sputtering of the copper contaminated sample with an argon ion beam for 5 minutes or exposure to oxygen during deposition did not affect the removal. Again, this is consistent with the removal of the dispersed copper but no removal of the copper islands. Figure 10 shows that etching of the sample at 20°C and then heating the sample to 250°C for 5 minutes did not affect the removal. This suggests that the greater removal observed with the 250°C etching was not a result of thermal diffusion.

The results for n-type polysilicon were very similar to those for undoped polysilicon. Figure 11 shows the XPS signals for the Cu(2p) emission at 20°C before and after exposure to a ClF_3 beam. Approximately 60% of the copper was removed with the Si sample at room temperature, and the removal occurred with etching of 6 nanometers or less polysilicon -- the copper removal was not increased by the removing more substrate Si.

The XPS signals for the Cu(2p) emission are shown for two different dosages of copper in Figure 12. The plots indicate that approximately 21% of the copper was not removed with the dosage of 3 monolayer of copper and that approximately 35% of the copper was not removed with the dosage of 15 monolayers of copper. In both cases, 25 nm of polysilicon was etched. This is consistent with the removal of the dispersed copper but no removal of the copper islands. The copper island should form a larger fraction of the surface as the copper dosage is increased, but is not linear in the exposure as the island has a thickness which also varies with dosage.

To test the hypothesis that copper islands remain on the surface blocking the copper removal, single crystal silicon samples were etched and Atomic Force Microscopy was performed to measure the roughness of the surface after etching. Shown in Figure 13 is a typical scan of such a surface. It can be seen that the surface is quite smooth with the exception of several spikes. We believe that these spikes are associated with the copper islands which block the etching. It should be noted that the vertical scale is exaggerated.

Using XPS, the F and Cl coverages after exposure to ClF_3 beams were measured, Figure 14. For all the cases with different sample temperatures and copper dosages, the surface was largely terminated with F and little Cl was observed. This is consistent with the Si-F bond being stronger than the Si-Cl bond.

The removal of copper was also studied for contaminants deposited on the native oxide of the silicon sample, Figure 15. After the sample exposed to ClF_3 at room temperature, the chemical shifts indicate that part of the F and Cu are bonded together, but other F is bonded to the Si and reduced copper (i.e. copper which is not reacted with a halogen) exists. After this surface has been sputtered lightly with an argon ion beam; the Cu-F bonds have been broken releasing the F which was bonded to the copper. Copper remains on the surface and with some F bonded to the silicon in the substrate. The sample was then heated up to 250°C and exposed to ClF_3. The copper signal has been reduced and a strong F signal exists. A light argon ion sputtering was then performed to drive off the F bonded to the copper allowing a quantitative measure of the copper. At these conditions, the native oxide was etched and copper removal is witnessed.

The removal of nickel from a polysilicon surface has been observed at 250°C sample temperature, as shown in Figure 16. However, it is not as efficient as copper removal since the nickel halides are even less volatile than the copper halides.

Conclusion

We have investigated the removal of transition metals using a room temperature ClF_3 beam to etch and clean silicon samples. Copper contamination catalyzes the etching of polysilicon using a ClF_3 beam. Copper removal from both Si and SiO_2 surfaces has been demonstrated. ClF_3 etches silicon spontaneously at room temperature and removes copper from the surface, while it etches SiO_2 at elevated temperature and removes copper. It is believed that the copper forms islands during deposition, and ClF_3 only removes the dispersed copper but not the copper islands.

We have established a process to reduce wafer surface contamination such as copper and nickel while an acceptable surface is maintained.

Acknowledgments

We would like to thank FSI International for its financial support and acknowledge John Hietzinger, Fred Hiatt, Ty Fayfield and Dave Gray at FSI for their guidance and useful discussions.

References

1. K. Suzuki, et.al., J. Appl. Phys. **77** (12), 6624 (1995)
2. D.E. Ibbotson, et. al., Appl. Phys. Lett. **44**, 1129 (1984).
3. Y. Saito, et. al., J. Vac. Sci. Technol. **B 9** (5), 2503 (1991).
4. A. S. Lawing , et. al., published elsewhere in this volume

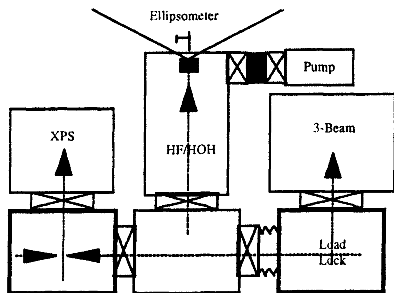

Figure 1: Schematic diagram of cleaning apparatus.

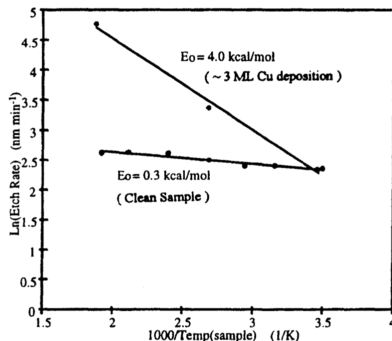

Figure 2: Arrhenius plot of the silicon etching rate for clean and Cu contaminated samples.

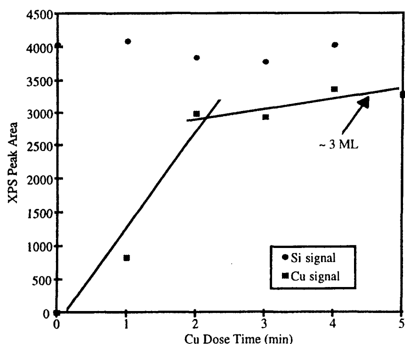

Figure 3: XPS signals for Cu(2p) and Si(2p) as a function of sputtered copper contamination level.

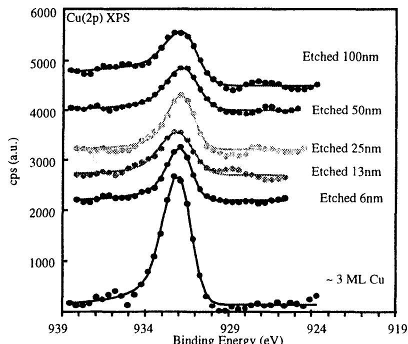

Figure 4: XPS signal for Cu(2p) from Undoped Poly-Si at 20°C

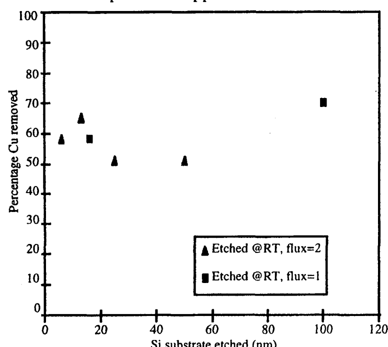

Figure 5: Cu removal efficiency from Undoped Poly-Si at 20°C

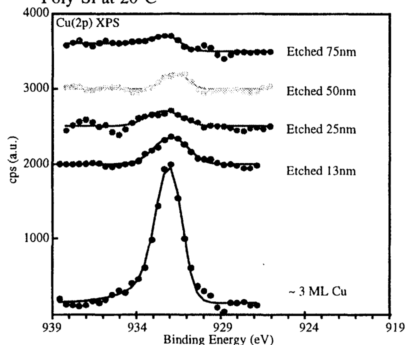

Figure 6: XPS signal for Cu(2p)from Undoped Poly-Si at 250°C

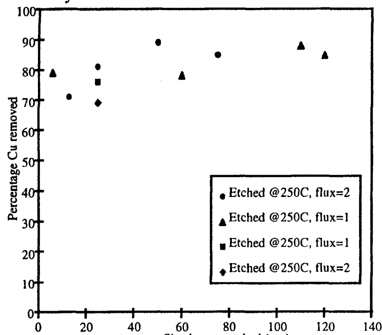

Figure 7: Cu removal efficiency from undoped Poly-Si at 250°C

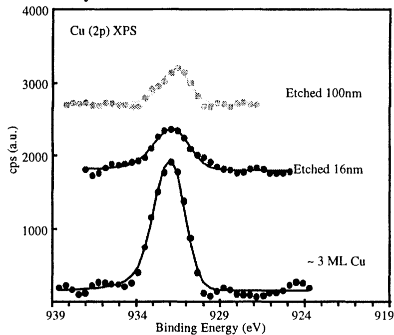

Figure 8: XPS signal for Cu(2p) from n-type Poly-Si at 250°C

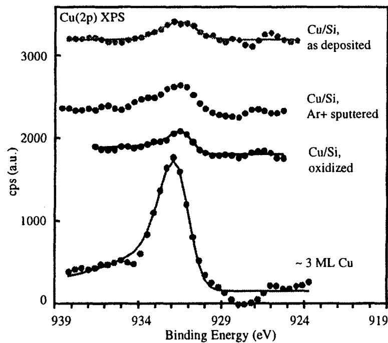

Figure 9: XPS signal for Cu(2p) from n-type Poly-Si at 250°C

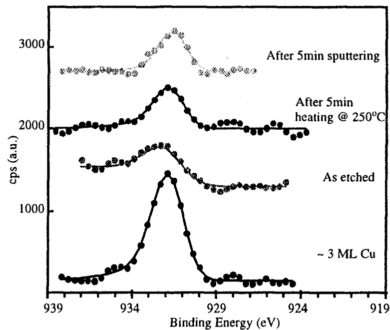

Figure 10: XPS signal for Cu(2p) from n-type Poly-Si at 20°C, different sample preparations

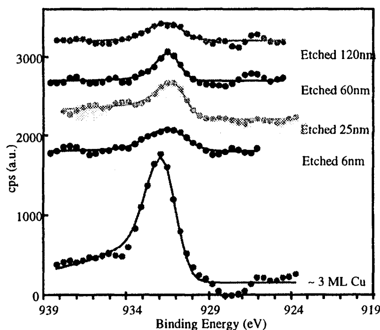

Figure 11: XPS signal for Cu(2p) from n-type Poly-Si at 20°C

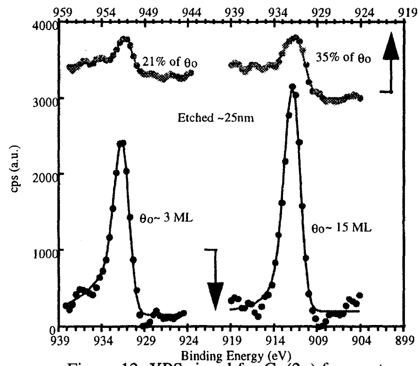

Figure 12: XPS signal for Cu(2p) from n-type Poly-Si at 250°C, two different dosages of copper.

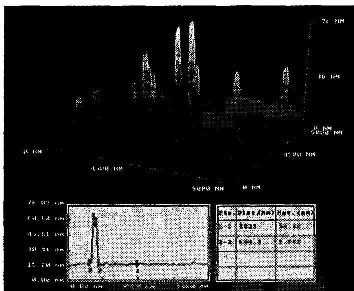

Figure 13: AFM image of copper contaminated Si surface after etching in a ClF3 beam. Copper forms islands during deposition.

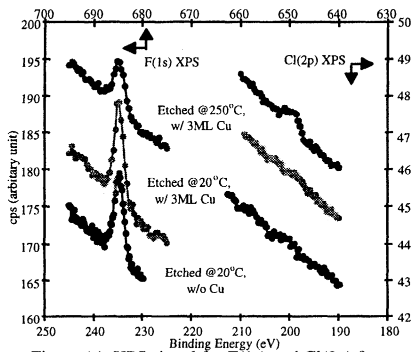

Figure 14: XPS signal for F(1s) and Cl(2p) for Polysilicon sample after exposure to a ClF3 beam.

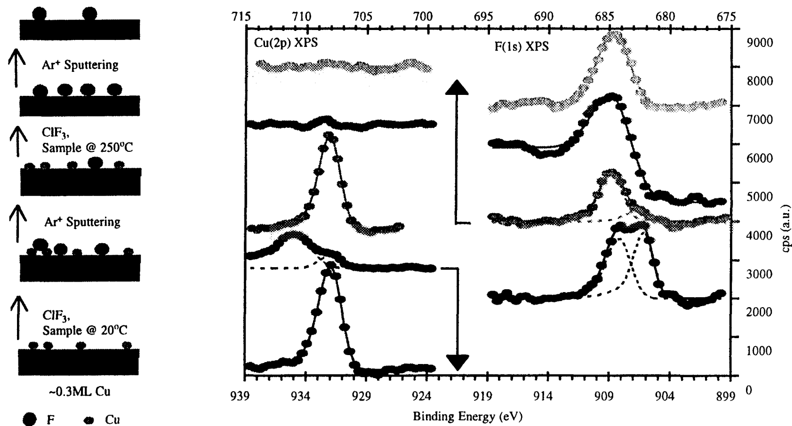

Figure 15: XPS signals of Cu(2p) and F(1s) from undoped Poly-Si sample with a native oxide under the sputtered copper. No measurable Cu exists after the sample is exposed to ClF_3 with the sample at 250°C.

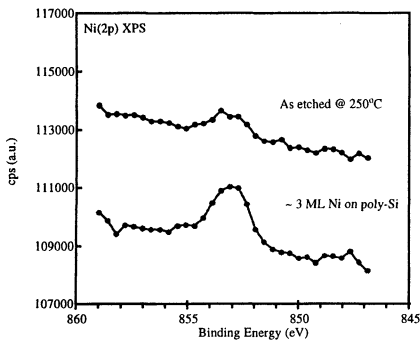

Figure 16: XPS signal for Ni(2p) from undoped Poly-Si at 250°C

SUB-MONOLAYER IRON AND COPPER REMOVAL BY EXPOSURE TO 1,1,1,5,5,5-HEXAFLUORO-2,4-PENTANEDIONE (H^+hfac)

S.E. Beck, M.A. George, K.M. Young, D.A. Moniot,
D.A. Bohling, A.A. Badowski, and A.P. Lane[†]
Air Products and Chemicals, Inc., Allentown, PA 18195
[†]Texas Instruments, Dallas, TX 75265

Sub-monolayers of iron and copper on SiO_2 and Si substrates were exposed to 1,1,1,5,5,5-hexafluoro-2,4-pentanedione (H^+hfac). The effects of exposure time, H^+hfac partial pressure, and carrier gas played a role in the removal of the surface contamination. For the particular process examined there is a lower limit to the removal. TOF-SIMS revealed the presence of trifluoroacetate, FeF^+, and FeC^+ suggesting some decomposition of H^+hfac on the wafer surface and the reaction of the decomposition products with surface species.

INTRODUCTION

With each new generation of microelectronic devices, more stringent requirements are placed upon the condition of the wafer surface before processing. Gas phase cleaning methodologies have been proposed as one way to improve the cleanliness of these surfaces. One of these methodologies is chemical vapor cleaning (CVC), a gas phase technique that removes transition metal contaminants from semiconductor surfaces.

Chemical vapor cleaning with 1,1,1,5,5,5-hexafluoro-2,4-pentanedione (H^+hfac) is a candidate for the gas phase removal of transition metals from silicon surfaces [1]. In this process, the gas (vapor) phase coordinating or chelating ligand (H^+hfac) reacts with a metallic species residing on the wafer surface forming a volatile coordination compound. This compound then desorbs from the wafer surface at low temperatures and is removed from the vicinity of the wafer by gas flow or vacuum. Previous work [2] with H^+hfac has focused on its reaction with copper oxide films where the typical reaction for the removal of the transition metal oxide is shown in Eqn. 1.

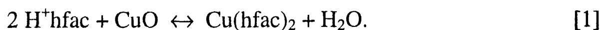

$$2\ H^+\text{hfac} + CuO \leftrightarrow Cu(\text{hfac})_2 + H_2O. \qquad [1]$$

Iron and copper are two of the most deleterious contaminants in microelectronics processing today. This work focuses on these two contaminants by extending previous work to the sub-monolayer level. By starting with fairly high surface concentrations of these contaminants (~10^{15} atoms/cm^2), we can gain insight into the mechanisms that may affect the removal of these contaminants.

EXPERIMENTAL

Iron and copper contaminated samples were prepared on bare and thermally oxidized 150 mm diameter, {100} silicon wafers. All wafers underwent SC1 and SC2 cleans before the intentional contamination step. Metals were deposited by evaporation with the wafers held at room temperature to ensure that the metals resided on the wafer surface prior to H^+hfac exposure. Three points on each wafer were analyzed by total reflection x-ray fluorescence (TXRF) before cutting them into 1cm × 1cm squares for processing. Additionally, several wafers were mapped by TXRF and the concentration of the primary contaminant was found to vary by less than 30% over the entire wafer. Typical contamination levels on the samples exposed to H^+hfac were 1.6×10^{15} Fe atoms/cm^2 and 1.1×10^{15} Cu atoms/cm^2 as determined by TXRF.

Exposures to the CVC chemistry were conducted in a vertical furnace capable of handling wafers up to 3 inches in diameter. A special pedestal was manufactured to hold the 1cm × 1cm samples perpendicular to the gas flow in the reactor. All exposures were performed in either N_2 or air (79% N_2/21% O_2) ambients at a total pressure of 7.6 torr and a temperature of 300 °C. A syringe pump (ATI Orion Sage Model M365) was used to inject H^+hfac into the process chamber through a 0.005 inch ID PEEK capillary at a rate of 0.05 to 0.2 ml/min. Partial pressures of H^+hfac were in the range between 0.32 and 1.13 torr. Exposure times varied from 6 to 60 minutes.

Surface concentrations after exposure to H^+hfac were determined by secondary ion mass spectrometry (SIMS) and TXRF. SIMS was performed using a 6 keV O_2^+ primary ion beam at 60° on a Perkin Elmer 6600 quadrupole SIMS system [3]. TXRF was done on a Technos TREX 610-T. SIMS performed on the as-deposited material always indicated lower surface concentrations compared to TXRF measurements on the same samples due to saturation of the secondary ion detector. Saturation of the detector did not occur on samples that were exposed to H^+hfac because of the lower metal concentration. X-ray photoelectron spectroscopy done on the as-deposited material revealed that most of the iron was in the state of either FeOOH or Fe_2O_3, while the copper was present as both CuO and Cu_2O.

RESULTS

Figures 1 and 2 depict the results of exposing the iron or copper on SiO_2 coated wafers to H^+hfac. Each data point represents the average surface metal concentration of three samples after H^+hfac exposure as determined by SIMS. The error bars reflect the scatter in these data. The final metallic concentration is clearly dependent upon the metallic species, the H^+hfac partial pressure, the exposure time, and the composition of the ambient. Note that a limit of removal is achieved for both types of samples ($\sim 5 \times 10^{12}$ cm^{-2} for the iron contaminated SiO_2 samples and $\sim 3 \times 10^{12}$ cm^{-2} for the copper contaminated SiO_2 samples). Exposures of iron on native oxide on silicon wafers for 20 minutes with an H^+hfac partial pressure of 0.61 torr in air results in a final surface iron concentration of approximately $3 \pm 1 \times 10^{13}$ cm^{-2}, almost one order of magnitude higher than the iron on thermal silicon dioxide after the same exposure.

Iron was always present at approximately 2×10^{14} cm^{-2} for the as-deposited copper on silicon dioxide samples used in this study. When these samples were exposed to H^+hfac the lowest final iron concentration detected was 4×10^{12} cm^{-2}, which is consistent with the lowest concentration results depicted in Figures 1 and 2. Copper was always present on the as-deposited iron on silicon dioxide samples at approximately 1×10^{11} cm^{-2}. Exposures of these samples to H^+hfac did not reduce the level of the copper contamination.

Previous work [4] using XPS as an analytical tool revealed carbon and fluorine on Si and SiO_2 surfaces after H^+hfac exposure. The F(1s) portion of the XPS spectra always contained two peaks (metallic fluoride and organic fluoride), while the C(1s) spectra contained adventitious carbon and a peak related to CF_x. Time-of-flight SIMS (TOF-SIMS) [5] was used in the present study to further our understanding of these observations by XPS. Negative ion mode TOF-SIMS detected the presence of FeF^- and the trifluoroacetate anion, while positive ion TOF-SIMS revealed FeC^+ on the Fe contaminated samples (See Table I). Intact hfac on the exposed surfaces is inferred from the presence of $C_5F_6O_2H^-$. The fluorinated species were not identified on as-deposited samples, while the FeC^+ signal increased after H^+hfac exposure.

DISCUSSION

Iron contaminated samples required longer exposure times than the copper samples to reach a minimum value. This is most likely due to differences in the reaction kinetics of the two metallic species with H^+hfac. Previous work with metal oxide powders exposed to H^+hfac showed that the reaction rate of copper oxides was higher than iron

TABLE I Ions detected by TOF-SIMS performed on an iron contaminated sample exposed to H^+hfac.

Ion Detected (amu)	Species Identified
67.93	FeC^+
68.99	CF_3^-
74.93	FeF^+
85.00	CF_3O^-
113.00	$C_2F_3O_2^-$
207.07	$C_5F_6O_2H^-$

oxides [6]. It was proposed that the bulk metal oxide reaction rates are proportional to the cleaning efficiencies of these metals. The data presented here confirm this hypothesis. For the removal of surface contaminants the reaction of the iron oxides with H^+hfac may be sterically hindered by the need for an additional H^+hfac molecule as compared to the reaction with copper oxides. This hypothesis is further suggested by comparing Eqn. 1 with the idealized overall reaction of H^+hfac with Fe_2O_3 shown in Eqn. 2.

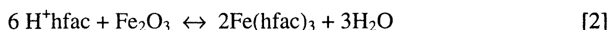

$$6\,H^+hfac + Fe_2O_3 \leftrightarrow 2Fe(hfac)_3 + 3H_2O \qquad [2]$$

The reaction may also be hindered by the cracking of the H^+hfac molecule on the wafer surface. Our TOF-SIMS results are a good indication that some of the H^+hfac molecules do crack on the wafer surface with the formation of carbonaceous and fluorinated species. These results are consistent with our work on thin iron oxide films where TOF-SIMS revealed these same by-product species after H^+hfac exposure [7]. The formation of Fe_3C would impede the removal of Fe, since this carbide is much less reactive with H^+hfac. Removal of iron by the formation of $Fe(tfaa)_3$ is also possible [7], but this molecule is less volatile than $Fe(hfac)_3$. As shown in Fig. 2, oxygen plays a role in the removal of iron from the SiO_2 surface, but is much less important in the removal of copper. These results may be indicative of several mechanisms occurring on the surface of the wafer. One possibility is that the presence of oxygen may change the state of the surface iron, converting it to a form that has a higher reactivity with H^+hfac. The oxygen may also assist in the removal of surface carbonaceous material that could impede the reaction of H^+hfac with the surface iron contaminant.

For the conditions examined, there is an optimum H^+hfac partial pressure for the removal of iron (around 0.6 torr). This is not as evident in the removal of copper. From these data we conclude that mass transfer and the chemical reaction rate at the wafer sur-

face must play a vital role in the removal of these metals. As noted above, the removal of iron may be sterically hindered compared to copper. The fact that an optimum partial pressure was observed indicates that among other potential variables affecting removal, the fluence of the reactant to the wafer surface, along with surface diffusion, are important to the removal phenomena.

The ultimate surface reaction efficiency may also be limited by the chemical state of the surface metal. For the as-deposited material, this state was known since the concentration of the contaminant was within the detection limits of XPS. Below 1×10^{13} cm^{-2}, the surface oxidation state and specific chemical environment is difficult to identify due to limitations in surface analytical techniques. As the surface concentration of the metal is decreased during CVC there are less metal oxide clusters and more individual unimolecular metal species that can react with the environment. It is possible that these individual molecules bond with substrate atoms, forming metal silicides and metal silicates which are much less reactive with H^+hfac. Additionally, it is also possible that these individual molecules react with the decomposing H^+hfac. A consistent limit to the removal process with different initial metal contamination concentrations (as observed above) is indicative of some reactive limit to the simple thermal removal process related to the surface concentration of the contaminant.

We also speculate that the differences in removal efficiency of iron with H^+hfac in the presence of oxygen versus nitrogen may be coupled to a complex competing surface reaction mechanism. From our data it is clear that the predominant reaction responsible for the removal of Fe^{n+} from SiO_2 surfaces is through the formation of $Fe(hfac)_3$ (see Eqn. [2] and reference [7]). Our observation of increased reaction efficiency with oxygen versus nitrogen, and decreased efficiency of the reaction at the highest H^+hfac partial pressures could be a probe into the rates of some potentially competing reactions at the surface. Iron as Fe^{II} likely can disproportionate under the reactive conditions seen in these experiments [7]. Depending on the gas phase environment, the resulting Fe^0 metastable species can react either with the solid state environment (most likely a slow process), oxygen in the ambient, H^+hfac, or some other surface adsorbed organic/fluoro-organic species. We believe that we are not actually seeing "burning" of the carbonaceous species from the surfaces at the process temperature of this study, but rather are seeing a competition between oxygen and H^+hfac with the Fe^0. Reaction of the iron with oxygen clearly would produce an iron oxide, likely aiding in the eventual removal of that metal as $Fe(hfac)_3$. In contrast, reaction of Fe^0 with H^+hfac will likely lead to a number of reactions, including formation of Fe_xC, $Fe(tfaa)_y$, and some FeF_z. Both the $Fe(tfaa)_y$ and the FeF_z will eventually lead to iron removal. However, the Fe_xC will likely remain on the surface. Exposure of the iron contaminated surface to high partial pressures of H^+hfac without gaseous oxygen will result in more side reactions and fewer reactions of the Fe^0 with matrix oxygen. This may explain why roughly half an order of magnitude difference is seen in the reactive efficiency of H^+hfac with iron versus copper doped samples.

Thermodynamics may also play a role in limiting the final concentration of the surface contaminant. The CVC process is, in its most general form, the reverse reaction of a chemical vapor deposition process. Preliminary calculations of the Gibbs free energy required for the CVC reaction indicate that the cleaning process is thermodynamically an uphill process [8]. If this is true, then the lower limit of removal may be due to achieving a steady state condition within the reactor. That is, an equivalent amount of removal and deposition is occurring during the process. This results in a final surface concentration above that required for microelectronics processing (i.e., 10^{12} cm^{-2} versus 10^{10} cm^{-2}) for the thermally driven process. The slightly higher Fe level after CVC may be a good measure of the extent of Fe_xC formation above the intrinsic thermal steady state reaction limit. This hypothesis should be subject to calculation and dependent on the concentration and purity of the incident H^+hfac.

CONCLUSIONS

Reactions of H^+hfac with sub-monolayer concentrations of iron and copper reveal that the removal process for these transition metals is complex and dependent on several mechanisms. These mechanisms are a complex function of the process ambient and the chemical state of the surface metal. Oxygen in the process ambient plays a significant role in the removal of iron. Entropic factors can somewhat explain the difference in the rates of removal of surface iron and copper. For both iron and copper a lower limit of removal was found after the simple thermal process (approximately 4×10^{12} cm^{-2} and 2×10^{12} cm^{-2}, respectively). This lower limit may be related to the formation of metal silicides and silicates or to achieving a steady state condition where removal and deposition occur at equivalent rates. Improvements to the lower limit of removal with this thermal process are a current topic of investigation in our laboratory.

ACKNOWLEDGEMENTS

The authors gratefully acknowledge many helpful discussions with J.G. Langan, S.W. Rynders, S.M. Fine (Air Products), D.A. Roberts (Schumacher), M.R. Frost, S. Novak (Evans East), J.M. Metz and P. Lindley (Charles Evans and Associates). This work was supported in part by the ARPA-National Center for Advanced Information Components Manufacturing Program administered by the Office of Naval Research (contract no. N0014-94-C-0076) and in part by Air Products and Chemicals, Inc. independent research funds.

REFERENCES

1. J.C. Ivankovits, D.A. Bohling, A. Lane, and D.A. Roberts, in Proceedings of the Second International Symposium on Cleaning Technology in Semiconductor Device Manufacturing, J. Ruzyllo and R.E. Novak, Editors, **PV 92-12**, p. 105, The Electrochemical Society Proceedings Series, Pennington, NJ (1992).
2. M.A. George, D.W. Hess, S.E. Beck, J.C. Ivankovits, D.A. Bohling, B.S. Felker, and A.P. Lane, J. Electrochem. Soc., **142**, 961 (1995).
3. M.R. Frost, in Contamination Control and Defect Reduction in Semiconductor Manufacturing III, D.N. Schmidt, D. Reedy, R.L. Guldi, and J.V. Martinez de Pinillos, Editors, **PV 94-9**, p. 339, The Electrochemical Society Proceedings Series, Pennington, NJ (1994).
4. S.E. Beck, A.G. Gilicinski, B.S. Felker, J.G. Langan, D.A. Bohling, M.A. George, J.C. Ivankovits, and R.M. Rynders, in Interface Control of Electrical, Chemical, and Mechanical Properties, S.P. Murarka, K. Rose, T. Ohmi, and T. Seidel, Editors, **Vol. 318**, p. 263, Materials Research Society Proceedings, Pittsburgh, PA (1994).
5. K.G. Standing, in Secondary Ion Mass Spectrometry: SIMS VI, A. Benninghoven, A.M. Huber, and H.W. Werner, Editors, p. 225, John Wiley & Sons, New York (1988).
6. D.A. Roberts, G.O. Voloshin, J.A.T. Norman, D.A. Bohling, S.E. Beck, S.W. Rynders, and M.A. George, in Environmental, Productivity, and Defect Issues in Semiconductor Manufacturing, p. 16.25, SEMI/Europe, 1994.
7. M.A. George, D.W. Hess, S.E. Beck, K.M. Young, G. Voloshin, D.A. Bohling, and A.P. Lane, *submitted to the J. Electrochem. Soc.*; and M.A. George, D.W. Hess, S.E. Beck, D.A. Bohling, D.A. Roberts, G. Voloshin, R. Vrtis, and A.P. Lane, *these proceedings.*
8. A.A. Badowski, M.A. George, and S.E. Beck, *unpublished.*

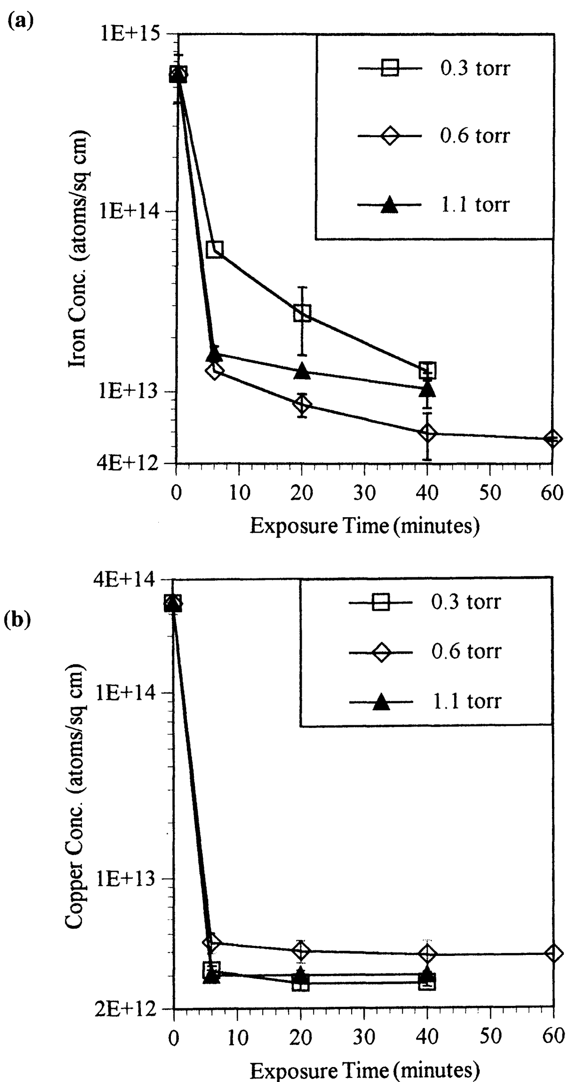

Figure 1. The final (a) iron and (b) copper surface concentrations after exposure to H^{+}hfac in air. Surface concentrations were determined by SIMS.

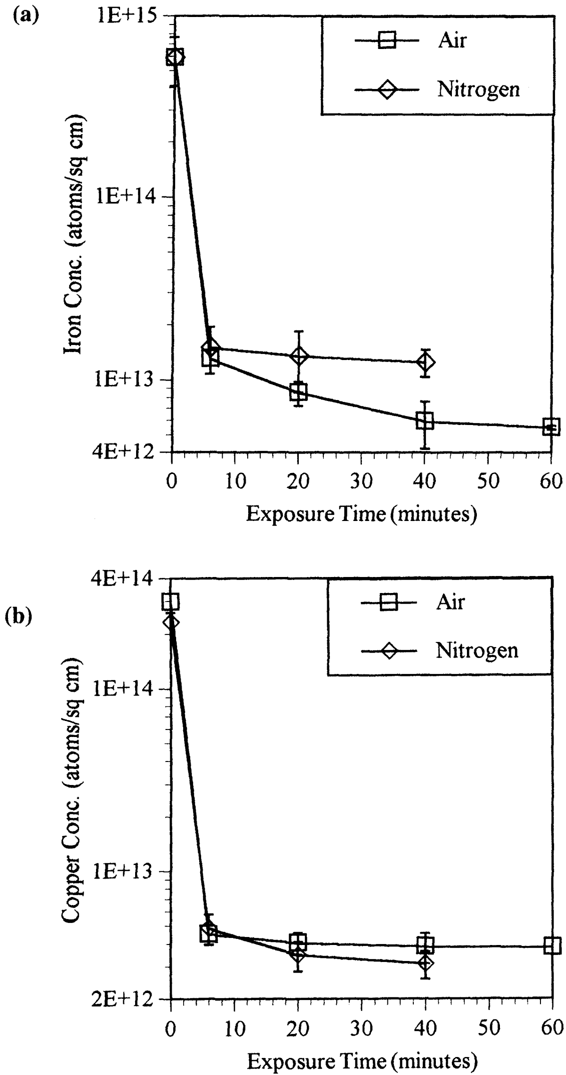

Figure 2. The final (a) iron and (b) copper surface concentrations after exposure to H^+hfac in air or N_2. The H^+hfac partial pressure was 0.61 torr for air exposures and 0.8 torr for N_2 exposures.

REACTION OF 1,1,1,5,5,5-HEXAFLUORO-2,4-PENTANEDIONE (H^{+}hfac) WITH IRON OXIDE THIN FILMS

M.A. George*§, D.W. Hess*, S.E. Beck§, K. M.Young§, D.A. Roberts†, R. Vrtis†, G. Voloshin†, D.A. Bohling§, and A.P. Lane‡
*Lehigh University, Dept. of Chemical Engineering, Bethlehem, PA 18015
§Air Products and Chemicals, Inc., Allentown, PA 18195
†Schumacher, Carlsbad, CA 92009
‡Texas Instruments, Dallas, TX 75265

ABSTRACT

The application of chelation chemistry to the removal of iron and iron oxide via heterogeneous gas phase reactions has been investigated. Reactions of iron and iron oxide with 1,1,1,5,5,5-hexafluoro-2,4-pentanedione (H^{+}hfac), and 1,1,1-trifluoro acetic acid (H^{+}tfaa) provide insight into the mechanisms responsible for H^{+}hfac wafer cleaning. Substitutional nucleophilic exchange reactions are only partially responsible for the removal of Fe contamination. In addition, H^{+}hfac decomposition at the gamma carbon results in the formation of volatile Fe^{III} complexes of trifluoroacetates and hexafluoropentandionates. Although decomposition of the H^{+}hfac occurs, this decomposition appears to have little affect on the cleaning process.

INTRODUCTION

The continuing decrease in integrated circuit (IC) pattern sizes demands significant advances in manufacturing technology. Since single wafer integrated processing approaches can result in improved process control and thus improved IC yield compared to batch processing (1,2), much emphasis has been placed on the replacement of liquid techniques by vapor phase methods. An important implication of these trends is the need to develop vapor phase cleaning chemistries. The β-diketone, H^{+}hfac, has been explored as a possible vapor phase cleaning agent for Fe and other transition metals such as Cu, Ni, and Cr (3). This approach to vapor phase cleaning exploits the high vapor pressure of metal-β-diketonate complexes (4,5). While mechanisms for the formation of $Fe^{III}(hfac)_3$ coordinated complexes in liquid solutions are well documented, the surface mechanisms involved in iron etching using the free β-diketone ligand have yet to be determined (6,7). The intent of this paper is to report results of an investigation which focused on the mechanisms of a vapor phase cleaning technique based on chelation (coordination) chemistry for iron oxide thin films. In order to develop chemical processes which rely on this particular chelation chemistry, it is necessary to understand the relationship between the chemical state of the species to be removed (iron) and the

heterogenous reactions observed (8).

In a previous paper, we investigated the use of H^+hfac to etch copper thin films through a heterogeneous gas-solid reaction (9). In this paper, the interactions of the coordinating complexes of H^+hfac, and H^+tfaa with iron oxides are examined. X-ray photoelectron spectroscopy (XPS), Fourier transform infrared spectroscopy (FTIR) and time-of-flight secondary ion mass spectroscopy (TOF-SIMS) were used to investigate the reactions of these compounds with iron thin films of various oxidation states.

EXPERIMENTAL PROCEDURES

Three types of iron oxide thin films were prepared by annealing in atmospheres consisting of O_2 or mixtures of CO and CO_2; a film of Fe_2O_3, a film with stoichiometry near Fe_3O_4 (Type I) and a film with stoichiometry between Fe_3O_4 and FeO (Type II)(10,11). Thin films of FeOOH were prepared by annealing sputtered FeO_x thin films in an ambient of H_2O. Ratios of Fe^{II} and Fe^{III} were determined for oxidized thin films by potentiometric titrations (12,13).

All reactions were conducted at a total pressure of 8 torr and a N_2 flow rate of 28 sccm and temperatures between 140 and 400 °C. Partial pressures of the coordinating compounds were: H^+hfac, 0.7 torr and H^+tfaa, 0.5 torr. A second reactor was used to identify volatile reaction products. Volatile byproducts from bulk iron oxide powders were trapped by condensation of the reactor effluent at 20 to 25 °C.

Surface analysis was performed on a Kratos XSAM 800 hemispherical capacitor electron energy analyzer using $Mg_{k\alpha}$ radiation (1253.6 eV). Fe(2p), O(1s), C(1s), Si(2p) and F(1s) chemical state information was deduced by shifts in the relative binding energy of the respective line positions (14). The Fe(2p) spectra was background subtracted according to the method of Shirley (15). For Fe(2p) spectra, the following peak assignments were used: 706.7 eV for $Fe^{(0)}$, 709.7 eV for Fe^{II} and 711.3 eV for Fe^{III} (16,17).

RESULTS

Thin film iron oxides, obtained directly from the oxidation furnace, exhibit significant adventitious carbon contamination, as observed via an XPS peak at 284.6 eV. Upon exposure of these oxide films to H^+hfac at temperatures above 180 °C, curve fitting of the C(1s) spectra reveals a new peak at 283.8 eV. This binding energy is consistent with a metal carbide bond that could be due to the presence of adventitious carbon. To study this phenomenon in more detail, surfaces were cleaned by an Ar/O_2 plasma at 140 °C. This process removes a significant quantity of adventitious carbon, but also oxidizes the incompletely oxidized surface of type I and type II iron oxide thin films to Fe_2O_3. After H+hfac exposures each spectrum exhibits peaks at 292, 288, and 286 eV, characteristic of CF_3, C=O, and C-O groups, respectively. The H^+hfac treated surface still shows an

additional peak at 283.8 eV, which is not observed in reactions with H^+tfaa, and is consistent with carbide formation.

Significant changes are also observed in the O(1s) spectrum for each thin film. Spectra from iron oxide thin films reacted with H^+hfac or H^+tfaa exhibit peaks at 529, 531, and 533.5 eV. A shift of the spectra to higher binding energy and peak broadening are observed in all cases. The most surface sensitive spectra (smallest takeoff angle) reveals an increase in intensity of the peak at 533.5 eV which arises from the H_2O reaction byproduct. Another feature observed in the O(1s) spectrum of iron oxide surfaces reacted with H^+hfac is a peak at 536 eV. The appearance of this peak is elucidated only after subtracting the contributions of the lower binding energy peaks. This feature is attributed to $\pi \rightarrow \pi^*$ shakeup satellites for the carbonyl groups of the hfac ligand (18,19,20).

Fe(2p) spectra for iron oxide thin films reveal significant bond disruption upon reaction with either H^+tfaa or H^+hfac. In each case, the films show an increase in the amount of Fe^{II} after reaction. The ratio of Fe^{II}/Fe^{III}, determined by curve fitting, increases with analysis depth. Figure 1 shows this ratio versus take-off angle for reactions of H^+hfac and H^+tfaa with different oxidation state iron oxide thin films at 300 °C. This increase in Fe^{II} relative to Fe^{III} indicates that reaction of the thin films is mediated through some type of reduction process of the metal oxide. Growth of an iron carbide peak at 706.7 eV, whose presence is inferred by the peak at 283.8 eV in the C(1s) spectra, is not observed in the Fe(2p) spectra. This is consistent with the presence of oxygen nearest neighbors in the iron thin films.

F(1s) spectra revealed peaks at 688 and 686 eV; we assign CF_3 and Fe-F_x bonds to these, respectively. In these studies, no Fe-F_x bonding was detected for iron oxide films comprised mostly of Fe^{III} reacted with H^+hfac. In contrast, type II thin films contain substantial amounts of Fe-F_x, but this amount was lower than that for films reacted with H^+tfaa. As shown in Figure 2 this ratio is smallest for the near surface region. Fluorination of Fe therefore is not expected to account for the observed increase of Fe^{III} on these surfaces, as depicted in Figure 1.

Samples of type II thin film oxides reacted with H^+hfac and H^+tfaa were analyzed by positive ion TOF-SIMS (21). Mass spectral analysis revealed a signal at 67.93 amu which is attributed to FeC^+. While this is not conclusive evidence for carbide formation, it is consistent with observations made by XPS.

Experiments exposing bulk powders of mixed iron oxide ($Fe^{(0)}$,FeO, Fe_2O_3 and Fe_3O_4) to H^+hfac reactions were conducted. Figure 3 shows a FTIR spectrum of condensate trapped from this reaction. For reference, the IR spectrum for anhydrous $Cr(hfac)_3$ is also included. $Cr(hfac)_3$ and $Fe(hfac)_3$ have similar spectra in this region (22,23). Curve fitting of the IR spectra revealed several peaks in the symmetric stretching region of C-O.

The appearance of several peaks in this region indicates a different reaction product than stoichiometric $Fe^{III}(hfac)_3$.

The C(1s) spectrum of the condensate clearly shows CF_3, C=O and CH bonds at 292, 288 and 285 eV respectively. These same features are also observed after reaction of H^+hfac and H^+tfaa with iron oxide thin films. Analyzing ratios of atomic species identified in the XPS spectrum reveals a fluorine deficiency in the condensate as compared to that expected for stoichiometric $Fe(hfac)_3$. Further analysis of the powder sample by potentiometric titration for Fe^{II} and Fe^{III} revealed no Fe^{II} above the background level in the 1M HCl solution (1 ppm). This indicates that the volatile reaction product responsible for iron oxide etching is comprised solely of Fe^{III}. Since the reaction product is deficient in fluorine and composed of all Fe^{III}, ligands other than hfac are likely present in the reaction byproduct.

DISCUSSION

To explain the observations described above, plausible mechanisms for reactions of H^+hfac and H^+tfaa with various iron oxides are proposed. These results and propsosed mechanisms have important implications for the further development of chemical vapor cleaning (CVC) of surfaces in semiconductor manufacture (24).

The formation of a carbide species is inconsistent with a substitutional nucleophilic reaction and is indicative of a decomposition of H^+hfac. Identified through XPS and TOF-SIMS surface analysis techniques, the formation is due solely to reactions of hfac ligands with iron oxide. From the structure of the H^+hfac molecule, one can deduce a logical scheme of events that can lead to ligand decomposition. Figure 4 depicts a plausible mechanism for the formation of two tfaa species along with additional H_2O from the decomposition of the hfac ligand. Negative ion TOF-SIMS surface analysis of a type II iron oxide reacted with H^+hfac revealed a peaks at 112.99 and 207 amu which we attribute to $tfaa^-$ and $hfac^-$, respectively. This observation of tfaa motivated an investigation of the reaction of iron oxide thin films with H^+tfaa.

The utilization of H^+tfaa for removing Fe contamination from a wafer surface has been explored previously (3,25). For H^+tfaa the expected reaction is the formation of the relatively volatile iron(III) tristrifluoroacetate ($Fe^{III}(tfaa)_3$) complex and H_2O. The volatility of the tfaa complex is less than that of the hfac complex which suggests that hfac would constitute a more useful cleaning agent(26,27). Reactions of H^+tfaa with the iron oxide films lead to the formation of $Fe\text{-}F_x$ bonds observed in the F(1s) spectra; the formation of these Fe-F bonds indicates some surface decomposition of the H^+tfaa.

The absence of $\pi \rightarrow \pi^*$ shakeup satellite in the O(1s) spectra of the H^+tfaa reacted surface is consistent with a bidentate form of the tfaa complex on the surface. Indeed, this bidentate form of $Fe(tfaa)_3$ has been identified through IR and Raman spectroscopies

(28). The presence of surface bound H_2O reaction product is confirmed by the appearance of a peak at 533.5 eV in the O(1s) spectra.

The analysis of volatile reaction products provides another indication of mechanisms involved with H^+hfac reactions. XPS analysis of reactor effluent condensate indicates that the reaction byproducts are deficient in fluorine compared to that expected for $Fe(hfac)_3$. This observation is consistent with an iron complex containing both hfac and tfaa ligands in various ratios. If this is correct, trifluoroacetate ligands should be observed in the reaction products. FTIR spectra of tfaa and hfac ligands are similar, except for the C-O stretching regions (29). Curve fitted FTIR spectra of the trapped condensate reveals four peaks in the symmetric stretching region of the C-O bonds (Figure 3). While not definitive, these peaks (1422, 1439, 1451, and 1467 cm^{-1}) are compelling evidence for a mixture of hfac and tfaa ligands. The C-O stretch in $Fe^{III}(hfac)_3$ has a single peak at 1430 cm^{-1} and $Fe^{III}(tfaa)_3$ has a single peak at 1435 cm^{-1} (22,28). Peak broadening and shifting would be expected for mixed ligand systems due to reduction in overall complex symmetry at the metal center.

F^{19} NMR spectroscopy can differentiate between tfaa and hfac ligands. However, a technique to separate the ligands from paramagnetic Fe is necessary. A sample of reactor effluent condensate was dissolved in methanol (CH_3OH) and Fe^{III} precipitated as FeOOH by adding excess ammonium hydroxide (NH_4OH). A F^{19} spectrum of the supernatant liquid reveals several peaks, the most intense being centered at -76.1 ppm and -77.8 ppm relative to a reference of $CFCl_3$(0 ppm). These two peaks coincide with chemical shifts observed for standard solutions of H^+tfaa and H^+hfac, respectively. The intensity ratio of hfac:tfaa for these peaks is 3:1, indicating an overall ratio of 3 hfac ligands for each H^+tfaa ligand in the reactor effluent condensate. Several other unidentified less intense peaks are observed in the F^{19} spectrum (-87, -86, -85, -77, and -73.5 ppm) which have chemical shifts consistent with fluoro-methyl groups. These data confirm that other fluorinated ligands, of which H^+tfaa is the most abundant, are also responsible for forming volatile Fe^{III} complexes.

Relative amounts of metal fluoride and carbon fluoride coupled with data on the relative amounts of Fe^{II} and Fe^{III} can provide insight into why H^+hfac decomposes. Detailed inspection of Figure 2 shows that more metal fluoride is formed for thin films with greater quantities of Fe^{II}. The volatile reaction byproduct has been identified as a Fe^{III} compound. How can Fe^{III} complexes be created from a material that is predominately Fe^{II}? We speculate that disproportionation of the $Fe^{II}O$ is responsible as illustrated in equation 1.

$$3Fe^{II}O \rightleftharpoons Fe^{III}{}_2O_3 + Fe^{(0)} \qquad [1]$$

We do not believe that $Fe^{(0)}$ actually exists in the film as an isolable species; rather, its reactivity is so great that it reacts in a concerted fashion with surrounding species from

either the film or the ligand. Indeed, the lability of Fe^{II} compounds is well-documented in Fischer-Tropsch catalysis (30). It is reasonable to expect some decomposition of the trifluoro methyl groups because of the reactive nature of reduced Fe. This decomposition is confirmed by analysis of the XPS results of the reaction of H^+hfac and $Fe^{(0)}$ where carbide, metal fluoride and $C\text{-}F_2$ are observed. The reduction of Fe and the subsequent decomposition of the ligand can account for the observation of metal fluoride bonds by XPS in oxide films.

The decomposition of the H^+hfac might be expected to reduce the effectiveness of the cleaning process. The etch rate of a type II iron oxide thin film was 0.07 nm/min at 325 ^oC, 0.7 torr H^+hfac and 7.6 torr total pressure; the entire film was removed to the underlying SiO_2, with a final surface concentration determined by SIMS of 6×10^{12} atoms/cm^2 +/-30%. Further work has shown that similar surface concentrations are achieved in similar reactions with monolayer coverages (31).

CONCLUSIONS

Reactions of H^+hfac with various oxidation states of Fe in the form of well defined thin films has been studied and the implications for a surface cleaning process has been discussed. The ideal chelation product desired for removing Fe contamination in this process is $Fe^{III}(hfac)_3$, due to its extremely high vapor pressure. In this study, we have shown that a nucleophilic substitution reaction may only be partially responsible for removal of Fe contamination.

A second reaction mechanism results in hfac ligand decomposition which leads to the formation of a mixture of tfaa and hfac ligands. While the volatility of this coordination compound is less than that of $Fe^{III}(hfac)_3$ the vapor pressure is still large enough to be effective for cleaning to surface concentrations near 5×10^{12} atoms/cm^2. Other decomposition products such as FeF_x and FeC are also observed on the surface. While the reaction of hfac with bulk FeF_3 to form a volatile coordination compound is expected, possible reactions for the removal of FeC are not obvious.

ACKNOWLEDGMENTS

This work was jointly funded by ARPA's National Center for Advanced Information Components Manufacturing (NCAICM) under Office of Naval Research (ONR) contract number N0014-94-C-0076 and by Air Products and Chemicals, Inc.

REFERENCES

1. The National Technology Roadmap for Semiconductors, Semiconductor Industry Association, Eds., (1994).
2. T. Ohmi, Proceedings of the 2nd International Symposium on Cleaning Technology in Semiconductor Device Manufacturing, J. Ruzyllo and R.E. Novak, Eds.,Electrochemical Society, Vol. 94-7, pp 3-14 (1994).

3. J.C. Ivankovits, D.A. Bohling, A. Lane, and D.A. Roberts, Proceedings of the 2nd International Symposium on Cleaning Technology in Semiconductor Device Manufacturing, J. Ruzyllo and R.E. Novak, Eds.,Electrochemical Society, Vol. 92-12, 105 (1992).
4. R.E. Sievers and Sadlowski, Science, Vol. 201(4352),pp 217-223 (1978).
5. T.P. Melia and R. Merrifield, J. Inorg. Nucl. Chem., Vol. 32, pp 2573-2579, (1970).
6. F.A. Cotton and G. Wilkinson, Advanced Inorganic Chemistry, Fifth Edition, John Wiley & Sons, New York, (1988).
7. F. Basolo and R.G. Pearson, Mechanisms of Inorganic Reactions: A Study of Metal Complexes in Solution, 2nd Edition, John Wiley & Sons, New York, (1967).
8. C.R. Helms and Heungsoo Park, Surface Chemical Cleaning and Passivation for Semiconductor Processing, G.S. Higashi, E. A. Irene and T. Ohmi, Eds. Mat. Res. Soc. Proc.Vol. 315, Pittsburgh, PA, pp. 287-297, (1993).
9. M.A. George, D.W. Hess, S.E. Beck, D.A. Bohling, B.S. Felker, and A.P. Lane, J. Electrochem. Soc. (1995).
10. H.T. Ellingham, J. of The Society of Chemical Industry, May, pp 125-133(1944).
11. D. R. Gaskell, Introduction to Metallurgical Thermodynamics, Chapter 10, McGraw-Hill, New York, N.Y., (1973).
12. D.G. Peters, J.M. Hayes and G.M. Hieftje, A Brief Introduction to Modern Chemical Analysis, W. B Saunders, Philadelphia PA, (1976).
13. L.S. Darken and R.W. Gurry, J. Am. Chem. Soc., **67**, pp 1398-1412, (1945).
14. C.D. Wagner, W.M. Riggs, L.E. Davis, J.F. Moulder, and G.E. Muilenberg, Handbook of Photoelectron Spectroscopy, Perkin-Elmer Corporation, Eden Prarie, MN (1979).
15. D.A. Shirley, Phys., Rev. **B5**, pp 4709 (1972).
16. C.R. Brundle, T.J. Chuang, and K. Wandelt, Surf. Scie., **68**, pp 459-468, (1977).
17. N.S. McIntyre and D.G. Zetaruk, Anal. Chem., **49**(11), pp 1521-1529, (1977).
18. Donnelly V.M. and Gross, M.E. J. Vac. Sci. Technol. A, **11**(1), Jan/Feb (1993).
19. Gardella, J.A. Jr., Ferguson, S.A., Chin, R.L.; Appl. Spectrosc., **40**, pp 224(1986).
20. M.P. Keane, S. Lunell, A. Naves De Brito, M. Carlsson-Gothe, S. Svensson, B. Wannberg, and L. Karlsson, J. Electron. Spectrosc. Rel. Mater., **56**, pp 313 (1991) .
21. K.G. Standing, Proceedings of the Sixth International Conference on Secondary Ionization Mass Spectrometry (SIMS VI), A. Benninhoven, A. M. Huber, and H.W. Werner, Eds., John Wiley& Sons, New York, pp 225-230, (1988).
22. R.W. Mosher, L. Morris and R.E. Sievers, Inorganic Chemistry, pp 411-412, (1963).
23. R.D. Hancock and D.A. Thornton, J. of Molecular Structure, **4**, pp 377-383, (1969).
24. S.E. Beck, D.A. Bohling, B.S. Felker, M. A. George, A.G. Gilicinski, J.C. Ivankovits, J.G. Langan, S.W.Rynders, J.A.T. Norman, D.A. Roberts, G. Voloshin, D.M. Hess and A. Lane, Proceedings of the 3rd International Conference on Cleaning Technology in Semiconductor Manufacturing, J. Ruzyllo and R.E. Novak, Eds., Electrochem. Soc., Vol. 94-7, pp 253, (1994).
25. J.C. Ivankovits, D.A. Roberts, J.A.T. Norman and D.A. Bohling, United States Patent 5,028724 (1992).
26. V.B. Lazarev, J.H. Greenberg, Z.P. Ozerova, and G.A. Sharpataya, J. of Therm. Anal., **33**, pp 797-799 (1988).
27. E.A. Mazurenko, A.I. Gerasimchuk, and Zh. N. Bublik, Ukrainskii Khimicheskii Zhurnal, **57**(10), pp 1011-1016, (1991).
28. H.G.M. Edwards and I.R. Lewis, J. of Molecular Structure, **296**, pp 15-20, (1993).
29. M. J. Baillie, D.H. Brown, K.C. Moss, and D.W.A. Sharp, J. Chem. Soc. (A), pp 3110-3114, (1968).
30. C.S. Kuivila, P.C. Stair, and J.B. Butt, J. Catalysis, **118**, pp 299-311, (1989).
31. S.E. Beck, M.A.George, D.A. Moniot, K.M. Young, D.A. Bohling, A.A. Badowski, and A.P. Lane, *This proceedings.*

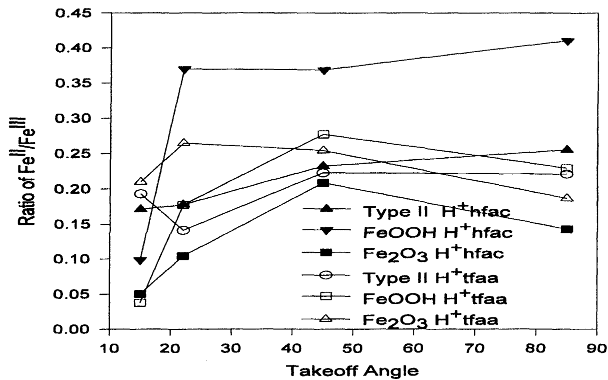

Figure 1. Ratio of Fe^{II}/Fe^{III} for different oxide films for reactions with H^+hfac and H^+tfaa at 300 °C.

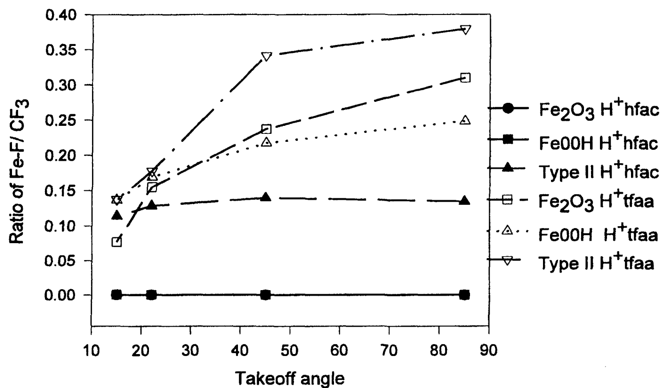

Figure 2. Ratios of CF_3/FeF for various iron oxide thin films with H^+hfac and H^+tfaa at 300 °C.

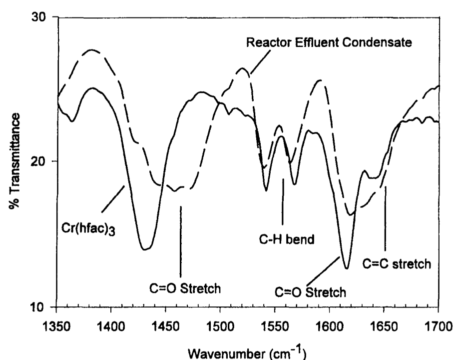

Figure 3. Transmission FTIR spectra of Cr(hfac)3 and reactor effluent condensate from reaction of H+hfac with iron oxide powder.

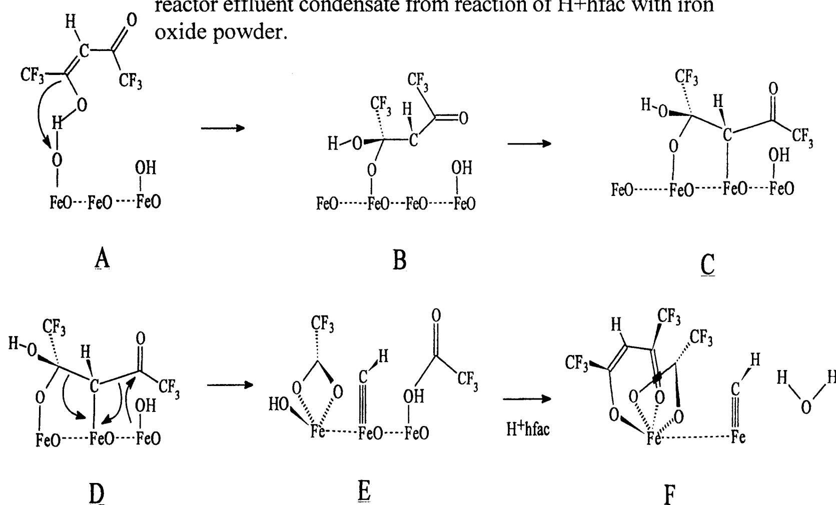

Figure 4. Hypothetical mechanism for the decomposition of H^+hfac on an iron oxide surface.

A: Initial chemisorption of H^+hfac between acidic proton and FeO_x surface.

B: Formation of sp^3 carbon through bridging surface oxygen.

C: Gamma carbon forms sp^3 carbon through bonding to iron.

D: Formation of surface carbyne or carbene with formation of chemisorbed H^+tfaa.

E: Protonation of surface FeO_x to chemisorbed H^+tfaa.

F: Reaction of second H^+tfaa with surface $Fe(tfaa)(OH)_{(ads)}$ forming mixed ligand complex of $Fe(tfaa)(hfac)_{(ads)}$ and H_2O. Iron "carbide" formation also occurs.

MONITORING OF SILICON SURFACE AFTER REACTIVE ION ETCHING

D.K. Hwang, J. Ruzyllo
Electronic Materials and Processing Research Laboratory
The Pennsylvania State University
University Park, PA 16802

E. Kamieniecki
QC Solutions, Inc.
Woburn, MA 01801

Silicon surfaces emerging from Reactive Ion Etching (RIE) of an oxide are covered with a fluorocarbon film and also physically damaged. Hence, they need to be properly conditioned prior to further processing. In this work the effect of post-RIE surface conditioning is monitored using non-contact surface charge and surface recombination lifetime measurements supported by XPS and Schottky diode current-voltage characterization.

INTRODUCTION

The chemistries used for selective Reactive Ion Etching (RIE) of silicon dioxide on silicon typically results in the deposition of a fluorocarbon film on the silicon surface [1]. RIE also involves ion bombardment of the silicon surface which results in surface damage and implantation of the elements in the etch chemistry [2]. Various methods have been used to characterize the surface after RIE and to evaluate the effectiveness of the surface conditioning procedures.

In this work, silicon wafers following RIE using a CHF_3 chemistry that resulted in the deposition of a surface fluorocarbon film were investigated. The fluorocarbon film was removed using a remote plasma oxidizing chemistry followed *in situ* with oxide etching. The objective of this work was to develop a methodology that would allow instant and easy monitoring of surface condition at various stages of the post-RIE surface conditioning process. Methods that are typically used to determine the outcome of the conditioning processes include electrical measurements of Schottky and MOS devices formed on etched surfaces [3,4], as well as methods allowing characterization of the chemical condition of the surface such as XPS. None of these methods, however, is capable of providing instant readings from the surfaces of the product wafers, and hence, none of them is useful for in-line monitoring of post-RIE surface treatments.

In this experiment, the condition of the silicon surface during treatments after RIE is monitored with a non-contact surface charge measurement method. The commercial system used in this study [5] also offers simultaneous measurement of the surface recombination lifetime. X-ray Photoelectron Spectroscopy (XPS) and Schottky diode current-voltage measurements were also used to characterize the condition of the silicon surface after the post-RIE cleans.

EXPERIMENTAL

Silicon wafers (p-type) with polymer approximately 95 Å thick were prepared by RIE in a CHF_3/Ar mixture at 75mTorr at a power of 400 watt. This process was performed on bare silicon wafers to simulate an oxide overetch process.

A laboratory style remote microwave plasma system, shown in Fig. 1, was used to condition the surface after the RIE. Microwaves at 2.45 Ghz were used to excite the process gases upstream of the wafer. The wafer is located inside a furnace where temperature can be controlled from room temperature to 1000°C. The system is pumped mechanically. All gas flows are controlled using mass flow controllers. The removal of the RIE polymer was achieved by using an O_2/Ar plasma. Previous work has shown that adding small amounts of NF_3 to this process greatly enhances the polymer removal process, therefore, this chemistry was used for this study [6]. The oxygen plasma clean results in a ultra-thin sub-oxide that was removed *in-situ* using an Ar/NF_3 chemistry. Etching of the sub-oxide using dilute HF (100:1) was also performed for comparison with the Ar/NF_3 remote plasma etch.

Characterization of the surface after cleaning was performed using surface charge measurements, Schottky diode I-V measurements, and XPS. Surface charge measurements were performed using a commercial Surface Charge Profiler (SCP) [5]. The measurement is based on the SPV effect which, in contrast to the similar methods, involves only a very thin (less than 0.4 μm) layer at the surface. In addition to SCP characterization, Schottky diodes were fabricated by thermal evaporation of Ti through a shadow mask onto the front surface of the wafer. Thermal evaporation of Al on the backside was used to form the back contact. Direct information concerning chemical composition of the surface was obtained by means of XPS, while surface roughness was evaluated using Atomic Force Microscopy (AFM).

RESULTS AND DISCUSSION

Figure 2 shows XPS spectra of the silicon surface during various steps of the cleaning process. The top spectrum labeled (a) represents the surface of a wafer after RIE. This surface shows coverage mainly by fluorine and carbon. The silicon peaks are

very weak indicating that the film covering the surface is fairly thick (95Å thick as indicated earlier). The spectrum of the surface after the O_2 plasma clean is labeled as (b) in Fig. 2. The carbon and fluorine coverage have been greatly reduced while oxygen coverage has increased significantly. The silicon peaks are more distinct indicating that the polymer film thickness on the surface has decreased. The decrease in film thickness is also supported by ellipsometry measurements. The remaining film is approximately 25Å thick as measured using a fixed index of refraction of 1.465. The XPS survey scans do not give much quantitative information concerning bonding of elements at the surface, however, the shoulders on the Si peaks indicate that the oxygen is bonded to silicon, which suggests that the remaining film has oxide-like qualities. The XPS spectrum of the surface after the Ar/NF_3 plasma exposure is labeled as (c) in the Fig 2. As shown, carbon, fluorine, and oxygen coverage have decreased after the etch. The silicon peaks in this case are very distinct indicating that the coverage of the surface by residual species is minimal. Since the wafers had to be removed from the process chamber and transferred to the XPS system for measurement the presence of adventitious carbon and oxygen could not be avoided. The presence of fluorine is most likely due to the Ar/NF_3 etch process.

Schottky diodes are sensitive to the condition of the silicon surface and in this study they are used to give a qualitative indication of differences in the surface condition due to changes in the surface conditioning procedures. The effects of the Ar/NF_3 etch on silicon wafers that did not receive an RIE process was also characterized using Schottky diodes. These I-V measurements were used to establish a baseline for comparison with the silicon samples that received RIE processing and also for comparison with surface charge measurements that will be discussed later.

Although the XPS results show that the relatively thick polymer was removed by the remote plasma cleaning process, further characterization using Schottky diodes fabricated on the etched surfaces indicate that the surface condition is different from the case of the control wafer. Figure 3 shows the I-V characteristics of Schottky diodes fabricated on silicon that did not receive RIE processing, but did go through the Ar/NF_3 remote plasma cleaning step. The I-V curves shown depart further from the curves for the control structures with increases in the NF_3 flow rate. Surface roughness is among the factors that may affect the I-V characteristics of the metal semiconductor contact. As the Ar/NF_3 remote plasma etch was found in this experiment to etch silicon (Fig. 4), the possibility of surface roughening had to be taken into account. To clarify this issue, Atomic Force Microscopy (AFM) was performed on the etched wafers to determine the extend of the possible surface roughening. Figure 5 shows the Rms values of roughness for different flow rates of NF_3 during the remote plasma Ar/NF_3 etching process. As seen, the wafer that was exposed to Ar remote plasma only did not show any increase in roughness as compared with the control wafer which was not exposed to any plasma processing. When NF_3 is added to the process gas flow however, roughening of the surface occurs. As the flow rate of NF_3 was increased the surface roughness continued to increase slightly (Fig. 5).

Figure 6 shows the I-V characteristics of the Ti contacts to the RIE processed surfaces after various steps during the post-RIE surface conditioning process. The surface after the O_2/Ar plasma exposure does not show a rectifying characteristics. The sub-oxide remaining on the surface after this cleaning step is preventing intimate contact of the metal to the surface and is acting as a resistor. Remote plasma processing steps used to etch the sub-oxide was found to result in a diode with rectifying characteristics. For comparison, a dip in dilute HF (100:1) was used to etch the sub-oxide. An I-V plot of this sample is shown in Fig. 6. The I-V characteristics in this case indicate that the surfaces are different after the polymer cleaning step. Different NF_3 flow rates during the Ar/NF_3 step affected the final surface condition.

The fabrication of Schottky diodes requires deposition of a metal on the silicon surface which may alter its condition. Therefore, an alternative method of silicon surface characterization was also applied in this study. This method involves non-contact measurement of surface charge using a commercial system [5]. For this system further preparation of the sample prior to measurements was not required. Figure 7 shows a schematic representation of the Surface Charge Profiler (SCP). Based on SPV measurements, the system measures surface depletion width which is directly related to the surface charge.

Figure 8 shows the depletion width of silicon samples that were exposed to the Ar/NF_3 remote plasma. Surface charge measurements show that process temperature changes the charge on the surface. Adding NF_3 to the process further changes the near surface region. SCP measurements indicate that the depletion width increases when NF_3 is added to the process gas. Since it was found that adding NF_3 to the process results in silicon etching and surface roughening it is possible that the increase of the surface roughness causes an increase of the surface charge leading to the increased depletion width. However, surface roughening is only one possible cause for the change in surface charge. The chemical state of surface can also have an effect on the density of surface charge. For instance, the surface charge measurements on the surface of chemically cleaned silicon have shown that surface charge varies significantly depending on the cleaning recipe as well as quality of chemicals used [7,8]. Based on the results obtained in this study however, more detailed conclusions in this regard cannot be drawn.

Figure 9 shows the depletion width of the RIE processed samples that went through the remote plasma cleaning procedure described earlier. Note the relatively high values of depletion layer width in this case which may be an indication of surface damage and/or contamination. However, it is also possible that the RIE process affected concentration of dopant in the silicon surface region. Other works have shown that the effective doping concentration in the near-surface region after RIE of p-type wafers is decreased due to boron deactivation by hydrogen and to the creation of donor-like defects near the surface [9,10]. The decrease in the surface effective doping concentration would result in a large depletion width such as that measured by the SCP. The large depletion

width is probably due to a combination of many factors with surface roughening during the oxide etch process having further impact. Remote plasma processing on bare silicon wafers indicate that surface roughening is occurring during the Ar/NF_3 process which causes an increase in the surface charge. In fact, the SCP measurements conducted on the RIE wafers show that the depletion width continues to increase with the increase of NF_3 content in the process gas flow (Fig. 9). The SCP measurements indicate that the surface after remote plasma cleaning using different NF_3 flow rates result in surfaces exhibiting different surface charge, probably due to surface roughening and different chemical state of the surface.

SUMMARY

In this study, cleaning and conditioning of RIE processed silicon surfaces was investigated. The CHF_3/Ar RIE chemistry resulted in the deposition of a polymer on the surface which was removed in a remote plasma process involving oxygen and NF_3. The silicon surface after the cleaning process was characterized using Schottky diodes and surface charge profiling. The results indicate that the surface condition is dependent on the cleaning process parameters, particularly the amount of NF_3 in the process gas mixture. Surface charge measurements indicate that there may be some dopant deactivation occurring on the samples that received the RIE process and that surface roughening inflicted during the remote plasma Ar/NF_3 exposures appears to further increase the surface charge. Cleaning of the surface after RIE further alters the surface, as indicated by changes in Schottky diode I-V characteristics and surface charge values. It was also shown that surface charge measurements in this study can provide a quick quantitative measure of the surface condition following RIE as well as during post-RIE surface conditioning.

ACKNOWLEDGMENTS

This study was supported in part by a grant from the Semiconductor Research Corporation. The authors would also like to thank Kevin Torek for assistance with the AFM measurements.

REFERENCES

[1] S.J. Fonash, J. Electrochem. Soc. 137, 12, 3885, 1990.
[2] G.S. Oehrlein, R.M. Tromp, Y.H. Lee, E.J. Petrillo, Appl. Phys. Lett. 45(4), 420, 1984.
[3] P. Spririto, C.M. Ransom, G.S. Oehrlein, Solid-State Electronics 29, 6, 607, 1986.
[4] Y. Ozaki, K. Ikata, Jap. J. Appl. Phys. 23(11), 1526, 1984.

[5] SCP Model 110, QC Solutions, Inc., Woburn, MA 01801.
[6] D.K. Hwang, J. Ruzyllo, R. Grant, ULSI Science and Technol. 1995, The Electrochem. Soc. PV95-5, 230, 1995.
[7] K. Torek, J. Ruzyllo, E. Kamieniecki, Proc. Third Intern. Symp. Cleaning Technol. in Semicond. Dev. Manufact., The Electrochem. Soc. PV94-7, 384, 1994.
[8] E. Kamieniecki, P. Roman, D. Hwang, J. Ruzyllo, Proc. Second Intern. Symp. on Ultra-clean Processing of Silicon Surface, ed. M. Heyns, M. Meuris, P. Mertens, p. 189, 1994.
[9] J.M. Heddleson, M.W. Horn, S.J. Fonash, D.C. Nguyen, J. Vac. Sci. Technol. B6(1), 280, Jan/Feb, 1988.
[10] X. Mu, S.J. Fonash, IEEE Electron Dev. Lett. EDL-6, 8, 410, 1985.

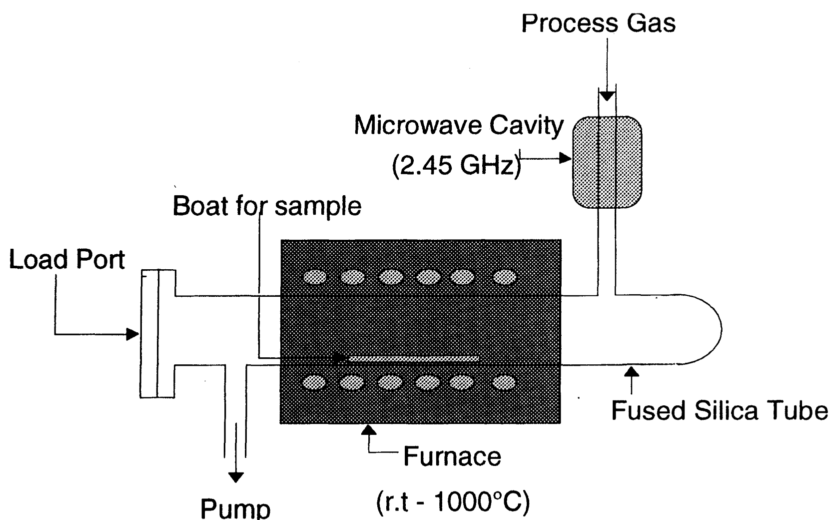

Figure 1: Schematic of the Remote Plasma System used in this study

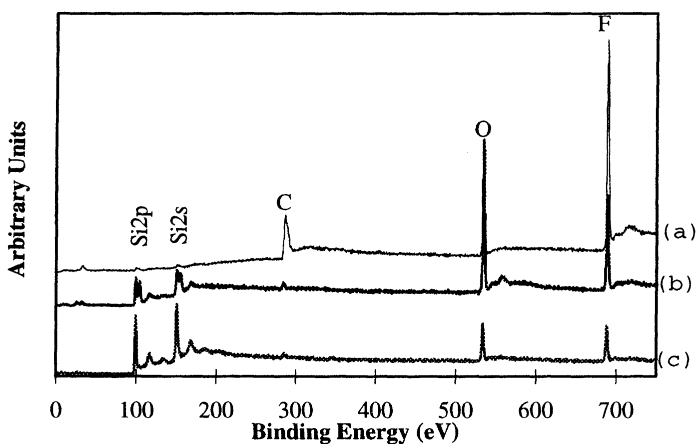

Figure 2: XPS spectrums of RIE processed silicon surface after various steps of the remote plasma clean (a) after RIE (b) after $O_2/Ar/NF_3$ remote plasma (c) after Ar/NF_3 remote plasma.

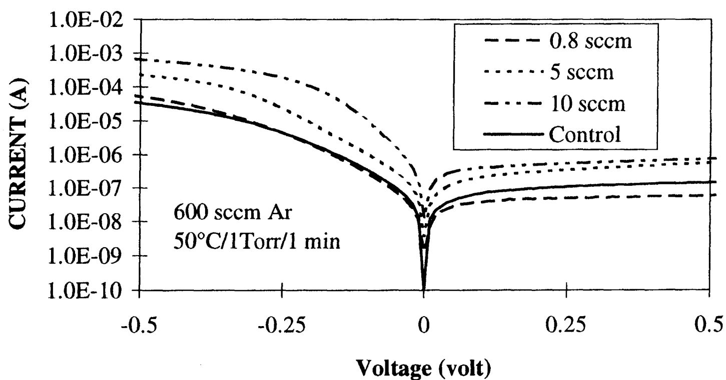

Figure 3: Characteristics of Schottky diode I-V of silicon wafers that have been etched using Ar/NF_3 remote plasma with different NF_3 flow rates.

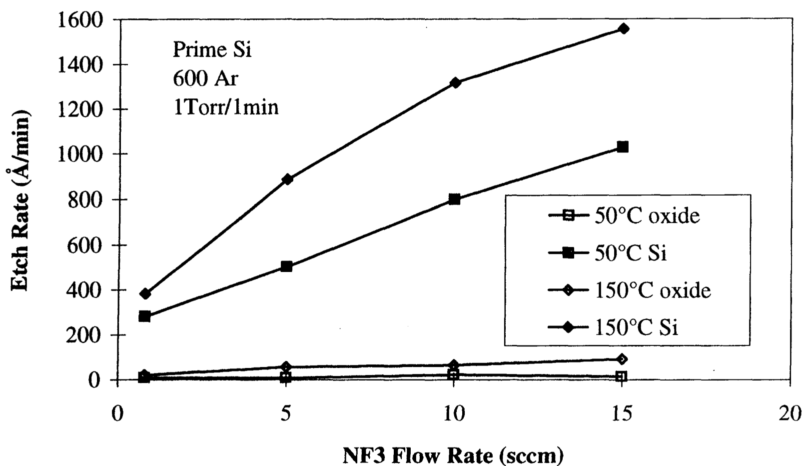

Figure 4: Etch rate of silicon and silicon dioxide in Ar/NF_3 remote plasma.

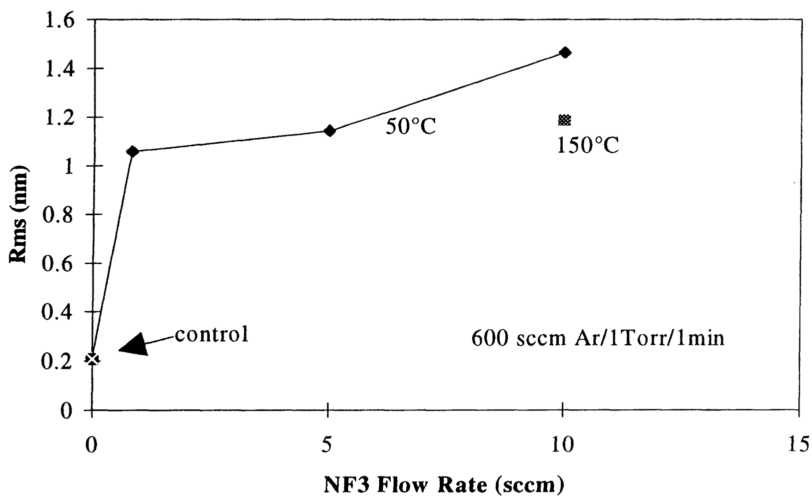

Figure 5: AFM measurements of silicon surfaces exposed to Ar/NF_3 remote plasma under different NF_3 flow rates.

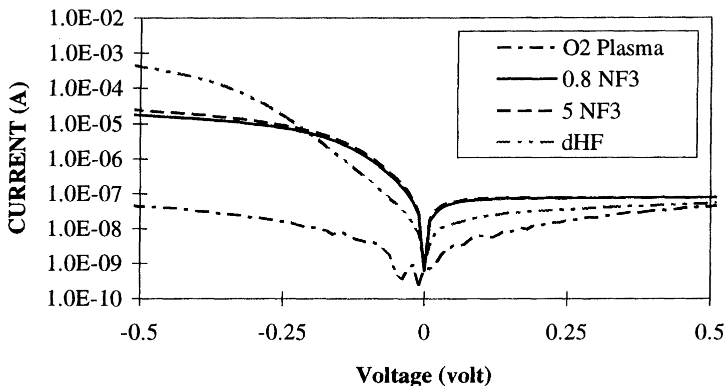

Figure 6: Characteristics of Schottky diode I-V of RIE processed Si wafers after various steps in the remote plasma cleaning procedure and also with different oxide etch steps.

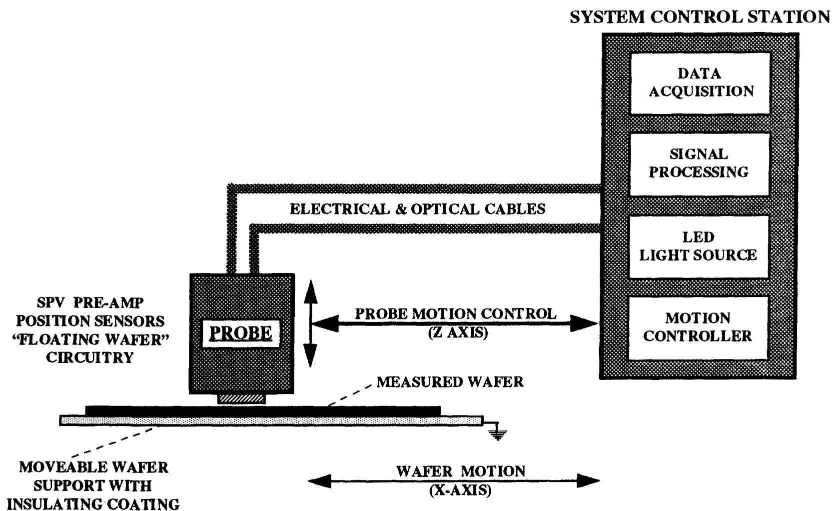

Figure 7: Schematic representation of the Surface Charge Profiler (SCP).

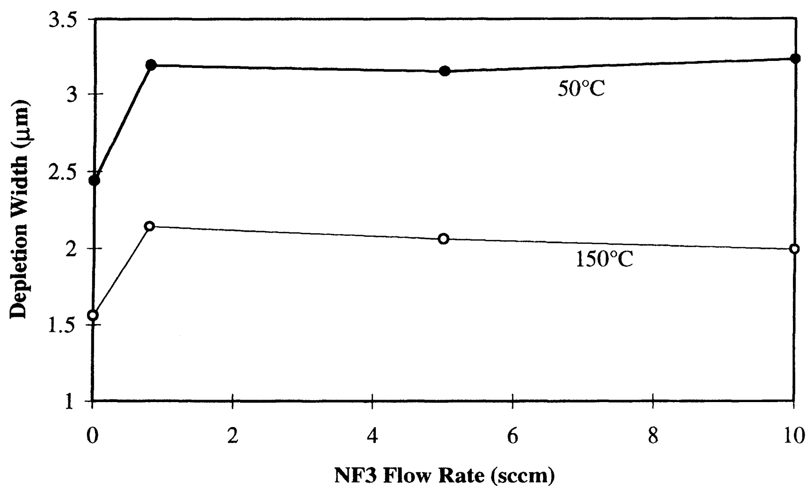

Figure 8: SCP measurement of depletion width of silicon wafers after exposure to Ar/NF_3 remote plasma at two different temperatures.

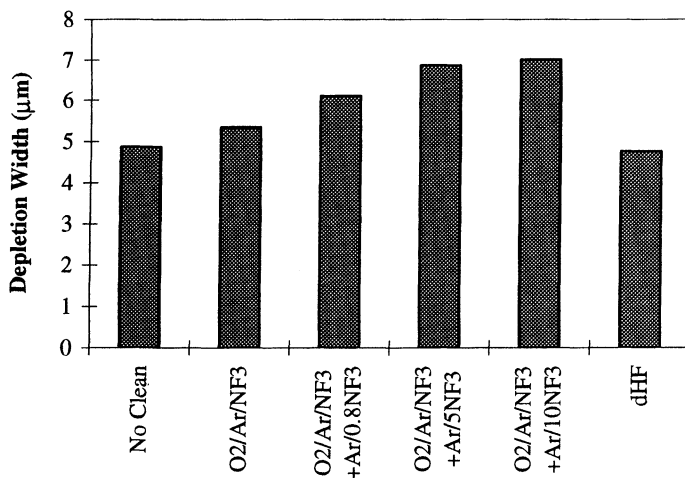

Figure 9: SCP measured depletion width of RIE processed wafers after various cleaning steps in the remote plasma system and after dilute HF etch.

Selective Etching For Making Cylindrical Capacitors Using Anhydrous HF Vapor Phase Chemistry

Jitesh R. Mehta, Tim Rogers

FSI International
322 Lake Hazeltine Drive
Chaska, Minnesota 55318-1096, U. S. A.

Satoshi Kikuchi

m·FSI Ltd
Japan

ABSTRACT

Recent proposals for 256 megabit and 1 gigabit devices promote the use of cylindrical or FINN capacitor devices. Typically, the production of these capacitor devices requires the ability to etch selectively (i.e., in the range of 50:1 to 200:1) among some of the commonly used silicon oxides. This has been made possible with the use of the anhydrous HF vapor phase etching technology, (also referred to as EXCALIBUR® technology). This paper shares etching and SEM results from a cylindrical capacitor-building process in order to show equivalent selectivity etching ratios of more than 200:1 between BPTEOS and non-densified TEOS. The process techniques used to achieve these selectivity ratios are also discussed.

INTRODUCTION

Stacked capacitors have been commonly used in the past generation of high density, 1 to 16 megabit devices. With increasing density a reduction in the memory cell area has become mandatory and thus a simple stacked capacitor is not sufficient to provide the necessary capacitance. To increase the capacitance with reduced memory cell area, device design engineers have come up with alternative capacitor structures with increased surface area of the storage electrodes. Two of these enlarged surface area structures are the cylindrical capacitor [1] and the FINN capacitor.

The cross section of a typical cylindrical capacitor is shown in Figure 1. The polysilicon capacitor is formed around a doped CVD oxide such BPSG, PSG or BPTEOS. The entire capacitor structure is developed over a denser dielectric CVD oxide such as HTO, TEOS or SiO_2. In the final step of the capacitor formation, the doped CVD oxide is completely etched from within the polysilicon structure. This final etching is very critical since only a limited amount of the dielectric layer under the capacitor should be etched to avoid undercutting the polysilicon structure. This final process in the formation of a cylindrical capacitor structure requires selective etching between the two oxides in the range of 50:1 to over 200:1.

ETCHING TECHNIQUES

A common method for achieving this selective etching is by using a resist mask over the dielectric layer, exposing the oxide within the polysilicon structure to liquid dilute HF or BHF chemistries, and following with a resist strip and cleaning process to remove the masking layer. The mask does not have to be a resist layer but could be any masking layer which is not attacked

by the dilute HF or BHF chemistries. This method requires multiple process steps which increase the cost of manufacturing and become possible sources of contamination.

An alternative process adopted in research environments uses HF vapor under low pressure to selectively etch the oxide within the polysilicon structure without having to mask the base dielectric oxide [1]. Selective etching ratios for BPSG to thermal SiO_2 of over 2000:1 have been claimed. The use of vacuum systems to control the partial pressure of H_2O in the reaction chamber makes it possible to control the amount of H_2O molecules adsorbed at reaction sites on the SiO_2 surface. One of the limitations of this HF vapor process is the requirement for pumps and all the associated vacuum components on the process tool. Another limitation is the need to move the wafer from the etching chamber into a separate DI water rinse chamber to wash away any CVD oxide dopants left on the wafer surface.

ANHYDROUS HF VAPOR PROCESS

The process described in this text uses anhydrous HF gas at atmospheric or slightly positive pressures and at room temperature or slightly elevated temperatures. This highly selective etching process does not require a mask to protect the underlying dielectric oxide. It is a single step process in which etching and rinse/dry are completed in the same process chamber.

The key to this highly selective etching process lies in the control of H_2O molecules at the reaction sites. The fundamentals of this process are described by Blackwood et al. [2]. The basic etching reaction involved in the use of anhydrous HF gas is as follows:

The etching reaction between anhydrous HF gas and SiO_2 is only possible in the presence of moisture. In case of dry (water vapor free) oxides and processes, the SiO_2 will not be etched [3].

The "science" behind the anhydrous HF vapor process is very simple. It is the "art" of controlling the kinetics of this reaction that makes the highly selective etching process possible.

It is important to understand the role of water vapor in order to appreciate the kinetics of the reaction. The etching of SiO_2 with HF will proceed only in the presence of water vapor. Water vapor is also generated as a product of the etching reaction. This water vapor is generated at the reaction sites and plays an important role in sustaining and propagating the reaction as long as HF molecules are available.

The precise control of the water vapor in the reaction makes this process possible and repeatable from wafer to wafer and lot to lot. It is necessary to control the water vapor content of the reactants, the water adsorbed at the reaction sites, the desorption of the reaction byproduct water from the reaction sites and the termination of the HF availability at the reaction sites. Thus the key to this process lies in understanding the etch initiation, propagation and termination for the two oxides, namely the doped CVD oxide contained within the polysilicon capacitor structure and the base dielectric oxide layer.

USE OF THE EXCALIBUR® ISR SYSTEM FOR ANHYDROUS HF VAPOR PROCESSES

The system used for this process is the EXCALIBUR® ISR Vapor Phase Processing System from FSI International. The ISR (in-situ rinse) system has the capability to follow the etch STEP with a DI water rinse and dry in the same process chamber. Because the wafers are not moved from an etch chamber to a rinse/dry chamber they are not exposed to the ambient air environment. This process can also be performed in the newly released EXCALIBUR® MVP Vapor Phase Processing System from FSI International.

The EXCALIBUR® ISR system is a single wafer processor. The vapor phase etch process consists of loading the wafer into a high molecular weight polyethylene or PVDF chamber, closing the chamber, purging with high flow (30 to 60 l/min) of nitrogen gas, introducing the anhydrous HF using nitrogen as a carrier gas, stopping the flow of HF gas after a controlled amount of time, purging with a high flow of nitrogen gas and concluding with an in-situ DI water rinse and spin dry. This entire etch/rinse/dry sequence can be repeated on the wafer without exposing the wafer to the ambient environment. This is made possible by the etch "looping" capability of the EXCALIBUR control software. The use of repeated etch process sequences in making cylindrical capacitors is henceforth referred to as "multiple etch loops."

ETCH CHARACTERIZATION RESULTS AND DISCUSSION

It is well understood and exhaustively documented that in traditional liquid HF etching, the etch rate is almost linear with respect to time. The etch rate is directly proportional to the HF concentration, the temperature of the substrate and the etching solution. In vapor HF etching the relationship between time and etch rate is not linear.

Figure 2 depicts the vapor HF etch rate as a function of time when no water vapor is added with the reactants. The concentration of water vapor in the reaction gases is less than 10 ppm. Figure 2 clearly shows the difference in the etch initiation between doped CVD oxides such as BPSG, PSG and BPTEOS and denser oxides such as HTO, TEOS and Thermal Oxides. Similar results are obtained when each type of oxide is individually exposed to the reaction gases. The differences in the etch initiation and etch rate acceleration between the two types of oxides plays an important role in making selective etching possible.

A thorough understanding of etch initiation and propagation is useful in achieving a highly selective etching process. In the case of doped oxides, the etch initiates almost instantaneously and accelerates rapidly until it stabilizes at a rate that is almost linear with increasing time. Water vapor inherently contained within the oxide acts as the necessary catalyst to get the etching reaction initiated. Furthermore, the doped CVD oxides are relatively porous and allow the adsorption of HF gas molecules within the oxide bulk structure. Once the HF gas molecules are adsorbed, etching propagates in a three dimensional mode resulting in a very rapid rate of acceleration until the reaction reaches a stable state.

The etch initiation and rate acceleration of denser oxides are much slower than that of the less dense doped oxides. Since no water vapor was added as part of the reaction gases, the etch initiation is dependent on the available vapor adsorbed on the oxide surface. The denser and the drier the oxide, the more slowly the etch is initiated. Once the etch is initiated water vapor is generated as a byproduct of the etching reaction. This vapor assists in increasing the etch rate. Furthermore since the oxide is dense, HF and water vapor are adsorbed only at the surface. This

keeps the etch propagation unidirectional and the etch rate acceleration at a much lower pace compared to doped CVD oxides.

The dashed lines in Figure 3 show the etch reaction rates for the same oxides when water vapor is added with the reaction gases. This experiment is important because it simulates the process conditions when two oxides are simultaneously exposed to reaction gases, as in the production of cylindrical capacitors. The key observation is that in the presence of water vapor the denser oxides show a much faster etch initiation than under the dry conditions used in Figure 2.

The water vapor generated as a byproduct of the etching reaction of the doped CVD oxides affects the vapor content of the reaction gases. When both the types of oxides are simultaneously exposed to dry reaction gases, the doped CVD oxide will show rapid etch initiation and propagation, as shown in Figure 2. This reaction generates water vapor as a byproduct. The reaction gases are no longer dry as originally introduced. The vapor generated as a byproduct of doped oxide etch now becomes available to adsorb on the surface of the denser oxide and work as a catalyst to initiate its etch reaction. This shortens the etch initiation time for the denser oxide, thereby reducing the selectivity window between the two oxides.

The goal of this highly selective process is to etch a large amount of the doped CVD oxide and a small amount of the denser dielectric oxide. To achieve this, the process must maximize the rapid etch initiation and propagation of the doped CVD oxide and stop the process before the denser oxide etch is initiated. Etch termination is made possible by discontinuing the flow of HF and purging the process chamber with nitrogen. This etch initiation and termination process can be repeated until the target amount of doped CVD oxide has been etched. Figure 4 is a diagram of the repeated etch initiation and termination process. Each cycle is referred to as a "loop" in the multiple etch looping process.

It is recommended that a rinse step be used between the etch loops since dopants are releases as the doped CVD oxide is etched. The dopants do not form volatile compounds as the SiO_2 does. These dopants have a tendency to accumulate on the surface of the unetched oxide and reduce its etch rate.

The benefit of a DI water rinse between loops is demonstrated in Figure 5. BPTEOS was etched using two dual etch loop processes, one with rinse and dry between the two etches and one with rinse and dry only after the second etch. Since the goal of this process is to etch the doped oxide as fast as possible and to minimize the etch of the denser dielectric oxide, the process with the largest delta is preferred. Rinse and dry after each loop proved to be very beneficial.

To eliminate all water vapor adsorbed on the denser dielectric oxide, a nitrogen purge is included prior to each etch step. Figure 6 shows the etch delta for TEOS after each etch loop in a 9 loop process. The etch delta is constant at about 10 Å. Furthermore, the rinse step does not affect the etch characteristics of the doped CVD oxide. Figure 7 shows the etch delta for BPTEOS using a 9 loop process. The etch delta for each etch loop is between 775 and 825 Å.

Figures 6 and 7 are representative of the etch consistency that can be achieved when the EXCALIBUR process tool is used to perform multiple etch loops. The number of etch loops to be carried out depends on the amount of doped oxide to be etched. In one particular application the BPTEOS contained within the polysilicon capacitor structure was about 4000 Å thick. Using the process conditions defined in Figure 7, 5 etch loops would be required for a "just etch" process. To assure that all of the doped oxide was etched from within the capacitor structure

would require 6 to 7 etch loops. Figure 6 shows that this would result in a TEOS etch of 60 to 80 Å. Because this is on the high side of acceptable dielectric oxide loss, further work was done to increase the etch selectivity.

Other parameters examined for further increasing the etch selectivity between the two types of oxide were: etch time for each of the etch loops, temperature at the reaction site and HF concentration.

Figure 8 shows the results of increasing the etch time for both of the loops for TEOS. The total etch delta for a two step process is almost independent of the etch time of the loops. The etch delta of BPTEOS increases linearly with increasing etch time. However, selectivity is not gained because the water generated during the etch of the BPTEOS is available to adsorb on the TEOS surface. Hence it is best to keep the etch times as short as possible.

Figure 9 shows the effect of wafer temperature on the TEOS etch delta. The higher temperature, 35°C, results in a lower etch delta for TEOS than 25°C. Other researchers have reported the same impact of temperature on the etch rate of vapor HF processes on thermal oxides [4]. In etch processes using liquid HF, the etch rate increases almost linearly with increase in temperature.

Figure 10 shows the effect of HF concentration and gas flow rate on the TEOS etch delta for different etch times. The TEOS etch delta is most dependent on the HF concentration and does not show much dependence on the total flow of the reaction gases. These results show that increasing HF concentration will reduce the process margin and cannot be used to minimize TEOS etch rate.

Figure 11 shows the effect of HF concentration and gas flow rates on the BPTEOS etch delta. As expected, increasing HF concentration resulted in increased BPTEOS etch delta. The BPTEOS etch delta also increases with increasing total gas flow rate, unlike the TEOS etch delta. This parameter, total gas flow rate, was used to further increase the selectivity between TEOS and BPTEOS. A nitrogen flow rate of 60 liter/min was selected for the actual process.

Figure 12 shows the effect of multiple parameters such as temperature, total gas flow, etch time and HF concentration on BPTEOS etch delta. These data verify the effect of increased etch time on BPTEOS etch delta, discussed earlier. The most important observation is that increasing the wafer temperature increased the BPTEOS etch delta. This is completely opposite to the effect observed with the denser TEOS oxide. Increased wafer temperature and increased gas flow rate were used in the final vapor HF process to make cylindrical capacitors.

To understand the contrary effects of total gas flow and temperature on the etch characteristics of TEOS and BPTEOS, it is necessary to go back to the discussion of adsorbed water vapor on the surface of the oxides and its impact on etch initiation and propagation. When no water vapor is added with the reactants, a higher flow of gases is able to desorb more vapor or desorb vapor more rapidly from the surface of the two oxides. In case of BPTEOS the etch rate is not dependent on the surface vapor since there is a relative abundance of moisture within the bulk of the oxide. But in case of TEOS the desorption of water vapor by the high nitrogen flow slows down the etch initiation. Further more, the increased gas flow rates may assist in diffusing the reaction products into the flow of gases and thus increase the overall etch rate of the BPTEOS.

Just as with high gas flow rates, increasing the temperature of the two oxides increases the desorption of moisture present at the reaction sites or slows the rate of moisture adsorption from

the chamber environment and the reaction gases. As already discussed, reducing water adsorption from the environment, the reaction gases and the byproducts of the BPTEOS etch slows the TEOS etch initiation. In case of BPTEOS, the increased temperature is insufficient to dehydrate the oxide. Instead the increased temperature may increase the etch rate, as in traditional liquid HF etching.

The SEM photographs in Figure 13 show cross sections of cylindrical capacitors that have been etched in the EXCALIBUR® ISR using an anhydrous HF process. The capacitors were etched with 2, 3 or 4 multiple loops, with each loop 3 seconds in duration. The process used 60 l/min of N_2 carrier gas and 1100 cc/min of anhydrous HF gas. No water vapor was added to the reaction gases. The SEMs show that the BPTEOS has been completely etched from within the cylindrical capacitor structure with no underetch of the base TEOS dielectric layer.

The BPTEOS to TEOS etch ratios for these three processes are shown in Table I.

Table I: Etch depths and selectivity ratios of an anhydrous vapor phase HF process with multiple etch loops

Number of etch loops	BPTEOS removal, Å	TEOS removal, Å	Selectivity ratio
2	4100	15	273:1
3	6144	30	204:1
4	8067	46	175:1

The use of multiple loops gives the vapor HF process a significant process margin. It is possible to overetch the BPTEOS to assure its complete removal from within the capacitor structure while maintaining acceptable amounts of etch at the polysilicon-TEOS interface.

In addition, the selectivity ratio can be further increased by using densified TEOS instead of non-densified TEOS. Besides TEOS and BPTEOS there are many other similar doped and non-doped oxides commonly used in the manufacturing of integrated circuit devices. Selection of oxides to be used in capacitor structures can be based on fundamental etching characteristics of the different oxides. Capacitor structures can be designed using those oxides which exhibit very high selectivity ratios, thereby providing very large margins in the semiconductor manufacturing process.

CONCLUSIONS

The use of cylindrical capacitors or similar increased surface area electrode capacitor structures holds strong promise for the near future. Development of these structures urgently requires a simpler manufacturing process with fewer steps. The process must have the ability to selectively etch doped oxides from within the capacitor structures without damaging the base dielectric layer. The anhydrous HF vapor process performed in the fab-proven EXCALIBUR® ISR system meets these requirements.

This paper has described an anhydrous HF vapor process performed in the EXCALIBUR® ISR system with selectivity between non-densified TEOS and BPTEOS in the range of about 200:1. SEMs of cylindrical capacitors etched by this process show that the BPTEOS has been completely etched from within the cylindrical capacitor structure with no underetch of the base TEOS dielectric layer. This selectivity ratio can be further increased through the careful

selection of the oxides used in the capacitor structure and the base dielectric layer. Use of oxides with high selectivity ratios can provide large process margins.

ACKNOWLEDGMENTS

The authors gratefully acknowledge the cooperation, confidence and patience shown by the customer in working jointly with FSI and m·FSI in developing the anhydrous HF process for their cylindrical capacitors. We appreciate the customer's efforts in providing us with test wafers and 200 mm device wafers and for sharing their SEM photographs for this paper.

REFERENCES

[1] Watanabe, T. Tatsumi, S. Ohnishi, T. Hamada, I. Honma, T. Kikkawa, IEDM 92-259, IEEE (1992).
[2] Blackwood, T. Biggerstaff, L. D. Clements, R. Cleavelin, United States Patent Number 4,749,440.
[3] Bersin, R. Reichelderfer, Solid State Technology, Vol. 20, No. 4, (1977).
[4] Wong, M. M. Moslehi and R. A. Bowling, "Wafer Temperature Dependence of the Vapor-Phase HF Oxide Etch," J. Electrochemical Society, Vol. 140, No. 1, (1993).

® EXCALIBUR is a registered trademark of FSI International, Chaska, MN.

Figure 1: A typical cylindrical capacitor structure

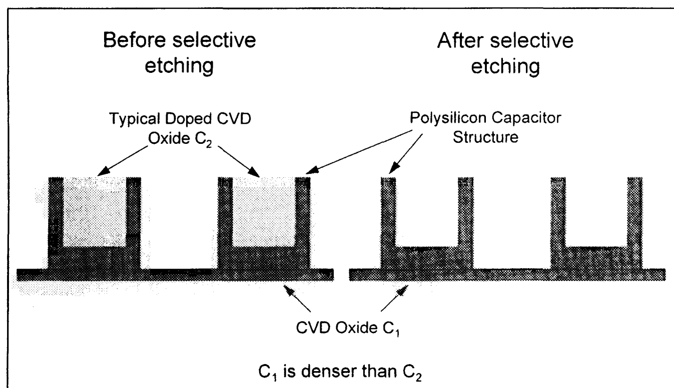

Figure 2: Etch initiation and propagation trends in a vapor HF process

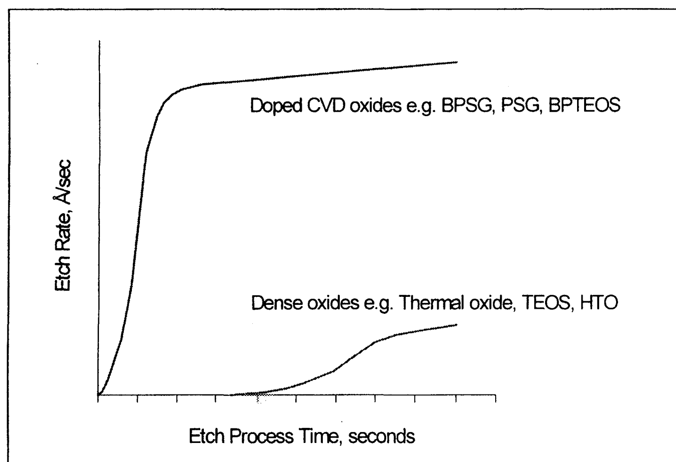

Figure 3: Effect of water vapor on etch initiation and propagation in a vapor HF process

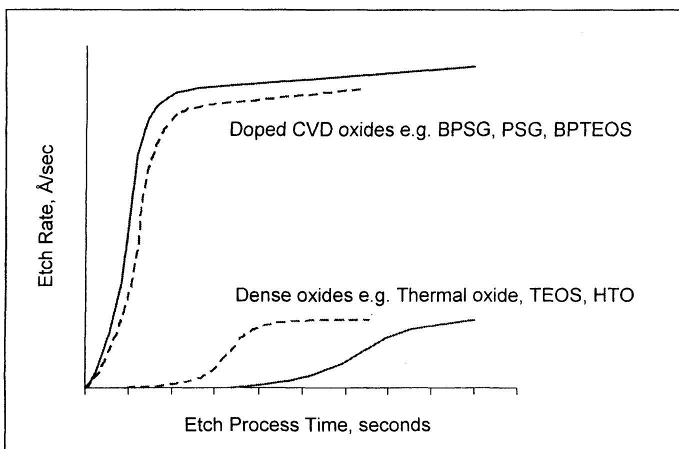

Figure 4: Use of multiple "short" etch process loops

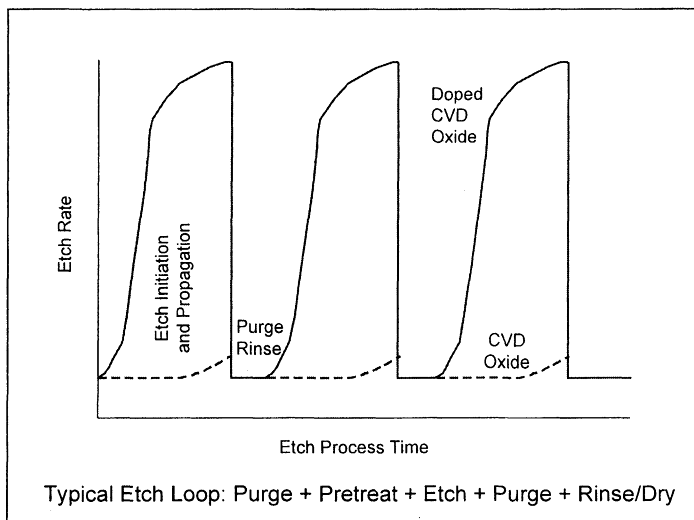

Figure 5: The effect of DI water rinse between multiple etches on BPTEOS

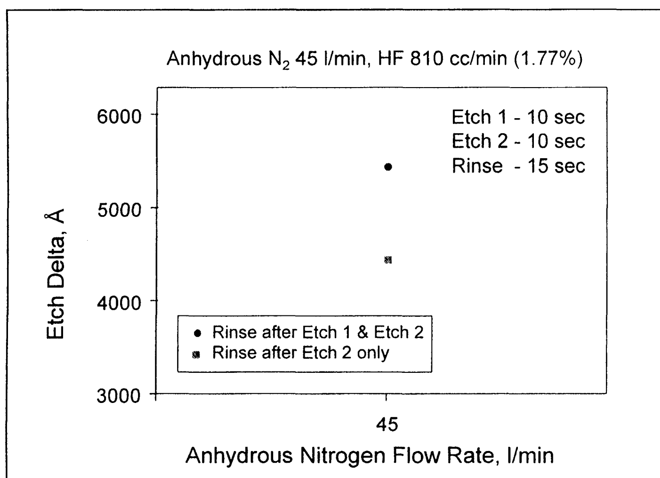

Figure 6: TEOS etch characterization using multiple loops

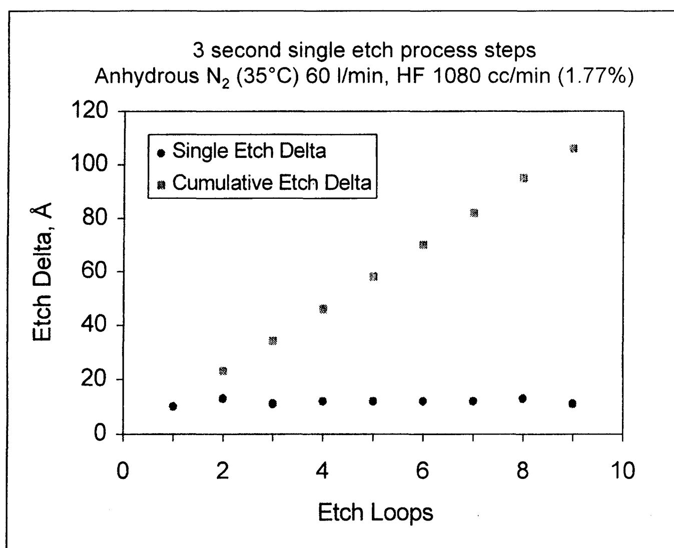

Figure 7: BPTEOS etch characterization using multiple loops

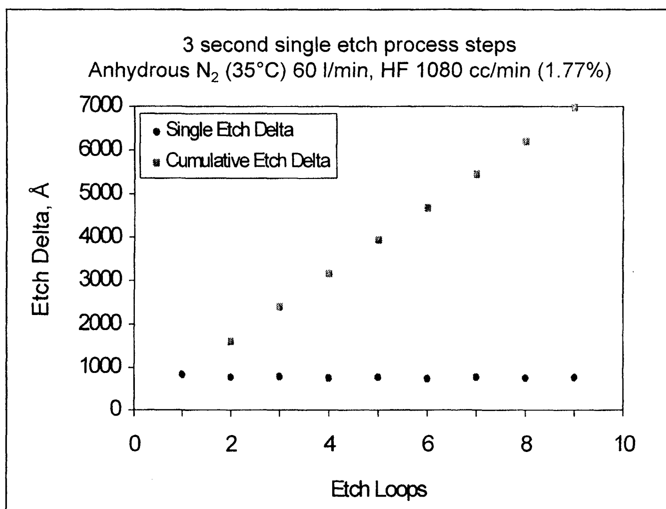

Figure 8: The effect of etch time on TEOS during multiple etch loops

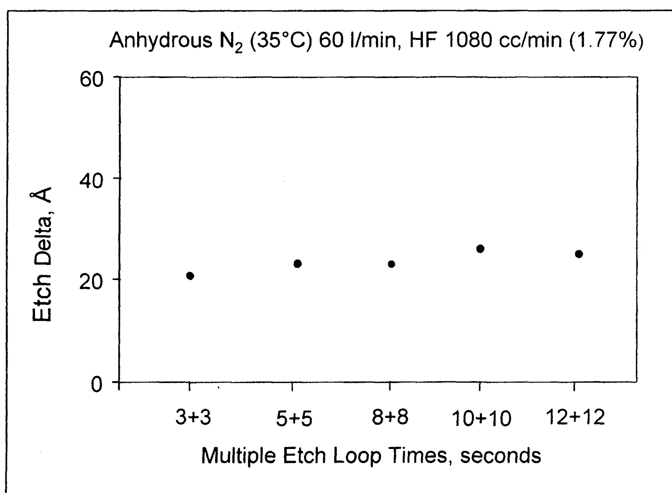

Figure 9: The effect of temperature on TEOS during multiple etch loops

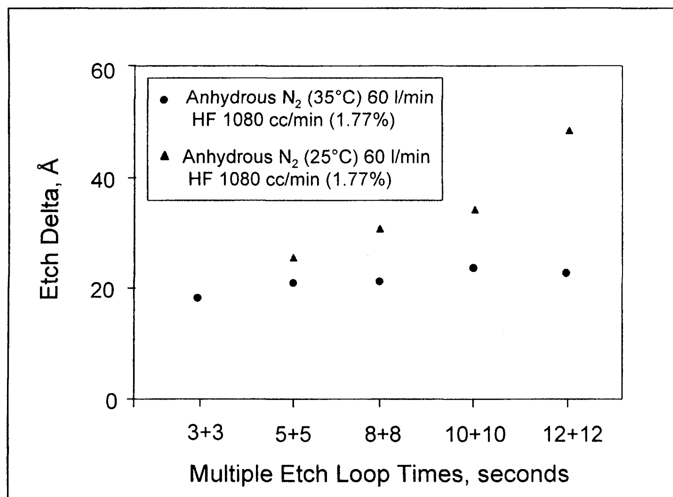

Figure 10: The effect of HF concentration and total flow on TEOS

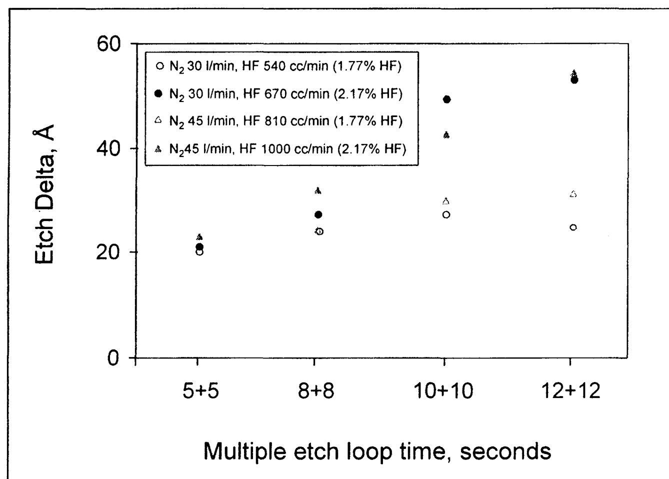

Figure 11: The effect of HF concentration and total gas flow on BPTEOS

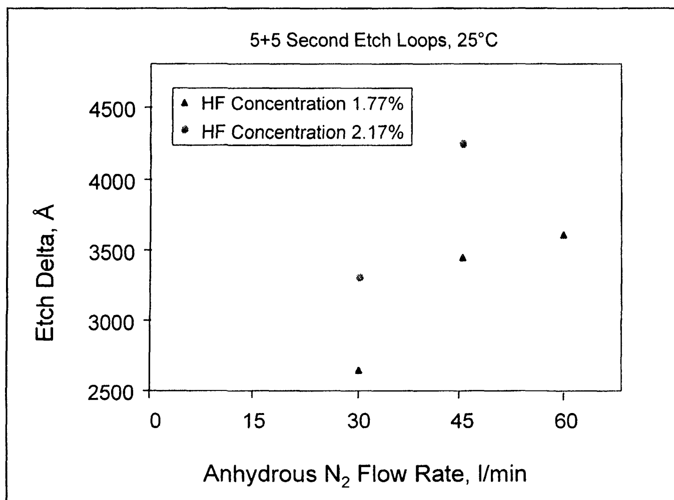

Figure 12: The effect of temperature, total gas flow, etch time, and HF concentration on BPTEOS etch in a dual etch loop

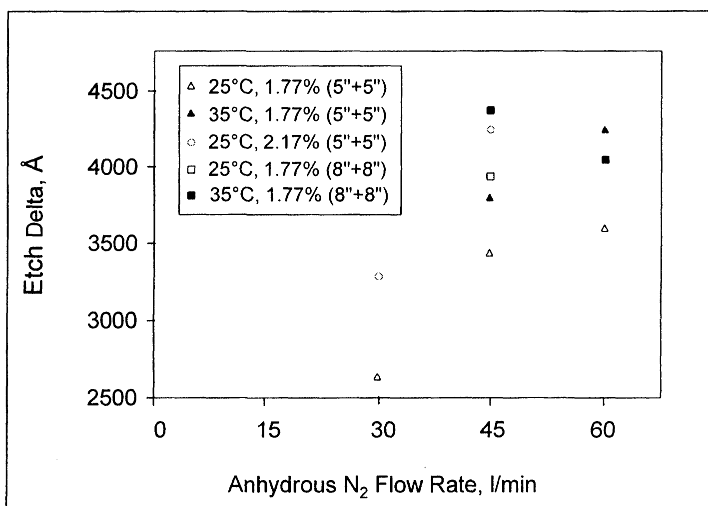

Figure 13: Cylindrical Capacitors produced in EXCALIBUR ISR using a vapor phase HF process

N_2 60 l/min + Anhydrous HF 1100 cc/min

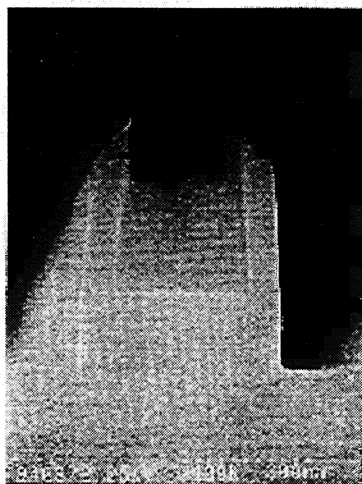

4100Å/BPTEOS 15Å/TEOS
3 sec x 2 loop

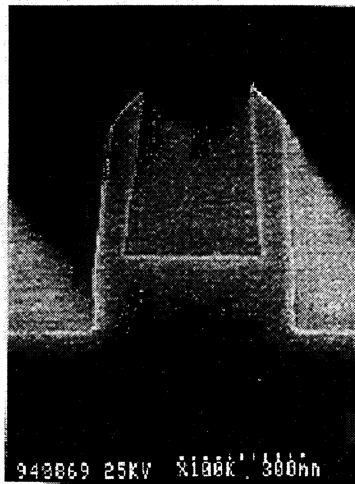

6144Å/BPTEOS 30Å/TEOS
3 sec. x 3 loop

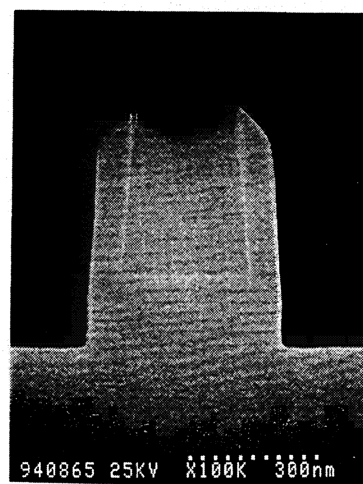

8067Å/BPTEOS 46Å/TEOS
3 sec. x 4 loop

EVOLUTION OF Si SURFACES AFTER ANHYDROUS HF:CH_3OH ETCHING

K. Torek, A. Mieckowski, and J. Ruzyllo

The Electronic Materials and Processing Research Laboratory
The Pennsylvania State University
University Park, PA 16802

The degree of changes of the chemical composition of the silicon surface following HF etching of chemical oxide is a measure of surface stability, and hence, can be used to derive information on the hydrogen termination of the surface. In this experiment, the surface evolution following anhydrous HF/methanol oxide etching was monitored using the Surface Charge Profiling (SCP) method.

INTRODUCTION

One of the important technological aspects of developing oxide etch processes concerns the evolution in ambient air of the Si surface after stripping the oxide (1). This work presents data on the stability of Si from which chemical oxide is removed by anhydrous HF(AHF)/methanol (CH_3OH) gas-phase etching (2,3). The data on the Si surface evolution in ambient air can be used to infer the chemical state of the Si surface. A Surface Charge Profiler (SCP) used in this study allows non-contact, non-invasive measurement of the Si surface charge vs. ambient air exposure time. The SCP results are compared with wetting angle measurements which were previously found to correlate well with XPS O_{1s} intensity and surface lifetime measurements (4,5).

Surface chemical information can be inferred as follows. Hirose et. al. (6) concluded that certain Si surfaces exposed to aqueous HF and rinsed may withstand long times (up to 300 min.) of ambient air exposure without being oxidized. Furthermore, they showed that the more stable surfaces were either fluorine-free, atomically flat Si terminated with silicon hydrides or had a significant percentage (about 12%) of relatively strong Si-F bonds passivating reactive atomic steps and kinks. The etching method in this study is likely to resemble the latter since the way to achieve an atomically flat, Si-H terminated surface was by pH-modified BHF solution. The purpose of this experiment was to investigate characteristics of anhydrous

$HF:CH_3OH$ etched silicon surfaces. By monitoring the changes of Si surface charge and wetting characteristics as a function of time of exposure to ambient air following etching, a sensitive and very convenient technique to assess the passivation efficiency of the etching recipe is realized.

The experimental approach in this study was possible due to the unique capabilities of the SCP tool (7,8) which allows measurements of surface charge at predetermined time intervals starting as soon as the wafer is removed from the etching module.

EXPERIMENTAL

Silicon wafers, CZ, p-type, <100>, 5-10 Ω-cm, 3 in. diameter were used. These wafers were etched without any additional pre-treatments. The commercial dry clean module in this experiment (9) could be fed with various gases at the reduced pressure. A sapphire window and IR lamps in the dry cleaning module allow shortwavelength UV and IR irradiation of the wafer front surface. The partial pressure ratio of AHF and CH_3OH, etch temperature, etch time, and post-etch treatments were used to alter the Si surface chemistry. Surface charge was measured using an SCP system which is a commercial non-contact, small-signal, surface-sensitive ac-SPV tool. Changes in the surface charge density were monitored as a function of time of exposure to the clean room ambient air (40% RH) following etching. In addition, wetting angles were measured after exposure to the same ambient and XPS characterization of etched surfaces was performed. As a reference, surfaces etched in $HF(1):H_2O(100)$ solution and rinsed/dried were used.

RESULTS AND DISCUSSION

In the first part of this investigation correlation between behavior of surface charge and wetting angle on the surfaces dry etched under various conditions was established. As an example, Fig. 1 shows the surface activity reflected by the variations of surface charge and wetting angle following an $AHF:CH_3OH$ chemical oxide strip at 40 ^{o}C. The results of this series of experiments are summarized in Table 1 showing values of surface charge density and wetting angle measured on the Si surfaces 10 minutes after etching. Both results in Fig. 1 and in Table 1 demonstrated differences in the condition of Si surfaces after the $HF:H_2O$ etch and $AHF:CH_3OH$ etch. In addition, they show that the lower temperature dry etch resulted in the surfaces displaying characteristics closer to those resulting from $HF:H_2O$ etch. The same results also indicate good correlation between surface

charge and wetting angle suggesting that instant, easy to carry out, and non-invasive measurements of surface charge using the SCP system can be used instead of time consuming, invasive measurements of wetting angle. In contrast to wetting angle measurements, the SCP measurements can be performed over a period of time on the same spot on the wafer surface without affecting the surface in any way, and hence, accurately reflecting evolution of the surface condition. Also, not practical would be the use of XPS for the purposes of this study. This is because besides purely technical problems and time constraints, cycling of the wafer surface between vacuum needed to perform XPS measurement and ambient air would alter its conditions rendering measurements of time related evolution of surface features inaccurate. Based on these considerations, the SCP system was used in the second part of this experiment to study other characteristics of Si surface evolution following oxide etching.

Figure 2 shows the evolution of surface charge with the time of exposure to ambient air for wafers etched under different conditions of the AHF:CH_3OH process and wafers etched in HF:H_2O solution. All surfaces display high positive charge. Initially, surface charge density on the dry etched surfaces is the same, or higher than on the HF:H_2O etched surfaces. However, surface charge on the dry etched surfaces remains stable for about 6 hours and then decreases in the same fashion for all etch conditions applied. At the same time charge on the HF:H_2O etched Si surfaces used in this study remain stable for much longer periods of time. It should be noted that length of surface stability period following HF:H_2O etch was found to differ substantially for wafers from different suppliers (10) as well as for wafers with different surface orientation.

The different behavior of the Si surface is an evidence of somewhat different surface chemistry resulting from HF:H_2O and HF:CH_3OH oxide etching. To determine the nature of this difference a more detailed study using XPS will have to be performed. Our initial XPS results did show Si_{2p} peak typically higher for HF:H_2O etched surfaces with Si_{1s} peak remaining virtually the same for both etch chemistries. In addition, at the detection limit of the XPS tool used, we have seen indications of slightly higher F_{1s} peak for the surfaces etched in AHF:CH_3OH. In the light of these initial findings it was concluded that changes in the surface charge density for dry etched surfaces shown in Fig. 2 are likely to be due to the higher susceptibility of these surfaces to oxidation. This observation leads to the indirect conclusion that under process conditions in this study AHF:CH_3OH etched surfaces are less hydrogen passivated than their HF:water counterparts. This conclusion

remains in agreement with the determination that wetting angles immediately after etching were consistently lower by a few degrees on AHF:CH_3OH etched surfaces than on HF:H_2O etched surfaces.

To study the effect of oxygen on the dry etched surfaces the UV/ozone oxidation was carried out inside the dry cleaning module following the AHF:CH_3OH etch. As Fig. 3 shows, slight oxidation of silicon following *in situ* dry etching of an oxide resulted in a small reduction of initial surface charge density and lower surface stability as compared to AHF:CH_3OH and HF:H_2O etched surfaces. Overall, these results indicate that the AHF:CH_3OH etch under the conditions applied in this experiment is not producing as strongly passivated surfaces as HF:H_2O (1:100) does. Passivation in the former case appears to result partially from physisorbed passivating species. On the other hand however, striking similarity in the evolution of AHF:CH_3OH etched surfaces and surfaces etched in weaker HF:H_2O(1:500) solutions was observed (10). This suggests that at the reduced pH of AHF:CH_3OH chemistries stronger surface passivation should be possible. During the future stage of the research reported in this paper parameters of the AHF:CH_3OH process, including CH_3OH/AHF flow rate ratio and HF partial pressure will be varied to accomplish this goal. In addition, temperature, pressure, degree of overetch, and post-etch treatments can be used to fine tune the process toward higher level of control over a Si surface chemistry.

SUMMARY

The results of this investigation can be summarized from the point of view of characteristics of the AHF:CH_3OH etched Si surfaces as well as usefulness of SCP methodology in instant evaluation of HF etched silicon surfaces. In the former case, the results obtained show a difference in the chemical condition of the silicon surface following AHF:CH_3OH and HF:H_2O (1:100) oxide etching processes. Additional research is needed to determine the exact nature of this difference. On the other hand, this study indicate that tools and chemistries used in dry oxide etching offer more latitude with respect to fine tuning of the surface features than the HF:H_2O processes.

Regarding performance of the SCP method, this experiment has proven that it is a very convenient tool in monitoring HF based processes. By allowing instant, very easy to implement monitoring of the process outcome, this tool fills the void in the arsenal of HF process monitoring methods which either XPS, or wetting angle measurements can not fill.

ACKNOWLEDGEMENTS

This study was supported in part by the Semiconductor Research Corporation. Also, authors would like to thank SubMicron Systems, Inc., and QC Solutions, Inc. for providing tools used in this experiment.

REFERENCES

1. A. Phillliposian, *J. Electrochem. Soc.*, **139**(10), 2956 (1992).
2. J. Ruzyllo, K. Torek, C. Dafron, R. Grant, and R. Novak *J. Electrochem. Soc.*, **140**(4), L64 (1993).
3. K. Torek, J. Ruzyllo, R. Grant, and R. Novak, *J. Electrochem. Soc.*, **142**(4), 1322 (1995).
4. J. Alay, S. Verhaverbeke, W. Vandervorst, and M. Heyns, *Ext. Abs. of the 1992 Conf. on Solid State Dev. Mat.*, Tsukuba, Japan, 1992, p. 123
5. P. Roman, D. Hwang, K. Torek, J. Ruzyllo, and E. Kamieniecki, *Proc. Ultraclean Semicon. Proc. Technol and Surf. Chem. Clean. and Passiv.*, Eds. M. Liehr, M. Heyns, M. Hirose, and H. Parks, Materials Research Society. vol. 386, 1995.
6. M. Hirose, T. Yasaka, M. Takakura, S. Miyazaki, *Solid State Technology*, 43, 1991.
7. SCP-110, QC Solutions, Inc. Woburn, MA 01801.
8. E. Kamieniecki, *This volume.*
9. Primaxx, SubMicron Systems, Inc., Allentown, PA 18106.
10. P. Roman, M.S. Thesis, Penn State University, 1996.

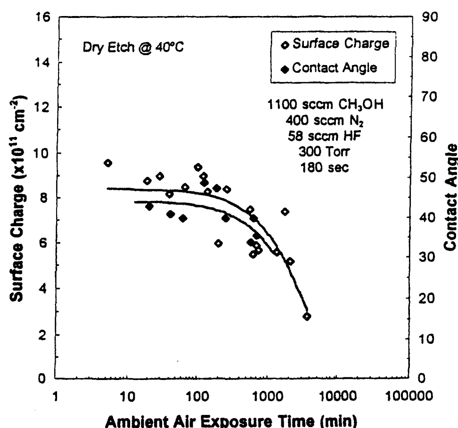

Fig. 1 Variations of surface charge and contact angles vs. time of ambient air exposure for Si surfaces dry etched at 40°C.

Table 1 Surface Charge Densities and Wetting Angles for Si Surfaces Etched under Different Conditions.

	$HF:H_2O$ (1:100)	$AHF:CH_3OH$ 20 °C	$AHF:CH_3OH$ 40 °C	$AHF:CH_3OH$ 60 °C
Surface Charge ($x10^{11}$ cm^{-2})	12	10	9.5	6
Wetting angle	68°	50°	46°	42°

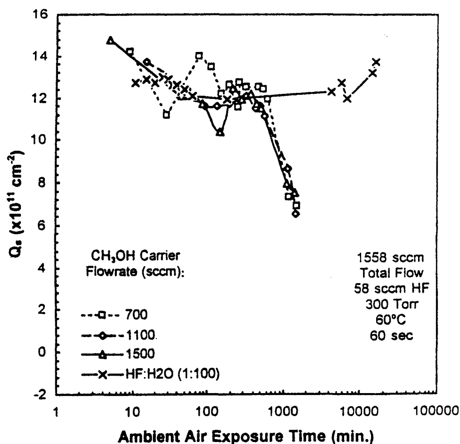

Fig. 2 Variations of surface charge density vs. time of ambient air exposure for Si surfaces dry etched at various methanol flow rates and wet etched.

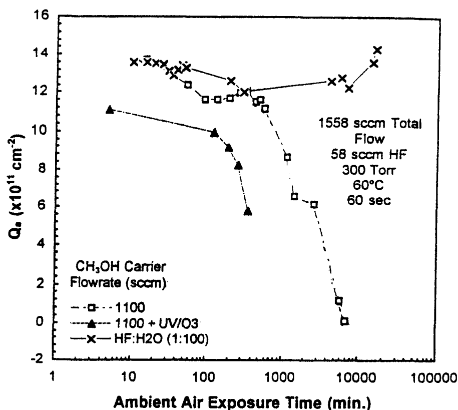

Fig. 3 Variations of surface charge density vs. time of ambient air exposure for Si surfaces dry etched, dry etched and then oxidized, and wet etched.

OPTIMIZATION OF PHOTORESIST AND POLYMER REMOVAL IN A VIA ETCH PROCESS

Steve Marks[1], Sandra W. Graham[2], Tinal Uk[3], C.C. Chang[3]
Claudia Geller[4], and Chiu Tse[5]

(1) Integrated Device Technology, Inc.
3131 NE Brookwood Pkwy., Hillsboro, OR 97124
(2) Semitool, 655 W. Reserve Dr., Kalispell, MT 59901
(3) GaSonics International, 2730 Junction Ave., San Jose, CA 95134
(4) Lam Research, 600 S.E. Maritime Ave., Vancouver, WA 98661
(5) EKC Technology, 2520 Barrington Court, Hayward, CA 94545

ABSTRACT

To achieve low via resistance and enhanced device performance, complete removal of residual polymer created during the via etch process is critical. This paper explores the contributions of several factors to the polymer removal process. Three different defects are identified and the factors that contribute to the formation of these defects are quantified. An optimized process flow is proposed based on the experimental results.

INTRODUCTION

Complete removal of photoresist and the etch residue ("residual polymer") that forms during the plasma etching of vias is critical to the performance of an integrated device. Photoresist is applied to the surface of a wafer prior to etching in order to mask the areas that are not to be exposed to the plasma. After etching, the photoresist must be removed before further device processing can take place.

Residual polymer, more correctly described as etch residue, is generated in conventional etching processes that utilize fluorocarbon gases as the primary etchant. A moderate amount of polymer buildup on the sidewalls of the via is desired in order to achieve a vertical etch profile [1, 2]. Residual polymer can also form on the bottom of the via. Incomplete removal of this residual polymer prior to subsequent metal deposition steps may result in unacceptably high via resistance. The sidewall polymer does not directly affect the resistance, however, incomplete removal may cause reliability concerns at the interface and process control issues at subsequent metal deposition steps.

In this paper, we discuss work performed in an effort to understand and optimize the post via etch photoresist and residual polymer removal process. The data was generated from shortloop wafers fabricated by IDT. The conclusions drawn are based on scanning electron microscopy (SEM) results.

EXPERIMENTAL SETUP

A fractional-factorial design of experiment (DOE) was performed to determine the impact of several variables on the polymer removal process. The process variables evaluated include: (a) the amount of CHF_3 in the via etch process, (b) the use of N_2 as a carrier gas in the etch process, (c) the type of gas(es) used in the ash process, (d) the order in which ashing and wet cleaning are done, (e) the type of chemicals used in the wet cleaning process and (f) the order in which the wet cleaning chemicals are used.

150 mm wafers with oxide deposited on a TiN/AlCu metal stack were patterned with photoresist. The wafers were then etched in a single wafer RF diode reactive ion etcher (RIE) with a split phase 400 kHz RF source (LAM Rainbow 4526). The etch parameters evaluated include the amount of CHF_3 in the feed gas and the addition or omission of N_2 as a carrier gas.

Wafers were ashed in a single wafer 2.45 GHz magnetron microwave reactor with a downstream source. Three different ash chemistries were evaluated: (1) oxygen (GaSonics 3510), (2) forming gas (a small amount of hydrogen in nitrogen) and oxygen (GaSonics 3510), and (3) O_2/NF_3 (GaSonics Aura 2000). Half of the wafers were ashed prior to wet cleaning and half were ashed post wet clean.

The wafers were wet cleaned in a batch spray solvent system with on-axis rotation (Semitool SST). Each wafer was treated with two chemicals: a photoresist stripper and a polymer removal solution. The wet cleaning process evaluated a total of three different chemicals: (1) a low temperature (95 °C) alkaline, organic based positive photoresist stripper (EKC 830), (2) a high temperature (110 °C) organic based positive photoresist stripper (EKC 837), and (3) an aqueous organic mixture designed to remove residues after via etch (EKC 265).

The sequence in which the wafers were processed as well as the type of chemicals used was defined by the experimental design. The process conditions for all wafers are listed in Table I.

Wafers were visually inspected with an optical microscope to look for gross amounts of unremoved polymer and photoresist. SEM photographs were used to evaluate the removal of residual polymer from the inside of the vias and to determine if TiN undercutting occurred.

RESULTS AND DISCUSSION

A fractional-factorial design is commonly used in screening experiments where there are a large number of factors to be evaluated. The goal of a screening experiment is to identify the most important factors and to quantify their effect on the responses, including interaction effects. This method is useful when evaluating a multi-step portion of a semiconductor fabrication process because it identifies significant interactions between discrete process steps.

This work evaluates the impact of 6 factors on 3 responses. There is a strong correlation between several of the factors and the responses that were studied. Some of the factors, however, were not statistically significant. The next several sections will discuss the factors that have a significant impact on the responses. This will be followed by a discussion of the factors that did not have a major impact.

Analysis of the processed wafers revealed three types of defects: (1) residual polymer on the sidewalls of the via, (2) undercut of the TiN metal layer near the bottom of the via, and (3) polymer nodules at the bottom of the via.

Polymer Formation

Via formation is achieved in this process by vertical anisotropic etching with CHF_3, CF_4, Ar and occasionally N_2. CF_4 in the plasma generates CF_x (x = 1, 2 and 3) ions and radicals, as well as F; and CHF_3 forms ions and radicals of CH_yF_x, CF_x and F atoms, where x and y are concentrations of F and H elements with respect to C elements [3, 4, 5].

These species can act as precursors for the deposition of residues on the bottom and sidewalls of vias during the etch process. Fluorocarbon polymer, composed mostly of CF_2 has been identified in the literature as the source of this residue [3, 4, 6].

Residual Sidewall Polymer

As discussed earlier, residual sidewall polymer is a byproduct of the etch process. The ability to completely remove the sidewall polymer is dependent on the conditions of etch process, the ash process, and the wet cleans process.

To quantify the amount of sidewall polymer remaining after the process was complete, wafers were SEM'ed and graded on a scale of 0 (no polymer) to 4 (heavy polymer). Figure 1 is an example of a via with heavy residual sidewall polymer.

Addition or omission of N_2 during the etch process had the largest impact on the amount of residual sidewall polymer. There were 16 wafers that had N_2 added to the etch process, with an average "grade" of 1.4. Another 16 wafers were processed without N_2, with an average "grade" of 2.9. Also noteworthy is that none of the wafers in the "with N_2" group received a grade of 3 or higher (heavy polymer), and none of the wafers in the "without N_2" group received a grade of 1 or lower (little to no polymer).

A statistical computer package (RS1/Discover) was used to evaluate the significance of the factors contributing to the existence of residual sidewall polymer. The omission of N_2 in the etch process is the only factor included in this experiment that is statistically significant to the severity of remaining sidewall polymer. An F-ratio of 24.83 implies a 99.5% probability that the cause and effect relationship between omission of nitrogen from the etch process and the severity of residual sidewall polymer is systematic.

Addition of N_2 to the etch process significantly decreases the severity of residual polymer on the via sidewalls. It is theorized that the nitrogen scavenges carbon atoms that would normally form a very hard polymer structure [7]. The nitrogen combines with the carbon to form cyanide (CN-) and cyanate (C_2N_2), both of which are volatile and therefore easily removed from the chamber.

Investigation of two-way interactions disclosed a minor correlation between the "addition of N2 - order of ash/wet" two-way interaction and the severity of remaining sidewall polymer. An F-ratio of 1.55 suggests a 75% probability that there is a cause and effect relationship between the two-way interaction and the amount of residual sidewall polymer. Addition of N_2 to the etch process combined with an ash then wet clean process sequence results in the least amount of residual sidewall polymer.

The other factors studied; the amount of CHF_3 in the etch process, and the wet cleaning and ashing chemistries; did not impact the amount of residual polymer.

TiN Undercut

TiN undercut occurs when there is preferential lateral attack of the interface between the TiN and an adjoining film. This results in a "mousebite" or indentation in the via sidewall at the interface.

Wafers were graded on a scale of 0 (no observable undercutting) to 2 (undercutting is severe enough to be a potential yield problem) based on SEM photographs (Table II). Figure 1 shows an example of a via with observable TiN undercut near the bottom.

The amount of CHF_3 flow in the via etch process is the only factor that significantly affects the occurrence of TiN undercutting at the interface. Wafers processed with high flow had an average grade of 0.875 and none of these wafers received a grade of 2 (heavy undercut). While wafers processed with low CHF_3 flow had an average grade of 1.25, and none of the wafers received a grade of 0 (no undercut).

RS1/Discover was used to evaluate the statistical significance of the factors studied. The amount of CHF_3 in the etch process was the only factor that had a statistically significant impact on the severity of TiN undercutting. An F-ratio of 6.82 implies a 98% probability that the cause and effect relationship between the amount of CHF_3 in the etch process and the severity of TiN undercutting is non-random.

High CHF_3 flow in the via etch process resulted in the smallest occurrence of TiN undercutting. The other factors studied; the addition or omission of N_2 to the etch process, the wet cleaning and ashing chemistries, and the wet cleaning and ashing process sequence; had little impact on the severity of TiN undercutting.

Polymer Nodules

We have defined "polymer nodules" to be residual clumps of polymer remaining at the bottom of the via. Wafers were assigned a grade of "yes" or "no" based on the presence or absence of these polymer clumps or nodules. The grading was based solely on SEM photographs of the wafer. The results are included in Table II. Figure 2 shows an example of a via with polymer nodules.

Three of the 32 wafers included in the experiment had polymer nodules. These wafers (#5, #12, and #17) had several process parameters in common: (1) N_2 was added

to the via etch process, (2) the wafers received a wet clean, followed by an ash, and (3) the wafers were ashed with O_2/NF_3. Wafer #11 also received these three process conditions, however, polymer nodules were not observed on this wafer.

Residual polymer forms during the etch process. The purpose of the wet clean and ash processes are to remove this polymer residue. It is believed that condition (2), a wet chemical clean followed by an ash process, is the primary contributor to the formation of (or lack of removal of) polymer nodules. The ash chemistry may contribute to the lack of removal, however, it is not believed to be a significant contributor.

The existence of polymer nodules may result in high via resistance and degraded device performance, and therefore, is a condition that should be avoided. To ensure complete removal of any residue that forms at the bottom of the via, the post etch process sequence of ashing followed by wet cleaning is recommended.

Gross Defects

Wafers were visually inspected at all process steps for gross defects. Unremoved photoresist on the surface of the wafer was the only gross defect observed. Wafers that received wet cleaning prior to ashing had photoresist remaining on the surface after the first wet clean process. However, this residual photoresist appeared to be completely removed by the second wet clean process. Inspection of wafers that were ashed prior to wet cleaning did not have any residual photoresist following the initial wet cleaning step.

Wet Cleaning

The factors that were modulated within the wet cleaning process did not have a significant impact on defect formation. The order in which the chemicals were used (stripper followed by polymer removal chemical vs. polymer removal chemical followed by stripper) did not contribute to the occurrence of defects. In addition, there is no statistical correlation between the type of stripper used (low temperature vs. high temperature) and the presence of the various defects.

Optimized Process Flow

The goal of this work was to optimize the via etch and post via etch cleans processes, taking into account any interactions between the discrete process steps. Based on the results of this study, the following process flow was recommended:

(1) Plasma etch with the high CHF_3 flow setting; include N_2 in the feed gas.
(2) Ash with oxygen and forming gas. Results with oxygen/forming gas were slightly better than results with oxygen only. These results are not statistically significant.
(3) Wet clean with a low temperature stripper (EKC 830) followed by a polymer removal chemical (EKC 265) wet clean.

CONCLUSIONS

We have evaluated the impact on photoresist and residual polymer removal of several factors in the via etch and post etch cleaning process. We have determined which of these factors have the greatest effect on residue removal and, therefore, on device performance. Our results indicate that N_2 addition to the etch process, low CHF_3 flow in the etch process, and ashing followed by wet cleaning (post etch) have the greatest impact on photoresist and residual polymer removal. An optimized process flow has been proposed.

REFERENCES

1. H. Shan, B. K. Srinivasan, D. W. Jillie, Jr., J. S. Multani, and W. J. Lo, "Effects of Deposition and Ion Scattering on Profile Control in Submicron Oxide Etch", J. Electrochem. Soc. **141**, 2904 (1994).

2. G. S. Oehrlein, Y. Zhang, D. Vender, and M. Haverlag, "Fluorocarbon High-Density Plasmas. I. Fluorocarbon Film Deposition and Etching Using CF_4 and CHF_3", J. Vac. Sci. Technol. A **12**(2), 323 (1994).

3. D. C. Gray, V. Mohindra, and H. H. Sawin, "Redeposition kinetics in fluorocarbon plasma etching", J. Vac. Sci. Technol. A **12**(2), 354 (1994).

4. J. W. Butterbaugh, D. C. Gray, and H. H. Sawin, "Plasma-surface Interactions in Fluorocarbon Etching of Silicon Dioxide", J. Vac. Sci. Technol. B **9**(3), 1461 (1991).

5. J. W. Coburn, "Role of Ions in Reactive Ion Etching", J. Vac. Sci. Technol. A **12**(4), 1417 (1994).

6. Y. Hikosaka and H. Dugai, "Radical Kinetics in a Fluorocarbon Etching Plasma", Jpn. J. Appl. Phys. **32** 3040 (1993).

7. LAM Research Internal Technical Report.

Table I
Experimental Setup

wafer #	N2 in via etch	amount of CHF3	order of ash/wet	type of strip chemical	order of strip and polymer removal	Ash process
4	yes	low	wet/ash	837	837/265	H2/N2/O2
5	yes	high	wet/ash	837	265/837	O2/NF3
6	yes	high	ash/wet	837	265/837	H2/N2/O2
7	yes	high	ash/wet	830	265/830	O2
8	yes	high	ash/wet	830	830/265	O2
9	no	high	ash/wet	830	830/265	H2/N2/O2
10	no	low	ash/wet	830	830/265	O2/NF3
11	yes	low	wet/ash	830	830/265	O2/NF3
12	yes	high	wet/ash	837	837/265	O2/NF3
13	no	high	ash/wet	837	265/837	O2/NF3
14	yes	low	ash/wet	830	265/830	H2/N2/O2
15	no	high	wet/ash	830	830/265	O2
16	no	low	ash/wet	837	837/265	H2/N2/O2
17	yes	low	wet/ash	830	265/830	O2/NF3
18	no	high	wet/ash	837	837/265	H2/N2/O2
19	no	low	ash/wet	837	265/837	H2/N2/O2
20	no	low	wet/ash	830	265/830	H2/N2/O2
21	no	low	wet/ash	837	837/265	O2
22	yes	low	wet/ash	837	265/837	H2/N2/O2
23	no	high	wet/ash	837	265/837	H2/N2/O2
24	yes	low	ash/wet	837	265/837	O2
25	no	high	wet/ash	830	265/830	O2
26	yes	low	ash/wet	837	837/265	O2
27	yes	high	wet/ash	830	265/830	H2/N2/O2
28	yes	high	ash/wet	837	837/265	H2/N2/O2
29	no	high	ash/wet	830	265/830	H2/N2/O2
30	yes	low	ash/wet	830	830/265	H2/N2/O2
31	yes	high	wet/ash	830	830/265	H2/N2/O2
32	no	high	ash/wet	837	837/265	O2/NF3
33	no	low	ash/wet	830	265/830	O2/NF3
34	no	low	wet/ash	830	830/265	H2/N2/O2
35	no	low	wet/ash	837	265/837	O2

Table II
Experimental Results

wafer #	are polymer nodules present	amount of sidewall polymer	amount of TiN undercut
4	no	2	2
5	yes	2	1
6	no	0	0
7	no	1	0
8	no	2	1
9	no	4	1
10	no	2	1
11	no	2	1
12	yes	2	1
13	no	3	1
14	no	2	1
15	no	3	1
16	no	4	1
17	yes	2	1
18	no	3	1
19	no	4	2
20	no	2	2
21	no	3	1
22	no	0	1
23	no	4	1
24	no	1	2
25	no	2	1
26	no	2	1
27	no	2	1
28	no	2	1
29	no	4	1
30	no	1	1
31	no	0	1
32	no	2	1
33	no	3	1
34	no	2	1
35	no	2	1

Key: Amount of sidewall polymer
0 = none 3 = moderate
1 = specs 4 = heavy
2 = light

Amount of TiN undercut
0 = none
1 = observable
2 = heavy

Figure 1 (Top): Via with heavy sidewall polymer and TiN undercut.

Figure 2 (Bottom): Via with polymer nodules.

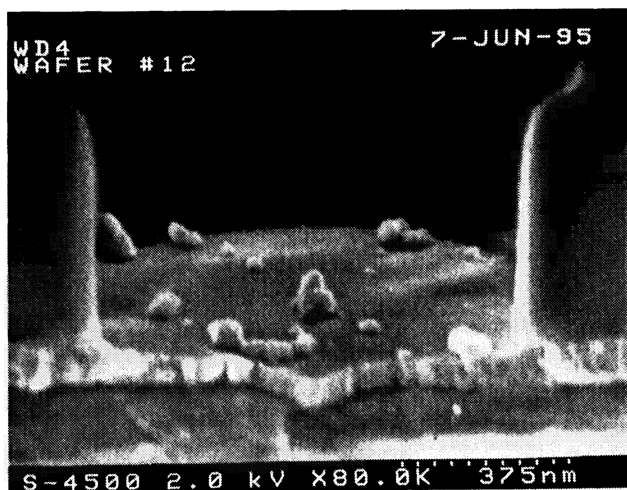

DAMAGE DURING ASHING: A CHARACTERIZATION OF SEVERAL MODERN ASHERS

Lee M. Loewenstein, Srikanth Krishnan
and George A. Brown

Semiconductor Process and Device Center, Texas Instruments,
P.O. Box 655012, Dallas, Texas, 75265

ABSTRACT

We have measured the effects of ashing photoresist using several new reactor configurations (inductively coupled plasma and microwave/reactive ion etch). These reactors also offer oxygen-fluorine chemistries that can remove post-ash residues from wafer surfaces. We have measured breakdown voltages, Fowler-Nordheim tunneling survivor rates, antenna charging and other electrical characteristics to determine the suitability of these tools and process chemistries for as replacements of standard microwave ashing combined with post ash sulfuric acid (piranha) and SC1 (NH_3, H_2O_2 solution) treatment. Our data show that the new plasma methods do not damage wafers to any significant extent, provided the RF power of the microwave/reactive ion etch method is low enough (<350 W). We do not find, however, that the plasma-rinse process is an equivalent substitute to plasma-SC1 treatment, since their breakdown voltages and Fowler-Nordheim survivor rates were lower than the control values.

INTRODUCTION

Photoresist ashing is facing several new choices. New plasma generation methods are being applied with the hope of reducing damage and improving aspects of the process such as removing the carbonized layer formed in ion implantation. Fluorine-containing gases are also being added during portions of the strip sequence to remove residues. The literature includes investigations of plasma-induced damage due to contamination and residues[1] There also is discussion of trapped charges and oxide interface states[2]. Some work looks specifically at the electrical effects of resist ashing.[3] In this work, we examine the consequences of the plasma and chemistry on device properties.

The standard process sequence for removing photoresist from silicon wafers prior to metallization involves removing the photoresist in an asher, followed by wet cleaning to remove remaining residues. Since the photoresist is used as a mask for an etching or ion implantation, it has species in it which do not oxidize to volatile species in an atomic oxygen ambient. The most common way to remove these residues consists of a sequence

of immersions in hot H_2SO_4 (piranha) and NH_3/H_2O_2 solutions (SC1). This sequence serves to oxidize any remaining oxidizable materials, and to remove residues.

By combining resist and residue removal in a single processing tool, we may be able to achieve a more cost-effective process. By adding a fluorine-containing gas to the gaseous discharge in the asher, atomic fluorine is generated which can remove many of the residues left on the wafer after oxygen ashing. This modification of the cleanup sequence causes etching of other exposed films such as silicon dioxide, however, and may damage the wafer surface. Before using such a process, electrical measurements must be made to assure acceptable performance.

We have studied several new tools for photoresist ashing. One tool uses an inductively coupled plasma (ICP) to generate the active oxygen and fluorine. The other uses reactive ion enhanced plasma and a microwave discharge and (RIE/μW). We compare the results of these tools with microwave (μW), high pressure triode (HPT), and barrel ashers. We have previously shown that all processes result in surfaces free of residue as observed by SEM.[4]

We designed process flows to challenge the ash processes. One process sequence involved stripping implanted photoresist from a silicon dioxide surface. This oxide was stripped from some wafers and a new oxide grown, or left as processed on other wafers. MOS capacitors were formed. This sequence demonstrated the ash process interaction with an oxide surface. In previous work, we have carried out similar tests with photoresist on a Si surface.[4]

Testing included MOS capacitor breakdown voltage, mobile ion, interface trap density, lifetime, and antenna charging. The antenna structures were on a proprietary test chip known as PREDATOR with antenna ratios from 10,000 to 200,000.[5] We measured threshold voltages, V_t, for p and n channel transistors, and compared them as a function of antenna ratio. We also measured gate leakage.

EXPERIMENTAL

Ashers

A brief description of the ashers and processes used is presented in Table I. The GaSonics and Branson ashers represent our laboratory's then current resist stripping capability, and are not the most up-to-date products available from these companies nor necessarily representative of μW and barrel methods. The ICP design, being new to resist ashing applications, is shown in Fig. 1.

Wafers passing through plasma residue removal steps still require a wet rinse to remove water soluble residues on the wafer surface. We do this by spin rinse drying (SRD). Wafers receive a 5 min rinse in DI water, followed by a drying sequence of 10 min length. The reactors which have residue removal processes in addition to bulk resist removal can be run with just the bulk removal process. In this case, these wafers need to pass through standard wet cleanup (SC1).

Table I. Types and properties of photoresist ashers.

Asher	Plasma Freq. (MHz)	Plasma Location	Batch size	Bulk resist removal	Residue removal	Manufacturer & Model
μW	2450	Ceramic tube upstream from wafer	1	O_2+N_2O	None	GaSonics Aura 1000 (μW1), Fusion 200MPC (μW2)
ICP	13.56	Quartz tube upstream from wafer	2	O_2	O_2+C_2F_6	Mattson ASPEN II
HPT	13.56	Between metal grids near wafer	2	O_2	O_2+C_2F_6	Mattson ASPEN
RIE/ μW	13.56 2450	At wafer (RIE) and in quartz tube upstream (μW)	1	O_2 (RIE) and O_2+H_2/N_2 (μW)	O_2+CF_4 + H_2/N_2 (μW)	ULVAC Phoenix
Barrel	13.56	Between metal cage surrounding wafers and reactor wall	25	O_2	None	Branson

Wet process

Wafers undergoing wet cleanup are placed in hot sulfuric acid (60 °C) solution for 45 min. They then are placed in SC1 solution (NH_3: H_2O_2:H_2O in a 1:1:5 ratio) at 60 °C for 20 min while receiving megasonic energy of 250 W. Following this, the wafers are spin-rinse-dried.

MOS capacitor fabrication sequence

We fabricated MOS capacitors as a test of the cleaning procedures described above. The fabrication sequence involved the following:

- Grow 60 or 500 Å oxide on 150-mm Si wafers (both p and n-type).
- Coat and bake 2 μm photoresist on wafers.
- Implant 1×10^{16} P^+ ions/cm^2 at 150 KeV into photoresist.
- Ash photoresist using reactors in Table I.
- Perform wet cleanup process *or skip.*
- Strip and regrow gate oxide *or skip.*

After this, all wafers had 2700 Å polysilicon deposited, implanted (P, 7×10^{15}/cm^2, 80 KeV), patterned and annealed to form top gate electrodes. (One set of wafers with 500 Å oxide had aluminum gates sputtered and patterned.) Aluminum was sputtered onto wafer backsides for electrical contact.

Antenna structure fabrication

We constructed antenna structures and used them at several places to measure charging effects. The antenna structure comprised an array with perimeter and area intensive structures. The ratio of the charge-collecting electrode to active area (antenna ratio) spanned a wide range from 10 to 200,000 and the perimeter varied from 440 μm to 99,000 μm. The antennas were connected to active devices, including transistors, MOS capacitors and differential amplifiers. P-type wafers were processed using a CMOS process flow targeted for the 0.35 μm technology node.

ELECTRICAL CHARACTERIZATION

MOS capacitor testing

Electrical measurements on the MOS capacitors included ramp voltage breakdown (RVB), high-low frequency MOS C-V characterization, mobile ion density analysis, and transient capacitance-time Zerbst measurements of carrier generation rates.

The RVB data was taken on arrays of 0.02 cm^2 capacitors. Both n-type and p-type wafers were included. Both types were tested so as to accumulate the substrate silicon; that is, n-type wafers were tested with positive voltages and p-type wafers with negative voltage applied to the gate electrodes. For the 60 Å gate oxides, ramp voltage breakdown data actually employed a staircase sequence of 0.33 V steps, starting from 0 V, and continuing with current checking at each step until a current consistent with a current density of 100 mA/cm^2 or greater was sensed. Voltage ranges reported here as breakdown voltages therefore do not necessarily indicate destructive breakdown, but may be only that voltage at which non-destructive Fowler-Nordheim conduction is observed at the 2 mA level. To clarify this situation, a second low-voltage test is done on each capacitor immediately following the sensing of the current limit to establish destructive breakdown. Low-leakage, non-shorted units found in this second test are classified as *survivors*. The percentage of such units for each process group has been found to be a useful monitor of oxide quality. A similar procedure was used for the 500 Å oxides, except that 2.0 V steps were used for the staircase ramp.

High-low frequency MOS capacitance-voltage characteristics were measured on 0.001 cm^2 capacitors on one p-type and one n-type wafer from each process group. Normally, four units per wafer were measured. For these 60 Å oxides, oxide capacitance was measured at 4 V of accumulating bias voltage, with a voltage sweep from 3 V into inversion to 3 V into accumulation. Voltage sweeps of ±5 V were used for the 500 Å oxide capacitors. From the high frequency data, an electrical evaluation of oxide thickness was obtained, along with flat band voltage, from which an estimate of oxide-silicon interface fixed charge was computed. The combination of high frequency and quasi-static data was used to extract interface state density-energy profiles. In general, these profiles were featureless for these samples, so a midgap value of interface state density, $D_{it}(0)$, was used for process comparison.

Mobile ion density measurements to determine whether the plasma exposures were contaminating oxides with alkali ions were made by standard MOS C-V bias-

temperature stress techniques, using 300 °C, 5 min cycles with sequential stress voltages corresponding to oxide field strengths of +/- 0.5 MV/cm. Heavy metal contamination of the silicon surface was measured by conventional Zerbst capacitance-time analysis.

Antenna structure testing

We tested in-line prior to any sintering, both at the gate and metal level. The shifts in the electrical characteristics of these active devices were monitored and compared to that of the control devices. All antenna data presented here are with 5x0.35 μm (gate width by length) transistors on 60 Å gate oxides. Each experimental split consisted of two wafers.

Electrical testing of the poly and metal antennas was performed immediately after the ash and wet cleanup. Since the transistors were not completely defined at poly level, we proved NMOS transistors for plasma stress induced gate leakage current with -3 V on the poly gate (5 MV/cm accumulation). Due to the inaccessibility of the well at poly level, we did not probe P channel transistors. Metal level testing included threshold voltage and gate leakage current measurement on NMOS and PMOS transistors. We measured V_t in the linear region (V_{DS}=50 mV), defined as the gate voltage required for gate current of 0.1 μAxW/L, where W and L are gate length and width.

RESULTS

Breakdown Voltages

Breakdown voltages for 60 Å oxides are shown in Fig. 2. Several things are evident for all samples, regardless of ashing method. As-grown oxides have lower breakdown voltages than regrown oxides. n-Si shows less variation from sample to sample than the comparable p-Si samples. Also, n-Si wafer breakdown voltages are closer for as-grown and regrown oxides than are the breakdown voltages for p-Si wafers.

For regrown oxides, standard processing using plasma ashing followed by SC1 wet cleaning gives higher breakdown voltages than plasma-SRD processing. The barrel asher with SC1 was inferior to other plasma approaches. (Note that this was an approximately 10 year old reactor, and does not contain any possible design improvements that might give better results.) The RIE-SRD process gave higher breakdown voltage than did the ICP-SRD process.

For as-grown oxides, ICP-SC1 and μW-SC1 processes gave the largest breakdown voltages. The other processes resulted in breakdown voltages up to 1 V lower.

Breakdown voltages for 500 Å oxides are shown in Fig. 3 and Fig. 4. p-Si as-grown oxides are inferior to regrown oxides, but the n-Si as-grown oxides are actually slightly better than the regrown oxides. In all cases tool variations are very minor. Complete SC1 cleaning gives very slightly better results than just SRD.

Fowler-Nordheim Survivors

Fig. 5 shows the large differences in survivor rates for as-grown and regrown 60 Å oxides. The difference is typically more than a factor of 2. Among the as-grown

oxide samples, those processed by plasma-SC1, except for RIE-SC1, tend to fare best. SRD processes give lower survivor rates than their SC1 counterparts. The μW-SC1 and ICP-SC1 give very similar survivor rates. (Survivor data for the case of ICP-SRD as-grown oxide is missing.) n-Si substrates show lower survivor rates than p-Si for as-grown oxides, while they show higher survivor than p-Si rates for regrown oxides.

Figs. 6-7 show survivor rates for 500 Å oxides. In Fig. 6, as-grown p-Si oxides gave generally lower survivor rates than the regrown oxides. For p-Si wafers with as-grown oxides, sequences ending in SC1 gave higher survivor rates than those ending in SRD. The RIE-SC1 process gave the highest survivor rate.

Flatband voltages

Flatband voltages, which correlate to fixed interface charge densities, show little variation other than that due to substrate material type, as Fig. 8 shows. We see that slightly lower V_{fb} result from SRD sequences than SC1 sequences for as-grown oxides. It is possible that this may indicate a slight contamination resulting from SC1 treatment.

Carrier generation lifetime

Minority carrier generation lifetime data is shown in Fig. 9 for a limited data set. Regrown oxides show better behavior than as-grown oxides.

Antenna structures

Charging by the ashing process was tested using antenna structures. The processes used were variants of the plasma-SRD techniques. These used 200 to 300% overetch for the resist strip step, followed by the standard fluorine process chemistry and time for a representative residue removal process. Photoresist was spun onto the antenna structure wafers, patterned and baked, but not subjected to implantation or other processing. Figs. 10 and 11 summarize the gate leakage currents subsequent to ash in the RIE/μW asher. Although the leakage currents are low, there is a significant trend in the leakage current. The monotonic increase in this current with antenna ratio is a clear signature of shift in the oxide properties after the ash. This form of light damage is minimized in this particular instance by lowering the RF power to 350 W. We observe no increase in leakage currents or any systematic trend in leakage current with antenna ratio after ICP ash, as seen in Fig. 12. This indicates minimal damage associated with the ICP asher. This result is further affirmed at the metal level ash. Post-ash testing for the HTP and ICP modes showed negligible shift for antenna ratio up to 200,000 (Table II).

Table II. V_t, threshold voltage.

	Antenna ratio	HPT	ICP
NMOS	10K	0.53	0.53
NMOS	200K	0.51	0.52
PMOS	10K	0.51	0.52
PMOS	200K	0.51	0.52

Mobile ion and fixed charge densities

We measured mobile ion densities and fixed charge densities. We did not find that these values were sufficiently above our background detection levels to merit further analysis.

DISCUSSION

There are two questions that this data addresses: (1) Are ICP and μW/RIE plasma sources suitable sources for photoresist ashers? (2) Are plasma-SRD processes suitable cleaning methods for post-process cleaning?

Plasma sources

Standard processing uses the full wet processing sequence, so at a minimum the plasma-SC1 data should be used as a standard for comparison. In addition, normal MOS processing also strips a sacrificial oxide before regrowing the gate oxide. Thus, for the most pertinent comparison, the comparable processes that we performed should be evaluated. As variations in processing can lead to abnormal results for single lots, it is best to compare the test process to a well-known process which serves as control. In this case, the μW-SC1 process is our control.

Breakdown voltage is a simple parameter that measures the quality of the Si-SiO_2 interface. Any significant reduction in breakdown voltage indicates a problem. RIE-SC1 and ICP-SC1 processes had breakdown voltages identical to the control for both n- and p-Si substrates. For as-grown oxides, breakdown voltages are in the order ICP>μW>RIE>barrel. The difference from best to worse is greater than 1 V, and should be significant. Breakdown voltages for thicker oxides showed little difference between ashers. 500 Å oxides showed only small differences. The breakdown voltage results strongly support ICP processing.

Fowler-Nordheim survivor data for SC1 processes with regrown 60 Å oxides showed survivor rates with ICP≈RIE≈μW>barrel. With as-grown oxides, barrel>ICP>μW>RIE. While the barrel asher gave good results with as-grown oxides, the breakdown voltage did not improve as much as for other tools. 500 Å as-grown oxides showed different behavior: RIE>μW(2)>ICP>μW. There were no differences among regrown oxides. In another experiment where Al gates were made, survivor rates for as-grown oxides went ICP>μW>triode. Survivor rates for regrown oxides in this case were inexplicably low. The Fowler-Nordheim results are not completely coherent. They do show that both ICP and RIE give as good or better than μW processing.

Lifetime data show the new techniques to be as good as or better than standard μW stripping. The antenna structure data indicates that the ICP has no charging problems. The μW/RIE process has no charging problems provided the power is kept sufficiently low (<350 W).

Plasma-SRD cleaning processes

Comparison to determine the fitness of the ash plus fluorine processes for removing residues should be made between the plasma-SRD and plasma-SC1 processes. This provides a relative measure of the process effect. The role of as-grown oxides is to

point to deficiencies of the cleanup process sequence which can be masked by stripping the contaminated or damaged oxide and regrowth of a high quality oxide.

Breakdown voltages for 60 Å oxides show reduced performance when fluorine chemistry replaces SC1. Lower breakdown voltages occur both for as-grown and regrown oxides. Fowler-Nordheim survivor rates for virtually all samples show a similar problem for fluorine chemistries. As the defect in plasma-SRD processing does not seem to result from charging, according to the antenna structure results, it presumably results from other defects. Residue removal may not be good enough to give electrical properties as good as SC1 chemistry, as some particulates have been noted.[6]

CONCLUSION

We have studied several new tools for stripping photoresist and removing residues. ICP can safely replace commonly used methods such as μW processing. So can μW/RIE provided that the RF power is sufficiently low. We have not proven that either plasma technique combined with fluorine chemistry for a plasma-SRD process can replace plasma-SC1 processing. This does not mean that they cannot ever do so. There are several areas where process improvements can occur which will give substantially cleaner surfaces with less attack of the underlying oxide. We also must note that the tests performed here are artificially severe, and that their consequences may be unrealistic in most manufacturing scenarios. Nevertheless, the cautionary note is sounded.

ACKNOWLEDGMENTS

We thank Jackie Kemp for her processing assistance, and Helen Simon for her help in electrical measurements. We adapted Fig. 1 from a drawing provided by Mattson Technology.

REFERENCES

[1] G.S. Oehrlein, R.M. Tromp, J.C. Tseng, Y.H. Lee and E.J. Petrillo, *J. Electrochem. Soc.*, **132**, 1441 (1985).
[2] L.M. Ephrath and D.J. DiMaria, "Review of RIE induced radiation damage in silicon dioxide," Solid State Technol., p. 182, 1981.
[3] S. Fang, S. Murakawa and J.P. McVittie, IEEE Trans. Electron Dev., 41, 1848 (1994).
[4] L.M. Loewenstein and G. Brown, Proc. 2nd Int. Symp. Ultra-clean Processing of Silicon Surfaces, M. Heyns, M. Meuris and P. Mertens, eds., Acco, Leuven, Belgium, p. 331.
[5] S. Krishnan et al., to be presented at the IEDM, Dec. 10-13, 1995, Washington, DC.
[6] P. Mertens and L.M. Loewenstein, unpublished data.

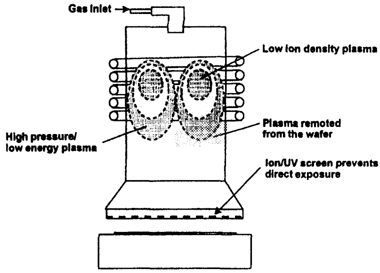

Fig. 1. Inductively coupled plasma source.

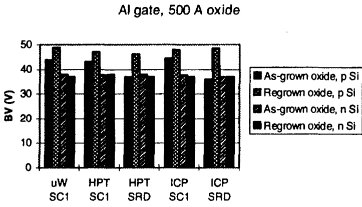

Fig. 4. Breakdown voltages for 500 Å oxides, Al gates.

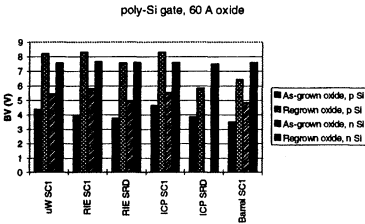

Fig. 2. Breakdown voltages for 60 Å oxides.

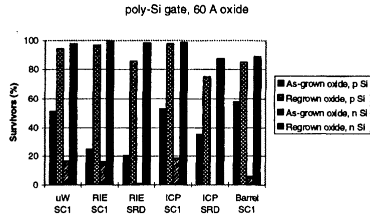

Fig.5. Fowler-Nordheim survivor rate for 60 Å oxides.

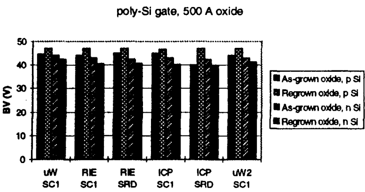

Fig. 3. Breakdown voltages for 500 Å oxides, poly-Si gates.

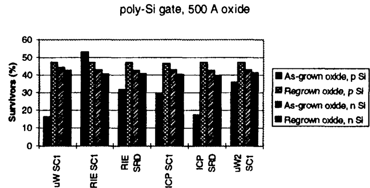

Fig.6. Fowler-Nordheim survivor rate for 500 Å oxides, poly-Si gates.

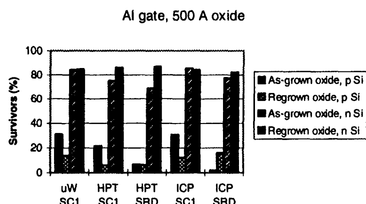

Fig. 7. Fowler-Nordheim survivor rate for 500 Å oxides, Al gates.

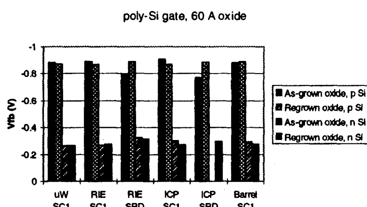

Fig. 8. Flatband voltages for 60 Å oxides, poly-Si gates.

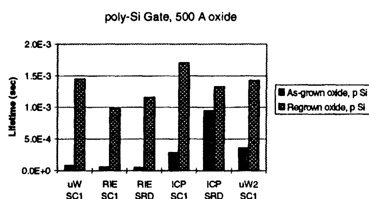

Fig. 9. Carrier generation lifetime for 500 Å oxides.

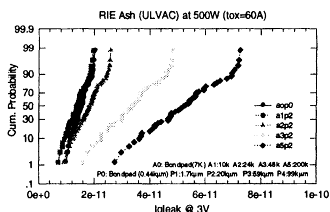

Fig. 10. Leakage current for RIE/μW.

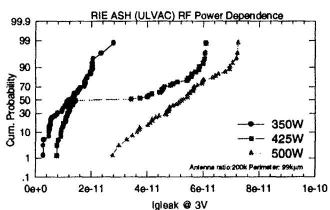

Fig. 11. RF power dependence of leakage current for RIE/μW.

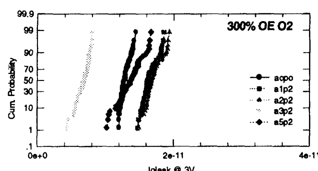

Fig. 12. Leakage current for ICP/μW.

Removal of Polymeric/Silicate Residues and Reduction of Contact Resistance for Inter-Metal Via Holes by Vapor Phase HF Cleaning

J. K. Tong, J. S. Martin, T. C. Rogers, D. J. Syverson

FSI International
322 Lake Hazeltine Drive
Chaska, MN 55318-1096, U.S.A.

ABSTRACT

In ULSI devices, electrical connection between metal layers is achieved by submicron via holes, defined by a dielectric RIE etch. A polymeric/silicate material often remains on the via hole sidewalls after the RIE process. SEM reveals that vapor HF can successfully remove this residue encapsulating the via openings and the via hole sidewalls. Additionally, vapor HF treatment reduces the metal-to-metal via contact resistance, presumably owing to the presence of AlF_3, formed by the reaction between the vapor HF and the Al/Al_2O_3 at the via base.

INTRODUCTION

In ULSI devices, electrical connection between metal layers is achieved by submicron via holes. Via holes are formed by cutting through interlayer dielectric (ILD) using anisotropic reactive ion etching (RIE) processes with CF_4 or CHF_3 chemistries and with inert gas mixtures. During the RIE process, a polymeric/silicate material, commonly referred to as RIE polymer or veil, formed on the sidewalls of the via hole to prevent lateral etching and thus greatly enhance the anisotropic aspects of the RIE etching process. Although this polymeric/silicate material is desirable for the directional RIE oxide etching process, it becomes a tenacious by-product for the downstream processing steps after the RIE process step. While the subsequent oxygen/ozone ashing process removes the bulk of the photoresist, it does not remove this sidewall polymer material. This is problematic as this polymer residue, in combination with the metal surface oxide at the bottom of the via holes, affects the subsequent metal deposition processes and leads to undesirable higher metal-to-metal via contact resistance. Therefore, a clean-up process has become necessary and inevitable, particularly given the rapid advances in device density and correspondingly higher via hole aspect ratios.

A successful clean-up process that is manufacturing applicable must at minimum meet four basic requirements: 1) complete removal of polymeric/silicate etch residues; 2) no significant degradation of the exposed ILD; 3) no significant alteration of the shape of the via holes and 4) comparable or better electrical properties.

This clean-up process is conventionally accomplished by solvent based or aqueous chemicals based bath processes, often times involving multiple steps, as illustrated in Figure 1. For solvent based processes, the removing mechanism is primarily by dissociating the metallic components in the polymeric material and the reaction can be described as:

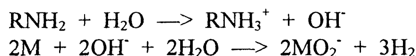

$$RNH_2 + H_2O \longrightarrow RNH_3^+ + OH^-$$
$$2M + 2OH^- + 2H_2O \longrightarrow 2MO_2^- + 3H_2$$

For aqueous HF based processes, HF is typically mixed with Ethylen Glycol (EG) and buffered with NH_4F. However, significant challenges remain for these types of solvent and wet clean-up processes including low efficiency of polymer removal, high and excessive variations of the via interface electrical resistance. Solvent safety and the high costs of solvents and their disposal are also becoming significant concerns in the industry.

Since Anhydrous vapor HF process has been successfully implemented in device manufacturing facilities for removing polymeric/silicate residues after metal RIE etch [1,2]. A logical extension is to apply the same processing technique to remove the residue formed during via dielectric RIE etch.

In addition, Al metals resides at the via hole base; however, this Al surface spontaneously oxides in the ambient environment to produce a 20-40Å, stable and electrically insulating Al_2O_3 layer. Accordingly, immediately prior to the subsequent metal deposition, a reverse-biased sputter etch is typically performed to remove this insulating material. For various reasons, it is highly desirable to minimize or eliminate, if possible, this reverse-biased sputter etch. To investigate the effects of vapor HF etching on Al surface, a series of experiments aimed at characterizing the pre- and post-vapor HF etched planarized Al surfaces were conducted and herein reported.

EXPERIMENT

Figure 2 shows the simplified plumbing diagram of the vapor HF process equipment used in the study. N_2 gas is used as carrier gas to introduce controlled amount of vapor HF and H_2O vapor mixture into the Teflon-made process chamber. An insitu DI water rinse is typically performed to rinse off etch byproducts and residues and followed by a high speed spin dry, all performed in the same process chamber.

For process characterization, various industry-common techniques such as SEM analysis, XPS measurements, TOF-SIMS measurements and electrical resistance measurements were used in this study.

RESULTS AND DISCUSSIONS

Removal of Sidewall Polymeric/silicate Residues

SEM micrographs, as shown in Figure 3, indicates that the vapor HF is capable of completely removing the via hole sidewall polymer residues due to its polymeric/silicate material and elemental composition. Notice also that no significant alteration of the shape of the via holes are seen as shown in the SEM micrographs. Figure 4 shows the characterization of ILD oxide loss, in this case PECVD TEOS, due to the vapor HF etching reaction of the TEOS. By precise controlling of the amount of vapor HF, the amount of H_2O vapor and the short duration of vapor HF exposure, the ILD oxide loss was minimized while still achieving the goal of complete removal of the sidewall polymer. Optimized process window for this process was determined to be 5 seconds of vapor HF exposure time with vapor HF flow rates of 60 to 100 SCCM which corresponds to PECVD TEOS loss of approximately 40 to 100Å. Figure 5 shows the significant reduction of metal-to-metal contacts resistance (normalized data) achieved by cleaning the via holes using vapor HF process, comparing with that using the process-of-record (POR) EG+HF mixture in a bath. Shown in Figure 6 is the normalized yield of the via contact chain, comparing the vapor HF process to the EG+HF process. In this case, significant yield improvement is achieved by using the vapor HF cleaning.

Removal of Surface Metal Oxide

It is believed that the complete removal of the sidewall residual polymer has significant contribution to the reduction of the via metal-to-metal contact resistance. But more importantly, it is speculated that the removal of the surface metal oxide at the bottom of the via holes are the primary reason for the reduction in the via contact resistance. Previous works have postulated that the reaction can be described as [3,4,5]:

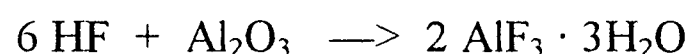

$$6\,HF + Al_2O_3 \longrightarrow 2\,AlF_3 \cdot 3H_2O$$

Representative high-resolution XPS spectrum of the Al metal surface pre- and post-vapor HF etching are shown in Figure 7. In the spectrum for the pre-vapor HF treated Al surface, the customary aluminum and aluminum oxide peaks appear at 71.8 and 73.8 eV, respectively. Note in this case these values are shifted by approximately 2 eV from their standard appearance engergies owing to surface charging. Of significance in the spectrum for the post-vapor HF treated Al surface, two peaks appear at 76.3 and 74.1 eV, which are consistent with AlF_3 and bare Al, strongly suggests that the HF/H_2O environment activates the Al/Al_2O_3 surface and replaces the Al_2O_3 with AlF_3. Interesting to note is that although AlF_3 is itself a stable and electrically insulating material, empirical evidence does indicate that significant reduction of via contact resistance was indeed obtained on the vapor HF treated Al surface. A speculative interpretation for this somewhat conflicting information is that the subsequent metal or barrier layer deposition more readily activates the Al-F bonds in the AlF_3 than the more stable Al-O bonds in the Al_2O_3. In point of fact,

further study is needed to fully understand the reasons for the improved electrical performance of the via contact holes cleaned by vapor HF process.

CONCLUSION

Vapor HF is successfully applied for the cleaning of submicron via holes which are used for electrical connection between metal layer in ULSI devices. The sidewall polymeric/silicate residues created by the dielectric RIE etch is successfully removed by the vapor HF etching followed by insitu DI water rinsing, with no significant alteration of the shape of the via holes and with minimized ILD oxide loss. Using vapor HF cleaning of the via holes, significant improvement in via contact electrical resistance and via contact chain yield were observed. Speculative interpretation is that the AlF_3, formed by vapor HF etching, is more readily activated by the subsequent metal deposition than that of the Al_2O_3, although further investigations are needed for complete understanding.

REFERENCES

[1] B. Bohannon, S. Poarch & D. Syverson, Proc. of Electrochem. Soc., Honolulu, HI (May, 1993)
[2] B. Bohannon, A. Bowling, S. Poarch, B. Wallace & D. Syverson, Proc. Vol. of the Institute of Environ. Sci., Las Vegas, NV (May, 1993)
[3] M.E. Straumanis & Y.N. Wang, J. Electrochem. Soc. **102**, 382 (1995)
[4] N. Hackerman, E.S. Snavely, Jr., & L. D. Fiel, Corros. Sci. 7, 39 (1967)
[5] M. Baverez & R. DeMarco, *Light Metals Conference Proceedings* (Metallurgical Society, New York, 1979)

FIGURE 1. Typical via cleaning process flow

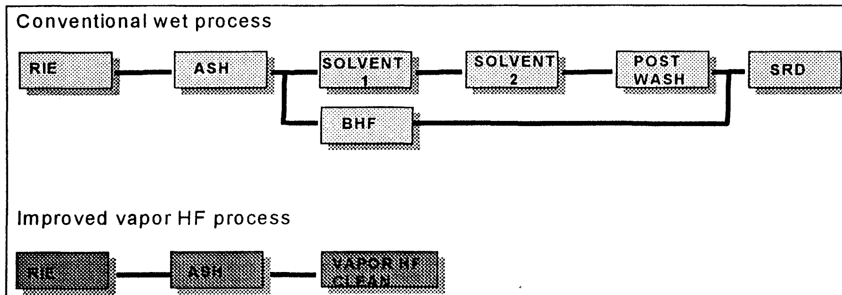

FIGURE 2. Simplified plumbing diagram of the vapor phase cleaning equipment

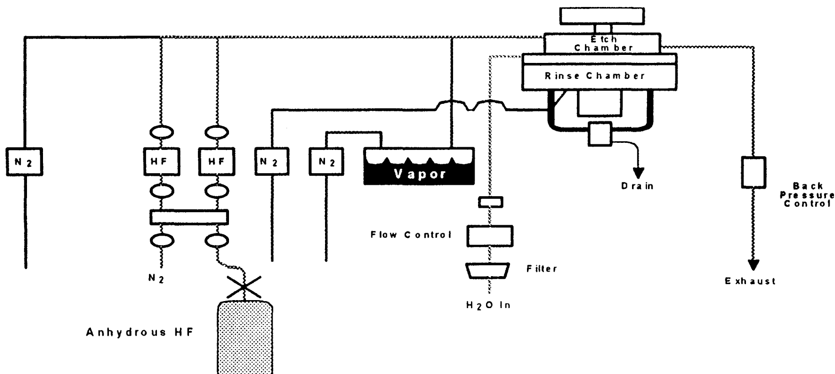

FIGURE 3. Via sidewall polymer removal pre- & post-vapor HF cleaning

Pre-cleaning | Post-Cleaning

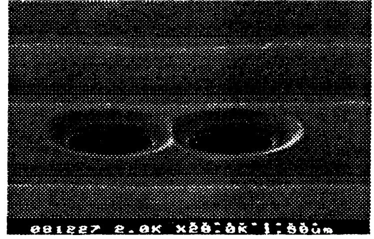

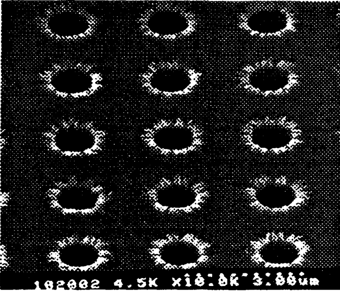

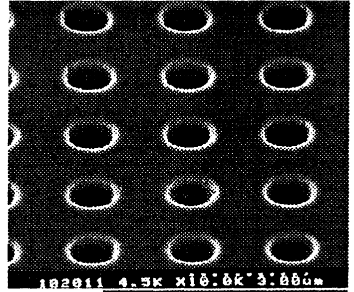

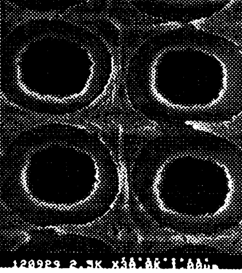

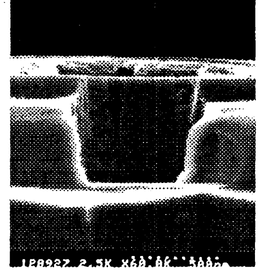

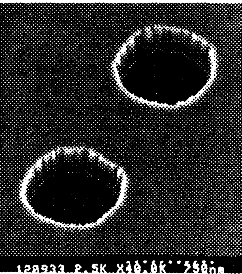

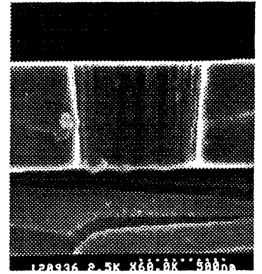

FIGURE 4. ILD PECVD TEOS loss characterization

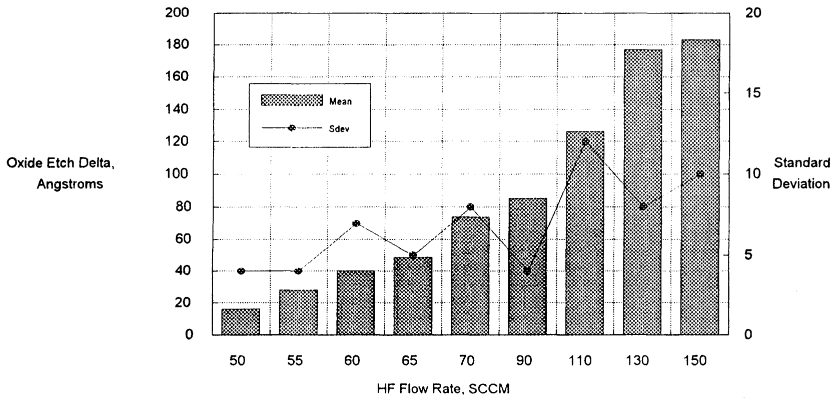

FIGURE 5. Normalized metal-to-metal via contact resistance

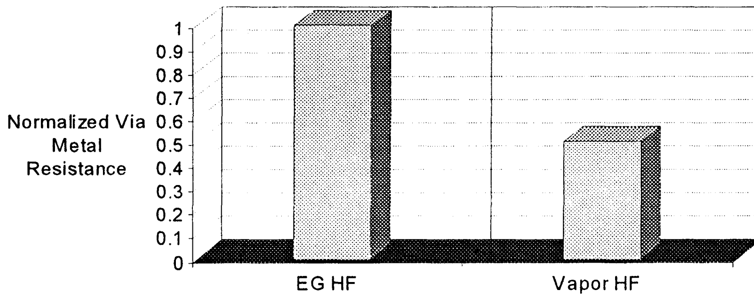

FIGURE 6 Normalized via contact chain yield

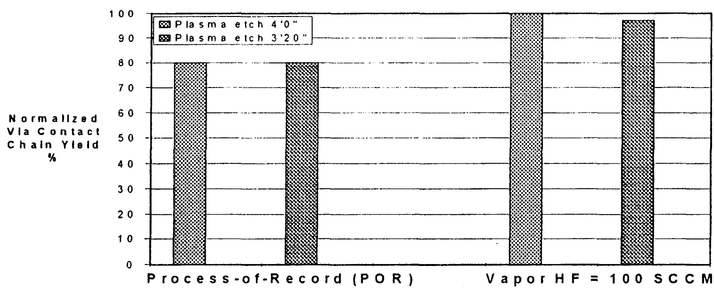

FIGURE 7. XPS spectrum of pre- and post-vapor HF treated Al metal surface

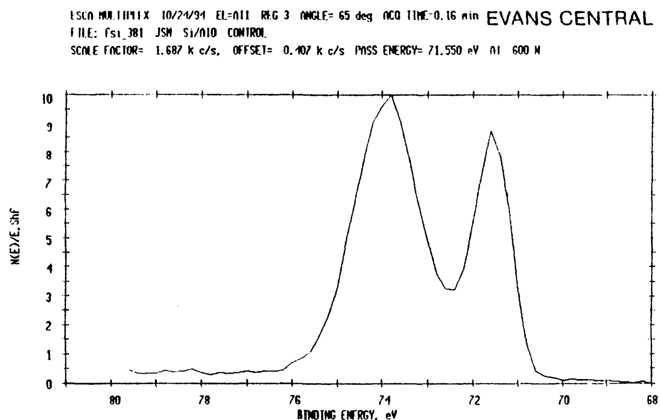

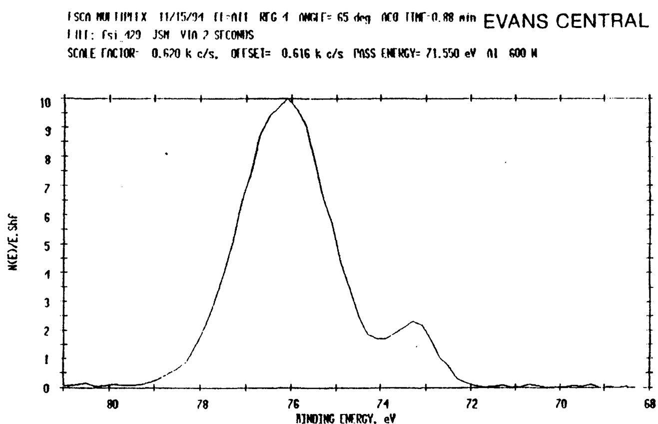

ANALYSIS AND REMOVAL OF POLYSILICON ETCH RESIDUE

Chang Weon Lee*, Sang Jun Choi,
Jae Jeong Kim, Hong Seok Kim, Woo Shik Kim
Jong Dae Lee**
Jong Wan Lee***

Advanced Technology Development Center, LG Semicon Co., Ltd., 1,Hayngjeong-dong, Hungduk-gu, Cheongju, Korea
** Department of Chemical Engineering, Chungbuk National University, San 48, Gaesin-dong, Cheongju, Korea
*** LG Electronics Research Center, LG Electronics Co., Ltd., 16, Woomyeon-dong, Seocho-gu, Seoul, Korea

The samples of 5000 Å polysilicon / 1000 Å thermal oxide / Si-substrate were patterned and etched with the gas chemistry of HBr, Cl_2, and He-O_2 and MERIE etcher. The dependence on gas flow rate was investigated and wet cleanings (RCA(SC1+SC2), HF) and dry cleanings (CHF_3/O_2, CF_4/O_2) were applied to evaluate the removal efficiency. The composition and chemical bonds of polysilicon etch residue were studied with XPS and SEM. The major components of polysilicon etch residue were Si and O and the residue existed as oxide-like structure (SiO_x) with considerable thickness. Post-cleaning processes were effective to remove etch residue.

INTRODUCTION

In dry etching process, the analysis of etch residue has been one of the main issues including etch rate, selectivity and etch profile to achieve high reliability of process and device performance. The residue has been investegated by many researchers for various materials such as silicon, silicon dioxide, GaAs and so on.[1,2] It has been recognized that the etch residue has large dependence on the process parameters such as gas chemistry, pressure, rf power, etc. When silicon and silicon dioxide are etched with fluorocarbon-based plasma, it is known that etch residue of CF_x polymer is generally

formed on the etched surface.[3~5] X-ray photoelectron spectroscopy is widely used to characterize the component and chemical bonding state in the near-surface region of the etched samples.[6,7]

In this paper, the composition and chemical bonds of polysilicon etch residue were studied with XPS and SEM. From these results, the formation mechanism of etch residue were discussed and post-cleaning processes for removal of etch residue were evaluated.

EXPERIMENTAL

Thermal oxide of 1000Å was grown on the pre-cleaned p-type silicon wafer and then polysilicon of 5000Å was deposited by LPCVD. Thereafter, the samples were patterned and etched with the gas chemistry of HBr, Cl_2, and He-O_2 and MERIE etcher. The dependence on gas flow rate was investigated and wet cleanings (RCA(SC1+SC2), HF) and dry cleanings (CHF_3/O_2, CF_4/O_2) were applied to evaluate the removal efficiency. The role of each gas during etch process was analyzed in order to investigate the formation mechanism of etch residue.

RESULTS AND DISCUSSION

The dependence of gas flow rate on the etch residue was investigated, especially, with He-O_2 gas. The amount of residue was increased linearly with He-O_2 gas flow rate and Figure 1 shows the effect of He-O_2 gas flow rate on the residue formation. Most of the residue was left on the top of etched structure and on the sidewall of photoresist mask forming rabbit ear-like shape, which was revealed to be chemically inert to PR strip processes of O_2 plasma ashing and SPM (O_3/H_2SO_4) cleaning. For the removal of residue, several wet and dry cleanings are processed and Figure 2 is the cross-section view of samples after post-cleanings. Figure 3, 4 are XPS results of etched and post-cleaned samples with varing the take-off angle. The three peaks of Si_{2p}, O_{1s}, and C_{1s} were detected from wide scan data and the deconvolution of each peak was done to find different binding energy in narrow scan data. For Si_{2p} peak, three peaks of 106eV (un-known), 104eV (Si-O), and 100eV (Si-Si) were detected and two peaks of 533.5eV (Si-O) and 536eV (un-known) in O_{1s} peak were shown in Figure 3. From XPS result with angle variation, it is considered that the residue was left on the top of etched structure to be in accordance with Figure 1. In contrast with etched sample, un-known peaks

(106, 536eV) were gone when the post-cleaning was applied. In depth profile (Figure 5), the etched sample was sputtered with Ar ion beam for 10 minutes and Si_{2p} and O_{1s} peaks were continually traced and un-known peaks (106, 536eV) decreased and disappeared with sputtering. As a result, un-known peak (106, 536eV) is attributed to the etch residue which is composed of Si and O complex with considerable thickness. Compared with wet cleaning, dry cleaning process remained new residue of CF_x on the surface which is shown as broad C_{1s} peak of Figure 4 (b). The reaction mechanism was studied with combination of gas chemistry and their ratio and it is revealed that etching is mainly attributed to Cl_2 gas and etch residue depends on He-O_2 gas. Also, it was found that HBr contributed some residue because of the lower volatility of brominated errosion product.

CONCLUSION

The major components of polysilicon etch residue were Si and O and the residue existed as oxide-like structure (SiOx) with considerable thickness. Post-cleaning processes were effective to remove etch residue but dry cleaning process using fluorocarbon-based plasma remained new etch residue on the wafer.

REFERENCES

1. P. H. Yih and A. J. Steckl, J. Electrochem. Soc., **140**, 1813 (1993).
2. G. S. Oehrlein, R. M. Tsang, Y. H. Lee and E. J. Petrillo, J. Electrochem. Soc., **132**, 1441 (1985).
3. G. S. Oehrlein, J. G. Clabes and P. Spirito, J. Electrochem. Soc., **133**, 1002 (1986).
4. G. E. Potter and G. H. Morrison, J. Vac. Sci. Technol., **B10**, 2398 (1992).
5. G. S. Oehrlein, S. W. Robey and J. L. Lindstrom, Appl. Phys. Lett., **52,** 1170 (1988).
6. A. M. Basrklund and H. -O. Blom, J. Vac. Sci. Technol., **A10**, 1212 (1992).
7. J. H. Thomas III, J. Vac. Sci. Technol., **B7**, 1236 (1989).

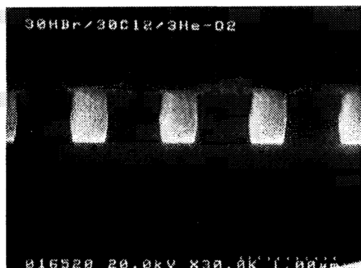

(a) 3 sccm

(b) 6 sccm

(a) 9 sccm

(b) 18 sccm

Fig. 1. He-O_2 gas flow rate dependence of the residue

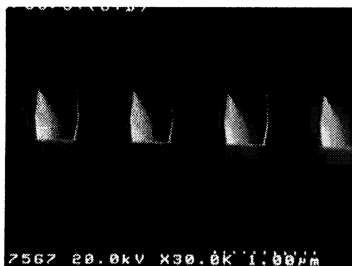

(a) SC1 + SC2

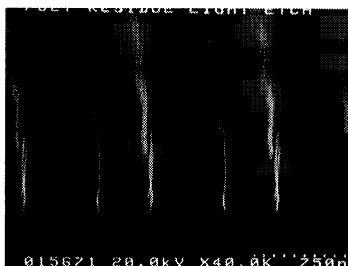

(b) HF

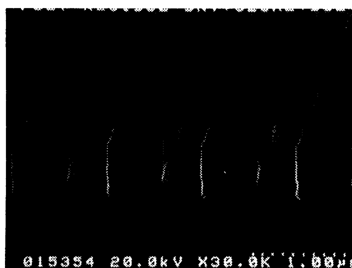

(a) CHF_3/O_2

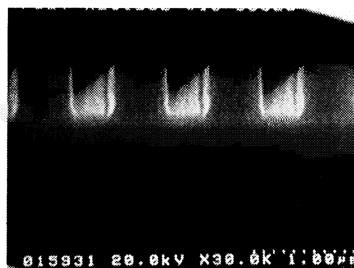

(b) CF_4/O_2

Fig. 2. SEM photographies after wet and dry cleanings

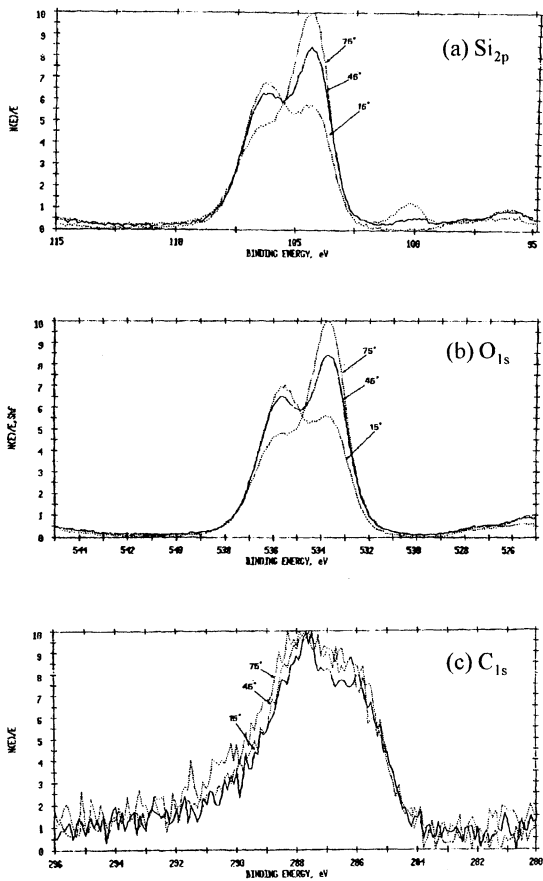

Fig. 3 The narrow spectra of XPS analysis after etch

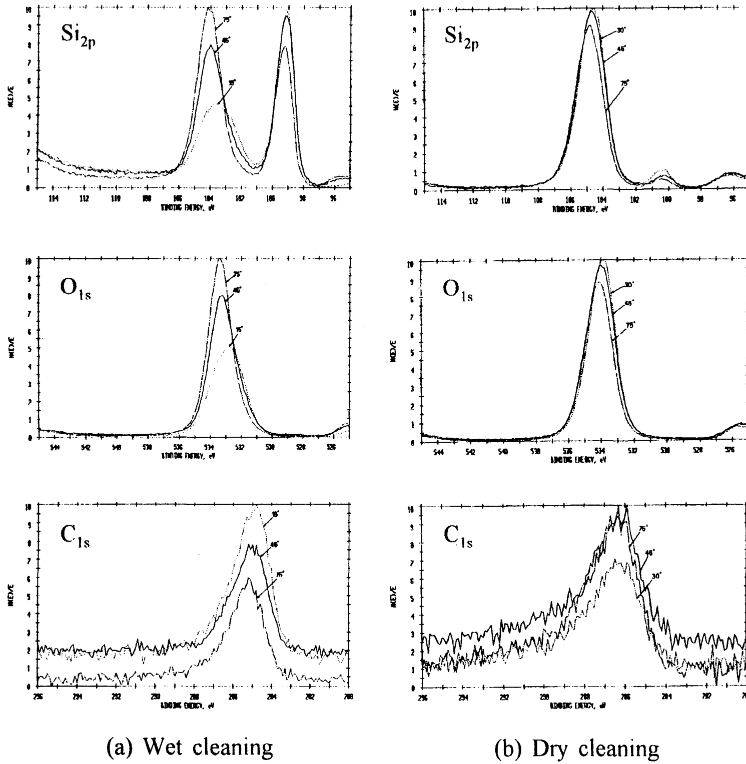

(a) Wet cleaning (b) Dry cleaning

Fig. 4 The narrow spectra of XPS analysis after post-etch clèanings

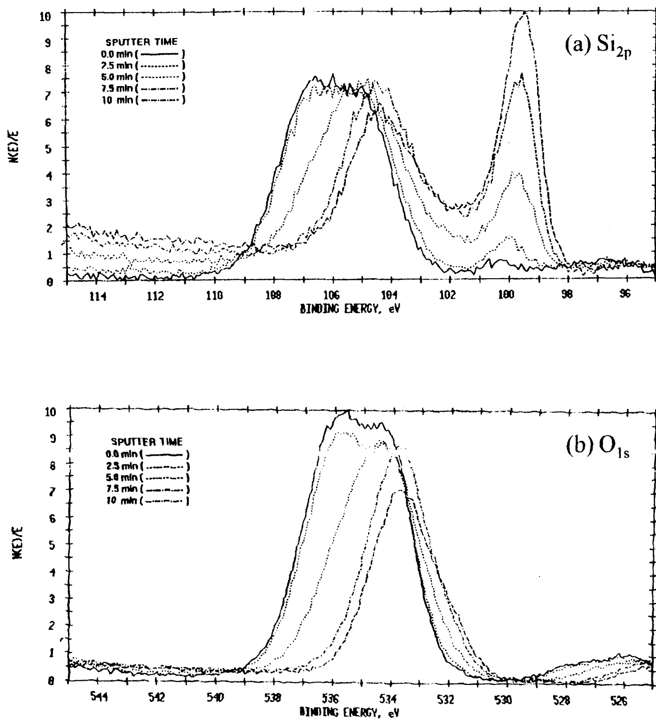

Fig. 5 The depth profile of XPS analysis after etch

Specialty Gas Interactions with Ultraclean Silicon Surfaces

Yasuyuki Shirai, Masakazu Nakamura and Tadahiro Ohmi

Dept. of Electronic Engineering, Faculty of Engineering, Tohoku University
Aza-Aoba, Aramaki, Aoba-ku, Sendai, 980 Japan
TEL : 81 22-217-7124, FAX : 81-22-263-9396
E-mail : shirai@sse.ecei.tohoku.ac.jp

We have studied surface reaction between various solid surface and specialty gases such as silane(SiH_4). Specialty gas decomposition characteristics such as decomposition temperature and decomposition rate were quite different due to the dilution gas species, specialty gas concentration and surface condition. In this report, we present the low temperature surface reaction mechanism based on ionization potential of gas molecule, the energy level of solid surface and experimental results.

INTRODUCTION

In order to establish scientific semiconductor manufacturing, we have been proposed ultraclean processing concept characterized by ultraclean wafer surface, ultraclean processing environment and perfect parameter controlled process(1),(2). The specialty gases such as SiH_4 and Si_2H_6 have been extensively used for thin film formation in the CVD process. However their physical and chemical properties are very complex and not well understood. Current manufacturing process, process parameters such as flow rates, concentration and temperature are mostly empirically determined. Thus we have studied reactive specialty gas interactions with various solid surfaces(3),(4).

EXPERIMENTAL

Fig.1 shows the schematic diagram of the experimental setup in order to evaluate the decomposition characteristics of specialty gases. All components used in this system are made of Cr2O3 passivated stainless steel(5),(6). Dead space in the integrated parts of valve was minimized as much as possible. Tube reactor was made of 1/2" x 40 cm Hastelloy-EP and was heated with electric sheath heaters wrapped with aluminum foil and insulation. The

temperature was controlled within ±2℃ by using several PID controllers along the tube reactor. The flow rate and dilution ratio were controlled by using precision mass flow controllers. A 100 ppm SiH_4 gas in mixture Ar gas was supplied to the tube reactor and concentration of SiH_4 gas came out from the tube reactor were measured using by FT-IR (Fourier Transform -Infrared Spectroscopy) or GC-TCD (Gas Chromatography-Thermal Conductivity Detector).

In this study, we prepared three types of Si surfaces : non-dope Si, n+ Si and p+ Si surface, on inner surface of tube reactor by means of thermal CVD method. The non-dope Si surface was formed by decomposition of SiH_4, n+ Si surface was formed by deposition with PH_3, and p+ Si by decomposition with B_2H_6. Every deposited Si thin film features (111) orientation. A predetermined gas is continuously introduced into the tube reactor with its inner surface covered with a predetermined thin film while the inner surface is not at all exposed to the clean room air. Thus we have evaluated specialty gas interactions with ultraclean Si surface. If we exposed Si surface to the clean room air, a large amount of moisture adsorbed on Si surface less than 1 second(7).

The flow rate was held constant until the exit concentration reached a steady state as indicated by FT-IR measurements. Then gas flow rate was changed for the desirable residence time. The residence time was calculated based on the reaction volume and the gas flow rate at the reactor temperature.

RESULTS AND DISCUSSION

Fig.2 shows the semi-log plots of SiH_4 decomposition characteristics on p+Si surface at various temperature. The vertical axis indicates the decomposition rate and the horizontal axis shows residence time. Due to the linearity plots, the decomposition rate follows the first-order kinetics. Its behavior can be reasonably well described by the equation

$$\ln[SiH_4]t/[SiH_4]t0=-kt \quad (1)$$

where k is the rate constant and t is the residence time of SiH_4 in the tube reactor, $[SiH_4]t0$ is the initial concentration of SiH_4 before introduced to the tube reactor and $[SiH_4]t$ is the concentration of SiH_4 from the tube reactor. From these results, all data were interpreted with first order kinetic equation in this study.

We measured 100 ppm SiH_4/Ar decomposition rate constant on non-dope Si, n+Si and p+Si surfaces as shown in Fig.3. SiH_4 is not decomposed on non-doped Si and n+Si surfaces at temperatures lower than 300°C. On the other hand, SiH_4

decomposed on p+Si surface even at extremely low temperature at 90°C to 100°C and their activation energy is 0.3eV from 90°C to 200°C. And decomposition rate constant (ˋ p+Si surface almost same to non-dope Si and n+Si surfaces about 400°C. We have considered the low temperature SiH_4 decomposition mechanism on p+Si surface as follows (Fig.4). The ionization potential of isolated SiH_4 molecules in gaseous phase is -11.6eV. But the SiH_4 energy level is changed from -11.6eV to -5.45eV due to wave function interference between gas molecules and p+Si surface when gas molecules getting close to the p+Si surface. Then the electron of adsorbed SiH_4 molecule received the thermal energy, 0.3eV, it recombines with the hole of p+Si surface and cause to SiH_4 decomposition. Furthermore we measured 100 ppm Si_2H_6 and Si_3H_8 decomposition characteristics on non-doped Si and p+Si surfaces as shown in Fig.5 and Fig.6 respectively. In these figures, we can observe that the decomposition rate constant of SiH_4, Si_2H_6 and Si_3H_8 on non-doped Si surface which increase in that order about 400°C. On the other hand, SiH_4, Si_2H_6 and Si_3H_8 have almost same decomposition rate constant due to the interactions with p+Si surface at low temperature. From these results, we consider that $-SiH_3$ group of Si_2H_6 and Si_3H_8 adsorbed on p+Si surface and cause to decomposition.

SUMMARY

In this study, we reported SiH_4 decomposition behavior on various Si surface. In particular, SiH_4 decomposed on p+Si surface at low temperature. We interpreted this surface reaction by means of change of energy level due to wave function interference when gas molecules adsorbed solid surface. To achieve scientific semiconductor manufacturing, it will be important to understand specialty gas molecule property in gas phase and adsorbed on solid surface.

ACKNOWLEDGEMENTS

This study was carried out at the Mini-Super Clean Room of Faculty of Engineering, Tohoku University.

REFERENCES

[1] T.Ohmi, 1989 International Electron Devices Meeting, Washington, D.C., pp49-52, December (1989).

[2] T.Ohmi, Microelectronic Engineering, Vol.10, pp.163-176, (1991).

[3] T.Watanabe, M.Nakamura, A.Ohki, K.Kawada, S.Miyoshi, S.Takahashi, M.S.K.Chen and T.Ohmi, International Conference on Solid State Device and Materials, pp.132-134, Tsukuba,Japan(1992).

[4] R.C.Weast,"CRC Handbook of chemistry and physics 62nd edition" CRC Press, Inc..

[5] T.Ohmi, A.Ohki, M.Nakamura, K.Kawada, T.Watanabe, Y.Nakagawa, S.Miyoshi, S.Takahashi and M.S.K.Chen, Journal of the Electrochemical Society, Vol.140, No.6, pp.1691-1699, June (1993).

[6] A.Ohki, Y.Nakagawa, M.Nakamura, K.Kawada, S.Miyoshi, T.Watanabe, S.Takahashi, M.S.K.Chen and T.Ohmi, Contamination Control and Defect Reduction in Semiconductor Manufacturing 1, PV92-21, pp.416-437, The Electrochemical Society Proceedings Series, Pennington, NJ(1992).

[7] H.Izumi, Y.Nakagawa, M.Nakamura and T.Ohmi, in proceedings of 41st Technical Meeting,Institute of Environmental Science, Anaheim, CA, pp.549-556, May(1995).

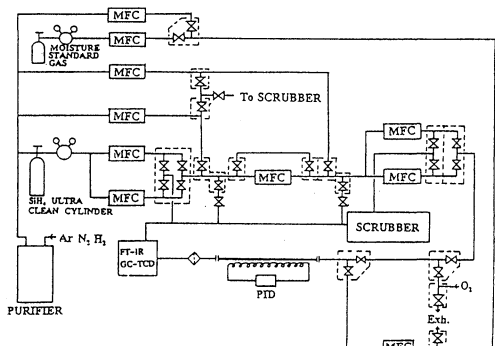

Fig.1 Schematic diagram of the experimental setup.

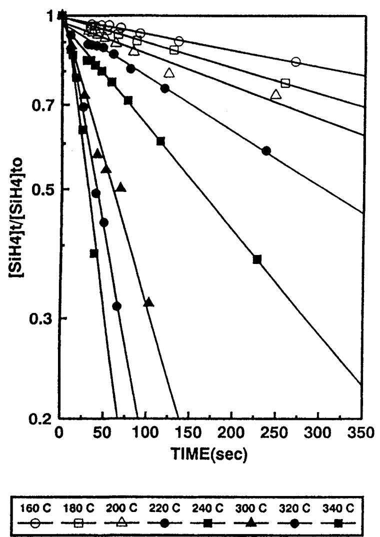

Fig.2 100ppm SiH4 decomposition characteristics on p+Si surface.

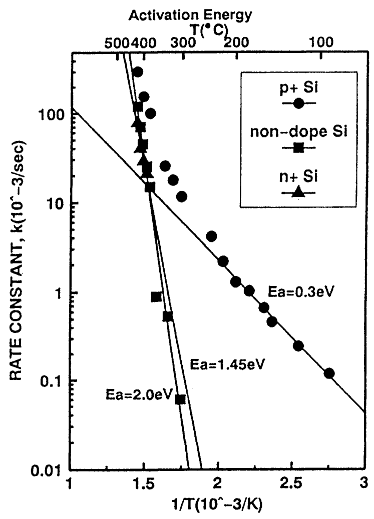

Fig.3 The activation energy of 100ppm SiH4 decomposition characteristics on non-dope Si, n+Si and p+Si surface.

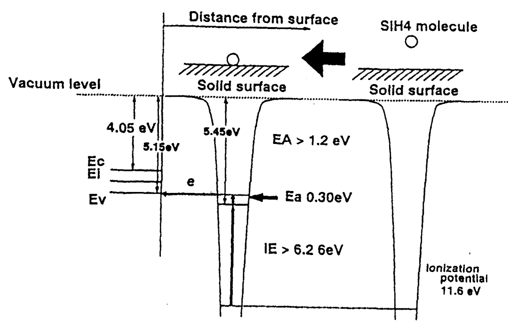

Fig.4 SiH4 decomposition mechanism on p+Si surface.

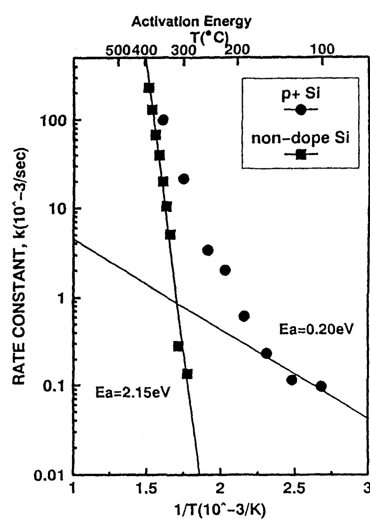

Fig.5 The activation energy of 100ppm Si2H6 decomposition characteristics on non-dope Si and p+Si surface.

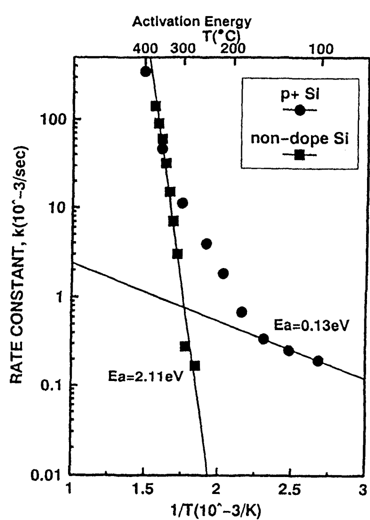

Fig.6 The activation energy of 100ppm Si3H8 decomposition characteristics on non-dope Si and p+Si surface.

ELECTROCHEMICAL DEPOSITION AND REMOVAL OF METALLIC IMPURITIES ON Si SURFACES

Hitoshi Morinaga
Mitsubishi Chemical Corporation, Kitakyusyu 806, Japan
and
Tadahiro Ohmi
Department of Electronics, Tohoku University, Sendai 980, Japan

The behavior of Cu deposition/removal onto Si surfaces in various solutions is investigated. The experimental results reveal the mechanism of electrochemical deposition and removal of noble metals on the Si surfaces. Based on the revealed mechanism, a metal-contamination-free advanced wet cleaning technology is developed.

INTRODUCTION

In order to establish the advanced and cost-effective wet cleaning technology, it is essential to reveal the mechanism of contamination adhesion and removal on Si surfaces in solutions. The main purpose of this study is to reveal the mechanism of metal deposition and removal onto the Si surface in wet processing, and to establish the advanced wet chemical processing which can achieve the Si wafer surface free from metallic contamination.

MECHANISM OF METALLIC CONTAMINATION ON Si SURFACES IN WET PROCESSES

It is reported (1-8) that the likelihood that a metallic impurity deposits on the Si surface in the wet process greatly depends on type of the metal, type of the solution, and type of the substrate (bare Si surface and oxide). It has been revealed that there are three deposition mechanisms when metallic impurities contaminate the Si wafer surface in solutions : (I) electrochemical deposition, (II) hydroxide precipitation, and (III) film inclusion. Cu is likely to adhere onto the bare Si surface in wet chemical processing. This has been believed to be because metals such as Cu, Ag and Au which exhibit higher electronegativity than Si, and which have a higher redox potential than hydrogen (i.e. noble metals) in solutions, are adsorbed directly on the Si surface by taking electrons from Si(1, 3). In Mechanism (I), noble metal is deposited on the surface due to an electrochemical reaction between its ion and Si. Meanwhile in a $NH_4OH/H_2O_2/H_2O$ (APM) solution, metals such as Fe and Al are very easy to deposit. As these metals form metal hydroxides in alkali solutions, their deposition is attributed to precipitation

of metal hydroxides on the substrate surface. This is Mechanism (II). In Mechanism (III), metallic impurities close to the Si surface are included into the oxide as the Si surface is chemically oxidized by oxidizing agents such as dissolved oxygen and H_2O_2. This Mechanism is more applicable to metals with higher oxide generation enthalpy(1).

Mechanisms (II) and (III) are relatively simple and easy to be addressed. In order to prevent metal deposition in alkali solutions, chelating agent should be injected to convert metals to a stable metal-chelate complex. Metal hydroxides deposited on the Si surface can be easily dissolved with acid. Metals (except for noble metals) included into the oxide can easily be removed by etching the oxide with Diluted HF.

On the other hand, Mechanism (I) is really critical because noble metals such as Cu deposit very easy on the Si surface in solutions (Figure 1), and because they, when deposited, deteriorate device performance such as recombination lifetime severely(9). It is essential to fully understand these deposition mechanisms in order to establish a metal deposition prevention technology and a cleaning technology.

In an attempt to understand the mechanism of the electrochemical deposition in wet processes, the behavior of Cu^{2+} deposition onto Si surfaces in solutions was investigated(5–8). It was found that Cu^{2+} ions deposit onto the bare Si surface in the form of particles (Figure 2). The result of XPS measurement revealed that the Cu particle features the metallic state. It has also been found that Cu deposition in HF solutions causes pits (Metal Induced Pits) being formed on the Si surface (Figure 3). The number and the diameter of the pits are almost the same as those of the Cu particles. In addition, in the case of the patterned wafer on which the Si surface and the SiO_2 surface coexist, selective Cu deposition onto the Si surface was observed. The experimental results reveal the Cu deposition mechanism shown in Figure 4 which is induced by the oxidation–reduction reaction between Si and Cu^{2+} ions. The Cu^{2+} ion has a much higher redox potential than Si. Therefore, Cu ions in the vicinity of the Si surface withdraw electrons from the Si, then deposit onto the Si surface in a form of metallic particle. The Si surface underneath the Cu particles releases as many electrons as required by the Cu ions to be charged, and oxidizes to become SiO_2 accordingly. In HF solutions, since the SiO_2 underneath the Cu particles is etched away by HF immediately, pits are made on the Si surface. This electrochemical deposition mechanism is considered to apply also to other noble metals.

TECHNOLOGY FOR PREVENTING METAL DEPOSITION IN WET PROCESSES

Effect of pH and Redox Potential of Solutions on Metal Deposition

The state of metals in solution can be described with the redox potential–pH diagram (Pourbaix diagram) when it is in thermodynamically equilibrium. Figure 5 shows the potential–pH diagram of the Cu–water system calculated from the equilibrium constants at 25°C (10). This diagram has been used to fully study two–phase system of metals and solution. The potential–pH diagram is effective in investigating metallic contamination on the Si surface. The diagram can not be applied as it is, however, because this investigation deals with three–phase system of metal, solution, and the Si

surface. A new approach of using this diagram must be developed which takes existence of Si into consideration. It should be also noted that the potential–pH diagram does not address reaction rate but that it just describes chemical equilibrium.

In order to establish a technology for preventing metal deposition, we have investigated the Cu deposition onto bare Si surfaces from various solutions with different pH and redox potential. To control the pH level and redox potential, acid, alkali, oxidizing agent, and reducing agent were injected to ultrapure water (Figure 6). The pH level and redox potential of solutions are measured by a pH and redox potential meter (PHL–10, DKK Corporation, Japan). Redox potential measurement were performed with a Pt electrode with an $Ag/AgCl_2$ reference corrected to the normal hydrogen electrode (NHE). Figure 7 shows the effect of pH and redox potential of solutions on the Cu deposition examined by testing various solutions used in this study. Cu deposition is found to be suppressed in the solutions which feature a pH lower than 7 and a redox potential higher than 0.75 V vs. NHE. This phenomenon can be explained in a following way. Cu is dissolved in a form of Cu^{2+} in the Cu–water system when the solution features a pH lower than 7 and a redox potential higher than 0.2 V vs. NHE. When Si is introduced in the Cu–water system, Cu^{2+} is reduced by Si and is deposited on the Si surface. When a strong oxidizing agent is injected in the solution, however, this reduction is affected by the oxidizing agent. Figure 8 shows the effect of redox potential of solutions on the amount of Cu deposition. Cu deposition is significantly suppressed when the redox potential exceeds 0.75 V vs. NHE. This is considered to be because, when the redox potential of the solution exceeds 0.75 V, the oxidizing agent features higher thermodynamic driving force than Cu^{2+} and captures electrons from Si. Figure 9 shows the mechanism of preventing Cu deposition by an oxidizing agent with ozone as an example. When ozone is injected in the Cu–water system, ozone takes electrons from Si with a higher thermodynamic driving force than Cu^{2+}. Therefore, Si is oxidized by ozone and Cu remains as Cu^{2+} in the solution. Even if Cu^{2+} ions can take electrons from Si to get deposited, the deposited Cu gets re–oxidized by the oxidizing agent to be ionized (dissolved) again. Electron exchange between the Cu^{2+} ion and Si is increasingly interfered as the Si surface gets oxidized to be covered with chemical oxide, which makes Cu deposition more and more difficult.

The redox potential E (V vs. NHE) is referenced against the reduction potential of H^+ in solution (0V). On the other hand, the electron energy level α_e (eV) (real potential) is referenced against the energy level of an electron in vacuum (0 eV). The relation between these two can be expressed as(11):

$$\alpha_e = - e (E + 4.44) \qquad [1]$$

Figure 9 shows value of α_e converted by using this equation. This value can be regarded as the Fermi level. The potential to prevent Cu deposition is 0.75 V vs.NHE, which is equivalent to −5.19 eV in α_e. This is almost the same as the energy level of the Si valence band. This means that when the redox potential of the solution exceeds 0.75 V vs.NHE, the energy level of an electron in solution gets lower than that of Si valence band. It is considered extremely easy for a solution to take an electron from the Si in

this state, which facilitates oxide growth.

As shown Figures 1, neither Fe nor Ni electrochemically deposit onto bare Si surfaces. Fe^{2+} and Ni^{2+} feature lower redox potential than the hydrogen ion in the solution. Ultrapure water and DHF, therefore, maintain sufficiently higher oxidizing force than these metals to keep them ionized in a stable way, even if bare Si is introduced into the system.

Effect of Anion Concentration

Figure 10 shows how HCl/KCl injection affects Cu deposition on the Si surface, pH level, and redox potential in ultrapure water with Cu of 1 ppm added. Unlike HCl injection, KCl injection hardly changes pH level or redox potential of ultrapure water. It also hardly prevents Cu deposition on the Si surface. Injection of acids or oxidizing agents can effectively prevent Cu deposition as it decreases the pH level and increases the redox potential in the solution. It is found, however, that raising the concentration of anions such as Cl^- does not at all prevent Cu deposition.

Prevention of Metal Deposition in HF Solutions

Cu deposition in DHF solution can be suppressed by injecting 3% HCl (12) or 1% H_2O_2(13). This suppression mechanism, however, is not yet revealed. It is speculated that raising the redox potential in DHF by injecting acids or oxidizing agents was effective in preventing the Cu deposition and examined how the redox potential affected the Cu deposition in a 0.5% DHF solution. Figure 11 shows the Cu deposition onto the Si surface from various DHF solutions as a function of the redox potential. It is obvious in Figure 11 that Cu deposition can be suppressed in DHF when the redox potential is raised by injecting acids or oxidizing agents. The redox potential needed to suppress the Cu deposition in the ultrapure water system (a system without HF) is 0.75 V vs. NHE while that in the DHF system is 0.85 V vs. NHE (Figure 12). This result indicates it is more difficult to suppress Cu deposition in the DHF system than in the ultrapure water system. In the ultrapure water system, an increase of redox potential not only facilitates Cu ionization but also prevents the oxidation reduction reaction between the Cu ion and Si as the Si surface gets covered with oxides. In the DHF system, on the other hand, oxides are promptly etched with DHF to make active bare Si surface constantly exposed to the solution. Figure 13 shows the effect of injecting various acids and oxidizing agents on Cu deposition in DHF solution. These additives raise the redox potential of solutions to 0.85 v vs. NHE or more, and suppress the Cu deposition. Injection of HIO_3 or KClO is also found effective in suppressing the Cu deposition.

Effect of Surfactant and Chelating Agent

Figure 14 shows how Cu deposition from a DHF solution with Cu of 1 ppm added is affected when 10% H_2O_2 or 0.1% anion-type surfactant is injected. It is revealed that Cu deposition can be suppressed by surfactant injection as well as by injection of oxidizing agents such as H_2O_2. The mechanism to suppress the Cu deposition by a surfactant injection has not yet been fully understood. It is speculated, however, to be as follows : (1) The surfactant covers the Si surface to locate itself

between the Cu ion and Si, which interferes the oxidation/reduction reaction between the Cu ion and Si. Or (2) The surfactant and Cu ion form a stable complex ion.

Figure 15 demonstrates that the Cu deposition onto the bare Si surface from ultrapure water with Cu of 1 ppm injected can be prevented by adding a chelating agent. EDTA (ethylenediaminetetraacetic acid) $\cdot 2K \cdot 2H_2O$ is used as a chelating agent in this experiment. Injection of the chelating agent is effective in suppressing the Cu deposition because the chelating agent and Cu ion form a very stable complex ion to stop the Cu^{2+}–Si reaction.

WET CLEANING TECHNOLOGY FOR METALLIC CONTAMINATION

Effect of Acid and Oxidizing Agent (pH and Redox Potential)

Figure 16 shows the effects of pH level and redox potential on Cu removal. Before cleaning experiment, a pre-cleaned bare Si wafer (Cu: 1 – 5 x 10^{10} atoms/cm^2) was dipped into ultrapure water with Cu of 1 ppm (using $CuCl_2$) injected for 3 minutes. The Cu concentration on the Si surface after being immersed in Cu-injected ultrapure water was 10^{14} –10^{15} atoms/cm^2, which was regarded as the initial Cu contamination in this experiment. Similar to the Cu deposition experiment, the solutions which feature a redox potential higher than 0.75 V and a pH lower than 7 are effective for removing Cu contamination. Figure 17 compares the conventional cleaning methods (SPM: $H_2SO_4/H_2O_2/H_2O$ and HPM: $HCl/H_2O_2/H_2O$), typical acids, and typical oxidizing agents in terms of Cu removal efficiency. Acids and oxidizing agents with a pH level of over 7 and a redox potential of over 0.75 V are found effective in removing Cu. They are not effective enough, however, in reducing the Cu concentration on the Si surface to the blank level (before it was immersed into Cu-injected ultrapure water: 1 – 5 x 10^{10} atoms/cm^2).

Removal of Metallic Impurities in Oxides

In an attempt to establish the technology to perfectly remove Cu, the authors have been studying various cleaning methods. Figure 18 shows the results of our studies. The Cu concentration could not be decreased to the blank level even by repeating the SPM cleaning four times. It is speculated that it was because some of the Cu was included in the chemical oxide when the chemical oxide grows in the SPM cleaning. In order to remove the Cu in the oxide, various HF cleanings were tried following the SPM cleaning to etch the oxide. The Cu concentration on the Si surface hardly decreased when the wafer was treated with a 0.5% DHF solution following the SPM cleaning. In a 0.5% DHF solution, it is possible that even if Cu in the oxide is ionized and etched off, it gets re-deposited on the bare Si surface. Therefore an $HF/H_2O_2/H_2O$ solution or DHF solution with surfactant of 0.1% injected was used to etch the chemical oxide as these two solutions were able to effectively prevent the Cu deposition. This time the Cu concentration was reduced almost to the blank level. These experimental results indicate that metallic impurities included in the oxide can be removed only by etching. It is also revealed that etchants to prevent the metal deposition must be used to remove metals such as Cu which easily get re-deposited on the bare Si surface.

Effect of Various HF/Oxidizing Agent Mixtures

Figure 19 shows the amount of residual Cu as a function of concentration of the oxidizing agent when the Si surface is cleaned with a DHF solution with various oxidizing agents injected. In every case, the Cu removal efficiency is poor when the concentration of the oxidizing agent is low. In general, a sufficient Cu removal efficiency is secured when the concentration of the oxidizing agent exceeds 1000 ppm. It is clear that Cu removal is affected not only by the redox potential but also by the concentration of the oxidizing agent. When the oxidizing agent is not sufficient in volume, the reaction rate is too slow for the oxidation/reduction system to achieve thermodynamic equilibrium in the 10-minute cleaning process. Besides the oxidizing agent in the vicinity of the Si surface is constantly consumed by repetition of Si oxidation and etching of the oxide with HF as well as by Cu ionization, which results in shortage of the oxidizing agent. In order to maintain the required amount of the oxidizing agent in the vicinity of the Si surface, it is necessary to increase the concentration of the oxidizing agent and to constantly deliver a fresh solution.

Si Surface Microroughness Induced by Noble Metal Removal

The HF/oxidizing agent mixture is very effective in removing metallic impurities as it features an etching function as well as a low pH level and a high redox potential. It must be noted, however, that the HF/oxidizing mixture roughens the Si surface due to local electrochemical reaction when it is used to clean the bare Si surface contaminated with noble metals. In order to remove Cu without increasing the surface microroughness, Cu on the Si surface is first removed with the oxidizing agent and then Cu included in oxide is removed with the etchant which can prevent Cu from being re-deposited. Table 1 shows the amount of residual Cu and microroughness (Rms) of the Si surface. Here Cu on the Si surface is first removed with the oxidizing agent such as SPM or ozonized ultrapure water. Then Cu included in the oxide is removed together with the oxide with an etchant, such as $HF/H_2O_2/H_2O$ or surfactant-injected DHF, which is very effective in preventing Cu from being re-deposited. This cleaning method can remove Cu deposited

Table I. The amount of residual Cu and microroughness (Rms: measured with AFM) when the Si surface contaminated with Cu is cleaned with various cleaning methods.

Chemical [Concentration]	Cu Remaining (atoms/cm^2)	Surface Roughness Rms (nm)
Blank	1-5E+10	0.09-0.13
Initial Contamination	1-10E+14	-
SPM	1.4E+11	0.11
HF/H_2O_2 [0.5%/10%]	1.5E+10	0.25
SPM + HF/H_2O_2 [0.5%/10%]	1.5E+10	0.12
O_3 + HF/H_2O_2 [0.5%/10%]	2.5E+10	0.12
O_3 + DHF with Surfactant	2.8E+10	0.11

on the bare Si surface in an almost perfect manner without increasing surface microroughness.

Removal of Metal-Oxide Particles

Metal oxides such as Al_2O_3 are chemically very stable. Is it possible to ionize and remove these metal-oxide particles deposited on the surface? Figure 20 shows the particle removal efficiency. In this experiment, the Si surface is intentionally contaminated with Al_2O_3 particles or Fe_2O_3 particles with an average size of 0.3 μm, and it is cleaned with HPM or APM. The particle count on the substrate surface is measured with a light-scattering particle counter. The particle removal efficiency is defined as the ratio of residual particles on the cleaned substrate. Figure 20 demonstrates that HPM, which is effective in removing metallic impurities, can hardly remove Al_2O_3 or Fe_2O_3 particles. These particles are chemically stable. Even in strong acid oxidizing solutions such as HPM, they can not be easily ionized in a 10-minute cleaning step. These stable metal-oxide particles must be brought apart from the substrate first to be removed. The APM cleaning is extremely effective in removing metal-oxide particles as it removes particles by combining two mechanisms : etching of the Si substrate and electrostatic repulsion between particles and the substrate in alkali solutions.

CONCLUSION

This study has revealed the mechanism of electrochemical deposition and removal of noble metals on the Si surface in wet processing. Once the mechanism was understood, we could apply the mechanism to cleaning technologies. Due to progress in the analysis technology and improvement of purity of ultrapure water, chemicals, and the substrate surface, it has become possible to analyze chemical reactions on the solid/liquid interface under ideal conditions. As a result, deposition/removal mechanism of trace impurities has been scientifically revealed. It is time to innovate the wet process on the basis of the chemistry of solid/liquid interface.

ACKNOWLEDGEMENTS

This research has been carried out in the Mini Super Clean Room at the Faculty of Engineering in Tohoku University, and in Mitsubishi Chemical Corporation.

REFERENCES

1. T.Ohmi, T.Imaoka, I.Sugiyama, and T.Kezuka, *Journal of Electrochemical Society,* Vol.139, p.3317, (1992).
2. T.Ohmi, T.Imaoka, T.Kezuka, J.Takano and M.Kogure, *Journal of Electrochemical Society,* Vol.140, No.3, p.811, (1993).
3. F.W.Kern,Jr., M.Itano, I.Kawanabe, M.Miyashita, R.W.Rosenberg and T.Ohmi, in *Proceedings of 11th Workshop on ULSI Ultra Clean Technology,* p.23 (1991).

4. F.W.Kern,Jr., *in Extended Abstracts of 184th Electrochemical Society meetings*, p.498, New Orleans, October, (1993).
5. H.Morinaga, M.Suyama and T.Ohmi, *Journal of Electrochemical Society,* Vol.141, No.10, p.2834, (1994).
6. H.Morinaga, M.Suyama M.Nose, S.Verhaverbeke and T.Ohmi, *Proceedings of Second International Symposium on UCPSS,* p.217, Bruges, September (1994).
7. H.Morinaga and T.Ohmi, in *Proceedings of 27th Workshop on ULSI Ultra Clean Technology,* p.43, Tokyo, June (1995).
8. H.Morinaga, M.Suyama M.Nose, S.Verhaverbeke and T.Ohmi, *J. Electrochem. Soc.,* submitted for publication.
9. M.Hourai, T.Naridomi, Y.Oka, K.Murakami, S.Sumita and N.Fujino, *Jpn. J. Appl. Phys.* **27**, L2361 (1988).
10. M.Pourbaix, "Atlas of Electrochemical Equilibria in Aqueous Solutions," Pergamon Press, London (1966).
11. S.Trasatti, *Pure and Applied Chemistry*, Vol.58 (7), p.956, (1986).
12. I.Oki, H.Shibayama and A.Kagisawa, in *Extended Abstracts of 184th Electrochemical Society Meetings*, Vol.93-2, p.473 New Orleans, October 1993.
13. T.Shimono and M.Tsuji, *in Extended Abstracts of Electrochemical Society meetings*, Vol.91-1, p.278, Washington, DC, May, 1991.

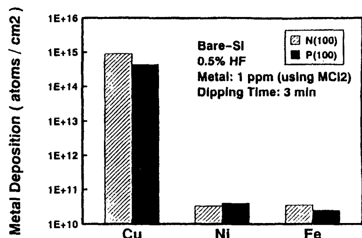

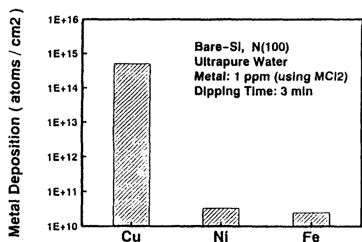

Figure 1. Metal deposition on the Si surface in DHF solutions and ultrapure water with Cu, Fe and Ni 1 ppm added.

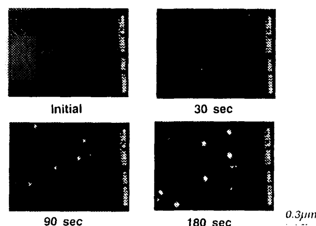

Figure 2. SEM images of the Cu particle growth process on the Si surface in a DHF (0.5%) solution [with Cu : 1ppm (using $CuCl_2$)].

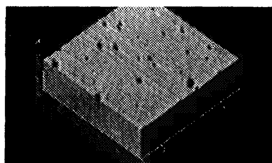

Figure 3. AFM image of the Si surface after Cu particles are removed by SPM cleaning (10 min). Cu was deposited in a DHF (0.5%) solution.

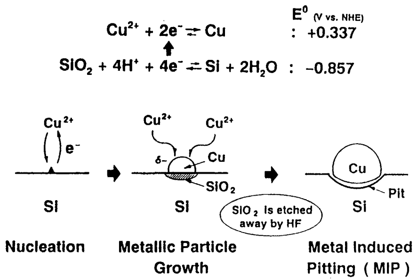

Figure 4. Mechanism of Cu deposition onto Si surfaces in solutions.

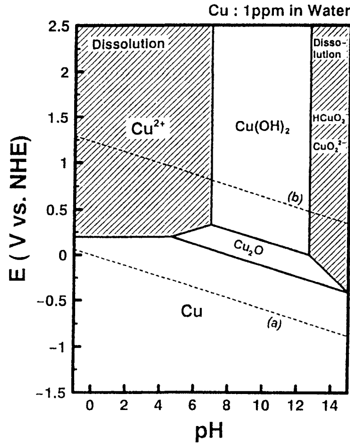

Figure 5. Potential–pH diagram (Pourbaix diagram) of the Cu–water system calculated from the equilibrium constant at 25°C.

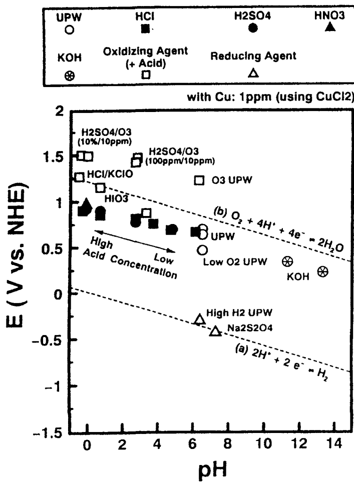

Figure 6. The pH level and redox potential of various solutions (measured value).

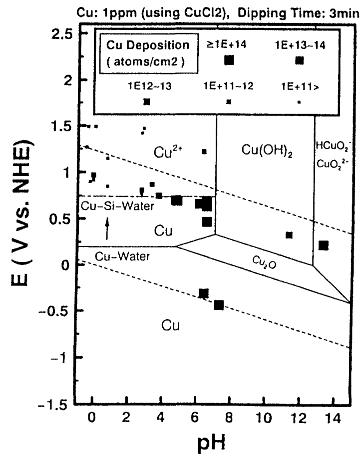

Figure 7. The effect of pH level and redox potential of solutions (ultrapure water with various chemicals added) on the Cu deposition onto the Si surface.

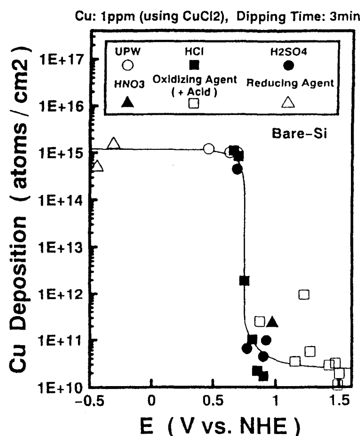

Redox Reaction	E^0 (V vs. NHE)	α_e (eV)
$O_3 + 2H^+ + 2e^- \rightarrow O_2 + H_2O$	2.076	-6.52
$H_2O_2 + 2H^+ + 2e^- \rightarrow 2H_2O$	1.776	-6.22
$Au^+ + e^- \rightarrow Au$	1.692	-6.13
$O_2 + 4H^+ + 4e^- \rightarrow 2H_2O$	1.228	-5.67
$Ag^+ + e^- \rightarrow Ag$	0.799	-5.24
$Cu^+ + e^- \rightarrow Cu$	0.520	-4.96
$Cu^{2+} + 2e^- \rightarrow Cu$	0.337	-4.78
$2H^+ + 2e^- \rightarrow H_2$	0.000	-4.44
$Pb^{2+} + 2e^- \rightarrow Pb$	-0.126	-4.31
$Ni^{2+} + 2e^- \rightarrow Ni$	-0.250	-4.19
$Fe^{2+} + 2e^- \rightarrow Fe$	-0.440	-4.00
$SiO_2 + 4H^+ + 4e^- \rightarrow Si + 2H_2O$	-0.857	-3.58
$Al^{3+} + 3e^- \rightarrow Al$	-1.663	-2.78
$Na^+ + e^- \rightarrow Na$	-2.714	-1.73
$Ca^{2+} + 2e^- \rightarrow Ca$	-2.866	-1.57
$K^+ + e^- \rightarrow K$	-2.924	-1.52

Figure 8. The effect of redox potential of the solutions (ultrapure water with various chemicals added) on the Cu deposition onto the Si surface.

Figure 9. Mechanism of preventing Cu deposition by oxidizing agent (with ozone as an example).

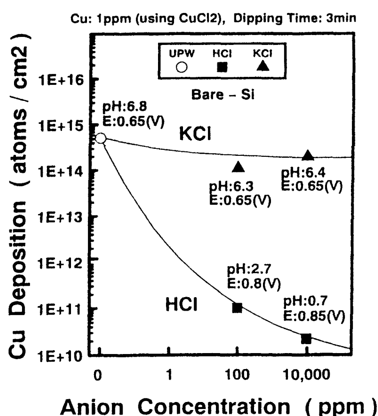

Figure 10. The effect of HCl/KCl injection on Cu deposition onto the Si surface, pH level, and redox potential in ultrapure water.

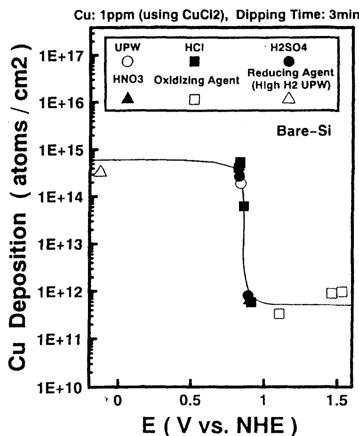

Figure 11. The effect of redox potential of the DHF solutions with various chemicals added on the Cu deposition onto the Si surface.

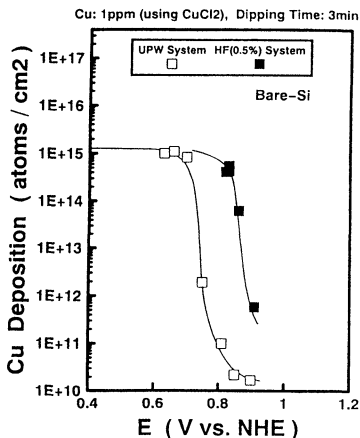

Figure 12. The comparison of the ultrapure water system and the DHF system in terms of the effect of redox potential on Cu deposition. Redox potential is controlled by HCl injection.

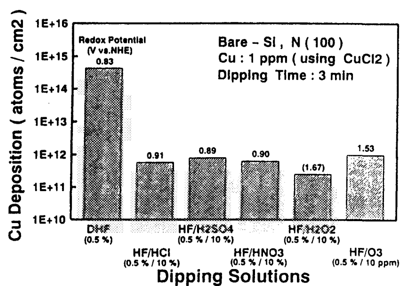

Figure 13. The effect of injecting various acids and oxidizing agents on Cu deposition onto the Si surface in DHF solution.

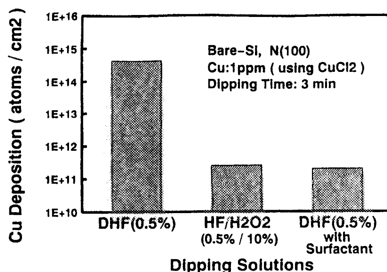

Figure 14. The effect of injecting H_2O_2 or anion-type surfactant on the Cu deposition onto the Si surface in DHF solution.

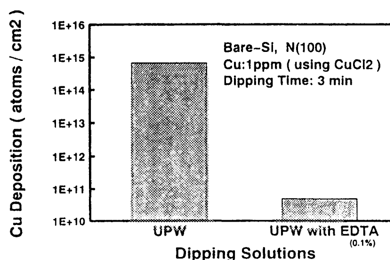

Figure 15. The effect of chelating agent injection on the Cu deposition onto the Si surface in ultrapure water.

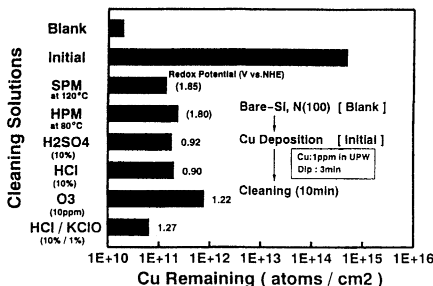

Figure 16. The comparison of the conventional cleaning methods (SPM and HPM), typical acids, and typical oxidizing agents in term of the Cu romoval efficiency.

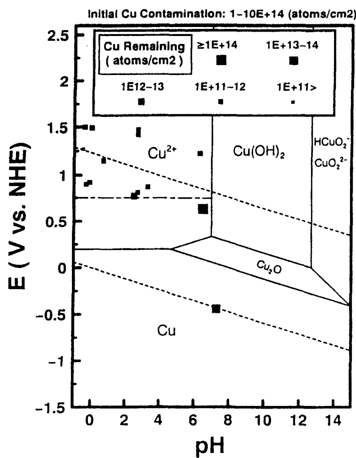

Figure 17. The effect of pH level and redox potential on the Cu removal from the Si surface.

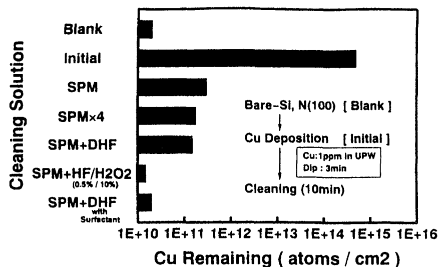

Figure 18. The effect of various cleaning methods on the removal of Cu included in oxide.

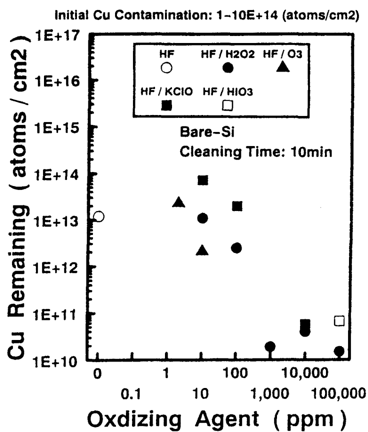

Figure 19. The amount of residual Cu as a function of concentration of the oxidizing agent when the Si surface is cleaned with DHF solution with various oxidizing agents injected.

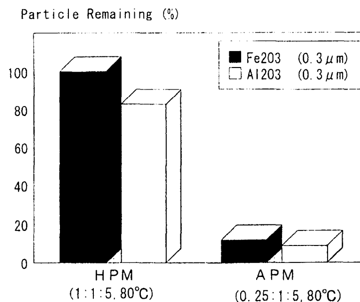

Figure 20. The effect of HPM or APM cleaning on the removal of metal-oxide particles.

METAL ION ADSORPTION MECHANISM ON SI WAFER

Y. Takahara, A. Saito and H. Oka

Production Engineering Research Laboratory, Hitachi, Ltd.
292 Yoshida-cho, Totsuka-ku, Yokohama 244, JAPAN

The mechanism by which metal ions in a cleaning solution are adsorbed on the Si surface was clarified both by calculation and experiment. Metal ions were found to be adsorbed mainly by coulomb interaction with the Si surface. The adsorption energy of the metal ion relative to the Si surface changed as a function of the solution pH. Adsorption energy was higher in an alkaline solution than in an acidic solution, and metal ions were easily adsorbed to the Si surface in an alkaline solution. Calculation results indicated that adsorption energy was reduced in the presence of electron-donating ligands. Calculation results were confirmed experimentally. Consequently it is thought that metal ion contamination can be reduced by adding electron-donating ligands to the solutions used in the wet processes of semiconductor manufacturing.

INTRODUCTION

Metal ion contamination on the Si wafer surface was first investigated by Kern in 1970(1). Since then, numerous attempts have been made to clarify this phenomenon because metal ion contamination has become increasingly detrimental to device performance, especially as integration density increases. For example, such contamination degrades both leakage current density and minority carrier lifetime. At present, the allowable concentration of metal contamination on the Si surface is less than 10^{10} atoms/cm^2. For 256MB DRAM fabrication, it is necessary to reduce this concentration to less than 10^9 atoms/cm^2 (2). However, contamination of the Si surface by metal ions following CVD, dry-etching or ion implantation is usually on the order of 10^{12} atoms/cm^2 (3). The reverse side of the Si wafer is contaminated more than the surface side because it comes into contact with the wafer handling system. Therefore, there is an urgent need for semiconductor manufacturing to develop cleaning technology capable of reducing metal ion contamination on Si wafers.

In order to develop a new cleaning technology, it is first necessary to clarify the mechanism by which metal ions are adsorbed on the Si wafer. We therefore used ab-initio molecular orbital calculation in an attempt to clarify the adsorption state of metal ions on the Si surface and to find a method for preventing metal contamination. The calculation results were then confirmed by experiment.

CALCULATION

Calculation Model and Method

The following model and assumptions were used for the calculation. It has been reported (4) that almost all (99.9%) of the Si surface treated by an HF cleaning solution is terminated by H, and the remaining area (0.1%) is terminated by OH. The type of OH termination changes depending on the pH of the solution. The termination is an OH_2^+ in an acidic solution (pH<2), OH at the isoelectric point (2<pH<3) and O^- in neutral and

alkaline solutions (pH>3). The surface structure assumed for the calculation is illustrated in Figure 1. Fe and Cu were used for the calculation because they were detected as contaminants in the semiconductor manufacturing process. Fe and Cu are known to exist as Fe^{2+} and Cu^{2+} at a concentration of 1 ppm.

The calculation was carried out using an ab-initio molecular orbital program called HONDO7 (5). An approximation of the ECP (effective core potential) (6) was incorporated into the calculation because of the large number of orbitals. The inner shell orbitals, which did not participate in the reaction, were thus replaced by core potentials. Each electron orbital was described by a DZP (double zeta polarization) function (7) in order to take into account the polarization effect.

The adsorption energy (E_{ads}) was obtained by subtracting the total energy at the optimized bond distance between the metal ion and the surface atom (E_{ts+m}) from the total energy of the dissociated state ($E_{ts}+E_{tm}$), as shown in equation [1].

$$E_{ads} = E_{ts}(\text{Si surface}) + E_{tm}(\text{metal ion}) - E_{ts+m}(\text{Si surface with metal ion}) \qquad [1]$$

The adsorption energy calculated by the above approximation was over-estimated, but it was still possible to make a relative comparison between the adsorption energies of the calculations.

Adsorption State

The adsorption energies of Fe^{2+} and Cu^{2+} obtained by the calculation are shown in Figure 2. It is impossible for a metal ion to be adsorbed at an OH_2^+ site on the Si surface because of the strong coulomb repulsion that exists between the positive charge of the ion and the positive charge on the Si surface. A metal ion can be adsorbed at the OH site on the Si surface because of coulomb attraction between the negative charge on the O atom and the positive charge of the metal ion. At the O^- site on the Si surface, the metal ion will be strongly adsorbed due to the large coulomb attraction between the negative charge on the O atom and the positive charge of the ion. In neutral and alkaline solutions, metal ions are easily adsorbed on the Si surface. In acidic solutions, however, metal ions do not adsorb on the Si surface.

Even though H sites have relatively low adsorption energies, as shown in Figure 2, these sites account for most of the sites on the Si surface. Therefore, adsorption at the H site must also be take into consideration, as well as adsorption at the OH site. It should be noted that the H site adsorption energy does not change throughout a wide region of pH values.

Adsorption of metal ions on the Si surface was found to be caused by coulomb interaction between the positive charge of the metal ion and the negative charge on the Si surface. Two approaches are available for preventing metal ions from being adsorbed on the Si surface. One is to change the pH of the solution, but this is difficult to do without adversely affecting semiconductor processes. The other is to somehow reduce the charge of the metal ion. In this paper, we investigated the possibility of reducing the charge of the metal ion.

Ligand Effect

In aqueous solutions, metal ions are coordinated with water molecules. The adsorption energy of the metal ion coordinated with water molecules was calculated ab-

initio with respect to the Si surface. Figure 3 shows the adsorption energy at the O^- site and H site. The energy was reduced by half when the ions were coordinated with water molecules compared with the adsorption energy of free metal ions (Figure 2). The reason is that an electron from the O atom of the water molecule was transferred to the metal ion, this neutralizing of the positive charge on the metal ion. Therefore, a ligand having a high electron-donating capacity could be used to reduce the positive charge of metal ions.

Porphyrin is an electron-donating ligand. The degree of coordination was calculated between the Si surface and the metal ion with the porphyrin. The electron-donating part of the porphyrin was expressed as $(NH_2)_4^{2-}$. The results are shown in Figure 4. In the case of Fe^{2+}, the adsorption energy was reduced to 1/3, compared with a water-coordinated metal ion. In the case of Cu^{2+}, the potential even became repulsive. Therefore, the electron-donating ligand should prevent the metal ion from being adsorbed on the Si surface.

EXPERIMENT

A model contamination solution was prepared with a concentration of 6×10^{-5}M NH_4Cl, and NH_4OH or HCl were added to adjust the pH and prevent etching or oxidation, respectively. The temperature of the solution was maintained at 23℃. The metal ion used as the contaminant was Cu^{2+} since the calculation results showed that its potential would become repulsive as a result of porphyrin coordination. A 4-inch Si wafer was treated with HF solution (0.5vol%) for 2 minutes and rinsed for 10 minutes. The Si wafer was then immersed in the contaminated solution, rinsed again for 10 minutes and dried by spin drying.

The metal concentration on the surface was detected by total reflection x-ray fluorescence spectroscopy. The detection limit was 10^{10}atoms/cm^2.

RESULTS AND DISCUSSION

The relationship between the pH of the model contamination solution and metal ion adsorption on the wafer surface was evaluated. Si wafers were immersed for 30 minutes in various solutions contaminated with 0.1ppm Cu^{2+}, where pH was adjusted from 2 to 10. The results are shown in Figure 5. The number of metal ions adsorbed on the Si surface in alkaline solutions was higher than in acidic solutions. The experimental results were in good agreement with the calculation results.

To further clarify the adsorption reaction, the dependence of surface contamination on immersion time was evaluated. Figure 6 shows the relationship between metal ions adsorbed on the Si surface and immersion time in Cu^{2+}-contaminated solution (0.1ppm) at pH10. Adsorption increased with immersion time, reaching an asymptotic state after about 20 minutes.

Figure 7 shows the relationship between Cu ions adsorbed on the Si surface and Cu^{2+} concentration in a pH10 solution for a 30-minute immersion. The surface concentration of the metal contaminant increased as the metal ion concentration in the solution increased. The relationship in Figure 7 was not a Langmuir type. However, in

the high concentration region above 10^{-4} ppm, the slope described a Langmuir curve. The reason for this was assumed to be that adsorption had occurred at the O^- site on the surface in the low concentration region, and at the H site on the surface in the high concentration region. The adsorption energy at the O^- site was larger than that at the H site. If the activation energy is proportional to adsorption energy, then the first adsorption step would be on the O^- site and the adsorption site would become fully occupied by the metal ion contaminants as evidenced by the fact that the surface coverage at the O^- site was about 10^{12} atoms/cm^2. The second step would then occur slowly at the H site because of the low adsorption energy. The reaction for adsorption is thus a complex reaction consisting of two interactions, one at the O^- site and the other at the H site.

Based on the calculation results, it should be possible to reduce the adsorption energy of the metal ion by adding an electron-donating ligand. This effect was evaluated by adding TCPP (Tetrakis (4-carboxyphenyl) porphine) to the contaminant solutions. The relationship between the Cu^{2+} concentration in solution with TCPP and Cu adsorbed on the Si surface is shown in Figure 8. TCPP was added to the solution at a molar ratio ([TCPP]:[Cu]) of either 2:1 or 5:1. Cu ion adsorption was reduced by 90% following the addition of TCPP.

When coordinated with TCPP, the metal ion did not adsorb at the O^- site nor at the H site on the Si surface. It was possible to reduce metal ion adsorption on the Si surface by adding greater quantities of ligands.

CONCLUSIONS

The mechanism of metal ion adsorption was clarified by both ab-initio molecular orbital calculation and by experiment. Adsorption was seen to occur by means of coulomb interaction between the metal ion and Si wafer surface. In an alkaline solution, the wafer surface was highly contaminated due to the strong adsorption energy. In an acidic solution, the contamination was lower than that in an alkaline solution. The adsorption reaction in the alkaline solution occurred at both the O^- and H sites.

The addition of an electron-donating ligand was effective in preventing metal ion adsorption. This effect was clearly demonstrated when TCPP was added to a model contamination solution. Therefore, because many of the wet processes in semiconductor manufacturing use solutions that are either neutral or alkaline, the use of ligands is thought to be highly effective in preventing metal ion contamination.

REFERENCES

1. W. Kern, RCA Review, **31**, 234(1970).
2. A. Hiraiwa and T. Itoga, IEEE Trans. Semiconductor Manufacturing, 7, 60(1994).
3. T. Ohmi, T. Imaoka, I. Sugiyama and T. Kezuka, J. Electrochem. Soc., **139**, 3317(1992).
4. O. Takahagi, Oyobutsuri, **59**, 1441(1990).
5. Quantum Chemistry Program Exchange, Program No. 544.
6. S. Topiol, J. W. Moskowitz and C. F. Melius, J. Chem. Phys., **68**, 2364(1978).
7. H. Tatewaki and S. Huzinaga, J. Chem. Phys., **71**, 4339(1979).

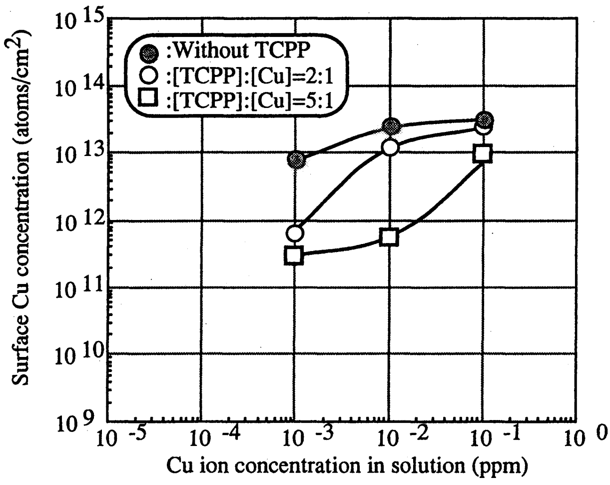

Figure 8. Effect of adding TCPP to contaminant solution

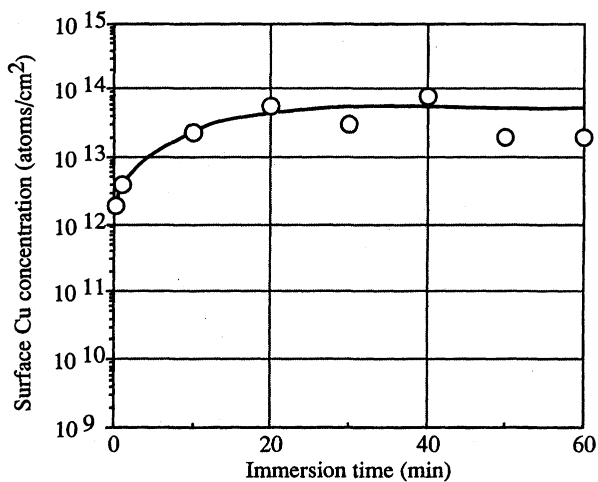

Figure 6. Relationship between immersion time and surface Cu concentration

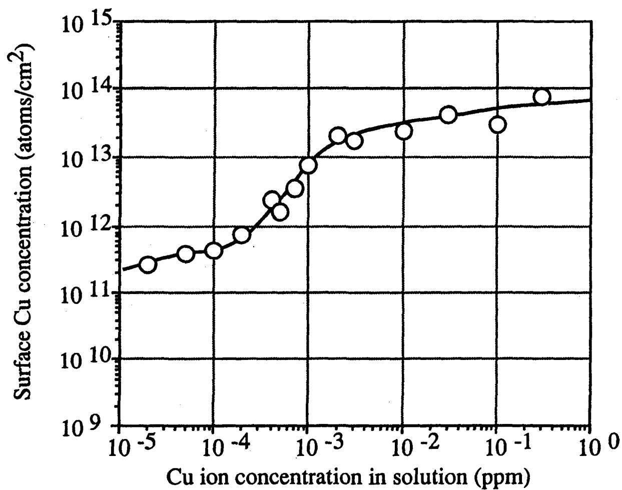

Figure 7. Relationship between Cu ion concentration in contaminant solution and surface Cu concentration

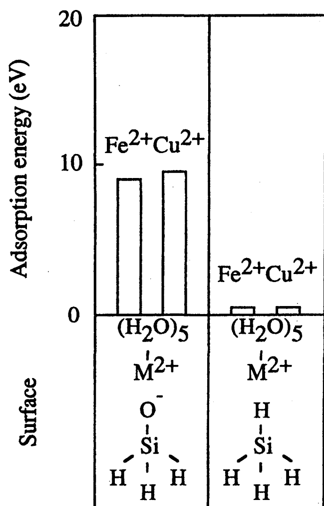

Figure 3. Adsorption energy of metal ions with $(H_2O)_5$ ligands

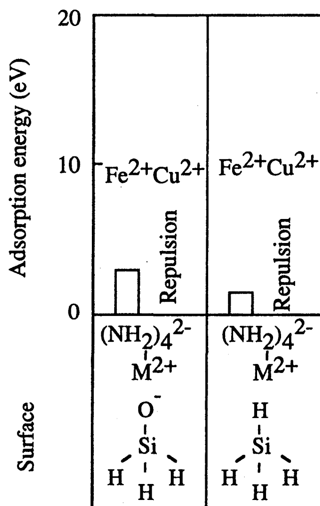

Figure 4. Adsorption energy of metal ions with $(NH_2)_4^{2-}$ ligands

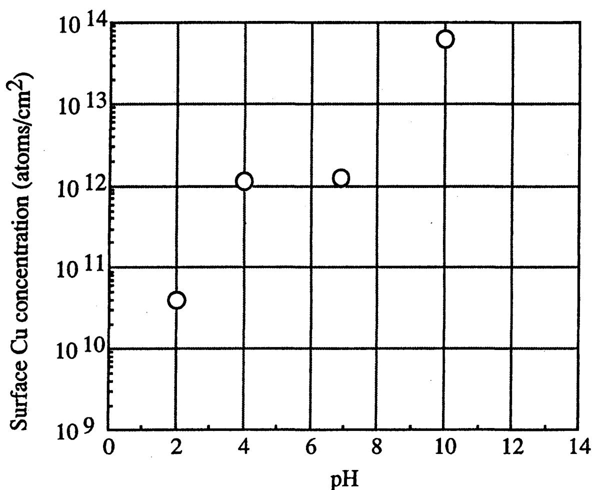

Figure 5. Relationship between pH of contaminant solution and surface Cu concentration

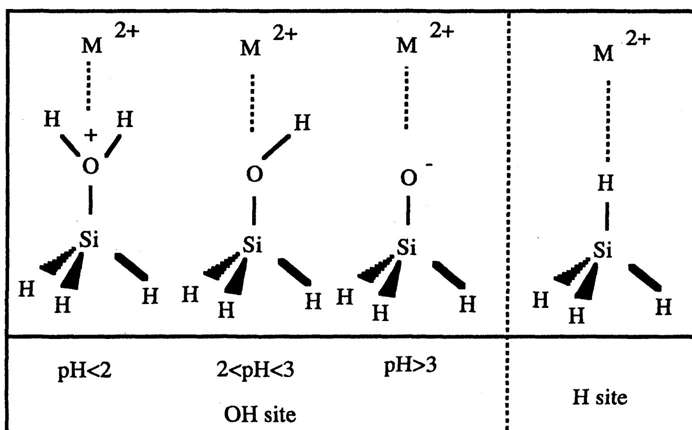

Figure 1. Surface and metal adsorption model for ab-initio calculation

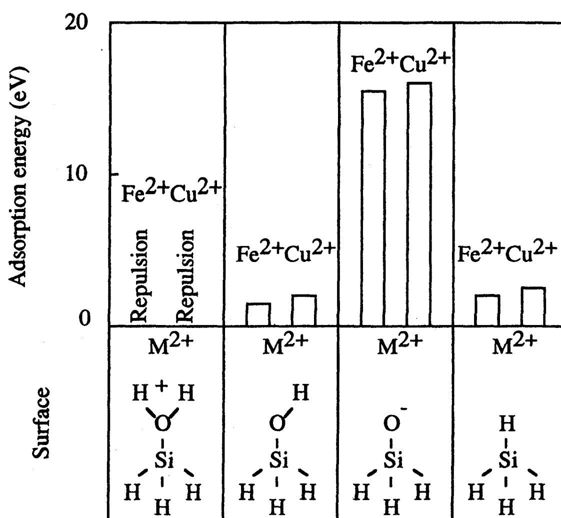

Figure 2. Adsorption energy of metal ions on Si surface

Metal Interactions with Silica (SiO_2) Surfaces: Adsorption and Ion Exchange

T.Q. Hurd[1], H.F. Schmidt, A.L.P. Rotondaro, P.W. Mertens, L.H.Hall[2], and M.M. Heyns
IMEC, Kapeldreef 75, B-3001 Belgium.
[1] on assignment from Texas Instruments, 13546 N Central, Dallas, TX 75243 USA
[2]Texas Instruments, 13546 N Central, Dallas, TX 75243 USA

Abstract

Deposition of Fe, Ca, and Cu onto SiO_2 surfaces is investigated as a function of pH and type of SiO_2 surface (chemical and thermal oxide). The relative deposition efficiencies are understood in the context of both the ion exchange properties of the surface silanol groups and the adsorption of metal hyrdrolysis products. Metals with high charges and the ability to form polydentate complexes are favorably complexed at the silica surface. The discussion is then extended to explanations of the observed metal deposition and removal by wafer cleaning solutions.

Introduction

Metal contamination on wafers is of major concern in semicondutor manufacturing. Advanced ULSI fabrication technologies demand metallic contamination levels below 10^{10} at/cm^2 [1]. Significant effort is spent on cleaning operations and in many cases the cleaning is performed to correct the metal contamination from the prior cleaning solution. In order to make improvements in cleaning and to meet the requirements of future generations of devices it is necessary to understand not only the chemistry of the ions in solution but also the chemistry of the ions at the surface of the wafer. Both chemistries will play an important role in cleaning. In this paper two coexisting mechanisms are proposed to describe and explain the deposition of metal contamination onto silicon oxide surfaces. Solutions of various pH's are spiked with different metals at various levels and the deposition behavior is explained in terms of the models.

Theoretical

It has been recognized as far back as 1925 that metal ions would attach to silica gel surfaces [2]. As research in the area progressed it became apparent that the silica gel could behave as a weakly acid ion exchange resin. The surface of silica gel is known to be covered by silanol (=Si-$(OH)_2$) groups. The silicon atoms in a silicon dioxide network have a valence of 4+ and thus show a high electron affinity. This results in a lower electron density around the attached oxygen atoms than would be the case were the oxygens bound to a metal atom. This means that even though the H^+ is bound fairly strongly (the silanol is weakly acidic), it can be substituted by a positive metal ion, as shown in the following reaction:

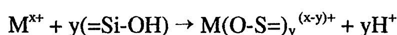

$$M^{x+} + y(=Si\text{-}OH) \rightarrow M(O\text{-}S=)_y^{(x-y)+} + yH^+$$

This mechanism has been confirmed at pH's ≤ 8 by experimental work performed in the past four decades. As metals levels grow on the surface, H^+ is released in direct relation to the number of metal atoms adsorbed [3,4]. In general, $y = x^+$ as long as $x^+ \leq 2$. It is most likely, however, that $y > 2$ is prohibited by steric hindrance. Models based on this mechanism have been developed which correlate closely to experimental observations [5].

It has also been proposed that metal ions can adsorb at the oxide water interface. This proposal was developed largely in response to the fact that metals, in general, commence attaching to silica surfaces close to the pH at which they begin forming hydrolysis products. Evidence for this proposal comes from several observations. First, usually there is little or no adsorption of hydrolyzed metals at or below the PZC (point of zero charge). Below the PZC a surface is positively charged and since metal hydrolysis products tend to be positive, it makes sense that very little adsorption would take place. Second, as metals attach to the silica surface in increasing numbers, they can cause charge reversals of the silica surface [6]. Finally, silica gel coagulation studies have led to the conclusion in the case of some metals that the species causing coagulation (directly related to surface adsorption) have charges higher than would be possible for an unhydrolyzed

metal cation. For example, studies with Al showed that the coagulating species had a charge of 4^+ which is not possible for Al. Further investigation led to the conclusion that the active species was the polynuclear Al hydrolysis product $Al_8(OH)_{20}^{4+}$ [7,8] A model based on adsorption has also been developed which correlates with experimental results up to pH 11-12 [9].

Both approaches are able to address experimental results that the other has difficulty with and it is likely that both are needed to explain what is observed during wafer cleaning. After more than half a century of work, the full picture of metal interactions at silica surfaces is not fully understood [10]. Both models lead to some of the same practical conclusions, however. The propensity of metals to attach to silica surfaces follows most closely their tendency to hydrolyze, as is evident from the fact that silica shows a rapid increase in uptake of most metal ions when the pH is raised to within 1-2 units of the pH at which the first hydrolysis products form [3,6,10]. The pH of hydrolysis, in turn, trends with the ratio of charge to ionic radius of any given metal ion. This provides a general guideline for which metals will be the most likely to deposit and therefore the most difficult to remove from silica surfaces. For the metals included in this study this leads to the expectation that Fe will begin to outplate strongly at pH 2, Cu at pH 5, while Ca only begins to ouplate at pH 8 [3,5,6]

Experimental

Silicon wafers, CZ, p-type, <100>, 1-30 Ωcm, 125 and 150 mm diameter were prepared in two ways. The first method consisted of cleaning the wafers with a full clean in a spray tool (SPM-HF-SC1-SC2) followed by a 30 minute, 900° C oxidation which resulted in the growth of 13 nm of thermal oxide. The second method consisted of stopping the above sequence after the clean in the spray tool. This resulted in one set of wafers with a thermal oxide and a second set of wafers with a chemical oxide. Following this, the wafers were dipped in solutions of varying pH that had been spiked with GFAA standard

metal solutions. In general, the pH was varied from high to low by addition of HCl. Depositions were carried out at room temperature, with a dipping time of 10 minutes and a rinse time of 2 minutes followed by spin drying. Analysis was performed using VPD-DSE-TXRF (Vapor Phase Decomposition - Droplet Surface Etching - Total reflection X-Ray Fluorescence).

Results and Discussion

Figure 1 shows the concentration of iron remaining on chemical and thermal oxides following immersion in HCl solutions spiked with iron. The iron level shows a large increase in the region of pH 2-4 which is very close to what has been shown in the literature for silica gel [3,6]. The difference of ~0.5 pH units is attributable to differences in experimental conditions, more precisely, the ionic strength of the solutions that were evaluated. Interestingly, the chemical oxide does not show the strong outplating behavior that is seen on the thermal oxide. In fact, the thermal oxide provides results which are more consistent with the models proposed for silica gel than the chemical oxide. This difference in the behaviors of thermal and chemical oxides toward metal ions can also be seen in the case of calcium as shown in Figure 2. In this case, the chemical oxide attracts more Ca than the thermal, but again, the thermal oxide behaves more in accord with the theory, as Ca does not begin to strongly outplate on silica gel until pH~8 [6]. It is possible that the chemical oxide is showing deviant behavior due to anion contamination (or possibly cations that are not detected by TXRF). It was noted in reference 3 that silica gels from different sources showed very different metal capture characteristics. These differences could be eliminated by repeated washing with 5 M HNO_3 and/or 5 M HCl at 80-90° C followed by a long rinse in distilled water. The gels were then dried for 20 hrs at 100° C. The reason for the differences was attributed to the silanol groups not being completed protonated prior to the acid washings as well the possibility of unknown cations or anions being present on the surface. Figure 3 shows a comparison of iron, calcium, and copper outplating onto thermal oxide from HCl solutions individually spiked

with 100 ppb of each metal. The results conform well to expectations. Fe shows the highest increase, beginning at pH 2, [3,6] while Ca and Cu are both low and approximately equal (after subtracting the initial Ca) which is to be expected as Cu only begins strongly attaching to silica gel at pH5-6 while Ca does not begin to attach until pH8 [5,6].

Conclusions

Metal outplating onto silicon wafers covered with chemical and thermal oxide was characterized as a function of pH. The results were shown to conform to what is known about the behavior of metals with silica gel. A remarkable difference was noted in the behaviors of chemical and thermal oxide with thermal oxide being closer to silica gel results. This was explained as being due to differences in the level of anions and/or non detectable cations on the surface. It was proposed that repeated washing of the chemical oxide in hot HNO_3 or HCl would result in it behaving more like thermal oxide. Most importantly, it has been demonstrated that the widely studied chemistry of silica gel can be used to understand the behavior of silicon dioxide in cleaning solutions.

Acknowledgements

A.L.P. Rotondaro would like to thank CNPq (Conselho Nacional de Desenvolvimento Científico e Tecnológico) Brazil. The assistance of Karine Kenis, Christian Wilms, and Ann Opdebeeck is gratefully acknowledged by all of the authors.

References:

1. O.J. Anttila, M.V. Tilli, M. Schaekers, and C.L. Claeys, *J. Electrochem. Soc.* **139** (4) 1180 (1992)
2. W.A. Patrick and E. H. Barclay, *J. Phys. Chem.* **29** 1400 (1925)
3. S. Ahrland, I. Grenthe, and B. Noren, *Acta Chem. Scand.* **14** 1059 (1960)

4. D.L. Dugger, J.H. Stanton, B.N. Irby, B.L. McConnel, W.C. Cummings, and R.W. Maatman, *J. Phys. Chem.* **68** 757 (1964)
5. P.W. Schindler, B.Fuerst, R. Dick, and P.U. Wolf, *J.Colloid Sci.* **55** 469 (1976)
6. R.O. James and T.W. Healy, *J.Colloid Sci.* **40** 42 (1972)
7. E. Matijevic, F.J. Mangravite Jr., and E.A. Cassell, *J.Colloid Sci.* **35** 560 (1971)
8. G. Johansson, *Acta Chem. Scand.* **14** 771 (1960)
9. R.O. James and T.W. Healy, *J. Colloid Sci.* **40** 65 (1972)
10. R.K. Iler, *The Chemistry of Silica*, (John Wiley & Sons) 665 (1979)

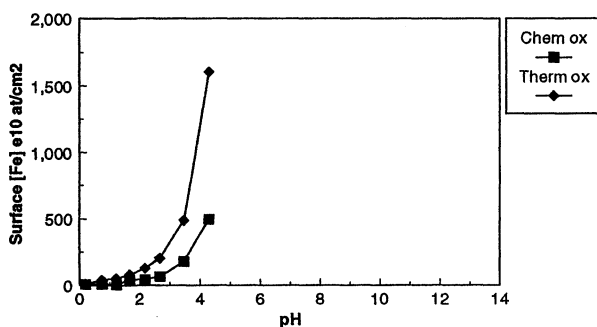

Figure 1: Iron concentration remaining on chemical and thermal oxide surfaces following 10 minute immersion in 100 ppb spiked HCl solutions of varying pH.

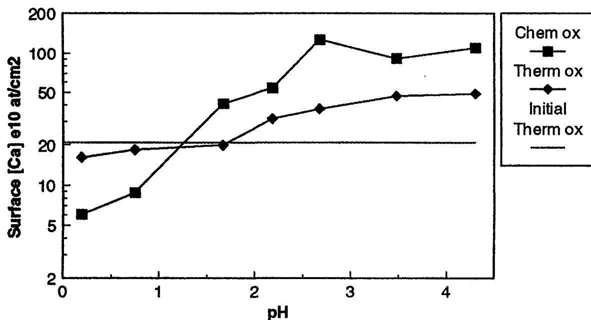

Figure 2: Concentration of calcium remaining on chemical and thermal oxide surfaces following 10 minute immersion in 100 ppb spiked solutions of HCl of varying pH.

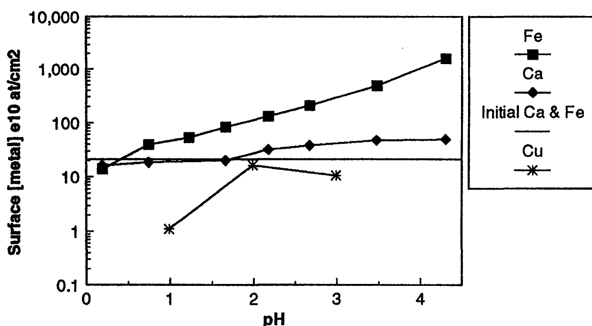

Figure 3: Comparison of iron, calcium, and copper outplating onto thermal oxide surfaces. Wafers were immersed in HCl solutions of varying pH that were spiked to 100 ppb of each metal. Metals were spiked individually so as to avoid interference between metals.

IMPACT OF THE ELECTROCHEMICAL PROPERTIES OF SILICON WAFER SURFACES ON COPPER OUTPLATING FROM HF SOLUTIONS

I. Teerlinck, H.F. Schmidt, A.L.P. Rotondaro, T.Q. Hurd*, L. Mouche,
P.W. Mertens, M. Meuris, M.M. Heyns, D. Vanhaeren and W. Vandervorst
IMEC, Kapeldreef 75, B-3001 Leuven, Belgium.
* on leave from Texas Instruments, 13546 N Central, Dallas TX, 75243 USA.

The impact of light on the copper outplating from aqueous HF solutions on various types of silicon wafers is investigated. A new mechanistic model describing noble metal plating onto silicon is proposed which takes the semiconductor properties of the silicon substrate into account.

INTRODUCTION

Copper ions present in aqueous HF solutions are known to plate out on Si wafer surfaces [1-8]. However, a lot of scatter in the reported data is observed. Copper deposition onto Si from aqueous HF solutions is an electrochemical process occurring at the wafer surface. Since mobile charge carriers are involved, it can be expected that Si semiconductor properties play an important role in this process. In this study this topic is investigated by evaluating the effect of illumination of the Si wafer surface on the copper outplating behaviour. A model for the copper outplating based on the semiconductor properties of the Si substrate is suggested which clarifies the importance of illumination.

EXPERIMENTAL

In the experiments 150 mm diameter Cz grown p-type (B doped) and n-type (P doped) Si(100) wafers (10-20 Ω·cm) were used. In all experiments Ashland GigaBit™ grade chemicals were used. Prior to the HF step the wafers received a pre-treatment consisting of an immersion in a H_2SO_4/H_2O_2 (volume ratio 4/1) solution at 100°C followed by a 0.5% aqueous HF dip at 19°C and overflow rinsing (IMEC clean [9]). This procedure results in an oxide free surface with surface metal contamination below 10^{10} atoms/cm^2 as measured by Vapour Phase Decomposition Droplet Surface Etching Total Reflection X-Ray Fluorescence (VPD DSE TXRF) analysis.

Then the wafers were immersed for different times (5 - 600 s) in an opaque polypropylene (PP) tank containing 8 liter of a 0.5% aqueous HF solution at 19°C. This HF solution was intentionally contaminated with various amounts of copper ions (10 - 1000 w-ppb) added from a 1000 mg/l copper(II)nitrate Merck standard solution. The experiments were done under two different illumination conditions. In a first set of experiments the wafers were immersed in the dark, *i.e.* with clean room lights turned off and with an opaque PP lid on the PP tank. For the second condition the immersion was done under illumination using a 35 W tungsten halogen lamp and with the clean room lights turned on. The experimental setup is schematically shown in figure 1.

The resulting copper surface concentration was measured by direct TXRF analysis. No VPD DSE was used since this procedure might introduce errors with regard to the collecting efficiency of the DSE droplet. The TXRF analysis was performed by means of an Atomika XSA 8010 instrument, operated with a Mo anode at 50 kV and 40 mA. Under these conditions the critical angle for total reflectance (θc) was 1.83 mrad. The angle of incidence of the exciting X-rays at which the sensitivity for a particulate type contamination equals the sensitivity for a film type contamination (θiso) was 1.3 mrad. In addition Angle Resolved - TXRF (AR-TXRF) measurements were performed by varying the angle of incidence (θ) between 0.3 and 1.5 mrad. By this technique one can differentiate between a film type and a particulate type of contamination [10]. Some wafers were inspected by Atomic Force Microscopy (AFM) using a Digital NanoScope instrument operated in TappingMode.

RESULTS AND DISCUSSION

p and n-type Si wafers were immersed for 600 s, in darkness and under illumination, in a 0.5% HF solution containing various amounts of copper ions. Figure 2 shows the resulting copper surface concentration under different illumination conditions as a function of the weight-concentration of copper ions. It is found that illumination of the wafer surface results in an increase of the copper surface concentration by at least an order of magnitude. p and n-type Si wafers have a nearly identical behaviour.

The effect of immersion time on the copper surface concentration was investigated using a 0.5% HF solution containing 100 w-ppb of copper ions. The results for p and n-type Si wafers are shown in figure 3 (a) and (b) respectively. When the wafers are immersed in darkness the copper surface concentration increases only very weakly with time within the experimental time frame from 5 to 600 s. Under illumination, however, a strong increase of the copper surface concentration is observed after about 15 s immersion. For shorter immersion times no significant difference is observed. The p-type and n-type Si wafers used in our experiments show again a nearly identical behaviour.

AR-TXRF measurements were performed on p-type Si wafers which had been immersed for 10, 30, 60 and 600 s, in darkness and under illumination, in a 0.5% HF solution containing 100 w-ppb of copper ions. The results are shown in figure 4 (a) and (b), which show the angular dependence of the normalised measured copper surface concentration after immersion in darkness and under illumination respectively. The copper surface concentration is normalised to the surface concentration measured at $\theta=\theta iso$ and is plotted as a function of the incident angle normalised to θc. During immersion in darkness the copper surface contamination forms mostly a film type contamination. This is attributed to the presence of only small copper nuclei, as evidenced by AFM analysis. A typical AFM result of a p-type Si surface after a 600 s immersion in darkness is shown in figure 5 (a). When the wafers are illuminated during the immersion, the contamination evolves as a function of time towards a more particulate character. This is due to the presence of large copper deposits as can also be seen by AFM analysis. A typical AFM result of a p-type Si surface after a 600 s immersion under illumination is shown in figure 5 (b).

In figure 6 the particulate like character of the copper contamination is plotted as a function of the copper surface concentration resulting from immersion in darkness or under

illumination. The "particulate like character" is defined as the ratio of the copper surface concentration measured at θ=0.5 mrad and at θ=θiso. The closer the value of this parameter approaches to unity the more particulate like the contamination is. It is found that the copper deposited onto the wafer surface obtains a more particulate like character with increasing copper surface concentration independent of the illumination condition. This indicates that copper ions tend to deposit preferentially at existing copper nuclei independent of the illumination condition. The major effect of illumination is an enhanced growth rate of the copper nuclei. The growth of copper nuclei after a nucleation period has been reported in Refs. 6 and 7. However, it must be noticed that previous studies did not take the illumination condition into account .

The importance of illumination can be explained by looking into more detail in the basic mechanisms that govern the copper outplating. The reduction of copper(II) ions in solution consists of two consecutive single-electron steps according to (with their respective standard redox potentials U referred to the Normal Hydrogen Electrode (NHE)):

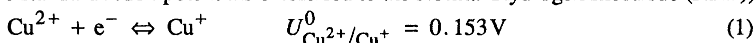

$$Cu^{2+} + e^- \Leftrightarrow Cu^+ \qquad U^0_{Cu^{2+}/Cu^+} = 0.153\,V \qquad (1)$$

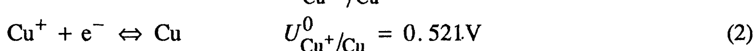

$$Cu^+ + e^- \Leftrightarrow Cu \qquad U^0_{Cu^+/Cu} = 0.521\,V \qquad (2)$$

of which the first reduction step (1) is rate determining. On the other hand, the electrochemical dissolution of Si in an HF solution is proportional to the hole concentration at the Si surface and proceeds, under conditions close to the open circuit potential, according to (see Refs. 11 and 12):

$$Si + 2HF + 2h^+ \Leftrightarrow SiF_2 + 2H^+ \qquad (3)$$

Basically, the charge transfer mechanism can occur via the conduction band, the valence band or through interface states [8, 13]. The probability of the charge transfer and therefore the rate of the outplating reaction is determined by the amount of overlap between occupied electron energy states at the Si wafer surface and unoccupied electron energy states of the metal redox system. This is schematically illustrated in figure 7 for two different metal redox systems M1 and M2 with their respective redox Fermi levels E_{M1} and E_{M2}. The relationship between the redox Fermi level E_{Mi}, referred to the energy of an electron at rest in vacuum (E_0), and the redox potential U_{Mi}, referred to the NHE, is given by:

$$E_{Mi} = -eU_{Mi} + E_{NHE} \qquad (4)$$

where E_{NHE} is the energy level of the NHE referred to E_0 [13].

When the Si wafer is immersed in an aqueous HF solution the equilibrium of the electrochemical potential between the wafer and the HF solution results in the creation of a space charge layer in the Si substrate which depends on the doping type and level of the Si wafer [13]. For both the p and n-type Si wafers used in our experiments the space charge region is depleted of majority carriers [12], as shown by the energy band diagrams in figure 8. In darkness, copper plating on the Si wafer surface is possible through metal ion reduction via a valence band mechanism (M2 in figure 7), *i.e.* metal ion reduction accompanied by hole injection into the Si substrate. The more positive the redox potential (*e.g.* gold ions added as $HAuCl_4$), the more likely it becomes that electron transfer via the valence band will occur (according to M2 in figure 7). The very slow copper deposition in darkness can be attributed to the fact that there is only a very small overlap between

occupied valence band electron energy states at the wafer surface and unoccupied electron energy states of the Cu^{2+}/Cu^{+} system. By illumination with light having a photon energy higher than the Si band gap (±1.1 eV) electron-hole pairs are generated. These are separated by the electric field in the space charge region (figure 8) resulting in an increased surface concentration of minority carriers. Therefore, under illumination, photoplating by metal ion reduction via a conduction band mechanism becomes possible. The drastically enhanced copper deposition under illumination is explained by the large overlap between occupied and unoccupied electron energy states at the Si surface and copper ions in solution respectively when the plating mechanism is driven by a conduction band mechanism.

CONCLUSIONS

The outplating of copper on Si wafer surfaces in HF solutions is shown to be substantially affected by the illumination condition of the wafer surface. When Si wafers (n,p-type; 10-20 Ω·cm) are immersed in darkness, the copper surface concentration increases only very weakly for immersion times between 5 and 600 s. This results in very small copper nuclei on the wafer surface. For short immersion times, *i.e.* of 5 to 10 s, the presence of light does not affect the copper surface concentration. In contrast, for an immersion time longer than 15 s, illumination strongly increases the rate of copper deposition. The behaviour for p and n-type Si wafers used in our experiments was nearly identical. The importance of illumination could be clarified by a model which takes into account the basic electrochemical properties of the Si substrate.

ACKNOWLEDGEMENTS

The assistance of K. Kenis, M. Baeyens, G. Doumen, I. Cornelissen, A. Opdebeeck and M. Lux is gratefully acknowledged by all authors. A.L.P. Rotondaro would like to thank CNPq Brazil for financial support.

REFERENCES

1 T. Ohmi *et al.*: J. Electrochem. Soc. **139** (1992) 3317.
2 H.G. Parks *et al.*: Mater. Res. Soc. Proc. **318** (1993) 245.
3 K.K. Yoneshige *et al.*: J. Electrochem. Soc. **142** (1995) 671.
4 L. Mouche *et al.*: to be publisched in J. Electrochem. Soc..
5 H. Aomi *et al.*: Mater. Res. Soc. Proc. **315** (1993) 333.
6 H. Morinaga *et al.*: J. Electrochem. Soc. **141** (1994) 2834.
7 O.M.R. Chyan *et al.*: UCPSS 1994 Proc. (Acco, Leuven, 1994) p. 213.
8 J.E. Turner *et al.*: Ext. Abstr. **95-1** (ECS, Inc., Pennington, 1995) p. 518.
9 M. Meuris *et al.*: Proc. ECS Fall meeting 1993 (ECS, Inc., Pennington, 1994) **94-7** p. 15.
10 H. Schwenke *et al.*: Adv. X-ray Anal. **32** (1989) 105.
11 H. Gerischer and W. Mindt: Electrochimica Acta **13** (1968) 1329.
12 P.C. Searson *et al.*: Electrochimica Acta **36** (1991) 499, and refs. therein.
13 J. Koryta *et al.*: Principles of Electrochemistry Second Edition, (John Wiley & Sons Ltd., England, 1993).

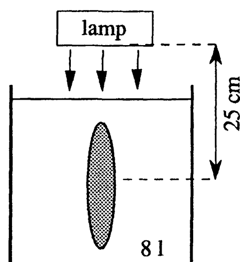

Figure 1. Schematic drawing of the experimental setup.

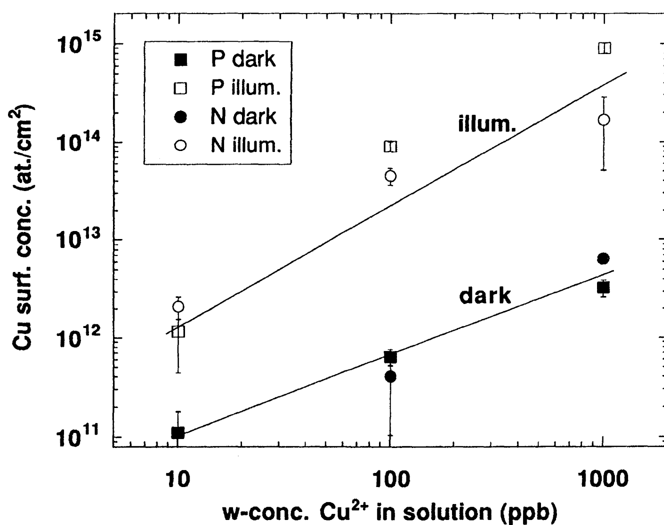

Figure 2. The copper surface concentration on p-type and n-type Si wafers as a function of the copper ion weight concentration in a 0.5% HF solution after 10 min immersion in the dark or under illumination of the wafer surface.

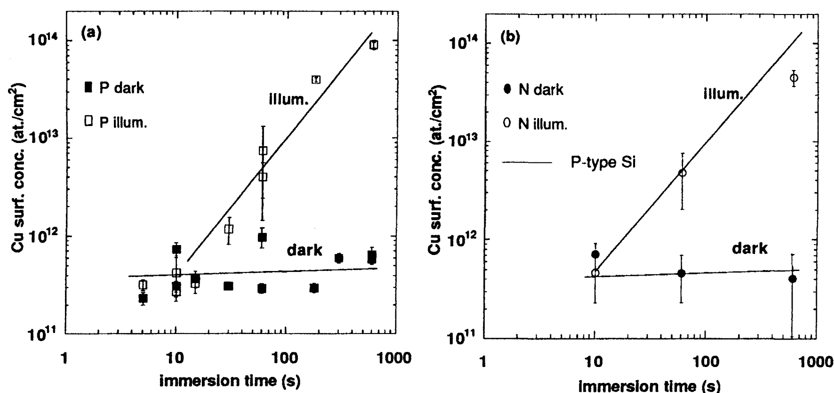

Figure 3. The copper surface concentration on p-type Si (a) and n-type Si (b) as a function of immersion time in darkness or under illumination in a 0.5% HF solution containing 100 w-ppb of copper ions.

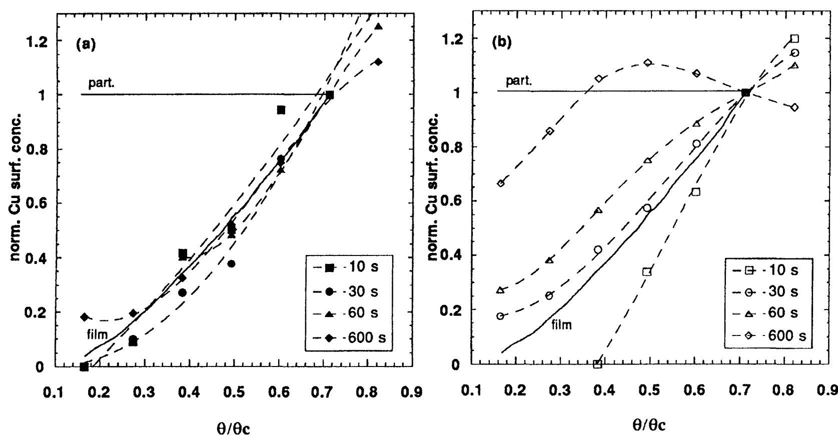

Figure 4. The normalised copper surface concentration on p-type Si as a function of the ratio of the angle of incident X-rays θ and the critical angle for total reflectance θc. The wafers were immersed for various times (10, 30, 60, 600 s) in a 100 w-ppb copper ions containing 0.5% HF solution in darkness (a) and under illumination (b). The plain lines represent the expected shape of the curves for a film and a particulate type of contamination.

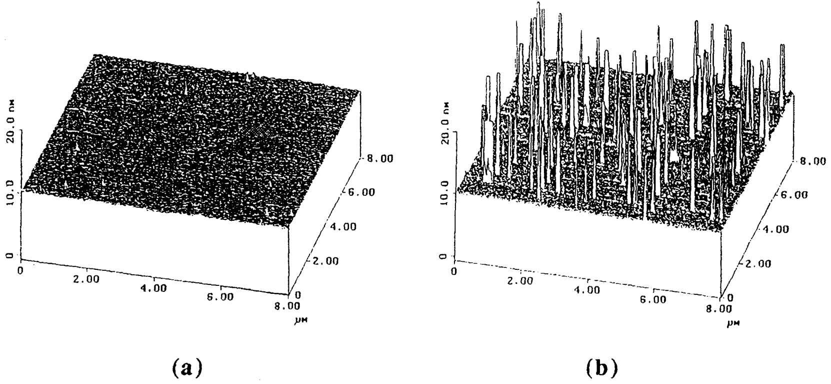

Figure 5. AFM plot of a p-type Si wafer surface after 10 min immersion in a 0.5% HF solution containing 100 w-ppb copper ions. The immersion was performed in darkness (a) or under illumination of the surface (b)

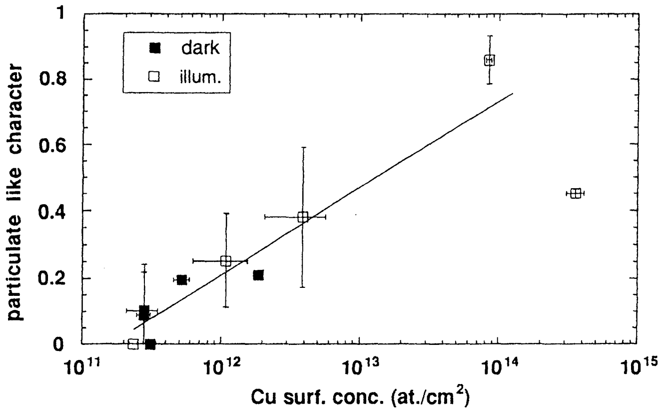

Figure 6. The particulate like character of the copper surface contamination on p-type Si as a function of the copper surface concentration after immersion in copper contaminated (10 - 1000 w-ppb) 0.5% HF solutions in darkness and under illumination. The particulate like character is defined as the ratio of the copper surface concentration measured at θ=0.5 mrad ant at θ=θiso.

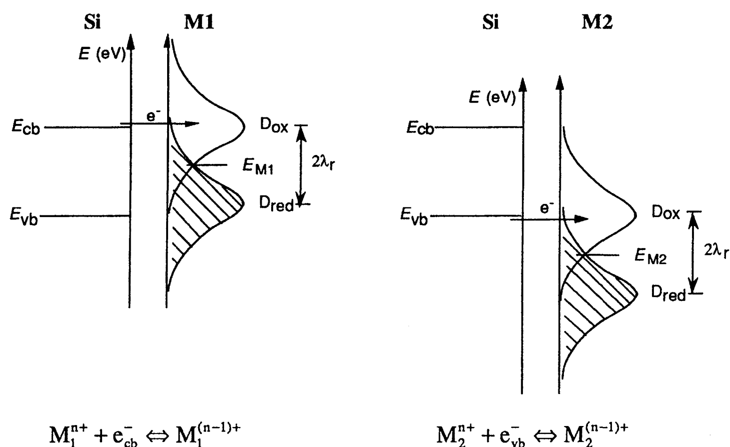

$$M_1^{n+} + e_{cb}^- \Leftrightarrow M_1^{(n-1)+}$$

$$M_2^{n+} + e_{vb}^- \Leftrightarrow M_2^{(n-1)+}$$

Figure 7. Comparison of the energy level distribution in the Si semiconductor and a $M^{n+}/M^{(n-1)+}$ redox system. E_{M1} and E_{M2} indicate the redox Fermi level, λ_r indicates the reorganisation energy. D_{ox} and D_{red} (hatched area) represent the distribution functions of the unoccupied and occupied electron energy states respectively. We distinguish between metal ion reduction via the conduction band (M1) and the valence band (M2).

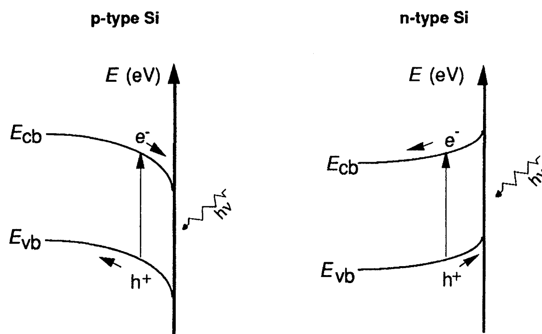

Figure 8. Qualitative band diagram of a p-type and n-type Si substrate immersed in a 0.5% HF solution. E_{cb} and E_{vb} indicate the energy levels corresponding to the conduction and valence band respectively.

Analysis of Cu Adhesion onto Silicon Wafer Surface Using Electrochemical Impedance Measurement.

Kenichi Uemura, Kengo Shimanoe
Electronics Research Laboratories, Nippon Steel Corporation,
3434 Shimata, Hikari, Yamaguchi 743 JAPAN

Cu adhesion to a silicon wafer in HF solution has been studied using electrochemical impedance measurements. The energy bands bend at rest potential, since the Fermi level shifts toward the cathodic potential. Consequently, the concentration of electrons near the silicon surface increases. Cu ions in HF solution receive the electrons and adhere to the silicon surface. It was also found that Cu adhesion depends on the resistivity of silicon.

Introduction

HF solution is widely used to remove a trace metal contamination and a native oxide on a silicon wafer surface. [1] However, it is known that Cu ions in HF solution adhere onto the wafer surface. [2] In this study, we report an analysis of Cu adhesion onto the silicon wafer surface using electrochemical impedance measurement. In addition to the amount of Cu adhesion in 1 wt% HF solution, a difference in the resistivity of the silicon wafer is demonstrated using atomic adsorption spectrophotometry (AAS).

Experimental

The silicon wafers examined in the present work are n-CZ single crystals with a polished (100) face. The resistivity was 1 ohm · cm, 10 ohm · cm and 100 ohm · cm. The wafers were chemically etched in 1 wt% HF solution in order to remove native oxide after cleaning in SC-1 solution ($NH_4OH : H_2O_2 : H_2O = 1 : 1 : 5$) to eliminate organic contamination. For measuring electrochemical impedance in 1 wt% HF solution, aluminum layers were deposited as the ohmic contact electrodes on the oxide free backside silicon. These silicon working electrodes were sealed in a bored polypropylene film. The electrochemical impedance measurement, i.e., Mott - Schttoky plots in 1 wt% HF solution,

were performed in a cell (Fig. 1) using solartron 1260 and 1287. On the other hand, other cleaned silicon wafers were immersed for 1 minute in 1 wt% HF solution containing 5 ppb Cu ion. The surface Cu concentration was determined using atomic adsorption spectrophotometry (AAS).

Results and discussion

When a silicon wafer is immersed in an aqueous solution, some ions become adsorbed. Additionally, the Helmholtz double layer (HDL) and the space charge layer (SCL) are formed on the surface of and in the silicon, respectively. Taking into account these formations, an equivalent circuit which models the silicon surface in solution may be as indicated in Fig. 2. The capacity C in an equivalent circuit is in agreement with the capacity of SCL, because the capacity of SCL is connected in series with that of HDL and the value of capacity is much too small. Cole-Cole plots of the frequency dependence of the impedance modeled by the circuit of Fig. 2 are shown in Fig. 3, which gives the capacity of SCL and an interface state. Fig. 4 shows Cole - Cole plots for 10 ohm · cm silicon measured in 1 wt% HF solution. An ideal circle was obtained in the anodic potential range between 0.1 and 0.5 V. The measured impedance associated with the combination of space charge capacity and interface state capacity can be evaluated from Mott - Schottky plot (Equation (1)). Fig. 5 shows the square of reciprocal capacitance for 10 ohm · cm silicon as a function of the electrode potential, where the capacitance was measured in the frequency between 0.2 Hz and 20 kHz. The linear dependence of the square of reciprocal capacitance on the anodic potential region is then obtained. From the extrapolation of a straight line and the square of reciprocal capacitance, the flatband potential is evaluated to be +0.071 V vs. Ag·AgCl in 1 wt% HF solution. The energy band diagram of 10 ohm · cm silicon at flatband potential in 1 wt% HF is shown in Fig. 6. The conduction band and the valence band are situated at -0.209 and +0.891 V vs. Ag.AgCl, respectively. However, since a rest potential of the silicon wafer in 1 wt% HF solution is -0.42 V, the Fermi level shifts toward the cathodic potential and the bands are bent at a further up portion there of, as is shown in Fig. 7. The Fermi level crosses the edge of the conduction band and silicon surface accumulates many electrons. Therefore, it is considered that silicon, which is a semiconductor, can behave like a metal.

In the same way, the Mott - Schottly plots are shown in Figs. 8 and 9 for 100 and 1 ohm · cm silicon, respectively. The square of reciprocal capacitance increases with the

electrode potential for 100 ohm · cm silicon. However, for 1 ohm · cm silicon, the capacitance is constant at a potential from 0.2 V to 0.4 V vs. Ag.AgCl. This seems to be due to the interface state. This interface state will become fully occupied at rest potential, but it is assumed that it is difficult to move the electron from the interface state to the Cu ions because the interface state is located in a more anodic potential than the Cu redox couple. From the results shown in Figs. 3 and 4, the flatband potential was estimated to be -0.012 and -0.133 V vs. Ag.AgCl for 100 and 1 ohm · cm silicon, respectively.

A surface Cu adhesion property was obtained by immersing the silicon wafer in a 1 wt% HF solution containing 5 ppb Copper (Fig. 11). Surface Cu concentration is maximized on 10 ohm · cm silicon. We considered a silicon band model in solution relating to rest potential and flatband potential. In Figures 7, 10 and 12, a silicon band model of each resistivity is shown. These bands are each bent at a further up portion thereof at the rest potential in 1 wt% HF solution. Each silicon wafer surface shows an accumulation of electrons. Since the Fermi level is below the Cu redox couple, the surface electrons are considered to reduce Cu ions in HF solution. The amount of Cu adhesion should be related to the concentration of surface electrons. The gap between the Fermi level and conduction band edge corresponds to the density of surface electrons. It can therefore be presumed that Cu adhesion in 1 wt% HF solution is maximized on 10 ohm · cm silicon.

Conclusions

From the electrochemical impedance properties and adhesion of Cu onto the silicon wafer surface in solution, the following conclusions are drawn.

(1) From the results of electrochemical impedance measured for n-type silicon in 1 wt% HF, it is clear that the surface of silicon accumulates at rest potential.

(2) From the surface Cu adhesion property obtained by immersing the silicon wafer in a 1 wt% HF solution, it was found that Cu contamination depends on resistivity and the Cu concentration is maximized on 10 ohm · cm silicon. This adhesion properties of Cu was understood the silicon band with model in solution.

Reference

1. W. Kern, RCA Review, **31**, 234 (1970).

2. H. Aomi, ECS Honolulu Meeting Ext. Abst., 93-1, **788**, 1144 (1993).

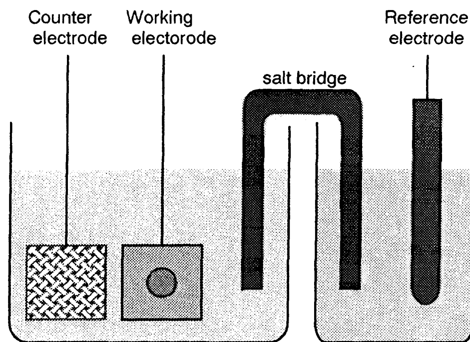

Fig. 1. Schematic illustration of electrochemical measurement cell.

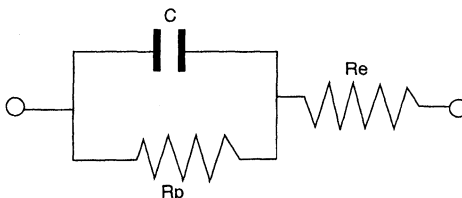

Fig. 2. An equivalent circuit which models the silicon wafer surface in solution. (Re : resistance of solution, Rp : resistance of polarization, C : capacitance of space charge layer.)

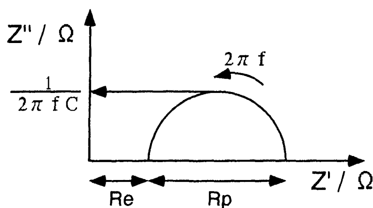

Fig. 3 . Cole-Cole plot of equivalent circuit .

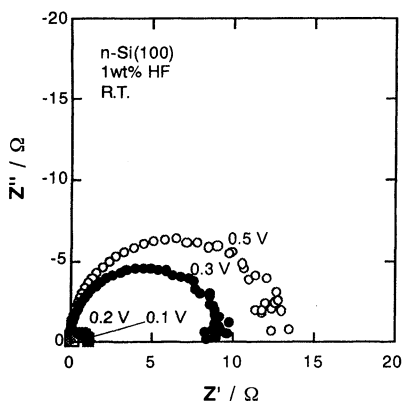

Fig. 4 . Cole-Cole plot for n-type 10 ohm · cm Si (100) in 1 wt% HF solution..

Mott – Schottky plot

$$\frac{1}{C_{SC}^2} = \left(\frac{2}{e\varepsilon\varepsilon_0 N_D}\right)\left(E - E_{fb} - \frac{kT}{e}\right) \quad (1)$$

C_{SC} : space charge capacitance

e : electronic charge

ε : dielectric constant

ε_0 : permittivity of free space (e_0 : 11.7)

N_D : dopant density

k : Boltzmann constant

T : absolute temperature

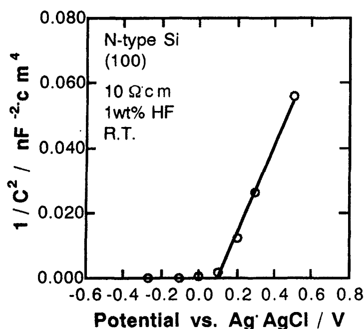

Fig. 5. Mott-Schottky plot for 10 ohm · cm silicon in 1 wt% HF solution.

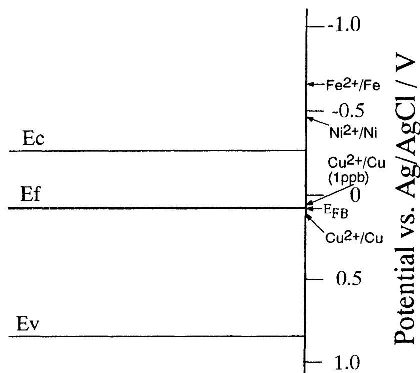

Fig. 6 . Schematic illustration of silicon band model for 10 ohm · cm silicon at flatband potential in 1 wt% HF solution.

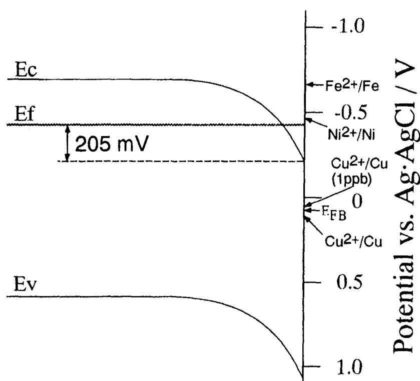

Fig. 7. Schematic illustration of silicon band model for 10 ohm · cm silicon at rest potential in 1 wt% HF solution.

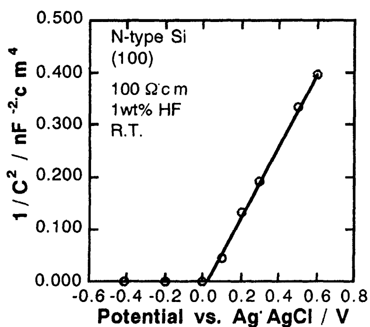

Fig. 8. Mott-Schottky plot for 100 ohm · cm silicon in 1 wt% HF solution.

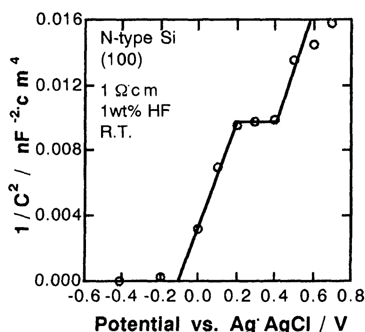

Fig. 9. Mott-Schottky plot for 1 ohm · cm silicon in 1 wt% HF solution.

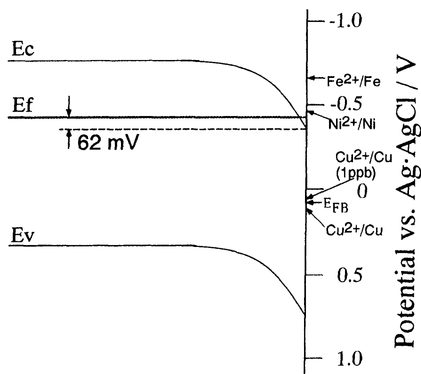

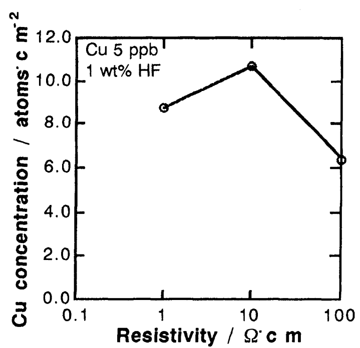

Fig. 10. Schematic illustration of silicon band model for 100 ohm · cm silicon at rest potential in 1 wt% HF solution.

Fig. 11. Surface Cu concentration after immersing in HF solution containing 5 ppb Cu.

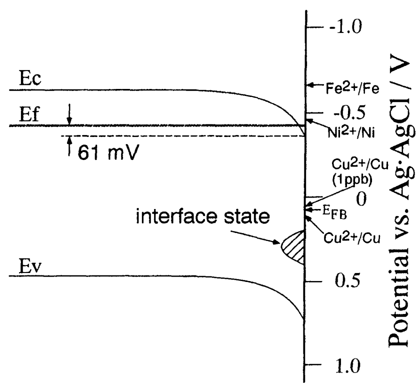

Fig. 12. Schematic illustration of silicon band model for 1 ohm · cm silicon at rest potential in 1 wt% HF solution.

THE EFFECT OF METALLIC CONTAMINATION AND SURFACE ROUGHNESS ON GATE OXIDE STRENGTH AND PRODUCT YIELD

Thomas Roche, Steve Adler, Rick Cosway, Stephen Schauer and Lisa Liu.
Motorola MOS 12, 1300 N. Alma School Rd., Chandler AZ 85224

Abstract

We examined some of the factors that affect the gate oxide strength in a manufacturing facility. This work shows the effect of preclean chemistry on surface metal contamination, surface roughness, charge-to-breakdown (Q_{bd}), optical thickness and circuit yield. Our results indicate that gate oxide strength can be best correlated with the amount of aluminum deposited on the surface by the pre-clean and, surprisingly, is not related to the roughness of the silicon surface.

INTRODUCTION

The critical surface clean processes are primary contributors to the strength of the gate oxide since they are the processes which prepare the surface on which the gate oxide is grown. The choices to be made for these cleans in a manufacturing facility must take into account the defectivity of the process, final metallic contamination of the critical surface, and the physical state of that surface. These analytical and physical results must be related to the electrical results, the ultimate objective of the surface preparation process.

The processes we considered included the use of HF containing etchants last, both BOE and dilute HF, the use of SC1 last or a complete "RCA" type clean including both SC1 and SC2. The objective of this work was to provide the best surface for gate oxide growth with the minimum number of steps. Thus the concept of the IMEC clean (1) with a minimum number of chemical processes necessary for a "perfect" surface was considered a benchmark.

EXPERIMENTAL

Process

All tests and experiments were performed in fully robotic Santa Clara Plastics (SCP) Model 9400 Surface Preparation System wet process stations installed in MOS 12, a 200mm wafer facility in Chandler, AZ. All processes described were accomplished sequentially with a water rinse between each process. The wafers were dried in SCP designed IPA dryers in these tools. The chemicals used in processing are "ppb Grade" chemicals supplied by Olin Electronic Materials using an FSI central distribution system to supply each of the tools.

Surface Analysis

TXRF. A Technos TREX 610T is used to measure metallic contamination on the wafer surfaces. A rotating tungsten anode X-ray source is used for these routine analyses. The elements which are normally quantified are: S, Cl, K, Ca, Ti, Cr, Mn, Fe, Ni, Cu and Zn. The detection limits for most of these elements is in the low e10 Atoms/cm ^{2} level.

The instrument was calibrated using standards obtained from GeMeTec. The certified concentrations of those standards are based on RBS measurements. The instrument at MOS 12 has been correlated with the similar instruments at other Motorola facilities, and the results have indicated that the different instruments and standards agree well.

SIMS. A Cameca IMS-5f is used to monitor the surface concentration of the lighter elements, which are not detectable by TXRF. An O_2^+ primary ion beam accelerated to 12.5 kV (8 keV impact energy) is used to sputter the sample. Positive secondary ions are detected, to maximize sensitivity. The elements analyzed are Li, Na, K and Al. Since we are analyzing surface contamination, each element is analyzed individually. In a sector instrument like the Cameca, if the elements were analyzed simultaneously, the results would be skewed to the first element analyzed.

Ion implant standards purchased from Leonard Kroko are used to calibrate the instrument daily. During the day, an in-house control is also run. The control used is a sample that was SC-1 cleaned, and has easily detectable levels of the elements of interest.

AFM. A Digital Nanoscope Dimension 5000 AFM was used to measure surface roughness. It has a large stage that can hold wafers as large as 200 mm. In the AFM measurements, tapping mode was used, and root mean square (RMS) roughness and peak-to-valley (R_{max}) values were detected for each wafer. Control wafers (as received wafers) were run periodically to check the AFM system.

Chemical Bath Analysis

In addition to the above techniques, we also have wet chemical analyses performed by our chemical supplier, Olin Electronic Materials. These analyses use ICP/MS and GFAA techniques to measure metal contaminants at levels typically on the order of 0.5ppb. Samples are taken on a regular basis from each of the chemical baths and rinse baths in all the wet process stations in the fab. In addition, samples are also taken from sample ports in each of the chemical distribution lines in the fab and all results are compared with the impurity specifications for the chemicals supplied.

Silicon Oxidation Experiments

Cleaned wafers were loaded into the gate oxidation furnace by grouping wafers with similar cleans together in groups. Only the thickness of the center wafers of a given group was used in determining the thickness offsets. This was to minimize the effects of wafers with other cleans changing the thickness of the wafer being measured.

Gate oxidations were performed in a 5-zone SVG/Thermco 7000 Vertical Thermal Reactor at 900°C in a mixture of O2 and HCl followed by an insitu anneal in N2. Wafers were pushed into and pulled from the furnace at 650°C. A 20 min. cool down followed the boat pull and preceded unloading.

Oxide thickness comparisons for the different cleans processes were made on a site-by-site basis. Since the wafers being compared were run in close proximity to one another,

(≤2.2 cm. separation in the furnace) this provided better resolution of the thickness variation since it minimized the impact of across the wafer nonuniformity in the dispersion of the data.

Electrical Tests

Charge to Breakdown. The charge to breakdown test involved forcing a ramped current through the gate oxide in the direction that biases the semiconductor substrate into accumulation. The test begins by forcing an initial current density through the gate oxide of 0.1 A/cm^2. The current is increased every two seconds at a rate of four steps per decade. The gate oxide is considered to have failed if the voltage across the gate drops by at least one volt when compared to the voltage measured at the end of the previous step. The current which has tunneled through the gate is then integrated to yield the total charge to breakdown.

Electrical Gate Oxide Thickness. Thicknesses were measured using a capacitance measurement technique. Gate oxide capacitors were biased into accumulation (5V)with the top plate tied low (ground) and the substrate is tied to the high side of the meter. A measurement frequency of 100 kHz was used.

RESULTS AND DISCUSSION

Process Results

The use of HF or BOE last processes was investigated in Gate Oxide Integrity (GOI) short flows but not used for product evaluation due to the relatively poor particle performance and the fact that no statistical difference was seen between the results for this clean and the clean chosen. Our results indicated that SC1 was necessary for particle free surfaces. Thus most of the effort was expended to determine the effects of SC2 in addition to SC1 and the comparison of dilute HF with BOE solution and the possible interactions of these processes. It should be noted that the etch solution in this clean serves three purposes. It is used to remove the sacrificial oxide grown and also to further pull back the field oxide to establish the effective width of the active area. In addition, it is part of the surface cleaning or preparation. Thus, the exposure to this HF containing solution is significantly longer than is necessary to simply remove the sacrificial oxide present.

The results of surface analysis on wafers treated with the processes under investigation indicated that the main effects of the use of SC1 were the addition of aluminum and zinc to the wafer surface. In order to characterize the effects of elevated aluminum levels (as measured by SIMS analysis on bare silicon test wafers), an experiment was run at pre-gate clean between two solutions which resulted in surface levels of 6E11 versus 1.5E12 $atoms/cm^2$ of aluminum. The final electrical results showed that the increased aluminum levels resulted in an electrical oxide thickness increase of 0.4 nm , which translated to a significant 30 mV increase in our n-channel MOS threshold voltage values. Tight threshold control is extremely important in our advanced device technologies, and additional variation due to this sort of contamination must be controlled.

The deposition of aluminum on the surface of the wafer is particularly prevalent with the SC1 solution due to the tendency of the aluminum to be incorporated in the oxide

grown during the cleaning process (2). The results presented in Figure 1 were taken from chemical and surface analysis monitors and indicate that even at levels below the detectability limit in the bath, the aluminum level on the surface can be as high as 10^{12} atoms/cm^2. This level can be shown to have an effect on the electrical characteristics of the gate oxide. As shown by the SIMS and TXRF data for the SC2 last pre-gate clean (Figure 2), the addition of the SC2 process resulted in the removal of the aluminum to a level below the detection limit. The removal of zinc was also seen, but the iron levels were not affected to the same extent.

Oxide variation

We also examined oxide thickness variations due to pre-cleans. These results are presented in Table I in which we compare oxide thickness variations to the Piranha/BOE/SC1/SC2 clean. Other have reported previously on the effect of surface clean on the oxidation of the silicon (4). As our results indicate, the elimination of piranha from this clean resulted in a negligible change in resultant oxide thickness while the use of Piranha/BOE resulted in approximately a 0.2 nm increase in oxide thickness. The greatest variation resulted from the use of Piranha/BOE/SC1, a 0.75 nm increase. In each case, the standard deviation of the difference determined on a site-by-site basis was small (0.02 nm) making the differences noted on the Piranha/BOE and Piranha/BOE/SC1 cleans statistically significant to the 95% confidence level.

Table I Effect of Pre-Clean on 15 nm Gate oxide Thickness

Clean Chemistry	Pir/BOE	Pir/BOE/SC1	BOE/SC1/SC2
Offset to Pir/BOE/SC1/SC2 Clean (nm)	0.22 ± 0.03	0.75 ± 0.03	0.03 ± 0.02

Surface Roughness

The surface roughness of the silicon produced by an etch is conceptually a factor in the quality of the oxide grown on the surface. Recently, surface roughness measurements have been made on silicon surfaces with attempts to correlate this with gate oxide strength. The results which we found for the BOE processes compared with the HF processes agree with some reports in the literature and indicate that the silicon is rougher with the BOE-treated surface (3). Our results are presented in Table II below.

Table II Surface Roughness of Cleaned Wafer Surfaces

Clean Process	Peak to Valley Roughness (nm)	Std. Dev. (nm)	Number of Samples
Pir+HF+SC1	0.55	0.10	8
Pir+BOE+SC1+SC2	1.45	0.41	10
BOE	2.06	0.71	8

The data indicate that the BOE-containing pre-gate clean results in a rougher surface than the dilute HF clean. This difference is due to the presence of BOE in the process and further processing results in a some decrease in the surface roughness. The results thus give a qualitative picture of the surface roughness but have not been directly related to any electrical property of the oxide.

The fact that we see improved electrical performance for a surface which measures rougher than the HF-treated surface is at first puzzling but when the AFM data is examined, the reason is apparent. Close examination of the data indicates that the periodicity of the roughening is significantly (≥10X) greater than the amplitude of the roughness. We believe that this indicates that the surface irregularities are so widely dispersed and, since they are due to faceting which is a crystal plane dependent process, that they are so regular that they do not appreciably concentrate the peak electric field created by the polysilicon electrode. Thus, significantly enhanced conduction is not seen at the asperities.

Electrical Results

GOI Wafers. Gate oxide integrity (GOI) wafers were used as an initial test of the effect of the cleans process on the gate oxide. These test flows included the same type of isolation used in the product wafers but were analyzed after deposition of gate polysilicon. Thus, these results are a good interpretation of the effect of the clean but do not take into account any further degradation of the gate oxide due to later implants or RIE etches used in the product flow.

GOI short flow split lots were used to examine the effect of the gate oxide pre-clean on the gate oxide strength. The result of a typical split lot is shown in Figure 3. In all lots tested, the Pir/BOE/SC1/SC2 split showed improved Q_{bd} values compared with the splits that utilized HF or ended with SC1.

Product Wafers. We used our single poly, 0.65μm CMOS process to investigate the effectiveness of using a PIR/BOE/SC1/SC2 clean compared with the PIR/HF/SC1 clean. A straight split was performed at both the pre-sacrificial oxide clean and the pre-gate oxide clean (15nm gate oxidation) on a number of different product flows.

The pre-clean split showed a number of reproducible electrical effects across all experimental lots. The PIR/BOE/SC1/SC2 pre-clean resulted in an electrical gate oxide thickness reduction of 0.3-0.45 nm across the lots when compared to the PIR/HF/SC1 pre-clean split (which agrees with the gate oxide data previously presented). The n-channel MOS transistor threshold voltages showed a 20 to 40 mV reduction in threshold voltage with the PIR/BOE/SC1/SC2 pre-clean, which correlated well with the reduction in gate oxide thickness. The p-channel MOS transistor threshold voltages showed much smaller reductions in threshold voltage (<10mV). These PMOS transistors were buried channel devices which show much less sensitivity to gate oxide thickness variation.

The largest parametric improvement was seen in our gate oxide charge to breakdown measurements, which are an important measure of gate oxide quality and reliability. Q_{bd} values (substrate and polysilicon injection) were obtained from all of the experimental lots with the following improvements seen on the PIR/BOE/SC1/SC2 pre-clean as compared to the PIR/HF/SC1 pre-clean. Q_{bd} for substrate injection improved on average 5.4 C/cm2 (from 11.2 C/cm^2 to 16.6 C/cm^2). Q_{bd} for polysilicon injection improved on average 5.7

C/cm2 (from 5.6 C/cm^2 to 11.3 C/cm^2). It should be noted that even though substrate injection shows higher Q_{bd} than does polysilicon injection, we obtained a nearly constant absolute Q_{bd} improvement (5.4 vs. 5.7 C/cm^2).

Probe yield was analyzed using JMP™ software, and at an alpha risk of 10% there were no significant difference in yield seen (See Figure 4) between the cleans splits on any of the product lots run.

CONCLUSIONS

Based on the analytical data presented we can see that even with the very pure chemicals available from suppliers, the contamination level on the wafer surface can have a significant impact on the electrical performance of the gate. In addition, since this level is below typical detectability limit for aluminum in the wet chemical, it cannot be controlled. As we have demonstrated, uncontrolled variations in the aluminum level can lead to uncontrolled variations in the electrical properties of the gate oxide.

The use of surface roughness measurements as a determining factor in the choice of pre-gate clean, although conceptually reasonable, does not appear to be justified. We have seen that in every case we investigated, the processes including BOE show significantly better gate oxide performance than processes which include dilute HF. The lack of dependence on surface roughness is believed to be due to the nature of the roughness which is believed to be based on anisotropic silicon etching by BOE.

Finally, our results indicate that the both SC1 and SC2 are still necessary for the preparation of a "clean" surface. Although the yield of product was not affected by these changes, better control of the product is obtained which is a major goal in a manufacturing facility.

ACKNOWLEDGMENTS

We would like to thank Oscar Gonzalez for the analysis of the GOI wafers and Chuck Davin for many of the surface analyses. We would also like to thank the members of the Cleans Engineering Group at MOS 12 for managing the split lot experiments.

REFERENCES

1. M. Meuris, S. Verhaverbeke, P.W. Mertens, H. F. Schmidt, A.L.P. Rotondaro, M.M. Heyns, and A. Philipossian in 3rd Intl. Symp. Cleaning Technol., J Ruyzyllo and R.E. White, Eds., PV 94-7 , p. 15 The Electrochemical Society Proceedings Series, Pennington, NJ (1994)
2. L. Mouche, F. Tardif and J. Derrien J. Electrochem. Soc. **142**, 2395 (1995).
3. G.S. Higashi, Y. J. Chabal, G.W. Trucks and K. Raghavachari Appl. Phys. Lett. **56**,656 (1990).
4. G. Gould and E. A. Irene J. Electrochem. Soc. **134**, 1031 (1987).

Figure 1 Bath and Surface analysis for SC1 Last Processes

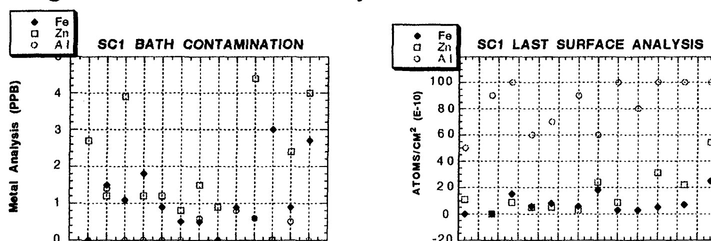

Processes were performed and samples taken over a ~3 month period.

Figure 2 Surface Analysis on SC2 Last Processes

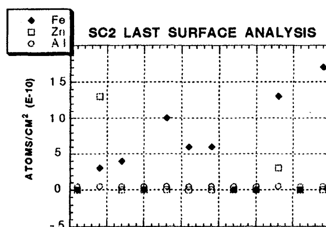

Processes were performed and samples taken over a ~3 month period. Note difference in Y axis compared with Figure 1

Figure 3 Analysis of Qbd Data from Split Among SC1 Containing Cleans

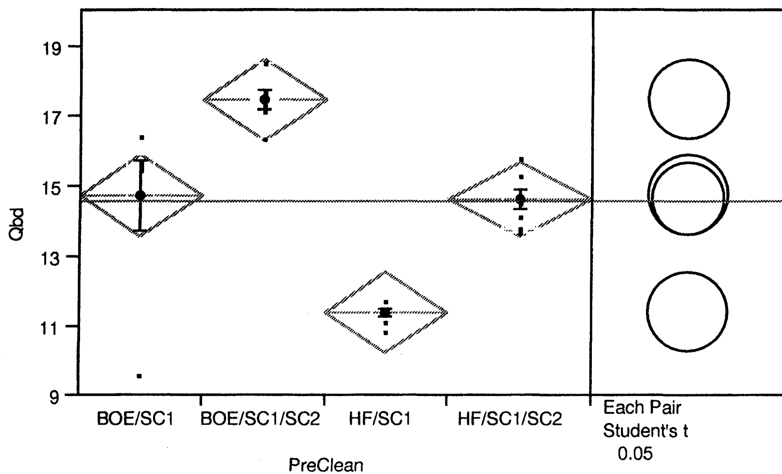

Figure 4 Analysis of Probe Yield Dependence on Pre-Gate Clean Process

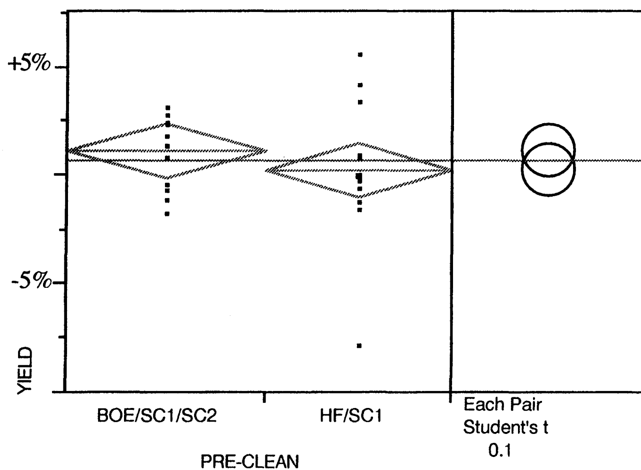

SURFACE METAL CONTAMINATION ON SILICON WAFERS MEASURED BY *SurfaceSIMS*.

Stephen P. Smith, C. J. Hitzman, and R.S. Hockett
Charles Evans and Associates, 301 Chesapeake Drive, Redwood City, CA 94063

The use of secondary ion mass spectrometry (SIMS) coupled with oxygen flooding of the silicon surface during analysis provides an accurate and highly reproducible analytical technique capable of detecting $\leq 10^{10}$ atoms/cm^2 of many surface elemental contaminants. Of particular importance in meeting the future needs of the semiconductor industry is the current ability to detect 5×10^8 atoms/cm^2 of Al and 1×10^9 atoms/cm^2 of Fe contamination on silicon wafers.

INTRODUCTION

Measurement of the surface metal contamination on silicon wafers is an essential part of IC manufacturing process improvement. As the critical dimensions of microelectronics devices steadily decrease, monitoring the improvement in the cleanliness of starting Si wafers and of IC process steps including ion implantation and resist strip is vital. Secondary Ion Mass Spectrometry (SIMS) provides such measurements because of the high sensitivity and good depth resolution of the technique.

Secondary Ion Mass Spectrometry (SIMS) using oxygen primary ion bombardment (O-SIMS) is frequently used to investigate surface cleanliness because of its high sensitivity for light elements such as Li, Na, Mg, Al, and K which cannot be readily detected by X-ray techniques such as Total Reflection X-ray Fluorescence (TXRF). However, to provide an accurate SIMS depth profile of near-surface contaminants, initial transient changes in secondary ion yields must be minimized. These initial variations which occur during the O-SIMS analysis of the first 10 to 20nm of a silicon sample are related to the increase toward steady state of the concentration of the implanted primary beam oxygen. Continuously exposing the sputtered surface of the sample to an external jet of oxygen gas will ensure that the surface is continually saturated with adsorbed oxygen, and that ion yields remain constant. This oxygen flooding procedure is important particularly for analysis of ion-implanted samples where some of the impurity or dopant atoms of interest may actually lie below the surface of the sample. The combination of oxygen flooding with other necessary analytical protocols are essential features of the measurement referred to as *SurfaceSIMS* at Charles Evans and Associates.

DETECTION LIMITS

Current surface contamination detection limits obtained by SurfaceSIMS using magnetic sector SIMS are listed in Table I, and are less than 10^{10} atoms/cm^2 for many elements. The few exceptions are for atmospheric elements (e.g. C) where the detection limit is influenced primarily by the partial pressure of species in the residual vacuum of the sample chamber.

TABLE I: Practical *SurfaceSIMS* Detection Limits for Surface Impurities on Silicon

Element	Detection Limit 10^{10} atoms/cm^2	Element	Detection Limit 10^{10} atoms/cm^2
Li	0.001	**V**	0.01
B	0.1	**Cr**	0.01
C	100	**Fe**	0.1
F	40	**Ni**	0.2
Na	0.01	**Cu**	1
Mg	0.1	**Zn**	0.5
Al	0.05	**As**	1
P	1	**Mo**	0.1
S	2	**Rh**	0.7
Cl	20	**Sn**	0.1
K	0.01	**Sb**	0.1
Ca	0.05	**Ta**	1
Ti	0.1	**W**	0.2

To obtain such low detection limits, several instrumental techniques must be used to separate interfering ions of the same nominal mass/charge ratio as the desired element. These techniques include careful selection of the isotope monitored, increased mass resolution of the secondary spectrometer, and the use of kinetic energy filtering ('energy offset').

The use of high mass resolution is essential to the achievement of the low detection limits listed in Table 1 for Al and Fe, since isobaric molecular interferences originating from BO, C_2H_3, BOSi, C_4H_6, and Si_2 are common. This fact presents an important practical limitation to the measurement of surface contamination with SIMS instruments using quadrupole-based mass analysis.

Present requirements of the semiconductor industry for individual metal contamination on starting Si wafer material are $<10^{11}$ atoms/cm^2 for Na, Al, and Ca, and $<5E10^{10}$ atoms/cm^2 for Fe, Ni, Cu, and Zn (1). A 10% metrology capability requires

detection limits of 1 and 0.5 x10^{10} atoms/cm^2 respectively. The requirements are expected to decrease by a factor of four or five over the next six years. The current *SurfaceSIMS* detection limits for Na, Al, Ca, and in particular the transition metals Cr, Fe and Ni satisfy these requirements. Improved *SurfaceSIMS* protocols are being developed to match possible future requirements for lower detection limits.

REPRODUCIBILITY OF *SurfaceSIMS* MEASUREMENTS

To provide useable information for IC manufacturing process control improvement, measurements of surface contaminant areal densities should be capable of a relative precision of about 10% (1 sigma) or better. This level of precision will certainly allow reliable identification of samples with contamination levels differing by a factor of two (or indeed by as little as 30%, 3 sigma), which should indicate significant reduction in the contamination associated with a given process or process step. A summary of measurements used to evaluate the long-term reproducibility of the *SurfaceSIMS* technique is shown in Table II.

TABLE II: Long-Term Reproducibility of *SurfaceSIMS* Measurements of Na, Al, K and Fe on Silicon Control Wafers. Areal Density expressed in units of 10^{10} atoms/cm^2. Samples 1 to 10 ranked in order of Al concentration.

Control Sample	Al			Na			K			Fe		
	Mean Areal Density 10^{10} at/cm^2	N	% RSD	Mean Areal Density 10^{10} at/cm^2	N	% RSD	Mean Areal Density 10^{10} at/cm^2	N	% RSD	Mean Areal Density 10^{10} at/cm^2	N	% RSD
1	4470	58	8.4%									
2	3630	60	6.8%									
3	1300	18	12%	3	16	36%	2	13	65%			
4	107	5	5%	0.8	5	23%	0.5	5	108%			
5	33	72	8.2%	120	23	30%	93	19	29%			
6	27	10	16%	2.2	9	38%	0.6	7	106%			
7	12	5	16%	33	5	6%	24	5	17%			
8	5.2	3	7%	0.6	3	38%	3	3	166%			
9	3.9	5	22%	9	5	14%	6	5	14%			
10	0.5	110	85%	0.6	25	111%	0.2	20	113%			
11										17	16	11%
Calibration Standard	*121*			*344*			*285*					

SIMS measurement precision is monitored by repeat measurements of both control samples and unknown samples. Previous investigations have demonstrated that the long-term (several months to greater than two years) reproducibility of *SurfaceSIMS* measurements of Na, Al, and K was quite similar to that of conventional depth-profiling SIMS, ±10 to 20% (2,3). Some of the earlier results are repeated in Table II, together with some updated figures for Al, and a recent result from several months of data accumulated measuring the Fe contamination on a control wafer. The table lists the mean areal density of the impurity on each control sample, the number of measurements N, and the percent relative standard deviation (%RSD) of the N measurements.

The control samples for the Na, Al, and K measurements are calibrated on an 'in-load' basis using a Consensus Reference Standard (as defined by ASTM F 1569). This standard is a silicon wafer uniformly contaminated with controlled amounts of Na, Al, and K prepared by a spin-coating technique. The Na, Al, and K contamination levels on the standard (Table II) were determined by VPD/AAS (Vapor Phase Decomposition/Atomic Adsorption Spectrometry). The standard sample is measured in the same sample load as the control (and unknown) samples to determine in-load relative sensitivity factors (RSFs). For comparison with the control data, the %RSD values of the mean in-load sensitivity factors for Na, Al, and K measured over the same period of time are 29%, 20%, and 35%, respectively.

In contrast the the Na, Al, and K data, the measurements of Fe on the control sample #11 were calibrated using a constant sensitivity factor determined from an ion implanted reference material measured under SurfaceSIMS conditions.

For a given contaminant, the RSD values in the table tend to be larger for low areal densities. This trend is due to a combination of the increased statistical variability of measurements at low ion count rates, as well as to an increased likelihood of small-scale unintentional contamination of the surfaces at low concentration levels. Careful inspection of the data in the table shows that among the most heavily contaminated samples, the results for Na and K on control wafer #5 seem to contradict this pattern. This probably reflects some real variation in the intentional contamination across the wafer. The RSD for aluminum on control #3 also seems slightly high compared to data for the other samples, and may also reflect non-uniformity.

In general, the in-load procedure provides an improvement in calibration precision of at least a factor of two compared to the use of a mean sensitivity factor. The fact that the in-load control sample RSDs are substantially reduced means that much of the variance in the calibration sample sensitivity factor measurement is systematic variation due to differences in analytical conditions such as sputter rate. The relatively low RSD obtained for the iron control sample measurements despite the use of a constant RSF reflects the fact that during the four-month period of the latest control measurements, there has been less variability in the *SurfaceSIMS* analytical conditions.

It is important to realize that the %RSD values in the table combine contributions from any non-uniformity of the calibration standard and of the individual control sample, as well as from random variation in the measurement process. Data presented in Table III provide further information concerning the uniformity of the calibration standard, and on the precision of the measurement process for aluminum and iron.

TABLE III: Short-Term Reproducibility of *SurfaceSIMS* Measurements of Al and Fe. Data from individual sample loads using a 12-window sample holder. Areal Density expressed in units of 10^{10} atoms/cm^2.

Sample description:	Al, Calibration Standard	Fe, Spin-Coat, B724-3 Center	R/2	Edge
Number of windows loaded	12	4	4	4
Number of measurements	26	9	8	8
Mean areal density (10^{10} cm^{-2})	121.0	68.2	84.2	85.8
%RSD of all measurements	5.63%	5.06%	5.93%	2.85%
Average %RSD of measurements in a single window	2.51%	3.51%		

The aluminum data in Table III were obtained during a single analysis session from twelve pieces of the calibration sample loaded in one multiple-window sample holder. The precision of repeat measurements on a single sample in any one window is ±2.5% on the average. This number sets a limit on any variation in the Al contamination on the standard on a scale of 1mm (the typical separation of the repeat analyses). The %RSD of the total set of 26 measurements is somewhat larger, ±5.6%. This suggests that there is some systematic variation in the results obtained from the different windows. This may be due to variation in the Al contamination on a centimeter scale (the characteristic dimension of the area on the original wafer from which the samples were cleaved). Alternatively, departures of the faceplate of the sample holder from its ideal flat configuration may also contribute to the increased RSD of the total measurement set. The measured RSD provides an upper limit to the magnitude of either of these effects in this experiment. The still somewhat larger %RSD values (6.8% to 12%) obtained for the long-term measurements of control samples 1 to 3 (Table II) imply that the variability of the Al contamination on these samples is ±5 to 10% (on a 10 centimeter scale).

The Fe data in Table III were also obtained during a single analysis session. In this case, four pieces each from center, R/2, and edge locations were analyzed, and the data have been grouped accordingly. The overall statistics are quite similar to those for aluminum, with a %RSD calculated for analyses from several windows of about 5%, and a somewhat lower average %RSD of 3.5% for measurements in a single window.

ACCURACY

The accuracy of *SurfaceSIMS* measurements of Na, Al, and K areal density is estimated to be within a factor of ±2 based on the uncertainty of VPD-AAS measurements used to determine the Na, Al, and K levels on the standard wafer. The accuracy of the *SurfaceSIMS* calibration for other elements is less certain. Relative sensitivity factors for other elements are currently determined from ion implanted or bulk doped standards measured under *SurfaceSIMS* conditions. Most of the impurity element in the implant standards used to determine the RSFs lies below the surface of the sample. In contrast, accurate determination of an areal density of a surface contaminant depends on the first few data points of a concentration depth profile since it is often decreasing rapidly with depth. Although the *SurfaceSIMS* technique minimizes ion yield variations very near the sample surface, it is not clear that the variations are completely eliminated. Therefore it is not certain that the RSF determined from measurements of subsurface implanted impurity atoms is necessarily the appropriate value to use for areal density determinations of surface contaminants. However, parallel analyses by *SurfaceSIMS* and TXRF of Fe and Ca contamination on the same silicon test wafer agree to within about 50%, suggesting that the quantitation of these two techniques is in basic agreement. A limited number of comparisons of sensitivity factors for Na, Al, K, Ca, Fe, and Sn calculated independently from surface-contaminated and ion-implanted samples have been made (unpublished results). The results suggest that the *SurfaceSIMS* calibrations based on ion implants are accurate to within a factor of three or four.

FUTURE ADVANCES

SurfaceSIMS detection limits must be lowered to keep pace with the increasingly stringent demands of the semiconductor industry. Some improvement in the precision of the measurements may also be required. Maintaining or improving analysis throughput is desirable, and may provide a constraint on improvement of detection limits in some cases. *SurfaceSIMS* detection limits potentially may be improved by increasing the area of analysis, increasing the useful yield of secondary ions, or reducing backgrounds. The following discussion provides a more formal description of these possible improvements.

In the absence of any measurement background that would limit the detection of a given impurity, the sensitivity of the *SurfaceSIMS* measurement can be represented in equation [1] by the number of secondary ions detected for a nominal impurity areal density:

Detected Ions = (Areal Density) x (Analysis Area) x (Useful Ion Yield) [1]

The useful ion yield is an empirical yield (ions detected per atom sputtered). The number of detected ions is given by the absolute ion yield modified by factors including efficiencies of ion collection, transmission, and detection. For a high transmission magnetic sector SIMS instrument (e.g. CAMECA IMS 4f), the useful ion yields are about 0.1 to 10^{-5} ions/atom sputtered for most elements, and a typical detected area may be approximately 10^{-5} cm^2. For a nominal areal density of 10^{10} atoms/cm^2, the number of detected ions should therefore range from 10^4 to 1 in the absence of any significant background contribution.

If we rearrange equation [1] to solve for the impurity areal density, and define an operational detection limit of 30 integrated ion counts, then the minimum detectable areal density, here called **ADL** (for Areal Detection Limit) is given by equation [2] as:

ADL (Areal Detection Limit) = 30 x (**Area** x **Useful Ion Yield**)$^{-1}$ + (**Background**) [2]

In equation [2] we have added an explicit background term, since for some contaminants (e.g. carbon) this may be the controlling factor in setting current or future detection limits. Inspecting equation [2] it is clear that detection limits potentially may be lowered by increasing the area of analysis, increasing the useful ion yield, or reducing backgrounds.

Increasing the area of analysis is an option for unpatterned wafers, but not necessarily for patterned product wafers. The increase can be direct, by increasing the area from which ions are accepted by the secondary spectrometer, or possibly indirect, by using a pre-concentration technique like vapor phase decomposition. One or more orders of magnitude improvement in detection limit may be gained through analysis area increases.

Increasing useful ion yields may have less potential for improving detection limits except in specific cases. Significant increases in absolute secondary ion yields are not generally possible, except if a reliable post-sputter ionization step can be incorporated. For elements that must be analyzed at high mass resolution to eliminate interferences, an improvement of about an order of magnitude would be possible using a secondary spectrometer of improved design (capable of high transmission at HMR conditions).

Reducing measurement background is important now for certain elements, and probably will become important for many other elements as detection limits are improved by other means. Some improvement can come about through minimizing wafer handling, for example by employing a SIMS sample chamber capable of accepting a full wafer. Other avenues for improvement may come about through instrument modifications (such as improvements in UHV, modification of construction materials, and increasing the primary ion beam purity). Finally, attention can be paid to design of analytical protocols to minimize backgrounds from sources such as memory effects.

SUMMARY

SurfaceSIMS is an analytical technique capable of detecting 10^{10} atoms/cm^2 or fewer of surface contaminants on silicon. These contaminants include low-Z elements such as Li, B, and C, important species such as Na, Al, K, and Ca, cross-contaminants such as P, As, and Sb, transition metals such as Cr, Fe, Ni, and Cu, and high-Z metals such as Mo, Ta, and W. The precision of the measurements are comparable to those of conventional SIMS (±10% or better at moderate areal densities, and controlled by ion-counting statistics at low concentrations). The accuracy of the technique depends on the accuracy of standards used for calibration. Under consideration at Charles Evans & Associates are several approaches which may be combined to improve the areal density detection limits by an order of magnitude or more.

REFERENCES

1. The National Technology Roadmap for Semiconductors, p.113, Semiconductor Industry Association, San Jose, (1994).

2. S. P. Smith, in Secondary Ion Mass Spectrometry (SIMS IX), A. Benninghoven, Y. Nihei, R. Shimizu and H. W. Werner, Editors, pp. 476-479, John Wiley & Sons, Chichester (1994).

3. S. P. Smith, L. Wang, J. W. Erickson, and V. K. F. Chia, in Ultraclean Semiconductor Processing Technology and Surface Chemical Cleaning and Passivation, M. Liehr, M. Hirose, M. Heyns and H. Parks, Editors, in press, Materials Research Society (1995).

Depth Profile of Metallic Contamination Deposited on Si and SiO_2 Surfaces in APM Solution

Mikio Tsuji*, Yoshinori Muramatsu and Nahomi Aoto
ULSI Device Development Laboratories, NEC Corporation
1120 Shimokuzawa, Sagamihara, Kanagawa 229, Japan

*) present adress : Analysis and Evaluation Technology Center, NEC Corporation
1753 Shimonumabe, Nakahara-ku, Kawasaki, Kanagawa 211, Japan

ABSTRACT

In this study, we investigated the depth profile of metallic contamination on Si and SiO_2 surfaces deposited in APM solution by HF-vapor phase decomposition-atomic absorption spectrometry (HF-VPD-AAS) and X-ray photoelectron spectroscopy (XPS). Most of the Al contamination, approximately 99%, occurs on the surfaces of native oxides. A small part of Al, approximately 1%, was taken into native oxide during oxidation in the APM solution and distributed within a depth of 0.5nm Other metallic impurities (Fe, Ni, Cu, Zn) were not deposited into the native oxides and adsorbed only on the top of the oxide surfaces. Therefor all of the metallic contamination deposited in the APM solution can be completely removed by slight etching of naive oxide surfaces for a depth of 0.5nm.

INTRODUCTION

It is well known that metallic atom contamination easily occurs on Si surfaces in Ammonium hydroxide-hydrogen Peroxide-Mixture (APM) solution. It has previously been reported that, during APM cleaning, metallic impurities deposit in the native oxide which is formed in the APM solution. However, the characteristics of metallic contamination have not yet been sufficiently documented. In the present work, we studied the properties of metallic contamination by examining the depth profiles of metals both on Si and SiO_2

EXPERIMENTAL

Figure 1 shows the experimental procedure of this study. Si (100) wafers (CZ, B-doped, 15ohm-cm) of two types of surfaces condition were employed as samples; (1) diluted-HF (DHF) treated bare Si surfaces, and (2) 100nm-thick thermal oxide surfaces (SiO_2). Wafers were intentionally contaminated in APM solutions with added metallic impurities Al, Fe, Ni, Cu and Zn of 0~100 ppb for each element. Bare Si surfaces were chemically oxidized in the APM solution to produce the native oxide. Si surfaces with the native oxide are referred to as Si in the following. Figure 2 schematically shows the analysis methods. Metallic impurities adsorbed on the sample surfaces were analyzed quantitatively by the HF-Vapor Phase Decomposition-Atomic Absorption Spectrometry (HF-VPD-AAS) technique. In this technique, surface oxide layers were completely removed and all impurities in the oxides were analyzed on both the Si and SiO_2 surfaces (Fig. 2(a)).

For the depth profile analysis, the surface oxide layers were gradually etched in a DHF/H_2O_2 solution of 0.1%HF and 1% H_2O_2 in order to reveal the deeper site in the oxides. The etching depth was evaluated by ellipsometry. Figure 3 shows the relation of the etching depth and theetching time for SiO_2 by DHF/H_2O_2 solution of 0.1%HF and 1%H_2O_2. The etching depth increases lineary with the etching time. After each etching step, the impurities were evaluated with the HF-VPD-AAS technique, by removing the residual oxide layers (Fig. 2(b)). XPS analysis was also employed for the surfaces after each gradual etching step (Fig. 2(c)).

RESULTS AND DISCUSSION

Figure 4 shows the concentration of the metallic impurities, Al and Fe, on Si and SiO_2 surfaces as a function of the concentration of intentionally added impurities in the APM solution. There were no significant differences in the concentration of Al and Fe between Si and SiO_2. The difference was also negligible for the impurities of Ni, Cu and Zn.

These results indicate the following characteristics of metallic impurity deposi-

tion. In the APM solution, SiO_2 surfaces are etched but not further oxidized. Thus the metallic impurities deposit on the top surfaces. In contrast, surface oxidation and the oxide etching occurs simultaneously on Si surfaces in the APM solution. In this case, there is a possibility that impurities deposit in the surface native oxide layers as well as on the top surfaces. Thus the small differences in impurity concentrations between Si and SiO_2, shown in Fig. 4, suggest that major deposition occurs on the top surfaces and that metallic impurities are scarcely taken into the native oxides.

The impurity deposition in oxides was examined in detail by depth analysis methods. Figure 5 shows the concentration of Al and Fe evaluated by HF-VPD-AAS on both Si and SiO_2 surfaces depending on the gradual DHF-etching depth. Fe concentration is high only on the non-etched surfaces and drastically decreased to the detection limit after slight etching of less than 0.1nm. Al concentration has a similar depth profile on the SiO_2 surfaces. In contrast, on the Si surfaces a gradual decrease in the Al concentration is observed until the depth becomes approximately 0.45nm. Fig. 5 also shows that the quantity of Al deposited in deeper regions is almost 1% of that on the top-surface.

The impurities of Ni, Cu and Zn showed depth profiles similar to those for Fe. Thus only the Al impurity showed a depth distribution for the Si native oxide surfaces within a depth of approximately 0.5nm with a concentration of 1% of the top-surface concentration. In other cases, metallic impurities adsorbed only on the top surfaces.

Figure 6 shows the XPS spectra of Al-2p, Fe-2p, and Zn-2p on the Si native oxide surfaces after gradual DHF-etching for 0nm (initial), 0.075nm, 0.45nm and 0.9nm. Oxide-related peaks of Fe-2p and Zn-2p disappeared after slight etching of 0.075nm, while the oxide-related peak of Al-2p spectra becomes smaller but did not disappear until the etching depth becomes 0.45nm. These XPS results are consistent with the results of HF-VPD-AAS shown in Fig.5.

It is thought that the difference in depth profiles between Al and other impurities is due to the higher oxide formation enthalpy of Al than others. Al atoms with high oxide formation enthalpy are easily deposited and become Al_xO_y in the native oxide layers formed during oxidation in the APM solution.

CONCLUSION

The depth profile of metallic contamination on Si and SiO_2 surfaces deposited in APM solution was investigated. Most of the Al contamination, approximately 99%, occurs on the surfaces of native oxides. A small part of Al, approximately 1%, was taken into native oxide during oxidation in the APM solution and distributed within a depth of 0.5nm. Other metallic impurities (Fe, Ni, Cu, Zn) were not deposited into the native oxides and adsorbed only on the top of the oxide surfaces.

Therefor all of the metallic contamination deposited in the APM solution can be completely removed by slight etching of naive oxide surfaces for a depth of 0.5nm. This information is applicable in designing wet cleaning processes for ULSI fabrication which needs surface etching control as well as micro-contamination control.

ACKNOWLEDGMENT

The authors would like to thank Drs. M. Kamoshida, M. Kikuchi and A. Ishitani for their encouragement and advises

REFERENCES

1) J.Atsumi, et al : Proc. of the 1st International Symposium on Cleaning Technology in Semiconductor Device Manufacturing, p.59 (1989)
2) O.J.Anttila, et al : J. Electrochem. Soc., **139**, p.1180 (1992)

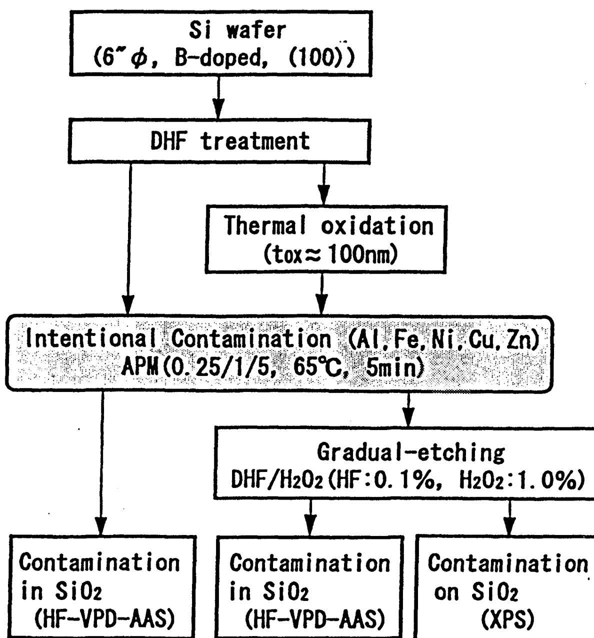

Figure 1 Experimental procedure of this study.

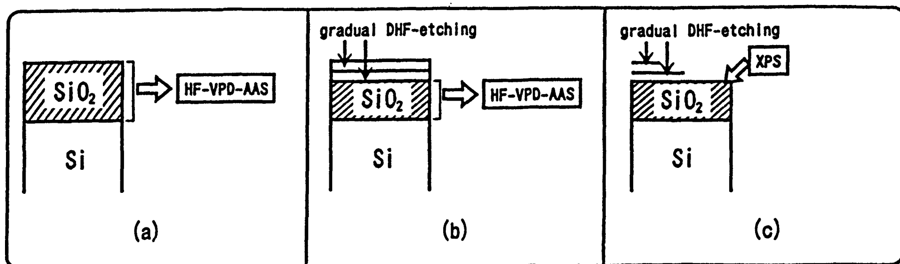

Figure 2 Schema of the analysis methods.

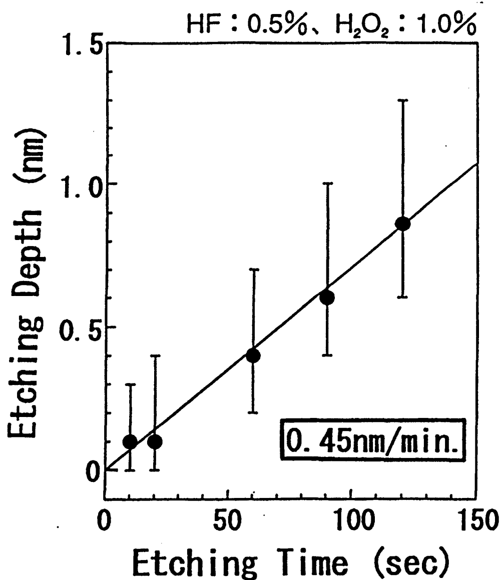

Figure 3 Relation of etching depth and etching time for SiO_2 by DHF/H_2O_2 solution.

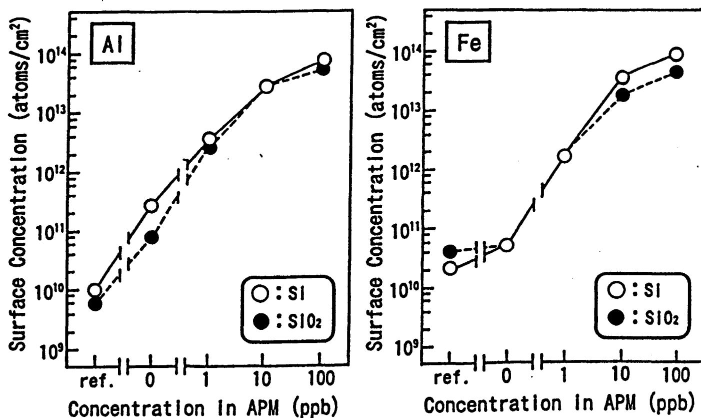

Figure 4 Concentration of Al and Fe on Si and SiO_2 surfaces as a function of their concentration in the APM solution.

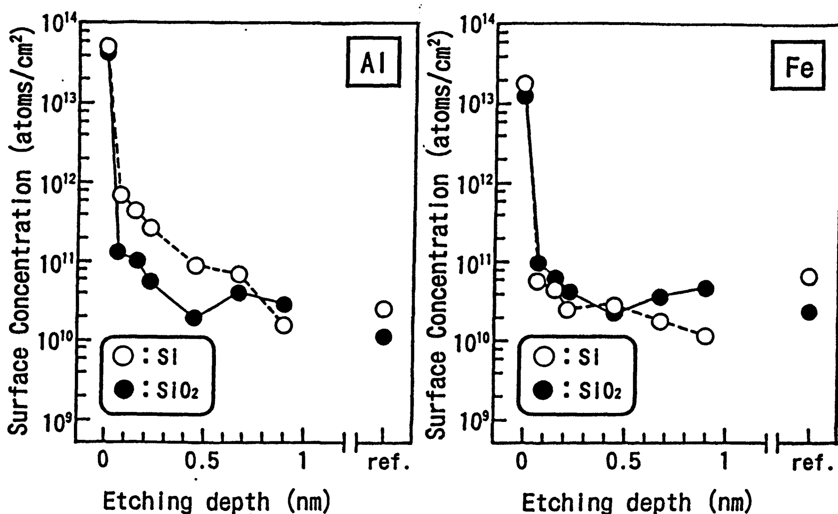

Figure 5 Concentration of Al and Fe on Si and SiO_2 surfaces, after gradual DHF-etching, in relation to the etching depth.

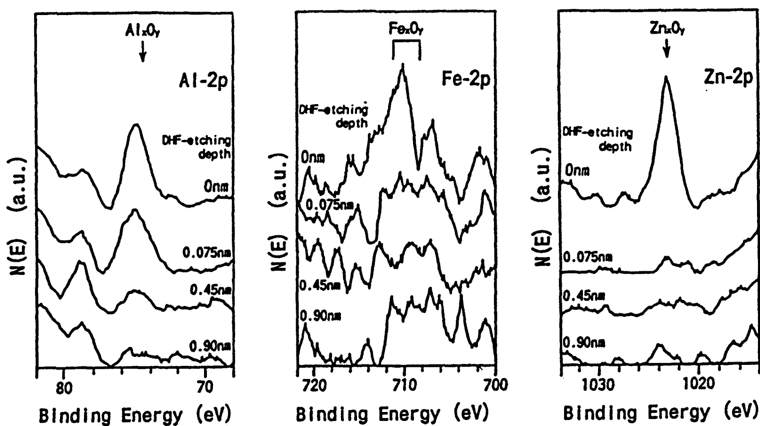

Figure 6 XPS spectra of Al-2p, Fe-2p and Zn-2p on the Si native oxide surfaces after gradual DHF-etching.

ANALYTICAL METHODS FOR ORGANIC IMPURITIES ADSORBED ON SILICON WAFER SURFACES

Ayako Shimazaki, Makiko Tamaoki and Yumi Sasaki*
Integrated Circuit Manufacturing Engineering Dep.
Toshiba Corporation
*ULSI Process and Material Technology Dep.
Toshiba Microelectronics Corporation
1, Komukai Toshiba-cho, Saiwai-ku, Kawasaki 210, Japan

Recently, airborne contaminants such as organic impurities in cleanroom air have affected the ULSI manufacturing process and device performance. A new approach for wafer surface organic contamination analysis, TD-GC/MS or TD-APIMS is introduced, which is, at present, the most practical evaluation method for qualifying and qantifying organic compounds adsorbed on silicon wafer surfaces with high sensitivity. With this method, it has been proved that several specific organic compounds in cleanroom air tend to adsorb on silicon wafers. These compounds include dioctylphthalate(DOP) and other esters and high molecular compounds. And we have also found that these organic contaminants adsorbed on the wafer surface cause a reduction in the breakdown field strength of an insulating SiO_2 layer. It is evident that this new method of analysis will also contribute to improving the wafer contamination control technology.

INTRODUCTION

It has been well known that even a trace of contamination on silicon wafer surface seriously affects the fabrication yields, performances or reliabilities of ULSI devices. The origins of these contaminants are various kinds of processing environments such as processing materials, processing equipments, or clean room ambients.

With the progress of the device fabrication, particularly size reduction, the requirements for wafer surface cleanliness is becoming increasingly rigorous. Not only metallic impurities but also organic impurities adsorbed on silicon wafer surface should be precisely controlled throughout the ULSI device fabrication processing. Organic impurities from the wafer processing ambients also turn out to be potentially harmful contaminants and are recently emerging as sources of serious problems(1,2). For the con-

trol of these organic contamination, highly sensitive surface analysis is of essential importance.

In this paper, the present methodology of wafer surface organic contamination analysis is discussed, particularly with reference to chemical analysis. And the details of our new method which is presently conceived as the most sensitive for detecting and quantifying organic impurities adsorbed on silicon wafer surfaces is introduced. Also examples of its practical application, the effect of this method on fabrication processing, and its future development are discussed.

ANALYTICAL METHODS

The methods for analyzing organic contaminants adsorbed on silicon wafer surfaces are shown in Table 1. These are typical methods for practical contamination analysis. We developed TD-GC/MS and TD-APIMS for organic contaminants on wafer surfaces by applying TD-GC(3) and TD-APIMS(4). Among them, it is possible to separate the compounds and quantify them by using GC/MS. Thus it is useful for clarifying the origin of organic contaminants.

The above methods, TD-GC/MS and TD-APIMS which we developed, consists basically of two steps, namely desorption of organic impurities from wafer surfaces by heating and its detection by gas chromatography / mass spectrometry (GC/MS) or atmospheric pressure ionization mass spectrometry (APIMS).

These thermal desorption methods are compared with conventional TDS in Table 2. The characteristic of the above methods is that they are capable of analyzing whole wafer samples under atmospheric pressure condition while conventional TDS (Thermal Desorption Spectrometry) must be carried out under vacuum condition. Therefore with these methods the organic compounds adsorbed on the very surfaces can be evaluated with high sensitivity.

TD-GC/MS OR APIMS ANALYTICAL SYSTEM

Figure 1 is a schematic diagram of our TD-GC/MS system. Sample wafer is heated to max. 1000°C with IR lamps in the quartz chamber under a flow of helium carrier gas. The gas is purified by adsorbent trap in liquid nitrogen. Impurities desorbed from the wafer surface are swept by the helium gas into the TENAX tube and organic compounds are collected there selectively. Later, the TENAX tube is

crease with increasing exposure time.

Phthalic anhydride, observed in Figure 3, is generally unstable in contact with the atmosphere, so it is supposed that these components are decomposition products under thermal desorption conditions. The original contaminants are thought to be compounds consisting of C_8H_{16}, octanol and phthalic anhydride.

Figure 5 shows TD-GC/MS chromatogram of a silicon wafer on which dioctyl-phthalate (DOP) in ethanol solution was deposited. Peak A, B and C in Figure 5 are identical to those of Figure 3, thus proving that components A, B and C are thermally decomposed products of DOP. Peak 3 in Figure 5 was not present in Figure 3, but the compound causing peak 3(C_8H_{16}) is a structural isomer of peak 1 in Figure 5. We also analyzed the DOP-deposited wafer by TD-APIMS, confirming that DOP decomposed to several fragments and showing APIMS peaks including m/z=104, 83, 149, 112.

We also evaluated the above airborne organic contaminants adsorbed on the wafer surfaces with other methods. One of them is the extraction method using an organic solvent. In this method, adsorbates are extracted with an organic solvent such as dichloromethane, concentrated and then analyzed with GC/MS. This method has enabled us to detect DOP without decomposition and other compounds such as dibutyl-phthalate (DBP) on wafer surfaces.

Another one we tried is ATR-FTIR (Attenuated Total Reflection - Fourier Transform Infrared spectroscopy) using silicon (111) crystal prism for sampling as silicon wafer. The peak heights detected increase with increasing exposure time. And the peak pattern matches that of DOP reported in data book. But the sensitivity is lower than GC/MS because of the existence of some organic contaminants within the system and the ensuing background signals are high. Thus the background should be suppressed by clean system for higher sensitivity.

It was shown that several specific organic compounds in cleanroom air tend to be adsorbed on silicon wafers including dioctyl-phthalate (DOP), dibutyl-phthalate (DBP), other esters and high molecular weight compounds.

We have also found that these organic contaminants adsorbed on the wafer surfaces cause a decrease in the breakdown field strength of an insulation SiO_2 layer. The relationship between the amount of organic contamination and reduction in the breakdown field is summarized in Figure 6.

heated to 250° C to release the adsorbed compounds and they are once again collected in the cold trap chilled to -130° C. Through this two-step concentration process, the desorbed compounds are collected in a narrow band. They are then swept into the GC/MS and analyzed. With this system, whole 8-inch wafers can be analyzed.

Figure 2 is a schematic diagram of our TD-APIMS system. This system is capable of analyzing whole 6-inch wafers. Sample wafer is heated to 900° C at a rate of 20° C/min. Nitrogen carrier gas sweeps desorbed compounds to the APIMS, where they are analyzed simultaneously. With this system, the desorption temperature can be elucidated.

Key point of the systems for high sensitivity, is how to suppress the background. Carrier gas is purified at the point of use and the chemical filter which traps organic impurities in air is set above the sample chamber to prevent the environmental contamination when the sample wafer is set into the chamber.

The sensitivity of these systems is several tens of nanogram per wafer. It is extremely high because organic contaminants within the system is completely purged and the ensuing background signals are nil. TD-GC/MS system is capable of concentrating the impurities, on the other hand APIMS needs higher volume of carrier gas than GC/MS so the impurities are diluted. Though APIMS has higher sensitivity than GC/MS, with combination of TD system the sensitivity is similar to TD-GC/MS.

PRACTICAL APPLICATION IN ULSI PROCESS

Contamination from Cleanroom Air

Using the above methods, the adsorption behavior of airborne contaminants on the wafer surfaces was evaluated. Figure 3 shows TD-GC/MS chromatograms taken from the silicon wafers covered with the thermal SiO_2 layer exposed to the atmosphere in Cleanroom I for 1 to 3 days. In these chromatograms, it is clear that peak heights increase with increasing exposure time. Thus these compounds are certainly contaminants from the cleanroom air. From mass spectra of these peaks, peak A was assigned to C_8H_{16}, peak B to octanol, and peak C to phthalic anhydride.

Figure 4 shows the TD-APIMS spectrum of a thermal SiO_2 wafer exposed to the same cleanroom air for a week. In this spectrum, several thermal desorption peaks are visible, including m/z=104, 83, 149, 112. These components are also clearly adsorbates from the cleanroom air, since they in-

The origin of these organic contaminants was traced to the cleanroom inlet atmosphere, humidity control system and polymeric materials used for wafer boxes, carriers and other equipment. We succeeded in decreasing the organic contaminants by use of active charcoal air filtering, modification of the humidity control system and alteration of wafer carrier materials. We have confirmed that a decrease in organic contaminants resulted in an increase of dielectric breakdown field strength.

SUMMARY

With the progress of device design, the target of contamination control has been changed to include impurities adsorbed on silicon surface from ambient surrounded wafers such as gas molecules add to metallic and particulate contamination. In such situation, it has been proved that these methods are the most efficient and reliable methods for analyzing the organic impurities adsorbed on the wafer surfaces. It is applicable to practical analysis and the evaluation of contamination during fabrication processing, which affects device performances. And it is evident that these new methods of analysis will also contribute to improving the wafer contamination control technology.

On the other hand, the physical approaches for surface organic contamination analysis, the so-called beam analysis, such as XPS (X-ray Photoelectron Spectroscopy), TOF-SIMS (Time-of-Flight Secondary Ion Mass Spectrometry)(5) and ATR-FTIR(6), have various advantages such as capabilities of small area/chemical state analysis over chemical approaches. The most specific advantage of FTIR is the capability of its non-destructive analysis. But those physical approaches provide only chemical bonding or chemical group identification, not specific identification of the molecule. The essential advantage of chemical approaches, especially TD-GC/MS, over physical surface analysis is the extremely high detection sensitivities and quantification of many kinds of organic impurities. Thus, for practical problems on ULSI fabrication processing, these various kinds of physical/chemical approaches should be used in complimentary fashion to each other in the near future.

For further improvement of the detection sensitivity of chemical analysis for organic impurities, the detailed surface chemistry of silicon surface must be understood as in the case of metallic impurities. At the same time, the deeper understanding would bring further progress to the surface cleaning technologies. It is believed that

through these efforts, the detection sensitivity of chemical analysis would continue to be higher than those of physical methods.

ACKNOWLEDGMENTS

It is a pleasure to express my deep appreciation to Mr. M. Hotta for his useful discussion about ATR-FTIR. And also I appreciate to Messrs. Y. Fukasawa, K. Usuda and M. Iiri for their encouraging discussions in the course of the preparation of this article.

REFERENCES

1. A. J. Muller, L. A. Psota-Kelty, H. W. Krautter and J. D. Sinclair, "Solid State Technol.", 37(9), pp. 61, 1994.
2. S. R. Kasi and M. Liehr, "J. Vac. Sci. Technol.", A 10(4), pp. 795, 1992.
3. Lewis A. Fergason, Microcontamination, April 1986.
4. N. Yabumoto, K. Minegishi, K. Saito and H. Harada, Proceedings of 2nd UCT workshop, January 1990.
5. B. W. Schueler, Proceedings of Microcontamination 93, 1993.
6. N. Yonekawa, S. Yasui and T. Ohmi, Technical report of IEICE, SDM 94-9(1994-04).

Table 1 Analytical methods for organic contamination on Si wafers

Contamination	Methods	Sensitivity	Advantages	Disadvantages
molecules adsorbed on surfaces	- TD-GC/MS	10^{-10} g/cm^2	qualitativity	decomposition by heating
	- Extraction+GC/MS (Organic Solvent)	10^{-8} g/cm^2	high qualitativity non-decomposition	complicated procedure concentration
	- TD-APIMS	10^{-10} g/cm^2	desorption temperature profile	low qualitativity
	- Extraction+TOC (D. I. Water)	10^{-9} g/cm^2	conventional	total quantativity
	- ATR-FTIR	10^{-9} g/cm^2	non-destructive	low qualitativity
	- TOF-SIMS	10^{-11} g/cm^2	small area	low qualitativity
	- Contact angle	-	simple	indirect
molecules exist / occluded in films	- SIMS - TDS			
particulates adhered on surfaces	- μ-AES [Auger Electron Spectroscopy] - Fluorescence Micro-spectroscopy			

Table 2 Thermal desorption analytical methods

Methods	TD-GC/MS	TD-APIMS	TDS (QMS)
Desorption	atmospheric pressure (helium gas)	atmospheric pressure (nitrogen, argon, oxygen gas etc.)	vacuum
Sensitivity	100 ppb	10 ppt ～ 1 ppm	10 ppm
Qualification	compounds separated by GC mass spectrum of fragmentaion	mass number dependence of drift voltage	mass number
Detection	organic compounds	moisture gas organic	moisture gas organic

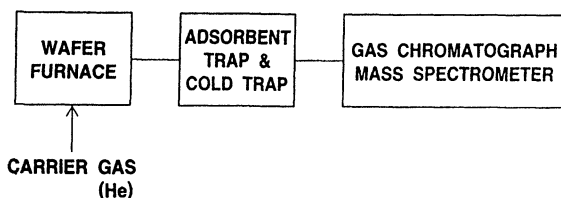

Fig. 1 Schematic diagram of TD-GC/MS

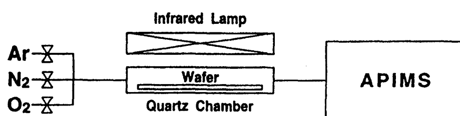

Fig. 2 Schematic diagram of TD-APIMS

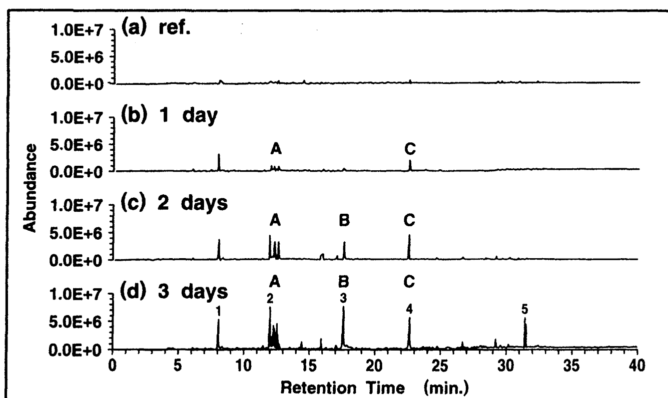

Fig. 3 Total ion chromatograms of TD-GC/MS from thermal oxide Si wafers exposed to Cleanroom I air for (a)0 day(ref.), (b)1 day, (c) 2 days and (d)3 days. Peak assignment; 1:butanol; 2:C_8H_{16}; 3:octanol; 4:phthalic anhydride; 5:diethyl phthalate

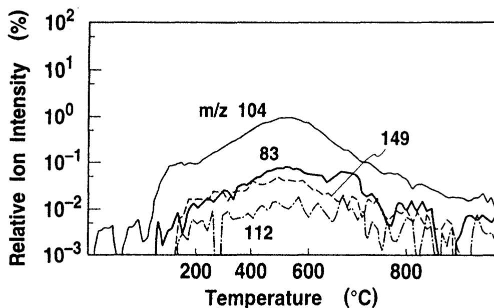

Fig. 4 TD-APIMS spectrum of Si wafer exposed to Cleanroom I for one week.

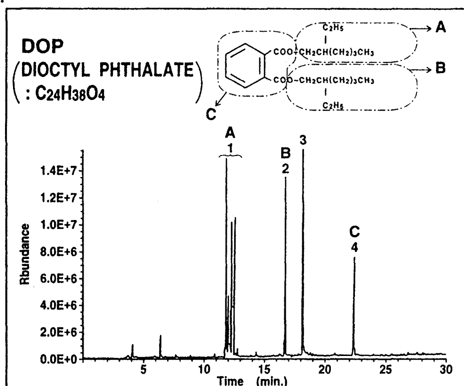

Fig. 5 Total ion chromatograms of TD-GC/MS from a wafer on which DOP(dioctyl phthalate) solution was dropped. Peak assignment; 1: C_8H_{16}; 2:octanol; 3: C_8H_{16}; 4:phthalic anhydride

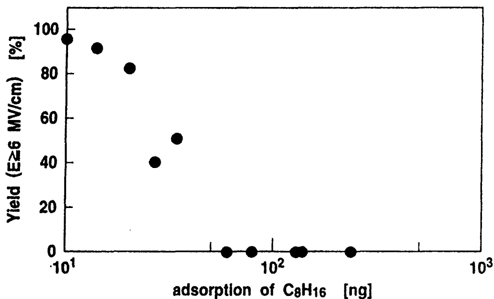

Fig. 6 Relation between amount of C_8H_{16} adsorbed on the wafer surface and yields of insulation SiO_2 layer.

NON-CONTACT ELECTRICAL CHARACTERIZATION OF SILICON SURFACES FOR TRUE IN-LINE MONITORING OF CLEANING PROCESSES

Emil Kamieniecki
QC Solutions, Inc.
Woburn, MA 01801

Effective in-line, real-time process monitoring is required to ensure adequate process reproducibility as well as early detection of potential process malfunction. This paper examines the basic requirements for a method for the in-line electrical characterization of Si surfaces and near-surface regions in the wafer cleaning processes. The indirect methods used in the wafer characterization are compared, regarding their applicability to surface cleaning evaluation. The in-line monitoring of cleaning is illustrated using a new non-contact ac-surface photovoltage instrument, the Surface Charge Profiler (SCP), that measures surface charge related parameters.

INTRODUCTION

As on-chip feature sizes decrease and wafer diameters increase, the value-content of an IC wafer in manufacturing rapidly increases. This results in increasing emphasis on improving IC wafer processing yields. The increasing complexity of ICs results also in increasing complexity of the manufacturing processes. Consequently, an in-line process monitoring that would allow instant detection of process malfunctions and prevent resulting losses is becoming increasingly urgent [1]. Considering that typically over 30% of the processes used in IC manufacturing are cleaning operations, cleaning should be considered a primary target for in-line monitoring.

According to the scaling rules, reduction of the lateral device geometries must be accompanied by an adequate reduction of its key vertical dimensions. In effect, devices become extremely shallow and the role of the silicon surface and near-surface region increases dramatically. Consequently, the role of manufacturing processes, such as cleaning, designed specifically to condition the silicon surface, becomes increasingly important. At the same time, the performance of these processes could be evaluated most effectively by in-line monitoring of silicon surface and near-surface region.

This paper examines the basic requirements for a method for the in-line electrical characterization of Si surfaces and near-surface regions following wafer cleaning. The discussion focuses mainly on the measurements of electrical parameters which provide the most complete picture of the condition of the silicon wafer. The methods used in wafer characterization are compared, regarding their applicability to in-line monitoring of

the surface cleaning processes. In this context, a new non-contact method of Surface Charge Profiling developed specifically for the purpose of in-line monitoring of cleaning processes is introduced and discussed.

IN-LINE MONITORING OF WAFER CLEANING BASIC REQUIREMENTS

The sampling of the performance of various processing steps in IC manufacturing is a common practice. It is performed on the designated test wafers which are added to the production lot. Because of the high cost, the number of such wafers, and hence, extent of process sampling is limited. Furthermore, since the history of designated test wafers is typically different from the history of the product wafers, monitoring using test wafers may not adequately reflect the process performance. Both reduction of testing costs and improvement of test reliability require use of the wafers that are not removed from the production lot. This approach is defined as an in-line process monitoring. Only when the test indicates a deviation from the specified process parameters, the wafer is removed from the production lot for further evaluation and for identification of the nature of the process malfunction (Figure 1).

To be acceptable for in-line process monitoring the method has to meet several basic requirements. Monitoring of cleaning processes in the case when the wafer surface is not protected, imposes even more stringent requirements on the measurement technique than other processes used in semiconductor production.

Non-contact

This requirement implies that no object can be brought into physical contact with the front surface of the wafer to perform measurement. At the same time both support and movement of the wafer must be compatible with standard means used in state-of-the art IC processing. This requirement eliminates any methods using even temporary contacts. The non-contact feature is particularly important in measurements after cleaning of the bare and unprotected wafer surfaces.

The non-contact character of the measurements implies that electrical characteristics of the wafer need to be evaluated using capacitive coupling combined with some kind of excitation of semiconductor with electromagnetic radiation.

Non-invasive

A method to be used for in-line monitoring of IC fabrication must not only be non-contact, but also must not alter the wafer surface making it unsuitable for further

manufacturing. Such external factors as corona charging, high voltage biasing of the wafer surface with an external voltage, or high intensity illumination may cause uncontrolled local non-reversible modification of the surface conditions interfering with intended process related changes. This requirement is particularly important in the case of cleaning of the unprotected wafer surfaces and maybe relaxed for some processes, in which the wafer surface is protected, e.g., with a thermal oxide.

In general, to ensure that monitoring of the cleaning process does not modify the wafer surface in any way, perturbation of the surface potential barrier by incident radiation or other factors must be well below thermal energy, kT.

Real-time

For true in-line process monitoring, the measurement should not interfere with the normal manufacturing process flow and should not require changes in the wafer transport scheme to accommodate measurements. Consequently, in-line monitoring should be compatible with the existing wafer transport scheme and become an integral part of the wafer handling procedure used in the IC manufacturing process. In a number of applications, particularly for in-situ measurements, such integration may be best accomplished only if the monitoring method is capable of performing testing on the wafer in motion.

Straightforward information

In order to meet requirements of in-line process monitoring the collected information must be adequate for instant detection, and not necessarily identification, of the process malfunction. The information should be also suitable for Statistical Process Control. It is desirable to limit the number of measured parameters to those that offer "go/no-go" information concerning integrity of the process, leaving identification of the nature of malfunction to off-line diagnostic and analytical methods. Commonly used diagnostics and analytical methods offer more specific information usually requiring complex data analysis, and therefore, are more time consuming, and are not useful in real-time monitoring.

ELECTRICAL MONITORING OF CLEANING PROCESSES COMPARISON OF MEASUREMENT METHODS

The critical feature of the cleaning operations in the front-end manufacturing is that they are dealing with an unprotected, frequently non-passivated, silicon surface. Consequently, monitoring of cleaning processes imposes more stringent requirements on the measurement technique than other processes used in semiconductor production. In

this section we will review basic features of the methods providing electrical characteristics of the wafers that are commonly considered for evaluation of the performance of cleaning processes [2]. The presented selection (Table I) includes photoelectrical techniques that, following considerations of the previous section, are the most suitable for in-line monitoring applications.

For historical reasons, most of the methods listed in the Table I are based on measurements of the minority carrier lifetime (minority carrier diffusion length). The conventional Surface Photovoltage (SPV) technique [3] is based on measurements of the variation of the surface potential barrier as a function of light wavelength. In a typical SPV approach, which is used to measure the minority carrier diffusion length, the light penetration depth exceeds several μm, and so measurements are dominated by the silicon bulk effects. Similarly, deep bulk penetrating light is used in other methods such as microwave photoconductive decay (μ-PCD) [4], and in the electrochemical method ELYMAT [5] that measures the photocurrent generated in the wafer when it is dipped in HF. The light penetration depth limits usefulness of these methods in extracting information specifically on surface characteristics. Since all of these methods actually measure bulk effects, extraction of information on the degree of surface contamination due to a cleaning process requires an additional thermal process after cleaning. Such a thermal process drives-in the contaminants from the surface into the bulk of silicon, where they can be detected using bulk-sensitive methods. Requirement of an additional processing after cleaning makes these bulk-oriented methods not suitable for the in-line monitoring of the cleaning operations. On the other hand, if a thermal treatment is an integral part of the device manufacturing process (e.g., thermal oxidation) then these methods may be useful in evaluating the entire sequence of operations including cleaning. The only problem is that in this case information concerning malfunction of the cleaning process is obtained after a batch of wafers undergoes irreversible alterations, and hence, the wafers are lost.

The Surface Charge Analyzer (SCA) uses the Surface Photovoltage induced by low intensity chopped illumination (ac-SPV) of the photon energy greater than the semiconductor bandgap [6]. Due to the shallow penetration depth of the incident light (1.5μm), the information extracted from the measurements is dominated by the surface of the wafer. In this technique, the surface characteristics are extracted from the measurements of the magnitude of ac-SPV as a function of externally applied bias. Physical contact of the probe with the wafer eliminates SCA as a in-line metrology tool. It may introduce chemical contamination or particles and cause mechanical damage to the surface. Therefore, SCA measurements are, as a rule, done on the designated test wafers. During measurements, the surface is biased between accumulation and inversion so that variation of the surface potential barrier may reach about 20 kT's (Table I). Such change of the surface potential in the presence of illumination may induce modification of the wafer surface leading to instability of measurements. For this reason, the method performs better when a protective thermal oxide is formed on the wafer. The high

external bias voltage (up to 1000V) required in SCA measurements may also induce ionization of air and deposition of ions on the wafer surface. Combination of contact probe and high voltage limits reproducibility of the measurements particularly in the case of bare wafers. Therefore, while the SCA method was found to be a useful tool in diagnostics of oxidation processes, it has only a limited usefulness in direct evaluation of cleaning processes.

Similar limitation as in the case of SCA may be expected for surface photovoltage (SPV) and Kelvin methods utilizing corona charging of the wafer surfaces. In this approach, the SPV and Kelvin methods are utilized in measuring height of the surface potential barrier by causing its collapse when the wafer is subjected to a high intensity irradiation. The variable corona charge deposited on the oxidized wafer surface modifies the height of the surface potential barrier [7], performing a function similar to the high voltage bias in the SCA method. Under those conditions (corona charge, high intensity illumination) the measurement is invasive, and hence, does not adequately represent the condition of the surface itself.

It follows from the discussion above that none of the electrical methods already described possess the basic features required for in-line monitoring of the cleaning processes. A new generation system, the Surface Charge Profiler (SCP), has been developed to fill this gap.

The Surface Charge Profiler (SCP), similarly to SCA, uses Surface Photovoltage induced by low intensity chopped illumination (ac-SPV) of the photon energy greater than the semiconductor bandgap [6]. Due to shallow penetration depth of the incident light (0.4μm), smaller than in any other method including SCA (Table I), the information extracted from the measurements is dominated by the surface of the wafer. Unlike SCA, the SCP method does not utilize external bias voltage and the probe does not make contact with the wafer during measurement. Instead of measuring the dependence of the ac-SPV as a function of the bias voltage, the surface properties of the wafer are determined from analysis of the real and imaginary components of the ac-SPV signal. The minority carrier surface recombination lifetime is determined from the ratio of the real and imaginary components (equivalent to the signal phase shift). The width of the depletion layer, W_d, is determined from the imaginary component corrected for the lifetime [6, 8]. The width of the depletion layer is used further to calculate total surface charge assuming that the doping concentration at the surface is the same as in the bulk of the wafer. In the case when the wafer surface is under inversion conditions, e.g., due to HF treatment, measurement of the maximum depletion layer width allows determination of surface doping concentration [9].

The SCP performs non-contact and non-invasive characterizations of electrical properties of silicon surfaces, and offers the possibility of direct, in-line monitoring of the wafers as a final step of the cleaning process. The measurement is performed in real-time

in a manner that does not impede the flow of the manufacturing process or the wafer motion. In the SCP system, simultaneous measurements of the surface charge density and the surface recombination lifetime are accomplished by passing the product wafer underneath the measuring probe. These two parameters allow characterization of both static and dynamic properties of the surface - change in the surface charge and modification of the surface recombination properties. While the surface charge is a dominating parameter in SCP applications, in certain cases, depending on the conductivity type of the wafer, the process type, and the type of contamination, only the surface recombination lifetime may be affected substantially, whereas the surface charge remains practically constant. The best results are achieved by considering the surface charge and surface recombination lifetime parameters as being complementary. Measurements of the two parameters could be taken in combination, or one could be emphasized over the other, depending on the specific application.

APPLICATION OF SCP FOR IN-LINE MONITORING OF WAFER CLEANING

In order to validate the use of the SCP system for in-line applications, the response of the SCP system to changes in wet wafer cleaning recipes was investigated. For this purpose, the parameters of various cleaning steps were deliberately altered, and the effect of these changes on the electrical characteristics of silicon surfaces was monitored. Results indicated that the SCP is capable of detecting changes in the process sequence as well as minute changes in the process recipes. As an example, Fig. 2 demonstrates changes of the surface charge vs. time of exposure to ambient air following two RCA-type (SC-1/ Rinse/SC-2/Rinse-Dry) surface treatments in which the only difference was composition of SC-1 clean (H_2O:H_2O_2:NH_4OH; 5:1:1 vs. 5:1:0.25) [10]. The stability of the measurements in the period immediately following cleaning is a good indication of the non-invasive character of the method. Note that differences in the charge resulting from different composition of the SC-1 clean are "remembered" by the wafer after SC-2 treatment, and remain even after prolonged exposure to the ambient air. Similar measurements stability of the SCP method was also reported for the HF treatment [10].

Each step in the cleaning sequence affects the surface in a different and distinctive fashion. The SCP measurements can be used to establish "process fingerprint" and monitor proper performance of each step in the sequence as well as the final outcome of the entire process. The results of the experiment illustrating change in the surface charge resulting from inverting sequence of two steps in the cleaning sequence are demonstrated in Fig. 3. Two n-type wafers from the same lot were subject to the modified RCA cleans. Wafer 1 was treated using SC-1/HF/SC-2 and wafer 2 with the SC-1/SC-2/HF sequence. The resulting charge for these two wafers was not only different immediately after cleaning but has remained different even after 12 hrs after the clean.

Since metal contamination is considered to be one of the most critical factors in IC manufacturing, the influence of heavy metals on the SCP measurements was investigated extensively [2, 11, 12]. It was found that metals such as Fe may affect both the surface charge, Q_s, and the surface recombination lifetime, τ, measured simultaneously using SCP. The results show (Fig. 4) that Fe deposited in SC-1 solution and measured, using TXRF and SCP, after SC-2/rinse/IPA-dry steps introduces negative charge on the surface (total surface charge, Q_s, decreases with increasing Fe concentration) and decreases surface recombination lifetime, τ.

Metallic contamination may affect both the surface charge and surface recombination lifetime. However, use of one or the other of these parameters may be appropriate depending on the measurement conditions itself. A typical example (Fig. 5) illustrating the selective use of one of these two parameters is the monitoring of HF/water treatment of p-type wafers [13]. In this case, the wafer was subjected to the HF/water solution for a very short time (~ 1 second). This treatment resulted in saturating the surface charge and inducing an inversion layer. Further etching of the chemical/native oxide layer did not modify the surface potential barrier (measured as the apparent surface charge). However, the HF etch dramatically affected the surface recombination lifetime, making this a very effective parameter in monitoring the HF treatment of bare p-type wafers including end point determination.

In the case of patterned wafers, the measurement of the front surface represents final averaged outcome of the entire processing sequence, and the effect of a single process step may frequently be not visible. The sensitivity to the single process can be improved by measuring how the single process affects the non-patterned back surface of the wafer. Since the SCP measures width of the semiconductor depletion layer that is dependent only on the atomic properties of the surface, it could be expected that SCP may be useful in monitoring of the cleaning processes by measuring the back surface of the wafer. This capability of the SCP method has been tested [14] comparing changes of the surface charge on the back surface of the wafer, with no mirror-like finish, with the changes of the charge observed for the front surface featuring a mirror-like finish. The surface charge on the front surface was shown before (Fig. 3) to respond with great sensitivity to any alteration of the wet cleaning process. The results shown in Fig. 6 indicate almost identical behavior of surface charge on the front and back surface of the wafer. As seen in this Figure, not only the direction of the observed changes, but also the values of the surface charge on both surfaces are virtually identical. These results indicate that the difference in the physical condition of the silicon surface on the macro-scale (fine-polished vs. rough-polished surface) is overshadowed by the variations of the chemical state of the surface on the atomic-scale. Therefore, the back surface of the wafer can be effectively used to monitor cleaning operations regardless of whether the front surface is patterned or not.

The results described above demonstrate the effectiveness of the Surface Charge Profiler as a new technology for in-line monitoring of cleaning operations used in semiconductor manufacturing.

ACKNOWLEDGMENTS

The author would like to thank Dr. Jerzy Ruzyllo for his helpful discussions and valuable suggestions.

REFERENCES

1. R.C. McDonald, Semiconductor International, July 1995, p. 344.
2. F. Tardif, JP. Joly and D. Waltz, to be published in Proc. Conf. ALTECH 95, Den Haag, The Netherlands, Sep. 28-29, 1995.
3. A.M. Goodman, J. Appl. Phys., 32, 2550 (1961).
4. A.P. Ramasa, H. Jacobs, F.A. Brand, J. Appl. Phys., 30, 1054 (1959).
5. V. Lehmann, H. Föll, J. Electrochem. Soc., 135, 2831 (1988).
6. E. Kamieniecki and J. Foggiato, in Handbook of Silicon Wafer Cleaning Technology, W. Kern, Editor, p. 497, Noyes Publications (1993).
7. R.L. Verkuil and M.S. Fung, Electrochem. Soc. Spring Meeting, Atlanta, May 15-20, 1988, Ext. Abs. 169.
8. Theory of Operation, Surface Charge Profiler, QC Solutions, Inc., Woburn, MA.
9. E. Kamieniecki and J. Ruzyllo, patent pending.
10. E. Kamieniecki, P. Roman, D. Hwang, and J. Ruzyllo, in Proc. Second Intern. Symp. on Ultra-Clean Processing of Silicon Surfaces UCPSS'94, M. Heyns, Editor, p.189, Acco, Leuven (1994).
11. I. Kashkoush, R. Novak, E. Kamieniecki, P. Roman, and J. Ruzyllo, 42nd American Vac. Soc. National Symp., Minneapolis, Oct. 16-20, 1995
12. P. Roman, I. Kashkoush, R. Novak, E. Kamieniecki, and J. Ruzyllo, in this Proceedings.
13. P. Roman, D. Hwang, K. Torek, J. Ruzyllo, and E. Kamieniecki, Proc. Symp. Ultra Clean Semicon. Technol., MRS Meeting, San Francisco, April 1995 (in press).
14. Application Note AN-3, Surface Charge Profiler, QC Solutions, Inc., Woburn, MA (November 1994).

Table I

Photoelectrical methods commonly considered for evaluation of the cleaning processes.

	SPV	μ-PCD	ELYMAT	SCA	SCP
CONTACT	NONE	NONE	HF	MYLAR	NONE
WAVELENGTH	830 ~ 1200 nm	900 nm	670 ~ 820 nm	560 nm	450 nm
LIGHT PENETRATION DEPTH	15 ~ 1000 μm	~ 30 μm	5 ~ 15 μm	1.5 μm	0.4 μm
TESTED REGION	BULK	BULK	BULK	SURFACE	SURFACE
PRETREATMENT REQUIRED	YES	YES	YES	YES	NONE
SURFACE BARRIER VARIATION or INJECTION LEVEL	<kT	MEDIUM to HIGH	HIGH	~20kT	<0.05kT
CLEANING MONITORING (1) THERMAL TREATMENT (2) LIQUID CONTACT (3) PHYSICAL CONTACT (4) SURFACE PASSIVATION - OXIDATION	INVASIVE (1)	INVASIVE (1)	INVASIVE (1), (2)	INVASIVE (3), (4)	NON-INVASIVE

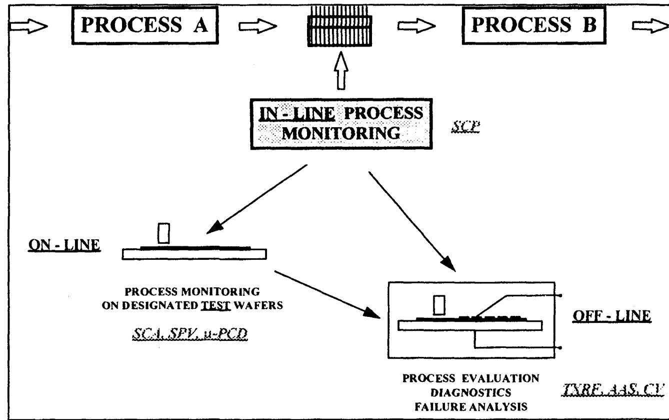

Figure 1. In-line process monitoring strategy.

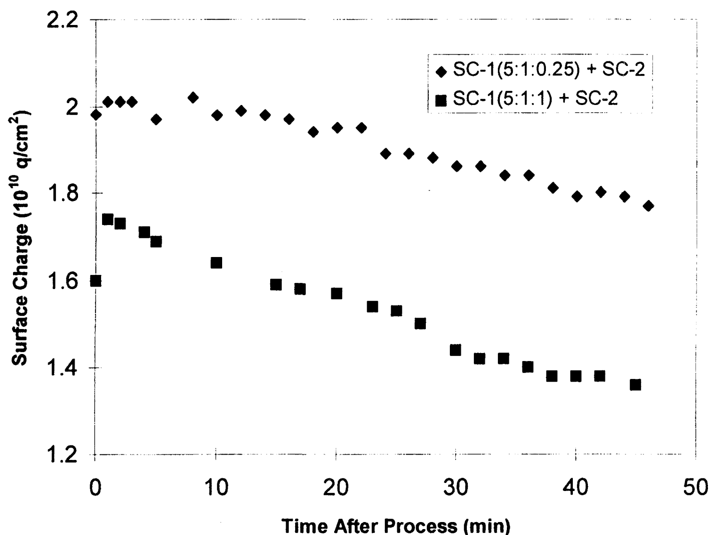

Figure 2. SCP measured evolution of surface charge after SC-1/SC-2 treatments as a function of time of exposure to ambient air.

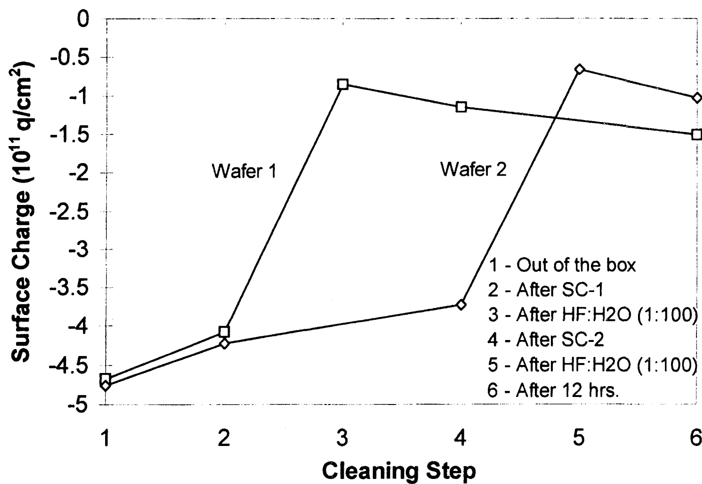

Figure 3. Surface charge after steps in two cleans for n-type Si.

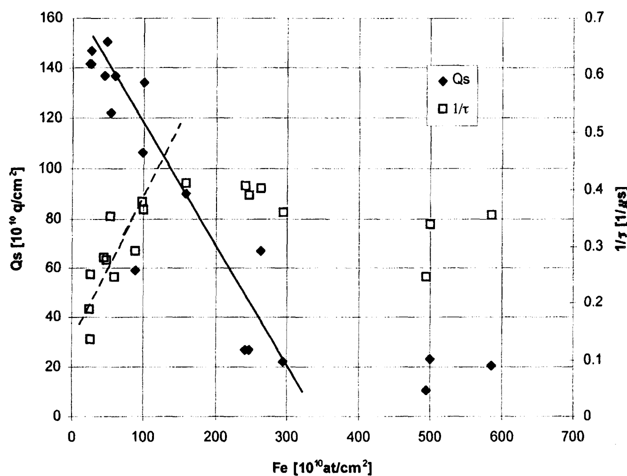

Figure 4. Surface Charge and Surface Recombination Lifetime vs. Fe Surface Concentration (TXRF) after Fe:SC-1/SC-2/Rinse/IPA-Dry steps.

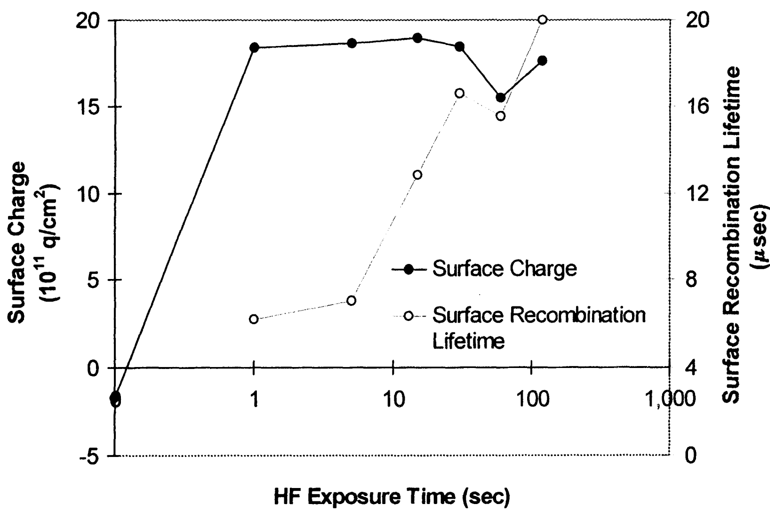

Figure 5. Surface charge and surface recombination lifetime vs. HF(1):H_2O(100) exposure time for p-type Si.

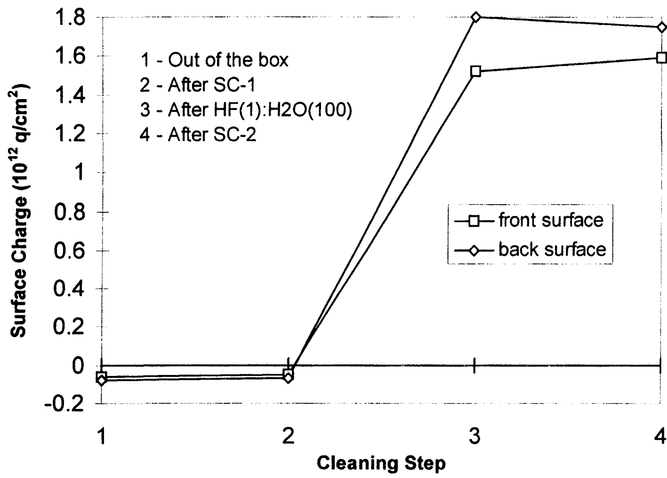

Figure 6. Surface charge after steps in SC-2-last clean for front and back surfaces of p-type Si.

MONITORING OF Fe CONTAMINATION ON Si SURFACES USING NON-CONTACT SURFACE CHARGE PROFILER

P. Roman, I. Kashkoush*, R. Novak*, E. Kamieniecki** and J. Ruzyllo

The Electronic Materials and Processing Research Lab
The Pennsylvania State University, University Park, PA 16802

*SubMicron Systems, Inc.
6330 Hedgewood Dr., #150, Allentown, PA 18106

**QC Solutions, Inc.
150 New Boston St., Woburn, MA 01801

The SCP (Surface Charge Profiler) method is used to monitor the surface Fe concentration on p and n-type Si surfaces following immersion in DI water, SC1 and HF:H_2O baths spiked with various levels of Fe. The system used provides immediate, non-contact measurements of both the surface charge and surface recombination lifetime. Wafers are also analyzed using TXRF (Total reflection X-Ray Fluorescence). It is observed that the surface charge and surface recombination lifetime are responding to the Fe concentrations in solution of less than 0.5 ppb.

INTRODUCTION

Metal contamination on silicon wafers is a major concern in microelectronic manufacturing. Among many metals that can be found in the IC manufacturing environment, iron is the most common impurity. The adverse effect of iron is multifaceted, but most notably iron degrades gate oxide integrity (1,2) and produces charges in the gate oxide (3), as well as degrades the bulk minority carrier lifetimes (4).

It is well known that iron can be added to the silicon surface during wet cleaning operations. Potential sources of Fe contamination during wafer cleaning include chemicals, the DI water and the chemical distribution systems. The detection of iron contamination at this stage is critical for the prevention of further processing of contaminated wafers. Therefore, a method is required that would allow immediate, non-invasive, in-line monitoring of Fe contamination on the bare Si surface following wafer cleaning operations. In this work, a commercial Surface Charge Profiler (5) is evaluated as a tool to monitor the level of Fe contamination on p and n-type wafers following immersion in DI water, SC1 solution and HF:H_2O bath spiked with various levels of Fe.

EXPERIMENTAL

The SCP method used in this study is based on the generation of the ac Surface Photovoltage (SPV) by illumination of the silicon surface with a beam of chopped low intensity light, having a photon energy higher than the silicon bandgap (6). The value of the SPV is related to the density of electric charge accumulated on the illuminated surface. From the magnitude of this signal, the system determines the depletion width and hence, the surface charge. Because low intensity illumination is used in this method, the perturbance of the surface potential barrier during measurement is kept well below room temperature thermal energy, and hence, the surface charge measurement in this case is non-invasive. A schematic diagram of the measurement setup is shown in Fig. 1.

Both p-type (CZ, <100>, 6-9 Ωcm, 100 mm diameter) and n-type (CZ, <100>, 1.32-1.98 Ωcm, 100 mm diameter) silicon wafers were used in this study. Using a commercial cleaning bench, three different solutions were used to add Fe to the wafer surfaces: SC1 (0.2:1:5, 60°C), DI H_2O (45°C) and HF(1):H_2O(100) (25°C). Wafers were dipped in baths that had been spiked with varying amounts of an ICP-MS standard Fe solution to vary the Fe concentration. The Fe concentration in solution was varied from 0 to 30 ppb. Depositions were carried out with a dipping time of 7 min and a DI water rinse time of 2 min, followed by air drying. Immediately after drying, SCP measurements were taken and then wafers were subjected to TXRF analysis.

RESULTS AND DISCUSSION

Iron Contamination from SC1

First, the deposition behavior of Fe in SC1 solution was determined. It was found to be similar to that reported in the literature (Fig. 2). A large deposition is observed, which increases linearly with Fe concentration in solution (except at high concentrations where it saturates). In this solution, the dominant Fe specie is $Fe(OH)_3$ which has a very low solubility limit. Therefore, the Fe precipitates and can deposit at the surface of the substrates due to the effect of van der Waals forces by physical adsorption (7).

The surface charge on the p-type wafers before adding Fe to solution is positive and decreases with increasing Fe concentration in solution (Fig. 3). Significant decrease in charge is observed for very low Fe concentrations below 0.5 ppb. In SC1 solution, the silicon surface is covered with an oxide. The iron at the surface is in oxidation level III. The iron III is easily incorporated in the native oxide (8) in which Silicon is in oxidation level IV. The decrease in charge is explained by hypothesizing that the Fe^{3+} ion is exchanged with Si^{4+} in the native oxide, resulting in a negative charge (3). Increased concentration of Fe on the surface adds negative charge which is responsible for the gradual decrease of the overall charge density (Fig. 3). The charge on the n-type wafer shows relatively little change with Fe concentration in solution. This is due to the fact

that the n-type wafer surface is near accumulation under these conditions, regardless of the surface iron concentration, and the surface charge is near the detection limit of the measurement.

It should be noted that, using the SCP method, the detection of Fe on the silicon surface following SC1 immersion and the rinse/dry process takes place without additional heat treatment aimed at driving Fe into the silicon.

Iron contamination from H_2O

In the second part of this study, the SCP system was used to detect Fe deposited on Si surfaces in DI H_2O spiked with iron. The deposition characteristics were found to be in general similar to those obtained in SC1 solution (Fig. 4). The slight difference between water and SC1 is explained by the difference in ionic strength of these two mixtures. Iron III (Fe^{3+}) precipitates in these media. At first, the precipitated molecules are isolated and neutral, and so can deposit on the silicon surface, which in solution remains negatively charged. But they can flocculate and give negatively charged particles in both of these mixtures (7). Therefore, there is electrostatic repulsion between the particles and substrate. The deposition is higher in SC1 where ionic strength is large, decreasing this electrostatic repulsion.

The surface charge results are also similar to those obtained in SC1 (Fig. 5). As in the SC1, the surface charge on the p-type wafer is initially positive and decreases with increasing Fe concentration in solution. Again, the silicon surface is covered with an oxide and this added negative charge is due to deposited Iron III, Fe^{3+} which is exchanged with Si^{4+} in the native oxide. The charge on the n-type wafer shows more pronounced change with Fe concentration in solution because of the initially less negative surface charge in the case of DI H_2O immersion.

Iron contamination from $HF:H_2O$ 1:100

For p-type Si immersed in the $HF:H_2O$ mixture, only two Fe concentrations in solution were studied (0 and 30 ppb). No Fe deposition was detected at these concentrations. In this mixture, the silicon surface is passivated by Si-H functions which are only slightly reactive except electrochemically (7). Iron is reduced to oxidation level II, but does not deposit as it is stable in Fe^{2+} form which does not precipitate in HF in the studied concentration range.

The surface charge on the p-type wafer has a large positive value and, in agreement with the above observation, remains independent of the Fe concentration in solution (Fig. 6). This result validates results presented above, and further confirms the reliability of the SCP method in the detection of very small amounts of Fe added to the Si surface in cleaning solutions.

SUMMARY

The detection of iron on the Si surface using the Surface Charge Profiler was investigated. The surface charge on the p-type wafers following immersion responds to the very small Fe concentrations in solution (<0.5 ppb) for both SC1 and water. The surface charge remains unchanged by Fe added to solution in HF where no Fe deposition takes place. Therefore, the SCP method can be used effectively for the monitoring of Fe contamination on the Si surfaces inflicted during wet cleaning operations. Due to the features of the SCP method, the monitoring can be carried out in-line on the product wafers. The Fe detection capability of the SCP method at lower surface iron concentrations remains to be determined.

ACKNOWLEDGMENT

The authors would like to thank F. Carillo and J. Phillips at SubMicron Systems for technical assistance in performing the experiments.

REFERENCES

1. T. Roche, S. Adler, R. Cosway, S. Schauer and L. Liu, in this Vol.
2. W. Henley, L. Jastrzebski and N. Haddad, in Cleaning Technology in Semiconductor Device Manufacturing/1993, J. Ruzyllo and R.E. Novak, Editors, **PV 94-7**, p. 487, The Electrochemical Society Proceedings Series, Pennington, NJ (1994).
3. H. Shimizu and C. Munakata, Appl. Phys. Lett., **62**, 276 (1993).
4. G. Zoth and W. Bergholz, J. Appl. Phys., **67**, 6764 (1990).
5. SCP Model 110, QC Solutions, Inc., Woburn, MA.
6. E. Kamieniecki and G. Foggiato, in Handbook of Semicond. Wafer Cleaning Technol., W. Kern, Editor, pp. 497-563, Noyes Publications, New York (1993).
7. L. Mouche, F. Tardif and J. Derrien, J. Electrochem. Soc., **142**, 2395 (1995).
8. R. Takizawa, T. Nakanishi and A. Oshawa, J. Appl. Phys., **62**, 4933 (1987).

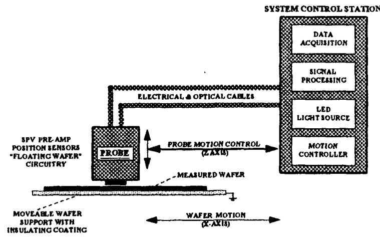

Figure 1 Schematic diagram of the SCP system

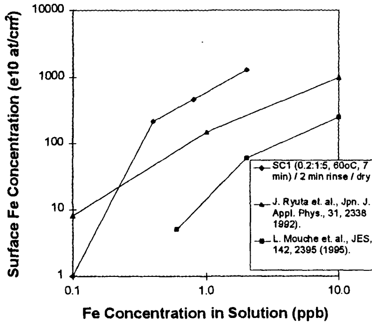

Figure 2 Surface Fe concentration vs Fe concentration in SC1 solution

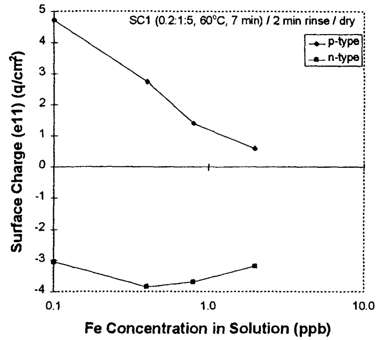

Figure 3 Surface charge vs Fe concentration in SC1 solution for p and n-type Si

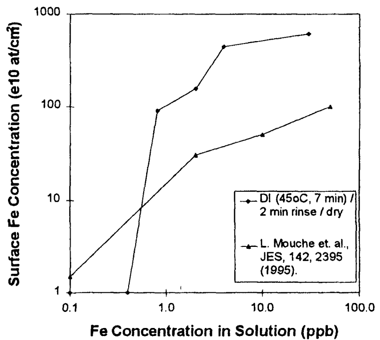

Figure 4 Surface Fe concentration vs Fe concentration in DI water

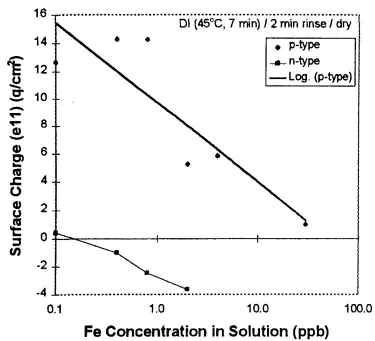

Figure 5 Surface charge vs Fe concentration in DI water for p and n-type Si

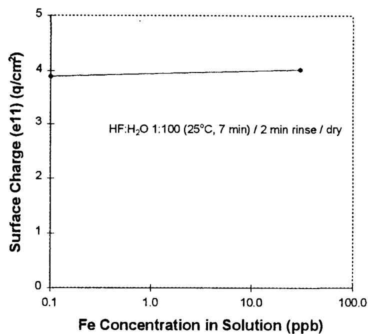

Figure 6 Surface charge vs Fe concentration in solution in $HF:H_2O$ 1:100 for p-type Si

IN-LINE MONITORING OF WET CLEANING PROCESSES USING RADIO FREQUENCY PHOTOCONDUCTANCE DECAY

G. J. NORGA, K. A. BLACK, M. R. BLACK, J. MICHEL, and L.C. KIMERLING

Materials Processing Center, Massachusetts Institute of Technology,
Cambridge, MA 02139

ABSTRACT

We use radio-frequency photoconductance decay (RFPCD) for in-line monitoring of wet silicon wafer cleaning. Today's high bulk lifetime (> 1 ms) CZ material allows high sensitivity detection of surface defects ($<10^8$ cm^{-2}). We perform *in-situ* studies of oxygen chemisorption on HF-passivated silicon and chemical oxide etching in HF. HF-passivated surfaces are stable in nitrogen ambient. Oxygen exposure immediately introduces surface states. We calculate a barrier height for oxygen chemisorption of 1.2 eV. Chemical oxide etching in HF obeys first order reaction kinetics. Using RFPCD in conjunction with TXRF and ICP-MS, we study copper deposition kinetics from HF solutions spiked with 10 - 400 ppb Cu. For the high spiking levels, Cu deposits more readily on p-type than on n-type silicon, consistent with a deposition process limited by silicon dissolution.

INTRODUCTION

Shrinking feature sizes and increases in process complexity have become characteristic trends of silicon IC technology during the last two decades. In today's submicron IC processing, the penalty for yield loss in the final product stage is substantial due to the the sunk costs of hundreds of unit processes. Early detection of contamination during front-end-of-line (FEOL) processes is considered indispensable for increasing both line and die yields. [1] In-line monitoring of process purity depends critically on analysis speed, detection sensitivity and noninvasiveness. Defect identification is desirable, but not essential; in-situ measurements are preferred because they obviate the use of monitor wafers. While non-contact carrier lifetime measurements are widely used for in-line detection of defects and impurities introduced during device processing, their scope has traditionally been limited to the control of bulk purity and perfection. In this paper, we report the use of photoconductance decay to detect silicon surface defects during wet cleaning.

Radio frequency photoconductance decay (RFPCD) measures the decay of excess minority carriers, generated by a light pulse of photon energy greater than the bandgap. An RF-coil, tuned to resonance, picks up the conductivity change of the wafer due to the excess carriers. The time decay curve of the reflected power directly yields the minority carrier lifetime. This lifetime is related to the bulk lifetime τ_b and surface recombination velocity (SRV) s by :

$$1/\tau_{meas} = 1/\tau_b + 2s/d \qquad (1)$$

where τ_{meas} is the measured lifetime and d is the wafer thickness. The surface recombination velocity is given by :

$$s=\sigma N_T v_{th} \quad (2)$$

where σ is the capture cross-section for minority carriers, N_T is the density of surface states (cm^{-2}) and v_{th} is the mean thermal velocity of the carriers.

As shown in Figure 1, the use of high bulk lifetime material permits sensitive measurement of SRV. Today's prime CZ silicon has typical lifetimes in the 5-10 ms range, allowing the measurement of SRV as low as 1 cm/s. In this review, we will demonstrate the use of RFPCD for (1) *in situ* kinetic measurements of chemical oxide etching in dilute HF; (2) reactivity of HF-passivated silicon (Si-H) in different ambients; and (3) in-line detection of metallic contamination during HF cleaning.

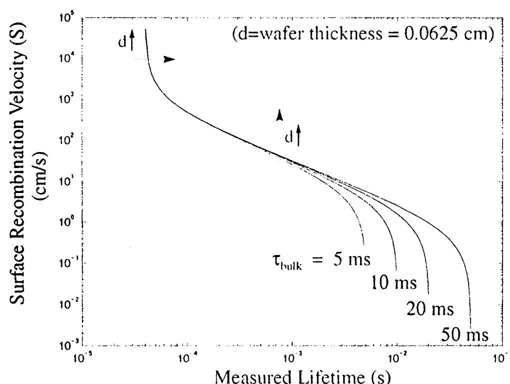

Figure 1 : The effect of wafer thickness, d, and bulk lifetime, τ_b, on the measurement of surface recombination velocity.

EXPERIMENTAL

We have constructed a contactless photoconductance decay apparatus to measure minority carrier lifetime in silicon wafers. The basic concept of this measurement technique is described by Miller *et al.* [2]. A more detailed description of the system used here can be found in references 3 and 4. The low attenuation of the carrier wave (50 -100 MHz) in insulating materials allows remote positioning of the coil outside the process vessel for *in situ* measurement. For enhanced sensitivity to surface defects, *ex situ* measurements are performed in 48 % HF to achieve effective passivation of silicon dangling bonds. [5]

High bulk lifetime (5-10 ms) single side polished CZ Si wafers were used for the experiments. The wafers (125 mm diameter, 625 μm thick, n-type, 11-25 Ωcm; and 150 mm diameter, 675 μm thick, p-type, 10-15 Ωcm) received a preclean consisting of 2 minutes

immersion in 1:100 HF; 4 minutes in 4:1 H_2SO_4/H_2O_2 at 90°C; 30s rinse in deionized water and 2 minutes immersion in 1:100 HF. All chemicals used were Ashland Chemical Gigabit™ grade.

IN SITU MONITORING OF CHEMICAL OXIDE ETCHING IN DILUTE HF

Dilute HF solutions are widely employed to remove chemical and native oxides prior to critical processing steps such as gate oxidation, epilayer growth and contact formation. To achieve complete oxide removal and avoid overetching, in-line control of etch time is essential. *Ex situ* monitoring of HF-treated silicon surfaces using surface charge measurements was reported elsewhere. [6] We present the use of RFPCD for *in situ* monitoring of chemical oxide etching during dilute HF clean.

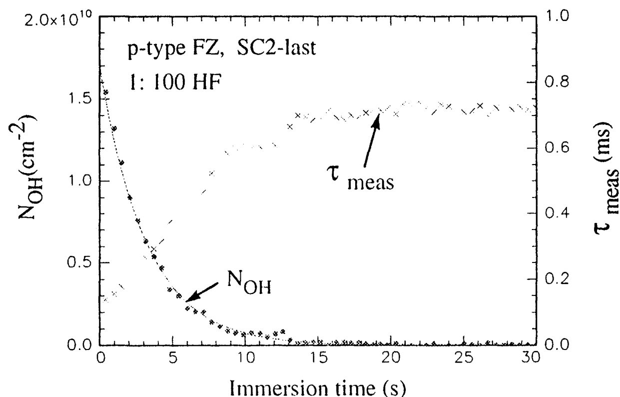

Figure 2 : *In situ* monitoring of oxide etching of an SC2-last, p-type FZ wafer in 1:100 HF. (N_{OH} is the calculated areal density of OH groups terminating the silicon surface.)

A p-type hydrophilic FZ wafer was immersed in 1:100 HF while its lifetime was measured continuously. The buildup of hydrogen passivation can be represented by the following reaction:

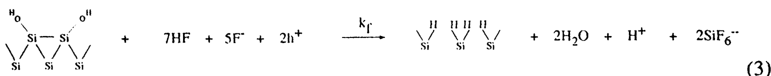

(3)

The polar Si-OH bond disturbs the sp^3 hybridization of the hydrogen passivated surface, creating surface recombination centers in the silicon bandgap. Assuming that surface recombination dominates, the OH coverage can be calculated from the measured lifetime using Eqs. (1) and (2). Figure 2 shows the calculated OH coverage assuming a minority carrier capture cross section, σ_n, of 10^{-15} cm^2. The OH coverage obeys a single exponential decay, indicative of first order reaction kinetics.

MEASUREMENT OF O_2 ADSORPTION ON Si-H

In recent years, the growth of native oxide on HF-passivated silicon has attracted significant research interest. Several studies suggest that H-passivation degrades only slowly in cleanroom ambient. [7-15] XPS studies [8,9] show that a monolayer of oxide is formed after 10 - 12 hours of exposure to cleanroom air. However, the use of a nitrogen ambient during cleaning and N_2-sealing during wafer transfer was reported to significantly lower the contact resistance of W/n^+Si contacts. The general use of controlled ambients during wet cleaning and wafer transfer has been proposed. [7] Free exciton photoluminescence (PL) studies on HF-passivated silicon revealed an immediate change in the PL spectrum when wafers were exposed to oxygen or cleanroom air. [14] The authors concluded that oxygen instantaneously attacks H passivation.

We studied the reactivity of the H-passivated silicon surface in different ambients. An n-type silicon wafer was cleaned and immersed in 48 % HF for RFPCD measurement. The HF immersed wafer was placed in a glovebox which was purged with N_2. Subsequently, the wafer was removed from 48 % HF solution and its lifetime was monitored continuously. Figure 3a shows the temporal change of the minority carrier lifetime. The measured lifetime drops from 6.0 ms, measured in 48 % HF, to 1.8 ms, immediately after exposure to nitrogen. The decrease in lifetime during the first 200 seconds and the ensuing increase is characteristic of wafers passivated in 48% HF. This behavior is not observed for wafers passivated in dilute (1-10 %) HF. After 300 seconds of N_2 gas flow the lifetime is stable. A stable lifetime is also observed when the passivated wafer is exposed to argon.

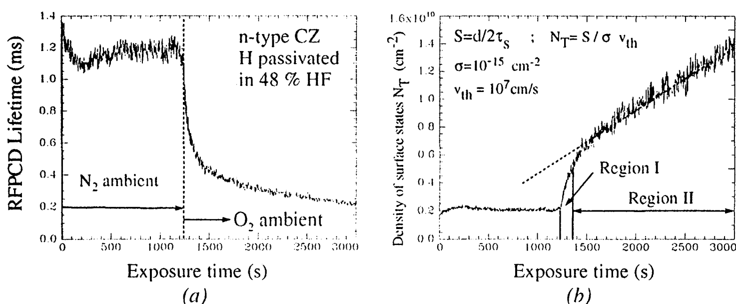

Figure 3 : (a) The effect of oxygen chemisorption on Si(100)-H on RFPCD lifetime and (b) density of surface states of a hydrogen terminated Si (100) surface, calculated from the data in 3a. A high and stable lifetime is measured while the H-passivated wafer is exposed to N_2.

After 1250 sec, the gas supply was switched from N_2 to O_2. An immediate decrease in lifetime is observed. Two kinetic regions were observed: (1) a region of rapid lifetime decrease during the first 40 - 50 seconds of oxygen exposure and (2) a region of slower decrease, lasting more than 10 minutes. The surface state density versus exposure time, assuming a cross section for surface recombination of 10^{-15} cm^2 , is shown in Figure 3b. If we assume that each Si-O bond introduces a single state in the bandgap, then the slope dN_T/dt can be used to calculate the sticking coefficient, f, for O_2 :

$$f = (dN_T/dt) / 2\Phi_0 \qquad (4)$$

where Φ_O, the flux of oxygen molecules impinging on the surface, is given by

$$\Phi_O = p/(mRT)^{1/2} = 6.8\times10^{23}\ cm^{-2}s^{-1} \quad (5)$$

($p = 1$ atm, m = molecular weight of O_2, R = ideal gas constant, $T = 300$ K). From the data shown in Figure 3b, we determine a sticking coefficient $f = 3.5 \times 10^{-18}$ for the slow process. This provides an estimate for the barrier height of the Si-H bond breaking and Si-O bond formation process : $-kT\ln f = 1.2$ eV. This large barrier height for oxygen chemisorption expresses the extraordinary stability of a hydrogen terminated silicon surface compared to bare silicon.

DETECTION OF METALLIC CONTAMINATION DURING HF CLEANING

The impact of metallic contaminants on device yield and reliability is well documented. [16,17] When present in silicon, heavy metals often act as generation-recombination centers, increasing the leakage current of junctions. Due to their high diffusivity and low solubility, they exhibit a strong tendency to precipitate and decorate extended defects, leading to junction shorting. Metals frequently cause deterioration of the gate oxide integrity. [18] Recently contamination by copper and noble metals during HF cleaning has attracted much attention because the dilute HF dip has gained popularity as the last cleaning step prior to gate oxidation. [19], [20]

Metal deposition on silicon from HF solutions is thought to occur by electrochemical outplating, where the electrons are provided by the dissolution reaction of the silicon :

$$M^{z+} + ze^- \longrightarrow M^0 \quad (6)$$

$$Si + 6F^- + 4h^+ \longrightarrow SiF_6^{--} \quad (7)$$

Because the Gibbs free energy of reaction (6) is given by :

$$\Delta G^o = -zFE_o \quad (8)$$

(where F = Faraday constant = 96,500 C/mol and E_o = standard reduction potential of metal), deposition only tends to occur for metals with positive E_o ($\Delta G^o < 0$) such as Cu ($E_o = 0.520$ V).

After cleaning, an n-type wafer was immersed in 1:100 HF and the lifetime measured. After 250 seconds, Cu (1000 ppm in 1% HNO_3, Atomic Absorption Standard) was added so as to obtain a Cu concentration of 10 ppb in the measurement solution.

Figure 5 shows the measured RFPCD lifetime vs immersion time. After approximately 2 minutes immersion, the measured lifetime saturates to a value of 1050 µs. After Cu is added to the solution, the measured lifetime starts to decrease. Spiking the solution with an equivalent amount of HNO_3 *without* Cu yields a stable lifetime, demonstrating that the lifetime degradation is due to the presence of copper ions in solution. We also performed similar spiking experiments with Fe, V and Au, as shown in Table 1. No degradation of the measured lifetime was observed for Fe and V, whereas exposure to the Au spiked solution caused a

remarkable lifetime degradation. These observations are consistent with E_0 values for the different metals .

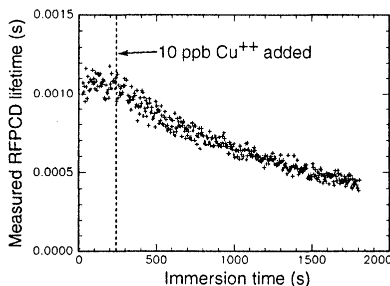

Figure 5 : In-situ detection of copper deposition from 1:100 HF solution.

Using RFPCD in conjunction with TXRF and ICP-MS, we investigated the effect of copper spiking level on surface copper concentration and carrier lifetime. After precleaning, wafers were immersed for 5 minutes in 1:100 HF solutions containing 30, 100 and 400 ppb Cu. Cu levels in solution were determined by ICP-MS. Immediately after the contamination treatment, carrier lifetimes were measured using 48 % HF for passivation. Subsequently, TXRF was performed on 5 locations. TXRF and RFPCD results for these experiments are summarized in Figure 6. At the high spiking level (400 ppb) , copper deposition occurs more slowly on n-type than on p-type material. As expressed by Eqs. (6) and (7), the deposition of copper requires the dissolution of a stoichiometric amount of silicon to maintain charge balance across the silicon/solution interface. Since the dissolution reaction of Si in HF is known to be exceedingly slow [23], silicon dissolution will be rate controlling for high copper levels in solution. Because silicon etching in HF is controlled by the flux of holes to the silicon/solution interface [24], silicon dissolution, and therefore also copper deposition, will occur at a higher rate on p-type material.

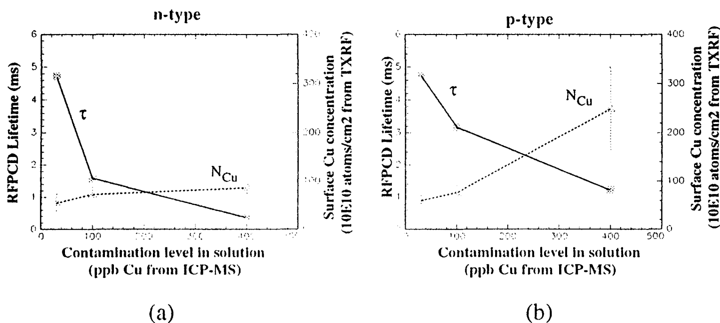

Figure 6 : Effect of spiking level on copper surface concentration and measured lifetime in 48% HF for (a) n-type, and (b) p-type CZ silicon. The error bars of the TXRF data are the standard deviations over the 5 analysis points.

	E_0(V)	τ_{meas}	0.5%HF exposure
Au	1.692	0.028 ms	100ppb, 5 min.
Cu	0.520	0.220 ms	1ppm, 10 min.
Fe	-0.440	5.0 ms	1ppm, 10 min.
V	-1.175	5.0 ms	1ppm, 10 min.

Tabel 1 : Standard reduction potential for the lowest charge state ion, and lifetime response after immersion in spiked 1:100 HF solution. All lifetimes were measured in 48% HF. Prior to immersion in the spiked solution, all measured lifetimes were greater than 5 ms.

SUMMARY

We demonstrated the use of RFPCD for high sensitivity, *in situ* detection of silicon surface reactions. Sensitive detection of surface defects ($N_T < 10^8$ cm^{-2}) is possible provided high bulk lifetime (>1 ms) material is used. We used RFPCD to monitor HF etching of chemical oxide and reactivity of HF-passivated silicon in different ambients. HF-passivated surfaces are stable in nitrogen. Oxygen readily attacks Si-H, increasing the surface recombination velocity. HF oxide etching obeys first order rate kinetics. Because metal deposition from HF solutions increases surface recombination, RFPCD can be used for detection of metallic contamination during wet cleaning. At the higher Cu levels in solution (400 ppb), we measured a higher copper deposition rate on p-type silicon. These observations are consistent with a deposition process which is rate limited by silicon dissolution.

ACKNOWLEDGEMENTS

Technical support from Ashland Chemical (Dublin, OH), Wacker Siltronic (Portland, OR), and SEH America (Vancouver, WA) is greatly appreciated. The authors would like to acknowledge Jieh Shyu, Steve Cheung, Jamie Rose and TS Sriram of Digital Equipment Corporation (Hudson, MA) for useful discussions as well as TXRF and ICP-MS support.

REFERENCES

[1] "SIA Semiconductor Technology - Workshop Working Group Reports", p. 78, Semiconductor Industry Association (1993)
[2] G.L. Miller, D.A.H Robinson, and J.D. Eiley, Rev. Sci. Instrum. 47, 799 (1976)
[3] H. M'saad, J. Michel, J.J. Lappe and L.C. Kimerling, J. Electron. Mat. 23, 487 (1994)
[4] H. M'saad, G.J. Norga, J. Michel, and L.C. Kimerling, AIP Conf. Proc. 306, 471 (1994)
[5] E. Yablonovitch, D.L. Allara, C.C. Chang, T. Gmitter and T.B. Bright, Phys. Rev. Let. 57, 249 (1986)
[6] P. Roman, D. Hwang, K. Torek, J. Ruzyllo, E. Kamieniecki, to be published in the

Proceedings of the Symposium on Ultra Clean Semiconductor Technology (MRS), San Francisco, April 17-19, 1995
[7] M. Morita, and T. Ohmi, Jpn. J. Appl. Phys. 33, 370 (1994)
[8] C. Okada, H. Kobayashi, I. Takahashi, J. Ryuta, and T. Shingyouji, Jpn. J. Appl. Phys. 32, L1031 (1993)
[9] M. Morita, T. Ohmi, E. Hasegawa, M. Kawakami, and K. Suma, Appl. Phys. Lett. 55, 562 (1989)
[10] M. Morita, T. Ohmi, E. Hagesawa, M. Kawakami, M. Ohwada, J. Appl. Phys. 68, 1272 (1990)
[11] B. S. Meyerson, F. J. Himpsel, and K. J. Uram, Appl. Phys. Lett 57, 1034 (1990)
[12] T. Konishi, T. Yao, M. Tajima, H. Ohshima, H. Ito, T. Hattori, Jpn. J. Appl. Phys. 31, L1216 (1992)
[13] D. Gräf, M. Grundner, R. Schulz, L. Mühlhoff, J. Appl. Phys. 68, 5155 (1990)
[14] T. Konoshi, K. Uesugi, K. Takaoka, S. Kawano, M. Yoshimura, and T. Yao, Jpn. J. Appl. Phys. 32, 3131 (1993)
[15] T. Ohmi, M. Miyashita, M. Itamo, T. Imaoka, I. Kawanabe, IEEE Trans. Electron Dev. 39, 537 (1992)
[16] S. Verhaverbeke, M. Meuris, P. W. Mertens, M. M. Heyns, A. Pilipossian, D. Graef, A. Schnegg in : Techn. Dig. IEDM, p 71, IEEE, Piscataway, NJ (1991)
[17] W. Bergholz, G. Zoth, F. Gelsdorf, B. Kolbesen, in: Defects in Silicon II, W. M. Bullis, U. Gösele, F. Shimura, Editors, ECS Proceedings Volume 91-9, p 21, The Electrochem. Soc.Softbound Proceedings Series, Pennington, NJ (1991)
[18] M. Meuris, M. Heyns, W. Kueper, S. Verhaverbeke, A. Philipossian, in: ULSI Science and Technology 1991, J. M. Andrews, G. K. Celler, Editors, ECS Proceedings Volume 91-11, p454, The Electrochem. Soc. Softbound Proceedings Series, Pennington, NJ (1991)
[19] E. Hsu, H. G. Parks, R. Craigin, S. Tomooka, J. S. Ramberg, R. K. Lowry, J. Electrochem. Soc. 139, 3659 (1992)
[20] O. M. R. Chyan, J. J. Chen, H. Y. Chien, *Proceedings of the Second International Symposium on Ultraclean Processing of Silicon Surfaces (UCPSS '94)*, (Acco, Leuven,1994), p. 213
[21] K. Y. Yoneshige, H. G. Parks, S. Raghavan, J. B. Hiskey, P. J. Resnick, J. Electrochem. Soc. 142, 671 (1995)
[22] H. Morinaga, M. Syama, T. Ohmi, J. Electrochem. Soc. 142, 2834 (1995)
[23] G. W. Trucks, K. Raghavachari, G. S. Higashi, Y. J. Chabal, Phys. Rev. Lett., 65, 504 (1990)
[24] R. Mlcak, PhD Thesis, Massachusetts Institute of Technology, September 1994

A METHOD FOR NATIVE OXIDE THICKNESS MEASUREMENT

K. Vepa, K. Baker, L.W. Shive
MEMC Electronic Materials, Inc
501 Pearl Drive, St. Peters, MO 63376

ABSTRACT

A new method of native oxide thickness measurement has been developed. This method is based on extraction of the oxide layer by the acid drop method (10% v/v HF), and then colorimetrically assaying complexed (with Molybdic Acid) silica in the aqueous phase. While the molybdenum-blue method has been known for years and is the preferred method for silica analysis, its application in the current context was limited due to the interference from the fluoride content. We have developed a procedure that minimizes fluoride and phosphate interference through pH control and complexing excess fluorine with boric acid. Then reduction of the silicomolybdate complex with stannous chloride results in a dark blue complex, that is assayed colorimetrically. We discuss the factors that minimize fluoride interference and yield reproducible results. We also compare ellipsometric measurements to thickness derived by this method and demonstrate its utility in wet cleaning of silicon wafers.

INTRODUCTION

Typically native oxide thickness measured by ellipsometry is reported to be around 6 to 12 A (1,2). There is considerable uncertainty in figures reported due to the method of oxide growth and the measurement method (3, 4). Ellipsometry is suitable for homogenous smooth reflective surfaces and SiO_2 thickness greater than (~)20 A. However, reflective losses due to substrate inhomogeneity and surface roughness influence the measurement. Consequently, thinner oxides cannot be reliably measured.

We have developed a method for oxide measurement, by acid extraction of the oxide layer followed by complexation and colorimetric assay of the silicomolybdate complex. Silica determination in water by such methods is well known, and extremely sensitive down to sub-ppm levels (5, 6). However, high fluoride content interferes with silica assay due to competitive reactions with molybdate (6, 7). We discuss the conditions needed to suppress fluoride ion interference to adapt this method for oxide thickness measurements on bare silicon wafers. We also compare this method to ellipsometry

EXPERIMENTAL

Colorimetry. Measurements were made in the visible range with a single beam Hach model DR/2000 spectrophotometer. P- and P+ (<100>) wafers were analyzed for oxide growth. All chemicals used are analytical grade reagents. DI water of 18 MΩ quality was used for all extraction and complexation procedures in Teflon® plastic ware. Blue color measurements were made at the absorption maxima of 750 nm.

The following reagents were used: 4%(w/w) solution of sodium molybdate solution in 0.5N H_2SO_4; 0.5 % (v/v) stannous chloride freshly prepared from 40 % stock solution in con.HCl and stored in amber bottles; saturated solutions of boric acid and sodium bicarbonate; 10 % HF.

Procedure. A 500 μl droplet of HF was used to extract the oxide layer, and this was then neutralized and with sodium bicarbonate solution. Excess fluoride was complexed with boric acid and pH of the mixture adjusted with 10 M H_2SO_4. Then sodium molybdate was added to the mixture and heated, to enhance complexation. The pH was further lowered by addition of 10M H_2SO_4 and stannous chloride added, resulting in a brilliant blue color. This complex is colorimetrically assayed after correcting for background absorbance with a blank. Silica standards were prepared by dilution of a 10000 ppm NIST standard in 10 %(v/v) HF.

Ellipsometry. Measurements were made on a Plasmos SD 1000 instrument at a wavelength of 632.8 nm, at an incident angle of 70°. Native oxide measurements reported are the average of nine spots across an eight inch wafer, with a spot size of 10 μm x 35 μm. Optical constants n_1 of 1.465 and k_1 of 0 for thin silica films (12 A), and n_2 of 3.865 and k_2 of -0.02 for the substrate, were used in a one layer model (8) for determining the native oxide thickness. The method for ellipsometric measurements have been discussed elsewhere (9). All measurements were made within a half hour of the sample drying under clean room conditions. Ellipsometric measurements were made on the same wafers that were subsequently assayed colorimetrically.

RESULTS AND DISCUSSION

Stable silicomolybdate complexes are formed in acidic media (7). However, ionic species such as fluoride and phosphates suppress silicomolybdate formation (6,7). To minimize this interference we had to bind the excess fluoride with boric acid (10,11).

Complexation of Excess Fluoride. Typically at low concentrations of fluorine, silicomolybdate formation is not suppressed. In this instance where HF is required to remove the SiO_2 film, considerable excess HF was present in a 10 % solution that was unreacted. Early on, we found that no color could be formed in the absence of boric acid addition after neutralization.

Effect of Solution pH on Molybdate Complexation. We had to optimize the pH both before and after molybdate addition to minimize blank absorption and suppress interference. Plasticware is a major source of phosphates, which can also cause interference. In Table I, is shown the effect of pH prior to molybdate addition on blue formation of a 10 ppm silica sample. In addition it was also necessary to suppress blank absorbance after molybdate addition by further lowering the pH (7). The blank reading was high when molybdate-complex pH was 2. However, when pH was 0 the blank remained colorless, which is important to improve detection limit. The concentrations of both sodium molybdate and stannous chloride in final solutions were based on results of previous work (7,11).

In Figure 1 is shown a calibration curve in the concentration range of 1 to 100 ppm of silica in 10 % (v/v) HF. It is apparent that the dynamic range and detection limit of this technique for oxide thickness estimation *are comparable if not superior* to ellipsometry. We also find that the calibration curve of the absorbance to silica concentration remains time invariant since we are nulling out the instrument. This is useful particulary in multi-laboratory comparison. Also shown on the second abscissa of this figure is the estimated oxide thickness on 200 mm wafer in the same silica concentration range.

Extraction Efficiency. 500 μl droplets of different HF concentrations were used for repeated extraction of the oxide layer (Table II). The first extraction transferred nearly all the surface silica and the residual absorbance was negligible in comparison. Furthermore, neither HF concentration nor dissolved oxygen content in solution had any effect on the final absorbance values attained.

Applications to Wet Cleaning. Interestingly, repeated wet cleaning of silicon wafers in SC-1 (13) resulted in no change of the oxide thickness (Table III). This data also demonstrates the reproducibility of this method. Finally, it was verified that P- wafers had much thicker oxides as compared to the P+ wafers after SC-1 cleaning (Table IV). This result is not surprising since etch rates and oxidation rates of the two wafers are known to be very different (12).

Comparison to Ellipsometry. In figures 2 and 3 are shown a comparison of the correlation of the absorbances obtained by the extraction procedure to ellipsometry. In both cases, there is a linear relationship between the two methods, in the range of this comparison. However, we found that the estimated thickness by the extraction procedure

was smaller compared to the ellipsometric method. This was similar to previous literature reports on comparison of XPS and ellipsometric data (14). In that instant also the film thickness reported by XPS was found to be smaller than that by ellipsometric measurements. On further analysis, there appears to be a dependence on the film growth conditions to the linear correspondence to ellipsometric data as evidenced by the difference in slopes in the two graphs and also in the film porosity as shown in Figure 4. The lower limit of the sensitivity of this method is also observed in Figure 4, where data for oxides grown in air-ambient on HF-stripped wafers is included. The thickness reported by ellipsometry was around 4 Å. We reason for the lower film thickness estimated by the extraction method is due to its sensitivity to silicon only, and is indifferent to the physical nature of the film.

Assuming that true film thickness to be the optical thickness, we estimated the porosity of films grown under different conditions shown in Figure 4. The dependence of the ambient to native oxide growth is clearly evident from the graph. It is clear that ozone oxides are denser compared to SC1 oxides, and air grown oxides are extremely porous. Measurement on the air-grown oxide was made after approximately 16 to 20 hours after being stripped by 10 % (v/v) solution of HF. The extremely low values of oxide thickness are not surprising, due to the stability of hydride terminated surfaces (15). On comparing the SC1 and ozone grown oxides we observed that resistivity effects were significant in SC1 baths, as already shown in Table IV. However, in the ozone bath, resistivity effect on oxide growth is not observed (difference between P+ and P-), which is indicative of a different oxidation pathway.

SUMMARY AND CONCLUSIONS

We have adapted a well known silica quantification method in wet analysis, for estimation of native oxide thickness, with great accuracy. In addition, we have shown it applicability for cleaning efficacy, and how it may be used to evaluate oxide growth. We have also shown the reliability of this technique and it's correspondence to ellipsometry. Finally, by combining the results of this technique with ellipsometry, we have evaluated the porosity of films grown in different conditions.

ACKNOWLEDGMENTS

The authors thank Bob Crepin and the Application Laboratory group for the ellipsometry measurements. We also thank MEMC Electronic Materials in supporting this work.

REFERENCES

1. M. Morita et.al. Jap. J. App. Phy., **29**, 2392 (1990).
2. M. Morita et. al. Appl. Phys. Lett. **55**, 562 (1989).
3. S. Kao, and R. H. Doremus, J. Electrochem. Soc., **141**,1832 (1994).
4. S.I. Raider et.al., J. Electrochem. Soc.,**122**, 413 (1975).
5. Y. Takaku et.al. J. Anal. Atom. Spectr.,**9**,1385 (1994).
6. R. K. Iler, The Colloid Chemistry of Silica: John Wiley, New York (1979).
7. R. Milton, J. Appl. Chem., **2**, S126, (1951).
8. Shou-Chen Kao and R. H. Doremus, J. Electrochem. Soc., **141**, 1832 (1994).
9. F. Lukes, Phys. Stat. Sol. (a) **93**, 223 (1986).
10. F.A. Cotton, G. Wilkinson, Mordern Inorganic Chemistry: John Wiley, New York (1972).
11. H. Bennet and R. A. Reed, Chemical Methods of Silicate Analysis: Academic Press, New York (1971).
12. H. Seidel et.al., J. Electrochem. Soc., **137**, 3626 (1990).
13. Kern, D.A. Puoteien, RCA Review,187 (1970).
14. S.I. Raider et. al., J. Electrochem. Soc. **122**, 413 (1975).
15. M. Morita et. al., Appl. Phys. Lett. **55**,(6), 562 (1989).

Table I. Effect of pH on Silicomolybdate Formation

Solution pH*	Blue Absorbance @
4.89	0.084
2.5	0.171
1.6	0.281

*pH of solution measured on addition of H_2SO_4, after boric acid step. The blank was then complexed (NaMo).
@ Absorbance measured at 750 nm.

Table II. Extraction Efficiency

Sample #*	HF Conc in % (v/v)	Absor- -bance
1	10	2.02
1	10	0.07
2	30	2.02
2	30	0.06
3	10 (degassed)	1.91
3	10 (degassed)	0.04
4	30 (degassed)	2.33
4	30 (degassed)	0.06

Table III. Effect of Repeated SC-1 Wet Cleaning on Oxide Thickness*

Wafer #	Run #	Absorbance
1	1	1.30
2	1	1.35
3	2	1.34
4	2	1.35
5	3	1.35
6	3	1.35

* Two wafers per cleaning run were analyzed after SC-1.

Table IV. Native Oxide Thickness*

Wafer Type	Absorbance
P-	2.02
P+	1.18

*The average value of repeated measurements after wet cleaning

APPENDIX

Conversion of Absorbance to Thickness

Vol to Density Calculations	Value	Units	Notes
density of fused quartz	2.20	gm/cc	CRC handbook
Area of 200 mm =	314.16	cm ^2	
1A =	1.00E-08	cm	
Vol per A of SiO2	3.14E-06	cm^3	
Mass per A of SiO2 =	6.91E-06	gm	based on fused quartz
Extraction volume =	0.50	ml	
Conc of 1 A =	13.82	ppm	(M/V)*10^6

Porosity Calculation

In figure 4, porosity was calculated as follows:

$p = \{(t_{ellip} - t_{abs})/t_{ellip}\} \times 100$

where p is porosity, and t is thickness in A

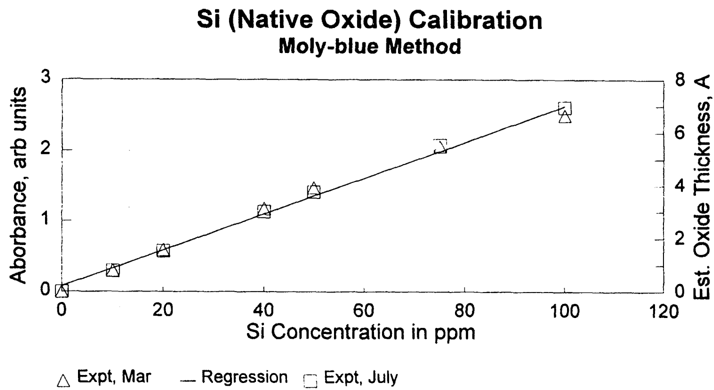

Figure 1. Absorbance calibration curve with NIST Si standards. (■) is a calibration run in March, and (▲) was run in July, to demonstrate the time invariance of the calibration.

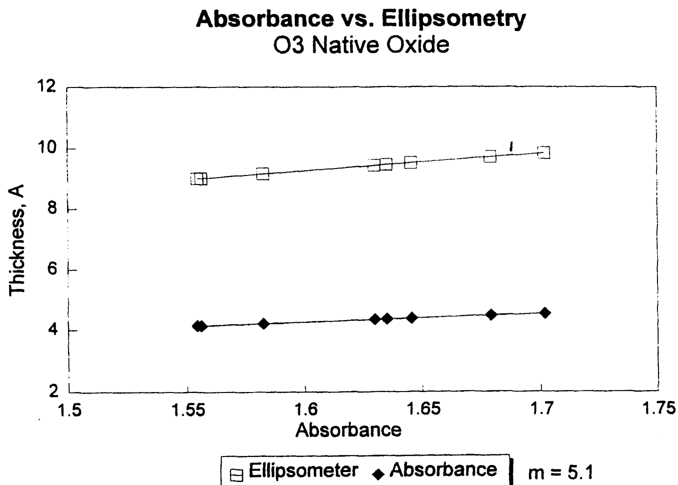

Figure 2. Comparison of ellipsometric and absorbance measurements for native oxide thicknesses, grown in an ozone ambient. The slope of line 1 (□) is 5.1.

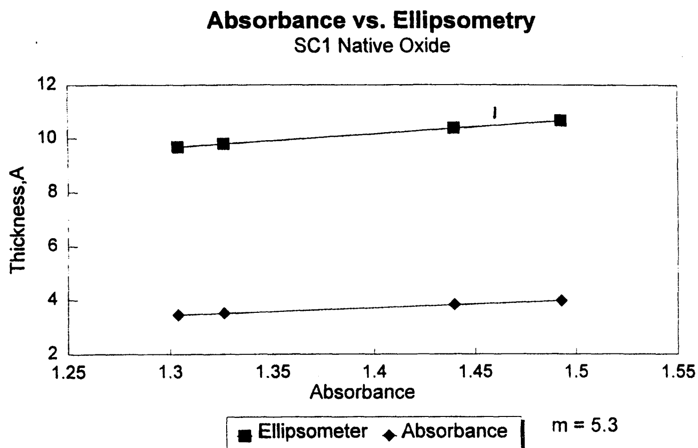

Figure 3. Comparison of ellipsometric and absorbance measurements for native oxide thicknesses, grown in SC1 ambient. The slope of line 1 (■) is 5.3.

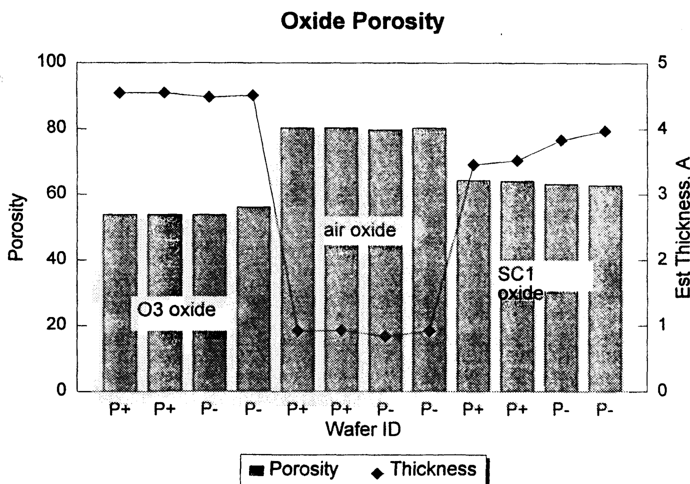

Figure 4. Estimated oxide porosity of oxides grown in different ambients. Also shown is the corresponding film thickness estimated from absorbance measurements.

CHEMICAL OXIDE CHARACTERIZATION

C. Paillet*, J.P.Joly and F. Tardif
GRESSI LETI (C.E.A), CEN/G,17, Rue des Martyrs
F-38054 Grenoble Cedex 9, France

K. Barla, P. Patruno, D. Levy,
*SGS/THOMSON Centre Commun F-38290 Crolles

The different oxidant cleaning steps leave a chemical oxide presenting different physico-chemical properties. It is very important for these characteristics to be known as it is widely acknowledged that critical processes depend on the final cleaning bath. Moreover, it is interesting for certain processes to adjust the quantity of oxide (poly emitter process for exemple). This paper deals with the optic thicknesses as measured by ellipsometry obtained with the different usual cleanings including ozonized mixtures and their chemical cohesion in terms of HF etching resistance.

EXPERIMENTAL

P-type <100> 100 mm wafers were first cleaned for 10 minutes in different oxidant cleaning mixtures such as : sulphuric peroxide mixture, nitric acid, ammonia peroxide (SC1 0.25/1/5), hydrochloric acid peroxide (SC2 1/1/5), peroxide in D.I. water, ozonated D.I. water, and finally D.I. water containing 1.5 ppm of dissolved oxygen.

MEASUREMENTS

A Rudolph FE III automatic ellipsometer was used to determine the thicknesses of the different oxides. The thickness was measured immediately after cleaning in order to avoid the impact of reoxidation and/or organic deposition on the wafers. Furthermore, the ellipsometer was calibrated at zero thickness with a freshly deglazed wafer. Nevertheless, the data obtained has to be considered as being relative due to the lack of standards in the very low range of thicknesses. However, only a slight shift was recorded for thin oxides during a cross-calibration campaign between TEM (Transmission Electronic Microscopy) and ellipsometer.
A home-made assembly comprising a conventional microscope was used for contact angle measurements. Microroughness was measured by an AFM Nanoscop III (Digital Equipment).

OXIDE THICKNESS

Various chemical oxides were analyzed, from conventional cleaning processes such as SC1 (0.25/1/5), SC2 (1/1/5), H_2O_3 30%, SPM mixtures and from other new cleanings such as DI water and sulphuric acid ozonated baths.

As is now well known, ozone can be used as oxidant instead of H_2O_2 as its electrochemical potential is higher (+2.07 instead of 1.78V). Ozone was injected via multiple holes at the bottom of a static bath to reach saturation at bath temperature (2 ppm at 20°C).
Figure 1 summarizes the various thicknesses obtained for the different cleaning treatments as measured by ellipsometry. It can be noted that the thickness values given by the ellipsometer for almost all the samples are quite close : between 0.6 and 1 nm. We can assume that chemical oxide quickly forms a layer impermeable to oxidant species. Nevertheless, a logical increase of the thickness is observed when the bath temperature is increased. The highest values were found for the two oxidant species in water : H_2O_2 and ozone (3 ppm), and the lowest values were found for D.I. water alone. The lower thicknesses from SPM 2/1 than from SPM 3/1 seem due to the higher decomposition rate of H_2O_2 in concentrated baths. The combination of D.I. water and ozonated D.I. water enables the whole range from 0.1 to 1 nm to be covered.

CHEMICAL COHESION OF OXIDES

A chemical oxide etch rate in 0.1% HF at 20°C is used to differentiate between the different chemical oxides. By ellipsometric measurements we verify that chemical oxides are homogeneous. As shown in figures 2 and 3, the oxide thickness decreases linearly with the etching time in HF.
Contact angle measurements on these oxides show large variations. The difference of chemical resistance could be attributed to a difference of chemical structure. For sulphuric peroxide cleanings (figure 4) no difference of resistance to HF can be seen in terms of the H_2SO_4/H_2O_2 ratios but a large difference can be seen according to the bath temperature : the higher the temperature, the higher the resistance. However, for the SC1, SC2 and ozonated D.I. water baths (figures 5 and 6), the process temperature has hardly any influence. The highest etching resistances are given by SPM mixtures at 140° and ozone in D.I. water. For oxidation obtained in water, etching is instantaneous.

SURFACE ROUGHNESS

Characterization of oxide cleanings by AFM measurements shows very little variations except for hydrogen peroxide/sulphuric acid cleanings which give larger roughness especially for temperatures between 90 and 120°C (figure 7). These high values can be explained by the behavior of these cleanings as a function of initial surface roughness. With SPM mixtures, when the surface is initially smooth, roughness is increased, whereas on the other hand when the surface roughness is initially high the surface is smoothed. As previously reported (1) SC1 and SC2 cleanings degrade the surface in all cases.

CONCLUSION

The oxide thicknesses after cleaning can be only slightly adjusted by varying the bath temperature. The different chemical oxides obtained by the cleaning baths present very different resistance behaviors to HF etching, the more resistant being sulphuric/peroxide cleanings.

REFERENCES

(1) K. Nakamura, T. Futatsuki, K. Makihira and T. Ohmi ECS proceedings vol 94-7 pp. 70-77.

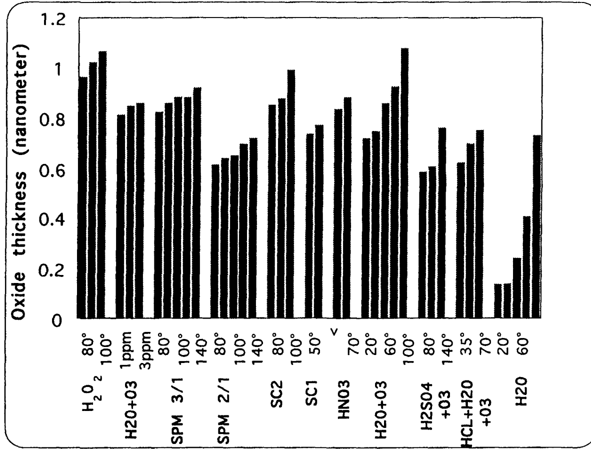

Fig. 1 : Oxide thicknesses obtained after different cleaning treatments as measured by ellipsometry (Rudolph FE III)

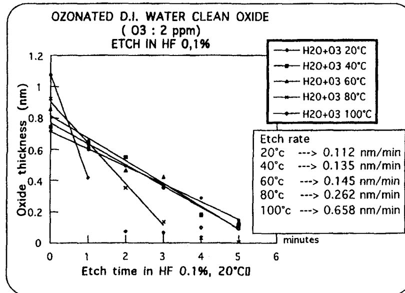

Fig. 2 : Oxide thickness evolution as measured by ellipsometry (Rudolph FE III) of ozonated DI water treated wafers, etched in 0.1% HF

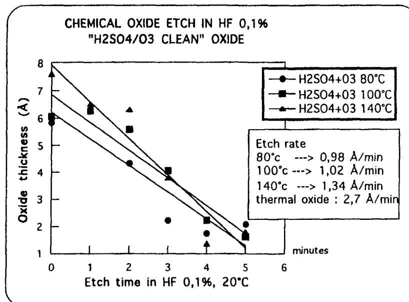

Fig. 3 : Oxide thickness evolution as measured by ellipsometry (Rudolph FE III) of hydrogen/peroxide treated wafers, etched in 0.1% HF.

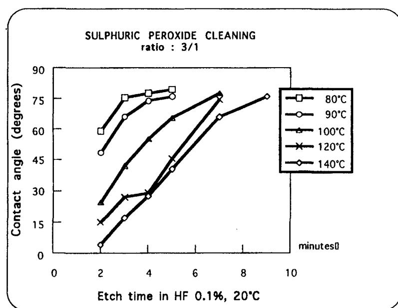

Fig 4 : Contact angle evolution due to 0.1% HF etching of the oxide left by sulphuric peroxide cleaning (ratio 3/1) for different temperatures

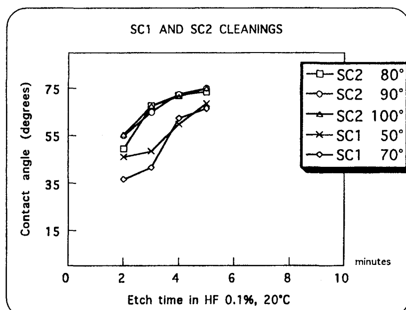

Fig 5 : Contact angle evolution due to 0.1% HF etching of the oxide left by SC1 and SC2 cleanings.

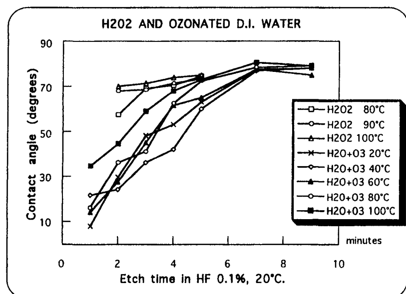

Fig 6 : Contact angle evolution due to 0.1% HF etching of the oxide left by H_2O_2 and ozone in D.I. water.

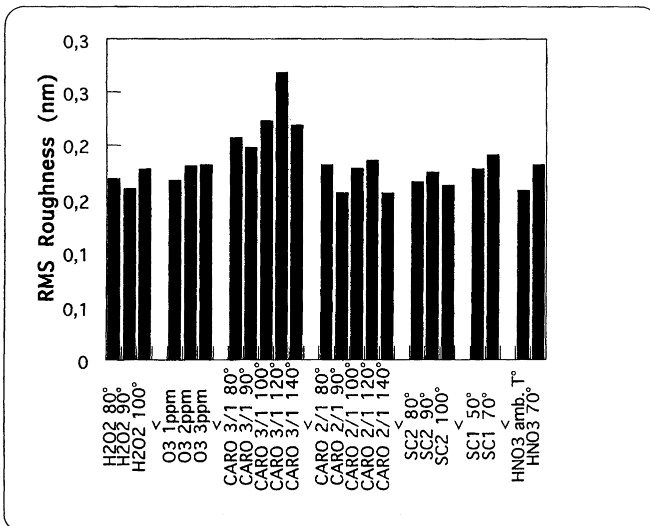

Fig 7 : Roughness of silicon by AFM measurements after various cleanings.

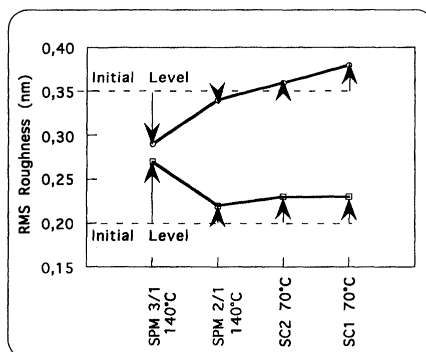

Fig 8 : Impact of cleanings on silicon roughness as a function of initial surface roughness.

CHARACTERIZATION OF SILICON OXIDE ETCHING IN GAS PHASE HF/VAPOR MIXTURES

Anthony J. Muscat, A. Scott Lawing, and Herbert H. Sawin
Department of Chemical Engineering
Massachusetts Institute of Technology
Cambridge, MA 02139

and

Jeff Butterbaugh, Dan Syverson, and Fred Hiatt
FSI, International
322 Lake Hazeltine Drive
Chaska, MN 55318

The objective of this work was to determine the correct coverage metric to use for gas phase etching of silicon oxide in mixtures of anhydrous HF and water vapor. The oxide film thickness was monitored in real time using *in situ* ellipsometry, and the relative concentrations of O, C, and F atoms after etching were measured using XPS. Measurements of pump down times after processing and film thicknesses on silica and sapphire suggest that etching occurs by a Langmuir-Hinshelwood mechanism. The etching rate response surfaces generated from a design of experiments study confirm this hypothesis by showing that the fraction of the saturation vapor pressure of both HF and water at the processing temperature is the correct metric to use for the surface coverages. Oxygen and fluorine atoms remained on the surface after every etching run, and the amount of carbon was unchanged.

INTRODUCTION

Gas phase cleaning processes may be required for the next generation of microelectronic devices built on a quarter micron design rule (1). The liquid phase cleaning technology now in use will not be acceptable for some processes because surface tension effectively excludes the etchant in an aqueous solution from small openings like contact holes and vias to underlying layers. Moreover, wet etching requires chemical baths which lack vacuum compatibility, hence can not be integrated with other processes in a single clustered system (2). These factors combined with stricter disposal regulations will accelerate the adoption of gas phase cleaning.

HF/vapor etching has been proposed as a replacement for liquid HF etching to remove oxide prior to silicon epitaxy and gate oxide growth (3, 4, 5). The reaction is thought to occur in a condensed vapor film on the surface (6), and the decrease in the etching rate with temperature observed experimentally (5, 7, 8) has been cited as evidence

for a liquid-like etching mechanism. This study was undertaken to better understand the etching mechanism, in particular to find the correct metric to scale the surface coverages of HF and water. The results of our Box-Behnken design of experiments study show that the etching rate response surfaces have the same functional form between 26 and 55 °C, when the fraction of the saturation vapor pressure of both HF and water is used to scale the surface coverages. This scaling removes the temperature dependence of gas adsorption from the surface reaction and shows that *increases* in the etching rate with temperature are possible. Using absolute partial pressures, instead, convolutes the temperature dependence of gas adsorption with that of the surface reaction and produces a monotonic decrease in the etching rate with temperature.

EXPERIMENTAL

The etching experiments were carried out in a stainless steel ultrahigh vacuum apparatus connected to a sample transport system for vacuum transfer. Samples were introduced via a load lock into the reactor module which had a base pressure between runs of 2×10^{-7} Torr. The load lock and the reactor were pumped using separate turbomolecular pumps. Metered amounts of anhydrous HF, water vapor using a nitrogen carrier, and dry nitrogen were introduced into the reactor via a temperature controlled gas handling system. The water bubbler and the gas handling line leading to the reactor were kept at the reactor processing temperature. The remaining gas handling lines and the mass flow controllers were kept at a fixed temperature of 65 °C to prevent condensation. The total pressure in the reactor was measured using a heated-filament capacitance manometer and fixed at 250 Torr for all of the etching runs reported. The exhaust gases were fed to a mechanical pump via a liquid nitrogen trap to remove condensables. Pressure control was accomplished using a throttle valve connected to set point electronics.

Oxide thicknesses were monitored in real time during each run using an *in situ* ellipsometer. The oxide films were prepared by conventional thermal techniques on 150 mm wafers which were diamond cut into 10 x 10 mm samples. Each sample was immersed for 60 s in aqueous 3:1 H_2SO_4:H_2O_2 (piranha), rinsed for 60 s with DI water, immersed for 30 s in 1:9 aqueous HF, rinsed again for 60 s with DI water, and blown dry with nitrogen. Storing the samples in a glass petri dish for at least one day prior to etching was found to give better reproducibility than using the samples immediately after the wet pretreatment. Dry nitrogen and the nitrogen/water vapor mixture for the run were used to pressurize the reactor to 250 Torr and maintained for 10 minutes. Etching of the oxide films which were nominally 3600 Å thick was initiated by flowing HF into the reactor. The change in the film thickness as a function of time was measured using an ellipsometer (J. J. Woollam M44) at 40 different wavelengths. The HF was run for 60 s at which time the chamber was exhausted of the process gases and all flows were stopped. After reaching a pressure in the 10^{-7} Torr range after 5-10 minutes, the sample was transferred under vacuum to an analytical chamber and X-ray photoelectron spectroscopy (XPS) was done.

HF and water vapor pressure fractions were chosen in the range from 1.5 to 4% and

10 to 25%, respectively, to complete a 17 run Box-Behnken design of experiments study. Response surfaces were generated using a quadratic fit of the resulting etching rates. The etching rate values are averages calculated by dividing the change in film thickness by the time needed to clear the oxide or by the total 60 s etching time if the oxide was not cleared. Endpoint was monitored in real time using the *in situ* ellipsometer.

RESULTS AND DISCUSSION

Experimental measurements of pump down times and film thicknesses suggest that a condensed film is not required to sustain oxide etching. Thinning of a condensed film on the oxide surface has been proposed in the literature to explain the drop in the etching rate with temperature (5, 7, 8). Pump down times to reach the 10^{-7} Torr range from the operating pressure of 250 Torr were on the order of 5-10 minutes after HF/water processing between 26 and 55 °C. Adsorption experiments using water vapor alone near its saturation vapor pressure lengthened the pump down time to 20 minutes or more and produced hangup in the 100-200 mTorr range. The times to reach the operating base pressure are inconsistent with the evaporation of a thick condensed water layer on the surfaces of the reactor and piping. Measurements of the water adsorption isotherm at 30 °C on silica using the *in situ* ellipsometer show a break near a saturation vapor pressure fraction of 0.6. The increase in slope or the amount of water adsorbed on the surface after this point suggests that this value marks the transition from monolayer to multilayer adsorption. A similar measurement using HF and water vapor is not as straightforward to make on silica because etching changes the underlying oxide thickness, but sapphire which is not etched by this mixture can be used. The ellipsometric signal for sapphire surfaces exposed to mixtures of HF and water vapor was constant with time which indicates that a condensed film did not form. These observations suggest that oxide etching proceeds by adsorbed HF and water molecules coming together on the surface, that is by a Langmuir-Hinshelwood mechanism.

The Langmuir-Hinshelwood mechanism expresses the dependence of the reaction rate, r, in terms of a single rate coefficient, k, and the surface concentrations of the adsorbates, here θ_{HF} and θ_{water}, as

$$r = k\, \theta_{HF} \theta_{water}\ .$$

The temperature dependence of the surface reaction is contained in the rate coefficient, which is usually expressed as the product of a pre-exponential factor and an exponential that includes the activation energy and temperature. The temperature dependence of adsorption is contained in the coverage terms, which are functions of the fraction of the saturation vapor pressures of each component. The surface coverages in a reaction that proceeds by a Langmuir-Hinshelwood mechanism can consequently be controlled using the saturation vapor pressure fractions of each component. Scaling the coverages with these fractions instead of with the absolute partial pressures decouples the temperature dependence of the surface reaction from the temperature dependence of adsorption. This hypothesis was tested by performing a Box-Behnken design of experiments using temperatures between 26 and 55 °C, HF fractions between 1.5 and 4%, and water fractions between 10 and 25% as variables. The resulting fit to the data was used to generate

response surfaces for the etching rate and XPS ratio.

The highest oxide etching rates for processing temperatures between 26 and 55 °C and a total pressure of 250 Torr occurred at intermediate pressures of HF and water in the intervals studied. The response surface in figure 1 was generated from a quadratic fit of the experimental design data and displays the oxide etching rate in Å/s at 26 °C as a function of the amount of HF and water admitted into the reactor expressed as a percent of the saturation vapor pressure, % p^o_{sat}, at the processing temperature. The response surface shows that the highest etching rates at approximately 200 Å/s occurred at intermediate HF and water fractions near 3% and 18%, respectively, not at the richest fractions used. Moreover, the etching rate varied more strongly with the water fraction than with the HF fraction. For process feed gas lean in both water and HF, the etching rate dropped sharply to approximately 70 Å/s. Otherwise, the rate dropped off more gradually from the maximum toward the limits of the reduced pressures studied.

The response surface at 40 °C has the same functional form as at 26 °C except that the etching rates are lower (figure 2). The etching rate exceeded 170 Å/s for HF and water fractions near 3% and 18%, respectively, of the saturation vapor pressures at 40 °C. These vapor pressure fractions represent absolute partial pressures of 47 Torr of HF and 10 Torr of water inside the reactor. The balance to reach a total pressure of 250 Torr was nitrogen. The highest etching rates were observed at intermediate HF and water fractions as at 26 °C. The drop in the etching rate at 40 °C has been reproduced experimentally, but it is not yet completely understood. One possibility is loss of control over the water partial pressure delivered to the system because of entrainment in the carrier stream. Although this condition was observed in particular instances, the bubbler and gas delivery tubing were checked carefully and no evidence for a condensate was found after an etching run.

The etching rate rose when the temperature was increased to 55 °C using the vapor pressure fractions to scale the gas phase concentrations (figure 3). The response surface at 55 °C has the same functional form as at 26 and 40 °C except that the etching rates are higher at comparable reduced pressures. The etching rate exceeded 290 Å/s at 55 °C for HF and water fractions near 3.5% and 18%, respectively, of the saturation vapor pressures for these compounds. This rate corresponds to the removal of over 70 silicon oxide layers every second, but the HF flux needed at the surface to sustain this rate is on the order of 10^{18} molecules/cm^2/s or an effective pressure of only 10^{-2} Torr. The vapor pressure fractions represent absolute partial pressures of 83 Torr of HF and 21 Torr of water at 55 °C. The high gas phase water concentration needed at this temperature did not extend pump down times which were on the order of a few minutes.

The etching rate response surfaces indicate that the vapor pressure fraction is the correct metric for the surface coverage. The vapor pressure fractions over which the etching rates between 26 and 55 °C reach their highest values are approximately the same (figure 4). Moreover, the functional shape of the response surfaces are the same: sharp drop off toward lean fractions, more gradual decent toward richer fractions. These observations are seen most easily by comparing the 2D projections shown on the floor of each plot. The equivalent shape of these curves indicates that the surface coverage is the

same throughout the temperature range from 26 °C to 55 °C at a given HF and water fraction. The vapor pressure fractions consequently establish the surface coverages of HF and water on the silicon oxide surface. Fixing the vapor pressure fraction fixes the surface coverage regardless of temperature.

We postulate that water adsorption on silica further polarizes a Si–O bond facilitating the rupture of the H–F molecule. Water adsorbed on oxide has a bond energy of 40-80 kJ/mole (9). This relatively strong, but nondissociative adsorption bond strength suggests that the underlying Si-O bonds are weakened by adsorbed water molecules. The weakening is brought about by the polar H^+-O^--H^+ water molecule which further polarizes a Si^+-O^- bond. The increased polarity overcomes the energy barrier to breaking the strong H-F bond. Etching occurs by the sequential insertion of the polar H^+–F^- into O^--Si^+ fluorinating Si and leading to new Si-F and O-H bonds, as depicted below. Neither water

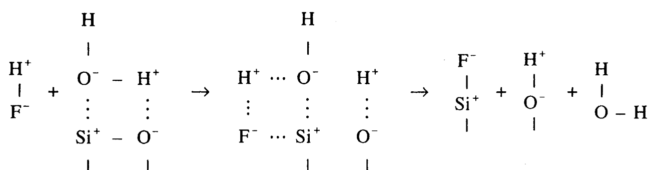

nor HF alone can etch oxide near room temperature, but the two in combination ultimately produce SiF_4, which is volatile, by repeating the proposed reaction. Understanding the reaction mechanism has practical applications since the gas introduction and pumping requirements are more stringent when operating in the condensation regime.

Vapor phase etching in HF/HOH left residual oxygen and fluorine, but did not change the surface carbon concentration. The response surface plot for the oxygen to silicon XPS peak ratio at 40 °C is shown in figure 5. The XPS spectra were recorded before and after etching in a separate chamber that was accessible by vacuum transfer. The highest O coverages remained after etching in lean HF/water mixtures due to incomplete removal of the film during the fixed HF processing time. The lowest coverages corresponded with the vapor pressure fractions at which the highest etching rates were observed. The fluorine XPS response surface (figure 6) shows a similar trend. The fluorine concentration rises toward the HF/HOH lean portion of the plot but was relatively insensitive to surface concentration at this temperature. The carbon XPS response surface (figure 7) was relatively constant as would be expected for a process that does not directly utilize carbon. All etching runs made using water vapor left residual oxygen on the surface in submonolayer quantities, which could have an impact on the utility of this process for contact cleans prior to forming barrier layers and pregate cleans.

CONCLUSIONS

The vapor pressure fractions of HF and water were shown to be the correct metric by which to scale the surface coverages for gas phase etching of silicon oxide. Further

polarization of the Si-O bond caused by water adsorption is proposed to facilitate breaking of the strong H-F bond, which leads to the sequential insertion of HF into Si–O bonds producing SiF_4. The reaction sequence proposed occurs in a single layer, or at most multilayer, on the surface, in contrast to the literature which assumes that a condensed layer is required to sustain etching. Pump down times and film thickness measurements as well as the adsorption bond strength of water on silica support the proposed mechanism. The high reactant flux available in a liquid phase is not required to produce the high etching rates observed in our study since an HF pressure of only 10^{-2} Torr at the surface can sustain an etching rate exceeding 290 Å/s. Oxygen and fluorine atoms remained on the surface after every etching run, and the amount of carbon was unchanged.

ACKNOWLEDGMENTS

We gratefully acknowledge support for this project from FSI, International and from NIST (Advanced Technology Program) via FSI.

REFERENCES

1. R. A. Bowling, S. C. O'Brien, L. M. Loewenstein, M. H. Bennett and B. K. Bohannon, Sol. State Tech., **January**, 61 (1994).

2. Y. Ma, M. L. Green, L. C. Feldman, J. Sapjeta, K. J. Hanson and T. W. Weidman, J. Vac Sci. Technol. B, **13**, 1460 (1995).

3. A. Izumi, et al., in *US Patent #5,022,961* (Dainippon Screen Mfg. Co., Ltd., USA, 1991).

4. A. E. T. Kuiper and E. G. C. Lathouwers, J. Electrochem. Soc., **139**, 2594 (1992).

5. K. Torek, J. Ruzyllo, R. Grant and R. Novak, J. Electrochem. Soc., **142**, 1322 (1995).

6. C. R. Helms and B. E. Deal, J. Vac. Sci. Technol. A, **10**, 806 (1992).

7. J. Ruzyllo, K. Torek, C. Daffron, R. Grant and R. Novak, J. Electrochem. Soc., **140**, L64 (1993).

8. H. Watanabe, H. Kitajima, I. Honma, H. Ono, R. J. Wilhelm and A. J. L. Sophie, J. Electrochem. Soc., **142**, 1332 (1995).

9. G. J. Pietsch, U. Kohler and M. Henzler, J. Vac. Sci. Technol. B, **12**, 78 (1994).

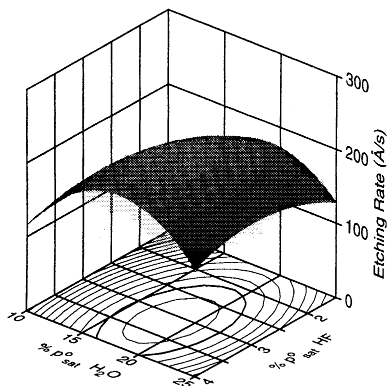

Figure 1: 26 °C etching rate response surface. The axes on the floor of the plot are scaled using the saturation vapor pressure fractions of HF and water.

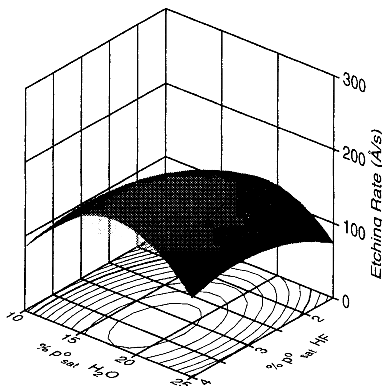

Figure 2: 40 °C etching rate response surface. The axes on the floor of the plot are scaled using the saturation vapor pressure fractions of HF and water.

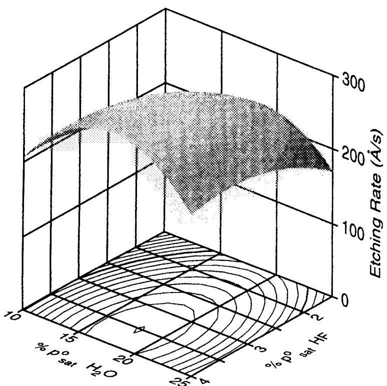

Figure 3: 55 °C etching rate response surface. The axes on the floor of the plot are scaled using the saturation vapor pressure fractions of HF and water.

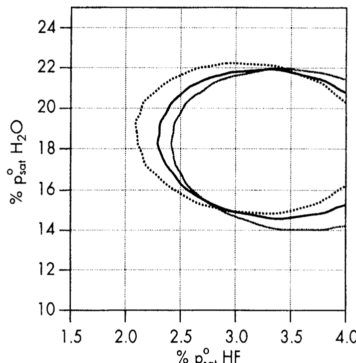

Figure 4: Maximum etching rate contour.

-------- > 200 Å/s at 26 °C

.... > 160 Å/s at 40 °C

——— > 260 Å/s at 55 °C

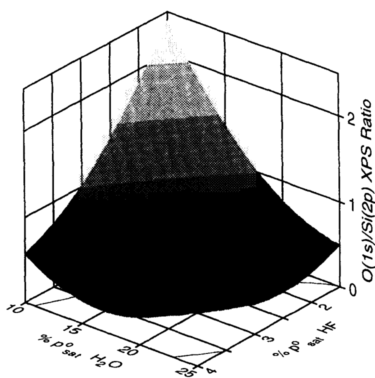

Figure 5: 40 °C O(1s)/Si(2p) XPS response surface after processing.

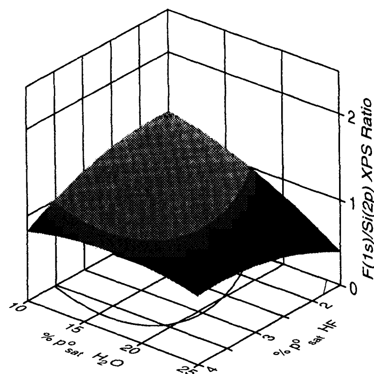

Figure 6: 40 °C F(1s)/Si(2p) XPS response surface after processing.

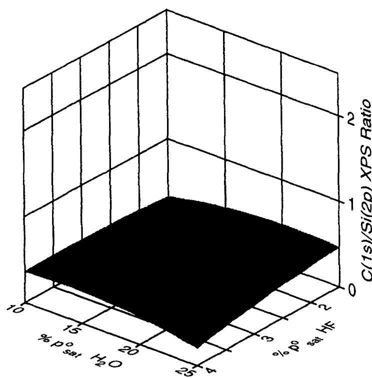

Figure 7: 40 °C C(1s)/Si(2p) XPS response surface after processing.

THE APPLICATION OF SURFACE ANALYSIS TECHNIQUES FOR MONITORING HYDROGEN TERMINATION CLEANING PROCESSES

Ronald A. Carpio and Burt W. Fowler
SEMATECH, Austin, TX 78741

Vasu Atluri and Nicole Herbots
Arizona State University, Tempe, AZ 85287

Philip R. Brierley
PIKE Technologies, Madison, WI 53719

ABSTRACT

The applications of attenuated total reflection-Fourier transform infrared spectroscopy, spectroscopic ellipsometry, surface wetting, and ion beam techniques for monitoring processes used to create hydrogen-terminated silicon (100) surfaces are discussed. A technique for preserving H-passivated surfaces during transport is described. Different HF/alcohol oxide etch solutions and alcohol rinses were compared to standard HF/H_2O cleans. Aqueous HF and HF/methanol solutions provided the most hydrogen termination. Ethanol and isopropyl alcohol rinses reduced adsorbed water and organic contamination during wafer transport. A new accessory was used to perform infrared spectroscopy on whole silicon wafers.

INTRODUCTION

Cleaning techniques used in integrated circuit (IC) manufacturing must be able to prepare chemically passivated silicon (Si) surfaces prior to growing epitaxial Si films and silicon dioxide (SiO_2) layers. Standard cleans (SC1 and SC2) used throughout the microelectronics industry leave a chemical oxide on the surface approximately 15 Å thick. Metal and hydrocarbon contamination must be removed and a smooth Si surface obtained prior to fabricating thin gate dielectrics by thermal oxidation, and all surface SiO_2 must be removed before growing high-quality epitaxial layers to eliminate crystalline defects. This can be done by thermally desorbing the oxide at temperatures ≥ 950°C. However, the current trend in IC manufacturing is toward low-temperature processing. To eliminate the high-temperature thermal desorption step, the chemical oxide can be removed with hydrofluoric (HF) acid. Both aqueous and vapor-phase HF techniques are used for this purpose. Vapor-phase cleaning is the subject of a companion paper in this conference [1], and is of special interest since such cleaning modules can readily be clustered with gate oxide and epitaxial reactors to eliminate exposure of the Si surface to air after the final passivation step [2,3]. The HF treatment leaves the Si surface terminated with hydrogen (H), which can be removed at temperatures of ~550°C. Hydrogen-passivated surfaces are strongly hydrophobic but are susceptible to particle contamination [4,5]. Complementary metal oxide semiconductor (CMOS) devices are fabricated on Si (100) surfaces to reduce the charge state density at the interface between the gate oxide and epitaxial Si. Whereas Si (111) surfaces can be made topographically smooth using HF-based treatments, it is more difficult to achieve this for Si(100) surfaces [6-8].

This paper addresses the use of optical, ion beam, and surface wetting techniques for monitoring Si (100) H-passivation processes involving HF/H_2O and HF/alcohol wet treatments. In this study, concentrated aqueous HF (49 wt%) was diluted with methanol, ethanol, and isopropyl alcohol, and these mixed solvent systems were used in the oxide etch step to generate H-passivated Si (100) surfaces. The hydrogen

passivation was characterized and compared to that obtained with a standard aqueous HF etch. In addition, different post-etch rinses using pure alcohol and deionized (DI) water were compared. Infrared (IR) spectroscopy was used to monitor residual carbon (C), adsorbed H_2O, and the relative amounts of silicon hydride (SiH_x) species after transporting four-inch, P-, Si (100) wafers receiving a modified RCA clean [9] followed by an HF/alcohol oxide etch and a rinse in either deionized (DI) H_2O or alcohol. The HF/alcohol concentration and the etch time were varied. The same type of alcohol was used in the etch and rinse steps. Wafers were immediately put into single-wafer carriers which were then heat-sealed in laminated, aluminized bags to reduce exposure of the passivated wafer surface to ambient during overnight transport. Ideally, the complete cleaning and bagging process should be done under N_2 ambient. It was found, however, that purging the single-wafer carriers and the bags during the sealing procedure with N_2 from a hand-held blower was adequate to preserve the surface for IR analysis. The stability in air of H-terminated surfaces after standard wet HF processing and 950°C H_2 annealing were compared using ellipsometry.

INFRARED SPECTROSCOPY

Multiple reflection techniques, such as attenuated total reflection-Fourier transform infrared (ATR-FTIR) spectroscopy, have been used extensively for characterizing H-terminated Si surfaces. These measurements provide detailed information on the nature of silicon hydride (SiH_x) bonding and hydrocarbon (CH_x) contamination. The vibrational assignments for the SiH_x bands have been published in several sources, the most recent being that of Y. Ogata *et al.* [10]. The integrated areas of the SiH_x stretching peaks provide a measure of the hydrogen coverage, and the relative amounts of monohydride (SiH), dihydride (SiH_2), and trihydride (SiH_3) bonding can be related to the surface topography [7,8]. Detecting hydrocarbon contamination can be difficult if the reference sample has similar amounts of contamination [11]. Special precautions, such as using a UV/ozone clean, can be taken to insure that the reference is free of organic contamination.

Implementation of ATR-FTIR has, in most cases, been achieved by beveling small Si pieces to form a trapezoid [12]. A similar multiple reflection structure can be formed by masking and etching techniques [13]. Recently, the use of p-polarized grazing angle reflection for H-passivation studies has been reported [14,15]. A germanium (Ge) crystal clamped against the Si surface to make optical contact can also be used [16,17], and this approach was adopted for this work. The key parameter controlling the spectral response is the optical contact between the Ge crystal and the Si wafer, which is affected by the applied pressure, wafer flatness, and particulates. The existence of surface irregularities will prevent perfect optical contact from being realized [18]. Using a pressure plate to apply high pressure will reduce the width of any air gaps. However, if adequate and reproducible contact is not made with the Si surface, it will be difficult to obtain quantitative data, as reported in the case of polymer studies [19].

A new accessory designed and manufactured by PIKE Technologies was used to make IR measurements on whole Si wafers ranging in size from 100 to 200 mm without breaking the wafer or performing any special processing to create a multiple reflection element. To the best of our knowledge, this is the first report of ATR-FTIR measurements on whole silicon wafers without special preparation. The accessory was installed in the sample compartment of a Nicolet Model 800 Infrared Spectrometer equipped with a liquid-N_2-cooled, narrow-band, mercury-cadmium-telluride detector. A 4 cm^{-1} resolution was employed and 256 scans were co-added. The samples were referenced against a wafer coated with a chemical oxide. Because the Ge crystal can be contaminated or scratched over time, and due to issues involving making reproducible contact, the best comparisons were obtained for measurements performed on the same day and with the same experimental conditions.

By using p-polarized radiation with a 60° Ge ATR element, components perpendicular to the surface are preferentially excited [16]. Figure 1 shows that the intensity enhancement obtained using p-polarization was approximately a factor of 2.4. These spectra were taken from a wafer that received an SC1

clean (H_2O:H_2O_2:NH_4OH, 20:4:1) at 80°C followed by a 1:50 HF:H_2O dip for 30 seconds. The trihydride peak, occurring at 2140 cm^{-1}, is quite prominent and the dihydride peak at 2108 cm^{-1} shows peak splitting.

Figure 2 shows ATR-FTIR spectra of a wafer that received a wet clean and HF/H_2O dip followed by a 950°C anneal in 100 Torr of H_2 for 30 seconds (top spectrum) and a wafer that was not annealed (bottom spectrum). The spectrum of the annealed wafer only has a narrow monohydride peak at 2088 cm^{-1}, indicating that the Si surface has undergone 2×1 reconstruction [13]. For the non-annealed wafer, a large absorption mode occurs near 900 cm^{-1}, corresponding to the SiH_2 scissors mode [10].

SPECTROSCOPIC ELLIPSOMETRY

An estimate of the reoxidation kinetics of H-passivated Si(100) surfaces can be made using spectroscopic ellipsometry [20]. The stability of hydrogen-terminated Si surfaces under ambient conditions is dependent on the surface orientation and extent of flatness [7,21]. Figure 3 shows the virtual oxide thickness as a function of time for two HF-dipped wafers (1:40 HF:H_2O for 30 seconds) with and without a 950°C H_2 anneal as measured using a Woollam Variable Angle Spectroscopic Ellipsometer (VASE [22]) operating over the range from 240 nm to 1000 nm. The "virtual" nature of this measurement arises from the neglect of surface roughness and the fact that the oxide was modeled as SiO_2. The similar slope changes for the two wafers indicates that the reoxidation process is similar for both types of surfaces. The initial portion of the curve is linear, followed by a second growth region having a different slope. Based on the initial, linear portion of the curve, the oxidation rate for the aqueous HF process was 0.018 Å/min and that for the H_2 annealed surface was 0.014 Å/min. These rates are similar to the average rate of 0.024 ± 0.007 Å/min obtained by Beechinor *et al.* for Si(100) surfaces after a 30-second 1:10 HF:H_2O dip [20].

Spectroscopic ellipsometry in the mid-IR range can potentially be used for in-line or *in situ* process monitoring since it is a non-contact measurement. There is also no need to use a reference spectrum. It has been shown that SiH_x modes can be detected using IR spectroscopic ellipsometry after a single reflection off the Si surface [15]. ATR-FTIR has been performed *in situ* in the laboratory during HF-based oxide etching [23], but the complications relating to using a multiple reflection element *in situ* may restrict its use to in-line monitoring. Experiments are now in progress to assess the ability of mid-IR spectroscopic ellipsometry to monitor H-passivation processes.

SURFACE WETTING MEASUREMENTS

Changes on Si and SiO_2 surfaces can be measured by wetting measurements. The contact angle of water droplets on H-terminated Si surfaces is sensitive to oxide, hydrocarbon and fluoride contamination [4,24]. The procedure used for this study is similar to that used by Utani *et al.* [25], where a droplet of water of constant volume is placed on the Si surface, and the sample tilted until the droplet falls off. A new tilting stage manufactured by PIKE Technologies was used. The tilt angle where the drop rolls off, Θ, decreases and the contact angle increases with an increase in the amount of H-passivation. Multiple 35 and 50 μl drops were typically placed on the diameter along the tilt axis. A linear dependence was observed between drop volume and tilt angle for H-passivated surfaces. The smaller drop volume produced the better sensitivity, but 50 μl drops were better for measuring hydrophilic surfaces. The tilt angle measurement is a low-cost technique that is less subjective than a contact angle measurement. The technique worked best for well-passivated surfaces where the droplet was well-beaded. For surfaces with significant amounts of oxide, instead of rolling off when the sample was tilted, the droplet spread-out prior to tilting and slid down the surface, leaving behind a visible water track.

NUCLEAR RESONANCE ANALYSIS

Ion beam techniques provide a quantitative measure of the total amounts of surface oxygen (O) and C. Using nuclear resonance analysis (NRA) in the ion channeling mode at a beam energies 3.05 and 4.27 MeV provides increased sensitivity for detection of O and C, respectively [9,26]. Surface hydrogen can be measured relative to a polystyrene standard by the elastic recoil of helium at 2.8 MeV. This technique cannot, however, determine whether the H is bonded as SiH_x or CH_x, but could be used to calibrate IR spectra in the absence of organic and moisture contamination. This points to more research needed in the areas of developing H-passivation standards for ion beam analysis and correlating total H, O, and C concentrations with the relative contributions of all IR spectral peaks involving these elements. Another calibration approach being evaluated is using SiO_x films containing various amounts of SiH_x groups, which can readily be characterized with NRA [27].

ALCOHOL PROCESSING STUDIES

Different HF/alcohol etch treatments and alcohol rinses were studied for their ability to remove chemical oxides, to H-passivate Si (100) surfaces, and to protect etched surfaces from ambient conditions. The types of alcohols studied were methanol (MeOH), isopropyl alcohol (IPA), and ethanol (EtOH). Using alcohol during the passivation step provides the ability to vary the OH^- radical and dissolved oxygen concentration, which are known to affect the oxidation kinetics of H-passivated surfaces [7,8,28], and is expected to aid the creation of a uniform, oxide-free surface since alcohols are effective wetting agents. Fenner *et al.* [29] obtained surfaces with low C and O contamination using a spin etch with HF-alcohol reagent and Kinosky *et al.* [30] found that a two-step etching process using HF/H_2O followed by HF/MeOH eliminated haze on epitaxial Si layers grown at very low temperature. This same, two-step clean was used by Lai *et al.* [31] to improved the dielectric integrity of thin gate oxides. Garrido *et al.* [32] found that HF/EtOH etches resulted in smoother Si (100) surfaces as compared to HF/H_2O etches. During HF-based oxide etching, SiH_xF_y species are present on the Si surface [23]. Most of these species remaining after the wet treatment may volatize quickly, leaving a minimal amount of F on the surface. If oxidation or Si deposition is to begin immediately after the HF etch and passivation step, a rinse may not be needed [30,31]. It is important to minimize rinsing in DI H_2O since this reduces H-passivation and etches Si (100) surfaces [7]. However, after an HF-based oxide etch, the H-passivated surface is susceptible to particulate contamination during transport in the clean room ambient and during reactor pump down [4,5]. Using alcohol-based rinses may reduce the uptake of airborne particles and can reduce the re-oxidation rate of H-passivated surfaces by decreasing the amount of physisorbed water on the surface. Physisorbed water molecules undergo dissociative chemisorption on silicon to form Si-OH and Si-H groups, and the Si-OH sites act as adsorption sites for additional water molecules and result in further oxidation [33]. This makes it important to investigate rinses other than those involving DI water.

Typical p-polarized FTIR spectra of wafers receiving a cleaning sequence consisting of SC1 + HF:H_2O (1:50) + SC2 + HF:MeOH (1:9) + MeOH steps are shown in Figure 4. The top spectrum is from a wafer after the SC1 and HF/H_2O steps. The dihydride peak is split into symmetric (2105 cm^{-1}) and anti-symmetric (2114 cm^{-1}) peaks, and the trihydride and monohydride stretching peaks are clearly present. These distinct features are lost after the SC2 clean (center spectrum). However, the surface H was not totally removed during the chemical oxidation process. The large peak at 2260 cm^{-1} is due to overlapping O_xSiH_y modes [17,34]. The bottom spectrum is typical of wafers dipped in HF/MeOH. The dihydride peak is no longer split as was the case for aqueous HF, but instead appears as a single peak at 2111 cm^{-1}.

Figure 5 shows that HF/H_2O and HF/MeOH etching solutions produce the most H-passivation. The HF/alcohol concentrations were 1:9 and the etch time was 1 minute in all cases. Five-minute rinses in alcohol or DI H_2O reduced the overall H-passivation compared to a quick DI H_2O rinse. Figure 6 shows that rinsing in EtOH and IPA can reduce organic contamination and H_2O physisorption as compared to

rinsing in MeOH. The wafer etched in HF/MeOH and rinsed in MeOH (top spectrum) shows pronounced H_2O peaks in the 3000 to 3600 cm^{-1} region and CH_x peaks near 2900 cm^{-1} as compared to the EtOH- and IPA-processed wafers which have nearly identical spectra.

Additional studies are in progress to explain these findings, but it is known that the use of mixed solvents such as water/MeOH modify the acidic or basic strength of the solvent and also change the dielectric constant of the solution. The wetting properties and the solubility for oxygen are also modified. Alcohols such as MeOH and EtOH are amphiprotic, and the main effect of adding them to water is to weaken molecular and anionic acids. The dissociation constant of HF will depend primarily on the basic properties of this mixed solvent. Two reactions must be considered

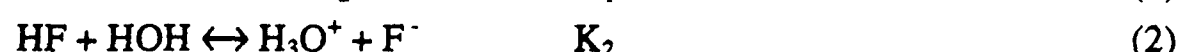

$$HF + ROH \leftrightarrow ROH_2^+ + F^- \qquad K_1 \qquad (1)$$

$$HF + HOH \leftrightarrow H_3O^+ + F^- \qquad K_2 \qquad (2)$$

where R stands for a alkyl group. The ratio K_1/K_2 will depend upon the basic strengths of the alcohol, ROH, and water. The dielectric constants and the autoprotolysis constants for the solvents of interest are listed in Table I [35]. Water behaves as both a stronger acid and a stronger base than MeOH and EtOH. The alcohols will show less tendency than water to protonate the very weakly basic fluoride ions in solution. The HF equilibria in aqueous HF solutions has been studied by Judge [36]. The net effect of the presence of an alcohol will be to modify the HF equilibria, which in turn controls the creation of SiH_x bond formation. This modification of acid/base equilibria is illustrated in non-aqueous titrations used in analytical chemistry [37]. More research is need to determine the effects of various alcohols on the dissociation constant of HF. Once dissociated, F^- can react with HF to form HF_2^-, which is thought to play a role in the uniformity of SiO_2 etching [38]. It has recently been proposed that H_2F_2 produced by the dimerization of HF may also etch SiO_2 [38]. Using alcohol to control the relative concentrations of HF, F^-, HF_2^-, and H_2F_2 during oxide etching may produce Si (100) surfaces that are smoother and less prone to particulate contamination.

CONCLUSIONS

ATR-FTIR spectroscopy was used to measure the degree of H-passivation on Si (100) surfaces after etching in three types of HF/alcohol solutions. Post-etch rinses in pure alcohol were compared with a standard water rinse. Aqueous HF and HF/MeOH etching solutions were found to provide more H-termination than HF/EtOH or HF/IPA. Rinsing in pure EtOH or IPA reduced hydrocarbon contamination and H_2O adsorption during overnight transport. Using spectroscopic ellipsometry, it was found that a 950°C anneal in H_2 did not significantly effect the re-oxidation kinetics of Si (100) surfaces etched in aqueous HF. ATR-FTIR spectroscopy provided the most specific information on H-passivation. More research and development is needed regarding the use of HF/alcohol mixtures in the etching of SiO_2 and the use of IR spectroscopic ellipsometry to provide a non-contact, in-line process monitor for H-passivation processes.

Table I. Dielectric constants and autoprotolysis constants for the solvents used.

Solvent	Dielectric Constant	pK_{auto}
Water	78.5	14.0
Methanol	32.6	16.7
Ethanol	24.3	19.1
Isopropyl Alcohol	18.3	

REFERENCES

1. J. S. Martin, J. M. Barnett, P. A. Grothe, R. A. Carpio, and B. W. Fowler, this proceedings (1995).
2. D.C. Frystak, J. Albone and P. Rumaine, "*Proceedings of the 1994 Advanced Semiconductor Manufacturing Conference*", IEEE/SEMI, Cambridge, MA, Nov. 14-16, p.28 (1994).
3. M. L. Green, Y. Ma, D. Brasen, and B. J. Sapjeta, "*Proceedings 3rd International Rapid Thermal Processing Conference, RTP'95*", R. B. Fair and B. Lojek editors, p. 141 (1995).
4. S. Verhaverbeke, J. Alay, P. Mertens, M. Meuris, M. Heyns, W. Vandervorst, M. Murrell, and C. Sofield, Mat. Res. Soc. Symp., **259**, 391 (1992).
5. V. B. Menon and R. P. Donovan, "*Proc. 1st International Symposium on Cleaning Technology*", ECS 1989, p. 167, Vol. 90-9 (1989).
6. K. Utani and S. Adachi, Jpn. J. Appl. Phys., **32**, 3572 (1993).
7. G. S. Higashi, Y. J. Chabal, K. Raghavachari, R. S. Becker, M. P. Green, K. Hanson, T. Boone, J. H. Eisenberg, S. F. Shive, G. N. DiBello, and K. L. Fulford, ULSI Symposium, 1993 Spring ECS (1993).
8. Y. J. Chabal, Mat. Res. Soc. Symp., **259**, 349 (1992).
9. V. Atluri, N. Herbots, S. Bhagvat, S. Whaley, R. Carpio and B. Fowler, 1995 Spring ECS (1995).
10. Y. Ogata, H. Niki, T. Sakka and M. Iwasaki, J. Electrochem. Soc., **142**, 195 (1995).
11. H. Bender, S. Verhaverbeke, and M. M. Heyns, J. Electrochem. Soc., **141**, 3128 (1994).
12. G. S. Higashi, Y. J. Chabal, G. W. Trucks and K. Raghavachari, Appl. Phys. Lett., **56**, 656 (1990).
13. O. Vatel, S. Verhaverbeke, H. Bender, M. Caymax, F. Chollet, B. Vermeire, P. Mertens, E. Andre, and M. Heyns, Jpn. J. Appl. Phys., **32**, L1489 (1993).
14. M. Nishida, M. Okuyama and Y. Hamakawa, Appl. Surface Science **79/80**, 409 (1994).
15. B. Drevillon "*Applications of Spectroscopic Ellipsometry to Thin Film Characterization*" to be published in World Scientific, 1995.
16. C. Bjorkman, M. Fukuda, T. Yamazaki, S. Miyazaki and M. Hirose, Jpn. J. Appl. Phys., **34**, 722 (1995).
17. L. Ling, S. Kuwabara, T. Abe, and F. Shimura, J. Appl. Phys., **73**, 3018 (1993).
18. S. D. Stuchebryukov and V. M. Rudoy, Vibrational Spectroscopy, **4**, 95 (1992).
19. R. W. Snyder and S. J. Fuerniss, Applied Spectroscopy, **46**, 1113 (1992).
20. J. T. Beechinor, P. V. Kelly, G. M. O'Connor and G. M. Cream, "*Proceedings of the Second International Symposium on Ultra-Clean Processing of Silicon Surfaces (UCPSS'94)*", M. Heyns, M. Meuris, and P. Mertens, editors, Acco Leuven, Amersfoort, p. 69 (1994).
21. N. Nishimura, T. Yamazaki, S. Miyazaki and M. Hirose, same proceedings as ref. 20, p. 358 (1994).
22. "VASE" is a registered trademark of J. A. Woollam Co., Lincoln, NE.
23. M. Niwano, Y. Kimura and N. Miyamoto, Appl. Phys. Lett., **65**, 1692 (1994).
24. A. Philipossian, J. Electrochem. Soc., **139**, 2956 (1992).
25. K. Utani, T. Suzuki, and S. Adachi, J. Appl. Phys., **73**, 3467 (1993).
26. A. T. Fiory, P. K. Roy, and G. E. Jellison, Mat. Res. Soc. Symp., **259**, 131 (1992).
27. B. W. Fowler and R. A. Carpio, "*Proceedings of the Syposium on Silicon Nitride and Silicon Dioxide*", ECS Vol. 94-16, May, 1994.
28. M. Egawa and H. Ikoma, Jpn. J. Appl. Phys., **33**, 943 (1994).
29. D.B. Fenner, D. K. Biegelsen and R. D. Bringans, J. Appl. Phys., **66**, 419 (1989).
30. D. Kinosky, *et al.*, Mat. Res. Soc. Symp., **315**, 79 (1993).
31. K. Lai, M. Hao, W. Chen and J. Lee, IEEE Electron Device Letters, **15**, 446 (1994).
32. B. Garrido *et al.*, Mat. Res. Soc. Symp., **259**, 119 (1992).
33. H. Ibach, H. Wagner, and D. Bruchmann, Solid State Commun., **42**, 457 (1982).
34. A. C. Dillon, M. B. Robinson, S. M. George, and P. Gupta, Mat. Res. Soc. Symp., **259**, 99 (1992).
35. I. M. Kolthoff and S. Bruckenstein "Treatise on Analytical Chemistry" Part I, 1, M. Kolthoff and P. J. Elving, Eds., Wiley-Interscience, New York, N. Y., 1959, Section B, Chapter 13, p. 484.
36. J.S. Judge, J. Electrochem. Soc.: Solid State Science, **118**, 1772 (1971).
37. H. A. Laitinen, Chemical Analysis, McGraw-Hill Book Co. Inc., New York, Chapter 4, pp. 57-83,1960.
38. S. Verhaverbeke *et al.*, Mat. Res. Soc. Symp., **315**, 457 (1993).

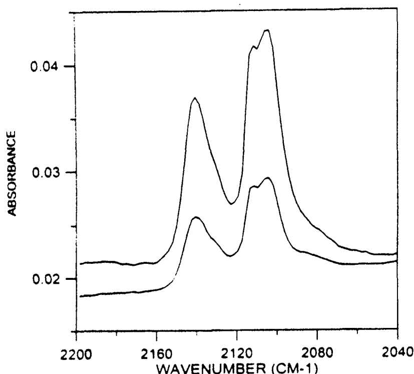

FIGURE 1. Comparison of p-polarized ATR-FTIR spectrum (top) with corresponding unpolarized spectrum (bottom). Wafer cleaned in SC1 followed by a 30 second dip in 1:50 $HF:H_2O$.

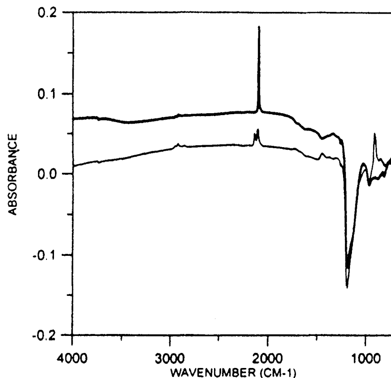

FIGURE 2. Overlay of p-polarized ATR-FTIR spectra for wafers treated with $HF:H_2O$ (1:40 for 30 s) with (heavy line) and without (narrow line) a H_2 anneal.

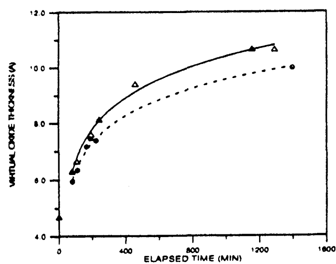

FIGURE 3. Comparison of changes in virtual oxide thickness change for aqueous HF process wafer (triangles) and hydrogen annealed surface (solid circles).

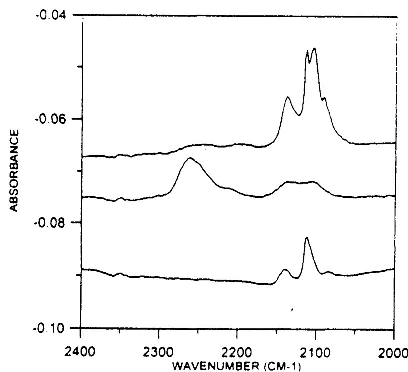

FIGURE 4. P-polarized spectra of SC1 + 1:50 $HF:H_2O$ (top) followed by SC2 (middle), and then followed by a 5-minute etch in 1:9 HF/MeOH (bottom).

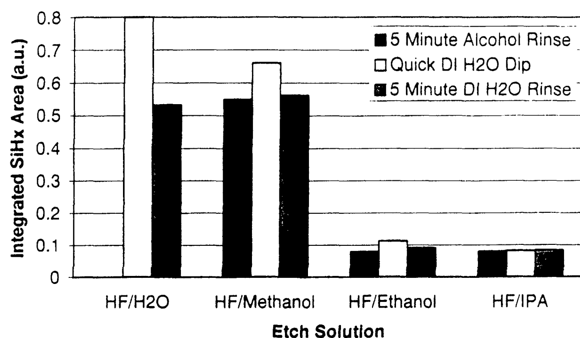

FIGURE 5. A comparison of different etch and rinse solutions.

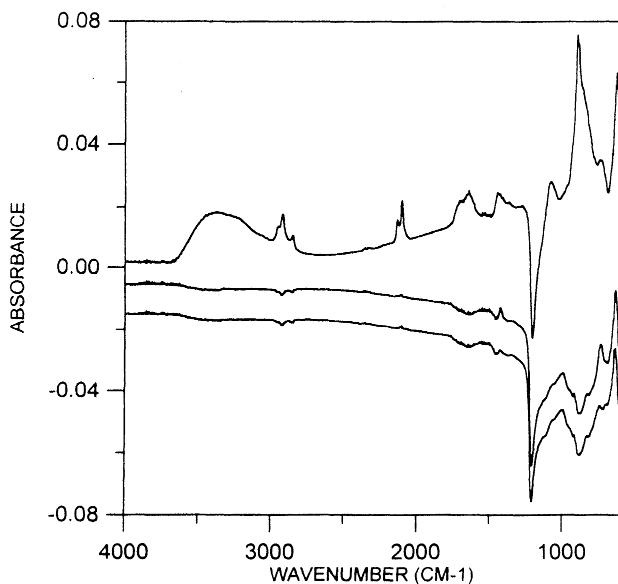

FIGURE 6. Overlay of unpolarized ATR-FTIR spectra for wafers treated with 1 min etch in 1:9 HF/Methanol (top), 1:9 HF/IPA (middle), and 1:9 HF/Ethanol (bottom) followed by 5 minute rinse in corresponding alcohol.

Trace Moisture Measurement in HCl using Near-Infrared LASER Absorption Spectroscopy

Yoshio ISHIHARA, Hiroshi MASUSAKI, Shang-Qian WU, Koh MATSUMOTO and Tetsuya KIMIJIMA

NIPPON SANSO Corporation, Tsukuba Laboratories
10 Ohkubo, Tsukuba, 300-33 JAPAN

We have developed a laser absorption spectroscopy with a near-infrared distributed-feedback (DFB) LASER diode as an in-situ and real time monitoring system. We have demonstrated that moisture (H_2O) in hydrogen chloride (HCl) gas can be precisely identified by measurement of a vibrational spectrum of H_2O. The limit of determination was obtained 500 ppb for 50 cm optical path length at a pressure of 100 Torr. Using this system, we have studied adsorption characteristics of H_2O in HCl gas onto Al_2O_3 surface, and compared that with in N_2 gas. The adsorption characteristics of H_2O in HCl gas is quite different as compared with that in N_2 gas. H_2O in N_2 gas is selectively adsorbed onto Al_2O_3 surface until 2.5×10^{14} molecules/cm^2 at 22 °C. On the other hand, H_2O in HCl gas does not adsorb onto Al_2O_3 surface. According to these results, it is speculated that H_2O in HCl gas forms a cluster by hydrogen association.

INTRODUCTION

Hydrogen chloride (HCl) gas has been widely used for cleaning process in Si epitaxy formation, dry etching and as an additive in dry oxidation processes [1,2] in present semiconductor manufacturing. Moisture (H_2O) is considered as a key impurity because it is extremely difficult to eliminate, and it affects many semiconductor fabrication processes [3]. Therefore, trace H_2O in HCl gas must be reduced to an extremely low level in order to establish highly reliable fabrication processes for sub half micron ultra-large scale integration (ULSI). In order to reduce the trace H_2O in HCl gas, it is important to develop both a purification technology and a measurement technology for trace H_2O in HCl gas. An in-situ and real time monitoring technology is also required in relation to future ULSI. The conventional analysis techniques of H_2O in HCl gas are dew point measurement [4], gas-chromatography. Either method, however, cannot be precisely determined trace H_2O in HCl gas [5]. It is also difficult to precisely measure the H_2O in HCl gas with high sensitivity by FT-IR [6], because the absorption peaks broaden and/or shift due to the presence of H_2O. Moreover, in order to develop a purification technology of HCl gas and effectively handling of HCl gas, it is essentially important to comprehend the characteristic of HCl in terms of the form of H_2O in HCl gas and its interaction with various surfaces.

In this study, we have developed a laser absorption spectroscopy with a near-infrared distributed-feedback (DFB) LASER diode, and measured H_2O in HCl gas. We have also studied the adsorption characteristics of H_2O in HCl gas using developed system. In this paper, we introduce the LASER absorption measurement of H_2O in HCl gas at room temperature, and describe the H_2O adsorption characteristics in HCl gas onto Al_2O_3 surface at room temperature.

EXPERIMENTAL

H_2O molecules have a vibrational absorption band at the region of 1380 nm [7] and can be detected by absorption spectroscopy using DFB LASER diode operating in 1380 nm at room temperature. A schematic diagram of an optical monitoring system using a LASER diode is shown in Fig. 1. We utilized a frequency modulation spectroscopy (FMS) combined with a conventional lock-in technique. A single mode DFB LASER diode with a threshold driving current of 30 mA operates at a typical power of 7.5 mW with 70 mA driving current. The driving current of the DFB LASER diode is modulated by dc-biased 4 kHz sine wave. The LASER beam is split into a sample cell, and into a reference cell and is detected by Ge detectors at room temperature. The second derivative of the absorption signal was observed by phase sensitive detector with a reference frequency of 8 kHz. An absorption path length and a volume of a sample cell was 50 cm and 500 cm^3, respectively. A reference cell with the length of 10 cm contains 20 Torr H_2O.

The developed system consists of the optical system, the gas supply system with dynamic dilution calibration function [8] and the system controller. The characteristic of the dynamic dilution of H_2O in N_2 gas was evaluated by using LASER spectroscopy, crystal oscillation moisture detector and atmospheric pressure ionization mass spectroscopy (APIMS). We had confirmed the excellent linearity between H_2O concentration and signal intensity at the wavelength of 1380.64 nm with the correlation coefficient of 0.999 in the range from 500 ppb to 250 ppm. In order to identify H_2O in HCl gas in the LASER absorption spectroscopy measurement, we scanned the wavelength from 1380 nm to 1381 nm in a step of 1.8×10^{-3} nm by varying the diode temperature from 25 °C to 36 °C in a step of 0.02 °C. H_2O level in HCl were varied in the range from 1 ppm to 70 ppm to obtain calibration curve between H_2O concentration in HCl gas and signal intensity from the absorption spectroscopy. HCl gas with various concentration of H_2O was flowed through the sample cell at 200 standard cm^3/min flow rate at 100 Torr. The wavelength was scanned from 1380.58 nm to 1380.7 nm by applying ramp current to a dc current from 75 mA to 90 mA in a step of 0.2 mA with the diode temperature of 31.5 °C. We defined the signal intensity as the difference between the minimum and the maximum of the output second derivative signal.

Figure 2 shows a schematic diagram of the experimental apparatus of an evaluation

on adsorption characteristic of H_2O in HCl gas. A filter made of Al_2O_3 ceramic with the surface of 8.95 m^2 was used as a sample. At first, the filter was baked at 200 °C for 24 hours while an ultra high-purity N_2 gas containing 1 ppb H_2O was flowed through the filter at 1000 standard cm^3/min in order to remove the H_2O from Al_2O_3 surface. The drying out of the Al_2O_3 surface was determined when the reading of a laser absorption spectroscopy becomes to constant 500 ppb at 200 °C. In next experiments, N_2 gas with 60 ppm H_2O or HCl gas with 1.3 ppm H_2O were flowed through the filter at 200 standard cm^3/min after baking at 22°C. H_2O concentrations in N_2 gas or HCl gas just after the filter were measured by a LASER absorption spectroscopy.

RESULT & DISCUSSION

H_2O Measurement in HCl

Figure 3 shows the LASER absorption spectroscopy signal at 1380.75 nm of each sample gases. The broken line in Fig. 3 shows the reference absorption line of H_2O simultaneously obtained from the reference cell. In spite of the H_2O concentration and the pressure are same in each samples, the peak shift is only observed with probing LASER power of 0.7 mW in HCl gas. Its peak position shifts to longer wavelength by 6×10^{-3} nm which is larger than the step size of the wavelength scan. The peak shift implies that the existence of the cluster formed by H_2O and HCl molecules. It is speculated that the cluster formation influences the vibrational spectrum of H_2O molecules.

In order to precisely identify a impurity in spectroscopic analysis, it is important to confirm the agreement of each peak positions between the sample and the reference. Figure 4 demonstrates the LASER absorption spectroscopy signals of 70 ppm H_2O added into HCl gas, and H_2O standard. The probing LASER power in this measurement is 2.05 mW. H_2O absorption lines are obtained at wavelength of 1380.17 nm, 1380.47 nm, 1380.64 nm and 1380.75 nm in each samples. Those show good coincidence between H_2O spectrum of 70 ppm H_2O added into HCl gas and that of H_2O standard. The ratio of each peak intensity shows also good agreement between two samples. Theses results mean that H_2O molecules in HCl gas can be measured precisely by applying the LASER absorption spectroscopy with a DFB LASER diode.

The strongest absorption line in the wavelength range from 1380 nm to 1381 nm is 1380.64 nm. The calibration curve between signal intensity at 1380.64 nm and H_2O concentration is shown in Fig. 5. The largest standard deviation of the signal intensities collected at each concentration is 4.8 % of signal intensities. Good linearity between the signal intensity and H_2O concentration is obtained, and the correlation coefficient is 0.99. The limit of determination of H_2O concentration in HCl gas is 500 ppb at the S/N ratio of 2 with a 50 cm optical path length.

H_2O Adsorption Characteristics

Figure 6 shows the H_2O adsorption characteristic in N_2 gas onto H_2O free Al_2O_3 surface at 22 °C. The vertical axis shows the H_2O concentration in N_2 gas. In this experiment, N_2 gas with the H_2O concentration of 60 ppm was flowed at 200 standard cm^3/min. As seen in Fig. 6, the H_2O in N_2 gas is not detected just after flowing N_2 gas, and increases with increasing the passage time until the equilibrium is obtained at 200 minute. This result suggest that the H_2O in N_2 gas is selectively adsorbed onto Al_2O_3 surface until the equilibrium between H_2O in the gas and the solid surface is obtained. Similar result already reported onto stainless steel surface [9]. By integrating the difference of the input and the output H_2O of the filter, the number of adsorbed H_2O molecules onto Al_2O_3 surface is calculated on 2.3×10^{19} molecules. The amount of adsorbed H_2O molecules for unit surface area is 2.5×10^{14} molecules/cm^2 because the surface area of filter made of Al_2O_3 is obtained as 8.95 m^2.

The H_2O adsorption characteristic in HCl onto H_2O free Al_2O_3 surface at 22 °C is shown in Fig. 7. The vertical axis shows the H_2O concentration in HCl gas measured by a LASER absorption spectroscopy. The H_2O concentration in HCl gas is almost kept constant just after flowing HCl gas which is quite different in the case of N_2 flowing. This result suggest that the H_2O in HCl gas does not adsorb onto Al_2O_3 surface. The H_2O adsorption characteristic is influenced by the characteristic of HCl gas itself. In HCl molecules, An H atom is positively charged relative to Cl atom because of electronegativity difference. An H atom in H_2O molecules is also positively charged relative to O atom. Therefore, it is possible that H_2O molecule forms cluster with HCl molecules by hydrogen association due to electronegativity difference in HCl gas. It is speculated that the difference of the H_2O adsorption characteristics onto Al_2O_3 surface between HCl gas and N_2 gas is originated by forming the cluster.

CONCLUSION

We have developed LASER absorption spectroscopy with a DFB LASER diode as an in-situ and real time monitor. Using this system, we have measured H_2O in HCl gas, and studied the adsorption characteristics of H_2O in HCl gas onto Al_2O_3 surface. We have demonstrated that the H_2O in HCl gas can be precisely estimated by measurement of a vibrational spectrum of H_2O. The calibration curve between the H_2O concentration in HCl gas and the signal intensity was obtained with good linearity with the correlation coefficient of 0.99 in the range from 1 ppm to 70 ppm. H_2O concentration was measured with the limit of determination of 500 ppb by only 50 cm optical path length at the pressure of 100 Torr. The adsorption characteristics of H_2O in HCl gas was quite different as compared with that in N_2 gas. H_2O in HCl gas does not adsorbed onto Al_2O_3 surface. According to the peak line shift of H_2O at low probing laser power and the adsorption characteristic of H_2O in HCl gas, it is speculated that H_2O in HCl gas makes a

cluster by hydrogen association.

ACKNOWLEDGMENTS

The authors would like to thank Prof. N. Takeuchi of Chiba University for the valuable discussions.

REFERENCES

[1] B. E. Deal, J. Electrochem. Soc., **125**, 576 (1978).
[2] D. W. Hess and B. E. Deal, J. Electrochem. Soc., **124**, 735 (1977).
[3] T. Ohmi, in Proc. 1986 SEMI Technology Symposium, A-1-1 (1988).
[4] E. Flaherty, C. Herold, D. Murray and S. R. Thompson, Anal. Chem., **58**, 1903 (1986).
[5] Y. Ishihara, T. Ohmi, H. Hasegawa, T. Ikeda, T. Takasaki, S. Yamane and R. Fukushima, J. Electrochem. Soc., **141**, 246 (1994).
[6] K. Miyazaki. Y. Ogawara and T. Kimura, Bull. Chem. Soc. Jpn., **66**, 969 (1993).
[7] J. H. Park, L. S. Rothman, C. P. Rinsland, H. M. Pikett, D. J. Richardson and J. S. Namkung, NASA Reference Publication **1188**, 157 (1987).
[8] N. Yabumoto, T. Amemiya, K. Kawai, T. Kimura, T. Shimono, T. Nakayasu, A. Nishina, Y. Mitsui, H. Mihira and Y. Sakakibara, in Proc. 180th Electrochem. Soc. Meeting, p.99 (1991).
[9] T. Ohmi, M. Nakamura, A. Ohki, K. Kawada and K. Hirao, J. Electrochem. Soc., **139**, 2654 (1992).

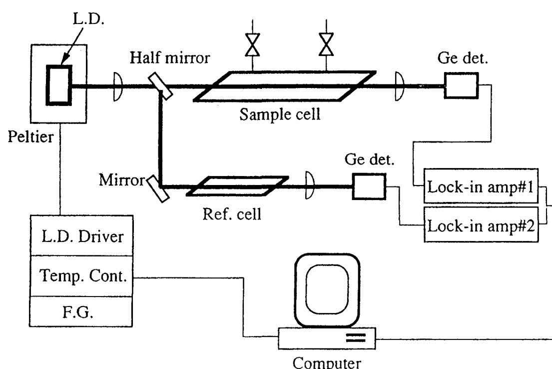

Fig. 1. Schematic diagram of the LASER diode optical system

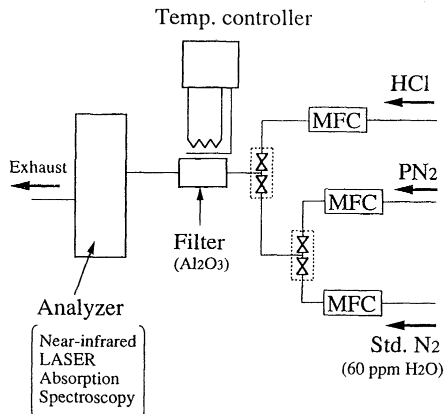

Fig. 2. Schematic diagram of the experimental apparatus

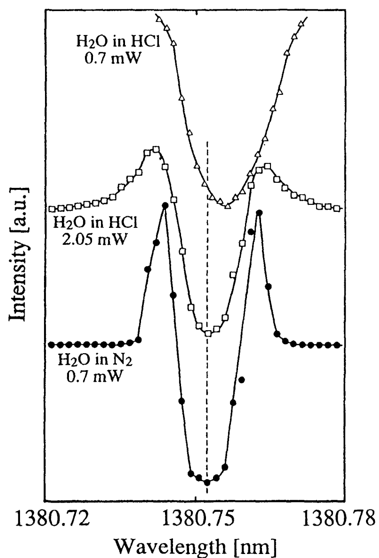

Fig. 3. LASER absorption spectroscopy signal of each sample gases at 1380.75 nm.

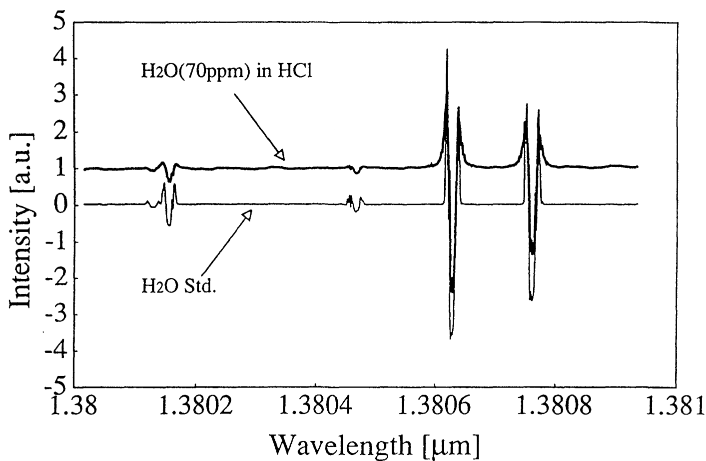

Fig. 4. LASER absorption spectroscopy signals of H_2O of 70 ppm added into HCl gas and H_2O standard.

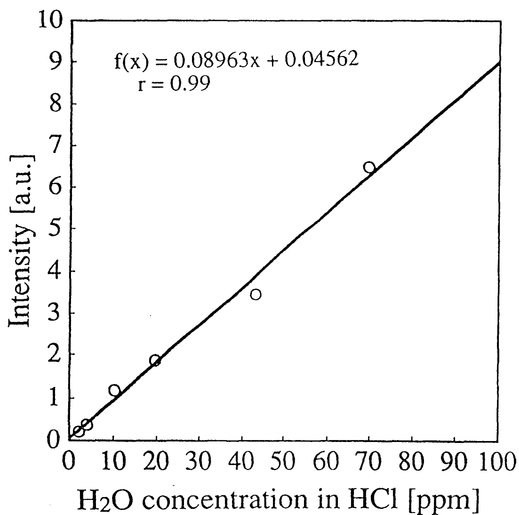

Fig. 5. Calibration curve between signal intensity at 1380.64 nm and H_2O concentration in HCl gas.

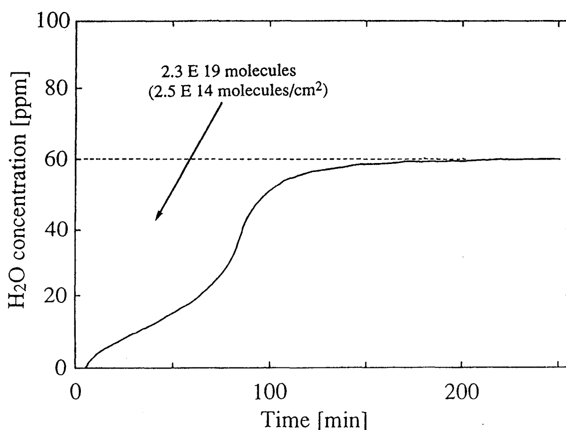

Fig. 6. Adsorption characteristic of H_2O in N_2 gas onto H_2O free Al_2O_3 surface.

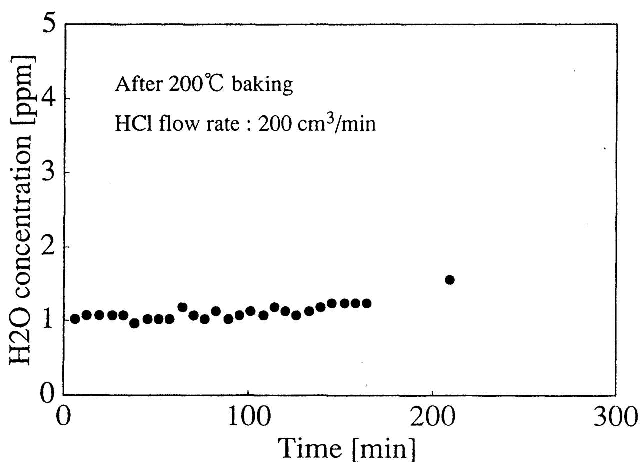

Fig. 7. Adsorption characteristic of H_2O in HCl gas onto H_2O free Al_2O_3 surface.

CHARACTERIZATION, PROPERTIES AND ANALYSIS OF VIA VEILS

K. Mocala, P. Crabtree, E. Mocala, R. Hegde, K. Lao and P. Laberge

MOTOROLA
Advanced Products Research and Development Laboratory
3501 Ed Bluestein Boulevard MD: K-10
Austin, TX 78721

ABSTRACT

Post Via Etch Residue (Via Veils) was studied using EDS analysis and dissolution experiments in several inorganic solvents. It was found that veil as formed is rich in Al and it dissolves in inorganic solvents like metallic Al. Fluorine content increases substantially when the residue is exposed to atomic Fluorine, and an AlF_3 passivation layer is most likely formed. Chemical Dry Etch was used to decorate via veils and its impact on veils composition and dissolution properties was shown.

INTRODUCTION

It is well known that many dry etch processes leave post etch residues on wafers. This residue may cause yield loss or decreased reliability of IC. Thus, understanding the properties of this residue is an important aspect of process development in IC manufacturing. In this paper, we will focus on post etch residues typically left after dry via etch processes. This residue is commonly called a veil or a fence. Although our main focus will be on understanding the properties of veils, some information will be given as to how they may be removed. Decoration of veils by Chemical Dry Etch (CDE) will be discussed and impact of that decoration on the properties of veils will be shown. Two types of veils will be discussed: veils formed in straightwall vias and those formed in taper vias.

It is commonly assumed that post via etch residue consists of C-F-O-Al polymer. Recently metallic like polymer was reported (1) but analytical details were not provided. For sure, veil formation, Fig. 1, is sensitive to many parameters like etch chemistry, type of etch tool, over-etch time, selectivity to underlayer, post etch treatment and others.

EXPERIMENTAL

Material Used

Five inch wafers with 12000Å TEOS film were patterned with the 0.8 micron vias using I-line photoresist. A patterned TiN/Al-Cu metal stack (250Å/6000 Å) was used below the isolator level.

Etch

Straightwall via veils were formed in an MERIE tool with CHF3/CF4/Ar chemistry. Straightwall veils are difficult to see and analyze without decoration. A special plasma decoration procedure was developed in a commercial CDE tool with CF4/O2 plasma. Taper via veils were obtained by etching the taper part of vias in the CDE tool with CF4/O2 chemistry followed by anisotropic etch in the MERIE tool.

Veils Analysis

Chemical analysis of the veils were obtained using Fison 310F Auger Nanoprobe equipped with a Fison/Kevex Energy Disspersive Spectrometer (EDS). All data was measured at 5 KV electron beam potential with a beam current of 2 nA. The most valuable information was obtained from taper via veils on thick SiO2 background. Some veils were also analyzed after special treatment to evaluate the impact of such treatment on veils composition. Dissolution properties of veils were analyzed in several inorganic solvents. Both whole wafers and/or small parts of wafers were used in dissolution experiments. Effectiveness of various treatments at removing the veils was checked using SEM.

RESULTS AND DISCUSSION

When silicon or TiN is used as a stop layer, veils are not observed for this via etch chemistry. Thus, veils are formed only when Al is the stopping layer for the processes investigated.

Fig. 2 presents typical straight wall veils decorated using CDE and typical, not decorated, taper via veils. Decoration using CDE technique changed some of the dissolution properties of the veils. This change of dissolution properties is caused by an increase of F content in the veils. Table 1 shows EDS results obtained from taper veils on thick SiO2 background. Since the background does not show any Al and F, all detected Al and F originate from the veils. Decoration of veils in F plasma increases F/Al content in veils by more than 4 times. On the other hand, as formed taper veils exhibit a 4X reduction in F/Al ratio when rinsed in hot DI water. These results suggest that as formed veil is multi-phase, with almost pure aluminum core and a small amount of AlF3 as a passivation layer. AlF3 is known to dissolve in hot water, so the decrease of F in veil after hot water rinse may be understood well. Increase of F content in veil after

isotropic plasma decoration by factor more than 4 clearly indicates that substantial amount of the analyzed volume was almost F free since the richest Al compound containing F known is AlF3.

Table 1.
Results of EDS analysis of taper via veils on thick SiO2 background.
Results expressed as an atomic(%).

Veil / Material	Al(%)	F(%)	Si(%)	O(%)	F/Al
As Formed	4.92	1.60	22.46	71.02	**0.33**
After CDE Decoration	9.85	13.95	21.14	55.06	**1.41**
After H20 Rinse	9.84	0.78	21.23	68.15	**0.08**
SiO2 Background	-	-	28.33	71.67	-
AlF3 Standard	28.17	71.83	-	-	2.54

Fig. 3 presents the different behavior of decorated straightwall and as formed taper veils in 10:1 BOE (NH4F:HF). Decorated straightwall via veils, rich in F, do not dissolve in BOE but taper via veils dissolve completely. This would agree with the fact that AlF3 does not dissolve in BOE but BOE does attack Al. Fig. 4 shows effect of KOH solution on taper via veils (not decorated by CDE). As may be seen from Fig. 4b, KOH which is known to etch Al dissolves taper via veils completely. Again this indicates that not decorated taper via veils behave similar to Al. Similar conclusion may be drawn from the results of dissolution experiment in wet poly-Si etchant, HNO3:HF (50:1). Two-three second dips of samples in this solvent were enough to dissolve all taper via veils, Fig. 5a, but could not dissolve straight wall veils, Fig. 5b. Again, Al may be dissolved in acids but acids do not dissolve AlF3.

CONCLUSIONS

Presented results indicate that decorated straightwall veil cannot show correct Al/F composition since decoration procedure substantially increases F content in veil. Taper via veils show Al/F ratio which is characteristic to straightwall etch process and overetch time. Taper via veils may be conveniently used in investigation of straightwall veils properties. As formed via veils behave similar to Al. Solvents which dissolve Al will also dissolve the veil. This makes it very difficult to remove veil without some loss of Al

substrate. However, when veil become rich in F, forming presumably AlF3 passivation layer, its dissolution properties change.

REFERENCES

1. H. Shan, B.K. Srinivasan, D.W. Jillie, Jr., J.S. Multani, and W.J. Lo, J. Electrochemical Society **141**, 2904 (1994)

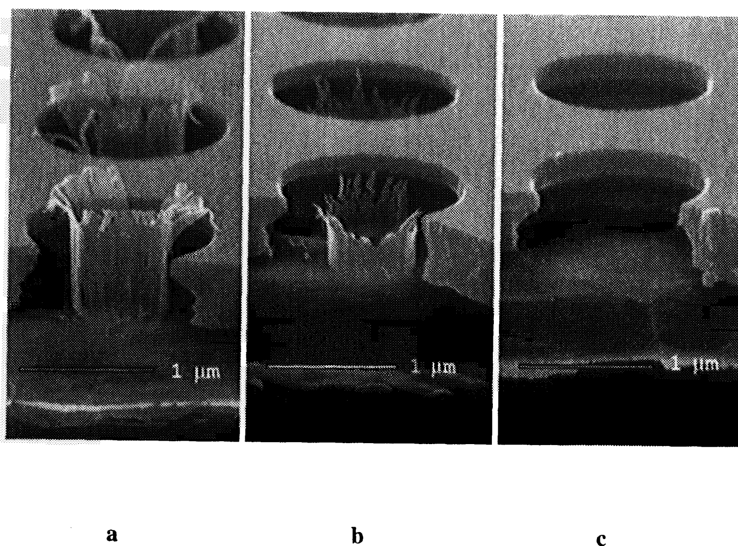

a b c

Fig. 1. Via veils formed in: (a) low RF frequency RIE tool, (b) MERIE tool and (c) veil free process in High Density Plasma etch tool. All samples were decorated by CDE.

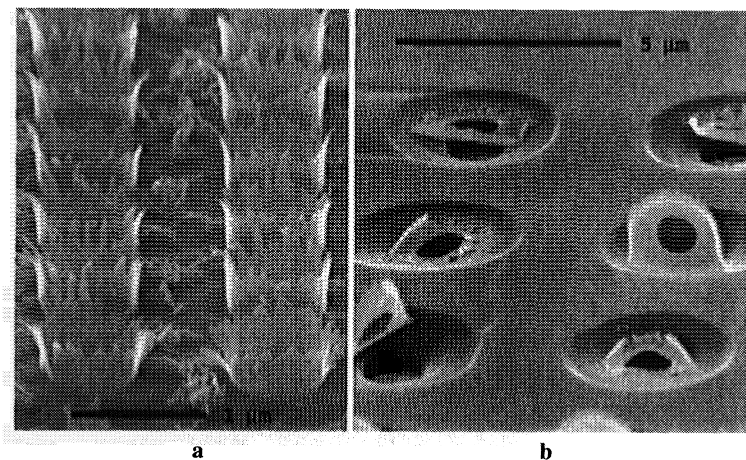

Fig. 2. Typical via veils formed in MERIE tool (a) straightwall via veils after CDE decoration and (b) taper via veils (without CDE decoration).

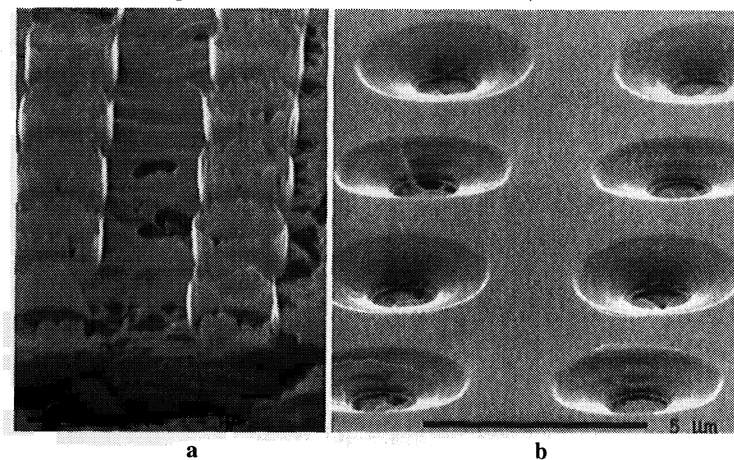

Fig. 3. Straightwall via veils after 20 sec 10:1 BOE treatment (a) and taper via veils removed after similar BOE treatment (b). CDE decoration of sample (a) was done before BOE treatment.

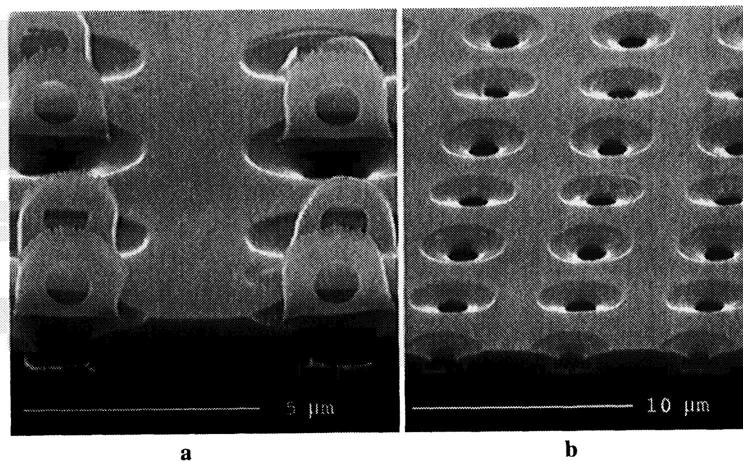

Fig. 4. Effect of KOH solution on taper via veils, sample before KOH treatment (a) and after KOH treatment (b).

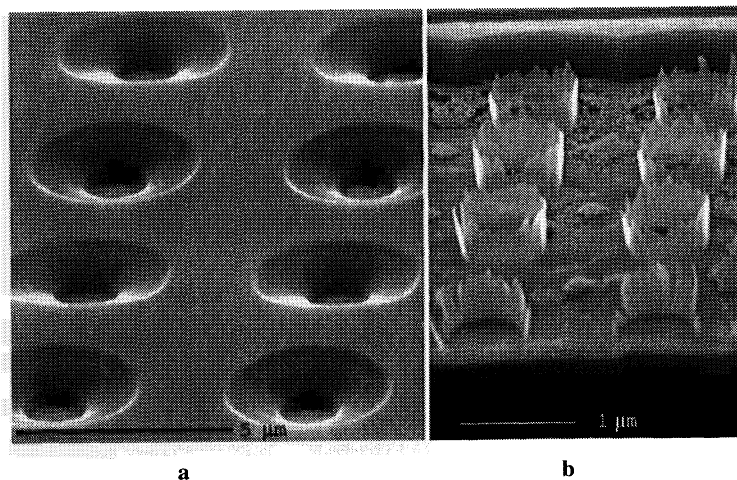

Fig. 5. Effect of two-three second dip in HNO3:HF (50:1) on taper via veils, veils completely removed (a), and on CDE decorated straightwall via veils (b).

DEFECT CHARACTERIZATION ON A BATCH CLEAN PROCESS USED AFTER PLASMA METAL ETCHING

K. E. Mautz
Motorola, Inc., Semiconductor Products Sector
505 Barton Springs Road, Suite 1050
Austin, Texas 78704

Defectivity addition on batch spray tool clean processes used after plasma metal etching was characterized. The defects studied were particulate and veil polymers on the wafer surface. Designed experiments were run on the process and equipment factors of the batch spray tool. Particle additions due to the spray tool recipe were reduced by process and equipment improvements. The clean solution step was characterized for oxide film removal etch and non-uniformity. Wafer streaking defects were identified and eliminated by changes in the clean process recipe.

INTRODUCTION

Defectivity addition from a batch clean step following a metal etch and ash process was characterized. The defects studied were particulate and veil polymer residue and were causing inspection failures and yield issues. Wet chemical spray batch processes are efficient in removing both defects with high throughput. Prior to introducing this tool into processing, characterizations were done to understand the mechanisms and process sensitivities to particle addition and removal, and veil polymer removal. These characterization results were used to create a process recipe to be used in volume processing of wafers. Metal etch processes use polymer-producing steps for corrosion control and maintaining sidewall integrity. These processes also produce particles due to particle flaking, or can trap other particles generated by mechanical movement. Veil polymers form on the surfaces of the metal lines and cannot be removed by DI water rinsing. The batch spray tool clean process is then relied on to remove all defects prior to the next deposition step.

EXPERIMENTAL

The equipment used for the clean process was a dual-chamber, batch spray tool that combined: 1) a preclean rinse wetting step, 2) a clean step, 3) an intermediate rinse, 4) a deionized (DI) water rinse, and 5) spin dry cycles. The clean chemistry was a dilute solution of buffered oxide etchant mixed with ethylene glycol and with or without a surfactant. The intermediate rinse was ethylene glycol at an elevated temperature. Experimentation on the equipment factors was done to determine baseline particle levels of the process chamber and the effect of various chemical flow and manifold purge cycles. Defects were measured and classified using particle metrology equipment, and optical and SEM inspections. The particle detection tool provided defect data on 0.5-5.0μ bins and

total adders. Designed experiments were run on the following: 1) preclean rinse step process parameters, 2) clean step process parameters, 3) intermediate rinse parameters, and 4) spin dry cycle parameters. Three cassette positions were used to obtain data. Process parameter characterization of the clean step was done using oxide film removal and non-uniformity as outputs. Automated oxide film measurements were made using 9 data point locations. The metal etch process that precedes the clean utilized a RIE hexode equipment set with a chlorine-based plasma chemistry. The ash was done using a stand-alone, heated chuck-rf downstream tool.

RESULTS AND DISCUSSION

The characterization was done on two fronts: particulate defectivity and process-induced defectivity. In some cases changes made to the equipment or processing to benefit one category had an beneficial effect on the other. Particle testing was done during the initial start-up and periodically during the process testing. Process testing was done in blocks, and clean solution chemistry changes were done between the block runs.

Particulate Defectivity Characterization

Particulate defectivity tests were run on the tool during the start-up phase and during volume production processing on both chambers. The initial particle tests were done using DI water only with bare silicon test wafers to establish a baseline prior to introduction of clean chemistries and processing wafers. Initial baseline counts ranged from 5 to 12 adders consistently on both chambers. The recipe used for this testing duplicated the production clean recipe in terms of flow times, pressures and chamber speeds, but substituted DI water for the clean and rinse chemicals. Three wafers were used in these tests, located at the forward (near door), middle, and rear cassette positions to sample the entire chamber space. The individual wafers were particle measured and the values were averaged to produce a reported number. No significant relationships in the particle bin size were found during this testing. During the clean process characterization period, particle tests were run once a day in each chamber. Particle levels then increased to 10-15 adders.

A significant increase in particles (averaging 25-45 adders) was found during the routine monitoring in one chamber near the completion of the clean process characterization. The other chamber was at a slightly higher, but not at a statistically significant level. Experiments were run to isolate the cause. Initially, running only the DI water process resulted in a small particle level reduction. The chemical tanks were drained, flushed, and refilled in conjunction with a filter change (using 0.2 micron grade). Particle tests after this action indicated little change. A hydrogen peroxide purge of the DI water lines, chemical manifolds and internal plumbing (up to but not including the chemical tanks) was done without much success. Since no assignable equipment cause was found, process recipe characterization was done to study the effects of the various steps and parameters on the overall particle level. These results indicated that the following steps and parameters had a significant effect on particle levels: 1) the drying time, 2) the nitrogen manifold purge steps after the clean and intermediate rinse steps, 3) the addition of a preclean rinse using the intermediate rinse, and 4) the length of time since the last DI water process was run in the chamber. After completion of this experimental

test, particle levels in this chamber increased significantly (averaging 50-100 adders). All plumbing and mechanical assemblies of this chamber were inspected, revealing the cause of the particle addition. A rotor seal had ruptured and had increasingly begun to shed particles into the process chamber. This was corrected by a rotor seal replacement and DI water purging of the chamber. The process recipe characterization was repeated after the particle levels stabilized and were found to have similar effects.

The drying step time affected particle levels after 150% of drying time. The drying time was determined by the disappearance of small droplets on the wafer edges between the rails of the teflon cassette. The presence of water left on wafers could cause defects in subsequent processes, especially thin film deposition operations by acting as nucleation points or ionic contaminant traps. After the 150% drying time particle levels would increase from the baseline level by approximately 50%. After 250% of drying time the particle addition effect was negligible above the initial increase. These particles were from the interior chamber walls as they dried and begun to shed particles as attractive forces within the chamber changed. The nitrogen manifold purge steps were found to have an effect on particle additions when these were used after the clean solution process step. An increase in large particle sizes was found from the baseline level up to 200%. These particles were created as the clean solution was blown from the manifold and the carrier solution evaporated producing precipitated particles that were spread over the spinning wafers. This purge step with nitrogen gas was eliminated without causing any detrimental effects on the overall process. The manifold was then purged during the intermediate rinse step, and after 5-10 seconds the intermediate solution would be free of any clean solution impurities. The wafers during this purge step would be spinning at a higher rate than the clean solution step to assist in removing the clean solution prior to the intermediate rinse. This caused a processing issue that will be explained later. On bare silicon wafers the manifold purge generated particles were easily removed by the intermediate solvent. On processed wafers particles were found in corners and ledges formed by lithography.

The preclean rinse step using the intermediate rinse solvent was found to remove particles that had been added to the wafers from previous processing steps or from wafer transport. A short duration rinse (15-20 seconds) was found to be sufficient for most fall-on particles. Particles held to the surface by other forces were more difficult to remove and longer preclean rinse times (60 seconds or longer) were not successful in removing these. This step was found to also be beneficial to the clean processing for wetting and will be discussed later. Particles were found to be affected by the length of time that the chamber was left in a static dry condition (i.e. without any other processing steps run or any designated rinse cycles designed to keep the chamber moist). Idle times exceeding 24 hours resulted in increased particle levels at 25-40% of the baseline levels. Periodic DI water rinse steps without drying steps were used to remove added particles from the chamber and keep the interior moist (lowering static charges that attract and hold particles on the surfaces). This also had an effect on the process that will be discussed later.

Clean Process Characterization

The clean process objective is to remove particles created during or remaining after the metal etch process and ash step, and to remove the post-etch artifacts (veil polymer) that decorate the top surfaces or sidewalls of the metal lithography. Fig. 1 shows an example of post-metal etch veil polymers. These polymers are produced by an interaction

of the metal etch plasma chemistry acting on the photoresist skin and from backsputtered aluminum and underlying oxide films. The polymer is an amorphous oxide ribbon with some organic components mixed within. The primary constituent has been identified as Al_2SiO_2 [1]. Various methodologies of wet chemical and vapor phase clean processes have been used to remove veil polymers and particles [1-3]. The clean step process was designed to remove the veil polymers without significantly damaging the underlying oxide surface and reduce the overall particle levels on the wafers (as compared to a DI water rinse only). Screening and characterization experiments were done using three oxides: 1) TEOS (PECVD), BPSG, and a thermal oxide (Fox). The primary outputs for this characterization were the oxide film removal and non-uniformities. Four clean solution compositions were tested: 1) 4:1 (EG:BOE) without a surfactant, 2) 4:1 (EG:BOE) with a surfactant, 3) 3:1 (EG:BOE) without a surfactant, 4) 3:1 (EG:BOE) with a surfactant. Three cassette wafer positions were used in this test, located at the forward (near door), middle, and rear of the cassette with bare silicon wafers occupying the other slots. The oxide wafers were measured and the values were averaged to produce a reported number. Table I displays the experimental clean step parameter inputs.

Table I. Clean Solution Characterization Parameters.

Parameter	Screening	Characterization
Data Value	-1, 0, 1	-1, 0, 1
Temperature, °C	22, 29, 35	24, 27, 30
Clean time, min.	0.5, 1.5, 2.5	1, 1.5, 2
Solution flow, psi	30, 39, 48	32, 38, 44
Cassette speed, rpm	30, 65, 100	40, 55, 70

The results of the clean process parameter experimentation were as follows. The effectiveness of the clean process was strongly affected by the: 1) temperature of the clean solution and intermediate rinse, 2) process step time of the clean solution, intermediate rinse and DI water rinse, 3) solution flow of the clean solution and intermediate rinse, and 4) spin speed of the clean, intermediate, and DI water rinse, listed in decreasing significance. Temperature strongly affects both the thickness removed and non-uniformity of all oxides. The 4:1 clean solution showed a stronger temperature effect than the 3:1 clean solution. As the temperature increased on both clean solutions, the non-uniformity improved (lower values). Temperature effects in spray clean tools have been found to increase the effectiveness of particle removal from surfaces [4]. Longer clean solution step times also resulted in higher effective oxide film removal and lower non-uniformities. Higher clean solution flow pressures had a mixed effect on oxide removal and non-uniformities. For the 4:1 clean solution, TEOS and BPSG oxide films showed no effect on oxide removal and a slight decrease in the non-uniformity. On the Fox film there was a slight increase in the oxide removal and no effect on the non-uniformity. For the 3:1 clean solution, all oxides increased slightly in oxide removal, and non-uniformity values increased on TEOS, decreased on BPSG and remained practically the same on the Fox film. Faster spin speeds caused a significant decrease for the 4:1 clean solution oxide removal and a slight decrease in all oxide non-uniformities. The 3:1 clean solution had lower oxide removal, with the BPSG and Fox film non-uniformities increasing and the TEOS decreasing with higher spin speeds. On spray clean tools the effects of an optimized rotation speed and cleaning time for removal of organics and metallic

contamination has been described [5]. Overall, the oxide removed was higher (as expected) on the 3:1 clean solution and the non-uniformities were lower. For the entire experiment, the spread of the data values for the BPSG and Fox non-uniformities were larger than expected. The clean step process parameters were chosen to minimize oxide loss and non-uniformity values using slower spin speeds with medium flows for short step times. Figures 2 and 3 display the results of the characterization for the 4:1 (EG:BOE) with surfactant and the 3:1 (EG:BOE) with surfactant, respectively.

The other process recipe steps were investigated in terms of process outputs and particles. Optimum drying step times without particulate additions were found to range from 115-145% of the time required for water droplet clearing from the wafer edges during the spin dry cycle. Decreasing the dry spin speed during the last half of the step reduced particle levels by approximately 5%. The maximum temperature of the drying gas (N_2) had a higher significance than the spin speed on the overall drying efficiency. The intermediate rinse step time was required to be greater than 1 minute with medium spin speeds and high flow to remove the clean solution and particles from the wafer surface. An elevated solution temperature (greater than 40C) was used to quickly and efficiently remove the clean solution from the wafers and prevent streaking. The DI water rinse time required greater than 3 minutes, slow spin speeds at medium flows for effective rinsing. The preclean rinse was found to possess a wide process window. A short step time (less than 45 seconds) was needed to adequately wet all wafers in the cassette. This step improved the clean step oxide removal non-uniformity by 1-2%.

Characterization of the veil removal times was done on test wafers with heavy veil formation. SEM analysis was used to determine the results after various clean solution exposure times, using the standard rinse and dry process. Veil formation was significantly reduced after 15 seconds of chemical exposure on all chemistries (using the baseline level for all other process factors). After 25 seconds all but the heaviest veils were removed. 35 second process times resulted in complete removal of all veil material. Surfactant addition had no measurable impact on the veil removal times. There was no apparent difference between the 4:1 and 3:1 (EG:BOE) clean solutions. Other process factor data indicated that damage to metal lithography was seen when using hot DI water rinses as opposed to cold (ambient) temperatures. There appeared to be a seasoning issue with the state of the process chamber. The process outputs were more consistent when running metal lithography tests on a chamber that was periodically rinsed during long periods of idle time as opposed to a chamber that was left dry for extended periods.

Two types of wafer streaking were observed. These were radial-caused by etched striations in the underlying oxide, and irregular-crystalline defects occurring in a random lines or areas. Radial wafer streaking occurred when the intermediate rinse was delayed or if the spin speed was increased prior to the intermediate rinse (done to promote removal of the clean solution). Radial streaking could also occur if the chemical manifold was purged (with the cassette still spinning) prior to the intermediate rinse producing etched striations in the underlying oxide. These were prevented by changes in the process recipe that eliminated these steps. The irregular crystalline defects were not due to the process recipe or any tool factor. These were produced from an interaction of a hot wafer surface and clean solution exposure. Following the ash step, wafers are exited at a temperature in excess of 200C in a teflon cassette. If these wafers/cassette are placed into the batch spray processor without an adequate cool-down period (between 5-10 minutes) the last wafers to be ashed would be at a temperature high enough to evaporate the carrier solvent leaving wedge-shaped crystalline defects (primarily consisting of ammonium

fluoride). This would serve as a mask on the underlying oxide that would replicate the wedge-shaped defects into the oxide prior to the ammonium fluoride re-dissolving into the solution. Veil removal on the metal surface was not affected due to the ability of the clean solution re-dissolve the crystal. The lifetime of the crystalline mask was less than 10 seconds. Analysis of the defects after completion of the process showed only the oxide background. The linear pattern of the defects was due to the spray pattern from the manifold. The insertion of the preclean rinse step to reduce the wafer temperature and provide better wetting prevented the defects from occurring, regardless of wafer temperature. Apparently there was no major stress on the wafers (breaking, cracking or chipping) produced by the rapid cool-down. Fig. 4 displays an optical photograph and SEM micrograph of the crystalline defect.

CONCLUSIONS

Defectivity characterizations were done on a batch spray tool to minimize particle addition and veil polymer. Particles were added on wafer surfaces during the nitrogen purges through the chemical manifold, and during the drying step. Particle levels rose slightly during clean processing cycles, and catastrophic increases were due to assignable equipment causes with particle additions returning to baseline levels after repair. Characterization of various clean solution concentrations with and without a surfactant was done to minimize oxide film removal and non-uniformity. Veil polymer was efficiently removed by all clean chemistries. Clean process recipes were modified to eliminate wafer streaking by the addition of a preclean rinse to prevent crystalline defects and deletion of the manifold purge steps to prevent radial striations in the underlying oxide film. A 50% reduction in the clean process particle levels was achieved due to process recipe and step modifications. The surface cleaning efficiency of the spray tool process was improved by optimizing each recipe step's parameters.

ACKNOWLEDGMENTS

The author wishes to thank Linda Hernandez and Tin Tran for their assistance in data collection and experimental analysis.

REFERENCES

1. B. Bohannon and B. Poarch, *Proc. Symp. Contam. Control Defect Red. Semi. Manufact. II*, **94-3**, 26 (1994).
2. S. O'Brien, et. al., *Proc. 3rd Intl. Symp. Cleaning Technol. Semi. Device Manufact.*, **94-7**, 233 (1994).
3. C. Draper, et. al., *Proc. 3rd Intl. Symp. Cleaning Technol. Semi. Device Manufact.*, **94-7**, 392 (1994).
4. K. Christenson, *Proc. 3rd Intl. Symp. Cleaning Technol. Semi. Device Manufact.*, **94-7**, 474 (1994).
5. N. Yonekawa, et. al., *Proc. 3rd Intl. Symp. Cleaning Technol. Semi. Device Manufact.*, **94-7**, 94 (1994).

FIGURES

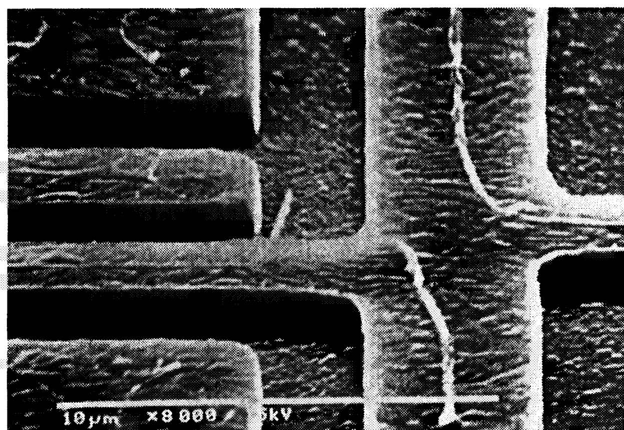

Fig. 1. SEM micrograph of veil polymer on top of metal lithography.

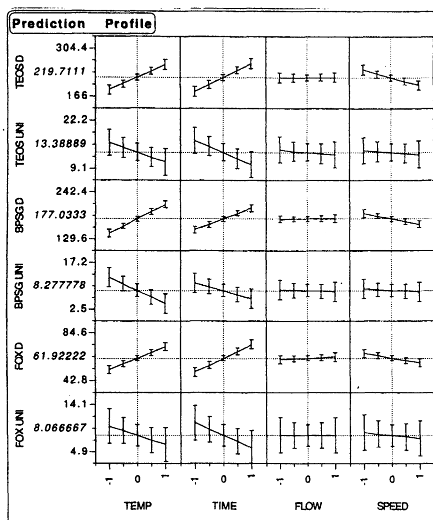

Fig. 2. Clean solution characterization results of 4:1 (EG:BOE) with surfactant.

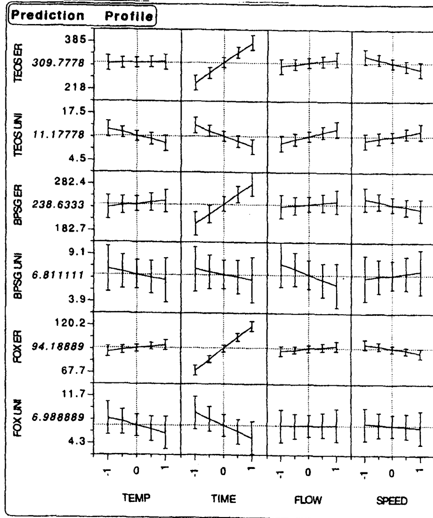

Fig. 3. Clean solution characterization results of 3:1 (EG:BOE) with surfactant.

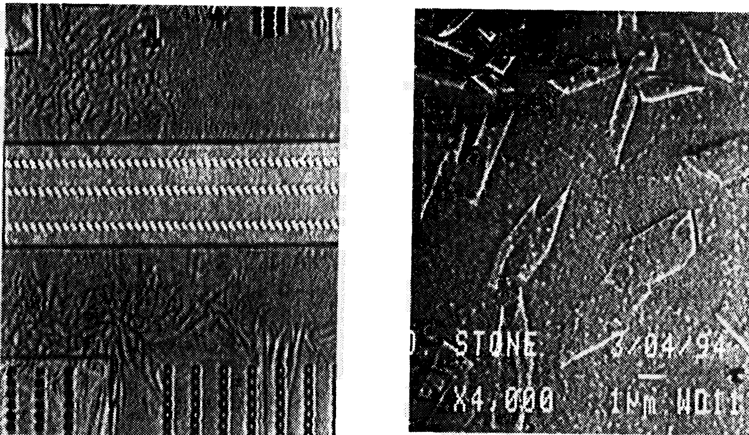

Fig. 4. Optical photograph (left) and SEM micrograph (right) of crystalline defects.

DOUBLE-SIDE WAFER SCRUBBING BEYOND POST-CMP CLEANING

Wilbur C. Krusell, Igor J. Malik, Fred Mohr, and Diane J. Hymes
OnTrak Systems, Inc., 1753 S. Main St., Milpitas, CA 95035

Double-side scrubbing has become the preferred cleaning process for wafers after Chemical-Mechanical Planarization (CMP). The popularity of this cleaning technology for post-CMP cleaning is due to a combination of high particle-removal efficiency, process robustness, and a favorable cost-of-ownership. The post-CMP particle performance (<20 particles >0.2 μm on a 200 mm diameter wafer) motivated the use of scrubbing in a variety of other cleaning steps in the device fabrication process. We give examples of post-cleaning particle and electrical defect density levels for a number of cleaning applications: after deposition of dielectric, metal and barrier layers, plasma etch of dielectric and metal layers, laser marking, and recovery of particle monitor wafers. A clear trend in scrubbing technology involves an addition of chemical cleaning capability so that the scrubbers evolve into "track" chemical cleaners. Surface metals removal capability down to levels interesting for pre-gate clean applications is demonstrated in another example. These developments make the double-side scrubber a single wafer cleaning alternative to wet benches in both front- and back-end applications.

INTRODUCTION

The manufacturing process for advanced integrated circuits typically includes 200-350 discrete steps. Up to 50 of these steps are wafer cleaning processes designed for removal of contamination deposited during previous steps and/or optimization of the surface state for subsequent processing. Liquid-based ("wet") cleaning methods have been competing with gas- and vapor-phase cleaning methods for a number of years. Despite some earlier predictions to the contrary, wet methods still dominate the cleaning processes implemented in manufacturing, in large part due to the inability of gas-and vapor-phase methods to remove particles. The wet cleaning approaches include immersion cleaning (chemical and rinsing action, often complemented by megasonic capability), spray cleaning (chemical and rinsing action), and contact cleaning (mechanical and rinsing action, often complemented by chemical

and megasonic capability). By far the most important contact method is double-side scrubbing using polyvinyl alcohol (PVA) brushes.

Double-side scrubbing has received a lot of attention recently (1-5) mostly because of its dominant position in post-CMP cleaning. The other application where scrubbing is well-established is the cleaning of hydrophilic polished and epitaxial Si wafers. Some of the recently published literature on wafer cleaning (6,7) underestimates the cleaning capability of scrubbers by not taking into account two crucial developments in scrubbing technology: 1. the fact that wafers are cleaned on front and back sides simultaneously (double-side vs single-side scrubbing), and 2. the new brush material (PVA vs harder materials like Nylon) removes submicron particles without any damage to the surface. The goal of this paper is to review the current status of double-side scrubbing technology with the emphasis on four applications referred to as general, i.e., non-CMP, fab cleaning. We discuss examples of scrubbing after different steps (non-CMP) in multilevel metalization, after laser marking through a Si_3N_4 layer, in Si wafer recovery, and in applications demanding very low surface metals levels (pre-gate, pre-diffusion cleans).

EXPERIMENTAL

The wafer cleaning was performed in an OnTrak Systems double-side scrubber DSS-200. Fig. 1 illustrates its layout and outlines the wafer cleaning process in the DSS-200: a cassette of wafers is placed in a wet input station where it is sprayed by deionized water (DIW); from here the wafers are sent individually through two brush boxes and a spin rinse/dry module into an output cassette. Inside the brush boxes the wafers are scrubbed with PVA brushes. DIW is supplied through the brush cores and penetrates the porous structure of PVA. The surface of the brushes has cylindrical nodules with open spaces between them to allow a sufficient DIW flow across the wafer surface. Dilute chemicals can be delivered to the brushes from teflon drip manifolds positioned above the top brushes; the chemicals are delivered at a rate of approximately 30 ml/min.

APPLICATIONS OF DOUBLE-SIDE SCRUBBING

Non-CMP Cleaning in Multilevel Metalization

Multilevel metalization chip designs are widely used in the manufacturing of both logic and memory devices. This metalization process includes a number of cleaning steps for which double-side scrubbing is a suitable technique. The chemical-

mechanical polishing of dielectric layers (SiO_2, BPSG, PSG) and W layers (W-plug formation) can now be considered a mainstream planarization method. Double-side scrubbing is the most widely used post-CMP cleaning technique for both dielectric layers and W-plugs as described recently (1-5). In addition to post-CMP applications, double-side scrubbing is effective in defect reduction after other multilevel metalization steps. In this section we discuss scrubbing after deposition of PSG, SiO_2 (TEOS), metal, and TiN/Ti, and oxide- and W-etchback.

Fig. 2 demonstrates the performance of double-side scrubbing for a metal 1 process sequence not using CMP: Short loop defect data for metal 1 from five independent split lot experiments are shown. The standard processing sequence has no cleaning steps; the experimental splits included three scrubbing steps with DIW only (no chemicals): after phospho-silicate glass (PSG) deposition, after W-etchback, and after metal 1 deposition. The lower defect densities achieved with the use of double-side scrubbing are obvious. The important point is that device yield data, as a rule, follow the same trend as the short loop defect density data, i. e., a significant yield advantage is likely after implementation of double-side scrubbing in device production.

Fig. 3 shows the short loop results for a metal 2 process in which the test wafers were scrubbed with DIW (no chemicals) after SiO_2 (TEOS) deposition, SiO_2 plasma etch, and metal 2 deposition. In this case, the scrubbing was compared to a standard wet bench cleaning process. A total of nine split lots were processed and evaluated for electrical defects using test comb structures similar to the metal 1 test structures (1.4 μm pitch, 0.7 μm line width). Again, a clear decrease in the defect density is seen as a result of the double-side scrubbing cleaning steps.

The normalized electrical defect density data (average ± standard deviation = $\phi \pm \sigma$) are summarized in Table I. It is important to look at the metal 1 and metal 2

TABLE I: Metal 1 and Metal 2 Short Loop Results - Electrical Defect Density Normalized to Mean of Standard Process

	Standard	**OnTrak**
Metal 1 (5 lots)	1.00±0.69	0.56±0.16
Metal 2 (9 lots)	1.00±0.70	0.51±0.40

split lot data not only from the point of view of an overall average of defects but also take into account the tighter distribution for the lots processed through the scrubber.

This reduction in σ is at least as important as the reduction in ϕ. Thus, the scrubber is shown to reduce the influence of variability of preceding production steps on subsequent process steps. It is also important to point out that the PVA brushes do not cause any damage to the printed pattern lines - if they did we would expect the electrical defect density after scrubbing to increase rather than decrease as is the case.

Another example of the use of scrubbing is as a cleaning step after the deposition of a TiN/Ti thin film stack (300 Å Ti - adhesion layer, 1000 Å TiN - diffusion barrier). Fig. 4 shows two Tencor 6420 particle maps (>0.2 μm) of the same TiN/Ti wafer: a) as deposited, and b) after double-side scrubbing using dilute ammonia solution. The particle count decreased from 729 to 59 as a result of cleaning. The particle data for 19 wafers processed in this experiment are summarized in Table II. Again, both ϕ and σ are significantly reduced, resulting in a more robust process.

TABLE II: TiN/Ti blanket wafer particle counts (>0.2 μm), Tencor 6420

As deposited	**After OnTrak scrub**
712±294	74±16

Post Laser Mark Cleaning of Si_3N_4

Laser marking is commonly performed at the beginning of the IC manufacturing process to record process lot information onto the surface of the Si wafer. Laser marking is accomplished using focused laser beams. In this experiment, the process flow consisted of thermal oxidation (500 Å oxide) of the Si wafers, LPCVD deposition of 1800 Å of Si_3N_4, and soft laser marking on the front surface. The subsequent cleaning was done by double-side scrubbing using a dilute ammonia solution; this cleaning approach was compared to a standard post-laser-mark clean consisting of a room temperature megasonic SC-1 bath ($1{:}1{:}4 = NH_4OH{:}H_2O_2{:}H_2O$) followed by DIW rinsing and drying in a spin-rinse dryer. The surface particles were measured by Tencor 6420 (>0.15 μm). Four microview maps of the laser mark region are shown in Fig. 5: a) wafer #02 no clean, b) wafer #02 after scrubbing, c) wafer #13 after standard (SC-1) clean, and d) wafer #13 after standard clean followed by scrubbing. The heavy contamination of the laser mark region immediately after laser marking is clearly visible in Fig. 5a; this contamination has to be dramatically reduced to prevent its release during subsequent wafer processing. Fig. 5b shows that scrubbing can achieve a dramatic defect reduction in the laser mark region while the standard SC-1 clean (Fig. 5c) results in only a marginal improvement. Fig. 5d shows

the defect levels after two subsequent cleaning steps (standard SC-1 followed by scrubbing); the residual defect level is comparable to Fig. 5b demonstrating that double-side scrubbing is capable of effective post-laser-mark wafers cleaning in a single step.

Recovery and Reclaim of Si Wafer Monitors

As the world-wide shortage of Si wafers is becoming more serious, recovery and reclaim of monitor wafers is getting a lot of attention. This is especially true for 200 mm wafers. Recovery is usually defined as recleaning (usually on-site) of contaminated wafers while reclaim involves removal of Si material by polishing followed by cleaning (usually off-site). A large number of bare Si wafers is used both by semiconductor equipment companies and IC manufacturers for monitoring the cleanliness of their equipment and/or process. Typically, after several rounds of experiments these wafers develop levels of particle contamination that make them unsuitable for further use as particle monitors. At this stage the wafers are either discarded (high cost), cleaned in wet benches with often unsatisfactory results, or sent out for reclaim (intermediate cost, very inconvenient).

A typical specification for 200 mm diameter wafers used for particle performance monitoring of CVD equipment is ≤40 particles >0.3 μm, or, for more sensitive applications, ≤40 particles >0.2 μm. Fig. 6 shows particle levels for 200 mm CVD equipment monitors (the cassette also includes several out-of-the-box rejects) before and after scrubbing using a dilute ammonia solution. Data for particles >0.3 μm and >0.2 μm measured by Tencor 6420 are shown. (Four wafers from this cassette were excluded from Fig. 6 because of surface damage due to extensive handling.) It is clear that despite a large spread of the initial particle counts the results after cleaning were uniform. The above cited specification (40 particles max.) is met for all wafers for particles >0.3 μm; 16 of the 20 wafers meet the stricter specification for particles >0.2 μm. Therefore, it is clear that double-side scrubbing is a suitable method for monitor wafer recovery.

Other applications where scrubbers proved useful include the recovery of wet bench rejects, out-of-the-box rejects, as well as CVD oxide and thermal oxide wafers processed in contaminated equipment.

Low Surface Metals Cleans

Two of the most challenging cleaning steps in semiconductor manufacturing

are the pre-gate and pre-diffusion cleans. We will refer to them as low surface metals cleans since in addition to particle removal the achievement of very low surface metals levels ($\leq 10^{10}$ atoms/cm^2) is required. The low metals requirement is due to the detrimental role residual surface metals play in gate oxide integrity (GOI) and charge carrier recombination lifetimes (8). The ability of double-side scrubbers to achieve very low particle levels (<2 particles >0.2 μm on a 150 mm hydrophilic Si wafer) is well established. However, the capability of the double-side scrubbers to remove surface metals needs to be demonstrated. This issue is discussed in the remainder of this section.

The first step in establishing the capability of double-side scrubbing to deliver wafers with low surface metals is to show that the tool itself is strictly metals-neutral when using DIW only. The second step is to demonstrate the actual surface metals removal capability. The first point was accomplished by measuring the metal ion concentration in DIW at two locations: 1. at the DIW input into the scrubber, and, 2. at the brush core through which DIW is delivered to the brushes. The results obtained by ICP/MS (Inductively-Coupled Plasma/ Mass Spectrometry) are summarized in Table III for the eight metals of highest interest to semiconductor processing: clearly, the DIW quality sampled at the brush cores shows no signs of degradation compared to DIW at the machine input. Therefore, we conclude that the scrubber parts coming in contact with DIW do not contribute measurable levels of metalic contamination.

TABLE III: DIW metals concentration (ppb) at DSS-200 input and at the brush cores as measured by ICP/MS (nd=not detected)

Metal	Detection limit	DSS-200 Input	DSS-200 Brush Core
Al	0.007	nd	nd
Ca	0.3	nd	nd
Cu	0.005	nd	nd
Fe	0.05	nd	nd
Ni	0.005	nd	nd
K	0.5	nd	nd
Na	0.01	0.1	0.1
Zn	0.008	0.012	nd

The plating of metals onto a hydrophilic (i.e., native-oxide-covered) Si surface is strongly dependent on pH (9). The low-pH (acidic) environment is desirable for cleaning metals while high-pH (alkaline) environment encourages particle removal.

The challenge then is to use the proper pH environment (or a sequence of them) to get effective cleaning of both metals and particles. For wafers with relatively low incoming particle levels the most promising strategy is the use of acidic chemistries. For wafers more heavily contaminated with particles the alkaline environment is needed; an addition of chelating agents then assures low surface metal levels.

The second point - surface metals removal capability - is demonstrated by the data listed in Table IV. We selected a set of experiments in which the surface metals were studied by two independent methods as a function of the cleaning conditions: TXRF and minority carrier lifetime (believed to be most sensitive to Fe). Group #1 is Si(100) p(-) polished wafers after a SC-1 clean. Ca, Fe, and Zn levels are high and the lifetime correspondingly low. Groups #2 and #3 are wafers processed through the same SC-1 cleaning as #1 followed by double-side scrubbing in the DSS-200. #2 represents the use of alkaline (with a chelating agent) and #3 acidic chemistry in the scrubber. Clearly, both #2 and #3 demonstrate surface metals removal capability of the scrubber based on both TXRF and lifetime data.

TABLE IV: Surface metals by TXRF and minority carrier lifetimes by microwave photoconductive decay method

		Metals in 10^{10} atoms/cm^2						in µs
Group	**Cleaning**	**K**	**Ca**	**Fe***	**Ni**	**Cu**	**Zn**	**Lifetime**
#1	SC1	<20	30	20	<1	<1	30	41
#2	SC1+DSS AMM+C	<20	<8	5	<1	<1	5	389
#3	SC1+DSS CIT	<20	<8	7	<1	<1	3	447

(*): The Fe levels measured by VPD-TXRF on wafers from the same groups were 9, 0.3, and 0.3×10^{10} atoms/cm^2 for groups #1, #2, and #3, respectively.

More data, especially data directly correlated to device yield, is clearly needed to establish double-side scrubbing as a method of choice for pre-gate and pre-diffusion cleans. However, the potential of using this method for applications requiring low surface metals together with low surface particles has been clearly demonstrated.

DISCUSSION

The current picture of the cleaning mechanism relevant to double-side

scrubbing includes a mechanical dislodgment of particles by the brushes followed by flushing of the particles over the edge of the wafer by DIW flowing through the brushes. Brushes can get loaded with particles - this would seriously shorten the brush lifetime (currently around 20,000 wafers, depending on the cleaning application). To prevent brush loading, it is important to use the zeta potential concepts (4,10,11) - to maximize the repulsive forces between particles, wafer surface, and brushes. Fig. 7 shows the zeta potential as a function of pH for several materials important in both CMP and non-CMP cleaning applications. The repulsive forces are maximized in an alkaline environment at pH>9, i. e., at pH higher than the PZC (point of zero charge) of the materials involved. As shown in Fig. 7, the approximate PZCs for SiO_2, PVA, Si_3N_4, and Al_2O_3 are 2.5, 2.5, 4.5, and 8, respectively (4,10,11). The alkaline environment ensures that the zeta potential of all the materials is strongly negative, therefore maximizing the mutually repulsive forces.

The cost of ownership (CoO), although difficult to calculate unambiguously, is in most calculations favorable for double-side scrubbers compared to other types of cleaning equipment. This is due to a combination of factors including low initial capital cost, small footprint, tool flexibility, high throughput, low DIW usage, and low chemical usage (if any). Of course, in cases when an increase in device yield can be directly tied to double-side scrubbing, CoO becomes even more favorable.

Future developments in double-side scrubbing will lead toward further enhancements of chemical capability in order to increase the versatility of this cleaning technology. In particular, the addition of well-established chemistries like SC-1, SC-2, and HF will undoubtedly lead to increased popularity of this cleaning method.

SUMMARY

We discussed the use of double-side scrubbing in several non-CMP applications. A variety of data obtained by different analytical techniques suggests that this cleaning method can produce excellent results in many cleaning steps in which scrubbing has not been used previously. The use of scrubbing after several non-CMP multilevel metalization steps resulted in clear improvement of short loop electrical yields; scrubbing after TiN/Ti deposition resulted in a sharp reduction of surface particles. Scrubbing after laser marking through a Si_3N_4 layer was shown to be superior compared to SC-1 cleaning. Recovery and reclaim of Si monitor wafers was discussed as another useful scrubbing application. And, finally, the potential of double-side scrubbing for pre-gate and/or pre-diffusion cleaning steps was demonstrated. A common feature for all the examples presented, and equally valid for post-CMP applications as well, is the robustness of the scrubbing process, i.e., the

consistency of the cleaning results even when starting with wafers with widely varying levels of contamination. This robustness of performance together with favorable cost of ownership makes double-side scrubbing a strong candidate for a variety of cleaning applications within the microelectronics industry.

ACKNOWLEDGMENTS

The authors would like to acknowledge the contributions of OnTrak customers, Prof. S. Raghavan's group (Univ. of Arizona, Tucson), and our colleagues from OnTrak J. J. Farber, J. Zhang, A. J. Jensen, R. Holbert, and J. Patterson.

REFERENCES

1. S. R. Roy, I. Ali, G. Shinn, N. Furusawa, R. Shah, S. Peterman, K. Witt, S. Eastman, and P. Kumar, J. Electrochem. Soc. **142**, 216 (1995).
2. W. C. Krusell, J. M. de Larios, and J. Zhang, Solid State Technol., 109 (June 1995).
3. D. L. Hetherington, P. J. Resnick, R. P. Timon, B. L. Draper, M. Ravkin, J. M. de Larios, W. C. Krusell, and A. F. Madhani, 156, Proc. of VMIC Specialty Conf. on Dielectrics for ULSI Multilevel Interconnection (DUMIC), Feb. 20-22, 1995.
4. I. J. Malik, J. Zhang, A. J. Jensen, J. J. Farber, W. C. Krusell, S. Raghavan, and C. Raghunath, Ultraclean Semiconductor Processing Technology and Surface Chemical Cleaning and Passivation, Materials Research Society Symposium Proc. (Spring 1995).
5. M. Ravkin, J. J. Farber, I. J. Malik, J. Zhang, A. J. Jensen, J. M. de Larios, and W. C. Krusell, ibid.
6. D. C. Burkman, D. Deal, D. C. Grant, and C. A. Peterson, p. 111, in Handbook of Semiconductor Wafer Cleaning Technology, W. Kern ed., Noyes Publications (1993).
7. V. B. Menon and R. P. Donovan, p. 379, ibid.
8. P. W. Mertens, M. Meuris, S. Verhaverbeke, M. M. Heyns, A. Schnegg, D. Graf, and A. Philipossian, in Institute of Environmental Science 38th Annual Meeting Proceedings, Vol. 1, p. 475 (IES, 1992).
9. H. Hiratsuka, M. Tanaka, and Y. Matsushita, 180th ECS Meeting Proceedings, 2nd International Symposium on Cleaning Technology in Semiconductor Manufacturing, Phoenix, AZ (1991).
10. I. Ali, S. Raghavan, and S. H. Risbud, Semiconductor International, 92 (April 1990).
11. D. E. Jan and S. Raghavan, J. Electrochem. Soc. **141**, 2465 (1994).

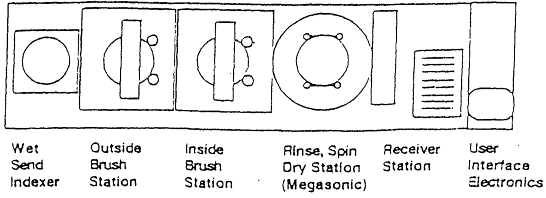

Fig. 1: DSS-200 double-side scrubber configuration.

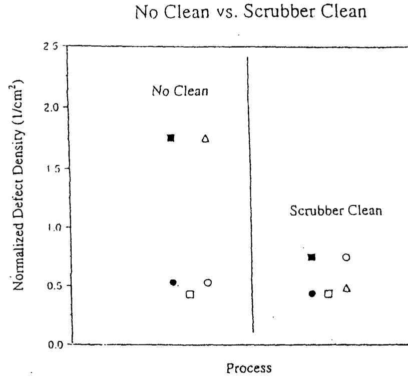

Fig. 2: Short loop electrical defect data for Metal 1.

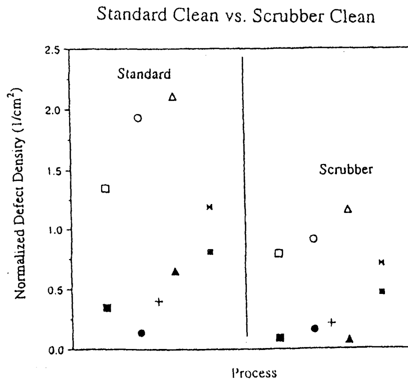

Fig. 3: Short loop electrical defect data for Metal 2.

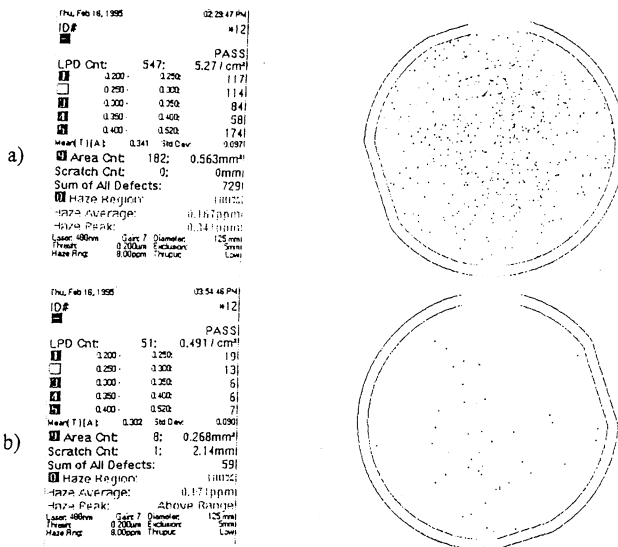

Fig. 4: Tencor 6420 defect maps (>0.2 μm) of a TiN/Ti film stack. a) As deposited. b) After double-side scrubbing.

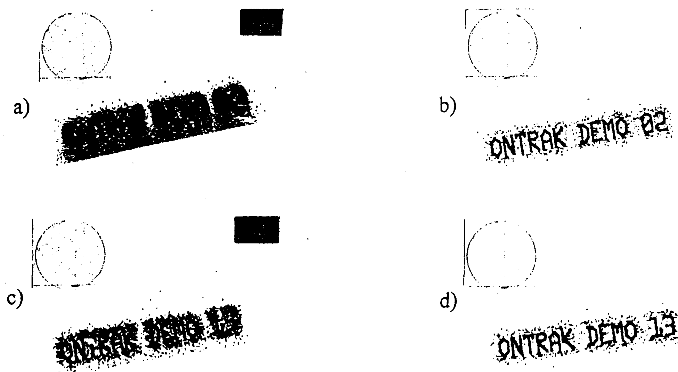

Fig. 5: Tencor 6420 microview maps (>0.15 μm) of the laser mark region. a) No clean. b) After double-side scrubbing. c) After SC-1 clean. d) After SC-1 clean followed by double-side scrubbing.

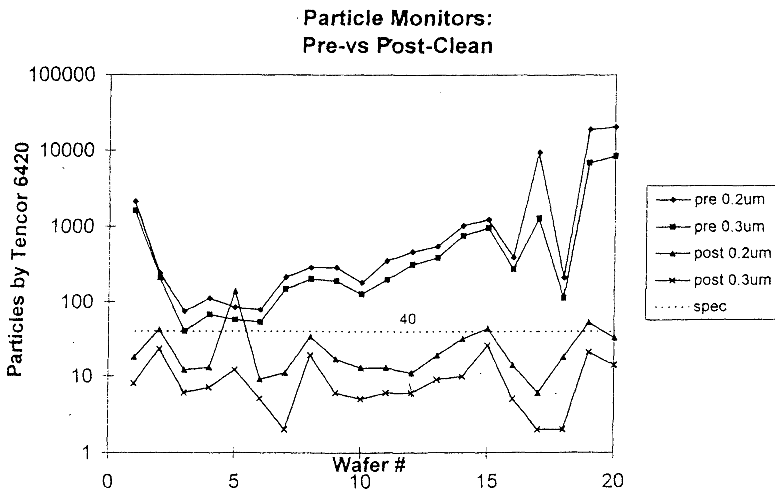

Fig. 6: 200 mm particle monitor wafers: Particle levels before and after double-side scrubbing for particles >0.2 μm and >0.3 μm. The dotted line (40 defects) represents a typical specification for particles >0.3 μm.

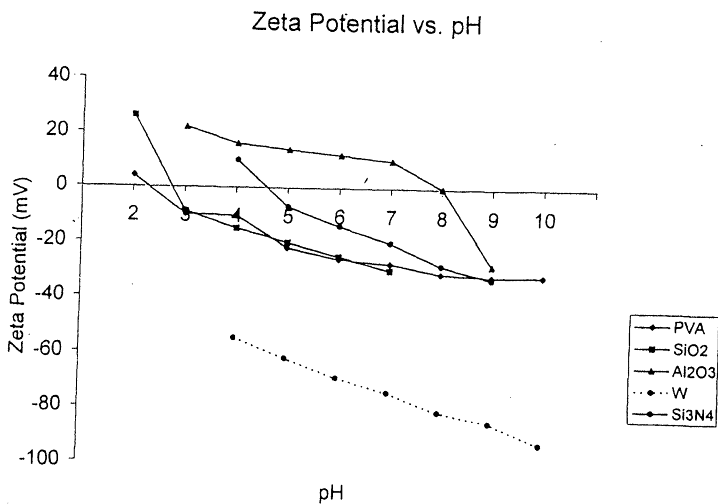

Fig. 7: Zeta potential as a function of pH for PVA, SiO_2, Al_2O_3, W, and Si_3N_4.

WATER CONSUMPTION AND RINSE CONSIDERATIONS IN SEMICONDUCTOR WET PROCESSING

Chris McConnell, Huw Thomas, Steven Verhaverbeke,
Steve Bay, and Jennifer W. Parker

CFM Technologies, Inc.
1381 Enterprise Drive
West Chester, PA 19380

A theoretical analysis of semiconductor wafer rinsing and DI water consumption is presented. Overall flow characteristics are compared with velocities and turnover rates assuming by-pass flow around the wafers. A CSTR model is used to predict rinse performance given desired initial and final contaminant concentrations. Finally, a simulation is used to estimate throughput and DI water consumption in wet processing systems that allow flexible dwell times.

INTRODUCTION

In recent years, increasing attention has focused on the environmental impact of semiconductor manufacturing. Once generally considered a clean, high-tech industry, wafer fabrication facilities now are being viewed more and more as chemical processing plants that consume copious quantities of water and use among the most dangerous chemicals known today (both liquid and gas). As the chip industry continues its historic expansion, this "chemical-plant" image is increasingly becoming a reality.

Although the industry is making significant progress in chemical conservation, water consumption has continued to grow at an alarming rate. This paper investigates scaling factors, modeling, design considerations, and performance expectations associated with water rinsing and DI consumption. Process choices for designing recipes that can significantly enhance rinsing speed and lower water consumption are also examined.

IMPACT OF RINSE TANK DESIGN

Two basic designs of wet processing systems are commonly used in the semiconductor industry for precision cleaning: immersion benches and plug-flow processors. Immersion tanks typically have relatively large tank volumes and 200mm wafers are spaced at 1/4" in a full load. In contrast, plug-flow processors are designed to have small vessel sizes and wafer pitch is half that of an immersion tank. For a given flow rate, a gross estimate of the effect of tank volume can be determined by calculating the turnover time, τ, for the vessel as a whole:

$$\tau = V / Q \qquad [1]$$

and, V = tank volume (gallons)
Q = volumetric flow rate (gpm)

The results of this estimate are shown in Table 1. Rinse tank volume is clearly linked to wafer diameter, but, it is also linked to inter-wafer spacing. In the move from 150mm to 200mm wafers, for example, wafer pitch in standard immersion systems increased 50%, from 3/16" to 1/4". While most direct material costs increased in proportion to the surface area, (i.e., by a factor of 1.78), DI water consumption rose by at least a factor of 2.67 (i.e., increase in surface area x increase in pitch $\approx$ 2 x 1.5). For the coming conversion to 300mm wafers, not only the effects of wafer diameter, but also the often-ignored impact of wafer spacing must be considered.

Recently, investigators have developed detailed chemical flow distribution (CFD) models that calculate flow characteristics and velocity profiles in conventional overflow tanks as well as in plug-flow processors [1-4]. In fully loaded systems, in both tank designs, DI flow tends to follow the path of least resistance and travels around the wafers rather than through the wafers because of open gaps at each end of the wafer stack. In the case of overflow tanks, this "by-pass flow" typically exceeds 85% [2]. In plug-flow systems, where the end gaps are minimized, by-pass flow is less than 13% [4].

The degree of flow by-passing the wafers has a large effect on rinsing effectiveness. Table I shows the ramifications of by-pass flow on rinsing; the turn-over time is estimated for the *flow through the wafers*, the flow to which wafer surfaces are actually exposed. This flow is modeled by assuming that the flow through the wafers is the total flow minus the by-pass flow. Additionally, the effective volume considered with by-pass flow is the volume available for water in the cylinder created by the wafer stack as given by:

$$V_{eff} = \pi r^2 50(p - \delta) \qquad [2]$$

where,

V_{eff} = effective volume with by-pass flow
r = wafer radius (100mm)
p = wafer pitch (1/4" for immersion tank; 1/8" for plug flow)
δ = wafer thickness (725μ)

The plug-flow vessel differs from the conventional rinse tank by a factor of three in overall volume and associated flow character; however, as a result of by-pass flow, this difference is greatly magnified at the wafer surface. The fluid velocity and volume turnover rate between the wafers is 13 times greater in the plug-flow system than in the overflow tank design.

RESISTIVITY MEASUREMENTS OF ELECTROLYTES

In order to fully understand rinse dynamics, the standard method for monitoring chemical concentrations in rinse baths, resistivity, must be considered. Resistivity is a measure of how many ions are present in a solution. The resistivity of a solution is dependent on how much an electrolyte dissociates (as indicated by the dissociation constant) as well as the inherent conductivity of each ion (as indicated by the ultimate equivalent conductivity). The dissociation constants and ultimate equivalent conductivities for a number of semiconductor cleaning reagents are given in Table 2. Using the values given in Table 2, the resistivity was calculated as a function of concentration for dilute solutions. These results are given in Figure 1. Note that these results are given in terms of ppb (i.e., a weight basis) and that the acids and basis actually dissociate on a molar basis, thus HF appears to be a stronger acid than H_2SO_4 only because for a given weight (or ppb level) there are more moles of HF than H_2SO_4. Table 3 provides a comparison of molarity and ppb levels.

When resistivity is used to determine chemical concentration, consideration of what chemical is being measured is critical. Figure 1 clearly indicates that for the same ppb levels, different chemicals will yield different resistivity readings. Additionally, carbonic acid is included to show the effects on resistivity measurements when solutions are exposed to a small amount of carbon dioxide, as in an open bath. The carbonate ion will readily alter the resistivity reading at the extremely low chemical concentrations levels desired in semi-conductor rinsing.

MODELS OF RINSING

Electrolyte Rinsing

In considering rinse dynamics of an over-flow tank, a CSTR model (continuous stirred tank reactor) provides a useful frame of reference. In this analytical model, any fluid that enters the tank becomes mixed instantaneously. Any fluid that exits the tank has a concentration identical to that within the tank. Recent studies[1-4] have indicated that mixing in a wet bench is not at all instantaneous; the CSTR model, however, provides a rough estimate of rinsing efficiency.

In ideal plug-flow, no mixing occurs and whatever is in the reactor is completely displaced by what enters the reactor in exactly one vessel volume. In actual plug-flow wet processing system, some mixing occurs and so the actual operating conditions are somewhere between ideal plug-flow and ideal-CSTR models. A CSTR model can also be used as a "worst case" model of a plug-flow processor.

Under the operating conditions of:

- constant volume, V,
- constant flow rate in and out of the bath or vessel, Q,
- initial concentration in the vessel of C_o, and
- no chemical reaction occurring in the bath (i.e., only dilution),

the following equation governs the concentration, C, in a CSTR at any time, t:

$$C = C_o * \exp\left[\frac{-Qt}{V}\right] \qquad [3]$$

Equation 3 can be used to estimate rinsing times for various bath configurations. Figure 2 indicates rinse times as a function of final bath concentration, C, given in terms of ppb. Assuming an initial concentration of 0.5% (e.g. 100:1 HF), an ideal 7.5 gallon. A CSTR (i.e., a standard immersion vessel) flowing at 10 gpm would require 11.6 minutes to reach 1 ppb. Due to the nature of dilution and the assumption of perfect mixing, increases in flow and/or decreases in tank volume have a direct impact on rinse time. For example, a 2.5 gallon CSTR (i.e., a standard plug-flow vessel) requires only 3.9 minutes to achieve the same result.

By-pass flow dramatically affects rinsing time. Using the models for by-pass flow presented in Table 1, the rinse times can be estimated using Equation 3. Dramatically different results are obtained with the immersion tank and the plug-flow reactor. The rinse time for the immersion reactor almost *doubles*, because the flow through the wafers is substantially reduced due to the relatively large end-gaps. In contrast, the rinse time for the plug flow reactor actually *decreases* as a result of the small operating volume in the plug-flow model. Clearly, the ratio of V/Q is critical in optimizing rinse time; V should be minimized while Q is kept as large as possible.

Particle Rinsing

Rinsing particles provides a completely different challenge than rinsing electrolytes since most wet processing systems do not include monitors for particle levels in the rinse water. No easy, cost-effective, on-line method exists to count sub-micron particles, today.

Prior to considering the rinsing dynamics of particles, determination of the possible starting concentration of particles is necessary. A mass balance for an SC-1 clean provides an estimate of such a starting level. Consider the removal of 5Å of oxide from a 200mm wafer with SC-1. The volume of material removed is 1.57e+7 μ^3 of SiO_2. SiO2 is known to precipitate out of solution at certain pH values[5]. The volume of a 0.2 μ diameter particle is 4.19e-3. Consequently, if this volume of material comes out of solution as 0.2 μ particles, then 3.75 billion particles would be generated!

The CSTR model can, again, be used to estimate rinsing times. In order to use this model, the correct initial and final concentrations must be approximated. The initial particle count can be assumed to be the particles generated by 100 surfaces (i.e., front and back of 50 wafers): 3.75 e+11 particles. These particles are assumed to be distributed throughout the entire volume of the immersion bath or the plug-flow vessel. In contrast, to calculate the final acceptable particle concentration, only those particles that are near to the wafers are of concern. Consequently, in our model we assumed that for particle rinsing only 10 particles should be in the vicinity of each wafer surface. In other words, 10 particles per wafer surface should remain in the volume defined by the wafer stack, the effective volume. Thus, C from Equation 3 is $10/V_{eff}$. The values for V_{eff} are given in Table 1.

Following the same arguments as used in the models of electrolyte rinsing, the estimated rinse times for particle rinsing from ideal tanks and tanks with by-pass flow can be generated. Figure 3 shows these results. A comparison of Figures 2 and 3 shows that the rinsing times for particles are all slightly longer than those for electrolytes, although certainly

within the same order of magnitude. The slightly longer times for particle rinsing are a direct result of the ratio of the initial to final concentrations. Although the initial concentration range for particles is much lower than that of electrolytes (if each molecule of electrolyte is considered a particle), the acceptable final particle concentration is much lower than that of electrolytes. Consequently, the ratio of C_0/C is more than 150 times greater for particles than for electrolytes.

WATER CONSUMPTION

The consumption of DI water during wet processing is an increasing concern for semiconductor manufacturers. Both plug-flow and conventional immersion systems are designed to conserve water when not in use by reducing flow rates substantially, down to the level of "idle bleeds." A direct comparison of the water consumed per batch and per wafer is presented in Table 4 based on conventional flow rates. The data for the plug-flow reactor in this table is for a dual vessel system, so flow rates as well as batch sizes are doubled. Use of a dual-vessel system in this model allows similar throughputs to a conventional immersion system to be compared. The data given in Table 4 is based on standard SC1-SC2 processing. The results presented in Table 4 clearly show that the plug-flow design conserves water, largely as a result of the small vessel volume. Also, shown in Table 4 is the effect of tool utilization; the more that the tool is used, the less water required per wafer. This result clearly shows the effect of idle bleeds.

Bleeds are required when tools are idle in order to reduce bacteria growth. Bacteria growth is minimized if the flow is turbulent within the tube or pipe. Figure 4 shows the flow rate as a function of tube size required for turbulent flow (i.e., Reynolds Number $\geq$ 2000). Clearly, the flow necessary to achieve turbulence increases with pipe diameter. The ratio of the required bleed to the maximum flow rate (i.e., 8ft/sec), however, decreases with diameter. In other words, a larger pipe delivers more flow with proportionally less bleed required. This result is shown in Table 5, where the bleed rates for different number of lines is shown on a equal flow basis. Clearly, one large pipe is substantially more efficient in terms of low water consumption during bleeds than many small pipes. Thus, a single rinsing vessel with a larger pipe uses less water for bleeds than a multi-bath system.

IMMERSION TANK RECIPE SIMULATIONS

Batch wet processors, like plug-flow systems, are relatively straightforward to analyze in terms of wafer throughput and DI water consumption. A fixed number of wafers are loaded into each batch, the process runs for a certain predictable time period, and DI consumption can be determined in a straightforward manner. Althogh considerable flexibility exists in terms of dwell times and DI consumption rates for each individual step. The overall process time and DI consumption is simply the sum of the values for all steps. As previously discussed idle-bleed rates must also be calculated.

Wet benches, on the other hand, are more difficult to analyze because different strategies exist for "loading" the system and managing throughput. At one extreme, a wet bench can be operated as a batch tool, one lot at a time, with complete flexibility. To increase throughput, a wet bench can be operated in continuous "lock-step" mode. In this case, the process conditions must be the same for all lots and dwell times for each bath must be identical.

An intermediate approach is to permit process flexibility while processing multiple lots. This strategy requires sophisticated computer scheduling to forecast and prevent conflicts. We have developed a simulation of conventional bench wet process dynamics. This model allows the user to define separate processes, rinse times, and rinse flow rates. Dwell times are not constrained. By simulating thousands of batches in a few moments, this simulator calculates wafer throughput and DI consumption for the entire system. During idle times in each rinse tank, the model assumes minimum DI flow rates required to achieve turbulence, such as those shown in Figure 4 and Table 5. Simulations using this model can account for chemical change-outs and other down times. The through-put of a wet bench (lots/hour) as well as the gallons/lot can be calculated with this model.

The results of simulations based on a typical RCA process (HF/rinse/SC1/rinse/SC2/rinse/dry with associated times of 3/10/10/10/10/10 minutes, respectively) are shown in Figure 6. Since the drying process is the rate limiting step, the simulations assume that the dryer is 100% utilized. As can be seen in Figure 6, initially the efficiency is 0 (no wafers/hour) until the first lot makes it through the process. At this point the gallons of DI water consumed per lot processed is very high. As the number of lots processed increases, a semi-steady state is reached. Every time a chemical change is required (10 minutes every four hours), the gallons/lot increase and the wafers/hour decrease even though only idle flow is used during the change. This oscillatory behavior must be accounted for when the true efficiency of a wet bench is considered.

The affect of specific recipes and chemical change-outs on throughput and water consumption is illustrated by the simulation results shown in Table 6. Changing chemicals drastically reduces through-put and increase water consumption. Experience in actual wet processing environments suggests that certain intermediate rinses can be radically shortened, or even eliminated. Other intermediate rinse steps must be thorough to avoid particle contamination. For example, in an SC-1 / HF / SC-2 recipe, the rinse between HF and SC-2 can be abbreviated without any harm to the wafers, but the rinse between the SC-1 and HF must be thorough. The effect of such short recipes can lead to substantial DI water savings. Typically, however, through-put will not increase since the drying process is the rate limiting step and is already fully utilized.

CONCLUSIONS

The water use associated with wet processing of semiconductor wafers is dramatically increasing despite efforts to control chemical consumption and minimize waste. Tank design has a huge effect on the volume of water required for wet processing. Small tank volumes and minimal pitch cut down on wasted water. Additionally, small tank volumes also minimize by-pass flow, leading to more efficient rinsing. Mass balances indicate that by-pass flow cause rinse times to be doubled in overflow tanks with large by-pass flows.

Mass balances on electrolytes and particles show that rinsing particles is as difficult as rinsing electrolyte impurities due to the extremely low final particles counts necessary to minimize yield loss. Additionally, resistivity is a useful tool for measuring electrolyte levels, whereas standard wet processing systems do not have on-line particle measurement systems for sub-micron particles.

Bleeds, low tool utilization, and chemical change-outs in wet benches can all dramatically increase the DI water consumed per wafer. Simulations indicate that there are ramp-up effects associated with every chemical change-out required on conventional immersion systems, causing such systems to consume more water per wafer processed than plug-flow processing systems. Optimized recipes can help to reduce water consumption even if throughput remains the same.

REFERENCES

1. A. Tonti, "Contamination by Impurities in Chemicals During Wet Processing," in Proceedings of the Second International Symposium on Cleaning Technology in Semiconductor Device Manufacturing, The Electrochemical Society, p. 409, 1992.

2. J.J. Rosato, R.N. Walters, R.M. Hall, R.G. Lindquist, R.G. Spearow, and C.R. Helms, "Studies of Rinse Efficiencies in Wet Cleaning Tools," in Proceedings of the Third International Symposium on Cleaning Technology in Semiconductor Device Manufacturing, The Electrochemical Society, p. 94, 1993.

3. S.N. Kempka, J.R. Torczynski, A.S. Geller, J.J. Rosato, R.N. Walters, and S.S. Sibbett, "Evaluation of Overflow Wet Rinsing Efficiency," in Conference Proceedings of MICRO '94, p. 225, 1994.

4. S.T. Bay, C.F. McConnell, H.K. Thomas, M.G. Izenson, and J. Murthi, "Computational Fluid Dynamic Modeling and Flow Visualization of an Enclosed Wet Processing System," presented at the MRS Meeting, Spring 1995.

5. S. Kubota, "Properties of Ultrapure Water," in Ultraclean Technology Handbook, Vol 1., ed. by T. Ohmi, Marcel Dekker, NY, p 45, 1993.

TABLES

Table 1. DI Rinse Flow Comparison

	Conventional Immersion Tank	Plug-Flow Vessel
Process Volume	7.5 gal	2.5 gal
Total DI Flow Rate	10 gpm	10 gpm
• Fluid Velocity	0.23 in/s	0.70 in/s
• Turnover Time	45 sec	15 sec
• Turns in 10 min.	13 x	40 x
DI Bypassing Wafers	>85% [2]	<13% [4]
Effective Volume	2.334 gal	1.016 gal
Flow Through Wafers	1.5 gpm	8.7gpm
• Fluid Velocity	0.07 in/s	0.86 in/s
• Turnover Time	93 sec	7 sec
• Turns in 10 min.	6 x	87 x

Table 2. Semiconductor Electrolyte Constants

Chemical Reagent	Equivalent Conductivity (S-cm2/mol)	Dissociation Constants
H_2SO_4	160.0	∞
H_2CO_3	44.5	$K_a = 4.3 \times 10^{-7}$
HCl	76.3	∞
NH_4OH	73.5	$K_b = 1.774 \times 10^{-5}$
HF	55.4	$K_a = 3.53 \times 10^{-4}$

Table 3. Comparison of ppm and Molarity Concentrations of Electrolytes

Chemical Reagent	Concentration at 12 MΩ-cm		Concentration at 16 MΩ-cm	
	ppb	mol/l (x 10^9)	ppb	mol/l (x10^9)
H_2SO_4	9.4	235	3.0	110
H_2CO_3	8.5	140	3.1	50
HCl	4.5	135	1.5	45
NH_4OH	4.0	125	1.9	40
HF	2.7	95	0.9	30

Table 4. Typical DI Flow Consumption

	Dual Vessel Plug Flow	Conventior Immersio
Idle Bleed	3 gpm	5 gpm
Fully Loaded	9 gpm	30 gpm
80% Utilization		
• Gallons/Day	11,200	36,000
• Gallons/Batch	220	520
• Gallons/Wafer	**4.4**	**10.5**
50% Utilization		
• Gallons/Day	8,600	25,200
• Gallons/Batch	270	590
• Gallons/Wafer	**5.4**	**11.7**

Table 5. Bleed Rates for Multiple Lines (Sized for Equal Flow)

	Flow Area (in^2)	Max. Flow (8 ft/s)	Req'd Bleed (Re=2200)
1x1" Pipe	0.79	20 gpm	0.70 gpm
4x1/2" Pipe	0.79 in^2	20 gpm	1.39 gpm
8x1/2" Tube	0.88 in^2	22 gpm	2.09 gpm
16x3/8" Tube	0.79 in^2	20 gpm	2.78 gpm

Table 6. Recipe Simulation Results

	Wafers/ Hour	Gallons/ Batch
Simple Rinse Dry (10 min.)	295	65
Full RCA Clean (infinite chemical life)	280	370
Full RCA Clean (4 hour chemical life)	175	415
Full RCA Clean (short exposures)	175	340
The short exposure process is HF/rinse/SC1/ rinse/SC2/ rinse/dry with associated times of 3min/4min/5min/12min/5min/8min/10min.		

Figure 1: Resistivity of Water Containing Trace Ions

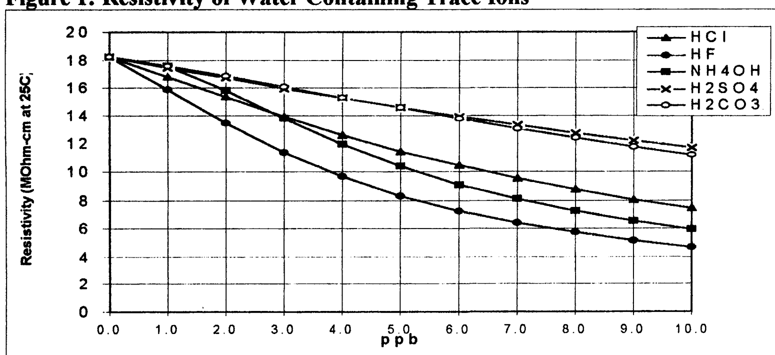

Figure 2. Electrolyte Rinsing Times for CSTR Models

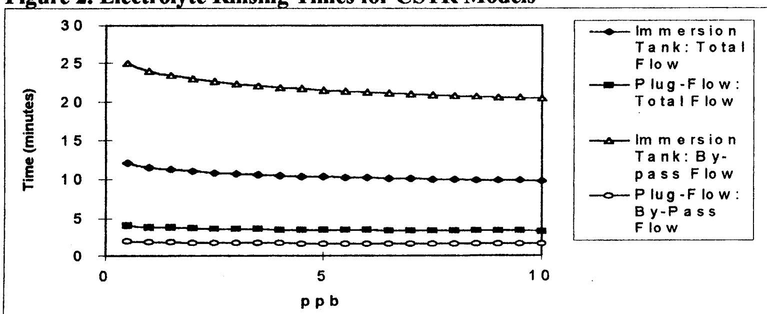

Figure 3. Particle Rinsing Times for CSTR Models

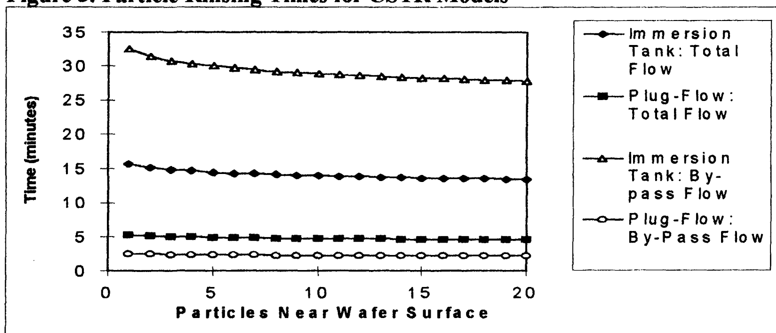

Figure 4. Minimum Turbulent Flow at Various Pipe Sizes

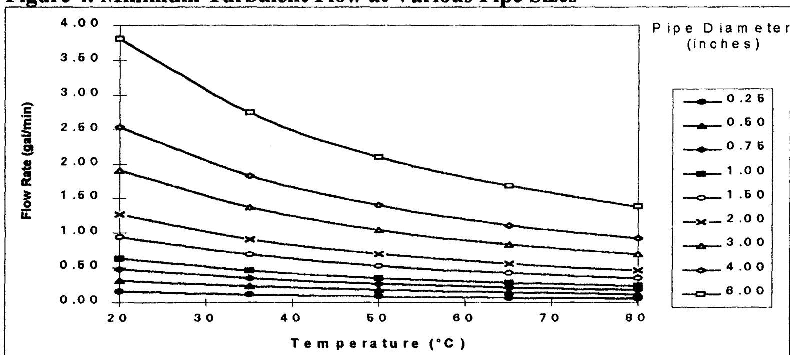

Figure 5. Conventional Wet Bench Simulation Results

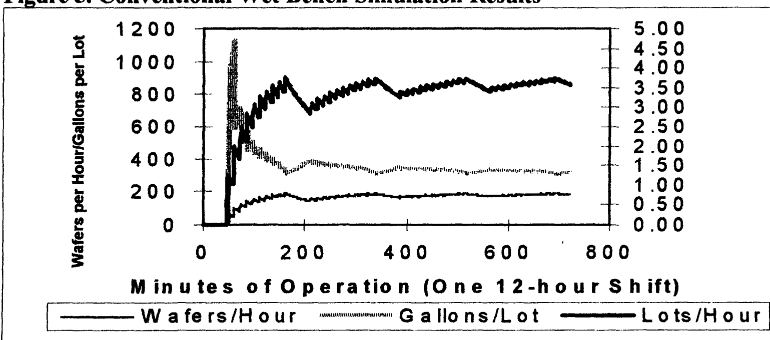

ETCH UNIFORMITY OF THERMAL OXIDE DURING HF-WET PROCESSES

I. Kashkoush, R. Novak, B. Rajaram, and F. Carrillo

SubMicron Systems, Inc., 6330 Hedgewood Dr., #150

Allentown, PA 18106

ABSTRACT

Thermal oxide etching from wafer surfaces is considered to be one of the more critical steps in the fabrication of IC devices. This removal of the oxide layer must be performed as uniformly as possible. In wet processing, HF aqueous solutions are typically used to remove oxide layers. It is the task of process engineers and equipment manufacturers to use the appropriate equipment design and the correct parameters to achieve the desired etch uniformity. In this study, we investigate how etch uniformity is affected by wafer transfer speeds, concentration, and fluid flow in the process tank. Preliminary results indicate that the etch uniformity is a strong function of the wafer transfer speeds and HF concentration.

1. INTRODUCTION

The process of complete or partial removal of an oxide layer from silicon surfaces is one of the critical steps in wet processing technology [1]. Although many researchers have focused their work on the kinetics of using HF to etch silicon dioxides, little research has been done on the uniformity of the oxide etching. Good etch uniformity is very important across the wafer as well as from wafer to wafer. The etch uniformity from lot to lot must be given the same attention. As wafer size increases and device sizes become smaller, etch uniformity will be more critical and harder to achieve using current wafer processing techniques.

Typically, silicon dioxide is etched in HF acid aqueous solutions. The use of BOE (Buffered Oxide Etchant) is commonly used to enhance the etch rate. This mixture of HF and NH_4F raises the pH of the solution to values between 3 and 5. This prevents the depletion of fluoride ions and leads to stable etch characteristics [1,2]. The silicon dioxide etch rate in BOE is 4-5 times greater than the etch rate in aqueous HF. Some surfactants are also added to BOE solutions to improve the wetting properties of silicon surfaces. Thin oxides are etched in dilute HF solutions while thick oxides are etched in highly concentrated HF chemistries. Process throughput and particle contamination are the

factors that determine the HF concentration. Most of these processes are typically performed at a temperature between 20-35 C.

Etch rate strongly depends on the HF concentration and bath temperature. It is safe to say that etch uniformity is a function of the etch rate, flow characteristics in the process tank, and other process parameters (e.g. speeds at which wafers are immersed into and lifted out of the process tank). Reported values of about 1.5-2% (1 σ) for etch uniformity seem to be acceptable by most IC manufacturers. The achievable etch uniformity values seem to be equipment specific.

2. EXPERIMENTAL

The variables considered in this study were: the immersion speed (S1), pull-up speed (S2), average velocity of fluid in the process tank and the concentration of the HF acid (which was varied between 0.5% to 5% by weight). A full factorial Design of Experiments (DOE), consisting of a series of 27 experiments, was designed for this purpose to investigate the variables that affect the etch uniformity across 200 mm wafers. A pre-diffusion clean wet processing system (GAMA-1™) was used in SubMicron's Class 1 Applications Laboratory, in Allentown, PA for these experiments. The station features cassetteless wafer handling which eliminates cassette shadowing and slot constraints during the etching process.

Wafers with approximately 6000 A° of thermally grown oxide were used for these experiments. HF solutions in concentrations of 0.5%, 2.5% and 5.0% (by weight) were used. A target oxide layer of 600 A° was removed at 24 °C. The test wafer was placed in slot #13; 49 dummy wafers filled the remaining slots. A series of experiments was conducted to ensure the repeatability of results at the selected slot (#13). Experiments were also conducted to examine the etch uniformity across the tank. In order to minimize the DOE matrix, the rinse cycle was not varied. Wafers were rinsed for 10 minutes and then dried in an IPA dryer. Wafers were pre-measured and post-measured at Rockwell International, Newport Beach, CA. 49 sites were measured in both cases and the mean thickness of oxide removed and standard deviation were recorded.

3. RESULTS AND DISCUSSION

3.1. Effect of Immersion and Pull-up Speeds

The effect of immersion and pull-up speeds on the etch uniformity is shown in Fig 1. The data show that the etch uniformity increases (σ% decreases) with the increase in both the immersion and pull up speeds at constant fluid velocity and HF concentration. For an immersion speed of 230 [units] and pull up speed of 500 [units], the percentage standard deviation was 2.215. However, for an immersion speed of 30 [units] and pull up speed of 30 [units], with all other experimental conditions remaining the same, the percentage standard deviation increased to 5.225. A similar trend may be observed in figures 2 - 6.

The following rough calculations demonstrate the theoretical limits of the dependence of etch uniformity on immersion and pull up speeds. Assuming that the maximum immersion speed (S1) is 230 [units] and the maximum allowable pull up speed (S2) is 500 [units], the time required to fully immerse and pull out a 200 mm wafer is = 200/S1 + 200/S2. Depending on the etch rate of the HF concentration and the target oxide layer to be removed, there will be a limit on the uniformity that is achievable (please see Table 1). These theoretical uniformity values will be reduced by a factor of 0.625 in the case of 150 mm wafers and increased by a factor of 1.5 for 300 mm wafers [3]. Table 1 below enumerates several cases that were examined:

Table 1. Calculated Theoretical Etch Uniformity Limits for 200 mm Wafers.

HF/BOE Concentration	Etch Rate (A°/s)	Etched Oxide (A°)[1]	Theoretical sd %[2]
100:1 (HF)	0.58	0.62	0.103
20:1 (HF)	2.79	2.97	0.495
40:1 (BOE)	4.166	2.78	0.463[3]

3.2. Effect of Fluid Velocity

The effect of average fluid velocity on the uniformity was also investigated. The average fluid velocity was varied by operating the recirculation pump at different supply pressures and hence changing the pump discharge. Three pressure levels --P2, P4, and P7 (20 psi, 45 psi, and 70 psi)-- were used. Figures 1 and 2 show the percentage standard deviation contours for the pressure levels P2 and P7. The data indicates that the fluid flow (within the given range of P2-P7) does not seem to be a major contributor to the variation in etch uniformity. As may be seen from figures 1 and 2, the lowest percentage standard deviation at pressure P2 is 2.215, and at P7 is 1.998. For these experiments, Reynolds Number, Re_D, (based on 200 mm wafer diameter D) was estimated to vary between 500 and 1000 from P2 to P7, respectively. In this narrow range of Re_D for the laminar flow, a strong dependence of the etch uniformity on the average fluid velocity was not obtainable at this time. More experimental data is required to confirm this observation.

[1] The amount of oxide etched from the bottom edge of the wafer during immersion and pull up while the upper edge is still in the air.

[2] A mean value of 600 A was assumed to have been removed.

[3] Only a time of 0.666 s for immersion was used in this calculation.

3.3 Effect of HF Concentration

The effect of the HF concentration on the etch uniformity can be obtained from figures 1,3, and 5. As shown in the figures, etch uniformity increases (σ decreases) as etch rates decrease (lowering HF concentration decreases etch rate). Uniformity values of 2.215 were obtained at 5% HF while values of 0.748 were obtained at 0.5% HF when tested under the same conditions.

Obviously, the etch rate plays an important role in the etch uniformity. The lower edge of the wafer enters the process bath first and is withdrawn last. As a consequence, there will be a "non uniformity" in the etch across the surface of the wafer [2]. For the purpose of rough estimates, the bottom edge of a 200 mm wafer will stay in the acid for approximately 1.26 s longer than the upper edge, at the experimental values of immersion and pull out speeds. An etch rate of 2.79 A°/s is expected in 5% HF at 24 °C. This means that an amount of 1.26 s x 2.79 A°/s = 3.5 A° more will be etched from the lower edge as compared to the upper edge of the wafer. The data shows that the lower etch rate results in better uniformity, as may be seen from figures. 1, 3, and 5 or figures 2, 4, and 6.

4. CONCLUSIONS

The following conclusions can be drawn:

- The etch uniformity is a strong function of immersion and pull up speeds.
- Etch uniformity also depends upon the HF concentration (or the etch rate of SiO_2).
- In this part of the study, the effect of the average fluid velocity on the etch uniformity is not clear. However, the etch uniformity is slightly improved by increasing the fluid velocity.
- It has been demonstrated that there is a theoretical limit to uniformly etching the thermally grown SiO_2. The theoretical limit is affected by the wafer size, immersion and pull up speeds, flow dynamics, and etch rate.
- The preliminary data shows that the etch uniformity can be improved by lowering the etch rate, increasing the immersion and pull-up speeds, and increasing the average fluid velocity on the wafer surface.

ACKNOWLEDGMENT

The authors would like to thank NCR Corp. and Rockwell International for their assistance in providing their tools for part of the experiments.

REFERENCES

1. Kern, W., Handbook of Semiconductor Wafer Cleaning Technology, Noyes, 1993.
2. Ruska, W.S., Microelectronic Processing, McGraw-Hill, 1987.
3. Kashkoush, I.I., SMS Technical Reports, Nov./Dec. 1994.

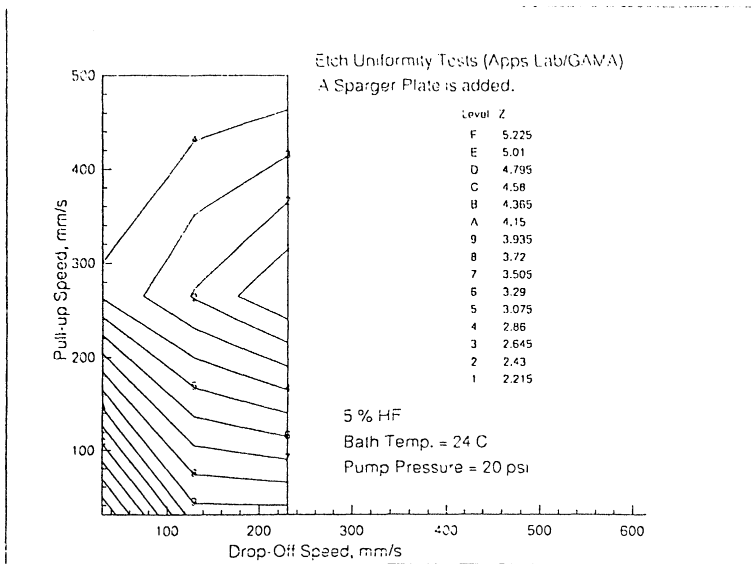

Figure 1: Variation of Etch Uniformity with Wafer Immersion and Pull-up Speeds (P2 and 5% HF).

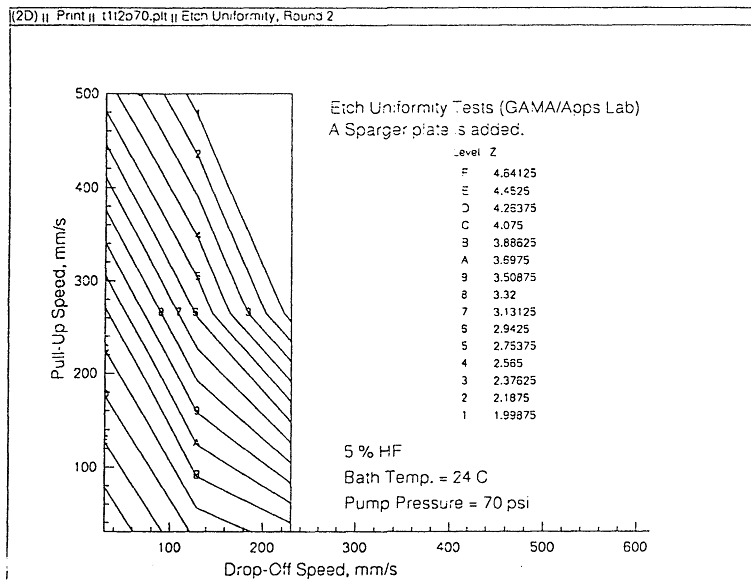

Figure 2: Variation of Etch Uniformity with Wafer Immersion and Pull-up Speeds (P7 and 5% HF).

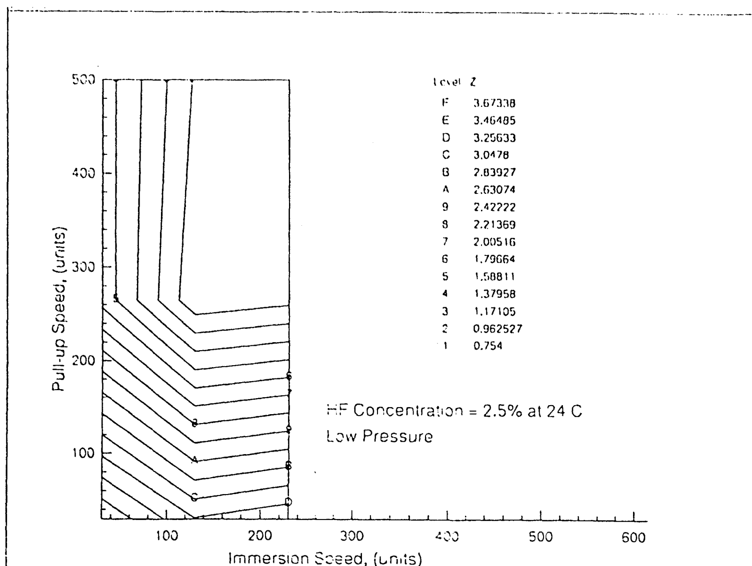

Figure 3: Variation of Etch Uniformity with Wafer Immersion and Pull-up Speeds (P2 and 2.5% HF).

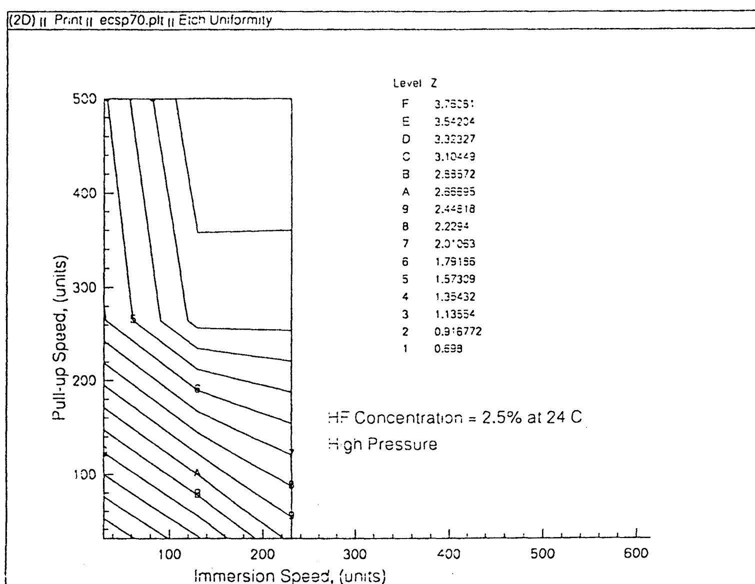

Figure 4: Variation of Etch Uniformity with Wafer Immersion and Pull-up Speeds (P7 and 2.5% HF).

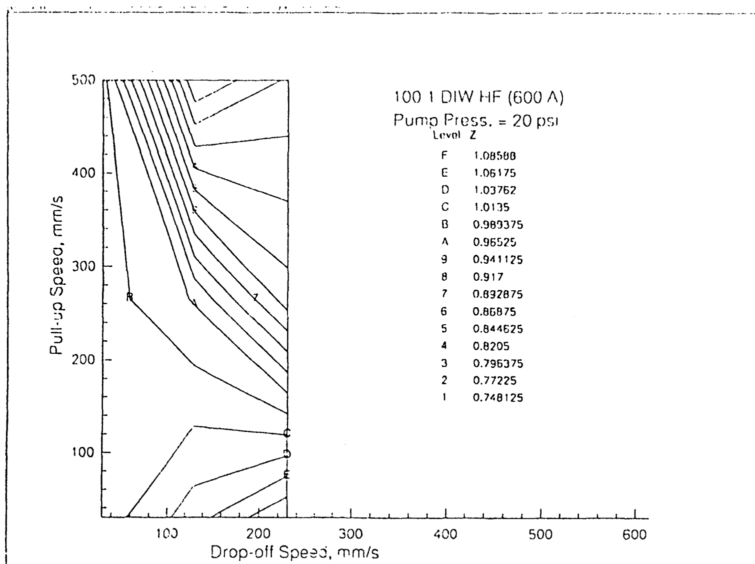

Figure 5: Variation of Etch Uniformity with Wafer Immersion and Pull-up Speeds (P2 and 0.5% HF).

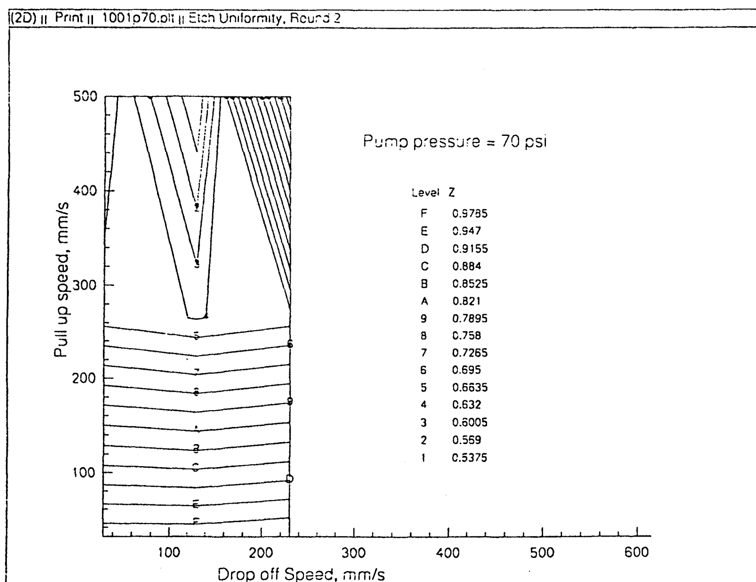

Figure 6: Variation of Etch Uniformity with Wafer Immersion and Pull-up Speeds (P7 and 0.5% HF).

SMOOTHING OF Si (100) SURFACE MICROROUGHNESS BY A NEW ETCHING SOLUTION BHF/H_2O_2

Yoshinori Muramatsu, Mikio Tsuji and Nahomi Aoto
ULSI Device Development Laboratories,
NEC Corporation
1120 Shimokuzawa, Sagamihara, Kanagawa 229, Japan

We propose a new buffered hydrofluoric acid (BHF) - mixed chemical solution, BHF/H_2O_2, for SiO_2 etching. With this mixture, the Si (100) surface microroughness is decreased and a smooth surface is achieved. It is due to Si surface oxidation and oxide etching that occur simultaneously in BHF/H_2O_2.

INTRODUCTION

The control of surface microroughness during the VLSI device fabrication processes is highly important subject in achieving high device performance and reliability. Among the conventional wet treatments, SiO_2 etching by buffered hydrofluoric acid (BHF), and cleaning by ammonia - hydrogen peroxide mixture (APM) are known to increase Si (100) surface microroughness [1] - [5]. Although the BHF treatment characteristics such as stable high etching rate are useful, the surface microroughness degrades the device performance [1] - [3].

It is well known that adding surfactant to the BHF effectively suppresses surface microroughness [4] [5]. The surfactant molecules, however, may remain on the wafer surface and cause carbonic contamination. Thus it is better if the surface microroughness is suppressed by BHF without adding surfactant.

In the present work, we examine a new BHF - mixed chemical solution, BHF/H_2O_2, for SiO_2 etching. With this mixture, a smooth Si (100) surface is achieved without surfactants. The etching rate of SiO_2 is sufficiently high as that of BHF. We studied the

phenomena of Si surface microroughness suppression by the BHF/H_2O_2 treatment and the relation with the Si etching rate. The origin of the surface smoothness was revealed by a simulational experiment.

EXPERIMENTAL

Phosphorus (P) doped n-type Czochralski-grown Si (100) wafers were used. The surface after native oxide etching by diluted hydrofluoric acid (DHF), whose average surface microroughness (Ra) is 0.12 - 0.22nm, were used as reference.

The wafers were immersed in BHF (HF : 6 weight percent, NH_4F : 30 weight percent, H_2O : 64 weight percent) at room temperature for 30 minutes. To the BHF solution, H_2O_2 (30 weight percent) was added to between 0.01 and 10 volume percent. For the comparison of H_2O_2-added BHF to just diluted BHF, H_2O-added BHF solutions were also prepared. Two types of samples with different initial surface microroughness were used : one type is with smooth surfaces treated by DHF, and another type is with intentionally roughened surfaces by BHF treatment. After these treatments, surface microroughness was measured by an atomic force microscope (AFM).

The relationship between surface microroughness and Si etching, was evaluated for the BHF-based solutions and the components of the solutions: HF, NH_4F, and H_2O_2. In this experiment, the concentration of added H_2O_2 or H_2O to BHF was fixed at 0.1 volume percent. These treatments were performed at room temperature.

For the investigation of the microroughness smoothing effect by adding H_2O_2, the alteration of Si surface microroughness was examined by repeating Si surface oxidation by H_2O_2 (30 weight percent) dipping and surface oxide removal by DHF (6 weight percent) dipping at room temperature. The dipping time in H_2O_2 was 5 minutes. DHF dipping was continued for 1 minute.

RESULTS AND DISCUSSION

Figure 1 shows the surface microroughness, Ra, as a function of concentration of

H_2O_2 or H_2O in BHF. The microroughness after the BHF/H_2O treatment increased to approximately 0.37 nm, which was about three times the reference value. In contrast, the microroughness after the BHF/H_2O_2 treatment was lower than that after the BHF/H_2O treatment.

Figure 2 shows AFM line plot images of the microroughness evaluated in Figure 1, after treated by : (a) BHF/H_2O (H_2O : 0.1 volume percent), 30 min., (b) BHF/H_2O_2 (H_2O_2 : 0.1 volume percent), 30 min. It is actually shown that the surface was roughened after the BHF/H_2O treatment. On the other hand, after BHF/H_2O_2 treatment, the microroughness was obviously suppressed and a smooth surface was achieved.

Figure 3 shows the immersion time dependence of the surface microroughness after treated by BHF/H_2O (H_2O : 0.1 volume percent) and BHF/H_2O_2 (H_2O_2 : 0.1 volume percent). By the BHF/H_2O treatment, the microroughness was increased to approximately 0.3 nm within 10 minutes. The microroughness maintained the increased level after the BHF/H_2O treatment longer than 10 minutes. In contrast, by the BHF/H_2O_2 treatment, the microroughness did not increased.

To clarify the influence of the H_2O_2 additive on surface microroughness, intentionally roughened Si surfaces of approximately 0.3 nm Ra were used as the initial surfaces. Figure 4 shows the alterations of Ra by BHF/H_2O (H_2O : 0.1 volume percent) and BHF/ H_2O_2 (H_2O_2 : 0.1 volume percent) treatments as a function of immersion time in the solutions. It is shown that the surface microroughness was decreased to approximately 0.15 nm by the BHF/H_2O_2 treatment with an increase in the immersion time. In contrast, the BHF/H_2O treatment did not alter the surface roughness. This indicates that the BHF/ H_2O_2 treatment has the effect of smoothing the initial surface microroughness.

For the investigation of the origin of the surface microroughness, the influence of each component of the solutions on microroughness was examined. Figure 5 shows the comparison of the microroughness for several solutions. The microroughness became higher after immersion in NH_4F (30 weight percent) and BHF/H_2O (H_2O : 0.1 volume percent) solutions than after immersion in BHF/H_2O_2 (H_2O_2 : 0.1 volume percent), DHF, or H_2O_2. The results indicate that the surface microroughness that occurs in BHF treatment is caused by the reaction with NH_4F. It is also indicated that H_2O_2 performs the effect of suppressing the microroughness.

The influence of each component on Si etching rate was also examined as shown in Figure 6. The NH_4F treatment etches Si at a high rate, which may cause large surface microroughness such as shown in Figure 5. By comparing BHF/H_2O_2 and BHF/H_2O, the

BHF/H_2O_2 treatment has a higher Si etching rate than BHF/H_2O (Figure 6), but causes less surface microroughness (Figure 5). Thus it is suggested that higher etching rates do not always result in more surface microroughness. Adding H_2O_2 both increases the Si etching rate and smooths the surface microroughness.

From the above mentioned phenomena, it is considered that the Si etching process of BHF/H_2O_2 differs from that of BHF. In the BHF treatment, the surface microroughness increased because the Si is etched by NH_4F. In contrast, in the BHF/H_2O_2 treatment, Si surface oxidation by H_2O_2 and oxide etching by HF occurs simultaneously. During the simultaneous oxidation and etching reactions, the Si surface microroughness is smoothed to suppress the initial surface microroughness.

To validate this model, the alteration of surface microroughness by simultaneous oxidation and etching in BHF/H_2O_2 was simulated by repeating Si surface oxidation by H_2O_2 and surface oxide etching by DHF. Figure 7 shows the surface microroughness after repeating the H_2O_2 treatment and the DHF treatment. The surface microroughness decreased gradually with repeated oxidation and etching.

With the results, we propose a model of Si surface alteration during the BHF/H_2O_2 treatment as illustrated in Figure 8. In BHF/H_2O_2, Si surface microroughness is smoothed by Si surface oxidation and oxide etching that occur simultaneously. It is supposed that peaks of the microroughness are oxidized more easily than the valleys because the oxidants diffuse from all around the peaks. Thus the microroughness are smoothed through oxidation and simultaneous etching.

CONCLUSIONS

BHF/H_2O_2 treatment acts to decrease Si (100) surface microroughness. This effect is considered due to the simultaneous occurrence of Si oxidation and oxide etching. It is essentially different from the Si surface reaction with BHF/H_2O, in which the surface microroughness increases due to the direct Si surface etching by NH_4F.

ACKNOWLEDGMENT

The authors would like to thank Drs. M. Kamoshida, M. Kikuchi and A. Ishitani for their encouragement and advices.

REFERENCES

1. T. Ohmi, M. Miyashita, M. Itano, T. Imaoka, and I. Kawanabe, IEEE, Trans. Electron Devices, **39**, 537 (1992).
2. M. Miyashita, T. Tsuga, K. Makihara, and T. Ohmi, J. Electrochem. Soc., **139**, 8 (1992).
3. T. Ohmi, K. Kotani, A. Teramoto, and M. Miyashita, IEEE Electron Device Let., **12**, 12 (1991).
4. H. Kikuyama, N. Miki, K. Saka, J. Takano, I. Kawanabe, M.Miyashita, and T. Ohmi, IEEE Trans. Semicond. Manuf., **3**, 99 (1990).
5. M. Miyamoto, N. Kita, S. Ishida, and T.Tatsuno, J. Electrochem. Soc., **141**, 10 (1994).

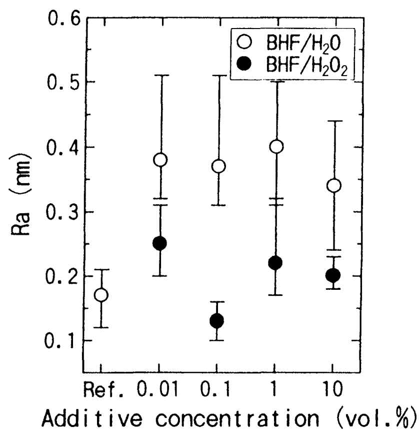

Figure 1. Relationship between surface micro-roughness and concentration of H_2O or H_2O_2 added to BHF, after a 30 minute BHF-based treatment by each solution.

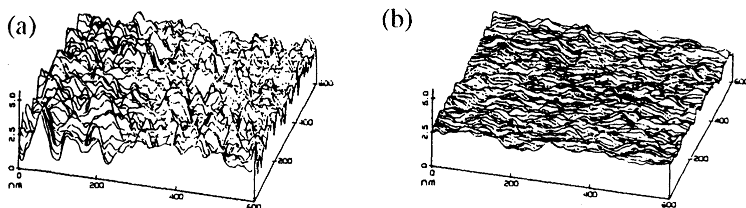

Figure 2. AFM line plot images after treated by :
(a) BHF/H_2O (H_2O : 0.1 volume %), 30 min.,
(b) BHF/H_2O_2 (H_2O_2 : 0.1 volume %), 30 min.

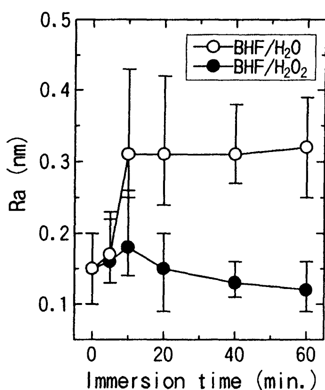

Figure 3. Relationship between surface microroughness and immersion time of H_2O or H_2O_2 (0.1 vol. %) added to BHF, with smooth initial surfaces.

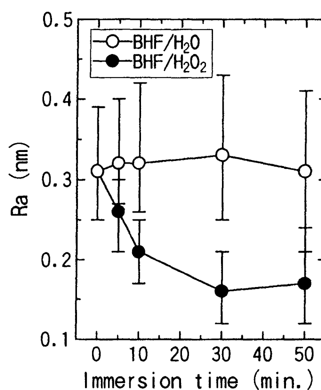

Figure 4. Relationship between surface microroughness and immersion time of H_2O or H_2O_2 (0.1 vol. %) added to BHF, with roughened initial surfaces.

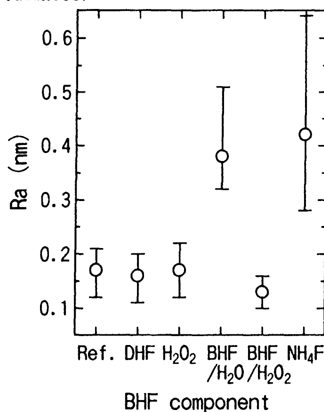

Figure 5. Relationship between surface microroughness and BHF-based solution and components of the solutions, after a 30 minute treatment by each solution.

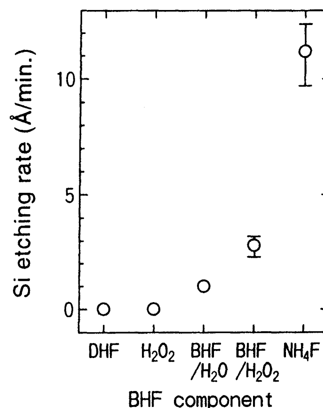

Figure 6. Relationship between Si etching rate and BHF-based solution and components of the solutions.

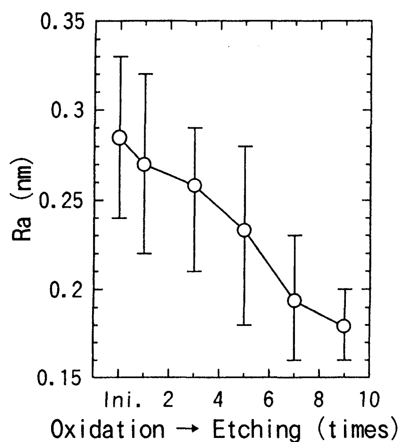

Figure 7. Relationship between surface micro-roughness and repeating times of Si surface oxidation by H_2O_2 (30 weight %) and oxide etching by DHF (6 weight %).

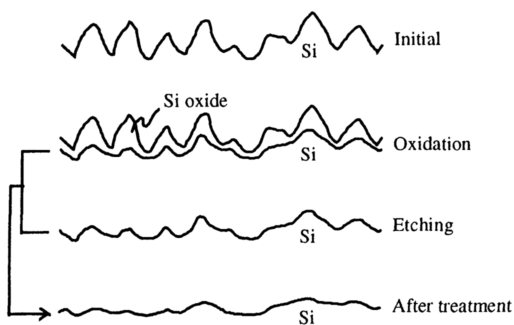

Figure 8. Model of Si surface microroughness smoothed in BHF/H_2O_2 by Si surface oxidation and oxide etching that occur simultaneously.

DETERMINATION OF THE H-PASSIVATION BUILD-UP TIME IN DHF-TREATMENTS

M. Meuris[1], H. Izumi*, K. Kubo*, S. Ojima*, T. Ohmi*, and M.M. Heyns

IMEC, Kapeldreef 75, 3001 Leuven, Belgium.
[1] *Work done at Tohoku University*
*Department of Electronics, Faculty of Engineering, Tohoku Univ., Aza-Aoba, Aramaki, Aoba-ku, Sendai 980, Japan

A quantitative model for the contact angle increase when etching silicon surfaces with DHF mixtures is proposed. The model agrees well with experimental data and can be used to measure the resistance of chemical oxides against DHF etching. It is shown that the etch time of an SPM oxide is longer than the one of an O_3/H_2O oxide and a SC1 oxide.

Introduction

Contact angle measurements are a measure for the amount of H-termination of the silicon surface [1]. The purpose of this study was to obtain a quantitative model to explain the relationship between the contact angle measurements and the hydrogen termination of hydrophobic silicon surfaces.

Model

When measuring the contact angle of a silicon surface covered with a (chemical) oxide as a function of the etch time in a DHF (Dilute HydroFluoric) solution, one expects the following curve (see Fig. 1). As long as more than one monolayer coverage of the chemical oxide is present, the contact angle will be lower than 5°. However, once the last monolayer of oxide is started to be etched by the HF molecule, the contact angle will gradually increase. The time to etch the chemical oxide down to this last monolayer is defined as t_0 and the time to obtain a complete hydrogen passivation (time to increase the contact angle from roughly <5° up to roughly 70°) is defined as t_1.

The contact angle θ is defined as the equilibrium of the forces acting on the liquid at the contact point of the liquid with the gas and the solid (see Fig. 2). The forces are F_{gs} (gas-solid), F_{gl} (gas-liquid) and F_{ls} (liquid-solid) [2]:

$$F_{gs} = F_{gl} \cdot \cos\theta + F_{ls} \qquad (1)$$

This equation means that in steady state conditions the sum of the forces acting on the liquid is zero. When rewriting eq. (1)

$$\frac{F_{ls}}{F_{gs}} = 1 - \frac{F_{gl}}{F_{gs}} \cdot \cos\theta \qquad (2)$$

At this point we make an assumption. F_{ls}/F_{gs} is the liquid-solid interaction force relative to the gas-solid interaction force acting on the liquid molecules. When looking to Fig. 2 one can observe that when reducing F_{ls} (or increasing F_{gs}) the contact angle will increase to obtain the equilibrium of forces. As mentioned in the introduction the contact angle

increases during the hydrogen passivation build-up of the silicon surface. Therefore it is reasonable to assume that F_{ls}/F_{gs} is equivalent to the concentration c_H of Si-H bonds on the silicon surface. Remark that the Si-H bonds only change the properties of the surface (not of the liquid or the gas) and therefore only can influence the forces F_{ls} (liquid-**solid** interaction) and/or F_{gs} (gas-**solid** interaction). The force F_{gl} will be constant because there is no change in the liquid or the gas.

$$F_{ls}/F_{gs} \sim c_H \qquad (3)$$

Also another consideration is necessary. In DHF mixtures, an HF molecule attacks a silicon atom of the last monolayer of the chemical oxide to create an Si-H bond [3]. In general this can be written as:

$$\text{Si-X} + \text{HF} \rightarrow \text{Si-H} + \text{Y} \qquad (4)$$

For the mathematical derivation here it is not necessary to define X and Y. If we assume that a Si-X bond is attacked by HF with a reaction rate k to form Si-H and [Si-H] = c_H, we can write:

$$\frac{dc_H}{dt} = k \cdot [Si - X] = k \cdot (1 - c_H) \qquad (5)$$

solving eq. (5) with $\tau = 1/k$ gives

$$c_H \sim 1 - e^{-(t-t_0)/\tau} \qquad (6)$$

The etching of the last monolayer starts at $t = t_0$. This means that t_0 is the time necessary to remove the chemical oxide in the DHF solution. Taking eq. (2), (3) and (6) with b as a constant gives:

$$1 - \frac{F_{gl}}{F_{gs}} \cdot \cos\theta = b \cdot (1 - e^{-(t-t_0)/\tau}) \qquad (7)$$

Because $\cos\theta \approx 1$ ($\theta < 5°$) when $c_H = 0$ (i.e. at $t = t_0$), we can write eq. (7) as:

$$\cos\theta = (1 - b) + b \cdot (1 - e^{-(t-t_0)/\tau}) \qquad (8)$$

This equation models the time dependence of the contact angle as a function of etch time when the last monolayer is etched to form the H-passivation of the silicon surface. The fitting parameters are t_0, τ and b. t0 is the time to etch the chemical oxide until the last monolayer and gives information how resistant the chemical oxide is against HF etching.τ is the time constant of the hydrogen passivation built-up. b is a value which is related to the value of the contact angle when a complete hydrogen passivation is obtained. Although in principal this value is unique for all contact angle measurements (and should not be fitted), it will be discussed later on why we need it as a fitting parameter in practice.

Results and discussion

As a first test for the model, the contact angle was measured as a function of dipping time for a SPM (sulfuric peroxide mixture) chemical oxide in 0.5% HF. In Fig. 3(a) the contact angle data are plotted. In Fig. 3(b) the cosine of the contact angle data are shown. The solid line shows the fitted curve through the data points using eq. (8). Only b, t_0 and τ is used as a fitting parameter. The value for (1-b) is 0.3, τ is 34 s and t_0 = 7.2 s. According to this fit, the etching time of a chemical oxide is extremely short, compared to the time constant τ

for the hydrogen passivation build-up. This is in agreement with the high etch rate for SiO_2 in DHF mixtures compared to Si.
Further, three different chemical oxides were made to measure the resistance of these chemical oxides against DHF etching. The chemical oxides were: an O_3 oxide (10 min immersion in 8 ppm O_3/H_2O at room temperature), a SPM oxide (10 min immersion in (4/1) H_2SO_4/H_2O_2 mixture) and a SC1 oxide (10 min in (0.05/1/5) $NH_4OH/H_2O_2/H_2O$ at 80 °C). To obtain sufficient resolution, a DHF mixture of 0.05 vol%HF was used, with 0.5 molar HCl added (to reduce the etch rate of the oxide). The contact angles were measured after every minute etching. Eq. (8) was applied for fitting the etching of three different chemical oxides. In Fig. 4 the contact angle measurements of the 3 different chemical oxides are shown. In Fig. 5 eq. (8) is fitted to the data of Fig. 4 with only b, t_0 and τ as fitting parameters. In table I, these parameters are tabulated (1-b=0.27 for all 3 oxides). One can observe that the etch time for removal of the chemical oxides (2 to 4 min) is very short compared with the time to etch the last monolayer of silicon, necessary to become Si-H bonds (12 to 14 min for 90% coverage). Note that a SPM oxide is more resistant to DHF etching (t_0=4.2 min) than a O_3 oxide (t_0=3.5 min) and a SC1 oxide (t_0=2.0 min).
Although these fitted curves agree well with the experimental data points, a remark is necessary to clarify a practical problem in determining accurately the contact angle on hydrophobic surfaces. When on a hydrophobic surface a droplet of DI-water is placed, one will observe a decrease of the contact angle as a function of waiting time due to the re-oxidation of the silicon surface by the contact of the water. Especially at high contact angles this effect becomes severe and a rapid reoxidation occurs (contact angles are dropping very rapidly by 3 to 5° and stay stable afterwards). This effect makes it very difficult to obtain accurate data when the hydrogen passivation is almost completed. This is leading to an inaccurate determination of the fitting parameter b in eq. (8).

Conclusions

In this study a model to explain the contact angle variation when etching the last monolayer of a chemical oxide was proposed. The method allows also to determine the resistance of a chemical oxide against DHF etching. It is shown that a SPM oxide needs longer etch times than a O_3/H_2O oxide and a SC1 oxide.

Acknowledgments

M. Meuris is indebted to the Japanese Society for Promotion of Science for the invitation to participate in the research at Tohoku University in the laboratory of Prof. Ohmi.

References

[1] S. Verhaverbeke et al., Proceed. MRS **259**, 391 (1992).
and J.L. Alay et al., Jpn. J. Appl. Phys. **32**, 358 (1993).
[2] T. Young, *Trans. R. Soc. London* **95**, 65 (1805).
[3] Y.J. Chabal, Proceed. MRS **259**, 349 (1992).

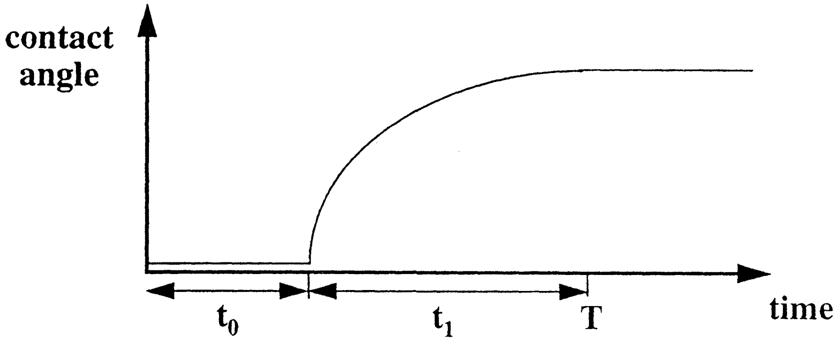

Fig. 1: Expected contact angle change as a function of DHF etching time for a chemical oxide on a silicon surface. the time t_0 is the time to etch the chemical oxide, the time t_1 is the time to etch the last monolayer of silicon and build-up of the H-passivation of the silicon surface.

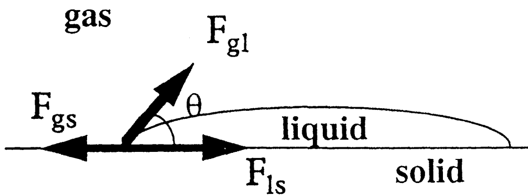

Fig. 2: Schematic of the forces acting on a liquid droplet placed on a solid surface (sessile drop technique). The liquid spreads out over the solid until (definition of the contact angle) an equilibrium between the forces is established (sum of forces = 0).

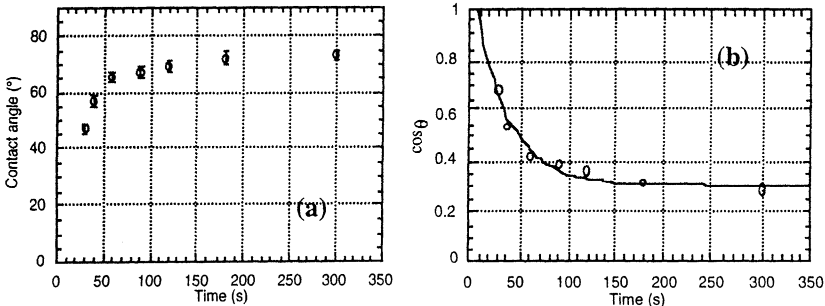

Fig. 3: (a) Contact angle measurements as a function of etching time in a 0.5% HF mixture of an SPM oxide. (b) The data of (a) fitted to the model of eq. (8).

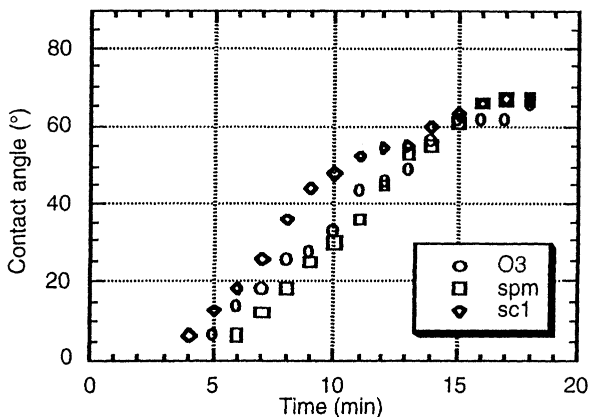

Fig. 4: Contact angle measurements as a function of etch time of 3 different chemical oxides, using a 0.05%DHF/0.5 molar HCl mixture.

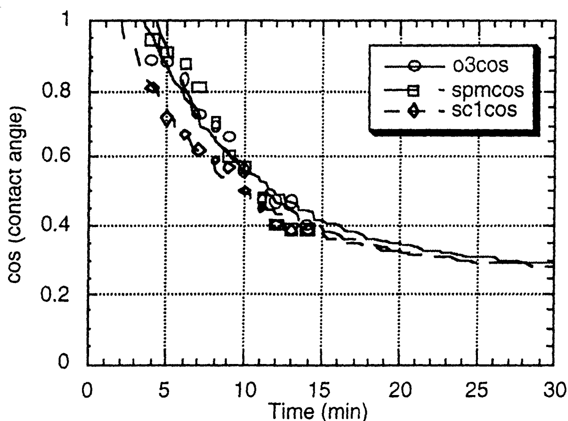

Fig 5: The data of Fig. 4 using eq. (8).

Table I: The fitting parameters for the curves of Fig.4 (1-b = 0.27).

oxide	τ (min)	t_0 (min)
SPM	6.1	4.2
O3	7.2	3.5
SC1	6.7	2.0

CHEMICAL OXIDE GROWTH AND ITS INFLUENCE ON SUBSEQUENT HF CLEANING

L. Li, E. Grieger, K. Griffiths, S. Byrne, R.C. Hawthorne

Micron Technology, Inc., 8000 S. Federal Way PO Box 6, Boise, ID 83707-0006

ABSTRACT

A chemical oxide growth process prior to the HF step is known to improve the performance of HF last wafer cleaning. This study relates to the treatment of bare silicon wafers in H_2SO_4:H_2O_2; H_2SO_4:O_3; and H_2O:O_3. Results are reported for growth rate and composition of the chemical oxide, the impurity content in the surface oxide layer, and the rinse efficiency for the treatment in these three oxidizing solutions. The metallic contamination and surface roughness after the oxide growth and HF clean is investigated by TXRF and AFM. And, the influence of various chemical oxide formations on the subsequent HF clean is discussed.

INTRODUCTION

In advanced cleaning processes for 256 Mbit technology, HF last clean is an attractive way to obtain reduced surface roughening while removing metallic contamination from the wafer surface.[1] Prior to the HF step, wafers are processed through an oxidizing solution to remove critical organic contamination, and to grow a fresh chemical oxide to improve particle removal in the subsequent HF clean.[2] Sulfuric acid/hydrogen peroxide (H_2SO_4:H_2O_2) mixtures are widely used for this application, but residues are difficult to remove by normal DI water rinse.[3] Ozonized DI water (H_2O:O_3) efficiently removes residual organic and grows an effective chemical oxide on the wafer surface.[4] In this work, a detailed study examines the treatment of bare silicon wafers in H_2SO_4:H_2O_2, H_2SO_4:O_3, and H_2O:O_3. Results are reported for growth rate and composition of the chemical oxide, the impurity content in the surface oxide layer, the rinse efficiency for the three treatments, and the influence of the various chemical oxide formations on the subsequent HF clean.

EXPERIMENTAL

The substrates used in this work are CZ, p-type Si (100) with resistivity between 1 to 10 Ω cm. All wafers were cleaned in 0.5% HF for 5 minutes to remove the native oxide, then rinsed and dried prior to the oxide growth experiments. The chemical solutions used

for the experiments were: 100:1 H_2SO_4:H_2O_2 at 125°C; H_2SO_4:O_3 at 125°C; and H_2O:O_3 at 25°C. High temperature (70°C) DI water rinse with megasonics (800W) was compared to room temperature (RT) DI rinsing to improve rinsing efficiency of the sulfuric acid chemicals. HF clean after chemical oxide growth was a five minute dip in 0.5% HF and room temperature DI water rinse. IPA vapor dry was used for all the experiments. The resulting chemical oxide thickness was measured by ellipsometer and verified by XPS. Light Point Defects (LPDs) were evaluated with Censor ANS100 and metal contamination was measured with VPD-DSE-TXRF. Surface roughness was analyzed by AFM.

RESULTS AND DISCUSSION

The growth rate of chemical oxide is shown in Figure 1. The oxide thickness for H_2SO_4:H_2O_2 and H_2SO_4:O_3 peaks at 10 minutes, while the H_2O:O_3 solution requires 20 minutes to reach the same thickness. These respective times were used for the experiments. The XPS measurements confirm the ellipsometric data and the composition analysis of the surface oxide layer shows there is no apparent difference between the oxides for the treatments in the three solutions. The XPS result of the H_2O/O_3 treated surface is shown in Figure 2. The LPDs on the wafer surface for the treatments in the three solutions are monitored immediately after the experiment or after a certain period of time stored in the cleanroom atmosphere (Table 1).

The H_2SO_4:H_2O_2 clean with a RT DI rinse leaves a relatively higher LPD counts on the surface and remains high five hours later. A tremendous increase in LPDs is found on H_2SO_4:O_3 cleaned wafers with RT rinse after five hours. Figure 3 shows the change of the surface LPD map with the storage time. However, these same cleans (H_2SO_4:H_2O_2 and H_2SO_4:O_3) with the high temperature megasonic rinse show low LPD counts, and the counts do not increase with time. The H_2O:O_3 simultaneous clean and rinse provides the lowest LPD counts on the wafer surface and the surface is very stable over time.

Surface metal contamination (TXRF) data for the comparative splits are shown in Table 2. A large amount of sulfur was found in the surface oxide layer formed in the H_2SO_4:H_2O_2 and H_2SO_4:O_3 solutions, even with the high temperature megasonic rinse. The contamination is reduced after an HF dip to remove the oxide. The wafers processed with the H_2O:O_3 solution and subsequent HF dip show the lowest surface contamination of metals except for calcium, which is very high. A detailed study will be done to identify the surface trapping mechanism of Ca for this situation. The AFM results in Figure 4 provide the surface microroughness after the HF clean. The wafer processed in the H_2SO_4:O_3, HF cleans shows a slightly rougher surface comparatively.

CONCLUSIONS

The different chemical oxide growth processes and subsequent HF dip are investigated to optimize the cleaning steps for Si wafer processing. The H_2O:O_3/HF with its simplicity and cost effectiveness offers a promising cleaning process.

ACKNOWLEDGMENTS

The support from T. Sorensen, G. Buhrer, D. Allgeyer, K. Johnson, C. Blackmer, W. Hagan, and D. Fillmore for the surface analysis is gratefully acknowledged.

REFERENCES

1. T. Hattori, Proceedings of the Second International Symposium on Ultra-Clean Processing of Silicon Surfaces, p. 13 (1994).
2. M.M. Heyns, *et. al*, MRS Symposium Proceedings, vol. 315, p. 35 (1993).
3. A.L.P. Rotondaro, *et al.*, Proceedings of the Second International Symposium on Ultra-Clean Processing of Silicon Surfaces, p. 301 (1994).
4. M. Kogure, *et. al*, PROCEEDINGS - Institute of Environmental Sciences, p. 380 (1993).

Table 1. LPDs (with a latex equivalent diameter of 0.12 - 0.22 μm) on the wafer surfaces immediately after the H_2SO_4:H_2O_2, H_2SO_4:O_3, and H_2O:O_3 cleans(*), or after five hours cleanroom storage (**). Both (a) RT DI rinsing, and (b) high temperature 70°C DI rinse with megasonics (800W) are applied after H_2SO_4:H_2O_2 and H_2SO_4:O_3 treatments .

H_2SO_4 / H_2O_2		H_2SO_4 / O_3		H_2O / O_3
(a)	(b)	(a)	(b)	
* 1403	772	771	766	732
**1421	774	5500	781	745

Table 2. Metallic contamination ($*10^{10}$ atoms/cm^2) on the wafer surfaces after different cleaning processes measured with VPD-DSE-TXRF.

ELEMENT	S	K	Ca	Fe	Cu
H_2SO_4 : H_2O_2	148.5	ND	0.19	0.11	0.22
H_2SO_4 : O_3	467.5	0.06	0.14	0.17	0.03
H_2O : O_3	5.5	0.06	0.17	0.25	0.06
H_2SO_4 : H_2O_2 / HF	1.93	0.03	0.06	0.11	0.11
H_2SO_4 : O_3 / HF	1.93	0.06	0.11	0.14	0.25
H_2O : O_3 / HF	1.93	0.01	1.1	0.06	0.08

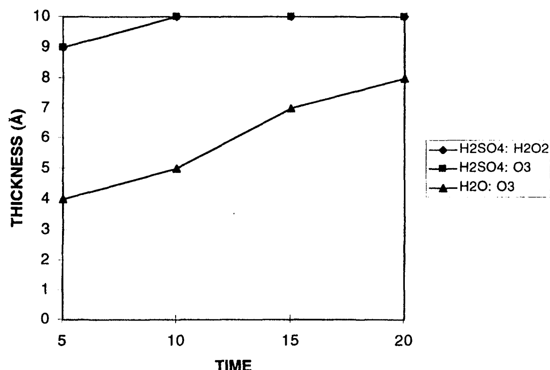

Figure 1. Chemical oxide growth on wafer surfaces as a function of treatment time in H_2SO_4:H_2O_2; H_2SO_4:O_3; and H_2O:O_3.

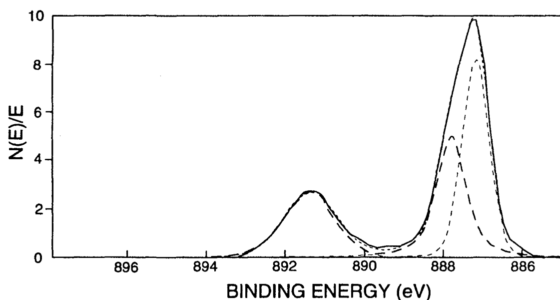

Figure 2. XPS Si2p spectra from H_2O:O_3 cleaned wafer surface.

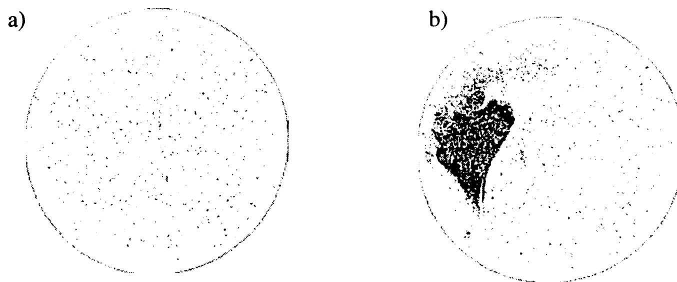

Figure 3. Map of LPDs with a latex equivalent diameter of 0.12 - 0.22 μm (a) on a wafer surface immediately after H_2SO_4:O_3 clean, and (b) after five hours storage in the cleanroom atmosphere.

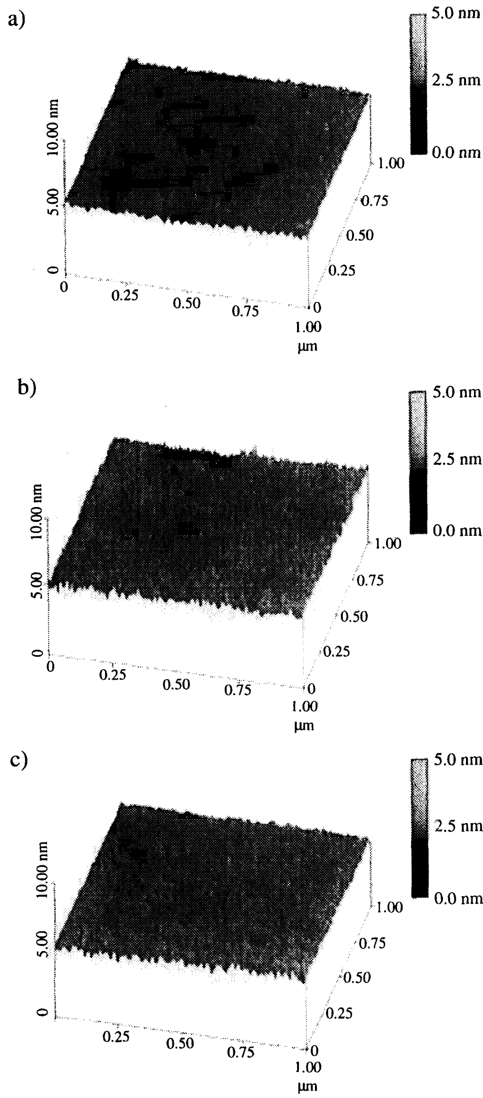

Figure 4. AFM profiles of the HF cleaned wafer surfaces with the pretreatment of (a) H_2SO_4:H_2O_2; (b) H_2SO_4:O_3; and (c) H_2O:O_3.

MECHANISM FOR THE CHEMISORPTION OF CONTAMINANTS ON HYDROGEN-TERMINATED SILICON SURFACES

Christopher E. D. Chidsey and Matthew R. Linford

Department of Chemistry
Stanford University
Stanford, CA 94305-5080

We elucidate a general mechanism for the chemisorption of contaminants onto hydrogen-terminated silicon surfaces. Under certain ambient conditions the relatively stable Si-H bond can be broken with the accompanying chemisorption of dioxygen, organic olefins and other unsaturated compounds present in the production environment, resulting in damage to the surface that can only be removed by further etching.

INTRODUCTION

In order to aid the optimization of wet cleaning procedures for silicon processing, we have begun a program to understand the mechanism of chemisorption of contaminants commonly found in production environments onto the HF-last or hydrogen-terminated silicon surface. Although the hydrogen-terminated silicon surfaces are reasonably stable in air (1), we find that many species do readily chemisorb on these surfaces, particularly if some of the Si-H bonds at the surface are first broken. Both ultraviolet light and low concentrations of radicals can facilitate reaction with the relatively stable Si-H bond. Prevention of this activation of the passive hydrogen-terminated surface is essential to prevent chemisorptive contamination.

We uncovered this mode of chemisorptive contamination in a search for convenient ways to form covalently bonded, monomolecular organic layers on hydrogen-terminated silicon single crystal surfaces (2-5). In that work, we studied the hydrogen-terminated Si(111) surface (H-Si(111)(1x1)) and found that organic radicals stimulate the chemisorption of α-olefins and α-acetylenes, species with the structure, $H_2C{=}CH{-}R$ and $HC{\equiv}C{-}R$ respectively, where R may be one of many different organic groups. The salient intermediate in these chemisorption reactions is probably the silicon dangling bond. Reaction of a dangling bond with the double bond of an olefin, presumably forms a secondary carbon radical, an even more reactive intermediate, which is energetic enough to extract the hydrogen atom from another silicon-hydrogen bond, thus activating another chemisorption event. This possible chain reaction suggests that very low levels of initial activation of the hydrogen-terminated silicon surface may lead to significant levels of reaction. The resultant surface species appear to be connected to the surface by a silicon-

carbon single bond and are chemically quite stable, withstanding hydrofluoric acid at room temperature, boiling in organic solvents and boiling in aqueous solutions of sulfuric acid or ammonia. Under ambient conditions, such adsorbates can only be removed by strong oxidants such as hydrogen peroxide/ammonium hydroxide (SC-1) (6,7).

We have subsequently found that radical activation is not essential and that light activation (and even in some cases no deliberate activation) is sufficient for chemisorption of unsaturated species. Here we report reactions of H-Si(111)(1x1) with dioxygen, and with olefins and other unsaturated organics that may be contaminants in the production environment. We discuss these reactions with an eye to their implications for silicon wet processing where such adsorbates are obviously undesirable contaminants.

All results reported here are for the H-Si(111)(1x1) surface, though we have previously found strongly analogous chemistry on hydrogen-terminated Si(100) (2). For initial studies such as these, H-Si(111)(1x1) offers the distinct advantage of having simpler bonding at the surface. We expect *even greater* reactivity on hydrogen-terminated Si(100) and will be exploring that surface more extensively in future work.

EXPERIMENTAL

The silicon was cleaned for 2 h at 100°C in 3:1 (by volume) H_2SO_4:30% H_2O_2, for 15 min at room temperature in 1:1 (by volume) 30% NH_4OH:30% H_2O_2 (SC-1) (6,7), and finally for 30 min at 100°C in 3:1 (by volume) H_2SO_4:30% H_2O_2. The silicon was rinsed thoroughly between and after each clean with water from a MilliQ 4-bowl purification train, with house DI water as feedstock. The silicon was dried with a jet of argon prior to immersion in an aqueous solution of 40% NH_4F (BOE) for 4 minutes to produce hydrophobic hydrogen-terminated silicon (111) (8). The silicon was then rinsed for 30 s with water and any remaining beads of water were blown off with argon.

In some illumination experiments (Figures 1, 4, and 5), an ozone-free (184.9nm-free) 253.7nm pen lamp with nominal intensity of 6 mW/cm^2 (intensity measured 3/4" from the lamp surface) from Jelight company (model 81-3306-2) was employed. The other illumination experiments shown in Figure 4 were performed with phosphor-coated pen lamps from Jelight company (5 mW/cm^2 intensity) that produce radiation (30-40 nm bandwidth) centered at either 351nm (model 84-2011-2) or 447nm (model 84-247-2). The spectra shown in Figure 6 were obtained from a monolayer prepared by illumination with a 253.7nm, ozone-free, 9 mW/cm^2 lamp (Jelight, model 823-3309-2), where the entire system was heated to 50°C. The results shown in Figure 7 were obtained with a 184.9nm/253.7nm 9mW/cm^2 lamp (Jelight, model 803-2049-2). In all experiments, the silicon was held in a narrow quartz cuvette and the lamps were placed a few millimeters from its surface so that the distance between the lamp and the silicon was ~1 cm. Illumination times are given in the figure captions. 1-dodecene (Aldrich (95%), Figure 7) was degassed by bubbling argon through it for 1.5-2 h. 1-octadecene (Wiley (95%),

Figures 5 and 6) was deoxygenated at ~$5x10^{-5}$ torr by rapid stirring for 3 h followed by vacuum distillation into the cuvette that held the silicon. The high vacuum was maintained until the end of illumination at which point the samples were rinsed extensively with ethanol and sonicated twice for 5 min in CH_2Cl_2 before XPS or IR measurements were made. The subsequent extraction experiments were performed by placing the monolayer-coated silicon substrate in ~100 mL of boiling $CHCl_3$ for 2 h.

The following is a brief review of the techniques used to characterize surface adsorbates on silicon, although a more complete account has been published (4). X-ray photoelectron spectra were obtained with a Surface Science Model 150 XPS spectrometer equipped with an Al Kα source, quartz monochromator, concentric hemispherical analyzer and multichannel detector. A take-off angle of 35° from the surface was used. The pressure in the chamber during analysis was between 1×10^{-9} and 5×10^{-8} torr. Ellipsometry was performed with a Gaertner Variable Angle Ellipsometer L116B using a helium-neon laser and an incident angle of 70°. Effective substrate optical constants were measured for freshly prepared hydrogen-terminated silicon and oxidized silicon. Infrared spectra were obtained with a Mattson RS-10000 research grade spectrometer and additional home-built external optics. After passing through a silicon attenuated total reflection (ATR) plate, the infrared light was directed to a mercury cadmuim telluride (MCT) detector (Graseby Infrared) with an associated preamp. Advancing water and hexadecane contact angles, which can be sensitive probes of adsorbate composition and structure, were measured with a Rame-Hart model 100 goniometer and the errors in these measurements are ±2°.

RESULTS

Photosensitivity of Hydrogen-Terminated Si(111) in Air

In order to explore the photosensitivity of hydrogen-terminated silicon surfaces, we first examine the x-ray photoelectron spectra (XPS) of a Si(111) wafer after etching and after illumination with a Hg lamp. Figure 1a shows the (XPS) of a Si(111) wafer as received, coated with a film of oxidized silicon (9Å by ellipsometry). We notice strong oxygen photoelectron and Auger peaks and their associated plasmon energy loss peaks (9). There is also a small carbon peak which corresponds to about half a monolayer of carbon atoms ($4x10^{14}$ atoms/cm^2). Following an oxidizing clean and a 4-minute etch with an aqueous solution of 40% (by weight) ammonium fluoride, the oxygen peaks in the XPS spectrum disappear, as does the carbon peak ($<1x10^{14}$ atoms/cm^2) (Figure 1b). This surface is known to be nearly ideally hydrogen-terminated (8). Finally, Figure 1c shows the result of 30 minutes of illumination of the wafer in air with 250nm light from a low-power Hg lamp. Notice that the oxygen peaks have returned, but that the carbon level is still quite low. Ellipsometry indicates that the surface is coated with 4Å of oxidized silicon.

Infrared (IR) spectroscopy has been found to be a complementary tool for examining silicon surfaces, particularly because it provides direct evidence for hydrogen species on the surface, which can not be detected by XPS. Moreover, IR spectroscopy can also discriminate among the various bonding patterns of hydrogen (8). A very sensitive way to obtain infrared spectra of the surfaces of IR-transparent samples is the attenuated total internal reflection (ATR) method (10,11). Figure 2 illustrates the trapezoidal Si single crystal we use for this purpose. The IR light is focused onto one of the bevels of the crystal and emerges after about 50 reflections at the other bevel. The light is then directed to a detector. Light polarized either in the plane of incidence (p-pol) or perpendicular to the plane of incidence (s-pol) can be used. The resultant spectra indicate the orientation of chemical species at the surface.

Figure 3 shows p- and s-polarized spectra of the hydrogen-terminated Si(111) surface relative to the surface obtained after an oxidizing clean. The narrow single peak at 2083.9 cm^{-1}, seen only in the p-polarized spectrum, is due to a Si-H bond oriented precisely perpendicular to the surface. The narrowness and p-polarization of this peak along with the absence of peaks assignable to SiH_2 or SiH_3 has been taken as an indication of the homogeneity of the surface and the low density of surface steps (8). The broad negative peak centered at 3500 cm^{-1} is due to O-H stretches from the oxidized background sample. Figure 4 shows the Si-H stretching region for hydrogen-terminated Si(111) samples following various treatments in air. Table I summarizes the fraction of Si-H bonds remaining after these and other treatments.

Table I Photsensitivity of Hydrogen-Terminated Si(111)

Illumination Conditions	Time	Fraction Si-H remaining
Dark in air	1 hour	0.99±0.01
450 nm in air	30 min each side	0.98±0.02
350 nm in air	1 min each side	0.97±0.02
350 nm in air	30 min each side	0.91±0.02
250 nm in air	2 min each side	0.79±0.02
250 nm in air	30 min each side	0.00±0.02
250 nm at 10^{-5} torr	2 min each side	0.72±0.02

The first spectrum in Figure 4 is of a sample held in the dark for 1 hour. No measurable change is observed in the spectrum, indicating that the Si-H bond is relatively stable in the dark. The next spectrum is of a sample illuminated on each side for 30 minutes with 450 nm light. Again, no significant change is observed. In contrast, the third spectrum shows a significant loss of the SiH stretch following illumination on each side for 30 minutes with 350 nm light. Note however that a 1-minute illumination at 350 nm has only a very modest effect (Table I). Finally, illumination at 250 nm is much more efficient at removing Si-H bonds, as shown by the complete loss of signal in the fourth spectrum in Figure 4. Table I shows that illumination for only 2 minutes removes

roughly 20% of the Si-H bonds. Interestingly, the final entry shows that a similar result is obtained with a 2-minute illumination in vacuum.

Clearly, hydrogen-terminated Si(111) is sensitive to illumination with 350-nm or shorter wavelength ultraviolet light. Moreover, the XPS results show that, at least in air, the hydrogen termination is replaced by a thin layer of oxidized silicon. These results lead us to ask whether species other than oxygen may also combine with the surface during loss of the Si-H bonds.

Chemisorption of Unsaturated Organic Compounds on Hydrogen-Terminated Si(111)

From our previous work, we were aware that organic olefins can combine with hydrogen-terminated Si(111) under appropriate activation (4). Recognizing that such unsaturated organic compounds are common contaminants in laboratory and production environments, we have examined the photoreaction of hydrogen-terminated Si(111) with olefins and acetylenes. Figure 5 shows an XPS spectrum of the film resulting from extensive 250-nm illumination of H-Si(111)(1x1) in contact with neat, deoxygenated $CH_3(CH_2)_{15}CH=CH_2$ (1-octadecene). The strong carbon peak corresponds to a coverage of about 20Å of hydrocarbon. Figure 6a shows the IR spectrum of a film prepared in the same way. The remaining Si-H on this surface has a broadened peak that is barely discernible, though it still represents 38% of the original Si-H peak area. Moreover, the spectrum shows strong hydrocarbon features, including two intense modes at 2850 cm^{-1} and 2918 cm^{-1} that correspond to the symmetric and asymmetric CH_2 stretches respectively. Figure 6b shows that this material is not removed even after 2 hours in boiling chloroform, establishing the chemisorbed state of the material. Such films are also stable to subsequent exposures to hydrofluoric acid at room temperature and to boiling water, acid, ammonia, and solvents (4). Similar results are obtained with α-acetylenes (HC≡C-R).

How much illumination is necessary for chemisorption of these unsaturated organic species? To answer that question, we have studied the time dependence of the growth of these films as shown in Figure 7. With a low-pressure Hg lamp, only a few minutes are required for half the final coverage to build up. On the other hand, the final coverage is not reached for more than an hour. In fact, a small fraction of the film forms even before the illumination is begun. We find that this fraction is strongly dependent on the amount of oxygen present. With more rigorous deoxygenation, the fraction of the film formed in the dark can rise as high as 30%. Oxygen seems to inhibit chemisorption of the unsaturated organics in the dark, possibly by breaking the radical chain reaction mentioned above.

DISCUSSION

The hydrogen-terminated silicon (111) surface is relatively robust and can be handled for some time in the laboratory environment without oxygen or carbon contamination. After tens of minutes in the air, XPS (Figure 1) and IR (Figure 3) both show very little contamination. After an hour in the air and in the dark, this surface shows no change in the intensity of its Si-H stretch (Figure 4). Figure 4 also shows that at wavelengths longer than 350nm, photooxidation of silicon in the air is not significant. We note that this cutoff corresponds to the Si-H bond strength (79 kcal/mol (12), 3.4 eV, or light at 360 nm light). However, under appropriate conditions, the surface can be degraded rapidly. After only 2 min of exposure to 250nm UV light, Table 1 shows that about 25% of the Si-H stretch disappears. Also, Figure 7 shows that only a few minutes are required to deposit a 6Å organic film when the silicon is exposed to an unsaturated organic compound and UV light.

We have hypothesized chemical mechanisms to rationalize the chemisorption of unsaturated species to the silicon surface (2,4). In these mechanisms, the silicon dangling bond is the key intermediate. As mentioned, the silicon dangling bond may be formed by UV light with more energy that the Si-H bond strength by desorption of surface hydrogen:

$$\text{Si-H} + h\nu \rightarrow \text{Si}\bullet + \text{H}\bullet \qquad [1]$$

The resulting silicon dangling bonds are highly reactive species and should couple easily with oxygen or an unsaturated organic compound. In the case of the unsaturated organic, the reaction would be:

$$\text{Si}\bullet + \text{H}_2\text{C=CHR} \rightarrow \text{SiCH}_2\text{CH}\bullet\text{R} \qquad [2]$$

If the resulting secondary carbon radical abstracts hydrogen from an adjacent Si-H group:

$$\text{SiCH}_2\text{CH}\bullet\text{R} + \text{Si-H} \rightarrow \text{SiCH}_2\text{CH}_2\text{R} + \text{Si}\bullet \qquad [3]$$

reactions 2 and 3 can be repeated many times, which would lead to a chain reaction on the surface. The dark reaction we observe with unsaturated organic compounds may be the result of such a chain reaction in which the initiation step is due to trace reactive species such as oxygen, ozone, chlorine or nitrogen oxides in the ambient environment. UV light may also facilitate a direct reaction between the Si-H group and an unsaturated organic compound. We plan a study of these possibilities in the near future.

This work is preliminary but it raises questions about the levels of ultraviolet light and organic compounds that are tolerable where hydrogen-terminated silicon surfaces are used. For example, it may prove useful to filter overhead fluorescent lights to cut out

ultraviolet light. Furthermore, the air often contains unsaturated organic compounds, such as terpenes from pine trees, that it may be desirable to filter, although a small amount of carbon contamination may not be an issue in gate oxide production if the silicon is heated in the presence of oxygen. However, in the case of silicon epitaxy and metal deposition, the utility of the hydrogen-terminated surface may depend on avoiding both oxygen and carbon contamination.

ACKNOWLEDGMENTS

This work was supported by Stanford University. We acknowledge the Stanford Center for Materials Research, which is supported by the Division of Materials Research of the National Science Foundation, for providing XPS instrumentation. M.R.L. thanks the Fannie and John Hertz Foundation for their kind support. C.E.D.C. is a Camille and Henry Dreyfus Teacher-Scholar.

REFERENCES

1. M. Niwano, J. Kageyama, K Kurita, I. Takahashi and N. Miyamoto, *J. Appl. Phys. 76*, 2157-2163 (1994).
2. M. R. Linford and C. E. D. Chidsey, *J. Am. Chem. Soc. 115*, 12631-12632 (1993).
3. M. R. Linford and C. E. D. Chidsey, US Patent No. 5,429,708 (1995).
4. M. R. Linford, P. Fenter, P. M. Eisenberger and C. E. D. Chidsey, *J. Am. Chem. Soc. 117*, 3145-3155 (1995).
5. M. R. Linford, P. Fenter, P. M. Eisenberger and C. E. D. Chidsey, unpublished results.
6. W. Kern, D. A. Puotinen, *RCA Review*, 187-206 (1970).
7. H. Akiya, S. Kuwano, T. Matsumoto, H. Muraoka, M. Itsumi, N. Yabumoto, *J. Electrochem. Soc. 141*, L139-L142 (1994).
8. G. S. Higashi, Y. J. Chabal, G. W. Trucks, K. Raghavachari *Appl. Phys. Lett. 56*, 656-658 (1990).
9. J. F. Moulder, W. F. Stickle, P. E. Sobol, K. D. Bomben, J. Chastain Handbook of X-ray Photoelectron Spectroscopy, Perkin-Elmer Corporation, 1992.
10. N. J. Harrick, *J. Opt. Soc. Am. 55*, 851-857 (1965).
11. N. Tillman, A. Ulman, J. S. Schildkraut, T. L. Penner *J. Am. Chem. Soc. 110*, 6136-6144 (1988).
12. J. M. Kanabus-Kaminsha, J. A. Hawari, D. Griller, C. Chatgilialoglu *J. Am. Chem. Soc. 109*, 5267 (1987).

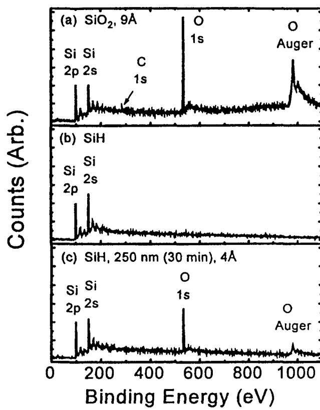

Figure 1. XPS spectra of Si(111) samples. (a) As received wafer. (b) Following NH_4F etch. (c) After 30 min illumination with 250nm lamp.

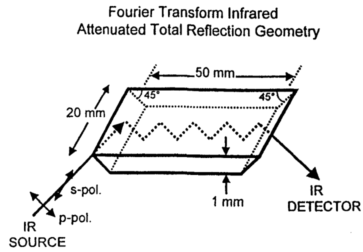

Figure 2. Path of infrared light through attenuated total internal reflection silicon element.

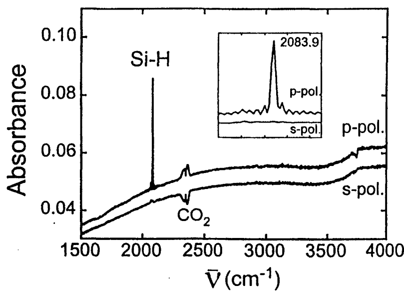

Figure 3. p- and s-pol infrared spectra of H-Si(111) (1x1).

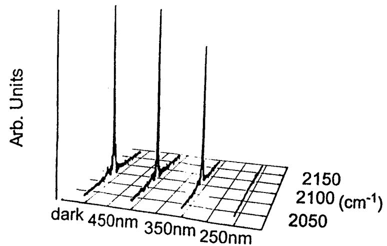

Figure 4. Infrared spectra of the Si-H region of H-Si(111) (1x1) samples kept in the dark for 1 h or exposed to various fluorescent lamps for 30 min each side.

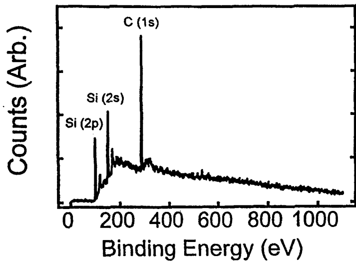

Figure 5. XPS spectrum of a 20Å film from 1-octadecene made with 2 h illumination.

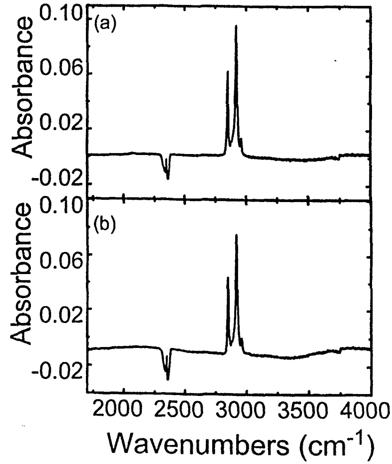

Figure 6. Infrared spectra of a 20Å film from 1-octadecene made with 2 h illumination before (a) and after (b) extraction for 2 h in boiling $CHCl_3$.

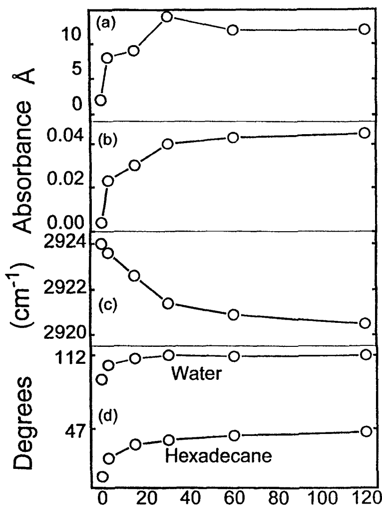

Figure 7. Monomolecular film formation from 1-dodecene as a function of illumination time showing ellipsometric thickness (a), asymmetric methylene stretching intensity (b), asymmetric methylene peak position (c), and advancing water and hexadecane contact angles (d).

REMOVAL OF THERMALLY GROWN SILICON DIOXIDE FILMS USING WATER AT ELEVATED TEMPERATURE AND PRESSURE

Geoffrey L. Bakker and Dennis W. Hess
Department of Chemical Engineering
Lehigh University
Bethlehem, PA 18015

ABSTRACT

The removal of thermally grown silicon dioxide films from silicon wafer surfaces with water at elevated temperature and pressure was studied using ellipsometry and X-ray Photoelectron Spectroscopy (XPS). Complete removal of 50 nm silicon dioxide layers was observed with XPS after exposure of the sample to de-ionized (18 M-ohm-cm) water at 280°C and 241 bar (3500 psi) for 30 minutes. To the detection limit of XPS (~0.5 atomic percent), no metal contamination was deposited on the surface. Removal rates were determined at temperatures between 260°C and 305°C at 138 bar (2000 psi). A surface reaction limited rate equation, used previously to describe quartz dissolution in water over a wide range of temperature, was used to estimate rate constants for silicon dioxide removal. An effective activation energy of 76.6 kJ/mol was calculated for the etching process, which is comparable to values reported for quartz dissolution under similar conditions(62.6 - 79.0 kJ/mol).

INTRODUCTION

Thermally grown silicon dioxide has many applications in the microelectronics industry including use as a dielectric material, a patterning mask, and a passivating layer. Removal of this oxide is therefore one of the fundamental steps in micromachining or in the production of microelectronic devices. Several processes are currently utilized for this purpose. The oldest and easiest to implement is immersion in aqueous HF solution. Such liquid methods have the advantage of being inexpensive and simple, but produce large amounts of contaminated waste and are difficult to incorporate into vacuum transfer systems. Immersion in basic solutions can be invoked to remove silicon dioxide, but removal rates are low and analogous problems to those experienced with HF solutions exist. "Vapor phase" HF/H_2O processes can also remove silicon dioxide and are more compatible with vacuum transfer systems. In general, these processes proceed through the formation of a thin liquid layer on the oxide surface where SiF_4 and H_2SiF_6 are generated[1]. When etching is complete, the products must be evaporated or rinsed from the surface. Finally, plasma techniques using fluorine-containing gases can be used to

remove thin layers of silicon dioxide[2,3], however, surface damage is a concern with plasma techniques.

In this study, a new method of stripping thermally grown silicon dioxide layers, which utilizes the solubility of SiO_2 in water at elevated pressure and temperature, is investigated. Thermally grown silicon dioxide films can be removed when exposed to deionized water at the proper conditions of pressure and temperature. Rate of removal can be adjusted through the choice of pressure and temperature. When optimized, this process may offer an alternative to competing technologies due to the high costs associated with waste disposal and chemical handling in traditional liquid and "vapor phase" methods. Deionized water is the only fluid used in the proposed process, and the only waste produced is water and silicon dioxide. Neither of these is hazardous or poses an environmental threat. Compatibility with vacuum transfer and integrated processing is possible despite the employment of liquid phase water. Because the process takes place at approximately 300°C, water in the chamber vaporizes and exits when the pressure is reduced and/or the chamber is purged with an inert gas.

BACKGROUND

The increase of silicon dioxide solubility in water as temperature and pressure are increased has been known for many years. In the 1950's, geologists studied reactions of water with minerals at elevated temperature and pressure to imitate conditions below the earth's crust. Solubility data of many substances were collected in order to model rock formation and other geologic phenomena. One of the most extensively studied systems was quartz(SiO_2) and water. Kennedy[4] (1950) presents a fairly complete report of quartz solubility data in the near critical region. Solubility data were obtained between pressures of 6.2 and 1750 bar (90 and 25,400 psi) over the temperature range of 160°C to 435°C. Since both quartz and thermally grown silicon dioxide share the same chemical composition (SiO_2), their solubility behavior in water is expected to be similar.

Although their chemical compositions are the same, the structures of quartz and thermally grown silicon dioxide are quite different. Quartz is a crystalline arrangement of silicon atoms tetrahedrally coordinated with oxygen atoms. In the bulk, each oxygen atom is bonded to two silicon atoms. At the surface, some of the oxygens are bonded to a single silicon atom neutralizing only one of the two negative charges associated with an oxygen ion. To neutralize the surface, hydrogen ions are adsorbed, forming SiOH groups. Silicon atoms at the surface can be singly, doubly, or triply bonded to the surface depending on the number of OH groups with which they are associated. Thermally grown silicon dioxide is amorphous. Silicon atoms are still tetrahedrally coordinated with oxygen atoms, but the arrangement of the tetrahedra is random. As with quartz, proton adsorption neutralizes the oxygen ions bonded to only one silicon. Silicon atoms which are only singly or doubly bonded to the surface are more likely in thermally grown silicon dioxide than in quartz due to the random structure.

Dissolution of silicon dioxide in deionized water proceeds when surface silicon-

oxygen bonds are broken. The primary mechanism by which this occurs is nucleophillic attack at a surface silicon atom[5]. An oxygen atom in a water molecule forms a bond with a surface silicon atom and loses a hydrogen ion to become an adsorbed hydroxyl group. Since the surface silicon atom is now bonded to five oxygen atoms instead of four, a bond between the surface silicon atom and a surface oxygen atom is broken. This surface oxygen atom bonds with the hydrogen ion lost by the water molecule and forms another hydroxyl group. The overall reaction is thus

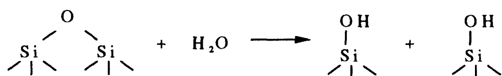

When all the bonds holding a silicon atom to the surface are broken, it is dissolved via the formation of a complex with hydroxyl groups. This complex is often written H_4SiO_4 [4,5,14]; $Si(OH)_4$ is used in this paper to be more chemically precise. Electrophillic attack of a hydrogen ion at a surface oxygen is also possible. Studies of quartz[6] in acidic solution show little or no increase in dissolution rate with decreasing pH, indicating this mechanism is not predominant.

SILICON DIOXIDE REMOVAL

Initially, experiments were performed to determine if it was possible to remove silicon dioxide from silicon surfaces using water at elevated pressure and temperature. A silicon 2p XPS spectrum of a 50 nm thermal oxide layer was recorded and the sample placed into the high pressure cell. Water was pumped into the chamber and conditions of 275°C and 241 bar (3500 psi) were established. After four minutes at these conditions, the pressure was reduced to atmospheric pressure, and another silicon 2p XPS spectrum recorded. The sample was placed back in the high pressure chamber, the temperature set to 280°C, and a pressure of 241 bar (3500 psi) established. These conditions were maintained for 30 minutes, the sample removed and a third XPS spectrum recorded. The XPS spectrum taken before water treatment shows only one peak at 104 eV, which is consistent with a silicon dioxide surface. After the 4 minute water exposure a small elemental silicon peak was detected at 99 eV. In this electron energy range, XPS is sensitive to a depth of approximately 10 nm, and thus the silicon dioxide thickness was most likely near this value. In addition, the silicon dioxide peak was shifted compared to the initial data, indicating reduced surface charging, and thus a thinner silicon dioxide surface layer after water treatment. After the 30 minute water exposure, the silicon dioxide peak was much smaller and the elemental silicon peak dominated. Additional peak shifting was also observed, indicating further silicon dioxide thinning. The silicon dioxide peak observed after the 30 minute water exposure indicates that approximately 1 nm of oxide remains.

XPS analysis is also useful for detecting contamination introduced onto samples during processing. Of particular concern in this case are metals (Iron, Chromium) which may be dissolved from the high pressure apparatus and deposited on the silicon substrate. Most of the samples mentioned in this paper (including the etch rate and surface roughening samples mentioned later) were examined using XPS. None of these samples had detectable metal contamination; all peaks could be attributed to carbon, oxygen, or silicon. For the case of iron and chromium this implies a concentration less than approximately 0.5 atomic percent. Since metal contamination at the ppb level can significantly affect electrical properties of microelectronic devices, these experiments do not resolve the issue of metal contamination. Further work is necessary to determine if special chamber materials would be necessary for this type of processing.

SILICON DIOXIDE ETCH RATES

To develop a better understanding of the silicon dioxide removal process, experiments were run to quantify the etch rate. Silicon wafers (B-doped, (100)) with approximately 50 nm of silicon dioxide were prepared via steam oxidation at 900°C. The wafers were cut into small (1 cm square) samples and the oxide thickness on each measured via ellipsometry. Samples were then exposed to water at varying conditions of pressure, temperature and time. The remaining oxide thicknesses were measured and oxide removal determined from the thickness differences.

Silicon dioxide removal data was obtained at temperatures of 260°C, 280°C, and 305°C. The data show an approximately linear removal of silicon dioxide over time, and an increasing removal rate with increasing temperature. Etch rates were calculated at each temperature from a linear fit of the data. The observed rates are 2.7 nm/min (260°C), 5.4nm/min (280°C), and 11.2 nm/min (305°C). Vapor and liquid phase HF processes can give a wide range of etch rates depending on concentration and temperature; however, both are capable of much faster rates than observed with elevated temperature and pressure water. Vapor phase HF etching rates of 120 nm/min[7], and liquid phase rates of 670 nm/min[8] have been reported. Higher temperatures and pressures will provide increases in etch rates using the current method, but film quality may suffer due to surface roughening.

Some of the data obtained when the remaining oxide film is less than 10 nm (more than ~ 35 nm removal) is not consistent with linear removal. Furthermore, for some samples, up to 10 nm of oxide remains when complete removal is expected. Data collected from samples which had less than 10 nm of oxide was ignored for the etch rate calculation, and several experiments were run to determine the source of the erratic data.

To evaluate the possibility of silicon and silicon dioxide surface roughening, several samples that had been treated with elevated temperature and pressure water were examined using scanning electron microscopy (SEM). Surfaces were examined on wafer samples with no thermally grown silicon dioxide present and on wafer samples with 50 nm of thermally grown silicon dioxide. Each type of sample was exposed to water at

temperatures of 260°C, 280°C, and 305°C. Etch rate data was used to predict the time necessary to etch 40 nm of oxide, leaving 10 nm of oxide on the oxide samples. XPS was used to confirm that approximately the correct amount of oxide remained after exposure. Experiments were also run with an etch time of five minutes to compare surface roughening as a function of temperature more directly. Each sample was examined at magnifications of 10, 100, 1000, and 10,000X.

Silicon dioxide samples exposed to water at 305°C showed surface pitting, while samples exposed at 260°C and 280°C did not. No comparison of etch time vs. roughening was possible at 305°C because the 50 nm oxide layer was completely removed in five minutes (as expected). The morphology of the silicon surfaces was very different than the silicon dioxide surfaces. At 260°C and 280°C crystalline structures each approximately 100 to 1000 nm across were present on the surface. XPS data indicate that these crystals are silicon dioxide. At 305°C the surface was covered by a patchy film of the silicon dioxide crystals. Preliminary AFM data gave similar results. Thermally grown silicon dioxide samples etched only partially at temperatures of 260°C and 280°C showed a fairly smooth surface (rms roughness of 1.7 and 1.8 angstroms respectively) with some features (~8/micron^2) approximately 4 nm high and 60 nm across. Silicon samples with no oxide present showed partial coverage of 0.1 to 1 micron silicon dioxide structures when exposed at the same temperatures.

The SEM and AFM results indicate that the silicon substrate, as well as the silicon dioxide, is attacked by the fluid. Microbalance measurements of silicon wafer samples were performed before and after water exposure to investigate this possibility. Samples exposed at 285°C and 241 bar (3500 psi) for 13 minutes were etched significantly. An etch rate of 154 nm/min was calculated assuming uniform silicon removal; this rate is approximately 25 times faster than that of silicon dioxide. At this rate of etching, significant amounts of silicon dioxide can accumulate in the fluid and subsequently precipitate when the pressure in the chamber is reduced. The silicon dioxide crystals observed in the SEM and AFM images described above were most likely formed in this manner. Furthermore, the erratic ellipsometry data noted for samples with thin silicon dioxide films remaining is also consistent with these results. Silicon samples with no thermally grown silicon dioxide remaining were attacked rapidly by the elevated temperature water, and displayed an increased precipitation of oxide when the experiment was terminated. Rapid etching of silicon under these conditions has important implications for potential applications of this technique. For instance, applications in which a silicon substrate is exposed to the water treatment will need additional or altered chemistry to be practical(control of dissolved oxygen, pH control, or chemical additives). Situations in which silicon is to be removed from silicon dioxide layers may be more practical with this approach.

Dove and Crerar[9] used equation [1] to describe the rate of quartz dissolution in water.

$$\frac{r_{Si(OH)_4}}{\gamma_{Si(OH)_4}}\frac{M}{A} = k_+\left(a_{SiO_2}\right)\left(a_{H_2O}\right)^2 - k_-\left(a_{Si(OH)_4}\right) \qquad [1]$$

where $r_{Si(OH)4}$ is the rate of molality increase of the dissolved species ($Si(OH)_4$) per unit surface area of quartz, M is the mass of water, A is the quartz surface area, $\gamma_{Si(OH)4}$ is the activity coefficient of the dissolved species, a_{SiO2} is the activity of quartz, a_{H2O} is the activity of water, $a_{Si(OH)4}$ is the activity of the dissolved species, k_+ is the quartz dissolution rate constant, and k_- is the quartz redeposition rate constant. Standardization of the equation to one kilogram of water (M = 1 kg) gives an expression for the molar rate of appearance of the dissolved species per unit surface area. Since the concentration of $Si(OH)_4$ is close to zero in these experiments, the activity (of the $Si(OH)_4$) and the activity coefficient were assumed to be zero and unity respectively. Activities of the quartz and water are assumed to be unity due to their high density (Poynting factor close to unity). The simplified equation with these assumptions is

$$\frac{r_{Si(OH)_4}}{A} = k_+ \qquad [2]$$

thereby directly relating the molar rate of $Si(OH)_4$ appearance to the forward rate constant. For the flat wafer samples used, molar removal rate (r_{SiO2}) per area (A) can be expressed as

$$\frac{r_{SiO_2}}{A} = \frac{\rho V}{Adt} = \frac{\rho Adx}{Adt} = \rho dx/dt \qquad [3]$$

where ρ is the molar density of silicon dioxide, V is the volume of silicon dioxide removed, and dx is the thickness of silicon dioxide removed. Since the silicon dioxide removal rate is equivalent to the appearance of $Si(OH)_4$, equations [2] and [3] can be combined to yield equation [4]

$$k_+ = \rho dx/dt \qquad [4]$$

an expression relating the forward rate constant (k_+) to the oxide thickness removed per unit time.

The logarithm of the etch rate constants calculated using equation [4] are -5.75 (260°C), -5.47 (280°C), and -5.16 (305°C). The equations of Dove and Crerar[10] were used to predict rate constants for quartz at the temperatures used in the present study resulting in values of -6.88 (260°C), -6.61 (280°C), and -6.27 (305°C). The rates for

thermally grown silicon dioxide from the present study are consistently higher than those predicted for quartz. This result is reasonable since thermally grown silicon dioxide is amorphous and thus less dense, with more sites for easy water attack when compared to quartz. Indeed, crystalline defects have an important effect on the observed rate of quartz dissolution because silicon atoms are more likely to be singly or doubly bonded to the quartz surface near defects[10,11].

An Arrhenius plot of the rate constants obtained for dissolution of thermally grown silicon dioxide yields an activation energy of 76.6 (+/-6.3) kJ/mol; activation energy values reported for quartz dissolution range from 65 to 95 kJ/mol[12,13,14]. For the temperature range 200°C to 300°C, Dove and Crerar[10] report a value of 71.3 (+/-8) kJ/mol. Our value of activation energy is within the range of the reported values for quartz. The agreement of the activation energies along with the similarity of chemical compositions suggests that the dominant mechanism for quartz and thermally grown silicon dioxide dissolution in elevated temperature and pressure water is the same.

SUMMARY AND CONCLUSIONS

The efficacy of water at elevated temperature and pressure to remove thermally grown silicon dioxide films from silicon wafer surfaces was investigated. Results from this study indicate that thermally grown silicon dioxide can be etched at a reasonable rate with deionized water at pressures above 138 bar (2000 psi) and temperatures above 260°C. XPS spectra indicate that a residual oxide layer similar in thickness to a native oxide is present on the surface after etching and air exposure. To the detection limits of XPS, no metal contamination from the stainless steel chamber was introduced onto the sample surface. Etch rates of the silicon dioxide films increase with increases in temperature in the range 260°C to 305°C, and are higher than values found in the literature for quartz dissolution under similar conditions. Some surface roughening and pitting was observed via AFM and SEM for silicon dioxide samples at 305°C; samples exposed at 260°C and 280°C showed little surface roughening. Silicon surfaces exposed at the same temperatures showed significant redeposition of silicon dioxide. Microbalance measurements indicate that silicon surfaces are etched approximately 25 times more rapidly than thermally grown silicon dioxide, thereby accounting for this behavior. Silicon dioxide etch rate data exhibit Arrhenius behavior with an activation energy of 76.6 kJ/mol. This activation energy is similar to the activation energy for quartz dissolution in water. Since quartz and thermally grown silicon dioxide share the same chemical composition and the activation energies for dissolution are similar, the dissolution mechanisms are probably the same.

ACKNOWLEDGEMENTS

This work was supported by Los Alamos National Laboratory under Subcontract No. 9-X52-X9139-1. We would like to thank AT&T Bell Laboratories for donating the

surface analysis system used in this study. Unilever Research U.S. Inc. is gratefully acknowledged for their fellowship support of G.L.B. The authors also thank Prof. F. Stein, M. George, and J. Martz for their suggestions and technical advice.

REFERENCES

[1] C. R. Helms, and B. E. Deal, in "Proc. Second International Symposium on Cleaning Technology in Semiconductor Device Manufacturing", The Electrochmical Society, Inc., 267(1992).

[2] O. Kesssi, and S. Nencib, J.Phys. D: Appl. Phys., **26**, 1516(1993).

[3] A. J. Lamm and M. Carrasco, Vacuum, **45**, 555(1994).

[4] G. C. Kennedy, Econ. Geol., **45**,629(1950).

[5] T. Hiemstra, and W. H. Van Riemsdijk, J. Colloid and Interface Science, **136**, 132(1990).

[6] K. G. Knauss, and T. J. Wolery, Geochim. Cosmochim. Acta, **52**, 43(1988).

[7] B. E. Deal, M. A. McNeilly, D. B. Kao, and J. M. deLarios, Solid State Tech., **7**, 73(1990).

[8] J. S. Judge, J. Electrochem. Soc., **118**, 1772(1971).

[9] P. M. Dove and D. A. Crerar, Geochim. Cosmochim. Acta, **54**, 955(1990).

[10] S. L. Brantley, S. R. Crane, D. A. Crerar, R. Hellmann, and R. Stalard, Geochim. Cosmochim. Acta, **50**, 2349(1986).

[11] A. C. Lasaga, and A. E. Blum, Geochim. Cosmochim. Acta, **50**, 2363(1986).

[12] A. J. Gratz, P. Bird, and G. G. Quiro, Geochim. Cosmochim. Acta, **54**, 2911(1990).

[13] J. D. Rimstidt and H. L. Barnes, Geochim. Cosmochim. Acta, **44**, 1683(1980).

[14] S. A. Greenberg, J.Phys. Chem., **61**, 960(1957).

IMPROVEMENT OF A POST-OXIDE CMP CLEANING PROCESS THROUGH THE USE OF DESIGNED EXPERIMENTS

Raj Shah, IBM assignee to SEMATECH
Jeanine Herrera, AMD assignee to SEMATECH
Shelley Peterman, TI assignee to SEMATECH
2706 Montopolis Drive
Austin, TX 78741-6499

The use of Chemical Mechanical Polishing (CMP) for the planarization of intermetal oxides is becoming a more commonly used technology as linewidths become smaller and lithographic depth of focus becomes more critical. As linewidths shrink, it becomes more important to remove the remaining particles and residues after the CMP process. The post-CMP clean must also maximize throughput and minimize cost to be a truly production-worthy process.

To achieve these goals, a series of two Designed Experiments were conducted on an OnTrak DSS-200 Series 1 wafer scrubber. These experiments tested the effects of chemical flow, brush speed, and wafer rotational speed on final polished-wafer particle counts. Results indicated that a low chemical flow and a medium to high brush speed produced the lowest possible particle counts on polished thermal oxide wafers.

BACKGROUND

Experiment Goal

The process of using Chemical Mechanical Polishing (CMP) on intermetal dielectrics to achieve highly planar surfaces has been in use for some time. As linewidths have shrunk to 0.35um and beyond, the use of CMP has become increasingly commonplace in high-volume wafer manufacturing. However, as linewidths decrease, the die yield per wafer becomes more and more sensitive to any particles or residues that remain on the wafer after CMP processing. Thus, a thorough and effective post-CMP clean is crucial to maintaining a consistently high die yield. In addition, the constraints of manufacturing require that the post-CMP clean process have a high throughput and low cost. The goal of the Designed Experiments described in this paper is to optimize a post-oxide CMP clean to minimize final polished-wafer particle counts while reducing processing costs and maximizing throughput.

Tool Description

The experiments described in this paper were conducted on a Westech 372 polisher, using a standard, commercially available set of consumables. All post-CMP cleaning experiments were conducted on the OnTrak 200 Series II Scrubber.

The OnTrak Series 2 scrubber is a belt-driven, single-wafer scrubber. The tool starts with a wafer load station on the left-hand side of the tool. Wafers lie horizontally in the load station and are sprayed with a constant stream of deionized (DI) water to keep them wet until they are cleaned. Wafers are loaded from the input station into two consecutive brush stations via a belt and motor transport system. Two cylindrical brushes scrub the tops and bottoms of the wafers in each of the two brush stations. Dilute chemical is dripped on top of the brushes during the wafer scrubbing process. Once the wafer has been scrubbed in each of the two brush stations, it is transported into the rinse/dry station. Once in the rinse/dry station, it is rinsed with DI water and dried using centrifugal force and heat. When rinsing and drying are complete, the wafer is placed into a cassette in the output station, using a multi-axial robot. The entire system is controlled by a touch-screen computer, located on the right side of the machine.

EXPERIMENT #1

Experiment design

Consideration of the mechanics of the tool and specifics of the cleaning process yielded three controlled factors as the most important for post-oxide CMP cleaning. These three factors were the flowrate of the basic chemical solution, brush rotational speed, and wafer rotational speed. Each factor was varied around the original settings which constituted the "standard" post-CMP cleaning process. In some cases, it was decided to vary the factor on only one side of the original setting, based primarily on past experience. Original and experimental settings are shown in Table I.

Table I - Factor Settings for Experiment #1

Factor	Original process setting	Experimental settings
Basic chemical flow	MEDIUM	LOW, MEDIUM, HIGH
Brush rotational speed	LOW	LOW, MEDIUM, HIGH
Wafer rotational speed	LOW	LOW, MEDIUM, HIGH

The experiment was designed as a full factorial with centerpoints, with two repeats of each split and three repeats of the centerpoint split, for a total of 19 splits. Each split was run with 4 wafers, for a total of 76 wafers in the experiment. Because chemical changes on the scrubber are not instantaneous, it was necessary to block the experiment for chemical flow, with 10 dummies run immediately after each chemical flow change, to be sure the chemical flow had stabilized before running a new split.

Experiment execution

The experiments were conducted using unpatterned eight inch wafers which had been thermally oxidized to a thickness of 7500Å. The wafers were polished to a final thickness of 5500Å on the Westech polisher, using a 1.5 minute polish on the primary platen, followed by a 1.0 minute final platen polish in DI water. After polishing, wafers were transferred immediately to the scrubber for the cleaning experiments, avoiding any drying of the wafers during transfer. Upon completion of the cleaning experiments, final post-polish particle counts were measured on a Tencor 7600, using a 0.2μm minimum particle size.

Analysis of results

Upon completion of the experiment, the effect of the factor settings on the final post-polish particle counts was analyzed using RS1 software. Note that all results are shown as final particle counts, that is particles left on the wafer surface and not particle count deltas. Results of this analysis are shown in Table II.

Table II - Analysis of Experiment #1 Results

Term	Coeff.	Std. Error	T-value	Signif	Transformed term
1	21.367	1.493			
CHEM	8.502	1.607	5.29	0.000 1	((CHEM-6.5)/3.5)
WFR	-0.596	1.607	0.37	0.711 8	((WFR-7e+01)/3e+01)
BRUSH	-3.310	1.607	2.06	0.043 2	((BRUSH-1.19e+02)/1.9e+01)
No. cases = 73	R-sq. =0.3215	RMS error=12.75			
Resid. df=69	R-sq.-adj. =0.2920	Cond. No=1.032			

The statistical analysis shown in Table II yields a rather low R-squared of 0.32, indicating that only 32% of the variability in the data is explained by the controlled factors. This was due primarily to the extremely low particle count levels that were seen on all splits. With particle counts of 20 per wafer and fewer at 0.2μm, such difficult to control factors as wafer handling, polishing variations, and measurement variations start to play a more important role. These difficult factors unfortunately could not be quantified enough to put into the statistical analysis. However, despite the low r-squared, two of the three factors still had a statistically significant effect on the final particle counts. These effects may be seen more clearly in Figures 1 and 2. Figure 1 shows a significant reduction in final particle counts when the chemical flow is decreased from the MEDIUM setting to the LOW setting. Figure 2 shows a similar reduction in particle counts when the brush speed is increased from MEDIUM to HIGH. Wafer rotational speed had no statistically significant effect on final particle count.

Conclusions

Results of Experiment #1 indicated that the optimal process used a LOW chemical flow and a HIGH brush speed. The statistics indicated that this optimal process would produce average particle counts of 10 per wafer or less (at 0.2μm). However, these optimal settings put the process at one corner of the experimental space. Thus it was necessary to design a follow-up experiment, both to verify the results of the first experiment and to better understand the variability of the process beyond the selected settings.

EXPERIMENT #2

Experiment design

Factors for experiment #2 included only those that were significant in experiment #1: chemical flow and brush speed. Settings for these factors were selected to go beyond the optimal process that was suggested by experiment #1. Thus, experiment #2 was designed with settings of MEDIUM, LOW, and LOWEST for chemical flow, and MEDIUM, HIGH, and HIGHEST for brush speed. This time, the experiment was designed as a face-centered central composite design, with 13 splits, 4 wafers per split, and 3 repeats of each split, for a total of 156 wafers in the experiment. Once again, the experiment was blocked for chemical flow, with 10 dummies run immediately after each flow change.

Experiment execution

Processing conditions for the execution of experiment #2 were identical to those for experiment #1. The same Westech 372 polisher and OnTrak scrubber were used, and final particle counts were collected from the same Tencor 7600 at a 0.2μm minimum particle size.

Analysis of results

The effect of chemical flow and brush speed on final post-polish particle counts was analyzed using RS1 software. Results of this analysis are shown in Table III below.

Table III - Analysis of Experiment #2 Results

Term	Coeff.	Std. Error	T-value	Significance
1	3.045	3.543		
CHEM	0.958	0.374	2.56	0.0113
BRUSH	0.0029	0.0215	0.13	0.8942
No. cases = 154	R-squared = 0.0419	RMS error=6.253		
Resid. df=151	R-squared adj=0.0292	Cond. No=16.2		

The most notable statistic from Table III is the very low R-squared number of 0.04, which indicates that very little of the variation in the data is due to the controlled factors. This may also be seen graphically in Figures 3, 4, and 5. These graphs show very low particle counts on all splits, with averages of less than 10 particles at 0.2μm and greater. Thus, there appear to be very few statistically significant differences between splits. One notable exception is in Figure 5, which graphs the effect of chemical flow on particle counts. In this graph, the MEDIUM flow setting has both a higher average and more variability than the LOW and LOWEST settings, indicating that lower chemical flows result in lower particle counts.

Conclusions

Several conclusions may be drawn from the analysis of experiment #2. First, the effect of chemical flow on particle counts was seen to be similar to that shown in experiment #1, with lower chemical flows resulting in lower particle counts. Second, brush speeds that were even higher than those used in experiment #1 did not prove to be

more effective at removing particles. Evidence from experiment #2 seemed to indicate that brush speeds in the MEDIUM to HIGH range would be best for particle removal. Finally, the particle count results from experiment #2 verify that the optimum process of LOW chemical flow and HIGH brush speed produces polished wafer particle counts of less than 10 particles per wafer. This may also be seen graphically in Figure 6, which displays the individual particle counts for all wafers in experiment #2 receiving the LOW chemical flow and HIGH brush speed. The average particle count for these 60 wafers was 5.9 particles, with 90% of the wafers having particle counts below 10. Thus the optimum process seems capable of producing polished wafer particle counts that are consistently below 10 particles, at a 0.2μm minimum particle size.

RECOMMENDED PROCESS

Based on the results of these two experiments, the recommended post-oxide CMP cleaning process uses a LOW to LOWEST chemical flow and a MEDIUM to HIGH brush speed. Any reasonable wafer rotational speed may be used.

ACKNOWLEDGMENTS

The authors would like to thank the people of SEMATECH Steve Eastman, Michael Sony, Tuyet Nguyen, Dean Patterson and Al Gonzales for their assistance in the execution of these experiments and the help of their administrative assistant Carolon Denman. They would also like to thank Fred Mohr and Norman Mertke of OnTrak Systems for their advise and assistance.

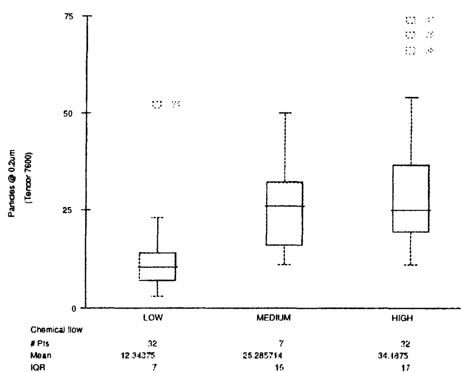

Figure 1 - Experiment #1 - effect of chemical flow on particle counts

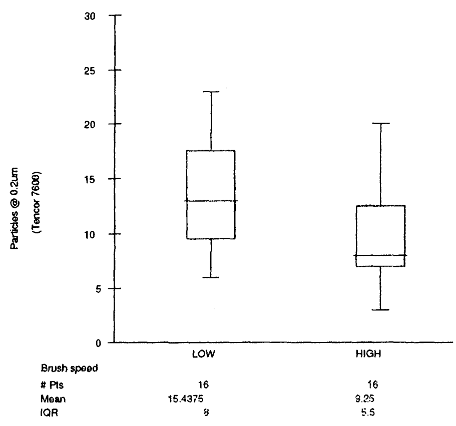

Figure 2 - Experiment #1 - effect of Brush speed on particle counts

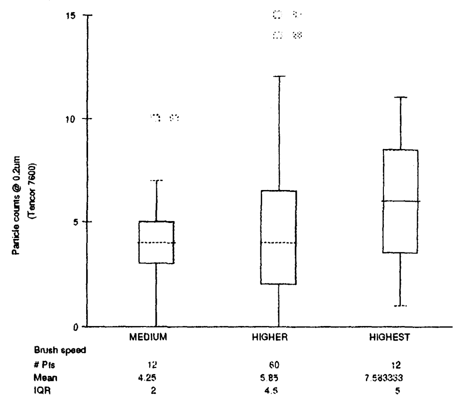

Figure 3 - Experiment #2, Brush speed vs.particle counts at low chemical flow

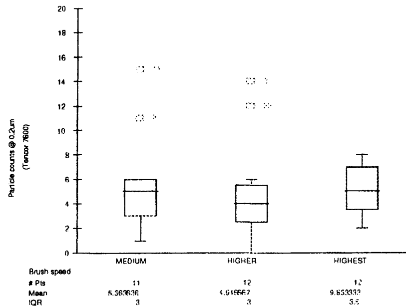

Figure 4 - Experiment #2, Brush speed vs.particle counts at lowest chemical flow

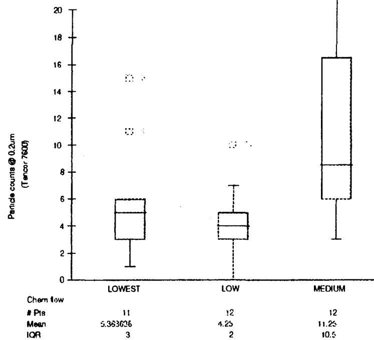

Figure 5 - Experiment #2, Chemical flow vs.particle counts @medium brush spd.

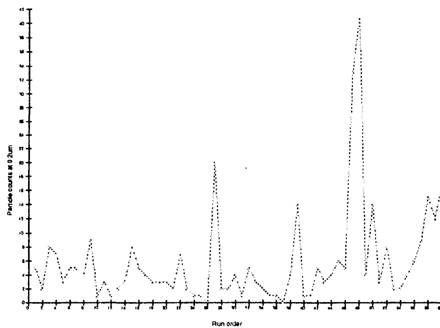

Figure 6 - Experiment #2, Individual particle counts for
LOW chemical flow and HIGH brush speed

IN SITU AND REAL TIME STUDIES OF WET CHEMICAL SILICON SURFACE CLEANING REACTIONS

H.F. Schmidt, I. Teerlinck, W. Storm,
H. Bender and M.M. Heyns

IMEC, Kapeldreef 75, B-3001 Leuven, Belgium

In this paper electrochemical Open Circuit Potential (OCP) measurements for in-situ characterisation of wet silicon surface cleaning processes is discussed. This technique provides unique information about the evolution of semiconductor surface reactions in wet chemical environments and allows to study the kinetics of oxidation and etching processes in real time. Very good agreement between results obtained by this technique and results from MIR-FTIR (Multiple Internal Reflection - Fourier Transform Infrared Spectroscopy), XPS (Photoelectron Spectroscopy), Spectroscopic Ellipsometry (SE) and contact angle studies were found and are presented in this paper.

1. INTRODUCTION

Real time monitoring and control of manufacturing processes for complex semiconductor devices has become increasingly important in developing and running a high yield manufacturing process. From the viewpoint of microcontamination control, metrology is urgently needed to qualify surface preparation steps in order to guarantee repeatability and also to minimise the costs related to the ever increasing surface purity needs. To satisfy these needs, expensive, ultra-clean chemicals for semiconductor applications have reached in the mean-time contamination levels in the sub-ppb range but often these chemicals are not very effectively used. This is mainly due to a lack of understanding of how long certain mixtures can be used and the non-existence of metrology tools to determine and/or monitor their efficiency over time (e.g. etch rate, oxidation rate). In this paper a technique, capable of monitoring reaction kinetics of semiconductor surface processes in real-time and in-situ is described. Earlier work has already shown that electrochemical OCP (Open Circuit Potential) measurements can assist significantly in optimising wet etchants for metals and silicides [1, 2]. A newly developed experimental set up allows now to monitor oxidation, dissolution and etching processes on semiconductor surfaces in-situ and in real time. A brief theoretical discussion can be found in ref. [3]. Experimental results, which are obtained until now give rise to the hope that this technique will assist in meeting the targets of future processing needs and also to provide basic insight in wet chemical cleaning mechanisms. In the following discussion, the applicability of OCP measurements to study wet chemical oxidation of Si by different SPM mixtures (96% H_2SO_4 / 30% H_2O_2 = 4:1) and the removal of the resulting oxides by HF mixtures (49% HF + high purity DI water) of different concentrations has been investigated and correlated with MIR-FTIR (Multiple Internal Reflection - Fourier Transform Infrared Spectroscopy), contact angle (water droplet on silicon surface), XPS (Photoelectron Spectroscopy) and SE (Spectroscopic Ellipsometry).

2. EXPERIMENTAL DETAILS

Silicon device-wafers, p/B-type, 125 and 150 mm, CZ, 16-24 Ωcm with <100> surface orientation have been applied as working electrodes. A good ohmic contact between the silicon electrode and the wiring was established by sputtering 700 nm Al on the backside followed by a sintering process at 435°C for 30 min. By using a specially designed single wafer holder made of PFA (per-fluor alkoxy copolymer) only the polished front side of the wafer was exposed to the electrolyte under investigation. As reference for most of the discussed measurements, different modified standard electrodes (Ag/AgCl based) were used for SPM and HF solutions. Due to the modifications made on the elctrodes, in some cases additional potential barriers were introduced. Because only the relative differences in the potential changes are relevant for the discussions in here, no further efforts were made to calculate the exact potentials of the used reference systems. Therefore the potentials are given vs. arbitrary reference ('a. ref.') and the mV-scales of the different graphs are in most cases not comparable to each other.
The working and the reference electrodes were connected through a mV-meter with a input impedance of > 10^{12} Ω and then immersed into different chemical mixtures. The experimental set-up is shown in Fig. 1.

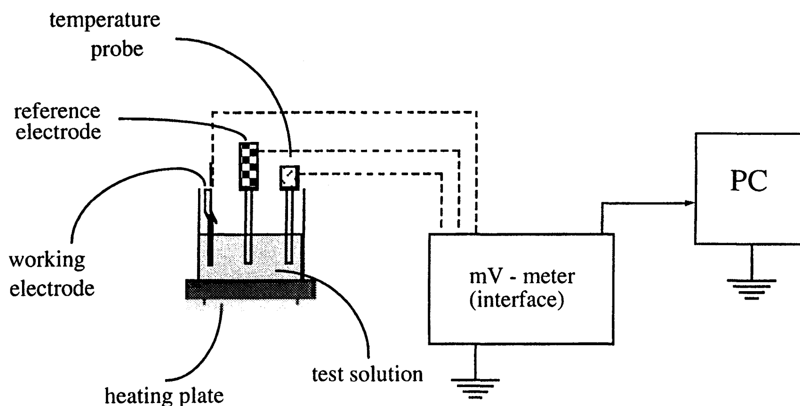

Fig. 1. Schematic drawing of the experimental set-up.

The interface to the PC allows also to monitor the temperature in the solution. High purity chemicals with typical contamination levels of <0.5 ppb or better were used in all experiments which were carried out under normal wet-bench light conditions, if not stated otherwise.

<u>MIR-FTIR:</u> Double side polished IR-samples (p-type, 10-25 Ωcm, <100>) were immersed one after each other into a 0.5% HF mixture after an SPM/DI-rinse pre-treatment. At pre-selected times, determined from the OCP curve, which was measured just before, the samples were taken out from the HF bath and immersed for max. 5 seconds into DI-water and then blow-dried with N_2. The samples were then transferred to a Mattson-galaxy FTIR

and measured within 20 minutes after preparation with p-polarised light and a resolution of 4 cm^{-1}. All samples are measured relative to the initial SPM oxide as reference.
SE: Si wafers of the same type as used for the OCP measurements (see above), were immersed together with the working electrode into the different SPM test solutions after an HF/DI-rinse pre-treatment. After the SPM, the wafers were rinsed for 10 minutes in DI-water and then blow-dried with N_2. Spectroscopic Ellipsometry measurements were performed immediately after sample preparation, using a SOPRA ES4Gt(photon energy range 2.76 - 4.86 eV in 21 equidistant points, angle of incidence: 80°). To obtain a better accuracy an averaging over 3 measurements per wavelength was performed.
XPS: Samples were prepared in the same way as described above for SE and then analysed, looking at the Si2p, O1s and the C1s lines.

4. RESULTS AND DISCUSSION

(a) OCP measurements in HF

In Figure 2 the typical time evolution and reproducibility of the OCP of a p-type Si-substrate immersed in a 0.25% HF solution after wet chemical oxidation and DI-rinse is presented. The same pre-treatment and measurement procedure was performed 6 times on 3 different days with 2 different Si-electrodes of the same type.

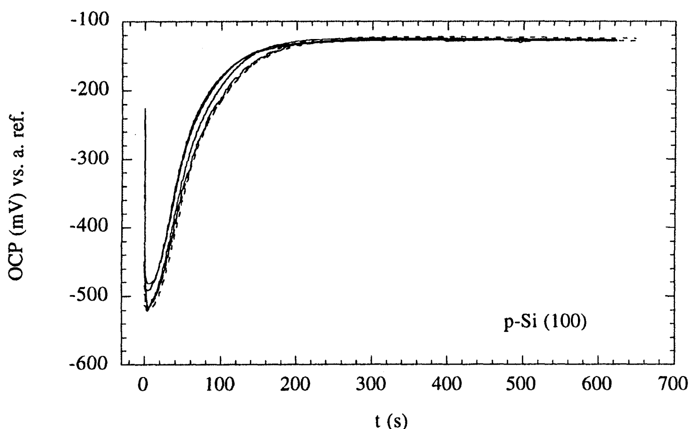

Fig. 2. Typical time evolution and reproducibility of the OCP of a p-type Si wafer when immersed into a 0.25% HF solution under clean room light conditions (pre-conditioning of the electrodes by the same wet chemical oxidation step for each measurement).

The start OCP value is difficult to quantify because of the finite time needed for immerson of the working electrode (around 1 second), but was found to have in general a value

somewhat more positive then the final steady state potential. In the initial stage of the reaction, the native oxide layer is dissolved, which results in a drift of the OCP to more negative values [4]. After reaching a characteristic minimum (called the PMP, Point of Minimum Potential), which is defined by several parameters (e.g. thickness of the oxide, etch speed, pH), the OCP turns into less negative direction until it reaches a quasi steady state potential. Here no major surface changes are happening anymore except a slow chemical corrosion of Si [4]. This results in a slow increase of the potential with time, depending on illumination and wafer doping [5].
Correlations with contact angle measurements (Fig. 3) and MIR-FTIR (Fig. 4 and 5) show, that around the PMP the build up of hydrogen termination starts to become the major potential determining step and that the quasi steady state potential indicates the completion of the hydrogen surface passivation layer. In Fig. 6 the integrated absorbance calculated from the curves in Fig. 5 is plotted versus the corresponding OCP values. The fit has been performed for values starting from the linear range of the OCP-time relationship untill the quasi-steady state range. As a result a linear correlation was obtained.

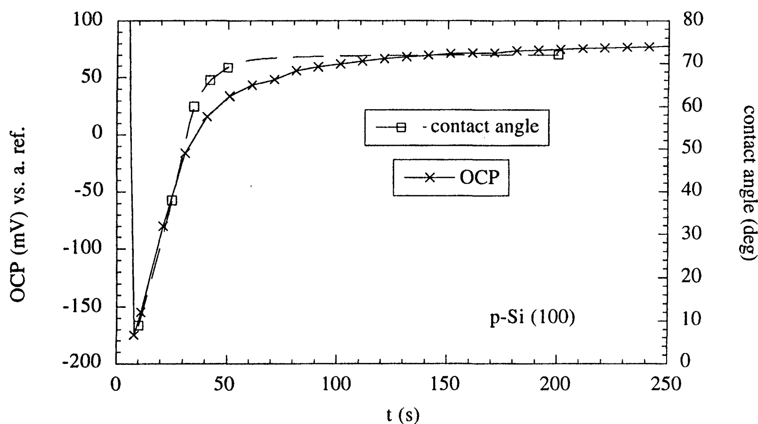

Fig. 3. Correlation between the time evolution of the OCP and the contact angle of a p-type Si wafer in a 0.5 % HF solution (clean room light conditions, pre-conditioning: SPM, 10 minutes at 95°C, followed by 10 minutes DI-water rinse).

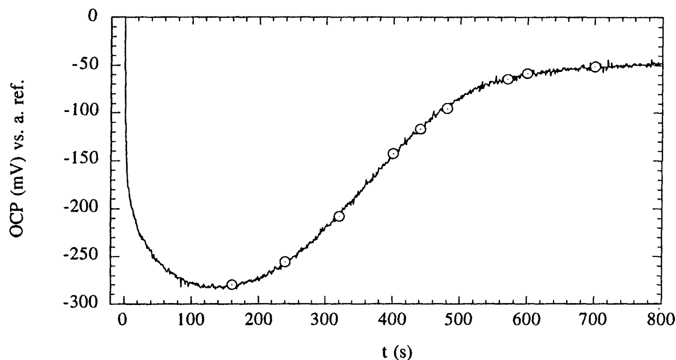

Fig. 4. OCP curve of a p-type Si wafer when immersed into a 0.1% HF solution under clean room light conditions with marks at the times where the samples for MIR-FTIR measurements (displayed in Fig. 5) were taken out from the HF bath (pre-conditioning: SPM, 10 minutes at 101°C, followed by 10 minutes DI-water rinse).

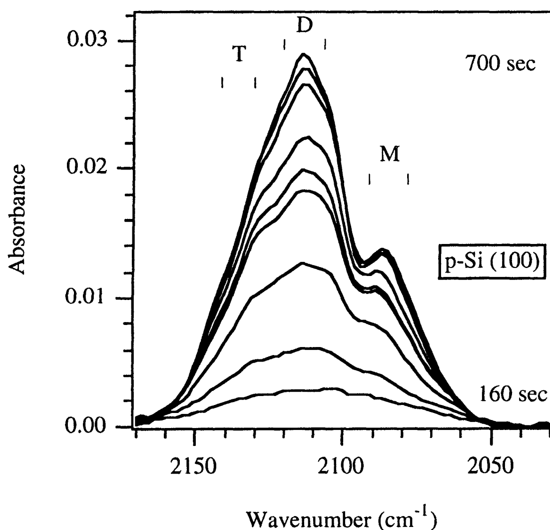

Fig. 5. p-Polarised SiH_x spectra as a function of the etching time in a 0.1% HF solution. Mono- (M), di- (D) and tri- (T) hydride peaks can be distinguished (sample pre-conditioning as in Fig. 4). The immersion times are marked in Fig. 4 and are represented by the spectra with increasing hight of the D-peak.

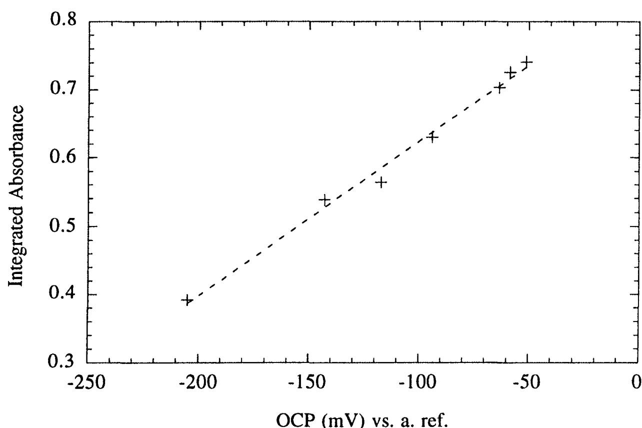

Fig. 6. OCP (from Fig.4) versus integrated absorbance of the MIR-FTIR spectra. The integration was performed over the whole range displayed in Fig. 5.

Figure 7 displays a very schematic and simplified representation of the major changes on the silicon <100> surface, when immersed in an oxidised state into an HF solution. In a first step the wet chemical oxide is dissolved by HF molecules forming SiF_6^{2-} ions in solution. The second major step is the etching of the top monolayer of Si, which is bonded to the bulk material. This results in the end in a stable hydrogen passivation of the remaining silicon surface [6, 7, 8, 9].

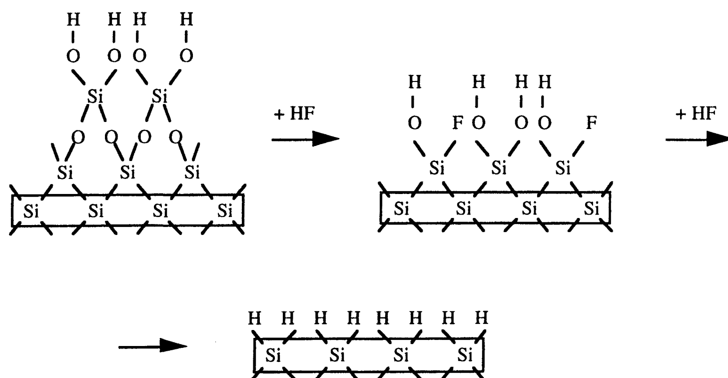

Fig. 7. Schematic and simplified two dimensional representation of the major changes on the silicon <100> surface, when immersed in an oxidised state into an HF solution.

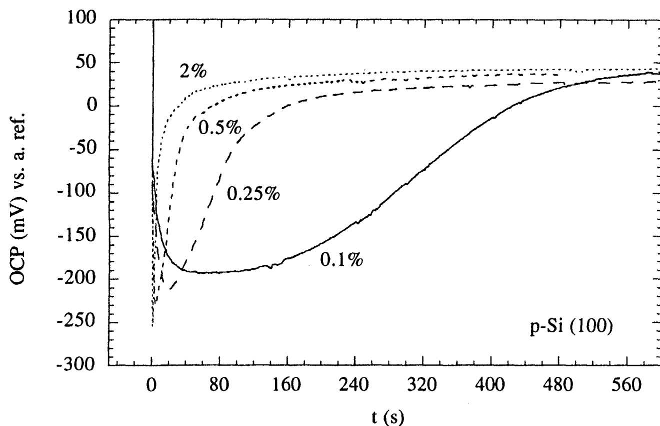

Fig. 8. Time evolution of the OCP as function of the HF concentration (pre-conditioning before each measurement as in Fig. 3).

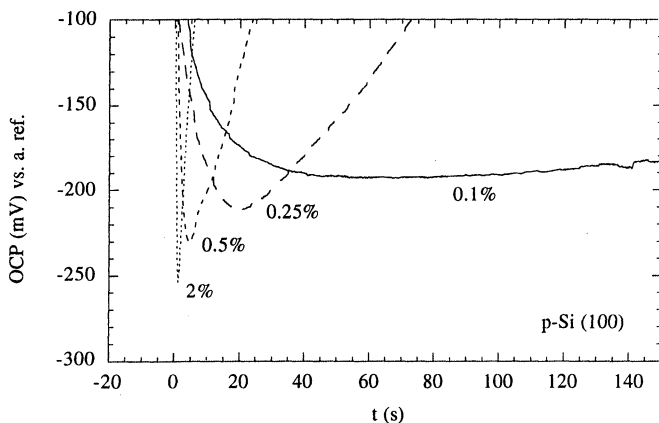

Fig. 9. Shift of the PMP's for the same wet-chemical oxide thickness as function of the HF concentration (re-scaled Fig. 8).

Figure 8 presents the results of an experiment, where the etching of equal wet-chemical oxides (SPM/DI-rinse) and the build up of H-passivation as a function of the HF concentration (i.e. total fluor concentration) has been studied. A significant change in the OCP curve before and after the PMP was obtained, which results in a major time delay for

reaching the PMP and the final surface passivation with a reduced HF concentration. Similar observations have been made by Bender et al. [10] by applying MIR-FTIR. Figure 9 represents a re-scaled Fig. 8 to enlarge the PMP region of the measurements. It can be clearly seen, that the PMP does not only have a time shift in direction of longer etch times but also a potential shift to more positive values for decreasing HF concentrations.

(b) OCP measurements in SPM

OCP measurements can also be applied for studying and monitoring of wet chemical oxidation processes on semiconductor surfaces. In Fig. 10 the very good reproducibility of a typical response from an OCP measurement is shown for the oxidation of Si in SPM. It should be noted here, that the general response of the OCP measurement is very similar in the case of Si oxidation as it is observed in the case of oxide removal (in HF). However a significant difference exists as the PMP is reached in a very short time which seems until now to be independent of the experimental conditions.

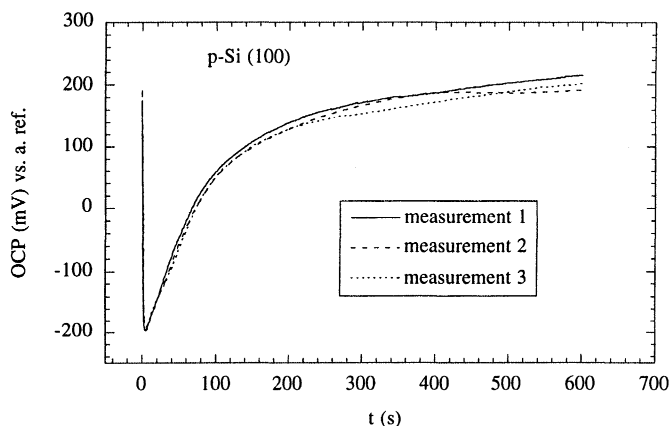

Fig. 10. Typical time evolution and reproducibility of the OCP of a p-type Si wafer when immersed into an SPM mixture at 95°C (pre-conditioning: 5 min 0.5% HF, followed by a 2 min DI water rinse).

Figure 11 represents results, where the oxidising power of an SPM mixture was tested as a function of bath age and temperature. Information which can be obtained from these curves is the slope of the potential change after the PMP and Δ_{OCP}, the absolute potential difference between the PMP and the final potential at which the steady state of the oxidation reaction is reached or the measurement is being stopped (i.e. where the sample is taken out from the solution). Investigations made with SE on these 2 oxides are showing a small but clear and significant difference in the oxide thickness (refractive index) and also relative to a H-passivated surface, which was measured additionally. An additional measurement has been carried out with an SPM mixture at 70 °C. In Fig. 12 the correlation between the oxide thickness, calculated from SE measurements and the Δ_{OCP} is displayed. XPS

investigations on the 2 different oxides from Fig. 11 confirmed the findings with SE (Fig. 13). These suggests, that the slope of the potential change after the PMP and the absolute difference between the PMP and the final potential (Δ_{OCP}) can be correlated to the oxidation speed and the resulting oxide thickness respectively.

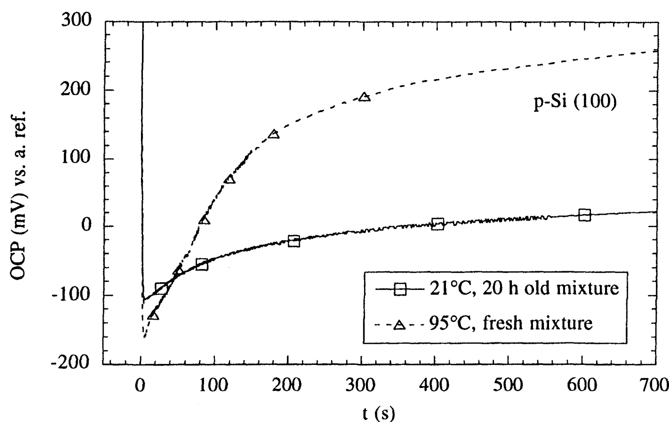

Fig. 11. Time evolution of the OCP of a p-type Si wafer as function of the age and temperature of an SPM mixture (pre-conditioning: as in Fig. 10).

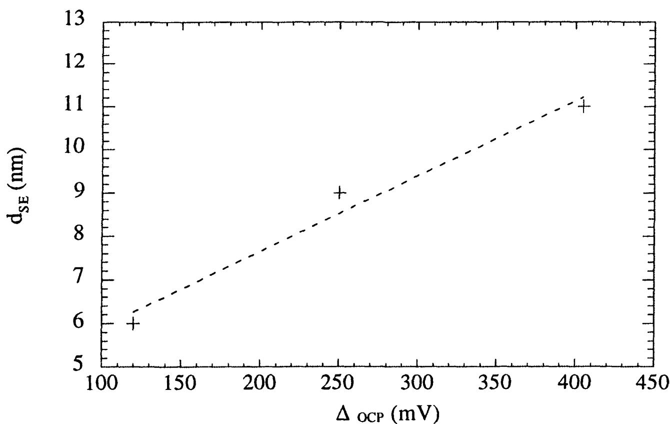

Fig. 12. Correlation between the Δ_{OCP} (potential difference between the PMP and the potential after 600 s immersion time) and the corresponding oxide thickness calculated from SE measurements (see Fig. 11).

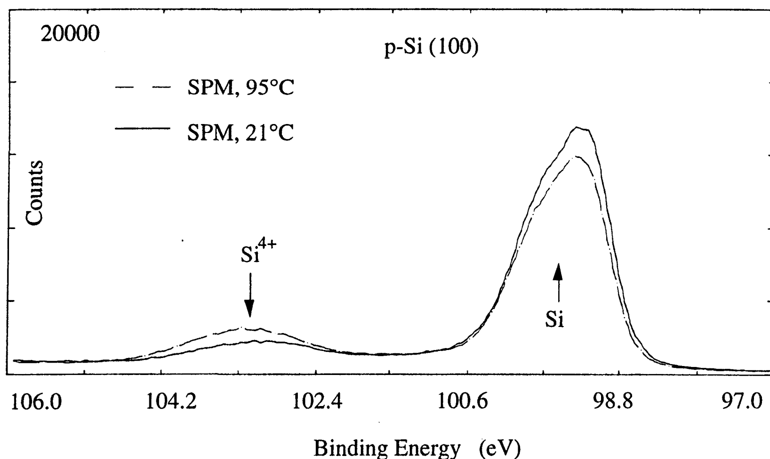

Fig. 13. XPS spectra for p-type Si samples treated in different SPM mixtures (see Fig. 11).

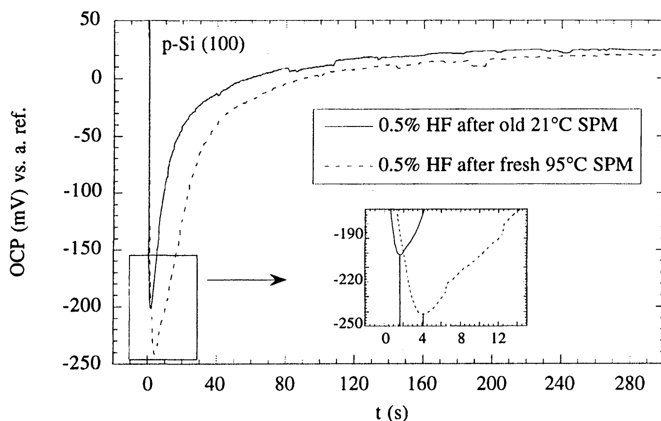

Fig. 14. Shift of the OCP curve to longer etch times and lower PMP with the thickness of wet-chemical oxides (pre-conditioning: Fig. 11).

Another way to estimate the difference in the thickness of native oxides on semiconductors is to use the OCP technique again. Figure 14 presents the results obtained, when the 2 different oxides under investigation (see Fig. 11) are etched off in 0.5% HF. A clear shift

of the PMP to more negative potentials and longer etch times is observed. This leads to a shift of the whole OCP curve. The sensitivity of this technique to determine relative differences in the oxide thickness, by comparing the time to reach the PMP of various samples can be strongly increased by using lower HF concentrations (e.g. see example in Fig. 8 and 9).

6. POSSIBLE APPLICATIONS OF THE OCP TECHNIQUE

At the moment several applications of this OCP technique can be envisaged. The first is to study the kinetics of wet chemical oxidation processes on semiconductor surfaces which was very difficult and time consuming until now, and also the dissolution and etching behaviour of semiconductor oxides and substrates [11]. More device fabrication oriented applications are under investigation at the moment for optimisation, control and end-point detection of wet chemical treatments in semiconductor device manufacturing. In the first step mixing ratios of chemicals, temperature, additive concentrations and other parameters can be optimised much faster and more precisely as was possible until now. As a result a response curve is obtained which is acting as a reference for the monitoring of the wet cleaning process with the OCP technique during the production process. This allows to control the status of the chemical bath (e.g. oxidising power, etch rate) and helps in optimising its lifetime to reduce chemical consumption and, with that, to reduce the chemical waste. Additionally the OCP response can be used as an end-point detector to optimise the process time as example by defining a certain slope of the OCP where the process should be stopped. Solutions for contamination issues from the reference electrode system, when being implemented as a real in-situ monitoring tool into a fabrication wet-bench are under investigation and will be reported elswhere.

7. CONCLUSIONS

A simple OCP measurement set-up was shown to be a useful metrology tool for in-situ monitoring of wet-chemical semiconductor surface reactions. This technique provides information about the evolution of semiconductor surface reactions in wet chemical environments and allows to study the kinetics of oxidation, dissolution and etching processes in real time. Results obtained until now show very good agreement with results obtained from MIR-FTIR, XPS, SE and contact angle studies and demonstrate very good repeatability and high sensitivity. This technique is also not limited to any particular chemical and the implementation into a fabrication wet bench for process optimisation and control to determine the time, when the chemical bath has to be replaced or refreshed, can be envisaged. Another application could be the determination of endpoints of oxidation and etching reactions in semiconductor wet chemical cleaning processes for throughput optimisation.

Acknowledgement: The contributions of Geert Doumen, Werner Poot (KU Leuven), Joost van Raaij (TU Eindhoven), Dimitrios Vassilakopoulos (NTU Athens), Felix Muniz Espada (Univ. de Valladolid, Spain) and Athina Kokkinidou (Univ. Thessaloniki, Greece) to this work are greatly acknowledged. H.F. Schmidt would like to acknowledge the financial support of his work by Ashland Chemical Corporation and the continuous support from Prof. H.P. Fritzer from the Institut für Physikalische und Theoretische Chemie, Technische Universität Graz, Austria. W. Storm receives grants from the Commission of the European Communities within the Human Capital and Mobility Program (ERB CHB GCT 930286) which he gratefully acknowledges.

References

[1] H.F. Schmidt, Diploma thesis, University of Technology, Graz, Austria, 1990.
[2] H.F. Schmidt, M. Hüttinger and E. Demm, presented at the NATO Advanced Study Institute on Semiconductor Materials and Processing Technologies, Erice, Italy, July 1-13, 1991.
[3] H.F. Schmidt, I. Teerlinck, M. Meuris, P.M. Mertens and M.M. Heyns, in Proc. Satellite Symp. to ESSDERC 95, The Hague/ The Netherlands, ALTECH 95, B.O. Kolbesen, C. Claeys and P. Stallhofer, Editors, Vol. 95-30, The Electrochem. Soc., Pennington, NJ (1995) p. 316.
[4] H. Gerischer and M. Lübke, Ber. Bunsenges. Phys. Chem. **92**, 573 (1988).
[5] H.F. Schmidt, unpublished results.
[6] H. Ubara, T. Imura and A. Hiraki, Solid State Communications **50**, 673 (1984).
[7] E. Yablonovich, D.L. Allara, C.C. Chang, T. Gmitter and T.B. Bright, Phys. Rev. Lett. **57**, 249 (1986).
[8] M. Grundner and R. Schultz, A.I.P. Conf. Proc. **167**, 329 (1987).
[9] V.A. Burrows, Y.J. Chabal, G.S. Higashi, K. Raghavachari and S.B. Christman, Appl. Phys. Lett. **53**, 998 (1988).
[10] H. Bender, S. Verhaverbuke and M.M. Heyns, J. Electrochem. Soc. **141**, 3128 (1994).
[11] G.S. Higashi and Y.J. Chabal, in Handbook of Semiconductor Wafer Cleaning Technology, W. Kern, Editor, Noyes Publication, Park Ridge, NJ (1993), p. 433.

SURFACE ANALYSIS OF Si(100) WAFERS PROCESSED IN VANADIUM SPIKED DILUTE HF SOLUTIONS

Jagdish Prasad, Jennifer Sees, Lisa Lester, Monte Douglas, Allen Templeton and Lindsey Hall
Texas Instruments, Inc.
P. O. Box 650311, MS 301
Dallas, TX 75265

Silicon wafers processed in vanadium spiked 5% HF solutions are characterized using TXRF, TOF-SIMS, SIMS and SPV techniques. The results of these experiments indicate that vanadium outplates on the wafer surface linearly with the vanadium concentration in the HF solution. Depth profiling of silicon wafers after processing in vanadium spiked HF solution clearly shows that vanadium diffuses into the bulk silicon to about 2000Å at room temperature. The depth profiles at different points of the same wafer show that the vanadium diffusion into the bulk is not uniform but varies from point to point. SPV measurements indicate that minority carrier diffusion length and thus the life time is reduced due to vanadium diffused into the Si bulk at room temperature.

INTRODUCTION

It is well known that metallic contamination can degrade the electrical performance of silicon devices. Metal impurities can affect gate oxide breakdown strength and can diffuse into the bulk of the silicon resulting in the reduction of minority carrier lifetime. All these factors will result in reduced device yield. Therefore, it is important to control metallic contamination in process chemicals to improve device yield.

A large part of previous research has focused on Cu, Fe, and Ni in process chemicals (1). Some metallic contaminants are studied very little, and others are not even suspected. One such unsuspected contaminant is vanadium (V). In a previous study, the effect of V on silicon solar cells (2) was investigated. In study reported V levels of about E13 atoms/cm^3 could be very harmful to solar cell performance, since V occupies the sites favorable for recombination processes. A more recent study conducted by spiking IPA with V during the drying process indicates that V in IPA results in the reduction of minority carrier lifetime (3). These studies strongly suggest that the effects of V contamination in process chemicals on a device's electrical properties should be more thoroughly investigated.

In this study we report the outplating efficiency of V from HF solutions and its effect on minority carrier diffusion length at room temperature as a function of time.

EXPERIMENTAL

V standard was prepared using V powder dissolved in 5% HF. Silicon wafers were processed in 5% HF solution spiked with V standard. The V contamination in processing solution was varied in the range of 0.2 to 1000 ppm. The concentrations of the spiked HF solutions were determined using inductively coupled plasma (ICP) technique.

The Si wafers used were B-doped p-type. The V concentration on the processed wafer surfaces was measured using total reflection x-ray fluorescence (TXRF), and time-of-flight secondary ion mass spectrometry (TOF-SIMS). To investigate the diffusion of V into the bulk, depth profiling was performed using secondary ion mass spectrometry (SIMS). The TXRF system used in this study was a commercial unit manufactured by Rigaku Corporation. The system uses a tungsten rotating anode and has two monochromator crystals. A PHI-Evans TFS 2000 TOF-SIMS instrument was used to characterize trace levels of V on the silicon wafer surfaces. SIMS analysis was performed using a Cameca ion microscope (IMS-3F) with a primary current of 0.320 μA and a primary beam O_2. The calibration of IMS-3F for concentration and depth was based upon the implanted standard from Hughes. The implant dose was 1E14 atoms/cc at an energy of 200 KeV.

SPV measurements were performed using a commercially available instrument from Semiconductor Diagnostics, Inc. model CMS III-A.

RESULTS AND DISCUSSION

TXRF (detection limit 1E10 atoms/cm^2) analysis of Si wafer surfaces processed in vanadium spiked HF bath with vanadium concentrations of 0.2, 1, and 5 ppm did not reveal vanadium on the wafer surfaces. However, vanadium on a silicon wafer surface was observed by TXRF at vanadium concentrations varying from 100 to 1000 ppm. This result indicates that at low concentrations, the vanadium on the wafer surface is below the detection limit of TXRF technique. To resolve the issue of TXRF detection limit, TOF-SIMS (detection limit 1E8 atoms/cm^2) analysis was performed on the same wafers that were used for TXRF analysis processed in HF solutions spiked with 0.2, 1, and 5 ppm of vanadium. The TOF-SIMS analysis data for Si wafer surfaces processed in 5%HF spiked with low concentrations of V (0.2, 1, and 5 ppm) are shown in Figure 1. Examination of Figure 1 clearly indicates that vanadium outplates on Si wafer surfaces and varies linearly with vanadium concentrations in HF solutions.

TXRF analysis of the wafer surfaces processed in HF solutions spiked with vanadium concentrations of 100 to 1000 ppm showed no correlation between the amount outplated on the wafer surfaces and the vanadium concentrations in the spiked HF solution. To explore the accuracy of TXRF data for vanadium, TOF-SIMS technique (which samples only the surface monolayer) was used. TOF-SIMS data (Figure 2) clearly indicate a linear relationship between the amount of vanadium outplated on the surface and the vanadium concentration in the HF solution. To determine the cause of discrepancy between TXRF and TOF-SIMS data, TXRF analysis was repeated as a function of incident beam angle. Three angles of 0.14, 0.12 and 0.10 degrees were used. It was found that an angle of 0.10 degrees gave the best correlation between TXRF (Figure 3) and TOF-SIMS (Figure 2) data. At this angle, the incident beam penetrates less into the bulk compared to the beam incident at 0.14 degrees and is probably more representative of the surface concentration.

SIMS data for depth profiling of processed silicon wafers are shown in Figure 4. The data shown in Figure 4 indicate that vanadium diffuses into the bulk to about 2000 Å at room temperature. Depth profiling at three different spots of the same wafer indicate that the diffusion of vanadium into the bulk is not uniform but varies from place to place from 500 Å to about 2000 Å. The extent of diffusion into the bulk depends on the time waited before analysis.

To study the effect of vanadium contamination and its diffusion into the bulk Si, the surface photovoltage (SPV) method was used to determine the minority carrier diffusion length . The results of SPV measurements are summarized in the following table.

Table 1: Summary of SPV measurements for diffusion length of Si wafers processed in vanadium spiked HF bath as a function of time and vanadium concentration. Diffusion length did not change with vanadium concentration.

State of the Wafer	Diffusion Length (μm)
Control	510 +/- 9.29
Just after processing in V/HF bath	483 +/- 8.26
14 days after processing	340 +/- 20.88
45 days after processing	285 +/- 5.59

Data presented in Table 1 clearly indicate that minority carrier diffusion length in Si wafers processed in 5% HF solutions spiked with vanadium decreases compared to that for control wafer. This SPV data is consistent with SIMS depth profiling data

since diffused vanadium may create recombination sites and thus decrease the diffusion length and minority carrier life time.

CONCLUSIONS

TXRF and TOF-SIMS analysis of silicon wafers processed in vanadium spiked 5%HF solutions indicate a linear relationship between the amount of vanadium outplated on the wafer surface and the vanadium concentration in the HF solution.

SIMS data show that vanadium diffuses into the bulk silicon to about 2000 Å at room temperature. The diffusion of vanadium is not uniform throughout the wafer but varies from place to place.

SPV measurements for minority carrier diffusion length indicate that diffusion length shortens as a result of vanadium contamination. This result is consistent with SIMS data that shows that vanadium diffuses into the bulk creating recombination sites and ,as a result, reduced diffusion length.

ACKNOWLEDGEMENTS

Authors would like to thank David Smith, Roy Beavers and Valerie Sewall for their help in analyzing the samples.

REFERENCES

1. E. Hsu, H. G. Parks, R. Craigin, S. Tamooka, J. S. Ramberg and R. K. Lowry, J. Electrochem. Soc., **139,** 3659 (1992)
2. R. H. Hopkins, R. G. Seidensticker, J. R. Davies, P. Rai-Choudhury, P. D. Blais, and J. R. McCormick, J. Cryst. Growth **42,** 493 (1977).
3. S. K. Yeo, et al., "Impact of Metallic Contaminants in IPA on High Temperature MCLT", Conference on Semiconductor Pure Water and Chemicals, February 21-23, page 275 (1995), Santa Clara, California.

Figure 1: TOF-SIMS signal vs. vanadium concentration in 5% HF process solution.

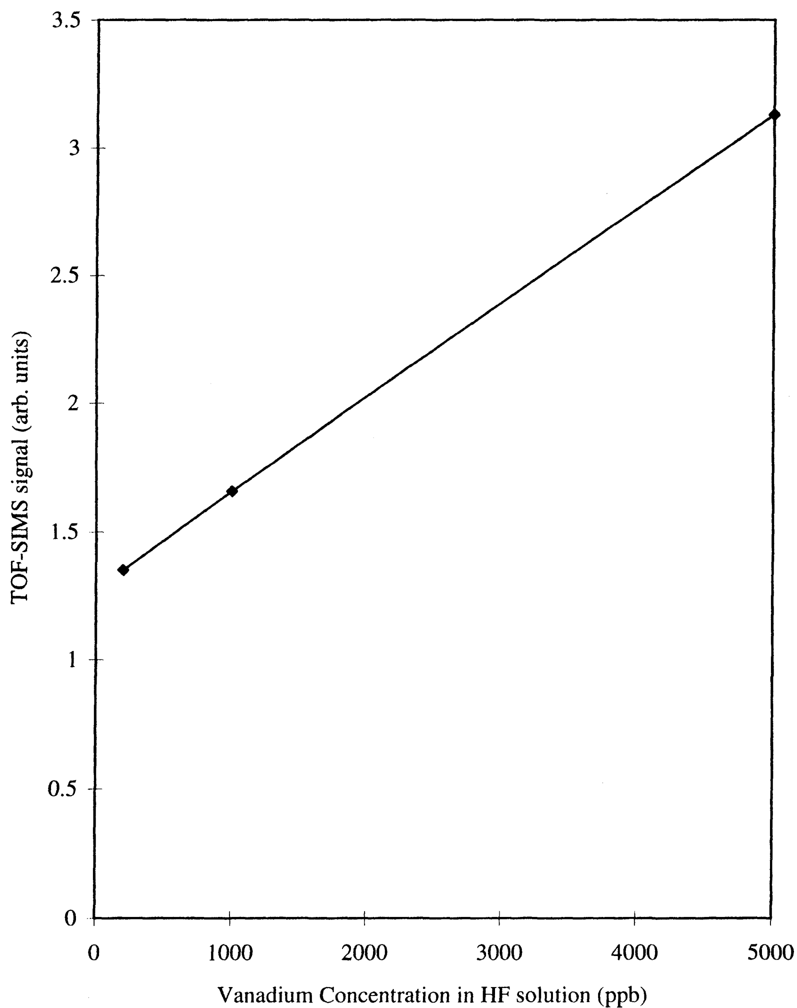

Figure 2: TOF-SIMS signal vs. vanadium concentration in 5% HF process solution

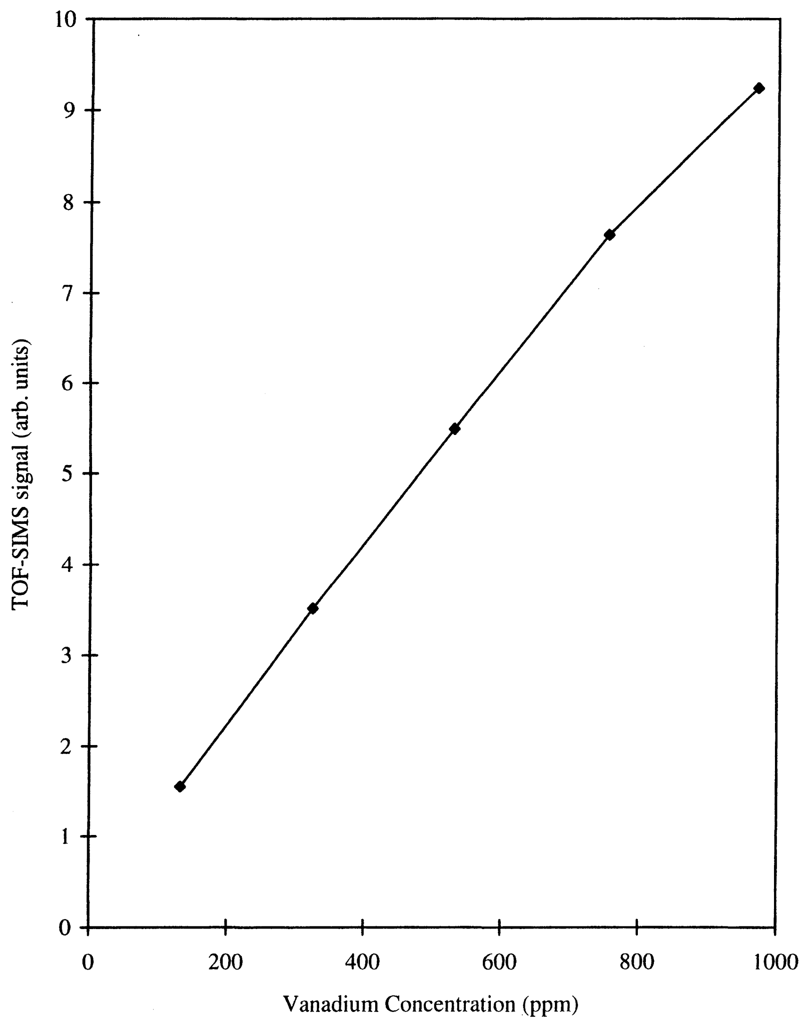

Figure 3: TXRF signal vs. vanadium concentration in 5% HF process solution

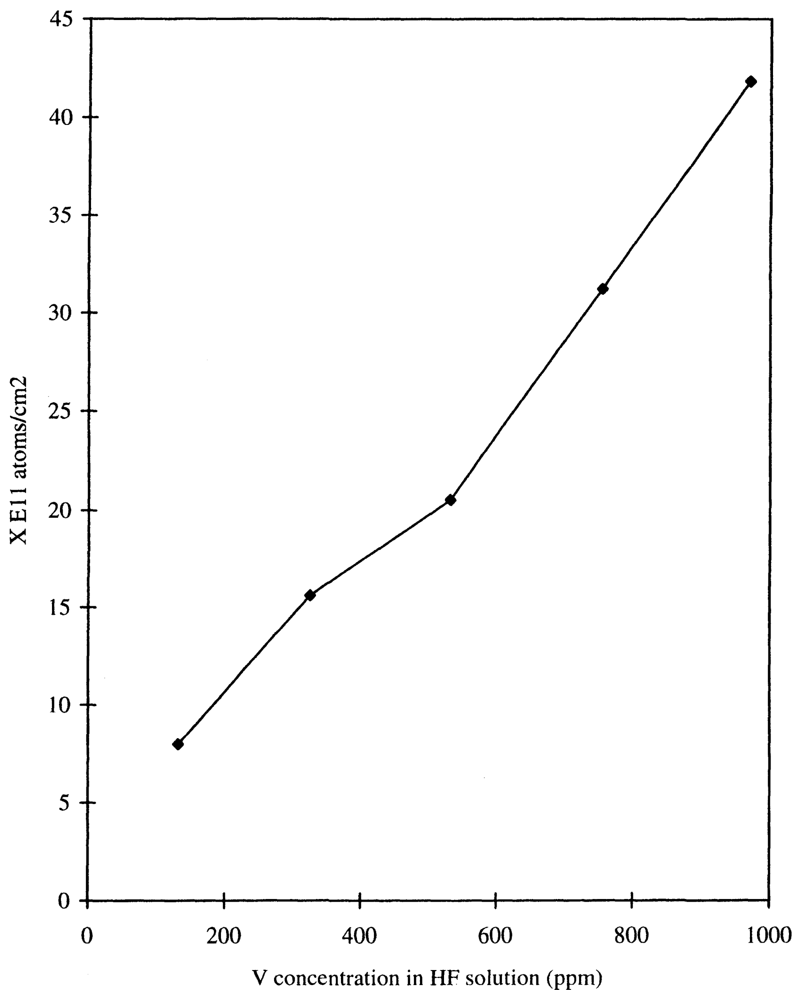

Figure 4: Depth profile of silicon wafer processed in 5% HF solution spiked with vanadium at room temperature. Vanadium concentration in HF was 132 ppm. Four curves represent four different spots on the same wafer.

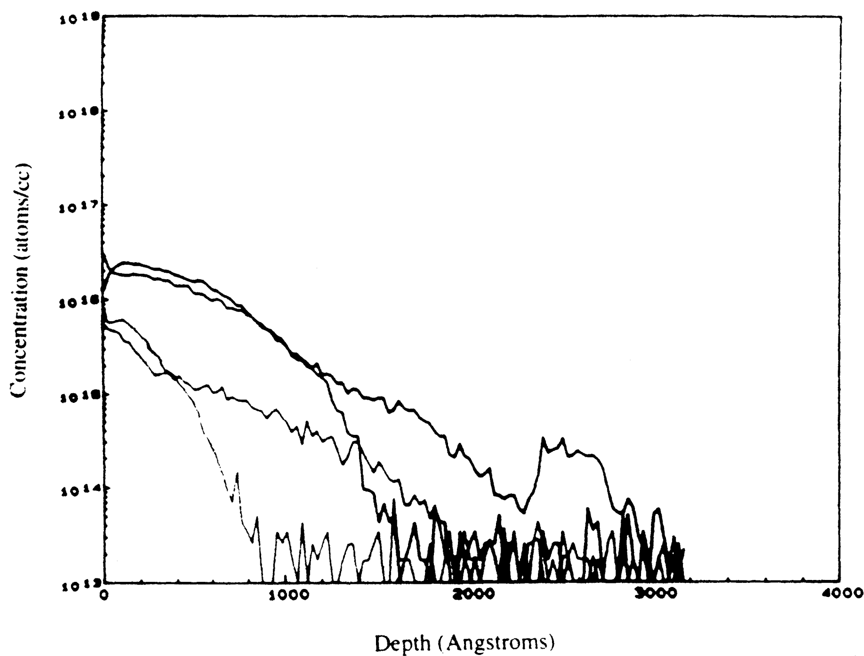

SURFACE SIMS ROUND ROBIN FOR NA, AL AND K ON SILICON WAFERS

R. S. Hockett
301 Chesapeake Drive
Charles Evans & Associates
Redwood City, CA 94063

and

Alain Diebold
2706 Montopolis Drive
SEMATECH
Austin, TX 78741

This paper presents the spoke-wheel round robin results, under the auspices of the ASTM F-1.06 subcommittee, for determining the precision of the ASTM test method F 1617-95 ("Test Method for Measuring Surface Sodium, Aluminum, and Potassium on Silicon and Epi Substrates by Secondary Ion Mass Spectrometry").

INTRODUCTION

Prior work [1, 2] showed that SIMS signals for surface metal impurities on polished silicon substrates could be linearly correlated to the amount of impurities deposited by the Spin-Coat method [3] and calibrated by Vapor Phase Decomposition (VPD) followed by Atomic Absorption Spectroscopy (AAS) [4]. This was significant for three reasons.

(1) Surface metal quantitative measurements by SIMS could be made without the need for polyencapsulation equipment [5] which had limited the widespread use of SIMS for this application.

(2) The already widespread capacity of SIMS instruments in the semiconductor industry could easily and quickly be applied to the control of surface metal contamination in semiconductor processing.

(3) Furthermore, the SIMS technique does not have the inherent chemical state collection problem of the Vapor Phase Decomposition (VPD) technologies which have arisen to meet the surface metal contamination control need. The problem is that for the VPD technologies to be quantitative one must assume the chemical bonding states of the contamination in order to estimate how much is collected, but the

chemical bonding states are not always known and this can result in an uncertainty in the accuracy even if the precision is very good [6,7]. However, the proper use of a sequence of different VPD chemistries designed to decompose a range of different chemical states can reduce this uncertainty.

Acceptable long term repeatability of the SIMS measurement was demonstrated for a 4 month period [8]. However, no interlaboratory precision study had been completed until now.

PARTICIPATING LABORATORIES

The following laboratories and scientists participated in this round robin study.

Winny McComas and Brian MacDonald, Advanced Micro Devices, Sunnyvale, CA

Steve Smith, Charles Evans & Associates, Redwood City, CA

Fred A. Stevie, AT&T Analytical Services, Allentown, PA

Greg Fitzgibbon, IBM Analytical Services, Hopewell Junction, NY

David Simons, NIST, Gaithersburg, MD

Thomas A. Anderson and Keenan Evans, Motorola Inc., Phoenix, AZ

Gabi Neubauer, Intel Corporation, Santa Clara, CA

Joy K. Watanabe, Motorola, Mesa, AZ

Michael R. Frost, Evans East, Plainsboro, NJ

Mark Anthony, Texas Instruments, Dallas, TX.

EXPERIMENTAL PLAN

Silicon wafer samples (125 mm diameter) with surface Na, Al and K were prepared by Sumitomo Sitix Corporation (Saga, Japan) using their Spin-Coat contamination process [3]. Each wafer was precleaned by SC-1 then SC-2 before the spin-coating. The intentional contamination was carried out within 3 hours after pre-clean. The wafers were segregated into groups of 5 (described later) and stored in double-packaged cassettes with an aluminum foil outer sealed package.

Each participant laboratory was provided with a sealed cassette containing five (5) wafers: one spin-coated REFERENCE wafer (called Sample D), 3 spin-coated TEST wafers (called Samples A, B, C), and one BLANK wafer (called Sample E).

This study was limited to the three elements: Na, Al, and K. The application of SIMS to the measurement of transition metal contamination, e.g. surface Fe contamination, is reported elsewhere in this proceedings [9]. The surface contamination levels determined by single-side VPD/AAS [4] at Sumitomo Sitix on two parallel processed wafers per target level are listed in Table 1.

Table 1. VPD/AAS Results for Round Robin Samples
(units of 10^{10} atoms/cm^2; ND means not detected)

Purpose	Sample	Al	Na	K
TEST	A	3,3	15,10	8,7
TEST	B	8,7	29,32	23,22
TEST	C	25,22	115,121	92,92
REFERENCE	D	118,124	334,353	288,282
BLANK	E	ND,ND	4,0.6	2,0.1

Round robin participants were given the VPD/AAS values for the REFERENCE wafers only; they were not given the values for the TEST or BLANK wafers. Participants were instructed to measure each wafer within a 50 mm x 50 mm square centered at the wafer centers, once per day for four days by SIMS. The participants were allowed some freedom to choose analytical conditions: oxygen leak, or not; energy filter, or not; and the mass resolution. The sputter rate was to be less than 0.01 nm/s. The reference wafer was to be used for the SIMS calibration. The test method which came out of this study is ASTM F 1617 [10].

Table 2 summarizes the equipment and measurement conditions used by each laboratory. Laboratory 5 made two sets of measurements under two different measurement conditions; these are called Lab 5 and Lab 5'.

STATISTICAL DATA SUMMARY

Statistical evaluation of the spoke-wheel round robin followed ASTM E 691 (Standard Practice for Conducting an Interlaboratory Study to Determine the Precision of a Test Method). Further details of the data and screening decisions can be found in the ASTM Research Report [11].

Table 3 summarizes the screened data statistics. The 95% repeatability, r, and reproducibility, R, limits are calculated by 2.8 times their respective standard deviations (s_r, S_R). Under ASTM E 691 rules:

<u>Repeatability</u> concerns the variability between independent test results obtained within a single laboratory in the shortest practical period of time by a single operator.

<u>Reproducibility</u> deals with the variability between single test results obtained in different laboratories.

TABLE 2

EQUIPMENT AND MEASUREMENT CONDITIONS
ASTM F-1.06 Round Robin for SIMS Measurement of Surface Metals on Silicon

	units	Magnetic Sector SIMS				Quadrapole SIMS						
		Lab 1	Lab 3	Lab 8	Lab 10	Lab 2	Lab 4	Lab 5	Lab 5'	Lab 6	Lab 7	Lab 9
System		4f	3f	3f	4f	6600	6600	6300	6300	6300	Riber	6600
O_2^+ Impact energy	KeV	3.5	8	5.5	3.5	6	4	6	6		7	3
Oxygen Leak		Y	N	Y	Y	N	Y	N	Y	N	N	N
Current	nA		50	50	18	50	3	3	3	8-9	10	30
Sputter Rate	nm/s	.007-.012		.008	0.006		.005			.007-.008	0.01	.012-.015
Sputter Crater	μm^2	100	500	250	250	400	500	500	500	700	10,000	750
Analysis Area	μm^2		150	60	60	120	100			350	100	225
Gating	%		70	76	76	70	80			50	90	70
Impact Angle	Deg.					60	60	60	60		60	60
e- Neutralization				N		N	N			Y	N	N
Na/integration time	AMU(s)	23( )	23(2)	23(1)	23(.5)	23(1)	23(1)	23(1)	23(1)	(5)	23( )	23(1)
Al/integration time	AMU(s)	27( )	27(2)	27(1)	27(.5)	27(1)	27(1)	27(1)	27(1)	(5)	27( )	27(1)
K/integration time	AMU(s)	39( )	39(2)	39(1)	39(.5)	39(1)	39(1)	39(1)	39(1)	(5)	39( )	39(1)
Si/integration time	AMU(s)	28( )	30(1)	30(1)	30(.5)	28(1)	30(1)	30(1)	30(1)	(1)	30( )	29(1)
Energy Filter (Quad)		-	-	-	-	Y	N	N	Y	N	N	Y
Field Aperature (M/S)	µm	30		750	750	-	-	-	-	-	-	-
Contrast Diaphram (M/S)	µm	150		50	150	-	-	-	-	-	-	-

Normally, the repeatability is less (lower variability) than the reproducibility. It is interesting to note that the SIMS X-Bar values in Table 3 agree well with the VPD/AAS results in Table 1.

TABLE 3. Summary Statistics for the SIMS Measurement of Surface Sodium, Aluminum, and Potassium (units of 10^{10} atoms/cm^2)

NA SAMPLE	X-BAR	s_r	s_R	r	R
A	10.68	2.240	2.791	6.273	7.816
B	33.64	3.339	4.931	9.348	13.81
C	112.1	16.19	19.79	45.32	55.41
E	0.665	0.359	0.861	1.005	2.410
AL SAMPLE	X-BAR	s_r	s_R	r	R
A	3.504	0.6865	1.107	1.922	3.100
B	9.425	0.7684	2.239	2.152	6.269
C	28.80	2.298	6.107	6.434	17.10
E	0.795	0.390	0.760	1.093	2.128
K SAMPLE	X-BAR	s_r	s_R	r	R
A	7.829	1.642	2.761	4.596	7.731
B	24.11	3.607	5.943	10.10	16.64
C	82.37	12.77	19.63	35.74	54.97
E	0.407	0.162	0.344	0.454	0.965

The significance of this round robin study is threefold:

(1) It is clearly possible to make acceptable Na, Al and K quantitative measurements on the surface of silicon wafers in conventional SIMS laboratories which are most often not clean rooms.

(2) It is possible to make the surface Al measurement down to the 10^{10}-10^{11} atoms/cm^2 range with both magnetic sector (high mass resolution) and quadruple (low mass resolution) SIMS instruments, as long as the quadruple instrument uses an energy filter in the secondary ion mass detection scheme to remove the $C_2H_3^+$ interference. If the energy filter is not used, then the measurement is not valid for Al. To detect surface Al below the 10^{10} atoms/cm^2 range requires a magnetic sector mass spectrometer.

(3) It is possible to make the measurement without an oxygen leak to stabilize the ion yields over the analysis period. (There may be a caveat in that the chemical native oxides on the reference and unknowns were all the same thickness. The effect of different chemical native oxide thicknesses is not known.)

An additional experiment by one of the participants revealed that for the PHI™ Model 6600 SIMS instrument with a primary beam incident at

60° the RSFs derived from Spin-Coat samples and from traditional ion implanted reference samples were identical for Na, Al and K [12]. This means that for this equipment and these elements, ion implanted reference samples (which are easier to obtain) are quite accurate reference samples for this measurement. It is not known whether this is true for other elements.

When evaluating the usefulness of an analytical technique it is important to understand the effect of variability in the measurement itself. For example, in order to use Statistical Process Control for a semiconductor process, the measurement capability itself must be evaluated for its usefulness. SEMATECH has described the method for this evaluation [13]. The ability of a measurement tool to keep a process under control is judged by the P/T ratio which equals 6 sigma/(UCL-LCL) where P/T of 30% is recommended, sigma is the measurement one standard deviation (short and long term variability included), UCL is the upper control limit and LCL is the lower control limit for the process.

To illustrate this method of evaluation, consider using an analytical tool to control the surface metal contamination on silicon wafers at an upper level of $1x10^{11}$ atoms/cm^2. The UCL is $1x10^{11}$ atoms/cm^2. The LCL is effectively zero. To achieve a P/T of 30%, the sigma must then be $5x10^9$ atoms/cm^2, or 1/20th of the control limit. Some others prefer to equate the P/T to 3 sigma/(UCL-LCL), and this leads to a sigma of 1/10th of the control limit, as used in The National Technology Roadmap for Semiconductors [14].

To further illustrate the issue from this SIMS round robin, we note Sample B had an ensemble Average surface Al of $9.4x10^{10}$ atoms/cm^2, and the one standard repeatability deviation, s_r, was $0.768x10^{10}$ atoms/cm^2, or 1/12th of the upper control limit. However, the s_r is an ensemble average of all the laboratories participating in this round robin. The individual laboratory ratio (sigma divided by the average) of course has a range.

REFERENCES

1. N. Fujino, H. Horie, K. Hiramoto, Y. Tanizoe, S. Sumita, and T. Shiraiwa, "SIMS Analysis of Contamination Elements in the Oxide Layer on VLSI Silicon Wafer," SIMS VII, edited by a. Benninghoven, C. A. Evans, K. D. McKeegan, H. A. Storms, and H. W. Werner, (John Wiley & Sons, New York, NY) pp. 527-530 (1990).

2. M. R. Frost, P. Gupta, and P. W. Davies, "Quantitation of Impurities near the Surface of Silicon Wafers Using SIMS/Comparison to TXRF and VPD/AAS," SIMS VIII, edited by a. Benninghoven, K. T. F. Janssen, J. Tumpner, and H. W. Werner, (John Wiley & Sons, New York, NY) pp. 637-640 (1992).

3. M. Hourai, T. Naritomi, Y. Oka, K. Murakami, S. Sumita, N. Fujino, and T. Shiraiwa, "A Method of Quantitative Contamination with Metallic Impurities of the Surface of a Silicon Wafer," Jpn. J. Appl. Phys. 27, pp. L2361-L2363 (1988).

4. T. Shiraiwa, N. Fujino, S. Sumita, and Y. Tanizoe, "Chemical Analysis of Metallic Impurity on the Surface of Silicon Wafers," Semiconductor Fabrication: Technology and Metrology, ASTM STP 990, Dinesh Gupta, editor, American Society for Testing and Materials, pp. 314-323 (1989).

5. R. S. Hockett and J. C. Norberg, "The Practical Use of Polyencapsulation/SIMS for Quantitative Surface Analysis of Silicon Substrates," SIMS VII, edited by a. Benninghoven, C. A. Evans, K. D. McKeegan, H. A. Storms, and H. W. Werner, (John Wiley & Sons, New York, NY) pp. 491-494 (1990).

6. R. S. Hockett, "High Sensitivity Characterization of Contamination on Silicon Surfaces Using TXRF," 1993 IES Proceedings, The Institute of Environmental Sciences, Mount Prospect, IL, pp. 238-244 (1993).

7. M. B. Shabani, T. Yoshimi, H. Abwe, M. Fukuda and Y. Sayama, "Development of One-Drop Sandwich Etching Method for Determination of Trace Impurities in Oxide and Bulk of Silicon Wafers by GF-AAS," Extended Abstracts Vol. 94-2, The Electrochemical Society, Pennington, NJ, Abstract No. 396, pp. 608-609 (1994).

8. S. P. Smith and R. S. Hockett, "SIMS Quantitative Measurement of Surface Metals on Silicon Wafers," ECS Extended Abstracts Vol. 93-1, (The Electrochemical Society, Pennington, NJ) Abstract 867, p. 1278 (1993).

9. R. S. Hockett, S. P. Smith, and C. J. Hitzman, "Surface Metal Contamination on Silicon Wafers Measured by Surface SIMS," this proceedings.

10. F 1617-95, "Test Method for Measuring Surface Sodium, Aluminum, and Potassium on Silicon and Epi Substrates by Secondary Ion Mass Spectrometry," Annual Book of ASTM Standards, Vol. 10.05, ASTM, Philadelphia, PA.

11. ASTM Research Report F01-1010, "Interlaboratory Test Study for the Determination of Surface Na, Al, and K on Polished Silicon Substrates Using Secondary Ion Mass Spectrometry," February 13, 1995, ASTM, Philadelphia, PA.

12. M. R. Frost, "On the Use of Quadrupole SIMS for the Measurement of Surface Metallic Contamination," Contamination Control and Defect Reduction in Semiconductor Manufacturing III, edited by Dennis Schmidt, ECS Proceedings Vol. 94-9, (The Electrochemical Society, Pennington, NJ) pp. 339-348 (1994).

13. S. A. Eastman, "Evaluating Automated Wafer Measurement Instruments," SEMATECH Technology Transfer Document #94112638A-XRF, SEMATECH, 2706 Montopolis Drive, Austin, TX 78741 (1994).

14. The National Technology Roadmap for Semiconductors, Table 26 Starting Materials, Footnote B, p. 113, The Semiconductor Industry Association (1994).

FEASIBILITY OF ANALYSIS OF SILICON SURFACE CLEANING USING TIME-OF-FLIGHT SECONDARY ION MASS SPECTROMETRY

S.D. Hossain-Pas [a], M.F. Pas [b], and M.A. Douglas [c]
[a] Manufacturing Science and Technology Center, M/S 350
[b] Semiconductor Processing and Device Center, M/S 944
[c] Corporate R&D, M/S 147

Texas Instruments, Inc.
Dallas, Texas 75265

ABSTRACT

Time-of-Flight Secondary Ion Mass Spectrometry (TOF-SIMS) is used to analyze the uppermost monolayer of silicon samples treated with wet cleaning sequences. Prior to surface cleaning, the wafers are photoresist-coated, ion-implanted, and plasma-ashed for bulk resist removal. The following standard wet process chemistries are evaluated individually or in combination: (a) NH_4OH:H_2O_2:H_2O (SC1) heated to 50°C and 80°C, (b) H_2SO_4 and O_3 (ozonated piranha) and (c) H_2O:HF. Dilute HF treatments are associated with improved photoresist removal, higher bromine contamination, less Al contamination, and the formation of silicon oxyfluoride in the uppermost monolayer of the native silicon oxide. Al contamination is observed after SC1 treatment. However, Al levels are reduced by as much as a factor of 100 when an HF process follows the SC1 treatment. Improved resist residue removal is observed when SC1 is heated to 80°C versus 50°C. SC1 at 50°C and ozonated piranha cleaning show similar results and exhibit the least effective resist residue removal properties compared to SC1 (80°C) followed by an HF process.

INTRODUCTION

Time-of-Flight Secondary Ion Mass Spectrometry (TOF-SIMS) is a sensitive analytical tool for molecular and atomic characterization of the uppermost monolayer of a surface. TOF-SIMS is used in this study to investigate silicon surfaces at the uppermost monolayer level for organic and inorganic, molecular and elemental species, as well as chemical alteration of the silicon native oxide surface with high sensitivity. An additional benefit is that no excess processing is required to prepare the wafer for analysis.

One feature of TOF-SIMS is its ability to detect elemental impurities from atomic mass Z=1 to 92, including all element isotopes. TOF-SIMS has demonstrated an elemental Fe detection limit of 1.0E8 atoms/cm^2 on a silicon substrate in a 100 μm diameter region [1]. Detection limits for Group I-A, II-A, III-A and VII-A elements are at least an order of magnitude better than for the Fe value. Currently, TOF-SIMS does not offer routine

quantification, although relative sensitivity factors (RSFs) are being evaluated for a silicon matrix to permit semi-quantitative analysis.

Time-of-Flight Secondary Ion Mass Spectrometry, TOF-SIMS, is a relatively new analytical method that is characterized by several attributes: (a) less than one parts per million (ppm) surface sensitivity, (b) single monolayer analysis depth, (c) about one percent monolayer sample consumption, (d) analysis of insulating material, (e) acquisition of organic and inorganic, molecular and elemental, chemical information, (f) chemical discrimination, (g) less than 0.2 μm lateral spatial resolution data acquisition and retrospective chemical imaging, (h) less than 200 Å lateral spatial resolution for refined physical imaging, (i) mass resolution greater than 10,000 when $m/z > 100$ at full transmission, and (j) at least 10 ppm mass accuracy. TOF-SIMS instrumentation and chemical analysis have been reviewed recently by several authors [2-3].

The goal of this investigation is to evaluate the use of the TOF-SIMS analytical technique for the purpose of comparing wet chemical processes. Contamination from other process steps such as photoresist coating, plasma ashing, and DIW rinsing or mechanisms such as wafer fab ambient, storage, and ambient during analysis will exist and may confound signal and intensities. As long as only comparisons are made between the different wet chemical processes, the comparison is valid. It is important to clarify that the term 'HF-only' refers to the fact that this step includes no chemicals other than HF but does include a DIW rinse following the HF etch.

PROCEDURE

P-type <100>, 1.6-1.9 ohm-cm, 150 mm silicon wafers are used in the study. The starting defect density for the silicon wafers is less than 0.09 defects/cm^2 at >/= 0.2 μm. The wafers are coated with 1.0-2.0 μm of photoresist. The resist is baked at 120°C for 60 minutes before ion implantation. As, B, and P are ion implanted into the silicon wafers coated with photoresist. The implanter used is a high current implanter. Ion implant conditions are As at a dose of 3.0E15 ions/cm^2 at 120 kV, P at a dose of 4.0E14 ions/cm^2 at 50 kV, and B at 2.0E15 ions/cm^2 at 20 kV. The wafers are ashed in a batch O_2 plasma asher and are then subjected to wet surface cleaning processes.

SC1 temperatures are 50°C (SC15) and 80°C (SC18). Process time is 15 minutes. A de-ionized water (DIW) overflow rinse is used at a temperature of 65°C +/- 5 post SC1 . Wafer drying is done using a spin rinse dryer (S/D), with N2 only during the drying process. Ozonated piranha (H_2SO_4:O_3) (O3P) process is a two-bath sequence and heated to 130°C +/- 5. Process time is 10 minutes in the first O3P tank and 15 minutes in the second O3P tank. The DIW rinse is an overflow rinse at a temperature of 65°C +/- 5. Wafers are dried in a spin rinse dryer, using N2 only during the drying process. The dilute HF (10:1 H_2O:HF) process temperature is 23°C +/- 3. The process time is 75 seconds. The wafers are rinsed in DIW at 25°C. The wafers are dried in an isopropyl alcohol vapor

dryer (IPA-VD). The silicon control wafers are as-received wafers from the material vendor with no further processing. The process sequence is shown in Table I. A more detailed description of the wafer preparation and defect density results is contained in reference [4].

Table I. Description of experimental processes

PROCESS	DESCRIPTION
HF	[HF > H_2O > IPA DRY]
O3P	[PIRANHA > PIRANHA > H_2O] - [S/D]
SC15	[SC15 > H_2O] - [S/D]
SC18	[SC18 > H_2O] - [S/D]
SC15-HF	[SC15 > H_2O] - [S/D] - [HF > H_2O > IPA DRY]
SC18-HF	[SC18 > H_2O] - [S/D] - [HF > H_2O > IPA DRY]

Each sample is analyzed in at least two different 100 micron diameter regions in both polarities for 20 minutes per region to avoid obtaining results associated with surface inhomogeneities. Typical primary ion doses in acquisition are less than 1E13 primary ions/cm^2. Thus each analysis consumes approximately one percent of a monolayer. This dose is below the static SIMS exposure limit, preserving the integrity of organic constituents on the substrate surface, an integral aspect of this study which is to examine variations in organic resist residue among wet chemical cleaning processes.

Almost all chemical information is derived from the uppermost monolayer of the silicon substrate surface (about 3-5 Å), in contrast to typical surface analytical tools, such as X-Ray Photo Spectroscopy (XPS), Auger, and Total X-Ray Fluorescence (TXRF) which acquire signal from the top 30 to 50 Å of the surface. While storage in fluoroware containers and other ambient factors may impact the levels of contaminants present on the surface and, therefore, the analysis itself, the results on which to focus are comparisons and trends between processes. Further insights will require additional work, using standards for calibration.

RESULTS

This study reports and discusses only data which are directly related to the types of cleaning sequences that are used. Analytical results that reveal a trend are noted. Differences in cleaning sequences and results which show relative efficiencies of the cleaning sequences are discussed.

The area of interest for this study is in post ash photoresist residue removal. The cleaning sequences evaluated comprise those which are either in standard semiconductor use, such as ozonated piranha or those which have shown some potential for this purpose in previous work [4]. 'HF only' processing by itself is not a standard post ash cleaning method. It is evaluated here to provide a comparison for analysis with cleaning methods

that result in hydrophilic Si surfaces rather than hydrophobic prior to DIW rinse. The 'HF only' process also increases the range of surfaces for study using TOF-SIMS analysis. At this step in semiconductor processing, the goal is to remove a maximum amount of surface organic residue and, if possible, metallic contamination.

Owing to high analytical sensitivity and high mass resolution of this method, data from a TOF-SIMS mass spectrum are abundant and require selection of the species of interest. For example, many mass peaks that correspond to saturated and unsaturated, unoxidized and oxidized hydrocarbons (CxHy and CxHyOz) are observed as positive and negative molecular ions. These species can be associated with carbon typically observed by XPS and Auger analysis. Selectivity to the uppermost monolayer tends to emphasize the presence of these species. Moreover, numerous inorganic elemental and molecular positive and negative ionic species are observed: NH4+, SixOy+, SixOyHz+, Al+, B+, F-, Cl-, S-, etc.

To characterize photoresist removal efficiency among the cleaning sequences, C6H5+ and C7H7+ molecular positive ions have been selected to assess relative photoresist residue levels since photoresist is largely comprised of phenolic resin, and C6H5+ and C7H7+ are aromatic positive ions typically observed in static SIMS spectra of phenolic materials. The C7H7+ ion is probably more directly associated with resist residue, since native levels of this ion are less intense. The above correlations are supported by observation of very low levels of these particular ions on the silicon control sample.

Figure 1 charts the normal ion intensity of C6H5+ and C7H7+ molecular ions versus cleaning treatments to characterize wet process efficiency with respect to removal of photoresist residue. The TOF-SIMS spectra is plotted in Figure 2 for the silicon control, SC15, O3P and SC15-HF samples for the value of m/z = 77.04 which corresponds to C6H5+. Figure 1 illustrates several interesting photoresist removal trends. SC18 is more effective than SC15 at removing resist residue. Resist residue removal is improved for both SC18 and SC15 by adding an "HF only" treatment after the SC1 process. Conversely, the dilute HF sequence is more effective if preceded by an SC1 sequence. SC15 and 03P exhibit similar resist residue removal efficiencies.

Figure 3 plots normal ion intensity versus cleaning sequence for select positive elemental ions. Data shows SC1 processing results in higher levels of Al as compared to the other processes evaluated. Conversely, dilute HF and ozonated piranha result in the lowest Al levels. Both Na and Al are reduced on silicon surfaces with SC1 processing when SC1 is followed by a dilute HF process. The sequence consisting of SC15 or SC18 and dilute HF results in the lowest levels of contamination for post ash resist removal cleaning. SC18 is better able to remove resist residue than SC15. SC1 at higher temperatures has been shown to be more effective at removing particulate and organic contamination [4]. Ozonated piranha results in contamination levels comparable to that of the Si control sample.

Figure 4 plots normal ion intensity versus cleaning sequence for select negative elemental ions. Br is observed only on samples exposed to "HF last" sequences. Br and S are not observed on the silicon control sample. F and Cl contamination are found on all samples. The impact of contaminants such as Br, S, F, and Cl and the levels of such contaminants required for such impact continue to be subjects of further study in many investigations.

Figure 5 graphs normal ion intensity of SiOxF negative molecular ions as a function of cleaning process, where x=1, 2. Dilute "HF-only " treatment alone or in conjunction with a preceding SC1 process increases the relative surface concentration of silicon oxyfluoride by at least a factor of ten. The silicon control wafer is void of these molecular ions. The atomic fluorine concentration does not vary among treatments.

CONCLUSIONS

This study illustrates the feasibility of employing TOF-SIMS analysis to characterize subtle chemical variations exploiting this method's high atomic and molecular sensitivity and monolayer analysis depth.

SC1 followed by dilute HF is associated with improved photoresist residue removal. Dilute HF is associated with Br contamination on the silicon surface. SC1 processing results in Al contamination of the silicon surface, presumably from the H_2O_2 component of the SC1 solution. However, SC1 followed by dilute HF reduces the Al level by up to two orders of magnitude. In general, the standard processing used in semiconductor manufacuring of Si consists of an ashing process for bulk photoresist removal followed by piranha. Heated SC1 solutions offer more efficient removal of organic residues and are under investigation by others.

TOF-SIMS analysis has been able to document very specific, subtle chemical differences among various chemical treatments with high sensitivity. It is critical to investigate the potential relationship between the above documented atomic and molecular, organic and inorganic ionic species, and electrical and device behavior with the use of this analytical technique with further work.

REFERENCES

[1] Schueler, B.W., "TOF-SIMS for Surface Organics, Ionics and Metals on Silicon Wafers with Metal Detection Capability of 10^8 atoms/cm^2, Proceedings of the 1993 Microcontamination Conference, 783 (1993).
[2] B.T. Chait and K.G. Standing, Int. J. Mass Spectrom. Ion Phys., 40, 185 (1981).
[3] D. Price and G.J. Milnes, Int. J. Mass Spectrom. Ion Processes, 99, 1-39 (1990).
[4] S. D. Hossain and M. F. Pas, "Comparison of Post Ash Cleaning Processes", ECS Fall Meeting, October 1993.

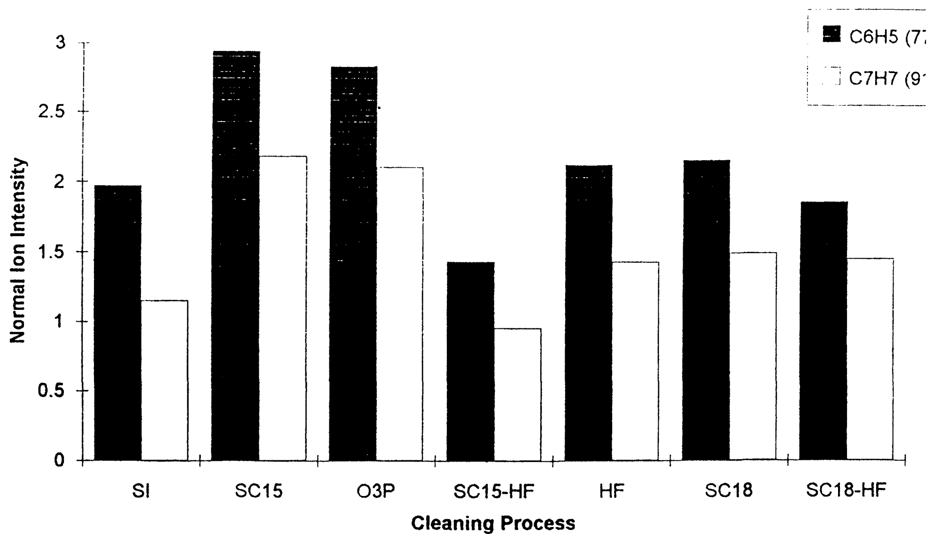

Figure 1. Normal Ion Intensity versus Clean for Photoresist Residue

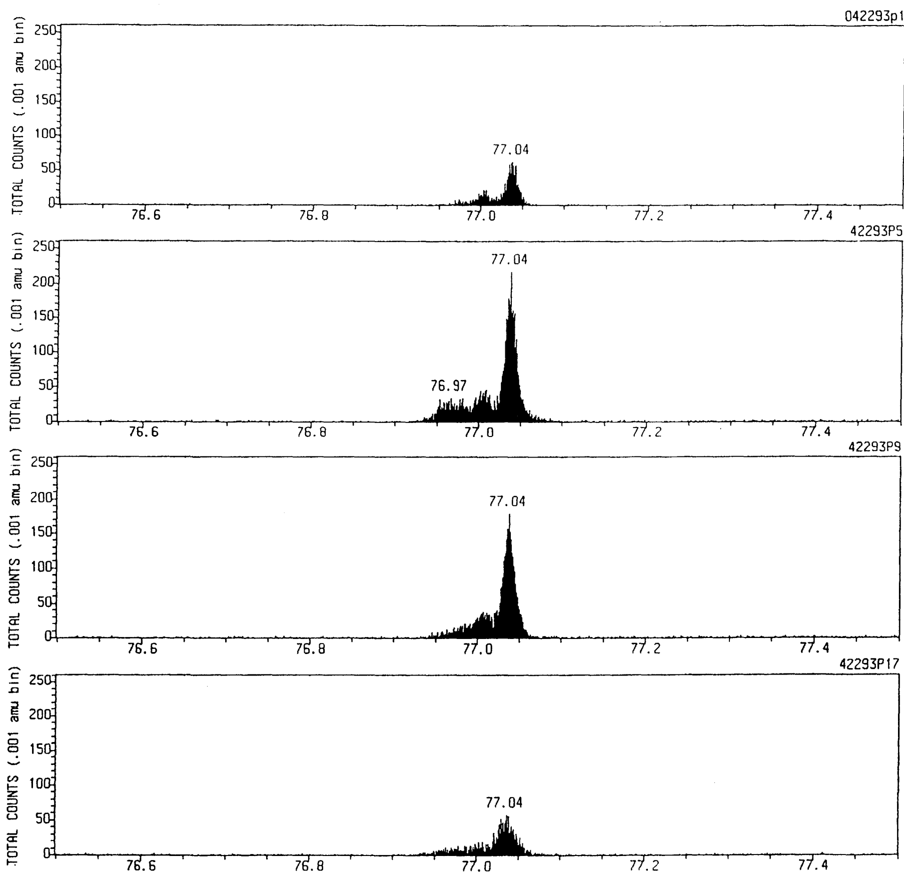

igure 2: TOF-SIMS spectra showing total ion counts versus m/z for a) Si control, b) SC15, c) O3P nd d) SC15-HF treatments.

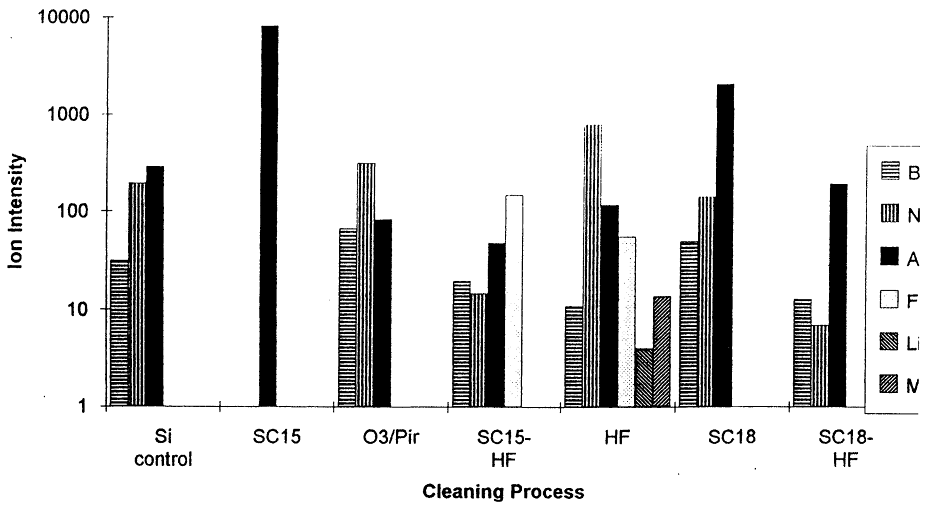

Figure 3. Positive Ion Intensity versus Clean Process

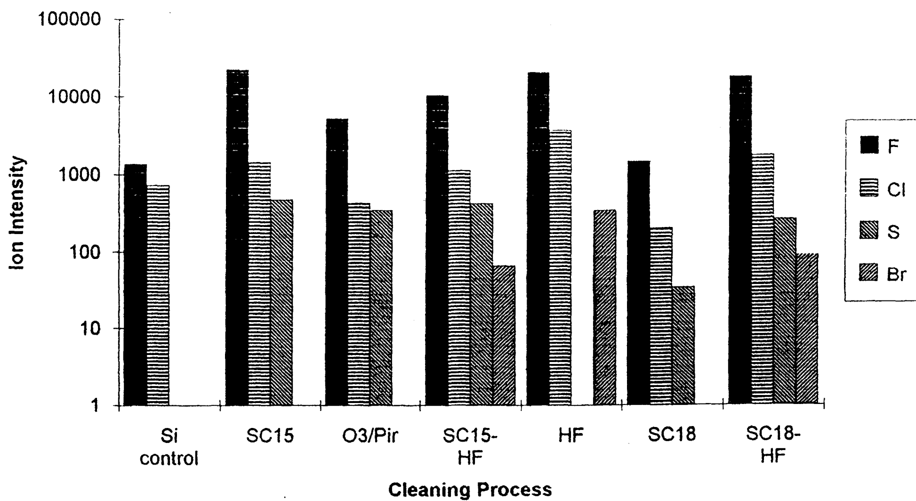

Figure 4. Negative Ion Intensity versus Clean Process

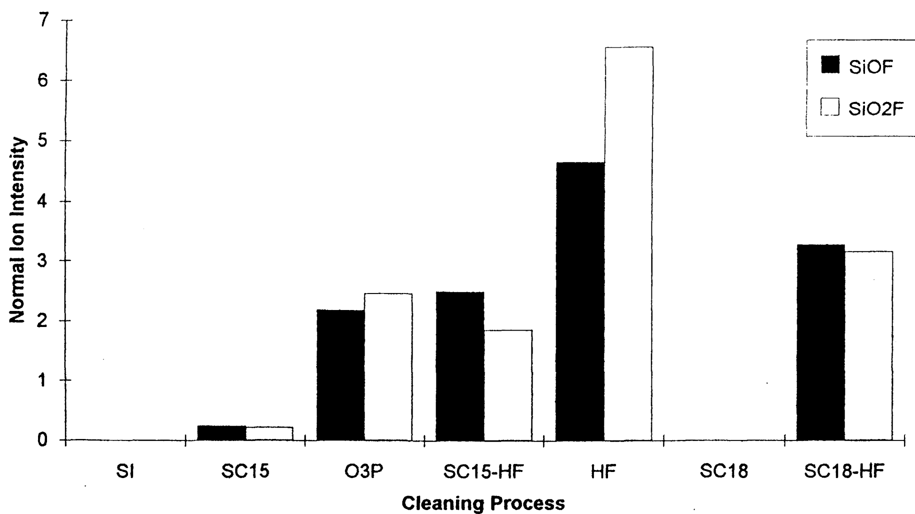

Figure 5. Normal Ion Intensity versus Clean for Fluorination of Native Oxide

ANALYSIS OF SUBMICRON ALUMINUM AND ALUMINA PARTICLES BY TIME-OF-FLIGHT SECONDARY ION MASS SPECTROMETRY (TOF-SIMS)

Patricia M. Lindley[a], Bruno W. Schueler[b], Alain C. Diebold[c], Richard S. Hockett[a] and George Mulholland[d]

[a] Charles Evans & Associates, 301 Chesapeake Dr., Redwood City, CA 94063
[b] Physical Electronics, 575 Chesapeake Dr., Redwood City, CA 94063
[c] SEMATECH, 2706 Montopolis Dr., Austin, TX 78741
[d] NIST, Gaithersburg, MD 20899

A series of submicron particles deposited on silicon wafers was analyzed by TOF-SIMS. The 0.5, 0.3 and 0.1 μm particles were identified in a static analysis mode using secondary ion maps of the Al^+ distribution. Aluminum and alumina particles were differentiated by obtaining depth profiles through the native oxide of the Al.

INTRODUCTION

Particle composition analysis is done to support process/tool development, pilot line integrated circuit (IC) yield improvement, and yield improvement during volume IC manufacture. Composition analysis is a key enabler when determining the source of contamination. One of the few in line/off line methods of composition analysis is scanning electron microscopy (SEM) equipped with energy-dispersive X-ray spectroscopy (EDS) and precision whole wafer sample stages. These systems are referred to as defect review tools (DRT). Optical microscopy is also used for in-line particle identification. Experienced microscopists use morphology and shape to categorize the particle. Focused ion beam (FIB) systems that employ SEM/EDS and precision, whole wafer sample stages for materials are used for characterizing of defect and particles buried by subsequent processing. High voltage (>5keV) SEM/EDS-based technology will not meet the analysis needs predicted for future IC generations.

Present x-ray detector technology limits analysis conditions. EDS detectors have modest energy resolution ($\Delta E \approx 50$ eV at 100-200 eV to 2-3 keV; $\Delta E = 130$ eV at 6 keV) and poor sensitivity to low energy x-rays (100-200 eV to 2-3 keV). Typical particle and defect analysis is done using high accelerating voltage electron beams (>10 keV, and often >20 keV) resulting in a large sampling volume for EDS based x-ray analysis. This is due to the inelastic scatter of electrons in the particle and sample. Characterization of small particles (sub 100nm diameter) and defects on patterned wafers will be difficult at these electron beam energies.

During 1994, the National Technology Roadmap for Semiconductors was developed (1). The requirements for particle detection equipment are listed in the Materials and Bulk Processes (MBP) part of the Roadmap. The Metrology Roadmap lists potential off line, in line, and in situ characterization solutions for the metrology needs specified in the Roadmap (2). Near- and long-term potential methods of particle composition analysis can be found in the MBP part of the Metrology Roadmap. The particle size requirements for several generations of IC technology are shown in Table I. Auger, time of flight-scanning ion mass spectroscopy (TOF-SIMS), and scanning near field optical microscopy (NFOM) are considered to be ready for development into whole wafer particle and defect composition analysis tools (i.e., DRTs). Longer term solutions include new x-ray detector technology to replace EDS and synchrotron x-ray source based micro-XANES (x-ray adsorption near edge structure).

Table I. Particle Size Roadmap for Particle Composition Analysis

Year of First Shipment	1995	1998	2001	2004	2007	2010
IC Design Rule	0.35μm	0.25μm	0.18μm	0.13μm	0.10μm	0.07μm
Particle Size	0.12μm	0.08μm	0.06μm	0.04μm	0.03μm	0.02μm

Evaluation of analysis capability required a set of reference samples. Using a custom deposition system, particles with similar effective size/charge characteristics are deposited at high densities on silicon wafers. The objective is to have samples that allow rapid location of particles at a magnification of 1000x. To evaluate light element characterization by TOF-SIMS, sets of 0.5, 0.3, and 0.1 μm diameter aluminum and aluminum oxide particles were analysed. This paper reports the method of particle deposition and the results of particle composition analysis.

PARTICLE DEPOSITION PROCEDURE

Particle deposition was done at the National Institute of Standards and Technology (NIST) on 2.54 cm (1 in) diameter silicon wafers. Particle suspensions were made of three different powders: $5m^2/g$ aluminum and 5 and $14m^2/g$ alumina. The numerical designation refers to the surface area per unit mass. To prevent oxidation, the aluminum powder was mixed with isopropanol. Stock solutions of the metal powders were made using 2 g of aluminum per 50 ml of isopropanol or 2 g of alumina per 100 ml of water. The 14 m^2/g alumina was used when targeting 0.1 and 0.3 μm but the $5m^2/g$ aluminum was used for the 0.5 μm size. The particle deposition system consisted of an aerosol generation system, a differential mobility classifier (DMA) for selecting a monodisperse size fraction, a condensation nucleus counter for monitoring the aerosol concentration,

and a cascade impactor for depositing the aerosol.

After the deposition was complete, the collection disk was taken to an optical microscope where the center of the deposit pattern was determined using 200X magnification. The magnification was increased to 1000X and the particles in one-quarter of the photograph area were counted in dark field to estimate if the intended density of particles was accomplished.

The CNC count average about $6/cm^3$ for the 15 minute deposition of 0.5 μm particles, so the total number of particles that entered the cascade impactor at 8.3 cm^3/s (0.5 l/min) was about 45,000. About 150 particles were observed in dark field in a 0.01 mm^2 moderately dense area of the collection disk for a density of $15000/mm^2$. Electron microscopy revealed a density of about $3000/mm^2$ for the same sample, but not necessarily at the same location.

EXPERIMENTAL

The experiments were performed on the PHI-EVANS TRIFT Time-of-Flight Secondary Ion Mass Spectrometer. A pulsed, rastered ^{69}Ga Liquid Metal Ion Gun (LMIG) was used as primary ion source. This ion gun produces short ion bursts to stimulate secondary ion production and is currently capable of achieving pulsed spot sizes down to about 1000Å at 60pA continuous current. Further improvements in pulsed beam diameter are expected. The pulsed primary ion beam stimulates the emission of sample specific secondary ions which are electrostatically extracted, focused through the energy compensating spectrometer and strike the detector. Ions created at the sample surface are accelerated to the same nominal kinetic energy. The spectrometer system is roughly equivalent to a drift region. Since all ions enter the spectrometer with the same kinetic energy, they will have different velocities according to the mass. Lighter ions will traverse the mass spectrometer faster than the heavier ones. The flight times to the detector are $t \sim (m)^{1/2}$, where m is the ion's mass. Ions of different mass will thus strike the detector sequentially but will still follow a similar path. Since the mass separation is only achieved by differences in flight times, TOF-SIMS offers in principle unlimited mass range. More importantly, TOF-SIMS provides high sensitivity surface analysis due to its inherent parallel detection capability, *i.e.* the analytical conditions can be chosen in such a way that practically <u>all</u> secondary ions of given polarity are also detected. This makes it possible to analyze surfaces with minimal primary ion beam damage. Typical ion doses required to perform a TOF-SIMS analysis are on the order of 10^{12} primary ions/cm^2 (static SIMS limit), making it possible to characterize both organic molecular and elemental contaminants.

RESULTS AND DISCUSSION

Location of the particles and initial data acquisition were accomplished with the instrument operated in a static SIMS mode, conditions that would be required to obtain organic molecular information. These conditions would be needed for the analysis of a particle of unknown origin. To distinguish Al from $C_2H_3^+$, the mass spectra were recorded in a higher mass resolution mode (shorter ion beam pulses of approximately 11 nanoseconds), resulting in a somewhat larger ion beam than longer pulse widths permit. In Figure 1, time-of-flight mass spectra illustrating the separation of Al and $C_2H_3^+$ are shown for a large raster area containing 0.5, 0.3 and 0.1 μm Al particles. In Figures 2 and 3, the differences in Al^+ signal intensity on and off 0.5 (Figure 2) and 0.1 (Figure 3) μm Al_2O_3 particles are shown.

Because the particles were composed of compounds having high secondary ion yields (Al_2O_3 and the surface oxide on Al), maps of the Al^+ distribution were most useful to locate the particles. The Si ion and total ion maps generally resulted in less useful images for particle location. In Figure 4, Al maps of 0.3 μm Al_2O_3 particles are shown. On one sample, containing 0.1 μm Al_2O_3, particles that were not alumina were observed in the pulsed ion images along with the expected A-containing particles. Examination of the spectra and subsequent ion image acquisition indicated that Na^+ and K^+ distributions were higher on these particles.

Both ion-induced secondary electron and total positive ion maps were able to locate the particles, but they were obtained using a continuous ion beam that would destroy organic molecular information on the surface. Since attempts were made to analyze the particles under static SIMS conditions (necessary for the analysis of unknown particles that might be organic/molecular), these images were not acquired until after the particles were located. Figure 5 shows a total positive ion image from the 0.1 μm Al particle sample.

In addition to locating particles on each of the samples, a second goal of this work was to differentiate the Al and alumina particles. However, under static SIMS conditions, the TOF-SIMS sampling depth of 1-3 monolayers (approximately 10 Å) would not penetrate beyond the native oxide layer of aluminum, meaning that surface spectra from the two types of particles are quite similar.

Al and Al_2O_3 could be differentiated by performing an analysis at depth in the samples. This was accomplished by obtaining a depth profile with the LMIG focussed on a single particle. For the alumina samples, the substrate oxide produced a relatively flat Al^+ profile (Figure 6). However, in the case of the Al samples, oxide enhancement of the Al^+ signal was lost below the native oxide, and the Al^+ signal intensity decreased significantly at that point (see Figure 7).

CONCLUSIONS

The selection of appropriate analysis methods depends on the application, but typically, analysis tools are expected to serve more than one function. Although defect review tools are presently applied to particle/defect characterization, future tools are expected to have expanded roles during contamination analysis. TOF-SIMS is capable of characterizing both particulate and non-particulate trace contamination. In addition, it is the only method capable of providing detailed analysis of organic contamination.

REFERENCES

1. National Technology Roadmap for Semiconductors, Semiconductor Industry Association, San Jose, CA, December 1994.

2. Metrology Roadmap: A Supplement to the National Technology Roadmap for Semiconductors, SEMATECH Technology Transfer Document #94102578A-TR, SEMATECH, Austin, TX, January 1995.

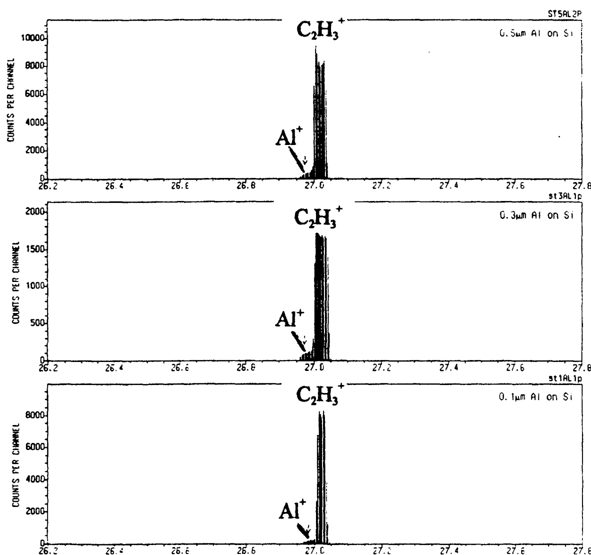

Figure 1. TOF-SIMS spectra showing Al^+ and $C_2H_3^+$ peaks for 0.5 (top), 0.3 (center) and 0.1 (bottom) micron aluminum particles.

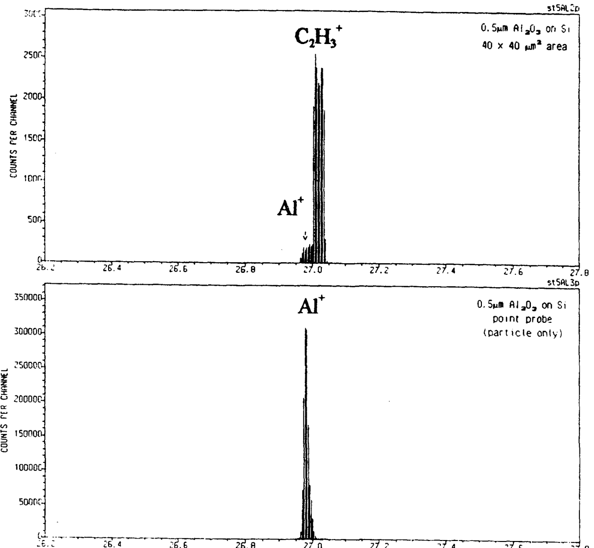

Figure 2. Difference in Al^+ signal intensity in a large field of view (top) and on a single 0.5 micron Al_2O_3 particle (bottom).

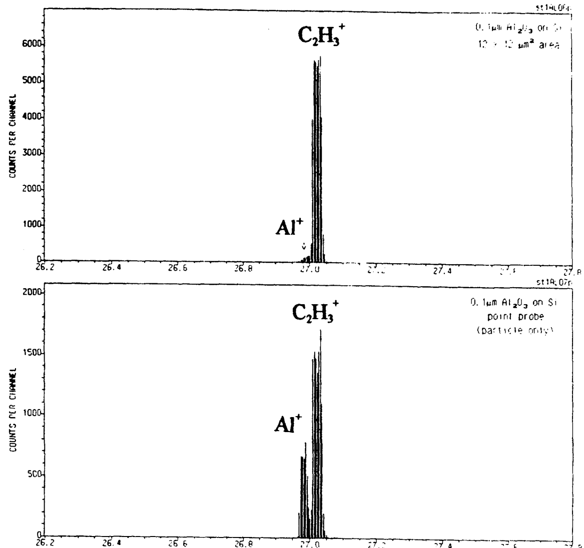

Figure 3. Difference in Al^+ signal intensity in a large field of view (top) and on a single 0.1 micron Al_2O_3 particle (bottom).

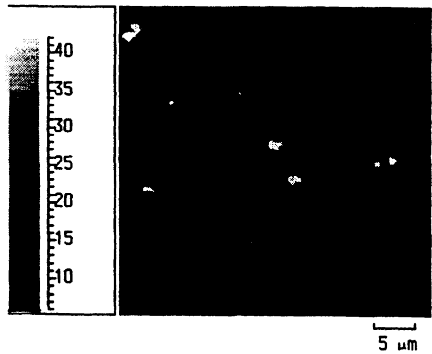

Figure 4. Al^+ ion map showing 0.3 µm Al_2O_3 particles in 40 x 40 μm^2 analytical area.

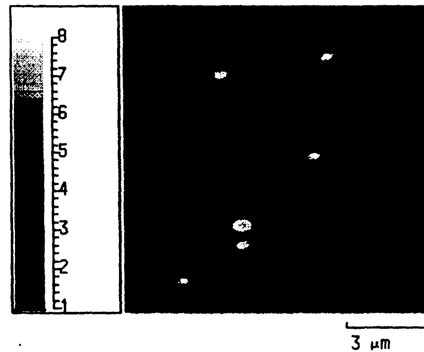

Figure 5. Total positive ion map from 0.1 µm Al sample.

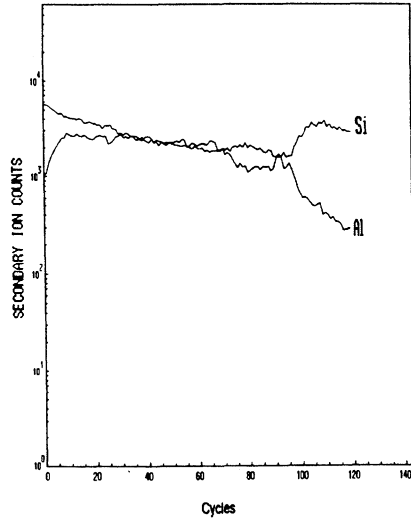

Figure 6. Depth profile of a 0.3 μm Al_2O_3 particle.

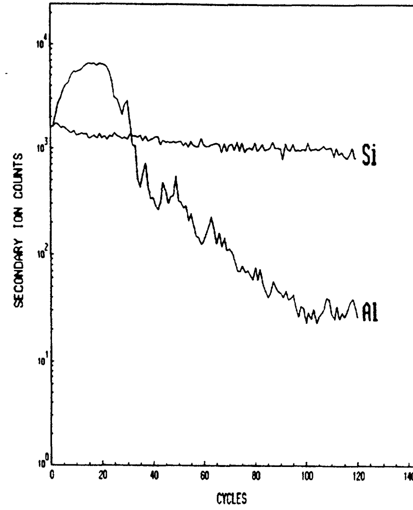

Figure 7. Depth profile of a 0.3 μm Al particle.

WET PROCESSING OF VIAS AND TRENCHES

Jennifer Parker, Steven Verhaverbeke, and Chris McConnell
CFM Technologies, Inc.
1381 Enterprise Drive
West Chester, PA 19380

The increasing aspect ratio of trenches and vias found in newer generations of DRAM chips heightens the concern over the ability to use wet processing for cleaning and etching of patterned surfaces. The wetting, rinsing, and drying of deep trenches are discussed. The contact angles formed between cleaning solutions and wafers are relatively low, leading to large capillary forces that drive the water into small trenches or vias. Diffusive forces, alone, are sufficient to remove chemicals and etching by-products from the bottom of trenches within seconds of beginning a rinse due to the extremely short lengths of trenches and vias. Drying is shown to be the most critical processing step; Complete removal of water by standard drying technology is impossible. The water in the trenches must be completely displaced with a drying fluid that will readily evaporate without leaving contamination.

INTRODUCTION

Wet cleaning is well recognized for its ability to effectively remove particles and metal contaminants on flat silicon surfaces. New generations of DRAM chips, however, continue to be developed with complex geometry, including small minimum features. The aspect ratios of trenches and vias are continuing to increase in new chip designs. The uneven structure of such designs and the increased depth to width (or diameter) ratio of the trenches raises concern about the applicability of wet processing for etching and cleaning of patterned surfaces.

Three distinct stages of wet processing, wetting, rinsing, and drying, must be evaluated with respect to the cleaning of deep, narrow trenches and vias. Complete wetting of vias is necessary to assure adequate cleaning or etching. Thorough rinsing of cleaning chemicals as well as reaction by-products must be achieved so that no residue remains in the trenches. Finally, wet processing must be completed with a drying cycle that assures all water is removed from the entire wafer surface including the deep vias or trenches.

WETTING

Wet cleaning of high aspect ratio vias (e.g., 4.0μm deep by 0.5μm wide) following dry etching and side-wall doping is critical for obtaining adequate capacitance. Complete wetting of the entire wafer surface, including vias, is required for thorough wet processing. If air pockets exist within trenches, wet cleaning cannot occur.

Consideration of capillary phenomena provides a useful model for the wetting of high aspect ratio trenches and vias. Whether a liquid rises or falls in a capillary tube is determined by the relative magnitude of the forces of cohesion between the liquid molecules themselves, and the forces of adhesion between the liquid and the walls of the tube. The relative magnitude of these forces determines the contact angle, θ, that the liquid makes with the capillary walls, as shown in Figure 1. If the angle is less than 90° then the liquid wets the surface and a concave

meniscus is formed. All solutions that are commonly used for wafer cleaning and etching form contact angles on silicon, silicon-oxide and silicon-nitride that are less than 90°. Table 1 contains examples of such contact angles.

According to the equation of Laplace, the occurrence of a curved surface leads to a pressure difference across the surface. The liquid in the surface rises until the weight of the liquid column just balances the pressure difference across the meniscus. The Laplace equation, given in equation 1, can be used to examine the large forces driving the wetting of a capillary tube:

$$\Delta P = \frac{(2\gamma \cos\theta)}{r} \qquad [1]$$

where,
- γ = surface tension of the liquid
- θ = contact angle of liquid the solid, and
- r = capillary radius

The pressure determined in equation 1 is the pressure that forces water into a via or trench. In Table 1, the size of the capillary force driving the wetting of deep vias is shown for a number of surfaces. Note that as the diameter of the via decreases, the force driving water into the trench actually increases.

Given the forces driving the water into the trenches, what happens to the air that is in the holes? A number of different factors lead to the complete displacement of the air. The capillary model indicates a strong force drives water into small contact holes and vias. This force results from the chemical affinity between the liquid and the wafer surface. The capillary force is strong enough to result in a significant reduction in the volume of the gas (i.e., the volume would be reduced by about a factor of two) that is in the vias prior to filling with water. Additionally, the same chemical affinity between the solid and the liquid that acts to create the capillary pressure causes the liquid to spread on the wafer surface, no matter what the geometry; thereby, displacing the air from the wafer surface and forming a bubble. The surface tension between the liquid and the air leads to a large pressure gradient across the bubble surface, as can be calculated from the equation of Young and Laplace:

$$\Delta P = \frac{(2y)}{r} \qquad [2]$$

where,
- γ = surface tension of the liquid, and
- r = bubble radius

The fluid on the concave side of the surface (i.e., the air in the bubble) is at the higher pressure. For an air bubble in water with a 0.5μm diameter, the pressure difference across the bubble interface is 83.5 psia. Clearly, such large pressure gradients will cause the bubble to rapidly dissolve in the water that is in and around the via. Diffusion gradients will also act to cause the bubble to dissolve. Such forces are discussed in detail in the Rinsing Section.

Filter Wetting

Filter wetting is another problem in wet processing that is similar to trench wetting. The same capillary forces active in trench and via wetting are involved during the filter wetting process. Teflon filters are notoriously difficult to wet with most aqueous solutions. This difficulty is a direct result of the large contact angle that water forms with Teflon. The contact angle of water on PTFE at room temperature is 108°, and so water will bead on Teflon and will not enter capillary pours. As indicated in Table 2, the capillary pressure actually acts to keep water out of pours in Teflon. In contrast, n-proponal readily flows into pours of Teflon and can then be displaced with water; other alcohols will act in a similar manner.

We have developed an algorithm for estimating the contact angles for other cleaning solutions on Teflon. Adamson [2] provides Zisman plots of contact angles as a function of surface tension for various homologous series. An equation that provides an estimate of this data, as well as the data given in Table 2 for water, is given by:

$$\cos\theta = 1.3925 - 0.023642 * \gamma \qquad [3]$$

Equation 3 can be used to estimate the contact angle of sulfuric acid on Teflon. At room temperature, the contact angle can be seen to be 85 degrees and so given time a PTFE filter will wet Teflon without pre-wetting the filter with alcohol. The surface tension of most liquids decreases in a linear fashion with increasing temperature, and so hot sulfuric acid, as typically used in wet processing, will wet a filter more readily than the data in Table 2 suggests.

RINSING

Once the trenches or vias are completely wet, etching or other cleaning processes can occur. For critical etching processes, the concentration of the etchant must be controllable both on the surface of the wafer and at the bottom of the trench or via. In order to achieve such control, efficient removal of the etchants and the by-products during rinsing is a requirement. Similarly, if the cleaning equipment used for wet processing is a continuous flow process, such as the Full-Flow™ system, the chemicals used for etching must reach the bottom of the trench at essentially the same time as they reach the wafer surface. In such equipment, the arrival of chemicals to the bottom of the trench at the beginning of the process is mirrored by the removal of chemicals at the end of the process. Precisely, the same forces govern the two transport steps, and so only rinsing will be detailed in this paper.

The high aspect ratio of the trenches and vias assures that convection occurring above the wafer surface does not lead to a substantial amount of convection at the trench bottom, no matter how fast the water is flowing over the wafer surface. Thus, convection can not be relied upon to remove chemical from a trench or via. Nakao et al. [4] modeled the effects of various flow rates across deep trenches in conjunction with chemical diffusion out of the trench. If the water flow across the wafer surface is 1.5×10^{-2} m/sec, then the resulting water flow at the bottom of a 0.5 x 4.0μm trench is only 1.5×10^{-12} m/sec. Consequently, water velocity across the top of the trench has very little direct influence at the bottom of a 4μm trench. Their results did show, however, that diffusion is a primary force driving chemicals out of the bottom of the trench.

Although diffusion is generally thought of as a slow process, the length of a diffusion path in a via is so short that even when diffusion is the only displacement force, rinsing can occur quite quickly. The flux of molecules resulting from a concentration gradient is governed by Fick's first law of diffusion:

$$J = -D_{AB}\frac{dn_A}{dx} \qquad [4]$$

where, J = flux of moles of species A in the x direction
D_{AB} = diffusion coefficient of species A in solvent B
n_A = mole fraction of diffusing species A in solvent B

Figure 2 indicates the effect of the length of a diffusion path on rinsing time for diffusion from a plane using a one dimensional model. Figure 3 indicates the apparent drop in concentration resulting from diffusion as a function of time for distances from the bottom of the trench. The results in both of these figures illustrate that when the diffusion path length is on the order of microns, thorough rinsing will occur in seconds.

Although the flow of water across the top of the trench does not directly create a flow at the trench bottom, water flowing across the wafer surface displaces the water directly above the trench with clear fresh water and consequently increases the concentration gradient from the bottom of the trench, dramatically decreasing rinsing time. Any mixing occurring above the wafer surface, such as those that result from megasonics, will also significantly speed up the diffusion process. The calculations performed by Nakao et al. [4] show that if the rinse water at the top of the trench is $1.5x10^{-2}$ m/sec, then the concentration at the bottom of the trench drops to 10^{-8} of the initial concentration within 1 second of rinsing. Clearly, complete rinsing of a via can occur within minutes of immersion in a rinsing solution.

Empirical results by Nakao et al. [4] as well as Fukazawa and Takase [5] substantiate the theoretical results presented above. Nakao et al. examined the effectiveness of rinsing buffered HF (NH_4:HF = 20:1) used to etch an HTO oxide deposited by LPCVD (a hydrophilic surface). The experiment was designed with a 3 minute delay in clean air between rinsing and drying to exaggerate the affect of any continued etching in the trench bottom resulting from remaining etchant that was incompletely rinsed. SEM photomicrographs of the cross-section of the etched trench indicated that uniform etching occurred throughout the trench. These results show that diffusion is dominant during the rinsing of trenches and vias, and sufficient for wet processing of high-aspect ratio geometries on wafers.

Similar experiments were run by Fukazawa and Takase. [5] These authors produced "trenches" of oxide with very high aspect ratios by placing an oxide blanket in a low aspect-ratio trench. Poly-silicon was then deposited on the oxide, and CMP was used to remove the Poly-Si and the oxide on the wafer surface, resulting in two parallel high aspect - ratio trenches of oxide. The trenches were then etched using either buffered HF or HF solutions. The etch rate of the oxide trenches was studied by comparing the result of four short etches to one long etch (i.e., one etch was completed by starting and stopping the etch 4 times, while another process was one long etch that was 4 times as long). The trenches resulting from the two distinct processes had the same depth. These results indicate that wetting of high aspect ratio trenches as well as complete rinsing is possible with wet

processing. The data of Fukazawa and Takase [5] also indicate that HF vapor etching process may be difficult to rinse leading to uncontrolled etching.

DRYING

Once the vias or trenches are completely rinsed, the water remaining in them must be removed during the drying process. Unfortunately, the same capillary forces that act to drive water into the deep trenches also act to keep the water in the trenches once the wafers are removed from a bath or wet processing unit. The large pressures indicated in Table 1 must be overcome for complete drying.

Traditional drying methods include spin drying, hot N_2, slow pull, and vapor drying. None of these drying methods provide a force that acts in a direction to pull the water out of the trench. As shown in Figure 4, the action in spin drying is perpendicular to the trench and so the capillary force will continue to hold the water in the via. Hot N_2 causes water to evaporate from the surface of the wafer. There may or may not be enough heat to evaporate the water from the via during the initial drying process, but eventually the water will evaporate. Undoubtedly, water marks will be left on the surface of the wafer and the via. Slow pull drying relies on the cohesive forces within the water to pull the water off the wafer surface. The process is done extremely slowly so that these cohesive forces are not overcome with fluid drag. Typically less than 1% of the initial *surface* water is left on the wafer. If the surface within the via is completely hydrophobic, the cohesive forces might be sufficient the pull the water out of the via. The surfaces within vias, however, are rarely sufficiently hydrophobic (i.e., the contact angle is relatively low) and the water will adhere to the side walls of the via rather than the bulk water with the same forces that create the large capillary pressures.

Standard vapor dryers condense a small amount of solvent vapor, usually isopropyl alcohol (IPA), onto the surface of a wafer. The solvent mixes with the water remaining on the wafer surface. The IPA acts to lower the contact angle and the surface tension of the water [6], helping the water to flow or "sheet" off the wafer. The reduction of surface tension and contact angle tends to make the wafer more "hydrophilic" and a thin layer of the IPA and water mixture adheres to the surface after drying. Within the via, however, the reduction of the surface tension and the contact angle will not cause the capillary pressure to become zero or negative and so water will remain in the via. Figure 5 shows the change in capillary pressure with IPA concentration. Consequently, standard vapor dryers are incapable of removing the water from the via or trench and leave water with a small amount of IPA in the via or contact hole. The affect of standard vapor dryers on vias and contact holes is schematically illustrated in Figure 6.

No currently available drying method is capable of directly removing the water from vias or trenches. In order to assure complete drying of the trench, however, the water in the holes can be readily displaced by a fluid that has a lower contact angle than water, one that completely *displaces* water. IPA is well known to have such a wetting property. The meniscus formed between a water and IPA layer is such that IPA will actually invert the meniscus that water typically forms with a wafer during withdrawal from a bath. The effect of the IPA layer is to increase the contact angle between the wafer and the water, such that the contact angle is greater than 90° so that the water "de-wets". The high spreading pressure of the IPA is the source of this change in contact angle. Bolster [7] measured the spreading pressure of a series of normal and branched alcohols and found that alcohols such as IPA can be expected to have very high spreading pressures with water, on the order of 40-50 dynes/cm.

The contact angle of IPA on hydrophilic and hydrophobic wafers is very small. [6] The IPA layer completely displaces the water even in a trench or via, as schematically illustrated in Figure 7. Once the water is displaced, the presence of hot IPA vapor is sufficient to assure that the IPA remaining in the trench flashes off, leaving no water marks. (8)

CONCLUSIONS

Wet processing of high aspect trenches and vias is possible with currently available technology. The relatively small contact angle of aqueous solutions on all types of wafer surfaces assures that water will readily flow into small trenches and vias as the result of strong capillary forces. In fact, for given aqueous solution and surface, the smaller the trench or via, the more easily the water flows into the space.

Diffusion is primary mode of transport during rinsing of trenches and vias. The high aspect ratio assures that any convection on the wafer surface is completely ineffective within the via itself. Although diffusion is a notoriously slow process, the extremely short lengths of vias (i.e., on the order of 5 microns) allows complete rinsing to occur within seconds of wafer contact with clean rinsing when diffusion is the primary transport mechanism. Although convection at the wafer surface does not directly act within vias, good flow across the wafer surface of fresh rinse water increases the concentration gradient within the via, and so substantially shortens the rinse process.

Standard drying methods are incapable of overcoming the capillary forces that hold aqueous solutions in small trenches and vias. In order to assure complete drying of wafers with complex geometry, the water on the surface and in trenches and vias must be completely displaced by a clean solvent with a high spreading pressure such as IPA. Once the water is displaced, the presence of hot IPA vapor is sufficient to evaporate all of the IPA from within trenches and vias.

REFERENCES

1. Verhaverbeke, S. "Improve rinsing efficiency after SBM by adding HF." UCPSS. 1994. p 201.
2. Adamson, A. W. "Physical Chemistry of Surfaces." Wiley-Interscience Publication. 1990.
3. Handbook of Chemistry and Physics, 57th edition, edited by Robert C. Weast, CRC Press, 1976-1977.
4. Nakao, I., et al. "A Simulation Model for Wet Cleaning of Deep Trenches." J. Electrochemical Soc. July, 1990. p. 2303.
5. Fukazawa, Y. and K. Takase. "Wet Processing for Sub-micron Deep Trench." The 21st Symposium of ULSI Ultra Clean Technology. Tokyo. 1994. p. 249.
6. Park, J-G., and S. Raghavan, Interfacial Characteristics of Silicon in IPA-Water Solutions and Their Significance in Particle Removal, Microcontamination Conference Proceedings, 1992. p. 543-554.
7. Bolster, R.N., "Removal of Fluid Contaminants by Surface Chemical Displacement." Surface contamination detection.. ed. K.L. Mittal, Plenum Press, NY. 1987. p.359-386.
8. US Patent # 4,984,597 - Process and Apparatus for Drying Surfaces

Table 1: Capillary Forces of Water in 0.5mm diameter capillary of various materials

Solid Surface	Surface Tension of Liquid (dynes/cm)[2]	Contact Angle (degrees)[1,2]	Capillary Force (psia)	Water Column Height (feet)
SiO_2	72	53	25	58
SiO_2 after hydration	72	17	40	92
SiO_2 after SC1	72	0	42	96
Si_3N_4 after sulfuric acid with peroxide	72	30	36	83
Si_3N_4 after HF last	72	0	42	96
Glass	72	1-2	42	96

Table 2: Capillary Forces of Various Liquids in 0.5mm diameter capillary of PTFE

Liquid	Surface Tension of Liquid (dynes/cm)	Contact Angle (degrees)	Capillary Force (psia)	Water Column Height (feet)
n-proponal	23[2]	43[2]	20	45
Water (@20-25 C)	72[2]	108[2]	-25 (depressed meniscus)	-59
Sulfuric Acid (98.5%)	55.1[3]	85 (estimated)	5.6	13

Figure 1: Rise in Capillary due to Contact Angle.

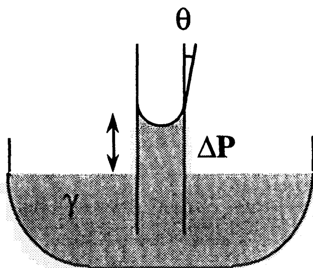

For g=72 dynes/cm, R=0.5μ
θ=10° ΔP = 100 feet
θ=70° ΔP = 34 feet

Figure 2: Effect of Path Length on Diffusion Time in One-dimensional Planar Model

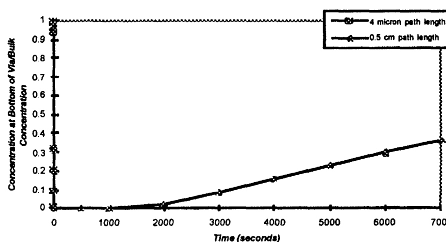

The contact angle of IPA on hydrophilic and hydrophobic wafers is very small. [6] The IPA layer completely displaces the water even in a trench or via, as schematically illustrated in Figure 7. Once the water is displaced, the presence of hot IPA vapor is sufficient to assure that the IPA remaining in the trench flashes off, leaving no water marks. (8)

CONCLUSIONS

Wet processing of high aspect trenches and vias is possible with currently available technology. The relatively small contact angle of aqueous solutions on all types of wafer surfaces assures that water will readily flow into small trenches and vias as the result of strong capillary forces. In fact, for given aqueous solution and surface, the smaller the trench or via, the more easily the water flows into the space.

Diffusion is primary mode of transport during rinsing of trenches and vias. The high aspect ratio assures that any convection on the wafer surface is completely ineffective within the via itself. Although diffusion is a notoriously slow process, the extremely short lengths of vias (i.e., on the order of 5 microns) allows complete rinsing to occur within seconds of wafer contact with clean rinsing when diffusion is the primary transport mechanism. Although convection at the wafer surface does not directly act within vias, good flow across the wafer surface of fresh rinse water increases the concentration gradient within the via, and so substantially shortens the rinse process.

Standard drying methods are incapable of overcoming the capillary forces that hold aqueous solutions in small trenches and vias. In order to assure complete drying of wafers with complex geometry, the water on the surface and in trenches and vias must be completely displaced by a clean solvent with a high spreading pressure such as IPA. Once the water is displaced, the presence of hot IPA vapor is sufficient to evaporate all of the IPA from within trenches and vias.

REFERENCES

1. Verhaverbeke, S. "Improve rinsing efficiency after SBM by adding HF." UCPSS. 1994. p 201.
2. Adamson, A. W. "Physical Chemistry of Surfaces." Wiley-Interscience Publication. 1990.
3. Handbook of Chemistry and Physics, 57th edition, edited by Robert C. Weast, CRC Press, 1976-1977.
4. Nakao, I., et al. "A Simulation Model for Wet Cleaning of Deep Trenches." J. Electrochemical Soc. July, 1990. p. 2303.
5. Fukazawa, Y. and K. Takase. "Wet Processing for Sub-micron Deep Trench." The 21st Symposium of ULSI Ultra Clean Technology. Tokyo. 1994. p. 249.
6. Park, J-G., and S. Raghavan, Interfacial Characteristics of Silicon in IPA-Water Solutions and Their Significance in Particle Removal, Microcontamination Conference Proceedings, 1992. p. 543-554.
7. Bolster, R.N., "Removal of Fluid Contaminants by Surface Chemical Displacement." Surface contamination detection.. ed. K.L. Mittal, Plenum Press, NY. 1987. p.359-386.
8. US Patent # 4,984,597 - Process and Apparatus for Drying Surfaces

Table 1: Capillary Forces of Water in 0.5mm diameter capillary of various materials

Solid Surface	Surface Tension of Liquid (dynes/cm)[2]	Contact Angle (degrees)[1,2]	Capillary Force (psia)	Water Column Height (feet)
SiO_2	72	53	25	58
SiO_2 after hydration	72	17	40	92
SiO_2 after SC1	72	0	42	96
Si_3N_4 after sulfuric acid with peroxide	72	30	36	83
Si_3N_4 after HF last	72	0	42	96
Glass	72	1-2	42	96

Table 2: Capillary Forces of Various Liquids in 0.5mm diameter capillary of PTFE

Liquid	Surface Tension of Liquid (dynes/cm)	Contact Angle (degrees)	Capillary Force (psia)	Water Column Height (feet)
n-proponal	23[2]	43[2]	20	45
Water (@20-25 C)	72[2]	108[2]	-25 (depressed meniscus)	-59
Sulfuric Acid (98.5%)	55.1[3]	85 (estimated)	5.6	13

Figure 1: Rise in Capillary due to Contact Angle

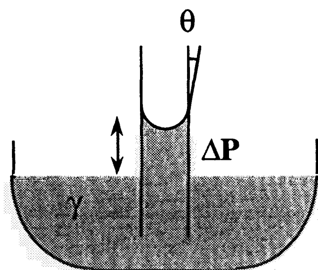

For g=72 dynes/cm, R=0.5μ
θ=10° ΔP = 100 feet
θ=70° ΔP = 34 feet

Figure 2: Effect of Path Length on Diffusion Time in One-dimensional Planar Model

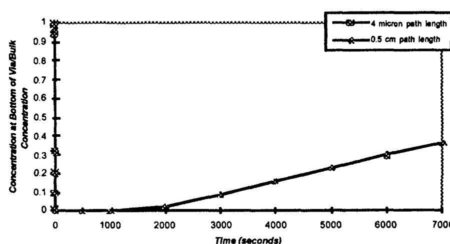

Figure 3: Diffusion Time for Relative depth in a Trench (One-dimensional model)

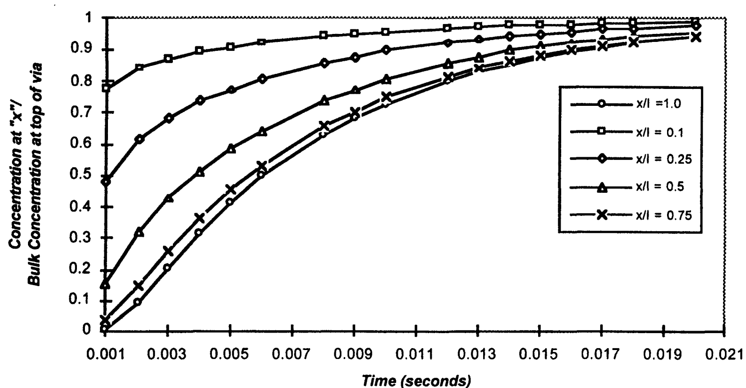

Figure 4: Schematic Illustrating Action of Forces in Spin-Drying

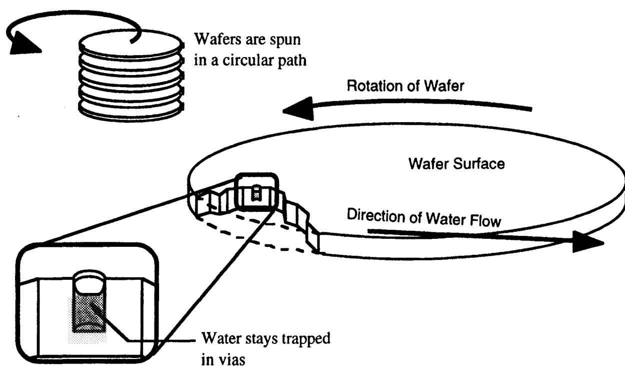

Figure 5: Change in capillary pressure with IPA concentration.

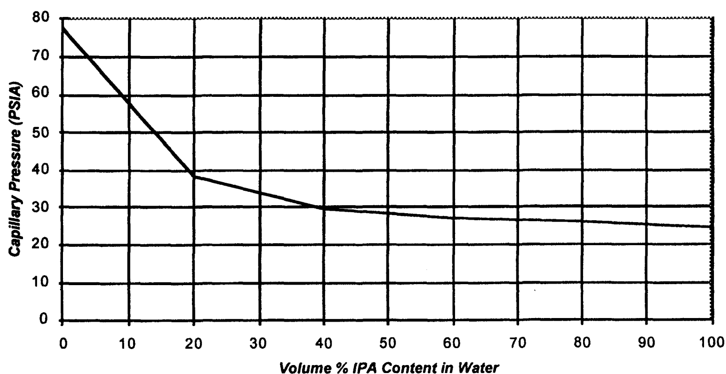

Figure 6: Illustration of the drawbacks of other drying techniques

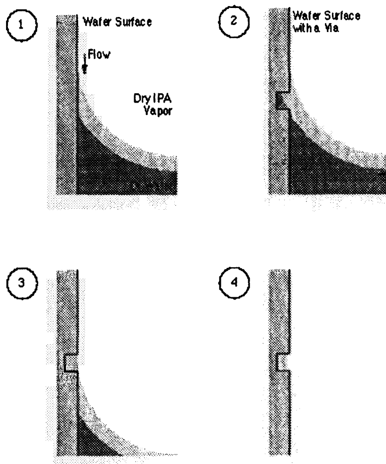

Figure 7: Schematic illustration of Direct-Displace™ drying of Trench or Via.

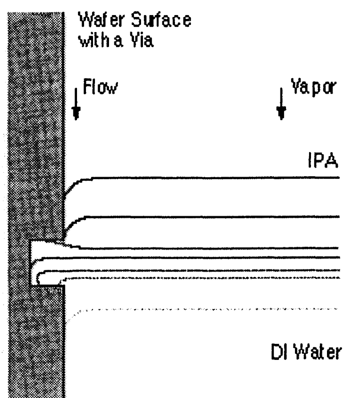

DEVELOPMENT OF ADVANCED CORROSION FREE ORGANIC STRIPPERS FOR ULSI PROCESSING

A.L.P. Rotondaro, K. Honda*, T. Maw*, D. Perry*, M. Lux, M.M. Heyns,
C. Claeys and I. Daraktchiev**
IMEC, Kapeldreef 75, B-3001 Leuven, Belgium.
* OCG, 200 Massasoit Av., E. Providence RI 02914, USA.
** OCG, Keetberglaan 1A, B-2070 Zwijndrecht, Belgium.

Corrosion free organic strippers were optimised. The addition of alkanolamino acids was used to control and suppress the corrosion of Al alloys, which is the major drawback of this class of strippers. Low particle and metallic contamination were obtained aiming for ULSI processing.

INTRODUCTION

Organic solvents are generally used to strip photoresist layers on wafers that have already received metallisation. In this case, the use of hot acid solutions is not possible as the corrosion of the metal lines would be catastrophic. Moreover, the organic solvents are the only class of cleaning solutions that can be used to remove contaminants from the wafer surface in the backend half of the device fabrication process. The majority of the organic strippers is composed of a polar solvent and an alkanolamine [1]. The amine is mainly responsible for the dissolution of the photoresist film and is a key component of the stripper. However, when in contact with water an alkaline media can be formed leading to the corrosion of Al and its alloys [2]. This drawback can be avoided by treating the wafers in isopropylalcohol (IPA) or other organic solvents prior to the rinse step, aiming for the complete removal of the amine from their surface. Although preventing corrosion, this approach requires an extra process bath, which increases the processing time and cost. A more suitable solution for the corrosion problem is to blend a corrosion inhibitor to the stripper. Acidic compounds can be used for this purpose when added to basic strippers [3]. In this paper, corrosion free alkanolamine based organic strippers are obtained by the addition of a new type of corrosion inhibitors to the solutions. The developed compositions were optimised aiming for ULSI processing.

EXPERIMENTAL

Silicon wafers, CZ, p-type, <100>, 1-30 Ωcm, 125 mm diameter were used to monitor the properties of the strippers. All tests were performed in a quartz tank without recirculation and filtration, thus characterising the worst case scenario for the use of the solutions. The stripping temperature was fixed at 90 °C. After processing, unless otherwise specified, the wafers were immediately rinsed in a room temperature DI water overflow tank for 10 min and spun dry.

The corrosion of Al alloys was evaluated by the change in the line resistance of meander structures made with 110 nm Ti/TiN + 700 nm AlSi(1%)Cu(0.5%) + 80 nm Ti/TiN (Stack) that have been exposed to the strippers. This allows the calculation of the average metal line width loss as the meander resistance (R) is related to its width (W) by:

$$R = \frac{L\rho}{W t} \tag{1}$$

where L is the meander length, ρ is the metal resistivity and t is the meander thickness. The baseline resistance of the meanders was determined on structures that have only received oxygen ashing in a PRS800 reactor for 45 min after the RIE treatment. The corrosion of Al lines was also measured by scanning electron microscopy (SEM) in top-view and cross-section mode with a Hitachi 4500 equipment. The Al alloy loss was evaluated by using the top and bottom Ti/TiN layers as internal reference representing the original size of the lines before stripping.

Metallic contamination was measured by Vapour Phase Decomposition - Droplet Surface Etching - Total Reflection X Ray Fluorescence (VPD-DSE-TXRF) [4] analysis on the wafers after treatment. The TXRF measurements were performed with an Atomika XSA8010 apparatus. The added particles were detected as Light Point Defects (LPD's) on the wafers with a Censor ANS100 light scattering equipment. LPD's bigger than 0.15 μm Latex Sphere Equivalent (LSE) diameter were measured.

The corrosion experiments were conducted in two phases: - In the first one stack meanders were treated in organic strippers without corrosion inhibitors (CIN) to determine the effect of the stripping time and the immersion time in stagnant water before the final overflow rinse on the corrosion of Al alloys; - In the second one, the worst case condition

regarding corrosion, as determined in the phase one, was used to evaluate the impact of the addition of different levels of CIN to the strippers on the attack of Al alloys. The metallic surface contamination and LPD addition studies were conducted using "standard" process conditions, meaning 10 min stripping immediately followed by 10 min overflow rinse in DI water.

The basic formulation of the advanced organic strippers consists of N-methyl-pyrrolidinone (NMP) as polar solvent, 2-(2 aminoethoxy) ethanol (AEE) as alkanolamine and tricine (trc) and bicine (bcn) as corrosion inhibitors.

RESULTS AND DISCUSSION

The stripping time has no influence on the width loss of the Stack meanders (figure 1). Even for 60 min immersion in strippers without CIN, negligible corrosion was noticed. On the other hand, when the wafers are dipped in stagnant DI water prior to the overflow rinse cycle the metal lines are attacked. This can be clearly seen on figure 1. The reduction of the metal line width increases with the immersion time in stagnant water between stripping and the overflow rinsing. This indicates that the corrosion of Al alloys mainly happens during the rinsing cycle.

Selecting the combination: 60 min stripping + 50 min immersion in stagnant DI water + 10 min overflow rinse as the standard process for the corrosion tests, the impact of the addition of different amounts of CIN to the strippers was studied. In figure 2 it is possible to observe that tricine and bicine are effective in reducing the corrosion of the Al alloy even at concentrations of 3%. Moreover, tricine appears to be more efficient in suppressing corrosion than bicine as reduced metal loss is noticed when the wafers are treated in the tricine containing compositions. This allows us to conclude that an NMP + AEE based stripper with 3% added tricine will present negligible corrosion of Al alloys and it would keep a good process latitude for variations in the rinsing process to occur.

The SEM analysis of the structures in cross-section confirmed the width loss calculated from the electrical measurements. Structures where negligible corrosion was detected by the electrical evaluation showed no appreciable loss of the Al lines when inspected in top-view or cross-section (figure 3). On the other hand, the samples where corrosion was detected by the electrical measurements presented a clear reduction in their Al line width (figure 4). Although a good correlation was observed between the two

techniques, more significant information is obtained from the electrical measurements as they provide mapping capabilities and take into account eventual non-uniform corrosion that might happen at corners or grain boundaries of the material.

The addition of CIN to the strippers does not result in the increase of the surface metallic contamination transferred to the wafers as can be seen for Fe in figure 5. In all cases, the Fe surface concentration could be kept below 10^{11} at/cm^2. Low metallic contamination was also observed for other metals like Cu and Zn indicating that the CINs do not contaminate the solutions.

Figure 6 shows the density of added LPD's on wafers treated in the different strippers. The LPD addition do not correlate with the % of added CIN. It is possible to notice that no significant increase in the number of added LPD's was measured. This indicates that the inclusion of CIN to the mixtures does not contribute to the LPD deposition on the wafers.

CONCLUSIONS

Advanced organic strippers have been developed. The corrosion of Al alloys is mainly related to the rinsing cycle and is independent on the stripping time. It was demonstrated that samples kept in stagnant water after the stripping treatment presented appreciable corrosion. On the other hand, when only a 10 min DI water overflow rinse was used no noticeble corrosion was measured. The addition of the corrosion inhibitors has shown to be effective to suppress the attack of Al alloys when the wafers are processed under corrosion favorable conditions. The addition of CIN to the strippers does not cause any increase to the contamination deposited on the wafers.

ACKNOWLEDGEMENTS

A.L.P. Rotondaro would like to thank CNPq (Conselho Nacional de Desenvolvimento Científico e Tecnológico) Brazil, for financial support.

REFERENCES

1. W.M. Lee, in Interconnects, Contact Metallization, and Multilevel Metallization, T.O. Herndon, K. Okabayashi and N. Alvi Editors, **PV93-25**, p.326, The Electrochemical Society Proceedings Series, Pennington, NJ (1993).
2. P.L. Pai et al., Proceedings of the INTERFACE'89, 137 (1989).

3. G. Schwartzkopf et al., in Reliability for Semiconductor Devices, Interconnects, and Thin Insulator Materials, H.S. Rathore, R.A. Susko and M. Kashiwagi Editors, **PV93-25**, p.379 The Electrochemical Society Proceedings Series, Pennington, NJ (1993)
4. P.W. Mertens et al., Proceedings of the 38th Annual Technical Meeting of the Institute of Environmental Sciences (IES'92), **1**, 475 (1992).

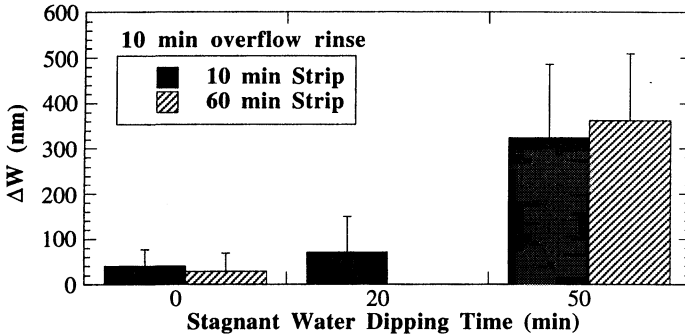

Figure 1: Stack meander width loss as a function of the immersion time in stagnant water after stripping. Two stripping times were used: 10 and 60min. The wafers received a final 10min DI water overflow rinse in all cases.

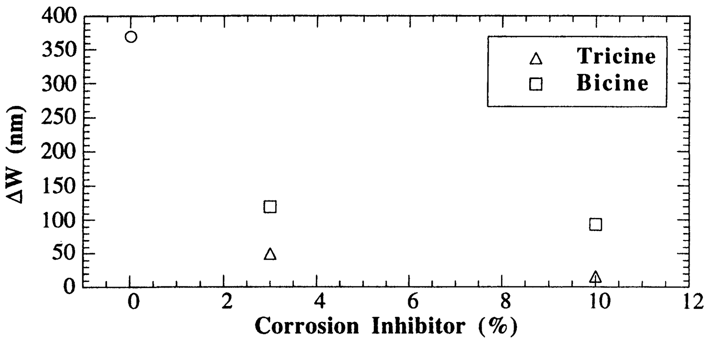

Figure 2: Stack meander width loss as a function of the amount of CIN added to the stripper. The wafers were processed for 60 min in the stripper, 50 min in stagnant DI water and received a final 10 min DI water overflow rinse.

Figure 3: Typical SEM cross-section picture of a non-corroded Stack meander line.

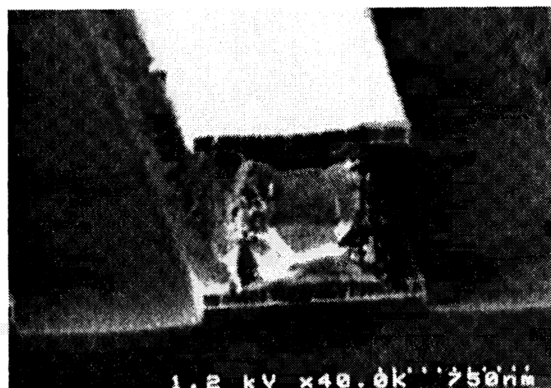

Figure 4: Typical SEM cross-section picture of a corroded Stack meander line.

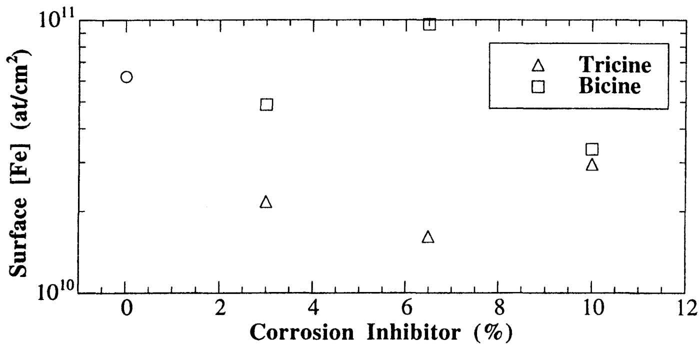

Figure 5: Surface [Fe] as measured by VPD-DSE-TXRF on wafers that have been treated for 10 min in the strippers and immediately received a 10 min DI water overflow rinse.

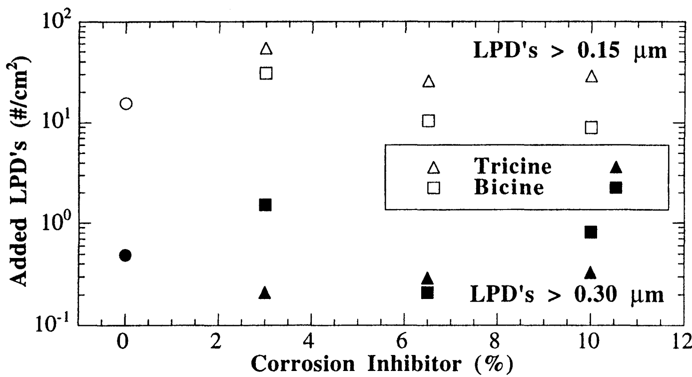

Figure 6: Density of added LPD's on wafers treated for 10 min in the strippers and immediately rinsed for 10 min in overflow DI water as a function of the amount of added CIN. Open symbols represent LPD's > 0.15 μm LSE. Full symbols represent LPD's > 0.30 μm LSE.

ETCHING SiO_2 FILMS IN AQUEOUS 0.49% HF

Sean O'Brien & Ambika Somashekar
Process Design and Control
Semiconductor Process and Device Center
Texas Instruments Dallas TX 75265

ABSTRACT

The wet etch of SiO_2 films shows surprising results depending on the film type and HF characteristics. The removal of undensified TEOS in 0.49% HF is extremely linear versus time with a slope near 150 Å/min in both unbuffered and 40% buffered HF. A 97 Å y-intercept corresponding to etch during the transfer and rinse is found with buffering, this zero-time intercept is only 13 Å without the NH_4F buffer. Thus it is impossible to etch less than 97 Å of TEOS in 40% BHF. Buffering increases the etch rate of thermal oxide from 20 to 65 Å/min, but the y-intercept is invariant. The selectivity of TEOS to thermal oxide is strongly time dependent. The rinse rate of TEOS in BHF does not depend on the flow velocity of the rinse water.

INTRODUCTION

This is the first in a series of papers which will investigate etch dynamics of HF and NH_4F for a variety of oxide films. Paper II will detail the impact of doping and thermal processing by studying the etch rate of BPSG and TEOS as a function of buffer concentration (1). Finally Paper III will study the true etch rate mechanism and rinse dynamics including rate limiting steps (2). This work will present a standard methodology for true etch rate and selectivity measurements. Traditional etch rate calculations are not sufficient to explain short process time etch dynamics, especially on deposited SiO_2 films.

EXPERIMENTAL

For this study SiO_2 was deposited on 6" silicon wafers using a furnace TEOS process at 700°C. No subsequent thermal annealing was done. HF immersion was in a stagnant tank without temperature control. The wafers were manually inserted into the HF, then transferred to the rinse water, rinsed for 5 minutes, then dried in a SemiTool Spin Dryer without water rinsing. Film thickness was measured using the ThermaWave Optiprobe. All wafers were measured at 9 sites. Etch delta was calculated on a site-by-site basis, followed by averaging of the 9 delta points. The precision of the thickness is near 2 Å, while the accuracy subtracts out for the delta. Repeatability is limited by the robotic wafer handler, which is crucial near the sharply varying edge of the TEOS wafer. Measurements were restricted to a 100mm diameter where the film is essentially flat.

HF ETCH CHEMISTRY AND MECHANISM

The chemical reaction between SiO_2 and HF is poorly understood. Throughout the semiconductor industry the overall chemical reaction is assumed to be:

$$6\,HF_{(aq)} \quad + \quad SiO_{2(s)} \quad <-> \quad H_2SiF_{6(aq)} \quad + \quad 2\,H_2O \qquad [1]$$

thus requiring 6 moles of HF to remove every mole of SiO_2. The implicit assumption is that reaction 1 goes to completion then stops, but this is an incorrect assumption. Fluosilicic acid (H_2SiF_6) etches silicon dioxide (3) and consequently a solution of H_2SiF_6 without HF can still etch SiO_2. The product of a complete reaction between HF and SiO_2 is not fluosilicic acid. The final product is decafluodisilicic acid produced through the reaction:

$$4\,H^+_{(aq)} + 5\,SiF_6{}^{2-}{}_{(aq)} \quad + \quad SiO_{2(s)} \quad <-> \quad 3\,F_4Si\text{-}SiF_6{}^{2-}{}_{(aq)} \quad + \quad 2\,H_2O \qquad [2]$$

Thus the overall reaction between HF and SiO_2 really requires only a 5:1 molar ratio:

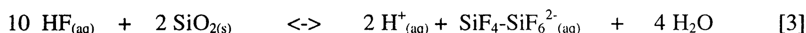

$$10\,HF_{(aq)} \quad + \quad 2\,SiO_{2(s)} \quad <-> \quad 2\,H^+_{(aq)} + SiF_4\text{-}SiF_6{}^{2-}{}_{(aq)} \quad + \quad 4\,H_2O \qquad [3]$$

Prevalent theories about the mechanism of SiO_2 etching center around the HF_2^- species, primarily because the addition of an NH_4F buffer to the HF will accelerate the etch of thermally grown oxide (4). An excellent review of HF etch references is given by Monk *et. al.* in their paper on etching mechanisms (5). Because buffering only marginally impacts the etch rate of deposited films a different mechanism seems to apply (6). Thus by increasing the concentration of the primary reactant species HF_2^- the selectivity can be tuned to a precise value. Previous work has measured the dependence of the etch rate on buffering for doped (7) and undoped (8) deposited oxide films, and recently the concentration dependence of key species has been calculated (9). Unfortunately it appears the calculation of etch rates in these papers was done improperly thus seriously confounding the entire analysis of etch rate and selectivity.

ETCH RATE MEASUREMENTS

The rate of removal of SiO_2 from a wafer surface can be easily measured, but the etch rate calculation cannot be based on a single point. As seen in Figure 1 the removal of TEOS is extremely linear with time, but a large zero-second intercept is found. Conceptually this intercept results from etching which occurs during the transfer from the BHF process tank to the water rinse tank and the subsequent rinse to pure water. Since it would take the BHF 40 seconds to etch 97 Å it is obvious that the rinse is a dramatic contributor to the etch process dynamics. It is essentially impossible to etch for less than 40 seconds, even if the HF immersion time is near zero.

For short process times (1-5 seconds) the correlation coefficient of this fit exceeds 0.9999. There are no discontinuous or non-linear effects for short times. The shortest possible process time will remove nearly 100 Å of TEOS, and every second in the etch tank will remove 144/60 or 2.4 Å more. Obviously 2 numbers (slope and intercept) cannot be obtained from a single measurement thus any etch rate calculation based on a single etch time is deficient and incomplete. It is only when the intercept is a minuscule fraction of the total etched thickness that the calculated etch rate approaches the true value. Since the etch of nearly 100 Å occurs in essentially 0 seconds this "faux etch rate" starts near infinity, and quickly plummets. 100 Å removal in 1 second is a 6000 Å/min etch rate. Figure 2 shows that even after a 30 minute etch this incorrectly calculated etch rate is still above the true value.

SELECTIVITY

Selectivity changes amongst the various different forms of oxide films as a function of HF and NH_4F concentration have been carefully measured in the literature, but unfortunately the single point etch rate was used. Measurement of selectivity leads to some surprising results. Figure 3 shows the etch curves for TEOS. The NH_4F buffering agent does not change the etch rate, only the zero time intercept is affected. Slight differences in slope as measured are well within experimental error. Figure 4 shows the exact opposite behavior is found for thermal oxide films, only the etch rate changes.

Table I lists numerical values obtained, along with the equivalent rinse time (intercept divided by slope). This approximates the time the wafers etch prior to the HF dilution by the rinse water.

The independence of TEOS etch rates on buffering shown in Figure 3 is a coincidence. The etch rate sharply increases as NH_4F is added, it peaks around 15% buffering, then decreases beyond that. At 40% it has decreased back to 159 Å/min.[1]

Table I   Etch Parameters for Oxide Films

Film	HF	Slope (Å/min)	Intercept (Å)	Equivalent Time (sec)
TEOS	0.49%	159 ± 10	13 ± 3	4.9
TEOS	BHF	144 ± 10	97 ± 10	40
Thermal	0.49%	20 ± 3	7 ± 2	21
Thermal	BHF	65 ± 5	8 ± 2	7

This opposite behavior for TEOS and thermal oxide leads to time dependent selectivity. The choice of HF must be based on the process time. As seen in Figure 5 for a process time near 25 seconds the selectivity is about 5:1 with or without buffering. For

shorter times the buffered HF has much higher TEOS selectivity, for longer times it is unbuffered HF which gives the higher value. Limiting values for selectivity are obtained for process times greater than 200 seconds.

RINSING

There are several process issues associated with rinsing HF from wafers. The primary reason for the rinse is to quench the etch, to quickly stop SiO_2 removal in a uniform and controlled manner. Other process issues include particles, and acid residue which may impact subsequent processing, device yield, or reliability. The most important non-process issue is safety. HF is dangerous, it must be removed from both the wafer and cassette quickly and efficiently. After safety comes equipment protection, most dryers contain exposed metal which can quickly corrode when exposed to acids.

It has always been assumed that the flow velocity of the rinse water (the rate at which clean new water is delivered to the wafer surface) strongly impacts the process. Both thickness and uniformity control are assumed to change drastically with rinse parameters. The truth is shown in Figure 6, rinse water velocity has no impact on either etch thickness or site to site uniformity. This data was taken for a single wafer, thus the volume ratio of HF carryover to available water is extremely small; however, the data is similar for a batch of 24 wafers. These data points are easily explained. The rate of diffusion of BHF out of the film and boundary layer is slow, so slow that the flow velocity parallel to the wafer will not significantly change it.

ZERO-TIME INTERCEPT

The non-zero intercept for the above analysis is easily assigned to etching during the wafer transfer and rinse to dilution. Unfortunately it appears this process requires a dramatic amount of time. The data in Figure 1 lead to the conclusion that the equivalent etch in the transfer and rinse is 40 seconds. Thus it is impossible to etch an undensified TEOS film for less than 40 seconds, even if the HF immersion time is minuscule.

The physical chemistry behind this process involves the film, since different films have different equivalent etch times. The data in Table I includes a conceptual etch time for the rinse. The wide variation in this time (5 to 40 seconds) indicates that the film and the HF chemistry dramatically influence this phenomena.

Rinsing velocity has been proven irrelevant, and thus diffusion of HF away from the wafer dominates this zero-etch time value. But what is not clear is whether the rate limiting diffusion is occurring within the oxide film, or simply out of the boundary layer at the wafer surface. A detailed series of experiments would be required to determine the actual process. First the activation energy of the HF etch process should be carefully measured as a function of dilution. Then the dependence of the intercept on rinse water

temperature must be measured. Deconvoluting out the HF etch rate dilution and temperature dependence would show the contribution of diffusion. Finally the dependence of film density and stoichiometry should allow separating out the difference between HF diffusing out of the oxide, and HF diffusing out of the boundary layer.

CONCLUSION

The removal of undensified TEOS from a wafer using buffered HF is extremely linear with process time, but the zero intercept is very large. The true etch rate of TEOS does not change with buffering, only the zero time intercept is changed. The etch of thermal oxide strongly depends on buffering concentration but the zero intercept does not. This leads to selectivity curves which change significantly with processing time. For a process which requires etch selectivity the choice of HF must be based on the etch time. The etch of TEOS in BHF does not change with rinse water flow rate.

ACKNOWLEDGMENTS

We would like to thank Jackie Kemp, Rajan Rajgopal, Chuck Roth, Jeff Large, Sharon Choice, and Debbie Weaver.

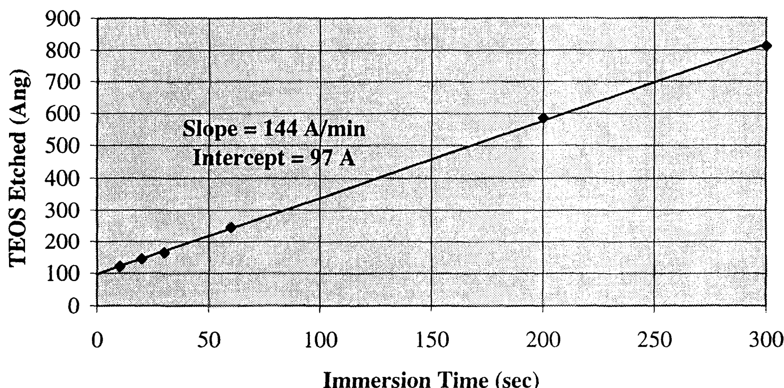

Figure 1 Etch of undensified TEOS in 40% buffered 0.49% HF. The correlation coefficient is > 0.999. Each data point is the average of 9 site-to-site subtracted measurements.

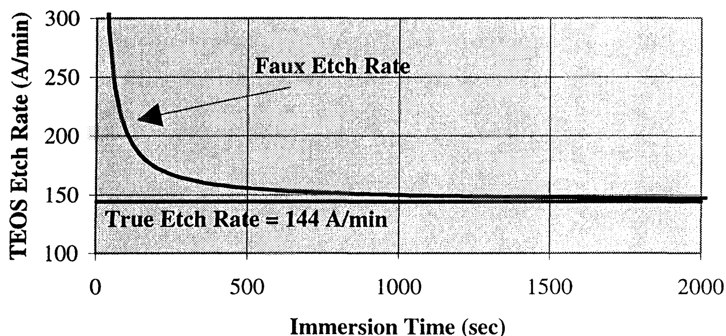

Figure 2 Traditional (and incorrect) single point calculation of etch rate using the data in Figure 1. The horizontal line is the slope of the graph in Figure 1.

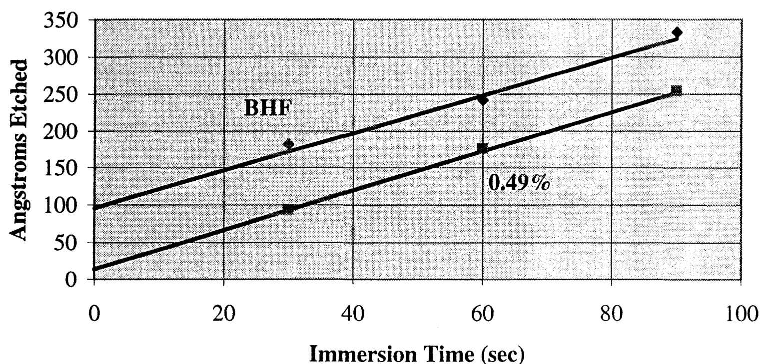

Figure 3 Etch of undensified TEOS in buffered and unbuffered 0.49% HF. The NH_4F buffer does not change the etch rate of TEOS (150 Å/min), only the zero time intercept.

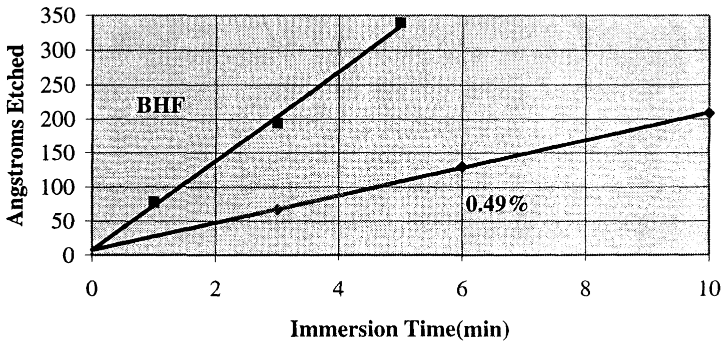

Figure 4 Etch of thermal oxide in buffered and unbuffered 0.49% HF. The NH_4F buffer does not change the zero time intercept, only the etch rate.

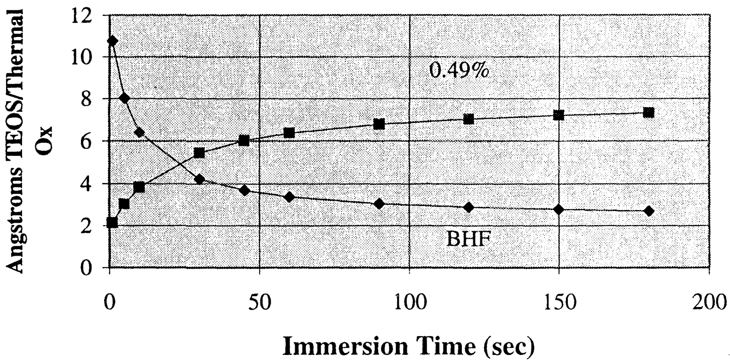

Figure 5 Selectivity of TEOS to Thermal Oxide as a function of process time for buffered and unbuffered 0.49% HF calculated from the slope and intercept data in Table I. The ratio of thickness at each process time is the selectivity.

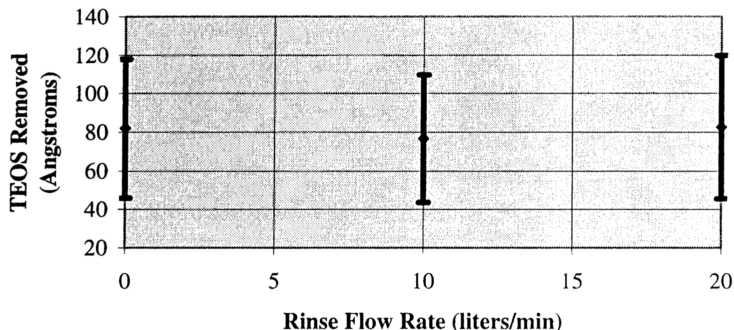

Figure 6 Removal of TEOS in a 1 second etch as a function of rinse water flow as measured on a single wafer. The error bars indicate the range of the 9 sites across the wafer. There is no evidence that rinse water flow velocity changes the rinse rate of BHF.

REFERENCES

1 S.C. O'Brien and A. Somashekar, Submitted to J. Electrochem. Soc. (1995).

2 S.C. O'Brien, Submitted to J. Electrochem. Soc. (1995).

3 S. M. Thomsen, J. American Chem. Soc. 74, p. 1690 (1952).

4 J. S. Judge, J. Electrochem. Soc. 118(11) p. 1772 (1971).

5 D. J. Monk *et.al.*, J. Electrochem. Soc. 140(8) p. 2339 (1993).

6 H. Kikuyama *et.al.*, IEEE Trans. on Semiconductor Manufacturing 4(1) p. 26 (1991).

7 H. Kikuyama *et.al.*, J. Electrochem. Soc. 139(8) p. 2239 (1992).

8 H. Proksche *et.al.*, J. Electrochem. Soc. 139(2) p. 521 (1992).

9 S. Verhavebeke *et.al.*, J. Electrochem. Soc. 141(10) p. 2852 (1994).

SURFACE EFFECTS DURING PROXIMITY RAPID THERMAL DIFFUSION OF PHOSPHORUS IN SILICON

S. Montandon, W. Zagozdzon-Wosik and Jia Li
Electrical and Computer Engineering Department, University of Houston, 4800 Calhoun, Houston, TX-77204

W. T. Taferner and B. Bensaoula
Space Vacuum Epitaxy Center, University of Houston, 4800 Calhoun, Houston, TX-77204

ABSTRACT

Rapid thermal diffusion was used to create shallow junctions in silicon. We investigated effects responsible for variation of the doping efficiency of phosphorus in a target wafer, which is placed in proximity to a dopant source wafer during the high temperature processes. Experiments have been done using different cleaning recipes of silicon wafers, thermal conditions, and ambient gases. The results indicate that, in an nitrogen ambient, the doping efficiency decreases for long purging times because of deposition of organic molecules, released from the spin-on-dopant source, prevent adsorption of doping species at the silicon surface. When oxygen is present in the chamber, this effect is reduced and doping improves. The best doping is obtained when the rapid thermal processor chamber is filled with oxygen, followed by the high temperature step performed in the nitrogen ambient.

INTRODUCTION

The need for more efficient, fast and complex integrated circuits (IC) has lead to a fast increase in packing density, which requires scaling-down horizontal dimensions of all devices present on a silicon wafer. This also calls for reduction of vertical dimensions of electrical devices to alleviate detrimental short-channel effects such as threshold voltage lowering or punchthrough. Consequently, very shallow junctions formation is indispensable in ultra large scale integration (ULSI). For a 0.25 μm gate length technology, the design rules require junction depths as small as 60 and 100 nm [1].

When the dopant source is in the gaseous phase, surface phenomena can play a role in the junction formation via adsorption of doping molecules at the silicon wafer. For instance, the dopant source in the form of PH_3, AsH_3, or B_2H_6, can be adsorbed at the silicon surface, and at high temperatures release P, As, or B atoms to diffuse into the substrate. The reactivity of the silicon surface can play a role in changing the adsorption kinetics and therefore doping efficiency. Diffusion sources can also be composed of dopant oxides, formed at the wafer surface in a reaction between Si and molecules such as P_2O_5 or B_2O_3 to create doped SiO_2 and dopants which can diffuse into the substrate. In this doping processes, surface effects can also play an important role since roughness,

cleanliness, or native oxide presence can be expected to affect adsorption of the dopant molecules.

It is well-known that cleaning processes of the silicon crystal have the influence on the surface roughness, native oxide formation and can result in the surface passivation [2-4]. However, no reports on the effects of silicon cleaning on the diffusion processes were found in the literature. Here, we study the surface effects that have an influence on the phosphorus doping efficiency in proximity rapid thermal diffusion (P-RTD) [5, 6]. It is a technique that can be used to create shallow junctions, without damage removal problems encountered in the ion implantation technique. A thin layer of a phosphorus doped oxide is grown on the surface of a p-type processed silicon wafer called a "target", by evaporating dopant oxide from another Si wafer, called a "source". The source is fabricated by coating the wafer with a spin-on dopant (SOD) and is placed in proximity to the target in a rapid thermal processor (RTP) chamber. High temperatures of P-RTD allow for the dopant release from the source in the form of P_2O_5, its transport through the separating gap, adsorption at the target wafer surface, and diffusion of phosphorus into the silicon substrate to produce an n-type layer.

The process is much less reproducible for the target as compared to the source wafers. Typical problems related to temperature measurements in RTP could not justify these results. We analyzed, therefore, the effects at the target surface to elucidate the reasons for differences in the doping efficiency of the both wafers. In order to understand these effects, we performed experiments in different thermal conditions while changing parameters such as ambient gas, purging time, and using various recipes for cleaning of the target wafers.

EXPERIMENTAL PROCEDURE

The source wafers were fabricated by deposition of a phosphorus spin-on dopant (SOD) at 2000 rpm on p-type, low doped, (100) oriented, clean silicon wafers. The wafers were baked in ambient air at 150 °C for 30 min, to maximize the doping efficiency by evaporating solvents and organics [6]. The same substrate wafers were used as the targets. The target was placed at a distance of 0.5 mm from the source in the RTP chamber. Both wafers were then heated at atmospheric pressure in an ambient of either nitrogen, oxygen, or air for 10 sec, at temperatures ranging from 850 °C to 1150 °C.

In order to study the cleaning effects on the doping efficiency, two target wafers were processed in every P-RTD process. One target of such pair was always cleaned using the IMEC clean [7], thereafter called "cleaning 1 & 2" and was used as a reference wafer. The first part of this cleaning uses H_2SO_4:H_2O_2 (4:1) to create a thin (15 Å) chemical oxide at the silicon surface that traps contaminants. The second step of this cleaning removes this oxide, using low concentrated HF (0.5 %) and 0.1 % of isopropyl alcohol (IPA) in DI water. This cleaning is supposed to leave the surface smooth and contaminant-free. The second target wafer used in the diffusion processes was cleaned using one of the following recipes: (A) cleaning 1 + cleaning SC-1, of the standard RCA

cleaning with $NH_4OH:H_2O_2:H_2O_2$ using 5:1:1 ratio, (B) wafer from the box, (C) cleaning 1 only, and (D) cleaning 1 + gaseous HF (49%). The source wafers were always prepared using the cleaning 1 & 2 before the SOD deposition.

Sheet resistance of the source and target wafers were measured using a four-point probe and the doped oxide created on the target surface was analyzed using Auger depth profile, XPS and FTIR methods. Thickness of this oxide was measured using an ellipsometer. Composition of the source was determined by low energy ion scattering (LEIS) and FTIR.

RESULTS AND DISCUSSION

In order to compensate for the influence of small temperature differences on doping, due to the temperature control problems typical in RTP, target sheet resistance measurements will be presented as a function of source sheet resistance. In such representation low sheet resistances correspond to high temperatures. Doping of the source wafers depends on temperature but is independent of the surface effects, since the cleaning is always the same, SOD thickness large, and the silicon surface is not in contact with the ambient gas. We verified that the system is symmetrical, so we can assume that the source and target wafers are at the same temperature. In addition, the doping efficiency is measured as a ratio of target (R_T) to source sheet resistance (R_S): R_T/R_S. Ideal doping should result in the same resistance values for both the wafers and this ratio should be equal to one.

The results of four different experiments using cleaning processes A to D are presented in Fig. 1 and 2. Purging of the RTP chamber prior the diffusion processes was done in N_2 for 20 sec and diffusion time was always 10 sec. The cleaning 1 & 2 was used for one target in each P-RTD for the reference purpose. The ratio of R_T/R_S varies from one experiment to another and the target doping is especially poor at high temperatures, as compared with the source wafers (large R_T/R_S ratio between 2.5 and 3). On the other hand, there is no significant difference between cleaning processes. However, for the high temperature processes in air, very large differences between experiments were observed when concentrated HF was used as the last cleaning step of the targets. This irreproducibility is possibly due to chamber contaminants, which are easily deposited on the oxide-free silicon surface.

While investigating the reasons for the poor doping at high temperatures, we found that the temperature in the RTP chamber during the purging step prior the diffusion process had an influence on the doping. The chamber temperature stabilizes around 350 ^{o}C after a few processes and is responsible for less efficient doping of the targets. On the other hand, doping can be improved (R_T/R_S closer to 1) if the chamber is completely cold during the nitrogen purging time. Fig. 3 shows the comparison of doping using the cold and warm chamber. The difference between the source and target doping becomes smaller at lower temperatures which correspond to higher source sheet resistances. In addition, thickness of the oxide formed on the target wafers shows also large differences

depending whether the warm or cold chamber was purged in nitrogen (Fig. 4). Therefore, we can conclude that the source of phosphorus for the target doping is limited by the oxide thickness which is formed at the target surface. This limitation is more pronounced at high temperatures, as the diffusion rates are larger.

At 1100 °C, the target doping is strongly affected by the nitrogen purging time in the range of 0 and 80 sec, as shown in Fig. 5. The oxide also becomes thinner as the purging time in the warm chamber increases, which means that the oxide growth is retarded. This blocking could be due to the deposition of organic contaminants still contained in the SOD source which would desorb above 300 °C. To verify this hypothesis, we analyzed the source composition, using FTIR. The results of these measurements, made after the SOD deposition, 150 °C baking and P-RTD processing, are presented in Fig. 6. After the baking process, there are still organic compounds in the source, but they almost disappear after the high temperature processing. The phosphorus bonding also changes from the form of P-O and P-O-C_2H_5 before P-RTD to P_2O_5 after the diffusion process.

In order to study desorption temperature of phosphorus and carbon compounds from the source, the SOD surface was analyzed using LEIS, while heating the sample from room temperature to 1050 °C to mimic the actual P-RTD process. At 150 °C the temperature was kept constant for 30 min to simulate the baking process (Fig. 7). We found that at 150 °C, the carbon content is reduced, but not entirely removed. At 1050 °C however, carbon is completely removed, and the phosphorus level at the surface, which was at its maximum value after the 150 °C step, also decreases. Some organic compounds are still present in the source at the beginning of the RTP process. The desorption of theses molecules takes place during the nitrogen purging step prior diffusion in a warm chamber. Their deposition on the target wafer surface can be the reason for the doping efficiency differences observed earlier. If this hypothesis is correct, loading the source wafer alone in the warm RTP and purging the chamber before placing the target would lead to better target doping as compared to the cold chamber purge. The organic molecules would desorb from the SOD but would not contaminate the target surface. Figure 8 shows a comparison of the target to source sheet resistance ratio (R_T/R_S) for diffusion temperature of 1100 °C. The doping of the target is the best when the source is loaded first in the RTP chamber, thus confirming that the surface blocking effects are due to the molecule desorption from the source.

Multiple internal reflection FTIR analysis have shown that the surface of the target wafer placed in proximity to the source in a warm chamber in ambient nitrogen, without diffusion, contained C_2H_5 molecules which presumably come for the SOD source. Using Auger depth profile, the phosphorus concentration in the doped oxide was also analyzed (Fig. 9). The maximum phosphorus concentration is located at the oxide-silicon interface, as reported by other authors [8, 9]. This concentration corresponds to about 10% of the other elements. Using XPS, we found that the phosphorus was in the P_2O_5 bonding configuration in the target oxide. As the target doping is limited by the organic molecules released by the source, it is possible to limit this deposition by purging the chamber with oxygen instead of nitrogen. These molecules can react with O_2 and be burned instead of being deposited on the target wafer. Results of the experiments using oxygen purging of the chamber for 30 sec, before the high temperature diffusion in

nitrogen, show that the doping is good and reproducible. The use of the nitrogen instead of oxygen ambient during diffusion maximizes the doping due to smaller growth of the thermal oxide which might mask the doping. Efficient doping (values of the R_T/R_S ratio is close to 1) have been obtained using this procedure, for the whole range of diffusion temperatures.

CONCLUSIONS

We have been able to understand and characterize the effects that limit the target doping in proximity rapid thermal diffusion. The correlation was found between sheet resistance and thickness of the doped oxide which is formed on the target surface. Differences in thickness of this oxide have been found to occur because of the deposition of organic molecules, released from the SOD, on the target surface. When organic contaminants are present on the surface, oxidation is retarded because time required for evaporating theses molecules from the surface, as described by Philipossian [10]. When the processing time is only 10 sec, this delay can influence significantly the oxide growth and therefore deteriorate doping. The oxide composition was analyzed using AES and XPS and phosphorus is found to be in the P_2O_5 form, with a maximum concentration at the silicon-oxide interface.

ACKNOWLEDGMENTS

This work was supported by Texas Higher Education Coordinating Board (ARP grant).

REFERENCES

1. B. El-Kareh, J. Vac. Sci. Technology, **B12 (1)**,172-178, (1994).
2. J. M. deLarios, D. B. Kao, C. R. Helms, and B. E. Deal, Appl. Phys. Lett., **54**, 715-717, (1989).
3. G. Gould, and E. A. Irene, J. Electrochem. Soc., **134**, 1031-1033, (1987).
4. T. Ohmi, M. Miyashita, M. Itano, T. Imaoka, and I. Kawanabe, IEEE Transactions on Electron Devices, **39**, 537-545, (1992).
5. W. Zagozdzon-Wosik, J. C. Wolf, and C. W. Tang, IEEE Electron Device Letters, **12**, 264-266, (1991).
6. W. Zagozdzon-Wosik, P. B. Grabiec, and G. Lux, J. Appl. Phys., **75**, 337-344, (1994).
7. M. Heyns, S. Verhaverbeke, M. Meuris, P. Mertens, H. Schmidt, M. Kubota, A. Philipossian, K. Dillenbeck, D. Graf, A. Schnegg, and R. de Blank, Surface Chemical Cleaning and Passivation for semiconductor Processing, p. 35-45, G. S. Higashi, E. A. Irene, and T. Ohmi, Eds. Mat. Res. Soc. Symp. Proc., **315**, Pittsburgh, (1993).
8. Y. Sato, M. Watanabe, and K. Imai, J. Electrochem. Soc., **140**, 2679-2682, (1993).
9. O. K. T. Wu, and A. N. Saxena, J. Electrochem. Soc., **132**, 932-936, (1985).
10. A. Philipossian, J. Electrochem. Soc., **139**, 2956-2961, (1992).

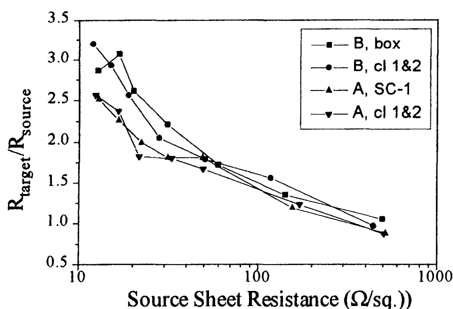

Fig. 1. Doping efficiency (R_T/R_S) vs. source sheet resistance for the experiments A and B. The cleaning 1 & 2 was used in all experiments for reference purpose.

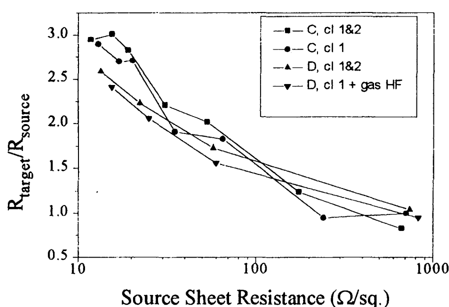

Fig. 2. Doping efficiency (R_T/R_S) vs. source sheet resistance for the experiments C and D. The cleaning 1 & 2 was used in all experiments for reference purpose.

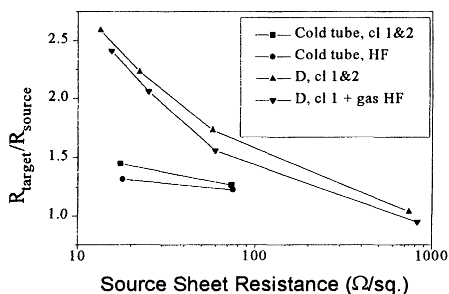

Fig. 3. Doping efficiency (R_T/R_S) vs. source sheet resistance for warm and cold chamber during the nitrogen purging period.

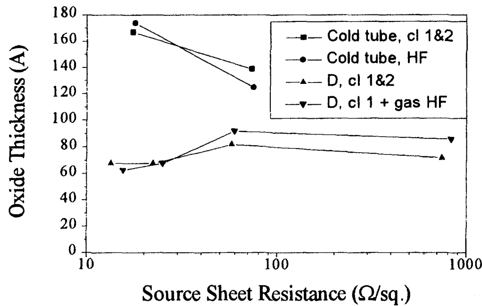

Fig. 4. Oxide thickness vs. source sheet resistance for warm and cold chamber during the nitrogen purging period.

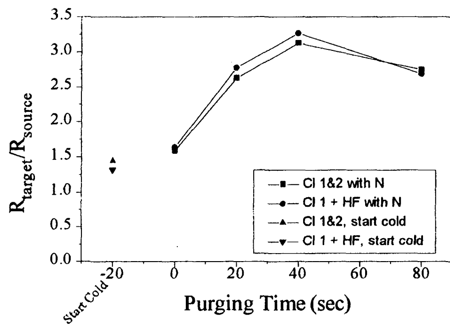

Fig. 5. Doping efficiency vs. purging time. The processing time is 10 sec, the temperature 1100 °C and the ambient gas is nitrogen. In the "start cold" process, the chamber is cold and purged with nitrogen for 20 sec.

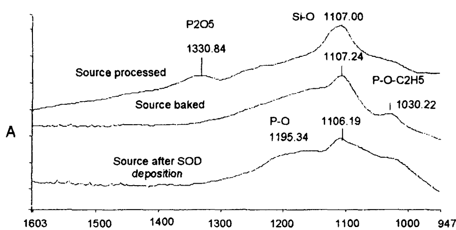

Fig. 6. Absorbance vs. wavenumber for the FTIR spectra of a source, taken after SOD deposition, after baking and after processing.

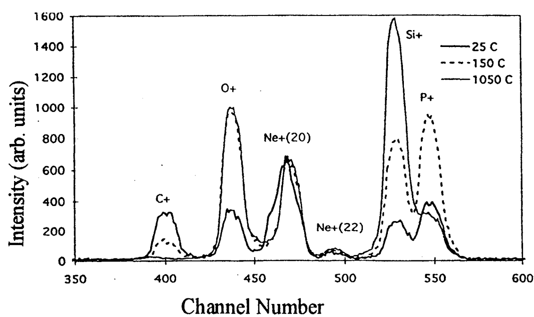

Fig. 7. LEIS spectra of a source, for three different temperatures.

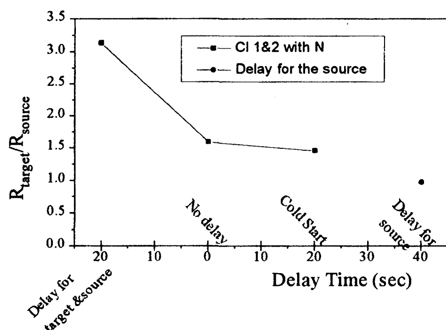

Fig. 8. Doping efficiency (R_T/R_S) for different purging times and conditions. The processing time is always 10 sec and the temperature 1100 °C.

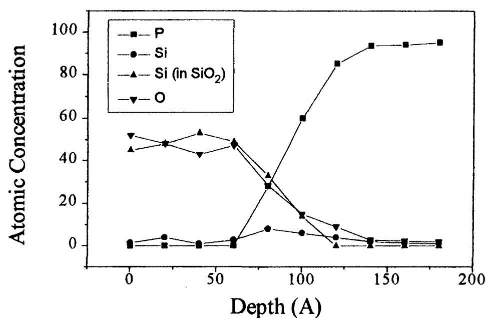

Fig. 9. Auger depth profile for a target, processed in air at 950 °C for 10 sec.

THE PARTICLE CONTAMINATION DURING WET CLEANING PROCESS ONTO VARIOUS WAFER SURFACES

Yasuki Sakata, Akihiro Ohnishi,
Gunji Kishi, Shouzou Izumo,
Hiroyuki Kondou and Akihiro Tomozawa

Hitachi Microcomputer System
Takasaki, Gunma 370, Japan

I Introduction

As the integration scale increases, it becomes more important to decrease particles on the wafer surface during fabricating VLSIs. During submicron-VLSIs manufacturing , RCA cleaning such as APM (Ammonia Peroxide of hydrogen Mixture) or HPM (Hydrochloride Peroxide of hydrogen Mixture) is widely used after photoresist-ashing process continued from dry-etching or ion-implantation in order to remove particles from wafer surfaces (Table.1).

There are many kinds of wafer surface in a half-micron-process fabrication line, not only the Si wafer but also other wafers on which SiO_2 (thermal or CVD) or Si_3N_4 or Poly-Si (metal) film is deposited. We found that the number of particles on a wafer surface during wet cleaning process was depended on the state of the wafer surface.Especially Si_3N_4-depo-wafers are the most sensitive to contamination in comparison with other wafers, that is, the number of particles on a Si_3N_4-depo-wafer after RCA cleaning is much more than that of SiO_2 wafer. And we also found that the number of particles on a Si_3N_4-depo-wafer surface was depended on its electrical capacity of Si_3N_4 film. These particles are coming off from the backside of other wafers, diffuse into the etchant, and re-adhere to the frontside of wafers (Fig.1)(1)(2).

And we observed this phenomenon mainly when RCA cleaning was applied in normal order, such as "HPM to APM". When the order of RCA cleaning was changed to "APM to HPM", the number of particles decreased, even on the Si_3N_4-depo-wafers. Particle distribution in wafer was depended on "liquid flow" in the cleaning vessel (Fig.2,3).

We tried to analyze these phenomena.

II Study

Zeta potential of various films at wafer state were measured in HCl/NaOH solution, in which an index number of hydrogen ion concentration (pH) is 2~8. Actually pH of APM is 10 and HPM is pH 1, so the values of Zeta potential in APM or HPM were extrapolated from pH 2~8 values.(Fig4)

The Zeta potential of Al_2O_3 which is presumed as main component of particles on the backside of wafers, as shown in the paper, has isoelectric point (zero-point) in pH9~10 area and is plus value under isoelectric point(Fig.5). When temperature of solution is 50~80℃, there is a

lowering in dielectric constant of solution depends on temperature, and isoelectric point will go up, so plus value will be continue until bigger pH area. So we can estimate that Zeta potential of Al_2O_3 particle in APM at 50~80℃ shows plus value(3)(4).

Various Si_3N_4-depo-wafers were prepared, changing source gas ratio, and Zeta potential of wafers were measured. (The ratio NH3/DCS : 6,10,20,30. DCS:DiChloroSilane) And surface charge per unit square of these wafers were measured using SCA (Surface Charge Analyzer).

III Results and Discussion

In APM solution, Zeta potential of SiO_2 wafer showed near zero value, and that of Si_3N_4 wafer showed -40mV. And in HPM solution, both of SiO_2 wafers and Si_3N_4 wafer, Zeta potential was plus value, that is, +15mV and +20mV. Among Si_3N_4-depo-wafers of various component ratio, Zeta potential values mutually related to capacitance.

In APM solution, Al_2O_3 particle has plus value of Zeta potential and SiO_2 wafer has near zero value. Then between Al_2O_3 particle and SiO_2 wafer, electrical attraction or repulsion power is small. So re-adhesion of particles to SiO_2 wafer surface in APM solution hardly happen. On the contrary, in the case of Si_3N_4-depo-wafer in APM solution, it has minus big value of Zeta potential and attracts Al_2O_3 particles. As a result, in APM solution re-adhesion of particles to Si_3N_4-depo-wafer surface easily happen.

In HPM solution, SiO_2 wafer, Si_3N_4-depo-wafer and Al_2O_3 particle, all has plus value of Zeta potential. So re-adhesion of particles hardly happen.

Si_3N_4-depo-wafer in APM has minus value of Zeta potential, and its potential is depending on the electrical capacitance ($\propto$dielectric constant), furthermore the number of re-adhesion of particles is depending on the value of Zeta potential (Fig.6).

IV Summary

In the wet cleaning solution, especially in APM, Si_3N_4-depo-wafer is the most sensitive to re-adhere particles from the backside of other wafers. And particle re-adhesion also depends on the electrical capacitance of Si_3N_4-depo-wafer. These phenomena are able to be explained by using Zeta potential.

References

1) A.Saito, K.Ohta and H. Oka : "Particle deposition mechanism onto silicon wafer"
Extended Abstracts of the 21st Conference on Solid State Devices and Materials, Tokyo,
pp.409-412 August 1989

2) A.Saito, K.Ohta and H. Oka : "Particle deposition mechanism onto silicon wafer"
Proceedings, 8th Workshop Ultra Clean Technology, Tokyo, Japan, pp.19-31, December 1990
3) T. Kezuka, M. Ishii, T. Unemoto, M. Itano, M. Kubo, T. Ohmi : "The behavior of particles in liquid chemicals and their deposition control onto wafer surfaces"
Ultra Clean Technology Vol.6 No.5/6 pp.19-24, 1994
4)A.Kitahara, K.Furusawa, M.Ozaki and H.Ohshima : "Zeta Potential" Scientist Ltd.Japan, January 1995

Step	Chemicals and composition	Temp. (℃)	Removal matter
APM	NH_3OH / H_2O_2 / H_2O	50～70	Particle, Organic Metal (alkali)
Rinse	UPW	Hot or R.T.	
HPM	HCl / H_2O_2 / H_2O	60～80	Particle, Metal
Rinse	UPW	R.T.	
Vapor dry	I.P.A.	80～85	

Table.1 Wet cleaning method of Sub micron ULSI fabrication.

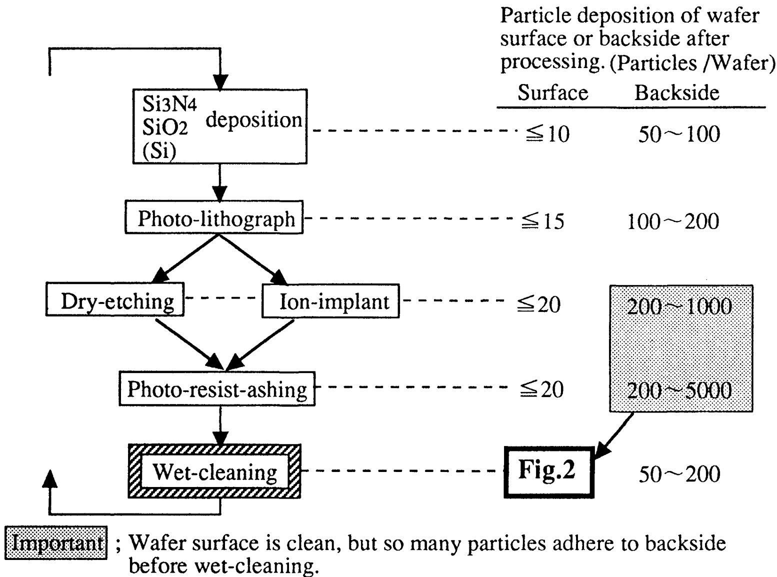

Fig.1 Number of particle of wafer surface or backside in the process flow.

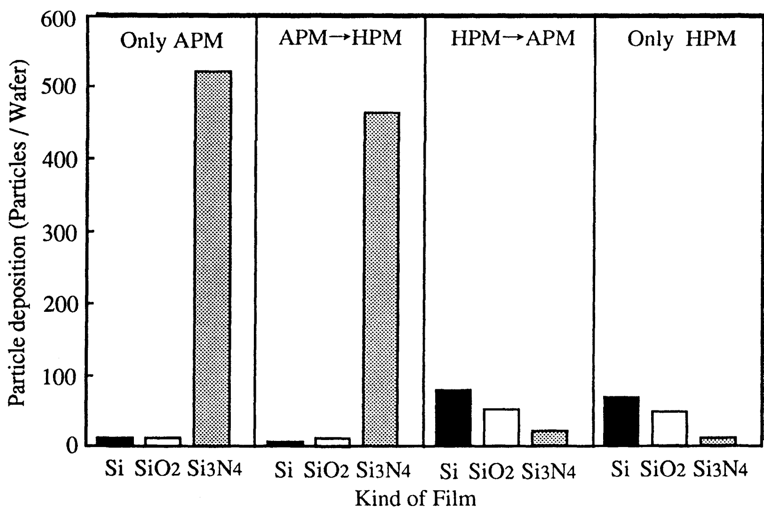

Fig.2 Particle contamination onto various wafer surfaces four kinds of cleaning methods.

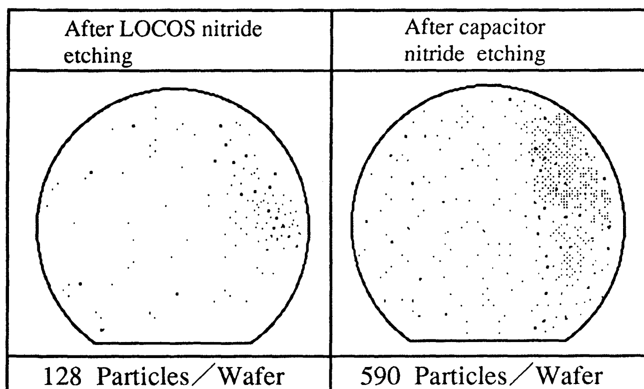

Fig.3 Particle contamination onto Si_3N_4 depo-wafer surface in special process after APM wet-cleaning.

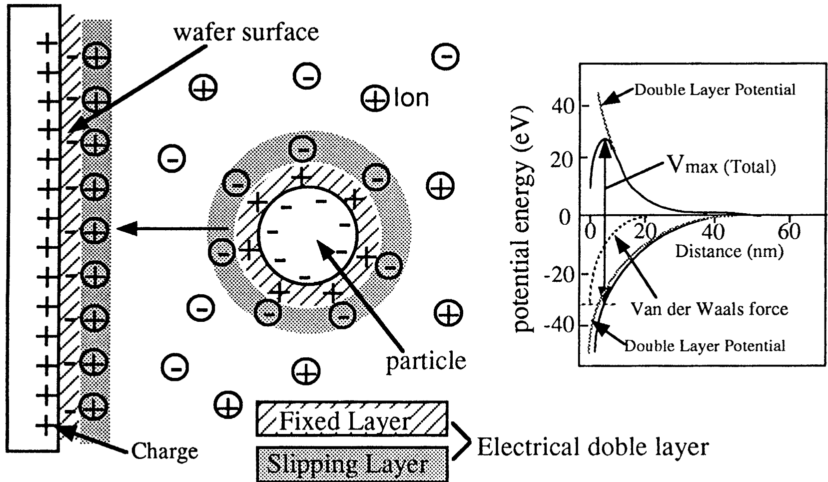

Fig.4 Zeta potential energy between wafer surface and particle in the cleaning solution.

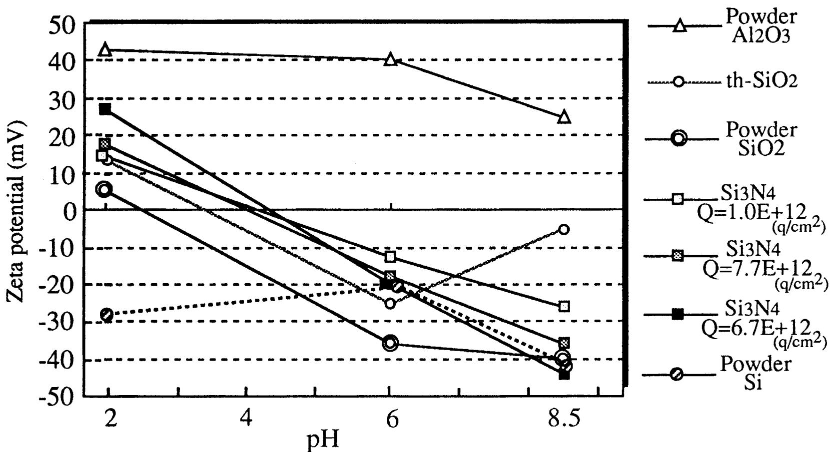

Fig.5 Zeta potential of various film on Si wafer and powder as a function of solution pH.

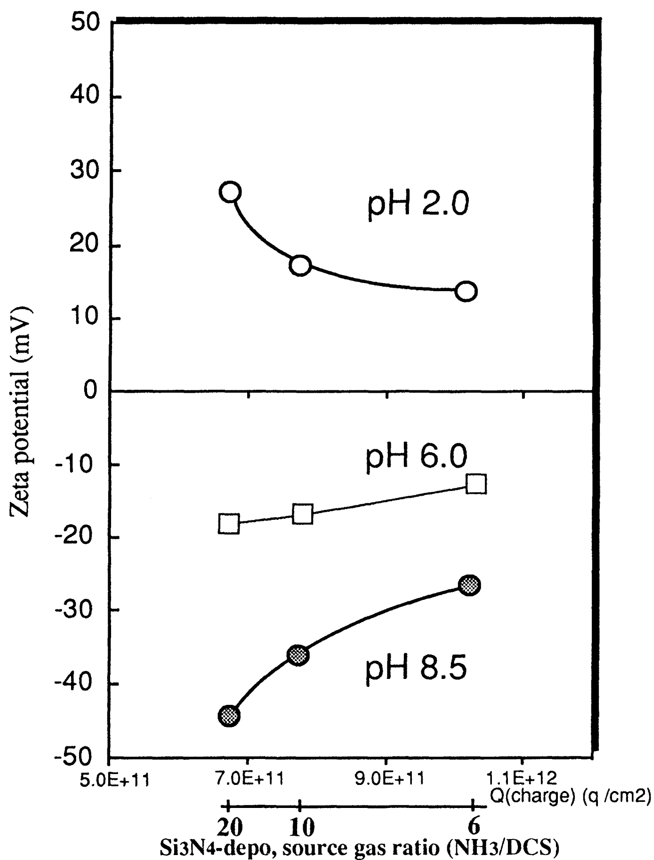

Fig.6 Zeta potential of Si_3N_4 film on Si wafer depend on surface electron capacitance or depo source gas ratio function of solution pH.

Q-Measure equipment: Surface Charge Analyzer

EFFECTS OF SEQUENTIAL CHEMISTRIES ON PARTICLE REMOVAL

K. K. Christenson, S. M. Smith, S. Nelson, B. Carlson, C. Bode* and K. Johnson**
FSI International, 322 Lake Hazeltine Dr., Chaska, MN 55318
* Univ. of Illinois at Urbana Department of Chemical Engineering
** Univ. of Minnesota Department of Chemical Engineering

ABSTRACT

This report compares the particle removal efficiency of an "APM Only" clean to that of HF Last (SPM, DHF, O_3) and B Clean (SPM, DHF, APM, HPM) cleaning sequences on Si_3N_4 particles in a spray processor. In the B Clean and APM Only cleans, the APM dispense time was varied from 3 to 12 minutes and the solution temperature at the spray post between 60° C and 95° C. Removal efficiencies for short APM dispense times were substantially better for those recipes containing a 90-second, 100:1 DHF etch. For a given removal efficiency, there was also less increase in surface haze for chemistry sequences containing DHF. With extended dispense times of 6-12 minutes, all chemistries were able to remove more than 98% of deposited Si_3N_4 particles >0.15 microns.

INTRODUCTION

Particle removal is one of the most widely studied aspects of wet chemical cleaning, particularly in the APM chemistry (1). The exact mechanism of removal in APM is unproved, but five factors seem to play an important role. First, the APM slowly etches the SiO_2, undercutting and releasing the particles. Second, the electrostatic charge, or Zeta potential, on the silicon wafer surface and most particles in APM solutions is strongly negative (2). These charges cause a repulsion between the wafer and particle, which enhances particle lift off and impedes redeposition. Third, the ionic strength of the solution affects the distances at which the repulsion is significant. Fourth, some types of particles could be dissolved by the APM. And finally, particles that are dislodged must be transported away from the wafer surface before they redeposit or dry in place (3). An etch of bulk SiO_2 or the native oxide by dilute HF is similar to an APM treatment in these factors, except that the Zeta potentials are positive. Therefore, etching the native oxide with DHF would remove a significant fraction of the particles.

EXPERIMENT

P type, <100>, 150 mm CZ wafers were initially pre-cleaned to near background levels in an FSI MERCURY® MP centrifugal spray processor with a B Clean chemistry

sequence (SPM, DHF, APM, HPM). Si_3N_4 particle challenge wafers were prepared by immersing cleaned wafers in DI water containing finely ground Si_3N_4 powder that had been dispersed by agitation in an ultrasonic bath (4). These Si_3N_4 wafers were prepared to conform to the particle removal challenge requirements laid out in the SIA road map (5). Counts of particles larger than 0.15 μm were measured on a Tencor Surfscan 6200, programmed for a 3 mm edge exclusion. Contaminated wafers typically had 10,000 to 20,000 light scattering defects, more than 50% typically registered between 0.15 and 0.3 micron diameter and 90% registered under 1.0 micron. The increase in surface haze, the diffuse light scatter normally associated with surface roughness, was determined by measuring the haze readings of pre-cleaned wafers before and after the cleaning treatment. Each run contained six Si_3N_4 contaminated and six bare silicon haze wafers in which particle removal and haze performance, respectively, were averaged.

A single run of each experimental treatment was carried out in the spray processor. See simplified plumbing diagram, shown in Figure 1. In the spray processor, Ashland SEMI grade chemicals and water were blended on-line and sprayed onto the wafers. In the APM Only portion of the experiment, the Si_3N_4 particle and bare Si wafers were exposed to 16 treatments in a 2x2x4 full factorial matrix of APM concentration, temperature and exposure times. The levels were 25:25:1500 and 125:125:1500 cc/minute NH_4OH:H_2O_2:H_2O for blend ratio; 60° C and 95° C for temperature at the spray post, and 3, 6, 9 and 12 minutes for APM dispense time. The following process sequence was used:

- 5 minute water rinse to preheat the wafers to the steady state process temperature
- 3 to 12 minute APM dispense at 60 RPM with 20 second, 500 RPM ramps every 90 seconds
- 4.5 - minute rinse in hot DI water, utilizing ramped rinsing (3)
- 6 - minute spin dry

Due to a 90 cc/minute practical lower limit on the flow systems, the H_2O_2 and NH_4OH were diluted 4:1 in the canister to achieve effective flow rates of 25 cc/minute for these chemicals when required. The in-line temperature at the spray post was varied between 60° C and 95° C using an in-line infrared chemical heater (6). Heat loss through processes such as evaporation reduced the on-wafer temperature from 60° C and 95° C to approximately 50° C and 70° C. A constant total APM flow rate of 1760 cc/minute was used for all treatments so that the transient and steady state on-wafer temperatures were the same (6).

In the B Clean portion of the experiment, the APM chemistry was preceded by a 90-second dispense of SPM and a 90-second dispense of 100:1 DHF. The APM within the B Clean sequence was varied in the same way as the APM Only treatments, a 2x2x4

full factorial matrix of APM concentration, temperature and exposure times. The APM was followed by an HPM to remove metallics. The HF Last / O_3 treatment consisted of a 90-second dispense of SPM, a 90-second dispense of 100:1 DHF and a 10-minute rinse in ozonated DI water (10 ppm).

RESULTS AND DISCUSSION

Figure 2 shows the variation of removal of Si_3N_4 particles for the APM Only treatments (7). Treatments in which labels do not include "+ IRH" had a spray post temperature of 60° C and those that include "+ IRH" are at 95° C. The removal of Si_3N_4 improves with increased temperature and dispense time, but is relatively unaffected by the concentration of the APM. The low removal efficiency during the first 3 minutes of the 95° C APM and 6 minutes of 60° C APM may be due to some minimum etch that is required to undercut the particles. The etch rates for bulk, thermal SiO_2 at 95° C and 60° C are 1 to 2 and 0.3 to 0.6 A/minute respectively (8). Both 95° C treatments achieved 99% removal after 9 minutes and 99.9% removal after 12 minutes.

Figure 3 shows the removal characteristics for various chemistry sequences including a DHF step. The HF Last treatment shown at "0" minutes of APM had a removal efficiency of 86% after removal of the native oxide. It remains to be determined whether the DHF is the sole particle removal agent or if the SPM and O_3 chemistries aided in the particle removal. In the B Clean sequences, there is little increase in particle removal at a 3 minute exposure time with concentrated (0.5:0.5:6) APM. This is consistent with the removal characteristic of APM only at 3 minutes. Further, the removal efficiency during the first several minutes is expected to be low because pre-heating was not used in the B Clean sequence as in the APM Only sequence. Both B Clean treatments with concentrated APM achieved 98.5% removal after 12 minutes.

Unlike the lack of effect in the first three minutes of *concentrated* APM mentioned above, there was an unexpected *reduction* in particle removal efficiency compared to the HF Last process when a 3 minute *dilute* APM was used in the B Clean sequence. One possible explanation is the redeposition of Si_3N_4 particles when the pH of the solution rises. In the low pH DHF solution, both the SiO_2 and the Si_3N_4 have positive Zeta potentials and will repel (2). In the high pH APM solution, both have negative Zeta potentials, resulting in a repulsive force. But during the transition from low to high pH, the SiO_2 will become negatively charged while the Si_3N_4 is still positively charged and the particles will be attracted to the surface. The range of this attractive force depends on the ionic strength of the fluid. Solutions with high ionic concentrations screen the charges of the wafer and particles over a shorter distance than do dilute solutions. Therefore, we would expect the attractive forces that drive redeposition to

have a longer range and to be more effective in dilute solutions. It may be possible to eliminate this effect by more thorough rinsing after the DHF so that there are no particles present at the beginning of the APM dispense.

Figure 4 shows the particle removal trends with APM dispense time for 4 B Clean and 8 APM Only recipes with varying APM concentrations and temperatures. The 8 APM recipes each have between 8% and 35% removal efficiencies with the initial 3 minute APM dispense. Removal efficiency improves substantially with increased APM exposure time in all cases. In contrast, the B Clean recipes have removal efficiencies between 62% and 88% with a 3 minute APM dispense; and the improvement in removal efficiency is not as rapid with increasing APM dispense.

Figure 5 shows the increase in surface haze as a function of particle removal efficiency for APM Only and B Clean sequences. Cleans employing the sequential B Clean chemistry showed significantly lower increases in haze than did APM Only cleans with equivalent particle removal. One possibility is that the increase in haze is due primarily to "nano-precipitates" of metals from the APM solution. These species would have been removed by the HPM step in all of the B Clean treatments. It has not been determined whether this represents a real lack of surface roughening or some other surface characteristic of APM Only wafers that increases the diffuse scatter of light.

There has been concern that wet chemical techniques will not remove small particles due to the lack of mechanical force supplied by fluid sheer, Megasonics, etc. Figure 6 shows the particle removal efficiency of the concentrated APM Only at 95° C broken out by particle size. There is no evidence that the small particles (>0.15 micron) are more difficult to remove than the large particles (1-5 micron). To the contrary, within the accuracy of this experiment, the larger particles are removed more slowly! This is consistent with the "under cut" theory of particle removal --- i.e., it is easier to under cut a small particle than a large one. This implies that the mechanical forces involved are of little consequence.

CONCLUSION

In a spray processor, sequential cleaning chemistries containing DHF are able to remove over 80% of the Si_3N_4 particles from a silicon wafer with a native oxide. While there is an interaction between the removal by DHF and a subsequent APM leading to decreased removal efficiency for short APM dispenses, removal efficiency is increased to greater than 98% by long APM dispenses after the DHF. Cleans employing the sequential B Clean chemistry showed significantly lower increases in haze than did APM Only cleans with equivalent particle removal. It has not been determined whether this represents a real lack of surface roughening or some other surface characteristic of

APM Only wafers that increases the diffuse scatter of light. Finally, the data indicates that the efficiency of the particle removal mechanism in the spray processor improves with smaller particles.

ACKNOWLEDGMENTS

Susan Cohen of IBM and Carol Adkins and Peggy Clews of Sandia provided guidance on the preparation of Si_3N_4 particle challenges. We would also like to thank Don Grant of CT Associates for suggestions regarding the experimental design and preparation of particle challenges.

REFERENCES

1. M. Itano, F. Kern, M. Miyashita and T. Ohmi, "Particle Removal From Wafer Surface in Wet Cleaning Process," *IEEE Transactions on Semiconductor Manufacturing,* 6:258 (1993).
2. R. Donavan in "Intensive Short Course in Semiconductor Wafer Cleaning Technology," presented in February 1993 in Austin, TX by Werner Kern Associates, East Windsor, NJ, (1993).
3. K. K. Christenson, "The Use of Centrifugal Force to Improve Rinsing Efficiency," *Proceedings of the Third International Symposium on Cleaning Technology in Semiconductor Device Manufacturing* edited by J. Ruzyllo and R. Novak (The Electrochemical Society, PV 94-7, Pennington, NJ, 1994) pp. 153-162.
4. Susan Cohen, Carol Adkins and Peggy Clews, private communications, 1995.
5. The National Roadmap for Semiconductors, Semiconductor Industry Association, San Jose, CA, (1994) p. 116.
6. K. K. Christenson, "The Effects of Increased Temperature in a Centrifugal Spray Processor," *Proceedings of the Third International Symposium on Cleaning Technology in Semiconductor Device Manufacturing* edited by J. Ruzyllo and R. Novak (The Electrochemical Society, PV 94-7, Pennington, NJ, 1994) pp. 474-483.
7. K. K. Christenson, S. M. Smith, C. Bode and K. Johnson, "Effects of SC-1 Dilution and Temperature on Various Particle Removal Challenges," *Proceedings of the Fourth International Symposium on Cleaning Technology in Semiconductor Device Manufacturing* edited by J. Ruzyllo and R. Novak (The Electrochemical Society, Pennington, NJ, 1994) to be published.
8. K. K. Christenson and S. M. Smith, "Effects of SC-1 Dilution and Temperature Variations on Etch Rate and Surface Haze," *MRS Spring Symposium Proceedings* edited by Liehr, Hirose, Heyns and Parks (The Materials Research Society, Pittsburgh, PA, 1995) 386, to be published.

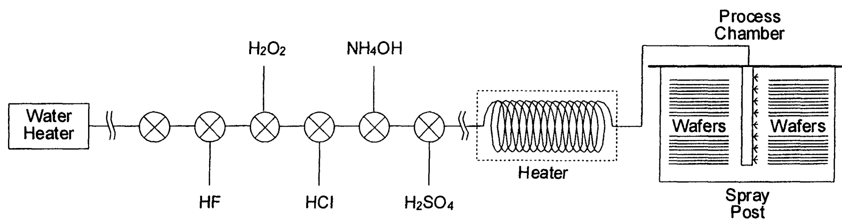

Figure 1: Simplified MERCURY MP Spray Processor Plumbing Diagram

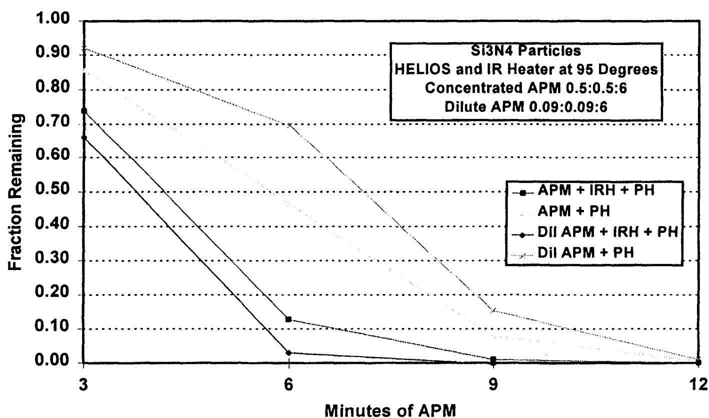

Figure 2: Variation of Particle Removal by APM with Time

Si_3N_4 Particles remaining after an APM in a FSI MERCURY MP vs time. "IRH" denotes infra-red heater and indicates a run at 95° C.

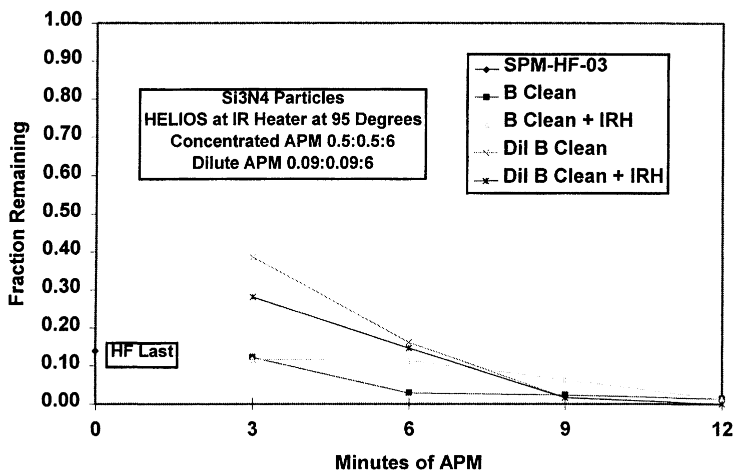

Figure 3: Particle Removal with B Clean and HF Last Chemistry Sequences

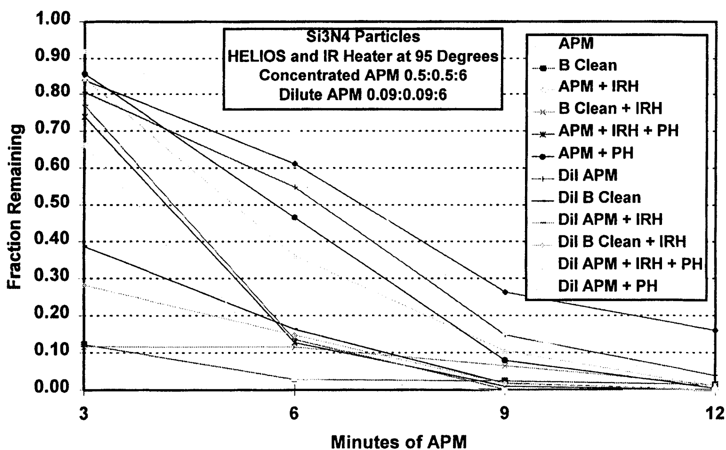

Figure 4: Particle Removal for APM Only vs B Clean Chemistry Sequences

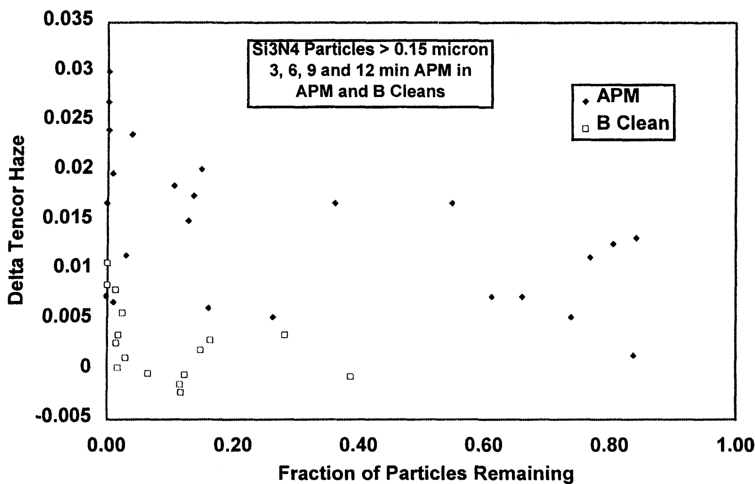

Figure 5: Delta Haze for All of the Treatments in Figure 4

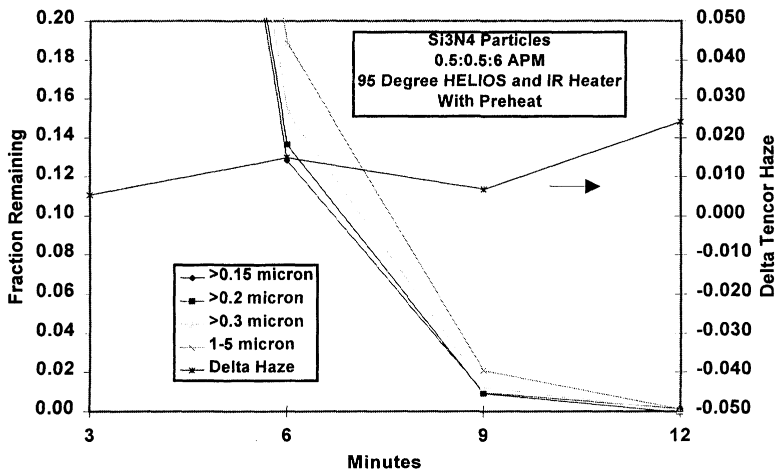

Figure 6: APM Particle Removal

PARTICLE IMPACT ON 7 nm GATE OXIDES

C. Paillet*, A.M. Papon, J.P.Joly and F. Tardif
GRESSI-LETI, CEN/G, 17, Rue des Martyrs
38054 Grenoble Cedex 9, France

D. Levy, K. Barla, P. Patruno
*SGS/THOMSON Centre Commun 38290 Crolles, France

ABSTRACT

The detrimental effects of particles are more and more important the thinner the gate oxide thickness. The influence of intentionally deposited particles on thin oxide infant breakdown depends on their nature and sizes. TEM observation with high magnification shows the presence of a peak which can explain this impact.

INTRODUCTION

Both particles and ionic contaminants have been drastically reduced during the last few years. Quantification of the impact of metallic contamination on gate oxide has been widely reported by many authors[1][2]. On the other hand the impact of particles on such gate oxide is not very well documented. This may be due to the low impact of particles on relatively thick oxide. But, as the gate oxide thickness decreases, we expect it to become increasingly sensitive to particles. Particles can of course contain metallic contamination and in this case we can refer to the work carried out in this field.
In this paper, the impact of different types of particles was studied on P-type <100> 14-22 Ω.cm. wafers. TEM observation of thin oxide grown under particles will be presented and an oxide destruction mechanism proposed.

PARTICLE IMPACT

The influence of particles was investigated by intentional contamination of two kinds of silicon wafers : hydrophobic after an HF dip or hydrophilic after an RCA cleaning process which leaves a 0.8 nm chemical oxide.
The contaminations were performed by dipping a large number of wafer-tests into D.I. water spiked with well characterised particles. In order to study the starch impact, SiO_2 and Al_2O_3 particles which are stable at high temperature were chosen (refractories). Furthermore, carbon particles were also used on hydrophilic wafers and "natural particles" from a non especially contaminated HF bath were also deposited on hydrophobic wafers. Surfscan 6200 (Tencor, Mountain View, USA) measurements were performed before and after contamination. Only the wafers which presented a fairly homogeneous particle distribution were kept (20%). The selected wafers were then heated to 900°C in dry conditions (no HCL or TCA) to grow a 7 nm oxide.

After patterning, capacitors of both 0.06 and 17 mm^2 were electrically tested. Ebd measurement performed on the small capacitors indicates good intrinsic performances with no detected correlation with the amount of deposited particles. On the other hand, the integrity of the larger capacitors was affected by infant breakdown referred to as "pinholes" . The defect densities D were determined from the obtained yields η using Poisson's law :

$$\eta = e^{-A \cdot D} \quad \text{With A: capacitor area.}$$

Figures 1 and 2 show that if the particles are uniformly spread at the wafer surface, then we verify that a linear correlation exists between defect density and particle concentration. On hydrophilic wafers, particles lead to less detrimental effects than on hydrophobic ones.
The importance of native oxide quality is also demonstrated. According to our experience, if we consider one particular cleaning, the 7 nm gate oxide sensitivty to particles is affected by both their physical nature and intrinsic thermal oxide properties. Furthermore, we suspect the ability of the different oxidant cleanings to separate the particles from the silicon by their capacity to "under-grow" their chemical oxide under the particles to have a decisive impact. Figure 3 shows the superiority in terms of pinholes of the higher oxidant cleaning : Sulphuric Peroxide Mixture as called Caro's acid. This behaviour has always been confirmed at Leti. Even with a high level of particles, the thin oxides grown after a Caro cleaning step always present a high yield at zero electrical field. This substantial advantage explains why this cleaning was quite popular before gate oxide : in a single bath, Caro mixture removes organics and a large amount of metals, smooths the surface, and desensitives oxide to particles.

DAMAGE MECHANISM

In order to understand the failure mechanism leading to electrical oxide integrity loss, hydrophilic wafers were intentionally contaminated with a very large amount of Al_2O_3 particles by drying a Di water solution contaminated with particles. After oxidation, a thick polysilicon embedding layer was deposited. The wafers were then cleaved and observed using an AKASHI 002B Transmission Electron Microscope (XTEM) working at 200 KV.
Cross-sections prepared using the usual mechanical polishing down to 30 µm thickness were then ion-milled at 6 KV. Extreme mechanical polishing (3) was also used to obtain a larger thin surface with several particles accessible.
In figures 4 and 5, we can see a particle, the silicon/oxide and oxide/polysilicon interfaces. We can clearly distinguish that the oxide layer presents an accident under the particle. The oxidation process was unexpectedly enhanced under the particle leading to a higher global quantity of oxide and the corresponding lack of consumed silicon. Near the particle boundary a very thick oxide is visible. Under the particle, a peak can be seen. This effect was checked on the other neighbouring particles (fig 6).

DISCUSSION

The hydrophobic surfaces seem to be more sensitive to particles than the hydrophilic ones. This behavior could be explained by the relative protection provided by a 0.8 nm chemical oxide.
The silicon protuberance observed under the particle could induce an electrical peak effect. As depicted on figure 7, aluminum contamination increases the oxide growth rate. Nevertherless, the enhancement of the oxide under the particle can only partially be explained by this effect.

CONCLUSION

All the studied particles deposited on wafers before 7 nm oxidation generate infant breakdown. The destruction efficiency is variable with the types and natures of the different particles. The highly oxidant cleaning Caro desensitives the following thermal oxide to particles.
The TEM cross-section under a particle reveals a silicon peak which could explain the electrical consequences.

REFERENCES

1. Critical aspect of wafer cleaning and gate oxide integrity. P.W. Mertens, M. Meuris, ECS proceedings p. 87, vol. 93-15.

2. Impact study of the use of ULSI, VLSI and MOS grade chemicals in the RCA cleaning process on MOS and bipolar devices, F. Tardif, J.P. Joly, ECS proceedings p. 114, vol. 93-15.

3. J.P. Benedict, S.J. Klepeis, W.P. Vandygrift and Ron Anderson, IBM, East Fishkill Laboratory, EMSA Bulletin 19: 2,74-1989)

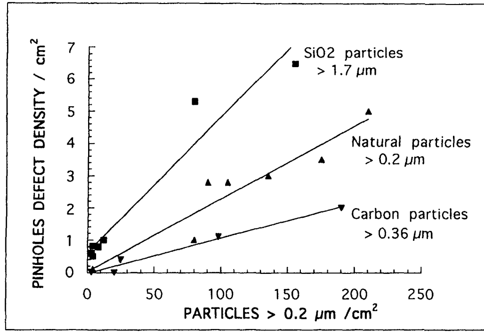

Figure 1 : Impact of particles on initially hydrophilic wafers

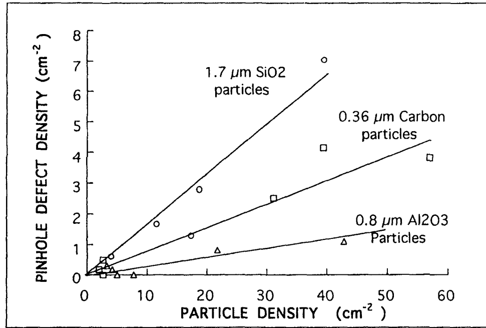

Figure 2 : Impact of particles on initially hydrophobic wafers

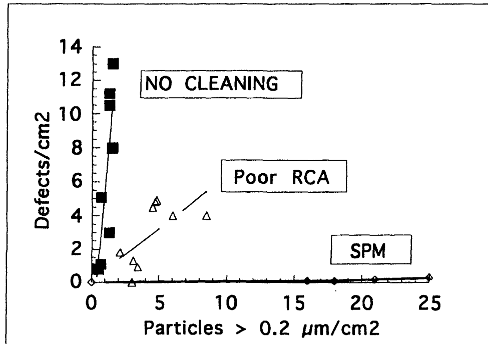

Figure 3 : Example of 7 nm dry oxide sensitivity to the same "natural" particles for different pre-gate cleanings.

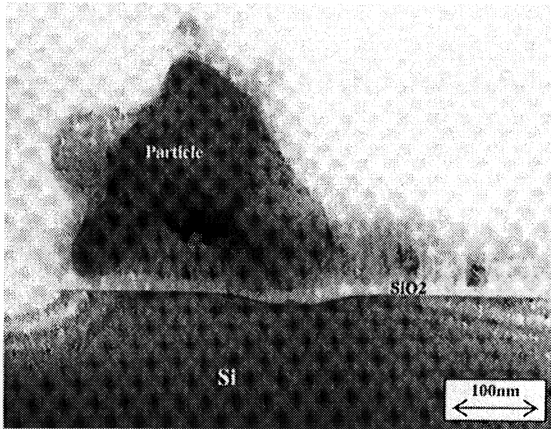

Figure 4 : TEM picture of a 7 nm gate oxide grown with an Al2O3 particle. Particles were deposited on a wafer presenting a 0.8 nm chemical oxide.

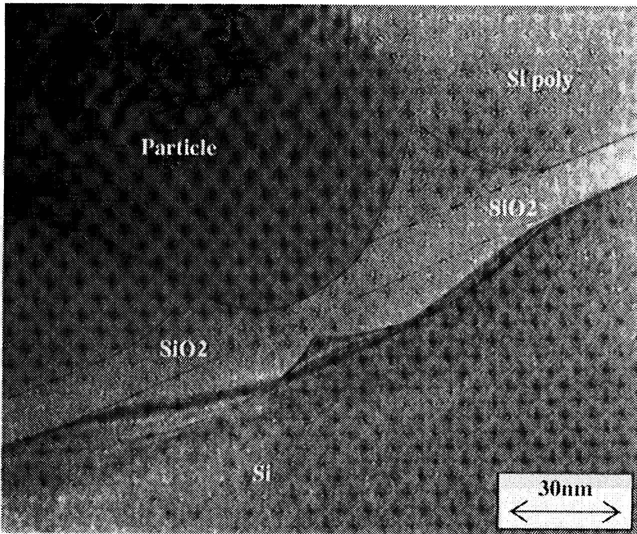

Figure 5 : Details of the same particle impact with typical features underlined.

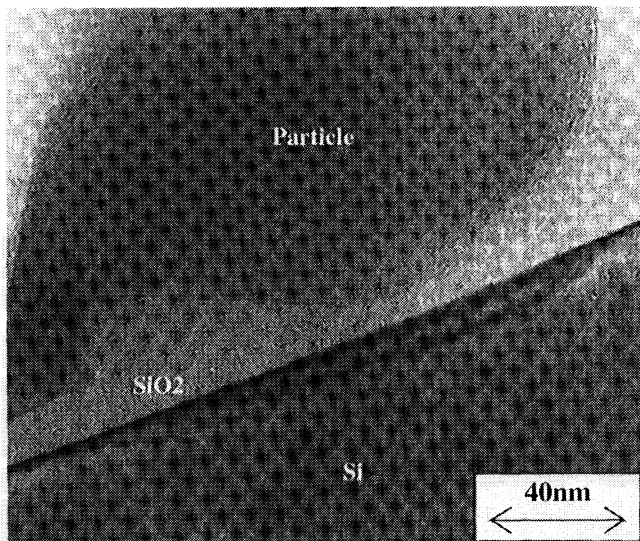

Figure 6 : Other TEM picture of 7 nm gate oxide grown with Al_2O_3 particule.

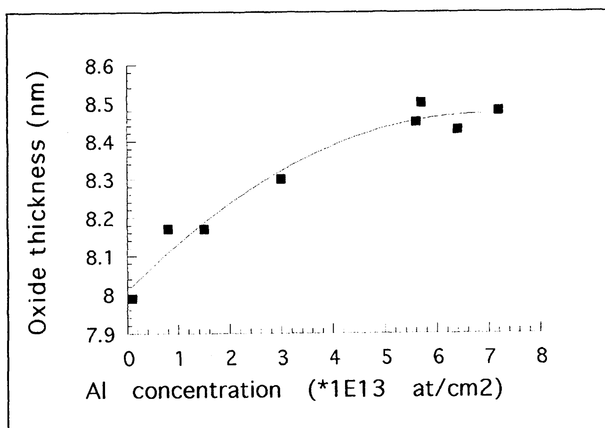

Figure 7 : Impact of Aluminum on oxide growth rate (900 °C, O_2)

ASPECTS OF ALUMINA PARTICLE DEPOSITION ONTO CVD TUNGSTEN WAFERS RELEVANT TO POST CMP CLEANING

Joong S. Jeon, Chilkunda Raghunath, Emil A. Kneer, and Srini Raghavan
Department of Materials Science & Engineering
University of Arizona
Tucson, AZ 85721

ABSTRACT

The electrochemical behavior of CVD tungsten wafer was investigated using a DC potentiodynamic polarization technique to elucidate the role of solution pH and H_2O_2 on the passivation characteristics of tungsten. Particle deposition experiments were performed to understand conditions which may affect the deposition of alumina particles onto CVD tungsten wafers. From a dispersion of high purity alumina particles (IEP=8.5) maintained at a pH of 4.1, tungsten biased as a cathode showed more particle contamination than that biased as an anode. As the value of pH increased from 4.1 to 9.5, the extent of particle deposition was decreased. The extent of high purity alumina particles deposited on cathodically biased tungsten decreased upon the addition of H_2O_2.

I. INTRODUCTION

Tungsten films deposited by LPCVD (low pressure chemical vapor deposition) find use as diffusion barriers, gate contacts and multilevel metal connections in integrated circuit devices.[1,2] The most widely used LPCVD method to form tungsten films on silicon is the hydrogen reduction of tungsten hexafluoride. The planarity of tungsten films is critical to the development of multilevel metallization schemes. Chemical mechanical polishing (CMP) process is attracting considerable attention as the planarization process of choice for tungsten films.[3,4] Colloidal alumina based slurries are favored for tungsten CMP. Using a particulate slurry containing $K_3Fe(CN)_6$ as an oxidant, ethylene diamine as a complexing agent and KH_2PO_4 as a pH buffer, it has been shown that the mechanism involved in CMP of tungsten is one of formation of a passive oxide layer followed by the removal of passivated layer through the abrasive action of slurry particles.[5] Rapid repassivation of bare tungsten surfaces exposed during polishing also appears to be an important criterion. Acidic alumina slurries ($pH \approx 4.1$) containing an oxidant such as hydrogen peroxide are currently used for tungsten CMP.

The deposition of alumina particles on tungsten surfaces during the polishing process is an important issue that needs to be characterized to develop post CMP cleaning techniques. This paper presents the results of electrokinetic, electrochemical

and controlled particle deposition investigations carried out to understand the conditions which may affect the deposition of alumina particles onto CVD tungsten wafers.

II. EXPERIMENTAL MATERIALS AND METHODS

LPCVD tungsten films (thickness $\approx 0.8\mu m$) were prepared by the reduction of WF_6 in a Genus reactor on 6" silicon substrates coated with a TiN adhesion layer (thickness $\approx 0.05\mu m$). For particle deposition experiments, alumina particle dispersions were prepared from high purity (99.9%) alumina particles.

The zeta potential of alumina powder was measured by an electrophoretic technique using a Laser Zee Meter (Model 501, Pen Kem). The electrokinetic properties of tungsten wafers were characterized by a streaming potential technique using an Electrokinetic Analyzer (Brookhaven Inst. Corp.) in conjunction with a specially designed cell to handle 6" wafers.[6] Electrokinetic measurements on CVD tungsten wafers were made after the following treatments; (1) etching in a K^3 etch solution [34g of KH_2PO_4, 13.4g of KOH and 33g of $K_3Fe(CN)_6$ in 1 liter H_2O],[7] and (2) anodic oxidation in a mixture of 0.4M HNO_3 and 0.04M KNO_3.[8]

Anodic potentiodynamic polarization of tungsten wafers was carried out using Potentiostat/Galvanostat (EG&G 273A) at a scan rate of 0.5 mV/sec. Tungsten samples were exposed to solutions using a flat cell, and the potential of tungsten samples was measured with respect to a saturated calomel electrode.

Alumina particle deposition experiments were performed by an electrophoretic method. A potential of 10 V was applied between a diced CVD tungsten wafer sample (15mm x 15 mm) and a titanium electrode separated by a distance of approximately 1 cm. The pH of alumina dispersions was maintained at 4.1, 6.8 or 9.5. During particle deposition, tungsten samples were biased anodically or cathodically. Some particle deposition experiments were also performed under no bias conditions (i.e., by dipping in the dispersions). Unless otherwise specified, tungsten samples were cleaned in DI water after particle deposition. Cleaning of contaminated tungsten samples was carried out using a dynamic contact angle analyzer (Cahn DCA 312) by immersing and then withdrawing the samples from DI water at a speed of 264 μm/sec. Contaminated and cleaned samples were characterized for particle level using a field emission-scanning electron microscope (Hitachi S4500).

III. RESULTS AND DISCUSSION

As a first step towards understanding the behavior of tungsten under solution conditions that prevail during tungsten CMP, thermodynamic data on tungsten species

were collected and analyzed through the construction of an Eh-pH (Pourbaix) diagram shown in Fig. 1. This diagram was drawn assuming an activity of 10^{-4} for all dissolved tungsten species. It may be seen from this figure that WO_3(s) is a stable phase only at pH values less than 2, while WO_2(s) exists over a wide range of pH values at moderately reducing conditions (slightly negative Eh values). Hydrogen peroxide based commercial tungsten CMP slurries are characterized by a pH value of 4 and an Eh value of 0.57 V. Under these Eh and pH conditions, $W_{12}O_{41}^{-10}$ is the most stable phase. If the dissolution of WO_2 to $W_{12}O_{41}^{-10}$ is slow, then the presence of WO_2 may be expected on tungsten during CMP.

The anodic potentiodynamic polarization behavior of tungsten at different pH values in 0.1 M KNO_3 solution is shown in Fig. 2. The polarization curves at all pH values indicate the formation of a passive layer that inhibits dissolution to varying degrees. The magnitude of the constant current density (passive current density ?) at a pH value of 2 was smaller than those at other pH values. This indicates that the surface layer formed at a pH of 2 has better passivation characteristics. It is interesting that a passive layer appears to form even at pH values higher than 4.5. It may be recalled that the Eh-pH diagram predicts the formation of WO_3 only at very acidic pH values. As pointed out earlier, the passive layer may well be WO_2 whose rate of dissolution is slow.

Fig. 3 shows the anodic potentiodynamic polarization behavior of tungsten in solutions containing hydrogen peroxide at a pH value of 4. It may be seen from this figure that the addition of H_2O_2 caused an increase in the open circuit potential of tungsten. As the concentration of H_2O_2 increased, the active as well as passive current densities were increased significantly. For example, addition of 1% H_2O_2 increased the passive current density value by two orders of magnitude. This indicates that H_2O_2 is actually etching rather than passivating tungsten.

Fig. 4 shows the results of zeta potential measurements carried out on high purity alumina powder and CVD tungsten wafers. The isoelectric point (IEP) of high purity alumina powder was measured to be approximately 8.5. Tungsten wafers cleaned by etching in a K^3 etch solution were characterized by a more negative zeta potential than the oxidized tungsten wafers, and both types of wafers exhibited negative zeta potential values of -10 to -50 mV in the pH range of 4 to 10. It may be concluded from this figure that the deposition of high purity alumina particles on a tungsten surface is favorable at pH values below 8.5.

Fig. 5 shows SEM micrographs of alumina particles deposited on CVD tungsten wafers in the absence of any electrical bias from dispersions containing 2.5 g/l high purity alumina powder at three different pH values. These contaminated samples were cleaned in DI water prior to SEM characterization. As the value of pH increased from 4.1 to 9.5, the extent of particle deposition was decreased. At a pH value of 4.1, the

tungsten surface was highly contaminated with alumina particles, while at a pH value of 9.5, only a few particles were found on tungsten surfaces. This result may be expected from the results of zeta potential measurement displayed in Fig. 4.

The results of particle deposition from dispersions containing 2.5 g/l high purity alumina powder under different bias conditions at a pH value of 4.1 are shown in Fig. 6. Experiments under applied bias conditions were carried out for two reasons; (i) to confirm the importance of electrostatic attraction in particle deposition, and (ii) to maintain the deposition surface as tungsten or tungsten oxide during deposition. CVD tungsten samples prepared under a cathodic bias condition were completely covered with alumina particles. Under no bias conditions, tungsten surface was only partially covered with alumina particles, while anodic bias resulted in the least amount of contamination. Higher amount of alumina deposition on tungsten under cathodic and no bias conditions is not surprising considering that the zeta potential of alumina particles at a pH value of 4.1 is positive, while the zeta potential of CVD tungsten wafers at the same pH is negative. This implies that the electrostatic interaction between alumina particles and CVD tungsten wafers play an important role in particle deposition.

The effect of H_2O_2 addition on particle deposition on CVD tungsten samples biased anodically or cathodically in dispersions containing 2.5 g/l of high purity alumina powder at a pH value of 4.1 was also investigated. The results of these experiments are shown in Fig. 7. As shown earlier (Fig. 6), in the absence of H_2O_2, a cathodic bias resulted in a much higher particle contamination. Micrographs in Fig. 7 show that increasing the amount of H_2O_2 added to dispersions resulted in a reduction of particle deposition. This may be due to the etching of tungsten by OH^- ions formed by the reduction of O_2 resulting from the decomposition of H_2O_2. Under anodic bias conditions, H_2O_2 did not seem to have a marked effect on the extent of particle deposition which, to begin with, was actually small.

An attempt was also made to investigate alumina particle deposition on anodically grown tungsten oxide surfaces. It may be mentioned that this oxide layer was grown in a mixture of 0.04M HNO_3 and 0.4M KNO_3 for 20 sec, and was confirmed to be WO_3 by a X-ray diffraction technique. Particle deposition on oxidized tungsten samples was conducted under an anodic, cathodic or no biasing condition in dispersions containing 2.5 g/l of high purity alumina powder at a pH value of 4.1. The results of these experiments are shown in Fig. 8. It may be seen from this figure that under a cathodic bias condition, WO_3 surface was significantly contaminated with alumina particles. However, comparison of Fig. 8 to Fig. 6 would reveal that the extent of contamination on WO_3 surface is lower than that on a bare tungsten surface. Under no bias conditions, contamination on WO_3 surface was also markedly lower than that on bare tungsten surface. More systematic experiments are required to propose a mechanism for the difference in particle contamination levels on tungsten and WO_3 surfaces.

IV. CONCLUSIONS

DC potentiodynamic polarization curves for CVD tungsten indicate the formation of a passive layer that inhibits dissolution. Addition of H_2O_2 appears to result in dissolution rather than passivation of tungsten. From particle deposition experiments carried out at different pH values and under different types of electrical bias, the importance of electrostatic interactions in deposition was established. The extent of alumina particles deposited from dispersions of high purity alumina particles on cathodically biased CVD tungsten wafers decreased as the H_2O_2 concentration was increased.

ACKNOWLEDGEMENT

The authors acknowledge financial support provided by SEMATECH to carry out this work. Appreciation is also extended to the National Science Foundation for providing FE-SEM facility under grant number DMR 9311302 at the University of Arizona.

REFERENCES

1. E. K. Broadbent, J. M. Flanner, W. G. H. Van Den Hoek, and I. H. Connick, IEEE Trans. Electron Dev., **35**, 952 (1988).
2. E. K. Broadbent and W. T. Stacy, Solid State Tech., 51, Dec., 1985.
3. W. J. Patrick, W. L. Guthrie, C. L. Standley, and P. M. Schiable, J. Electrochem. Soc., **138**, 1778 (1991)
4. S. Sivaram, H. Bath, R. Leggett, A. Maury, K. Monnig, and R. Tolles, Solid State Tech., 87, May, 1992.
5. F. B. Kaufman, D. B. Thompson, R. E. Broadie, M. A. Jaso, W. L. Guthrie, D. J. Pearson, and M. B. Small, J. Electrochem. Soc., **138**, 3460 (1991).
6. D. Jan and S. Raghavan, J. Electrochem. Soc., **141**, 2465 (1994).
7. J. L. Vossen and W. Kern, Thin Film Processes, p. 475, Academic Press, New York, (1978).
8. F. D. Quarto, A. D. Paola, and C. Sunseri, J. Electrochem. Soc., **127**, 1016 (1980).

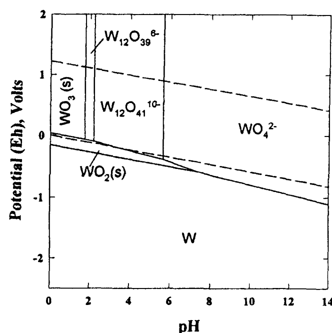

Fig. 1, Potential-pH equilibrium diagram for tungsten-water system at 25°C (dotted line represents water stability limits).

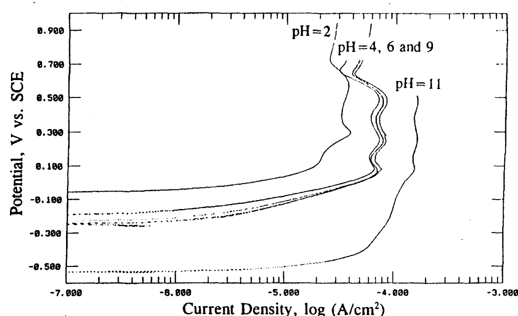

Fig. 2, DC potentiodynamic polarization curves for tungsten at different pH values.

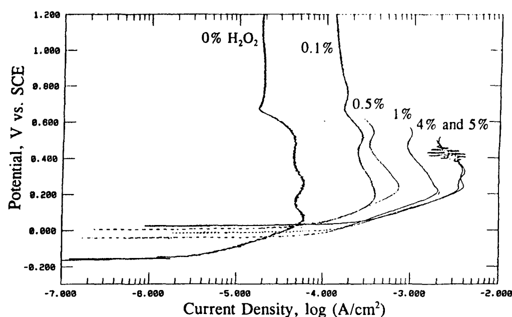

Fig. 3, DC potentiodynamic polarization curves for tungsten as a function of H_2O_2 concentration at a pH value of 4.

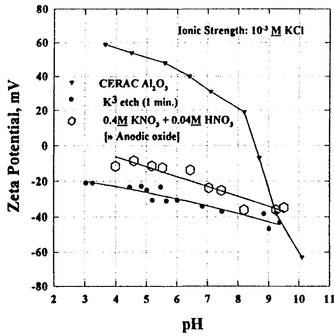

Fig. 4, Zeta potential of high purity alumina particles and CVD tungsten wafers subjected to different treatments.

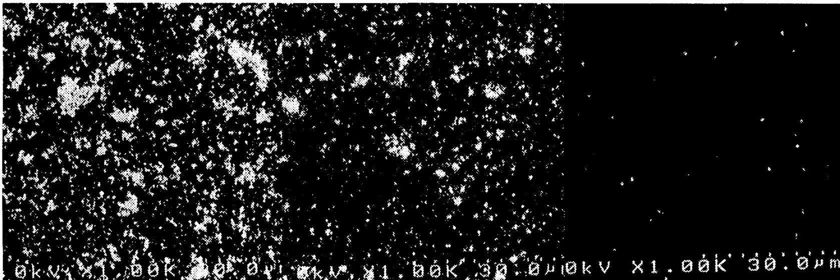

(a) (b) (c)

Fig. 5, Micrographs of alumina particles deposited on tungsten wafers in the absence of electrical bias. [pH: (a) 4.1, (b) 6.8 and (c) 9.5]

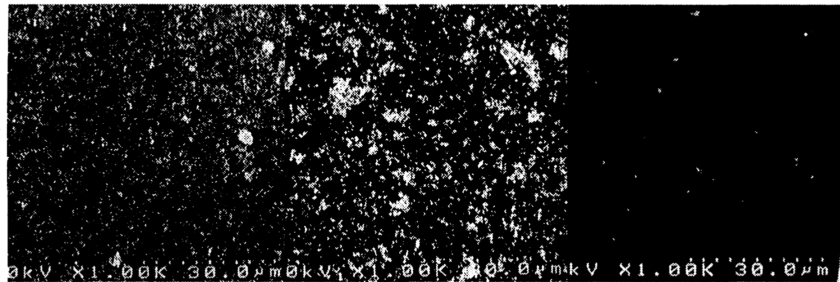

(a) (b) (c)

Fig. 6, Micrographs of alumina particles deposited on tungsten wafers at a pH of 4.1. [biasing condition: (a) cathodic, (b) none, (c) anodic]

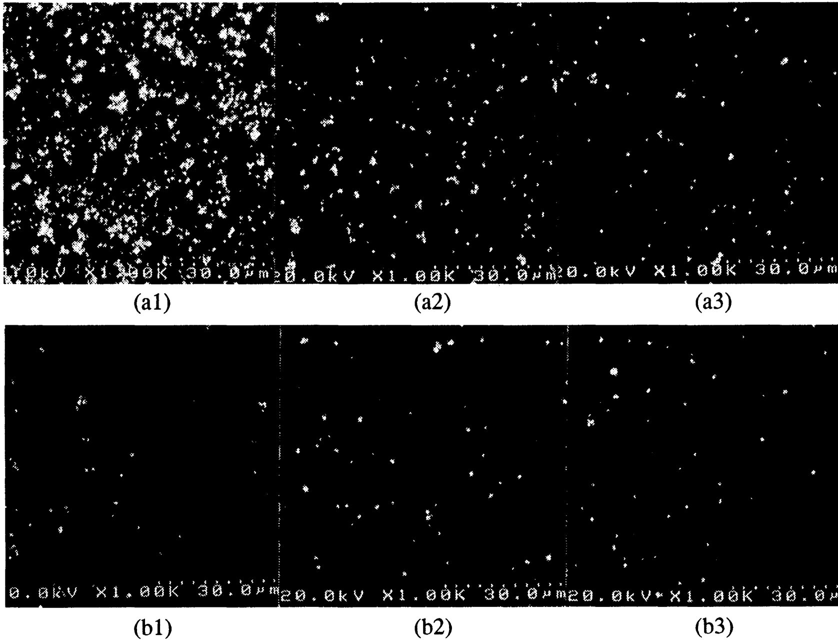

Fig. 7, Effect of H_2O_2 addition on particle deposition under cathodic (a) and anodic (b) biasing conditions at a pH of 4.1. [H_2O_2 concentration: (a1) and (b1): 10%; (a2) and (b2): 30%; (a3) and (b3): 50%]

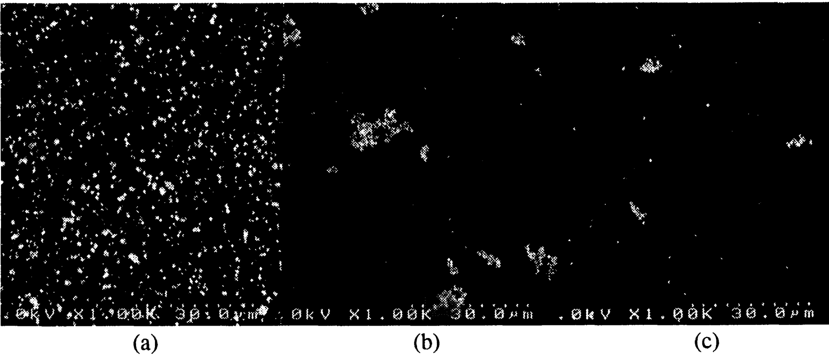

Fig. 8, Micrographs of alumina particles deposited on WO_3 surfaces at a pH of 4.1. [biasing condition: (a) cathodic, (b) none, (c) anodic]

A STUDY OF LIGHT POINT DEFECT REMOVAL BY SC-1 CHEMISTRIES*

P. J. Resnick, C. L. J. Adkins, C. A. Matlock,
M. J. Kelly, P. J. Clews, N. C. Korbe
Sandia National Laboratories
Albuquerque, NM 87185

ABSTRACT

Recent research has shown that dilute SC-1 chemistries, when combined with high frequency sonication (megasonics) can be highly effective for particle removal. The mechanism by which the SC-1 chemistry facilitates particle removal remains unclear. Experiments were performed under extremely dilute conditions in order to help elucidate a cleaning mechanism. Results indicate that hydrogen peroxide, under extremely dilute conditions, is not necessary for effective particle removal. The increase in haze commonly attributed to increased surface roughness is not observed when sufficiently dilute ammonium hydroxide (*e.g.*, 1:2700) is used. The role of hydrogen peroxide, when more concentrated chemistries are used, may be simply to mitigate surface etching and roughening, rather than to play an active role in particle removal.

INTRODUCTION

In a study of SC-1/megasonic cleaning for small particles (≤ 0.20 μm), an empirical response surface model was previously generated [1]. Megasonic power was the dominant factor for these cleans, with temperature and chemical ratio ($NH_4OH:H_2O_2$) modifying the effect of power. As a continuation to the original study, a matrix was constructed and performed using ultra-pure water without any SC-1 chemistry at various megasonic power and temperature set points. The particle removal response surface from the DI water experiments was substantially different than the response surfaces generated when dilute SC-1 solutions were used. The disparate nature of these two response matrices suggested that additional experimentation was warranted in the regime between water-only and the previously studied dilute chemistries such as 1:100:6900

*This work was performed at Sandia National Laboratories, which is operated for the U.S. Department of Energy under contract no. DE-AC04-94AL85000. This work was funded through a cooperative research and development agreement with SEMATECH.

($NH_4OH:H_2O_2:H_2O$). The objective of performing experiments in this "ultradilute" regime was not necessarily to optimize an existing clean, but rather to develop insight into the chemical action involved in the SC-1 megasonic clean. By developing a more fundamental understanding of the way in which the cleaning chemistry interacts with the wafer surface, optimized SC-1 chemistries can be used with more confidence for future generation device fabrication.

EXPERIMENTAL

A design of experiments (DOE) matrix was constructed to study particle removal efficacy with various ultra-dilute SC-1 chemistries in a megasonic bath. The study was performed in a Verteq focused beam megasonic, and particle metrology was performed on a Tencor Surfscan 6200. The NH_4OH and H_2O_2 concentrations were varied from 0 to 5000 ppm at fixed megasonic power and temperature (150 or 200 W, 25°C or 45°C). The addition of light point defects (LPDs) to pre-cleaned wafers was the measured response for these experiments.

Following the DOE, two chemistries with different oxidation potentials were selected with which to perform open circuit potential (OCP) measurements. The first chemistry was a 1:80:2600 dilute SC-1, and the second chemistry was a 1:0:2700 aqueous ammonia solutions (no H_2O_2 added). OCPs were measured with both n and p-type Si<100> (both high and low resistivity material), under both bright and dark lighting conditions. Bright light conditions were created by illuminating the sample with a Balzers 50 W tungsten halogen inspection lamp, positioned approximately 30 cm from the liquid surface. Dark processing conditions were created by covering the test cell with black plastic and turning off room lights in the bay. OCP data were recorded with an Accumet pH meter model 50. The values obtained from the pH meter were verified with a Keithley model 617 electrometer. Wafers were precleaned in 100:1 HF to remove any backside oxide. Contact to the backside of the wafers was made using indium foil pressed onto the wafers, and contact to the indium was made with a platinum disk. All measurements were made relative to a saturated calomel electrode (SCE).

Finally, cleaning efficacies for the removal of silicon nitride particles (0.11 - 0.30 μm) deposited from an aerosol were measured under conditions which produced substantially different OCP values. The wafers for these experiments were pre-cleaned in a 1:4:64 SC-1 solution at 45°C with 200 W applied megasonic power.

RESULTS

In the first experimental matrix, the addition of LPDs to pre-cleaned wafers processed in ultra-dilute SC-1 chemistries was studied. Because extremely dilute chemistries were used (ppm range), reproducible cleaning efficiency data were difficult to obtain. Therefore, the addition of LPDs to pre-cleaned wafers was the measured response. Light point defect addition increased as the concentration of hydrogen peroxide was increased and ammonium hydroxide reduced. Calculated solution pH values were found to vary primarily with the ammonium hydroxide concentration and only slightly as a function of the hydrogen peroxide concentration. LPD counts did not correlate directly to calculated solution pH values (based on a pH of 5.9 in equilibrium with cleanroom air). The solution oxidation potential was calculated using the method of Pourbaix [2]. The trend was found to be similar to the LPD addition trend, although no causal relationship can yet be deduced. These results are shown in Figures 1 and 2.

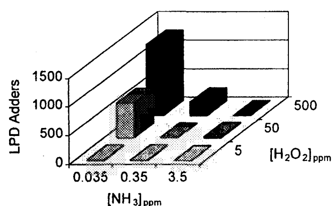

Figure 1. Light point defect addition as a function of process chemistry.

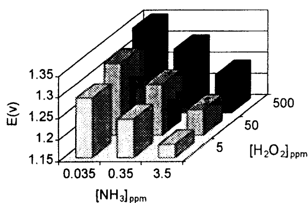

Figure 2. Calculated oxidation potentials (NHE) as a function of process chemistry.

Because LPD addition was observed to trend with the solution oxidation potential, additional electrochemical experiments were performed to assess the significance of electrochemistry in the SC-1 clean.

Open circuit potential values were obtained for both n and p-type silicon in 1:80:2600 and 1:0:2700 chemistries. These chemistries, which are significantly more concentrated than those used in the previous experiments, were chosen because they have similar pH values (9.7 and 10.6, respectively), and are in a concentration regime where moderate particle removal performance without applied megasonic power should be expected. The measured OCPs generally trended more positive with time, indicative of surface passivation. The OCP values are plotted in Figures 3 and 4. Most notable is that the OCP drifted very little when n-type silicon was placed in the aqueous ammonia solution (1:0:2700 chemistry), and the OCP values were essentially independent of wafer doping

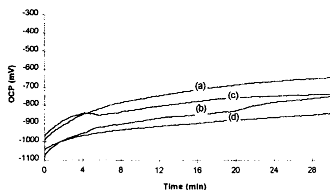

Figure 3a. OCP (wrt SCE) for n-type Si in 1:80:2600 SC-1 chemistry.

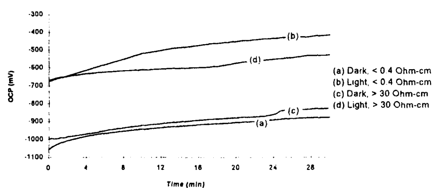

Figure 3b. OCP (wrt SCE) for p-type Si in 1:0:2700 aqueous ammonia.

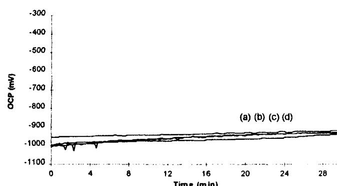

Figure 4a. OCP (wrt SCE) for n-type Si in 1:0:2700 aqueous ammonia.

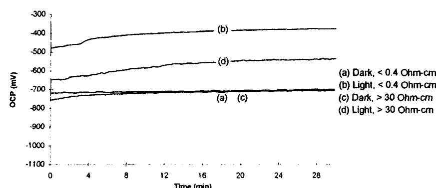

Figure 4b. OCP (wrt SCE) for n-type Si in 1:0:2700 aqueous ammonia.

level and ambient lighting conditions (Figure 4a). When p-type silicon was placed in the same solution, stable OCPs were obtained only under dark conditions (Figure 4b). These data indicate that photo-assisted redox chemistry, (*e.g.*, surface oxidation), does not occur when n-type silicon is processed in aqueous ammonia solutions (no hydrogen peroxide present). Thus, if surface oxidation/etching are requisite for an effective cleaning process, the cleaning efficacy of n-type silicon in dilute aqueous ammonia should differ significantly from the efficacy obtained in ammonia solutions containing hydrogen peroxide.

Cleaning efficacy data were collected for the removal of Si_3N_4 particles (0.11 - 0.30 μm) from hydrophilic Si <100> surfaces. The results from these experiments, which were performed at 45°C with no applied megasonic power, are shown in Figure 5. The mean cleaning efficiency is slightly higher when no hydrogen peroxide is present in the cleaning solution. There is no significant difference in these data between cleans which were performed under dark conditions and cleans performed under bright light conditions. Overall, p-type wafers had slightly higher cleaning efficiency and a significantly smaller spread to the data than n-type. The interquartile range (IQR) for p-type silicon was 7.2%, and for n-type the IQR was 18.9% (noting that all outliers were from n-type silicon). Although the differences in wafer type on cleaning performance are quite small, the processing appears to be slightly more robust with p-type silicon. No significant difference was noted between light and dark cleaning conditions for either n or p-type silicon. If cleaning efficacy is strongly influenced by an etch/oxidation

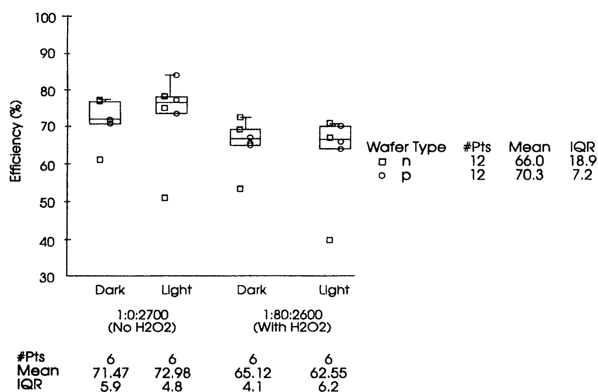

Figure 5. Particle removal efficiency with and without hydrogen peroxide under light and dark processing conditions.

mechanism, and assuming that the etch/oxidation processes are not kinetically limited, then some difference in cleaning performance should be noted under conditions where large differences in OCP were measured. Atomic force microscopy (AFM) methods to measure the extremely low etch rates expected under these conditions are currently being explored.

Historically, hydrogen peroxide has been added to the SC-1 clean to suppress surface roughness generated by the alkaline etch of Si<100>, and to aid in the removal of organic contamination. As this work has been focused primarily on particle removal, no effort has yet been made to study the impact on organic removal by reduction or elimination of H_2O_2. Although somewhat ambiguous, haze is commonly used as a metric for wafer cleaning performance. Haze can be defined as the ratio of light scattered from the surface to the light illuminating the surface (a source of noise in scattered light particle detection), and increased surface noise can be attributed to increased surface roughness [3]. In aqueous ammonia solutions at sufficiently dilute chemistries (*e.g.*, 1:2700 dilution), high cleaning efficiencies have been observed without producing measurable increases in haze. Haze delta values are shown in Figure 6. There are notable differences for wafers processed under bright and dark conditions. Higher haze values are produced when wafers are processed with H_2O_2 under dark conditions, or without H_2O_2 under bright conditions. The conditions which result in increased haze do not correlate with increased (or decreased) cleaning efficacy.

Finally, experiments were performed with dilute ammonia solutions using applied megasonic power to determine if acceptable particle removal efficiencies can be achieved

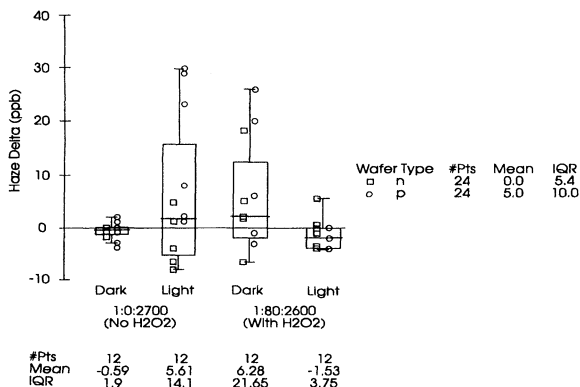

Figure 6. Delta haze values with and without hydrogen peroxide under light and dark processing conditions.

without hydrogen peroxide present. Cleaning efficiencies of greater than 95% were obtained at 45°C with 200 W of megasonic power applied. No significant increase in haze was measured on these wafers, indicating that the use of megasonic power did not promote surface roughness.

DISCUSSION

First, open circuit potential measurements have been used to determine conditions where passivation of the silicon surface is likely to occur. Ambient lighting, wafer type (n or p), and solution oxidation potential influence the passivation characteristics of the silicon surface in solution. Conditions have been identified where photo-assisted surface reactions are occurring. For example, n-type silicon, without peroxide present, appears quite stable (OCP is not effected by lighting conditions). However, p-type silicon without peroxide shows significant shifts in OCP when processed under different lighting conditions.

Second, the change in the haze values were also noted during these experiments. Although other surface phenomena can be attributed to increased haze (*e.g.*, organic films, grain boundaries), the only explicable source of haze during these experiments is surface roughness. The increase in surface roughness can be caused by incomplete etching of the chemical oxide on SC-1 pre-cleaned wafers, or the selective etching of the

Si<100> plane [4]. The latter mechanism assumes that the chemical oxide is etched away prior to the attack of the silicon substrate. According to Schnakenberg, *et. al.* [5], etching is facilitated by interaction of conduction band electrons with adsorbed H_2O_2, or increased population of the conduction band in p-type silicon with photoelectrons by illumination. The haze delta values were lowest when the Si<100> was processed without H_2O_2, under dark conditions. Low haze deltas were also observed when the wafers were illuminated during processing with H_2O_2 added to the cleaning solution. The former condition should give rise to very low etch rates (few photoelectrons and no adsorbed H_2O_2); the latter condition should give rise to a smooth etched surface [5]. The conditions which give rise to substantially increased haze are processing without H_2O_2 under light conditions, or dark processing with H_2O_2. These conditions result in either no adsorbed H_2O_2 or reduced photoelectrons. Increased haze under these conditions may be the result of preferential etching of the <100> plane when H_2O_2 is omitted, or incomplete etching of the native oxide when H_2O_2 is included in the cleaning solution and processing is performed under dark conditions.

It is important to note that, although systematic differences in haze and OCP values were observed depending on lighting and solution chemistry, no such systematic differences were observed in actual cleaning performance. These data indicate that surface modification, under conditions of dilute chemical processing, do not correlate to cleaning efficacy. These results are consistent with the findings of Itano, *et. al.* [6], who determined that particle removal efficiency is not always proportional to the silicon etch rate in SC-1 type chemistries.

When a sufficiently dilute aqueous ammonia solution is used, it is not clear what role hydrogen peroxide plays with respect to particle removal. Other researchers [7,8] have shown that iron deposition from SC-1 corresponds to iron concentration in the hydrogen peroxide. Thus, a desirable reduction in metal contamination caused by the SC-1 chemistry should be accomplished by reduction or elimination of H_2O_2 in the SC-1 clean.

CONCLUSION

Although lighting conditions, wafer resistivity and doping levels are seen to influence the removal of LPDs during processing in extremely dilute (ppm range) solutions, these phenomena are not observed when somewhat more concentrated chemistries (those which yield effective particle removal) are used. These appear to be second order effects that have little impact on cleaning performance in an otherwise efficacious clean. OCP data, along with haze values obtained during cleaning experiments, indicate that etching/passivation of the surface depends on both NH_4OH and H_2O_2 concentrations, as well as wafer type and lighting conditions. Process parameters conducive to etching do

not necessarily result in more efficacious cleans with respect to particle removal. Although etching of native oxide may be part of the cleaning mechanism when more concentrated chemistries are used, with dilute chemistries it appears that effective cleaning can occur with little or no removal of material from the wafer surface. In traditional concentration chemistries, the addition of H_2O_2 is required to suppress the surface roughness that is created by the selective alkaline etch of Si<100>. When sufficiently dilute aqueous ammonia solutions are used on hydrophilic wafers (without H_2O_2 addition), alkaline attack and roughening of the silicon is minimal, yet effective particle removal is still obtained.

REFERENCES

1. P. J. Resnick, C. L. J. Adkins, P. J. Clews, E. V. Thomas, S. T. Cannaday in Cleaning Technology in Semiconductor Device Manufacturing, J. Ruzyllo and R.E. Novak, Editors, p. 450, PV 94-7, The Electrochemical Society, Inc., Pennington, NJ (1994).
2. M. Pourbaix, Atlas of Electrochemical Equilibria in Aqueous Solutions, Pergamon, Oxford (1966).
5. J. C. Stover, Optical Scattering: Measurement and Analysis, p. 166, McGraw-Hill, New York (1990).
4. E. D. Palik, V. M. Bermudez, O. J. Glembocki, *J. Electrochem. Soc.*, 132, 871 (1985).
5. U. Schnakenberg, W. Benecke, B. Lochel, S. Ullerich, P. Lange, *Sensors and Actuators*, A25-27, 1 (1991)
6. M. Itano, F. W. Kern Jr., R. W. Rosenberg, M. Miyashita, I. Kawanabe, T. Ohmi, *IEEE Trans. Semiconductor Manufacturing*, Vol. 5, No. 2 (1992).
7 O. J. Antilla, M. V. Tilli, M. Schaekers, C. L. Claeys, *J. Electrochem. Soc.*, 139, 1180 (1992).
8 M. Meuris, S. Verhaverbeke, P. W. Mertens, M. M. Heyns, L. Hellemans, Y. Bruynseraede, A. Philipossian, *Jpn. J. Appl. Phys.*, 31, L1514 (1992).

EFFECTS OF SC-1 DILUTION AND TEMPERATURE ON VARIOUS PARTICLE REMOVAL CHALLENGES

K.K. Christenson, S.M. Smith, C. Bode* and K. Johnson**
FSI International, 322 Lake Hazeltine Dr., Chaska, MN 55318
* UIUC Department of Chemical Engineering
** Univ. of MN Department of Chemical Engineering

ABSTRACT

The removal of particulates is the primary use of the APM chemistry (NH_4OH:H_2O_2:H_2O). This report covers variations in particle removal efficiency of an APM solution as a function of NH_4OH and H_2O_2 concentration and temperature in a spray processor. Particle challenges include ashed photoresist, residue after a nitride strip, "HF dip" and Si_3N_4 particles. The removal of Si_3N_4 particles was also studied as a function of dispense time. Removal efficiency increased strongly with solution temperature and dispense time. With extended dispense times of 6-12 minutes, all chemistries were able to remove over 99% of deposited Si_3N_4 particles >0.15 microns. Other portions of the larger APM study covering the addition and removal of metals and the SiO_2 etch rate and surface roughening are published elsewhere (1 , 2 , 3). These response surfaces can be used to select the most promising regime of parameter space for further optimization of any particular process.

INTRODUCTION

Particle removal is one of the most studied aspects of the APM chemistry (4 , 5 , 6). The exact mechanism of removal is unproved, but five factors seem to play an important role. First, the APM slowly etches the SiO_2, undercutting and releasing the particles. Second, the electrostatic charge or Zeta potential on the silicon wafer surface and most particles in APM solutions is strongly negative (7). These charges cause a repulsion between the wafer and particle which enhances particle lift off and impedes redeposition. Third, the ionic strength of the solution affects the distances at which the repulsion is significant. Fourth, some types of particles could be dissolved by the APM. And finally, particles which are dislodged must be transported away from the wafer surface before they redeposit or dry in place (8). The complexity of the mechanism precludes simple predictions of a solution's particle removal efficiency. In this experiment, the particle removal efficiency of APM solutions is measured as a function of exposure time, temperature and NH_4OH and H_2O_2 concentrations for various particle challenges.

EXPERIMENT

N type, <100>, 150 mm CZ wafers were initially cleaned to near background levels in an FSI MERCURY® MP with a B Clean chemistry sequence (SPM, DHF, APM, HPM). Photoresist or "PR challenge" wafers were prepared by O_2 plasma ashing a 1 µm layer of photoresist. Two sets of photoresist challenge wafers were prepared in separate laboratories ("Source 1" and "Source 2"). Nitride strip residue challenge wafers were prepared by growing layers of SiO_2 and Si_3N_4, stripping off the layer of Si_3N_4 in hot phosphoric acid, stripping off the SiO2 layer with 10:1 HF and ending with a spin rinse dry. "HF dip" challenge wafers were prepared by immersing cleaned wafers for 10 minutes in ambient temperature, 10:1 HF (5.0 wt%) followed by two iterations of a spin rinse dry. All of the HF challenge wafers were prepared together before the experiment. Si_3N_4 particle wafers were prepared by immersing cleaned, p type, <100>, 150 mm CZ wafers in DI water containing finely ground Si_3N_4 powder (9). These Si_3N_4 wafers were prepared to conform to the particle removal requirements laid out in the SIA road map.

The first portion of the experiment consisted of exposing ashed photo resist, residue after a nitride strip and HF dip test wafers to 27 treatments in a 3x3x3 full factorial matrix of H_2O_2 and NH_4OH concentrations and temperatures along with a 28th "rinse only" treatment. Each experimental run contained 1 ashed photoresist wafer from each source, 1 nitride strip residue challenge wafer and 2 HF challenge wafers. Counts of particles larger than 0.15 µm were measured at on an ESTEK 8500 Wafer Inspection System programmed for a 6 mm edge exclusion.

The experimental runs were carried out in an FSI MERCURY MP centrifugal spray processor. A simplified plumbing diagram is shown in Figure 1. In the spray processor, Ashland SEMI grade chemicals and DI water were blended on-line and sprayed onto the wafers. The following process sequence was used:

- 5 minute water rinse to preheat the wafers to the steady state process temperature
- 3.25 minute APM dispense at 60 RPM with 20 sec., 500 RPM ramp after 85 sec.
- 4.5 minute rinse in hot DI water utilizing ramped rinsing (11)
- 6 minute spin dry

Chemical flow rates of 23, 92 and 320 cc/min were chosen to give two, approximately 4x, changes in concentration and a blend ratio range of n:m:5 with n and m ranging from to 0.06 to 1.45. Due to a 90 cc/min practical lower limit on the flow systems, the H_2O_2 and NH_4OH were diluted 3:1 in the canister to achieve effective flow rates of 23 cc/min for these chemicals when required. The in-line temperature at the spray post was varied over 20, 60 and 95° C with an in-line infrared chemical heater (10). Heat loss through processes such as evaporation reduced the on-wafer

temperature from 60 and 95° C to approximately 50 and 70° C. A constant total APM flow rate of 1760 cc/min was used for all treatments so that the transient and steady state on-wafer temperatures were the same (10).

In the second portion of the experiment, the Si_3N_4 particle wafers were exposed to a 2x2x4 full factorial matrix of APM concentration, temperature and exposure times. The levels were 25:25:1500 and 125:125:1500 NH_4OH:H_2O_2:H_2O for blend ratio, 60 and 95° C for temperature and 3, 6, 9 and 12 minutes for time. The process sequience was as above but with 20 second, 500 RPM ramps every 90 seconds for the duration of the dispense (11). Counts of particles larger than 0.15 μm were measured on a Tencor Surfscan 6200 programmed for a 3 mm edge exclusion.

RESULTS

Figure 2 and Figure 3 show the particle removal efficiency for nitride strip residue and HF dip challenge wafers respectively. The removal efficiency improves strongly with temperature, slightly with NH_4OH concentration and is unaffected by H_2O_2 concentration. Figure 4 shows the particle removal efficiency for the ashed photoresist wafers from Source 1. These particles were removed very easily; 90% were removed by the 0:0:5 blend which was in effect only a hot rinse.

Figure 5 shows all of the particle removal data plotted together. The runs were first arranged in increasing order of temperature. Then within temperature, in order of increasing NH_4OH concentration and within NH_4OH concentration, in order of increasing H_2O_2 concentration. The individual H_2O_2 flows are not listed on the x axis of the graph. There is a large difference between the responses of the three challenges. The particles remaining after ashing photoresist from either source were removed fairly easily - the least aggressive blends at 20° C typically removed over 90% of the particles. The nitride strip residue and HF particles behaved very similarly and were much harder to remove than the ashed photoresist. The most aggressive blends removed approximately 80% of the particles. The slope of the graph indicates that HF and nitride strip residue particle removal efficiency increases both with temperature and with the concentration of NH_4OH.

The Si_3N_4 particles were much harder to remove than the other challenges. Figure 6 shows that the removal of Si_3N_4 particles improves with temperature and time, but is relatively unaffected by concentration. The etch rate of the SiO_2 is also dominated by the solution temperature (3). This data supports the theory that the removal efficiency scales with the amount of material etched from the surface - that it is necessary to undercut particles in order to remove them from the surface (5). Particles, once broken free of the surface will be swept away during the 500 RPM ramps with little chance of redeposition (11).

The most interesting feature of Figure 6 is the high particle removal efficiency after 9-12 minutes of APM dispense. After 9 minutes, both concentrated and dilute APM solutions at 95° C meet the SIA requirement of 95% removal. With a 12 minute dispense, removal efficiencies for all concentrations and temperatures ranged from 99-100% for Si_3N_4 particles >0.15 μm; substantially better than the 95% required in the SIA road map.

CONCLUSION

The efficiency of particle removal by the APM solution varies strongly with the nature of the particle challenge. The particles from ashed photoresist were removed too easily and hence do not constitute an effective challenge. Nitride strip residue and HF particles were more difficult to remove and behave similarly. Their removal efficiency is controlled primarily by the temperature of the solution and weakly by the NH_4OH concentration. The concentration of H_2O_2 had little effect.

Processes which require high particle removal efficiency should use the highest available temperature and an exposure time varied to produce the required removal efficiency. Since removal efficiency is only weakly effected by NH_4OH and H_2O_2 concentration, dilute solutions should be used to reduce the environmental impact and cost of the cleaning procedure. Greater than 99% removal efficiencies on the SIA standard Si_3N_4 particle challenge are typical for APM dispense times of 9-12 minutes.

ACKNOWLEDGMENTS

We would like to acknowledge the generosity of Motorola Incorporated whose support made this work possible. In particular, we thank Robert Duffin and Kathy McCormack for their involvement in the FSI IRONMAN program. Susan Cohen of IBM and Carol Adkins and Peggy Clews of Sandia provided guidance on the preparation of Si_3N_4 particle challenges. We would also like to thank Brad DeSelms and Eric Persson of ATT, Jeff Glick of AMD, John Grant of Sharp and Scott Becker, Don Deal, Jim Oikari and Don Grant of FSI for suggestions on the design of the experiment and appropriate particle challenges.

REFERENCES

1 . Shelley Smith, K. K. Christenson and Dennis Werho, "Metal Addition of the RCA-1 Chemistry as a Function of Blend Ratio and Temperature," *Proceedings of the 1995 Semiconductor Pure Water and Chemicals Conference*, edited by M. Balazs (Balazs Analytical Laboratory, Sunnyvale, CA, 1995).

2 . K. K. Christenson, Shelley Smith and Dennis Werho, "Metal Removal of the RCA-1 Chemistry as a Function of Blend Ratio and Temperature," *Proceedings of the 1995 Semiconductor Pure Water and Chemicals Conference*, edited by M. Balazs (Balazs Analytical Laboratory, Sunnyvale, CA, 1995).

3 . K. K. Christenson and Shelley Smith, "Effects of SC-1 Dilution and Temperature Variations on Etch Rate and Surface Haze," to be published in Proc. of the spring 1995 MRS.

4 . M. Itano, F. Kern, M. Miyashita and T. Ohmi, "Particle Removal From Wafer Surface in Wet Cleaning Process," *IEEE Transactions on Semiconductor Manufacturing*, 6:258 (1993).

5 . M. Meuris, M. Heyns, P. Mertens, S. Verhaverbeke and A. Philipossian, "Investigating Techniques To Improve Gate-Oxide Integrity," *Microcontamination Magazine*, May 1992, p. 31.

6 . K. Mori, N. Ishikawa, T. Shihoya and A. Yamashita, "SC-1 Cleaning With Low Surface Tension Ammonia Water," in *Proceedings of the 1992 Semiconductor Pure Water and Chemicals Conference*, Balazs Analytical Laboratory, Sunnyvale, CA, pp 191 (1992).

7 . R. Donavan in "Intensive Short Course in Semiconductor Wafer Cleaning Technology," presented in February 1993 in Austin, TX by Werner Kern Associates, East Windsor, NJ, (1993).

8 . A. Tonti, "A Simple Model For Rinsing," in *Proceedings of the Second International Symposium on Cleaning Technology in Semiconductor Device Manufacturing*, The Electrochemical Society, Pennington, NJ, PV 92-12:41-47 (1992).

9 . Susan Cohen, Carol Adkins and Peggy Clews, private communication, 1995.

10 . K. K. Christenson, "The Effects of Increased Temperature in a Centrifugal Spray Processor," *Proceedings of the Third International Symposium on Cleaning Technology in Semiconductor Device Manufacturing* edited by J. Ruzyllo and R. Novak (The Electrochemical Society, **PV 94-7,** Pennington, NJ, 1994) pp. 474-483.

11 . K. K. Christenson, "The Use of Centrifugal Force to Improve Rinsing Efficiency," *Proceedings of the Third International Symposium on Cleaning Technology in Semiconductor Device Manufacturing* edited by J. Ruzyllo and R. Novak (The Electrochemical Society, **PV 94-7,** Pennington, NJ, 1994) pp. 153-162.

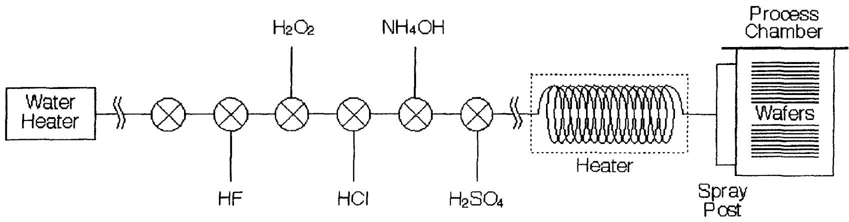

Figure 1: Simplified MERCURY MP Spray Processor Plumbing Diagram

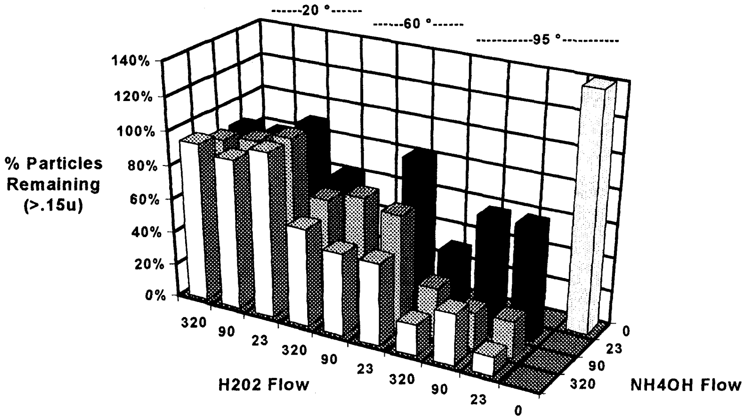

Figure 2: Particle Removal by APM From Silicon Nitride Challenge Wafers
Particles remaining after an APM in a FSI MERCURY MP vs NH_4OH and H_2O_2 flow rates and temperatures. Particles from Si_3N_4 stripped in hot phosphoric acid.

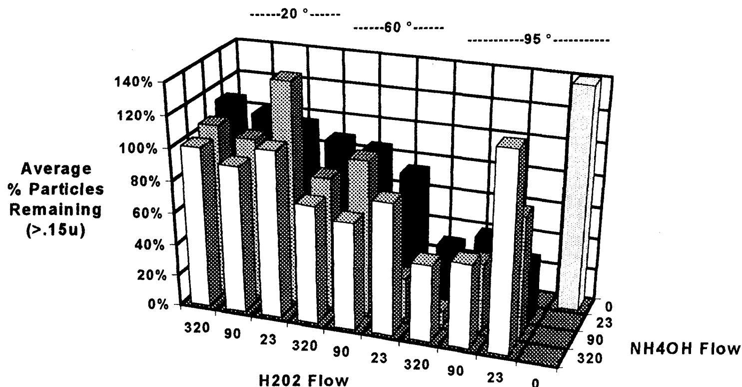

Figure 3: Particle Removal by APM From HF Dip Challenge Wafers
Particles remaining after an APM in a FSI MERCURY MP vs NH_4OH and H_2O_2 flow rates and temperatures. Particles from an HF dip followed by a spin rinse dry.

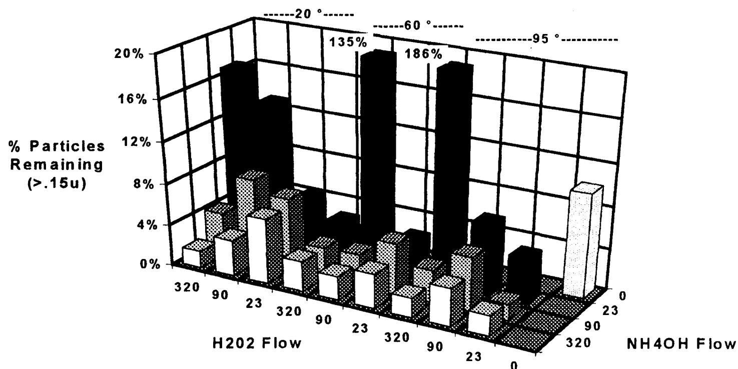

Figure 4: Particle Removal by APM From Ashed Photoresist Challenge Wafers
Particles remaining after an APM in a FSI MERCURY MP vs NH_4OH and H_2O_2 flow rates and temperatures. Particles from 1 micron of ashed photoresist (Source 1).

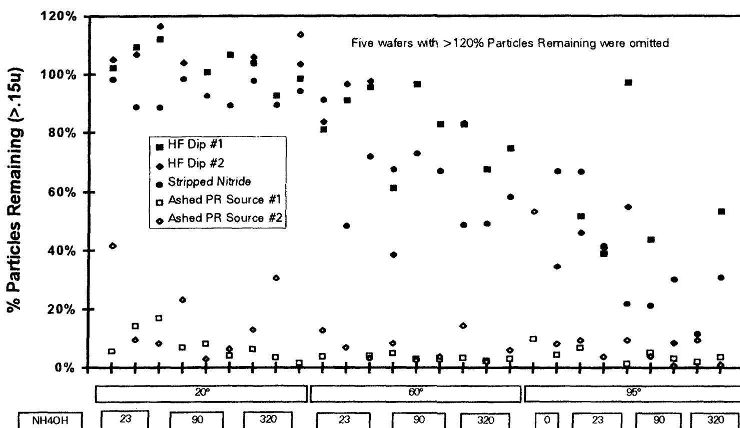

Figure 5: Summary of All APM Particle Removal Data

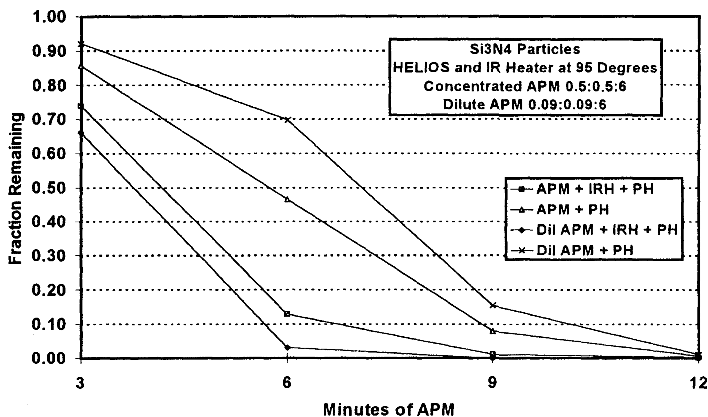

Figure 6: Variation of Particle Removal by APM with Time

Si_3N_4 Particles remaining after an APM in a FSI MERCURY MP vs time. "IRH" denotes infra-red heater and indicates a run at 95° C.

First Observation of 0.1μm Size COPs and Dusts on the Bare Si Wafers by Using AFM with Optical Scattering System

Naohiko Fujino, Isamu Karino, Junji Kobayashi, Kazuo Kuramoto,
*Masashi Ohomori,
**Masatoshi Yasutake, and **Shigeru Wakiyama

Mitsubishi Electric Corp., Advanced Technology R&D Center, 8-1-1 Tsukaguchi Honmachi, Amagaski, Hyogo 661, Japan
*SPC Electronics Corp., 25 Achigaya, Shimada, Shizuoka 427, Japan
**Seiko Instruments Inc., 36-1 Takenoshita, Oyama, Suntougun, Shizuoka 410-13, Japan

ABSTRACT

We have developed a new technique by using optical scattering phenomenon to link the coordinates of the commercially available wafer inspection system to the analyzer one with high precision of ±0.1μm. In this paper, we will report on the results about the first observation of 0.1μm-size particles such as dusts and crystal originated particles(COPs) on Si wafers by using the atomic force microscope(AFM) combined with this new technique.

INTRODUCTION

Even particles of 0.1μm-size have been believed to cause devise failure in 0.5μm VLSI processes. Therefore it has been required to reduce the number of such particles. The commercially available wafer inspection system(WIS) has been generally used to monitor particles on a Si wafer (Ref.1). However, It should be noted that the WIS could not give the detailed information such as shape and composition instead of the number, the size and the position of a particle. Recently, it has been strongly required to identify the nature of each particle by observing it directly or analyzing its composition. In order to realize them we have to establish the coordinates linkage system (Ref.2) which integrates the WIS and the analyzer such as the scanning electron microscope(SEM) and AFM via computer interface with high precision.

It is, however, very difficult to directly detect 0.1μm-size particles using SEM because the accuracy of the coordinates linkage is approximately ±100μm while the aria of the view field of at least 20μm is necessary for observing the 0.1μm-size particles using SEM, hence a considerable long time has been needed to detect a particular particle(Ref.3). In addition, it is difficult from SEM image to determine whether the particle is a pit or a

jut(Ref.4) because resolution of SEM is not sufficient enough to confirm the detail shape of the particles as small as 0.1 μm-size.

Therefore, AFM should be used as the observation tool of the particles which may cause a variety of problems in the 0.5μm VLSI processes because AFM has three-dimensional resolution for sizes as small as atoms. However, the scan aria(vision field) of AFM is narrow and a great deal of time is necessary to scanning for the mechanical probe.

We have developed a new technique on the basis of the optical scattering phenomenon which links the coordinates of a commercially available wafer inspection system to an analyzer one with a high precision of ±0.1μm. This new technique has been installed on a large sample AFM capable of observing wafers of 8-inch size(Ref.5). In this paper, we will report on the newly developed AFM and on the results of the first observation of 0.1μm-size particles such as dusts and COPs on Si wafers(Ref.6).

POSITIONING OF PARTICLES

OPTICAL SCATTERING METHOD

We can specify the positions of particles located on Si wafers by detecting the optical scattering from those particles with argon ion (Ar^+) laser light. Figure 1 shows a schematic illustration of optical scattering due to a particle in the dark field observed through an optical microscope. In this figure, E stands for errors when one link coordinates from the WIS to the AFM system using the conventional coordinate linkage system via computer interface. Firstly, the defocused Ar^+ laser beam is illuminated at a glancing angle on the region S(>E) around a specified particle on the AFM stage. Secondly, the scattering light due to the particle is detected in the dark field. Thirdly, the scattering light detected by a highly sensitive CCD camera through the optical microscope gives the position of the particle, which is registered into the coordinate system of the AFM. The theoretical accuracy of the position obtained by a detection of scattering light is approximately ±0.1μm which is mainly determined by the wavelength of Ar^+ laser beam (0.488μm). Finally, the measurement with the AFM is carried out around the registered position.

PROCEDURES OF COORDINATE LINKAGE

Figure 2 shows a schematic block diagram of the coordinates linkage with the large sample AFM and the WIS. The actual procedures of positioning would be further described here in detail. Firstly, we record the size and the coordinate of the each particle on the wafer using the WIS onto a floppy disk. Secondary, the coordinates are transferred into the AFM system using the conventional coordinate linkage system. The accuracy of this coarse coordinate linkage is about ±100μm which is mainly determined by the area of one pixel in the WIS (pixel errors). Finally, we perform coordinate linkage to confirm the position of the particles on the AFM coordinates system with the precision of ±0.1μm using the above mentioned scattering method. The scattering light due to the 0.10μm-size particle is observed by the ocular and objective lens with the magnification of 50 times and

20 times respectively. Figure 3 shows an example of the observation of a scattering light due to the 0.10μm-size particle such as COP at a glancing angle of 80 degrees.

EXPERIMENTAL

One of the most remarkable features of this newly developed instrument is the ability to observe the same position on a wafer before and after some processes. We will present three typical examples below. The sizes and locations of particles on a polished (100) CZ type of Si wafer (p-type, 8-inch in diameter) were measured by the wafer inspection system(ESTEK model CR80). The particles defined as large as 0.10μm and 0.12μm were observed by an AFM(Seiko instrument model SPA360) in the non-contact mode. The wafer was treated with SC1 cleaning (Ref.7) ($NH_4OH/H_2O_2/H_2O$=1:1:5) for 10 min at 75℃, then the particles were observed again by the developed AFM.

RESULTS AND DISCUSSION

Figures 4 and 5 indicate the AFM images of a 0.10μm-size COP before and after SC1 cleaning respectively. It has been originally presumed that this type of COP is a shallow unoriented pit. As clearly shown in Figure 4, our observation has indicated that the COP is a jut. The SC1 cleaning has turned it into a deep crystalline pit with the width of 91nm and the depth of 63nm. This pit runs parallel to the <110> axis of the wafer and has four facets with an angle of 54 degrees with respect to the surface of the wafer, which means that the facet is lying on the {111} plane.

It has been found out that whether a defect referred as COP in the WIS is a pit or a jut is dependent on the period of SC1 cleaning through a considerable numbers of observations of COPs before and after SC1 cleaning. Furthermore, it has been clarified that almost all the relatively large COP which exceeds 0.10μm in size is a chemically etched pit during SC1 cleaning and has four facets which are lying on the {111}, {112} or {113} plane.

Figures 6 and 7 shows the AFM images of a 0.12μm-size COP before and after SC1 cleaning, respectively. In this case a 0.12μm-size COP is a crystalline pit before SC1 cleaning with the width of 69nm and the depth of 30nm, and has the same four facets as in the 0.10μm-size COP after SC1 cleaning shown in figure 5. It is considered that this COP has already been turned into a pit in SC1 cleaning by the Si wafer supplier. The pit has grown larger and deeper to lie along on the {111} plane after our SC1 cleaning with the width of 117nm and the depth of 61nm. These results means that COPs are chemically grown to lie along on the {111} plane by SC1 cleaning. Figure 7 also shows a newly appeared COP which lies along on the {112} plane and has four facets with the angle 35 degrees with respect to the surface of the wafer. Before SC1 cleaning, shown in figure 6, there was apparently no COP at the position where the COP has newly appeared on the wafer after SC1 cleaning. However, a slight protrusion as small as surface roughness of

the wafer is recognized. The more detail results would be presented in future.

Figure 8 shows an AFM image of a 0.10μm-size dust before SC1 cleaning. It is clear that the real size is much bigger than the result (0.10μm) measured by the WIS. The difference is considered to be ascribed to the correction method in the WIS with 0.10μm-size polystyrene latex(PSL) standard particles. The size of a particle is estimated by comparing the intensities of the optical reflection between due to the particle and due to the standard particle. Actually, however, the optical reflectivities are different between these two particles. Our AFM results clearly indicate that we should regard the particle size by the WIS as a reference. It was confirmed by our developed AFM system that the dusts was removed after the SC1 cleaning process.

SUMMARY

(1) It has been confirmed that the AFM combined with an optical scattering system is useful for the evaluation of 0.1μm-size particles as well as the cleaning process of wafers.

(2) The COPs are inherently juts instead of pits , as was originally presumed. These COPs are chemically etched and become crystalline pits during SC1 cleaning.

(3) The actual size of the dust is much bigger than expected by using wafer inspection system.

ACKNOWLEDGMENTS

The authors would like to acknowledge Mr. Kazutake Yamasaki and Mr. Makoto Kurotobi of Canon Sales Co.,Inc. for monitoring particles by the wafer inspection system. We would also like to acknowledge helpful discussions with Dr. Yuuji Koezuka of Mitsubishi Electric Corp..

REFERENCES

(1) R. G . Knollenberg; SPIE, Vol. 774, pp. 32,(1987).

(2) T.Hattori et.al.; SPIE Proceedings of the Symposium on Microlithography, San Jose, California, vol. 1464, p. 365(March, 1991).

(3) N. Fujino et. al.; Europian patent application, Patent No. 95108440.9-2204.

(4) N. Fujino et. al.; UCPSS'92, FRI., 18 Sep., No. 18(1992).

(5) M. Yasutake et.al.; J. Vac. Sci. Technol., B12(3), May/June(1994).

(6) J. Ryuta et.al. ; J. J. A. P., Vol. 29, No.11, pp. L1947(1990).

(7) W. Kern et.al.; RCA Review, June(1970).

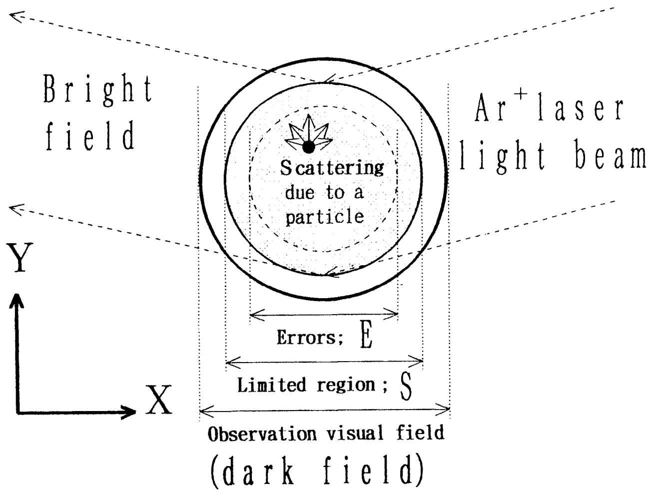

Figure 1. Schematic illustration of optical scattering due to a particle in the dark field observed through an optical microscope.

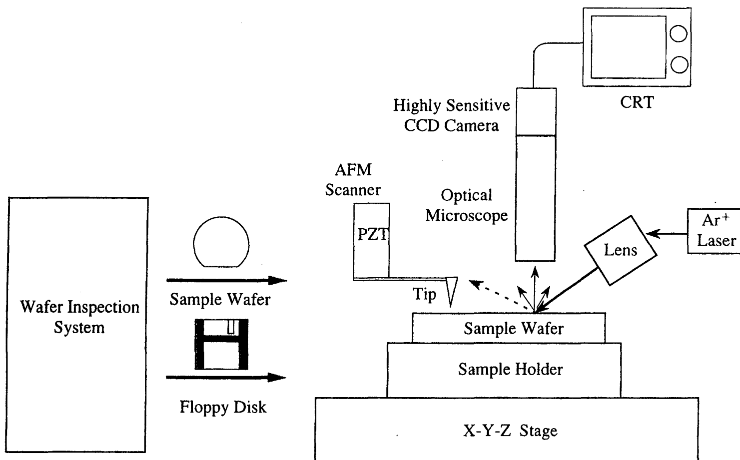

Figure 2. Schematic block diagram of the coordinates linkage with the large sample AFM and the wafer inspection system.

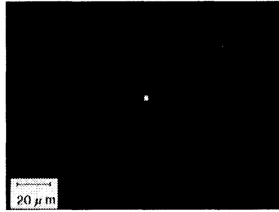

Figure 3. Photography of an observation of a scattering light due to the 0.10μm-size particle at a glancing angle 80 degree with Ar^+ laser beam (power of 15mw).

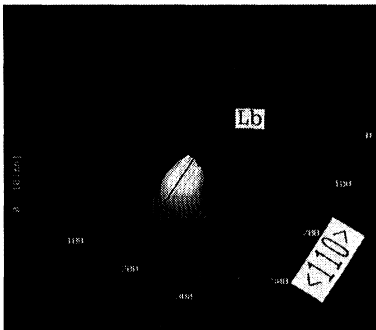

(a)

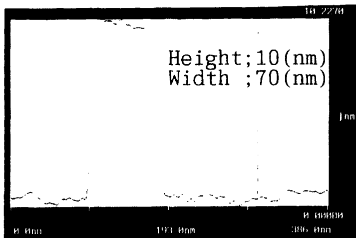

(b)

Figure 4. (a) AFM image of a 0.10μm-size COP before SC1 cleaning. Scan aria: $(400nm)^2$. (b) The software cross section along line"Lb" in (a).

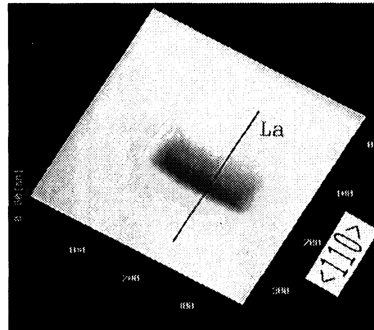

(a)

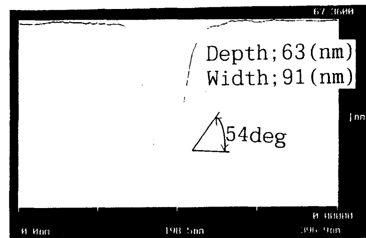

(b)

Figure 5. (a) AFM image of a 0.10μm-size COP after SC1 cleaning. Scan aria: $(400nm)^2$.(b) The software cross section along line"La" in (a).

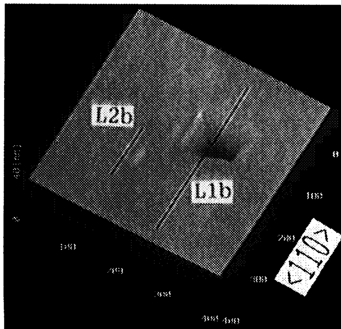

(a)

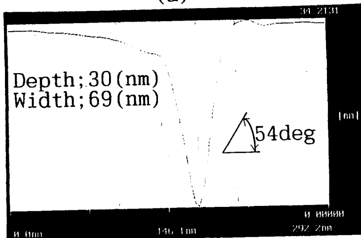

(b)

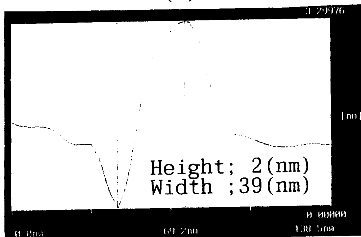

(c)

Figure 6. (a) AFM images of a 0.12μm-size COP before SC1 cleaning. Scan aria: $(400nm)^2$. (b) The software cross section along line"L1b" in (a). (c) The software cross section along line"L2b" in (a).

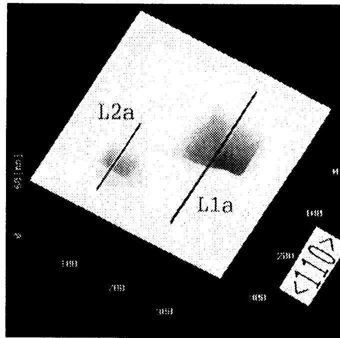

(a)

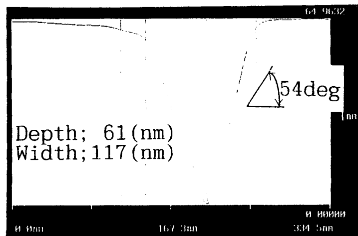

(b)

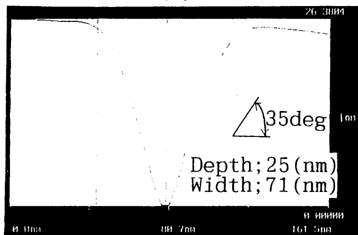

(c)

Figure 7. AFM images of a 0.12μm-size COP after SC1 cleaning. Scan aria: $(400nm)^2$. (b) The software cross section along line"L1b" in (a). (c) The software cross section along line"L2b" in (a).

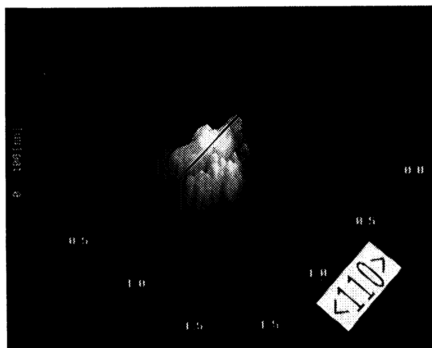

(a)

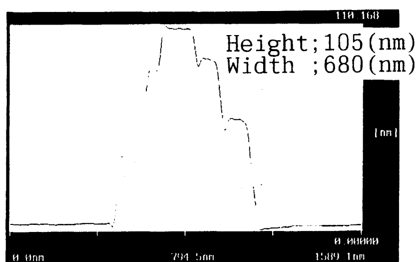

(b)

Figure 8. AFM images of a 0.10μm-size dust before SC1 cleaning. Scan aria: $(1700\text{nm})^2$. (b) The software cross section along line"L" in (a).

EXPLORATORY USE OF MICRO-XANES FOR PARTICLE DETECTION AND ANALYSIS ON SI WAFERS

C. R. Brundle
C. R. Brundle and Associates, San Jose, CA 95125
Y. Uritsky
Applied Materials, Santa Clara, CA 95054
A. Warwick
Advanced Light Source, LBL, Berkeley, CA 94720
R. S. Hockett, A. Craig
Charles Evans and Associates, Redwood City, CA 94063
C. Ayre
Intel Corporation, Santa Clara, CA 95052
D. Dunham, T. Droubay, and B. P. Tonner
Physics Dept., University of Wisconsin - Milwaukee, Milwaukee, WI 53201

An evaluation of the potential for the use of synchrotron radiation, in conjunction with an imaging electron microscope, to both detect and analyze small particles (0.1 to 0.5 microns) on Si substrates, has been carried out. The technique of X-Ray Absorption Near Edge Structure, XANES, was used. Test samples with particles typical of real wafer processing problems were evaluated (Cu, Fe, Al and C containing). Micro-XANES (i.e., XANES used in the microscopy mode) exhibits high contrast for elemental distinction, good chemical state distinction, and also in some cases phase distinction (i.e., structural information), demonstrating the essential technical viability of the technique for particle analysis. With the present prototype microscope spatial resolution is limited to about 0.2 microns, though theoretically this can be improved to less than 0.05 microns. Whether these attributes of the technique are sufficiently strong (and necessary) to outweigh the obvious difficulties of providing an analytical service at a government (DOE) facility remains to be seen.

INTRODUCTION

The current industry approach for determining the <u>origin</u> of particles on Si wafers is to transfer the full wafer (blank or patterned) to an SEM/EDS system, re-find particles originally detected and mapped by light scattering or imaging (Tencor, KLA, etc.), and then rely on <u>morphology</u> (SEM) and <u>qualitative elemental analysis</u> (x-ray analysis using EDS) for identification. Even for large particles this is sometimes not adequate for definitive identification of the particle (so that its <u>origin</u> can be determined and the source of contamination eliminated). As specifications change, and the particle

sizes to be dealt with get smaller, the SEM/EDS approach alone becomes less and less adequate for two reasons:

1) Though SEM can certainly handle morphology determinations down to very small particle sizes (much below 0.1 microns), x-ray analysis excited by the SEM electron beam is not a small-volume technique. The x-rays generated may come from as much as a 4 micron diameter volume, depending on the material and the electron beam voltage (the higher the voltage and the lower the material Z, the larger the volume). For sub-micron particles, therefore, the majority of the detected x-ray signal comes not from the particle, but from the substrate.

2) Some "particles" identified as such by light scattering, turn out to be thin film patches only 100's Å thick, often made up of low Z material (e.g., C,O,N). EDS is poor in dealing with low Z material in general (low intensities and no way of distinguishing one chemical form of C, for instance, from another) and for material only 100's Å thick often no observable additional signal over and above that of the background wafer is obtained.

Methods are needed which are capable of both providing good spatial resolution and elemental analysis, but also providing chemical speciation, being more surface sensitive than EDS, and being able to effectively handle low-Z material and organics/polymers.

X-Ray Photoelectron Spectroscopy, XPS, is a well-established analytical technique which has all of the above attributes, except the most important - sufficient spatial resolution. A technique closely related to XPS, X-Ray Absorption Near Edge Structure, XANES(1) (also known as Near Edge X-Ray Absorption Fine Structure, NEXAFS(2)) can, however, be operated in a highly spatially resolved mode, termed micro-XANES(3). In this technique a variable energy soft-x-ray photon beam floods the sample and has its energy scanned through the absorption-edge regions appropriate to the elements being searched for. Any absorption increase at an edge provides an elemental identification. There are several ways of detecting the absorption, but the one appropriate for looking at surfaces and particles on surfaces is to collect the electrons emitted as a result of the electronic de-excitation processes following the absorption excitation. The electrons are simply a signature of the absorption as a function of photon energy and do not need to be energy analyzed (though they can be). This is called the Total Electron Yield mode. Since most of the electrons emitted are low energy secondaries, plus Auger electrons, the analysis is surface sensitive (the absorption process itself is not - the soft-x-rays penetrate deeply). These electrons are collected in an imaging electron microscope, which provides the spatial analysis. Unfortunately, the only suitable source of high-brightness variable energy soft x-rays is synchrotron radiation, so micro-XANES is not an in-house laboratory option.

The elemental x-ray absorption edges have fine-structure associated with them which carries chemical state information about that element (rather like "chemical shifts " in XPS). Thus, in principle, the technique provides elemental identification and quantification (from absorption intensities) and chemical state identification.

EXPERIMENTAL

The synchrotron radiation source is an undulator beamline at the Advanced Light Source (ALS) of the Lawrence Berkeley Laboratory. Photon energies between the Al, 2p edge (≈78 ev) and the Cu 2p edge (≈930 ev) were used, though scanning this whole range required changing gratings in the monochrometer of the beamline. The x-ray beam from the monochrometer, which is ≈1 mm^2 in area, strikes a sample held below the lenses of the electron microscope (fig. 1). The whole system is under UHV. Electrons ejected from the surface of the sample are imaged through the microscope onto a channel plate electron multiplier detector. For this prototype instrument, which was designed and built by the University of Wisconsin group(3) and is owned by an IBM Almaden Research Center group, the maximum magnification achievable is ≈5,000X, with a spatial resolution of around 0.2 microns. In principle this can be reduced to below 0.05 microns in later versions of the instrument.

The prototype microscope is only capable of taking substrates up to 1 inch in diameter. For purposes of testing the technique we used high density deposits of different types of particles on small Si pieces. The high density eliminated any need for accurate co-ordinate information to find representative particles. The sample set included large (10 micron and larger) steel particles made by filing a screw-head; a graphite slurry with fullerine powder sprinkled on it; very small particles (<0.1 micron to 0.5 microns) of electrochemically deposited Cu and Ag; and a SEMATECH/NIST sample consisting of uniform 0.5 micron Al_2O_3 particles.

RESULTS AND DISCUSSION

Because of space limitations we will discuss only two examples from the set: the graphite/fullerine case and the 0.5 micron particle Al_2O_3 case. These are picked because they illustrate two of the important attributes of the technique - the ability to image small particles in real time and the degree of chemical state distinction available.

Fig. 2 shows the XANES spectrum obtained from the graphite/fullerine example. We do not show any images, because the surface turned out to consist of large patches of bare graphite and of fullerine. No individual particle regions were seen. The C(ls) absorption spectrum of the bare graphite is shown in fig. 2a, that of a fullerine

patch in 2b. Graphite is essentially a 2D layered structure consisting of hexagons of C atoms. Fullerine is a C_{60} cluster molecule. Clearly the electronic structure of the carbon atoms is sufficiently distinct in the two cases to provide reasonably different features in the near-edge structure, even though both materials consist entirely of carbon atoms. For imaging purposes, if one sits at a photon energy of 285.3ev any graphite within the field of view of the microscope (which can be as little as 25 microns at maximum magnification) will appear as a bright patch (greater electron emission) against a darker background. By changing the photon energy to 284.8 ev, i.e, a 0.5 ev energy decrease only(4), the fullerine patches will "light up" as the graphite darkens. The limit in spatial resolution is, of course, set by the microscope, and, as stated earlier is currently around 0.2 microns. With an entirely different approach where a Zone Plate is used to focus the photon beam to a small spot (i.e., a scanning approach, as opposed to an imaging approach), Ade(5) has demonstrated chemical state imaging resolution for carbon of down to 0.03 microns in thin block co-polymer films, where the absorption process is measured directly in transmission rather than reflection.

Fig. 3a shows an image, recorded by photographing the display screen (i.e, real-time imaging), of a 30 micron region on the SEMATECH/NIST 0.5 micron Al_2O_3 particle sample. The individual particles appear as bright spots over a wide range of photon energies, since the total electron yield is significantly higher than for the Si substrate (rather like SEM). However, when the photon energy passes over the Al 2p edge at 78.5 ev the particles brighten, then fade again. This is actually observable to the naked eye from the screen. Fig. 3b shows the recorded spectra across the Al 2p edge both on Al particles (two superimposed traces from two particles are actually shown), and on bare Si regions. The contrast in going over the Al 2p edge of a particle is about 30%, which is very high and much greater than is found in Scanning Auger Spectroscopy, for instance. The way the data in fig. 3b is actually obtained is to plot intensity, as a function of photon energy, for only the pixels from the region of interest by defining boxes on the screen. Information on all the particles on the screen could, in principle, be obtained and displayed simultaneously (in this case about 25 particles). In practice we are currently limited to six regions.

A dramatic feature of the data in fig. 3b is the very sharp structure contained in the Al_2O_3 XANES spectrum. By comparison with literature data on bulk standards an exact match is obtained for this structure with that of α-Al_2O_3 - i.e., not only is the particle identified as containing aluminum, it is identified as Al_2O_3 in the α (crystalline) form. Thus elemental, chemical, and phase information is supplied, along with real-time imaging.

CONCLUSIONS

Particle imaging, at video rates, for a field of view of 30 microns, with a spatial resolution of about 0.2 microns, has been demonstrated. Contrast at elemental edges is high and even with the present prototype microscope and non-ideal beam-line configuration, taking the relevant data over an absorption edge takes only a few minutes. Improvements in microscope design and optimization of a beamline for dedicated XANES usage should mean that similar data will be possible for spatial resolution down to a least 0.05 microns in the future.

In addition to imaging, micro-XANES provides direct elemental, chemical state, and sometimes even phase identification. There are a number of potential problems in implementing the technique as an analytical service, however. The biggest is simply whether an analytical facility acceptable to the semiconductor industry can be run at a government (DOE) installation. Worse, the primary commodity of the installation the synchrotron radiation is supplied to many beam-lines (and users) simultaneously, meanng that even if a custom-designed dedicated beam-line were available for a XANES analytical service, it would not have control over the radiation delivered to it. On the technical side there are two clear problems. First, the technique is unable to deal with large insulating particles (of several microns size). The high voltage between microscope lenses and sample results in severe charging and no electron emission from the insulating particle. Small insulating particles (such as the 0.5 micron Al_2O_3 particles discussed here) give no problem, however. This is also true for thin films of insulators (maybe up to 1000Å). Second, the technique is very surface sensitive; at least as sensitive as XPS, with the majority of the imaged electrons coming from the first 20Å or so of material. Therefore, in many cases, it will be necessary to couple micro-XANES with sputter profiling capabilities, preferably in a FIB mode, in order to distinguish the outer atomic layers from the core of even sub 0.1 micron particles.

ACKNOWLEDGMENTS

We are grateful to George Castro and Jo Stohr of IBM Research for making available to us the microscope facility for this work. We are also grateful to Alain Diebold of SEMATECH for providing the Al_2O_3 particle sample.

REFERENCES

1) A. Bianconi, Appl. Surf. Sci. **6**, 92 (1980)
2) J. Stohr, "NEXAFS Spectroscopy", Springer-Verlag, New York, (1991)
3) B. P. Tonner and D. Dunham, Nucl. Instr. and Methods in Physics Research, A347, 43, (1996)

4) Actually the absolute values of these energies may not be accurate, within a few eV, since this depends on grating alignment and requires calibration. Relative values, however, are very accurate.
5) H. Ade, to be published

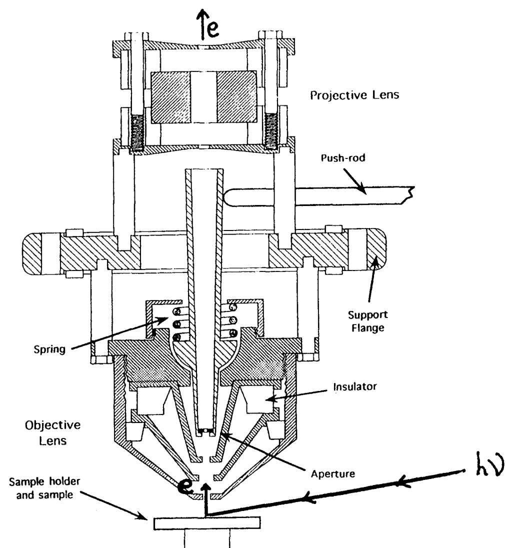

Fig. 1 Schematic of the imaging electron microscope. Photons from the synchrotron strike the sample and the ejected electrons are imaged through the microscope.

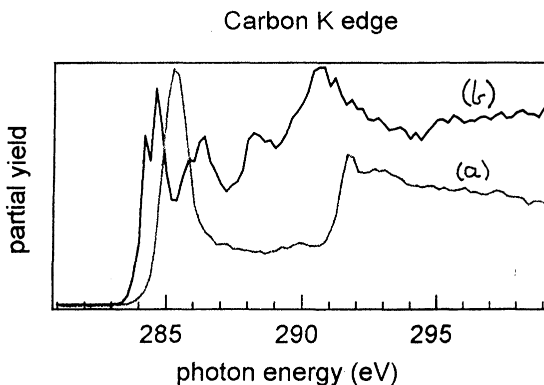

Fig. 2 C (1s) XANES of graphite patches (trace a), and fullerine patches (trace b) on a Si substrate.

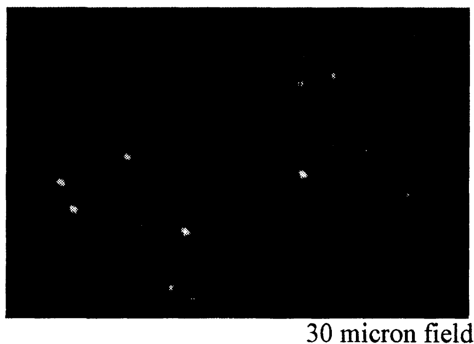

(a)

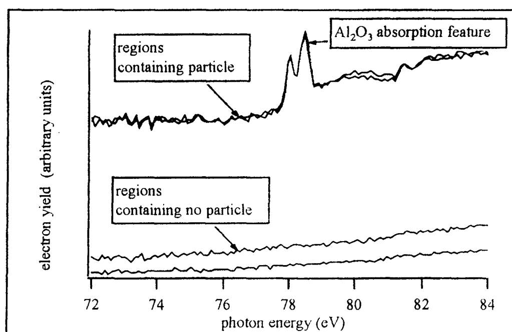

(b)

Fig. 3 (a) XANES image of 0.5 micron alumina particles on an Si substrate, taken at the Al 2p absorption edge photon energy (78.5ev for alpha-alumina). (b) XANES spectra in the Al 2p edge region for individual particles and for the silicon substrate.

Author Index

Adkins, C. L. J. 66
Adler, Steve 294
Aoto, Nahomi 310, 429
Atluri, Vasu 126, 372
Ayre, C. 606
Badowski, A. A. 166
Baker, K. 351
Bakker, Geoffrey L. 457
Barla, Kathy 28, 49, 359
Barnett, M. L. 126
Bay, Steve 414
Beck, S. E. 166, 175
Becker, D. S. 134
Bender, H. 473
Bensaoula, B. 545
Black, K. A. 343
Black, M. R. 343
Bode, C. 590
Bohling, D. A. 166, 175
Brierley, Philip R. 372
Brown, George A. 225
Brundle, C. R. 606
Butterbaugh,JeffreyW. 150, 158, 364
Byrne, S. 442
Carlson, B. 560
Carpio, Ronald A. 126, 372
Carrillo, F. 422
Chang C. C. 214
Chang, Jane P. 158
Chidsey, Christopher 448
Choi, Sang Jun 243
Christenson, K. K. 21, 560
Claeys, C. 530
Clarke, J. 142
Clews, P. J. 66
Cosway, Rick 294
Crabtree, P. 388
Craig, A. 606
Darakchiev, I. 530
Diebold, Alain C. 493, 511
Douglas, M. A. 501
Douglas, Monte 485
Elsmore, C. 142
Fleming, M. 60
Fleury, Alain 28
Fowler, Burt W. 126, 372
Fujikawa, Nobuyuki 74
Fujino, Naohiko 598
Geller, Claudia 214
George, M. A. 166, 175
Graham, Sandra W. 214
Green, M. L. 115
Grieger, E. 442
Griffiths, K 442
Grothe, P. A. 126
Hall, Lindsey 13, 277, 485
Hanger, G. F. 134
Hawthorne, R. C. 442
Hegde, R. 388
Herbots, Nicole 126, 372
Herrera, Jeanine 465
Hess, Dennis W. 174, 457
Heyns, M. M. 142, 277, 279, 437, 473, 530
Hiatt, Fred 364
Hiratsuka, Yutaka 74
Hitzman, C. J. 302
Hockett, Richard S. 302, 493, 511, 606
Honda, K. 503
Hossain-Pas, S. D. 501
Hurd, T. Q. 142, 277, 270
Hwang, D. K. 184
Hymes, Diane J. 402
Ishihara, Yoshio 380
Izumi, H. 437
Izumo, Shouzou 553
Jeon, Joong S. 574
Johnson, K. 590
Joly, J. P. 49, 359
Kamieniecki, Emil 184, 326, 338
Karino, Isamu 598
Kashkoush, Ismail I. 90, 338, 422
Kato, Masayuki 99
Kelly, M. J. 582
Kikuchi, Satoshi 194
Kim, Hong Seok 243

Kim, Jae Jeong	243
Kim, Woo Shik	243
Kimerling, L. C.	343
Kimijima, Tetsuya	380
Kishi, Gunji	553
Kneer, Emil A.	574
Kobayashi, Junji	598
Kondou, Hiroyuki	553
Korbe, N. C.	66
Krishnan, Srikanth	225
Krusell, Wilbur C.	402
Kubo, K.	107, 437
Kuramoto, Kazuo	598
Laberge, P.	388
Lane, A. P.	166, 175
Lao, K.	388
Lardin, T.	49
Laurens, Kwakman	28
Lawing, A. Scott	150, 364
Lee, Chang Weon	243
Lee, Jong Dae	243
Lee, Jong Wan	243
Lester, Lisa	485
Levy, Didier	28, 49, 359
Li, Jia	545
Li, L.	442
Lindley, Patricia M.	511
Linford, Matthew R.	448
Liu, Lisa	294
Loewenstein, Lee M.	225
Lux, M.	530
Ma, Y.	115
Malik, Igor J.	402
Marks, Steve	214
Martin, J. S.	126, 235
Masusaki, Hiroshi	380
Matlock, C. A.	66
Matsumoto, Koh	380
Mautz, K. E.	394
Maw, T.	530
McConnell, Chris F.	39, 519, 414
Mehta, Jitesh R.	194
Mertens, P. W.	142, 277, 279
Meuris, M.	142, 279, 437
Michel, J.	343
Mieckowski, A.	208
Mocala, K.	388
Mohr, Fred	402
Moniot, D. A.	166
Montandon, S.	545
Morinaga, Hitoshi	257
Mouche, L.	279
Mulholland, George	511
Muramatsu, Yoshinori	310, 429
Muscat, Anthony J.	150, 364
Nakamura, Masakazu	251
Nelson, G. C.	66
Nelson, S.	560
Niccoli, John	13
Norga, G. J.	343
Novak, R. E.	338, 422
O'Brien, Sean	537
Ohmi, Tadahiro	1, 107, 251, 257, 437
Ohnishi, Akihiro	553
Ohomori, Masashi.	598
Ojima, S.	107, 437
Oka, H.	269
Paillet, C.	49, 359
Papon, A. M.	568
Park, Jin-Goo	82
Parker, Jennifer W.	39, 519, 414
Pas, Michael F.	82, 501
Patruno, P.	49
Perry, D.	530
Peterman, Shelley	465
Prasad, Jagdish	13, 485
Raghavan, Srini	574
Raghunath, Chilkunda	574
Rajaram, B.	422
Resnick, P. J.	66
Roberts, D. A.	175
Roche, Thomas	294
Rogers, T. C.	194, 235
Roman, P.	338
Rotondaro, A. L. P.	277, 284, 530

Ruzyllo, J. 184, 208, 338
Saito, A. 269
Sakata, Yasuki 553
Sasaki, Yumi 317
Sawin, Herbert H. 150, 158, 364
Schauer, Stephen 294
Schleisman, Anthony 13
Schmidt, H. F. 277, 284, 473
Schubring, P. 60
Schueler, Bruno W. 511
Sees, Jennifer 13, 485
Shah, Raj 465
Shimanoe, Kengo 287
Shimazaki, Ayako 317
Shirai, Yasuyuki 251
Shive, L. W. 351
Smith, Shelley M. 21, 590
Smith, Stephen P. 302
Somashekar, Ambika 537
Storm, W. 473
Syverson, D. J. 134, 235, 364
Syverson, W. 60
Taferner, W. T. 545
Takahara, Y. 269
Tamaoki, Makiko 317
Tardif, F. 359
Teerlinck, I. 284, 473
Templeton, Allen 485
Thomas, Huw 414
Toda, Masayuki 99, 107
Tomozawa, Akihiro 553
Tong, J. K. 134, 235
Tse, Chiu 214
Tsuji, Mikio 310, 429
Torek, K. 208
Uemura, Kenichi 287
Uk, Tinal 214
Uritsky, Y. 606
Vandervorst, W. 279
Vanhaeren, D. 279
Varadarajan, Mohan 21
Vepa, K. 351
Verhaverbeke, Steven 39, 519, 414
Voloshin, G. 175
Vrtis, R. 175
Wakiyama, Shigeru 598
Warwick, A. 606
Wu, Shang-Qian 380
Xu, Han 158
Yasutake, Masatoshi 598
Young, K. M. 166, 175
Zagozdzon-Wosik, W. 545
Zhang, Zhe 158

Subject Index

Keyword	page #	Keyword	page #
1% HF + 1% HC1	50	depth profiles	316
acid processor	21	designed experiments	473
adsorption state	270	detection limits	309
AFM	606	dilute chemistry	569
alumina contamination	582	dilute SC1 solutions	39
aluminum contamination	302	dissolved oxygen	50
anhydrous HF	194	double-side scrubbing	409
anodic potentiodynamic polarization	583	dry cleaning	144
APM contamination	318	electrical monitoring/cleaning	334
APM	567, 597	electrochemical impedance	292
AR-TXRF	285	electrolyte rinsing	422
ATR-FTIR	380	elevated pressure/temperature etching	466
backside contamination	560	equilibrium constant	40
batch spray tool	401	etch initiation	196
BHF/H_2O_2	436	etch rate of oxide	545
BPTEOS	198	etch residue	243
brush scrubbing	472	Fe contamination H_2O	346
carbon contamination	555	FTIR	176
cavitation bubbles	93	FTIR-ATR	108
CFD models	422	gate oxide cleaning	54
charge to breakdown	119, 136	GOI	14, 85,304
chelating ligand	166	H^+hfac	166, 175
chemical oxide thickness	367	H_2O adsorption	390
chemical oxide	366, 449	H_2O in HCl	387
chemical vapor cleaning	167	haze	593
chemisorption	459	HC1 gas	387
ClF_3	158	HF passivated silicon	353
contact angle measurements	367	HF rinsing	547
contact angles	381	HF/alcohols	382
COO	145	HF/vapor etching	371
COP's	605	$HF{:}CH_3OH$	208
copper removal	153, 160	H-passivation	379
corrosion of Al	538	H-termination	444
Cu adhesion	292	hydrocarbons	511
Cu contamination	284	hydrogen passivation buildup	445
Cu deposition	259	hydrogen passivation	482
cylindrical capacitors	194	hydrogen terminated	127
D_0	136	hydrogen-terminated silicon	455
deposition kinetics on Si	252		

hydrophilic 575
hydrophobic 575
illumination 287
in situ monitoring 352
in-line process monitoring 332
ionic strength 42
kinetics/wet chemical process 490
LASER spectroscopy 388
ligands 272
light sensitivity 592
LPD's 538, 591
MCLT 84
megasonic irradiation 110
megasonic rinsing 68
megasonic 99, 590
metal adsorption 278
metal deposition 257
metal ion contamination 269
metal particles 263
micro-XANES 614
minority carrier lifetime 335
monolayer 510
MOS-CV 228
native oxide thickness 359
native oxide 358
non-contact 333
OH radicals 108
open circuit potential 480, 590
organic based positive photoresist stripper 215
organic contamination 23
organic strippers 537
overflow rinse 74
oxidation thickness 301
oxide etch uniformity 429
oxide etching 373,429, 544
ozonated water 450
ozone 4, 53, 449
ozone/water 83
parallel down flow rinsing 5, 77
particle analysis 521
particle contamination 575
particle removal efficiency 30, 570, 597
particulate defectivity 402
photoresist ashing 225
photoresist stripping 90
photosensitivity 457
point of zero charge 278
polarized SIRS 127
polymer nodules 218
post CMP cleaning 410
post LASER mark cleaning 412
post-CMP clean 472
post-RIE surfaces 184
Pourbaix diagram 583
radical formation 101
radio frequency photoconductance decay 350
rapid thermal diffusion 553
RCA cleaning 28
redox potential 3, 286
redox potential-pH diagram 258
reproducibility 310
residual polymer 214
rinse models 422
rinsing of vias 528
rinsing particles 423
round robin surface SIMS 500
SC1 Fe contamination 345
SC1 purity 15
selective etching 194
selectivity 546
SEM 605
Si_2H_6 251
sidewall polymer 217, 235
SiH_4 251
silica analysis 360
silica gel 281

silica surfaces 279
silicon etching 159
SIMS 24, 308
single wafer cleaning 135
SiO_2 solubility 465
space charge 293
spectroscopicellipsometry 381
spin on dopant 555
SPM 66
spray processor 567, 597
sulfuric cleans 60
sulfuric peroxide 450
surface charge profiler 332
surface charge 187, 210, 345
surface metal oxide 237
surface microroughness 437
surface roughness 33, 303, 367
surface SIMS 308
surfactant 260
TD-APIMS 324
TD-GC/MS 324
TEOS 198
time dependent haze 61
TOF-SIMS 176, 494, 508, 519
TTDDB 23
TXRF 23, 300, 494
ultradilute SCl 590
ultrasonic 90
UV activated HCl 143
UV/Cl_2 117, 150
UV/O_3 117
vanadium contamination 493
vapor HF 128, 236
vapor phase cleaning 115, 175
vapor phase HF cleaning 135
via drying 530
via veil material 397
via veils 395, 396, 403
via wetting 426
via 214
VPS-DSE 538
wafer reclaim 413
water marks 84
wetting 60
XANES 614
XPS 176,185, 244, 318
zeta potential 2, 560, 583